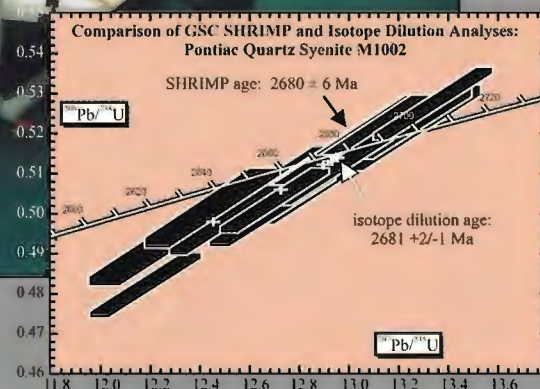
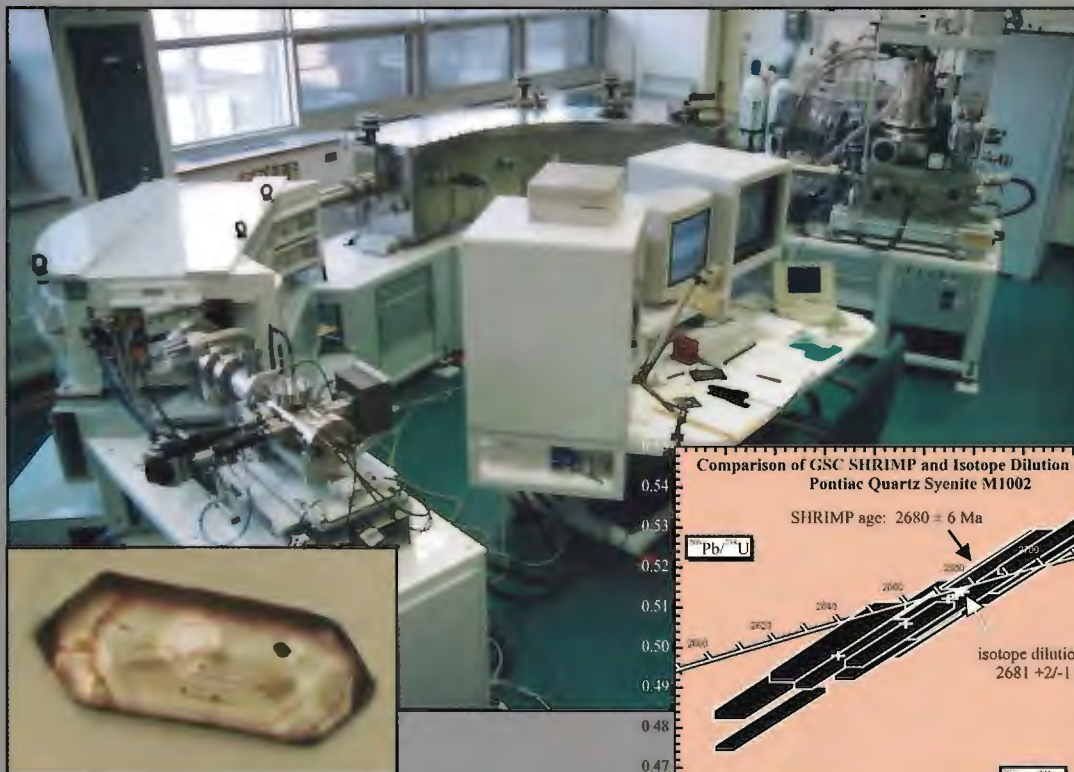




GEOLOGICAL SURVEY OF CANADA  
CURRENT RESEARCH 1997-F

**RADIOGENIC AGE AND ISOTOPIC STUDIES:  
REPORT 10**



1997



**STAFF, GEOCHRONOLOGY SECTION  
GEOLOGICAL SURVEY OF CANADA**

Research Scientists: Otto van Breemen  
Richard Stern  
Bill Davis  
Tom Skulski

Visiting Scientists: Mike Hamilton  
Dave Scott

Professional Scientists: Patricia A. Hunt  
Vicki J. McNicoll  
Réginald J. Thériault  
Mike Villeneuve  
Natasha Wodicka

Technical Staff: Diane Bellerive  
Jack L. Macrae  
Fred B. Quigg  
Klaus Santowski  
Ron Christie  
Gerald Gagnon

GEOLOGICAL SURVEY OF CANADA  
CURRENT RESEARCH 1997-F

**RADIOGENIC AGE AND ISOTOPIC STUDIES:  
REPORT 10**

1997

©Her Majesty the Queen in Right of Canada, 1997  
Cat. No. M44-1997/6E  
ISBN 0-660-16962-2

Available in Canada from  
Geological Survey of Canada offices:

601 Booth Street  
Ottawa, Ontario K1A 0E8

3303-33rd Street N.W.,  
Calgary, Alberta T2L 2A7

101-605 Robson Street  
Vancouver, B.C. V6B 5J3

or from

Canada Communication Group — Publishing  
Ottawa, Ontario K1A 0S9

A deposit copy of this publication is also available for  
reference in selected public libraries across Canada

Price subject to change without notice

#### **Cover illustration**

The top photograph shows the GSC's new SHRIMP II ion microprobe housed within the J.C. Roddick Ion Microprobe Laboratory. The bottom left photograph is a transmitted light image of a 200 µm long Paleozoic zircon, with a distinct core and rim, from which SHRIMP age determinations (15 µm diameter white spots) were obtained. The bottom right graph shows isotope age results on Archean zircons dated using the SHRIMP and the GSC's conventional TIMS method.

---

# CONTENTS

---

Introduction	
<b>R.J. Thériault</b> . . . . .	v
1. The GSC Sensitive High Resolution Ion Microprobe (SHRIMP): analytical techniques of zircon U-Th-Pb age determinations and performance evaluation	
<b>R.A. Stern</b> . . . . .	1
2. Modified chemical procedures for the extraction and purification of uranium from titanite, allanite, and rutile in the Geochronology Laboratory, Geological Survey of Canada	
<b>W.J. Davis, V.J. McNicoll, D.R. Bellerive, K. Santowski, and D.J. Scott</b> . . . . .	33
3. 2.70-2.58 Ga plutonism and volcanism in the Slave Province, District of Mackenzie, Northwest Territories	
<b>M.E. Villeneuve, J.R. Henderson, R.B. Hrabi, V.A. Jackson, and C. Relf</b> . . . . .	37
4. Sm-Nd isotopic study on mafic volcanic rocks from the Rankin Inlet and Tavani regions, District of Keewatin, Northwest Territories	
<b>R.J. Thériault and S. Tella</b> . . . . .	61
5. Preliminary U-Pb geochronology of the Hall Peninsula east of Iqaluit, southern Baffin Island	
<b>D.J. Scott</b> . . . . .	67
6. Timing of early deformation within the long-lived Elbow Lake Shear Zone, Trans-Hudson Orogen, Manitoba	
<b>K.M. Ansdell and J.J. Ryan</b> . . . . .	79
7. Thermochronology of hornblende and biotite from the Wekusko Lake area, Flin Flon Domain, Trans-Hudson Orogen, Manitoba	
<b>D. Marshall, K. Connors, and K. Ansdell</b> . . . . .	89
8. U-Pb age constraints on the timing of deposition of the Waugh Lake and Burntwood (Athabasca) groups, southern Taltson magmatic zone, northeastern Alberta	
<b>M.R. McDonough and V.J. McNicoll</b> . . . . .	101
9. U-Pb zircon ages of Tetagouche Group felsic volcanic rocks, northern New Brunswick	
<b>N. Rogers, N. Wodicka, V. McNicoll, and C.R. van Staal</b> . . . . .	113

10. New U-Pb data from the Laberge Group, northwest British Columbia: implications for Stikinian arc evolution and Lower Jurassic time scale calibrations <b>G.G. Johansson and V.J. McNicoll.</b> . . . . .	121
11. Laser $^{40}\text{Ar}/^{39}\text{Ar}$ ages of the Babine porphyries and Newman Volcanics, Fulton Lake map area, west-central British Columbia <b>M.E. Villeneuve and D.G. MacIntyre</b> . . . . .	131
12. U-Pb geochronology of stranger stones in Neoproterozoic diamictites, Canadian Cordillera: implications for provenance and ages of deposition <b>G.M. Ross and M.E. Villeneuve</b> . . . . .	141
Other publications containing geochronological data generated by the Geochronology Laboratory of the Geological Survey of Canada . . . . .	157

---

# RADIOGENIC AGE AND ISOTOPIC STUDIES: REPORT 10

---

## INTRODUCTION

This year's edition of "Radiogenic Age and Isotopic Studies" marks the tenth anniversary of its initial publication. Initiated in 1987, "Radiogenic Age and Isotopic Studies" has become a yearly tradition amongst researchers and staff of the Geological Survey of Canada. Once again, the Geochronology Subdivision, Continental Geoscience Division presents a collection of papers on various geoscience research topics within the fields of U-Pb,  $^{40}\text{Ar}/^{39}\text{Ar}$ , Sm-Nd, and Rb-Sr dating. Readers are reminded that the contributions often contain provisional results and interpretations of on-going research, or consist of completed studies of limited scope. Typically, articles of greater depth and magnitude are published in external journals, and a list of such recent works is provided at the end of this volume. Nonetheless, all reports herein present brief regional and local field settings, and relate data in an appropriate geological context.

The year 1996 was highlighted by the commissioning of the SHRIMP (Sensitive High Resolution Ion Microprobe), allowing micrometre scale age determinations on individual mineral grains. With the acquisition of the SHRIMP, new research horizons are attainable, promising discoveries on the age and evolution of Canada's landmass with unparalleled detail. Once in full operation, the SHRIMP laboratory was officially dedicated to the memory of the late Chris Roddick, who spearheaded the effort to bring the SHRIMP to the GSC. Since the passing of Chris, Richard Stern has led the SHRIMP program. With the capable help of Mike Gerasimoff, Richard oversaw the installation of the instrument, established an appropriate analytical standard and saw that the SHRIMP quickly matured to a fully operational research tool. Appropriately, the description, calibration, and operation of the SHRIMP are the object of the first paper of this volume.

Other papers presented in this volume exemplify the span of the Geochronology Subdivision's involvement, both in time through the geological eons and in space across the Canadian landmass. Included are reports on the age and evolution of the Archean Slave and Keewatin crust, which are the focal point of extensive recent and upcoming mapping efforts by the Continental Geoscience Division. Contributions on the Paleoproterozoic include papers on the Trans-Hudson Orogen in Manitoba and southern Baffin Island, and the

## INTRODUCTION

L'édition de cette année de *Radiogenic Age and Isotopic Studies* (Âges radiométriques et études isotopiques) marque le dixième anniversaire de cette publication. Lancée en 1987, la parution de cette publication est devenue un événement annuel pour les chercheurs et le personnel de la Commission géologique du Canada. Une fois de plus, la Sous-division de la géochronologie de la Division de la géologie du continent présente plusieurs articles sur divers sujets de recherche liés à la datation radiométrique par les méthodes U-Pb,  $^{40}\text{Ar}/^{39}\text{Ar}$ , Sm-Nd et Rb-Sr. Il est ici utile de rappeler aux lecteurs que les rapports regroupés dans la présente publication ne contiennent souvent que les résultats et les interprétations provisoires de recherches en cours ou qu'ils consistent en un compte rendu final d'études de portée limitée. En général, les articles plus approfondis et de grande portée sont publiés dans des revues scientifiques extérieures; une liste des articles publiés récemment est donnée à la fin de la présente publication. Néanmoins, tous les rapports contenus dans la présente publication renferment un résumé descriptif du milieu régional et local dans lequel les échantillons ont été recueillis et contiennent une interprétation qui place les données dans le contexte géologique approprié.

Le point saillant de l'année 1996 a été la mise en service de la microsonde SHRIMP, acronyme anglais de *Sensitive High Resolution Ion Microprobe* (microsonde ionique à haute résolution et à haut niveau de sensibilité), qui permet d'effectuer des datations à l'échelle du micron dans des grains individuels de minéraux. L'acquisition de la microsonde SHRIMP a ouvert de nouveaux horizons de recherche, laissant entrevoir des découvertes intéressantes sur l'âge et l'évolution de la masse continentale du Canada à un niveau de détail sans précédent. Lorsqu'il est devenu complètement opérationnel, le laboratoire qui abrite la microsonde SHRIMP a été officiellement inauguré à la mémoire du regretté Chris Roddick grâce à qui la CGC a fait l'acquisition de cet appareil. Depuis la disparition de Chris, Richard Stern a pris la relève à la direction du programme SHRIMP. Avec l'aide de Mike Gerasimoff, Richard a supervisé l'installation de l'instrumentation, établi une norme d'analyse adéquate et a veillé à ce que la microsonde SHRIMP devienne rapidement un outil de recherche complètement opérationnel. Il est donc à-propos que la description, l'étalonnage et le fonctionnement de la microsonde SHRIMP fassent l'objet du premier article de la présente publication.

Les autres articles apparaissant dans le présent volume illustrent l'éventail des travaux de la Sous-division de la géochronologie, tant dans le temps (à travers les grandes divisions des temps géologiques) que dans l'espace (à la grandeur de la masse continentale du Canada). Le lecteur trouvera également des articles sur l'âge et l'évolution de la croûte archéenne de la Province des Esclaves et du district de Keewatin, deux régions où la Division de la géologie du continent a entrepris des travaux de cartographie géologique de grande envergure. Les contributions sur le Paléoprotérozoïque incluent des articles sur l'orogène trans-hudsonien au Manitoba et

Taltson Magmatic Zone of northern Alberta. Also included are reports on the Ordovician Tetagouche Group of New Brunswick, and on aspects of Cordilleran evolution.

The continued vitality of the Geochronology Subdivision's program would not be possible without the diligent work of its support staff. Gerry Gagnon and Ron Christie produce pure mineral separates from rock specimens. Fred Quigg assures continued production of  $^{40}\text{Ar}/^{39}\text{Ar}$  data. Diane Bellerive and Jack MacRae perform the delicate procedures to extract nanogram levels of Pb and U from carefully selected mineral separates. Klaus Santowski meticulously measures isotopic ratios on a solid source mass spectrometer. Students Katherine Baker, Jasen Robillard, Nicole Sanborn, Steve Walker, and Shane Wilkinson provided invaluable help in mineral preparation. All are warmly thanked for their reliability and commitment.

dans le sud de l'île de Baffin, ainsi que sur la zone magmatique de Taltson dans le nord de l'Alberta. D'autres articles portent sur le Groupe de Tetagouche de l'Ordovicien au Nouveau-Brunswick, ainsi que sur certains aspects de l'évolution de la Cordillère.

La vitalité sans cesse renouvelée du programme de la Sous-division de la géochronologie ne saurait exister sans la diligence de son personnel de soutien. Gerry Gagnon et Ron Christie s'occupent de la production de concentrés de minéraux purs à partir d'échantillons de roches. Fred Quigg livre de manière ininterrompue les données  $^{40}\text{Ar}/^{39}\text{Ar}$ . Diane Bellerive et Jack MacRae réalisent les opérations délicates d'extraction de nanogrammes de Pb et d'U dans des concentrés de minéraux choisis. Klaus Santowski mesure avec minutie les rapports isotopiques sur un spectromètre de masse à source solide. Les étudiants Katherine Baker, Jasen Robillard, Nicole Sanborn, Steve Walker et Shane Wilkinson ont fourni une aide inestimable à la préparation des minéraux. Nous les remercions chaleureusement de leur travail consciencieux et de leur dévouement.

---

*Réginald J. Thériault*



# The GSC Sensitive High Resolution Ion Microprobe (SHRIMP): analytical techniques of zircon U-Th-Pb age determinations and performance evaluation

R.A. Stern<sup>1</sup>

*Stern, R.A., 1997: The GSC Sensitive High Resolution Ion Microprobe (SHRIMP): analytical techniques of zircon U-Th-Pb age determinations and performance evaluation; in Radiogenic Age and Isotopic Studies: Report 10; Geological Survey of Canada, Current Research 1997-F, p. 1-31.*

---

**Abstract:** Analytical methods of zircon U-Pb-Th age determinations using the newly acquired Sensitive High Resolution Ion Microprobe (SHRIMP) have been established and are reported in detail. In a SHRIMP analysis, an attempt is made to sample the smallest possible amount of zircon that can give useful age information, usually a spot selectively variable from about 5 to 30  $\mu\text{m}$  diameter and <1  $\mu\text{m}$  deep. Only 1-10 ng of zircon is sampled, three orders of magnitude smaller than a typical isotope dilution thermal ionization mass spectrometry (ID-TIMS) analysis. Causes and mitigation of the variable relative yields of Pb, U, and Th due to the sputtering process are discussed. Megacrystic zircon from the Kipawa syenite complex has been adopted as the current Pb/U and Pb/Th standard; the Pb/U age of the standard has been independently determined by ID-TIMS analysis at  $993.4 \pm 0.7$  Ma. SHRIMP data reduction and error propagation procedures are summarized.

The overall performance of the SHRIMP was evaluated by analyzing zircons of varying ages (0.5 to 2.7 Ga) using the new zircon standard to calibrate the Pb/U and Pb/Th ratios. Both  $^{207}\text{Pb}/^{206}\text{Pb}$  and  $^{206}\text{Pb}/^{238}\text{U}$  ages agree within error with the ID-TIMS ages. The  $^{208}\text{Pb}/^{232}\text{Th}$  are systematically younger and indicate unknown analytical problems. Under routine conditions,  $2\sigma$  age uncertainties for single spots in average zircons decrease from typically  $\pm 4\%$  at 0.5-1.5 Ga, to  $\pm 2\%$  at 1.9 Ga, and  $\pm 0.5\%$  at 2.7 Ga. The  $2\sigma$  errors on pooled analyses of relatively simple zircon samples decrease from  $\pm 1.5\%$  at 0.5-1.5 Ga,  $\pm 0.5\%$  at 1.9 Ga, and  $\pm 0.2\%$  at 2.7 Ga. For zircons <1.5 Ga, precise age determinations rely mainly on pooling of  $^{206}\text{Pb}/^{238}\text{U}$  ratios or regression on a Tera-Wasserberg diagram, whereas for zircons >1.5 Ga, ages are derived mainly from the pooled  $^{207}\text{Pb}/^{206}\text{Pb}$  ratios of concordant zircons. As a rule of thumb, it is generally possible to derive a SHRIMP zircon age that has an error of about five times that of a precise ID-TIMS analysis.

**Résumé :** Le présent rapport consiste en un compte rendu détaillé des méthodes analytiques qui ont été établies aux fins d'utilisation de la microsonde SHRIMP (microsonde ionique à haute résolution et à haut niveau de sensibilité), dont la Commission géologique du Canada vient de faire l'acquisition, pour la datation U-Pb-Th sur zircon. Lors d'une analyse à la microsonde SHRIMP, on tente d'utiliser la plus petite quantité possible de zircon qui puisse produire des données utiles sur l'âge, ce qui correspond dans les faits à un point de dimension variable préétablie d'environ 5 à 30  $\mu\text{m}$  de diamètre et de  $\mu\text{m}$  de profondeur. Le poids de

---

<sup>1</sup> Geological Survey of Canada, 601 Booth Street, Ottawa, Ontario K1A 0E8

l'échantillon de zircon analysé n'est seulement que de 1-10 ng, soit mille fois moins que celui nécessaire à une analyse typique par dilution isotopique et spectrométrie de masse à thermoionisation (ID-TIMS). Les causes de la variabilité des rendements relatifs de Pb, U et Th, qui est liée à l'érosion superficielle de l'échantillon, et les mesures à prendre pour atténuer ces effets sont abordées. Les gros phénocristaux de zircon du complexe syénitique de Kipawa ont été adoptés comme étalon des rapports Pb/U et Pb/Th; l'âge Pb/U de l'étalon a été indépendamment établi par analyse ID-TIMS à  $993,4 \pm 0,7$  Ma. Les méthodes de réduction des données et de propagation de l'erreur appliquées aux analyses à la microsonde SHRIMP sont décrites succinctement.

La performance globale de la microsonde SHRIMP a été évaluée par l'analyse de zircons d'âges variés (de 0,5 à 2,7 Ga) en utilisant le nouvel étalon de zircon pour calibrer les rapports Pb/U et Pb/Th. Les âges  $^{207}\text{Pb}/^{206}\text{Pb}$  et  $^{206}\text{Pb}/^{238}\text{U}$  coïncident, à l'intérieur de l'intervalle d'erreur, à ceux établis par analyse ID-TIMS. Les âges  $^{208}\text{Pb}/^{232}\text{Th}$  sont systématiquement plus récents et indiquent des problèmes analytiques de caractère non déterminé. Dans les conditions normales, les valeurs  $2\sigma$  de l'erreur qui entache les datations de points précis dans des zircons moyens diminuent de façon inversement proportionnelle à l'âge, passant typiquement de  $\pm 4\%$  à des âges de 0,5-1,5 Ga, à  $\pm 2\%$  à un âge de 1,9 Ga et finalement à  $\pm 0,5\%$  à un âge de 2,7 Ga. Les valeurs  $2\sigma$  de l'erreur sur les analyses groupées d'échantillons de zircon relativement simples diminuent dans le même sens, passant de  $\pm 1,5\%$  à des âges de 0,5-1,5 Ga, à  $\pm 0,5\%$  à un âge de 1,9 Ga et finalement à  $\pm 0,2\%$  à un âge de 2,7 Ga. Pour les zircons de  $<1,5$  Ga, des datations précises peuvent être obtenues surtout par un regroupement de déterminations individuelles du rapport  $^{206}\text{Pb}/^{238}\text{U}$  ou encore par une régression dans un diagramme de Tera-Wasserberg, tandis que pour les zircons de  $>1,5$  Ga, les âges sont surtout établis à partir du regroupement de déterminations individuelles du rapport  $^{207}\text{Pb}/^{206}\text{Pb}$  de zircons concordants. Règle générale, il est possible de dériver un âge sur zircon au moyen de la microsonde SHRIMP avec un intervalle d'erreur d'environ cinq fois supérieur à celui d'une analyse ID-TIMS précise.

## INTRODUCTION

On December 12, 1995, a  $^{208}\text{Pb}^+$  signal from a feldspar target was detected for the first time at the ion collector of the GSC's new Sensitive High Resolution Ion Microprobe (SHRIMP) occupying the new ground-floor facility, the J.C. Roddick Ion Microprobe Laboratory, at 601 Booth Street, Ottawa. This seemingly modest achievement nevertheless signified the beginning of a new era in geochronological research within the GSC, and marked the end of a two year long preparatory period during which the instrument was manufactured, exhaustively tested, and finally delivered to Ottawa. The GSC's SHRIMP II (Clement and Compston, 1989) is a second generation instrument, a modified version of the highly successful SHRIMP I prototype that was designed and built at the Research School of Earth Sciences, Australian National University (RSES-ANU; Clement et al., 1977). Clement et al. (1977) had one simple, but ambitious, goal in mind in designing the original SHRIMP: to build an instrument that would permit precise in situ measurement of isotopes in mineral grains.

Over the past 15 years, both SHRIMP I and SHRIMP II have proven highly successful performers throughout a range of analytical tasks, including the measurement of isotopes of U, Pb, Th, Hg, Ca, Ti, REEs, and S in several mineral targets. By far the most widespread application of the SHRIMPs, however, has been the determination of U-Pb isotopic ages of zircon (Compston et al., 1982, 1984). The zircon dating capabilities of the SHRIMP became more widely recognized following the discovery of the oldest zircons on Earth (Froude et al., 1983). The SHRIMP has been used to tackle the most complex geochronological targets, including the dating of the oldest rocks on Earth (Bowring et al., 1989).

The demand for an in situ isotopic age dating tool at the GSC stems largely from the increasing demand to date complex mineral targets, such as zircons with cores and overgrowths. It is possible to date parts of such grains with existing methods at the GSC, by physical isolation of zircon fragments followed by isotope dilution solution chemistry and thermal ionization mass spectrometry (ID-TIMS). Although this approach can precisely resolve many complex geochronological problems, the work is time consuming and it is not always possible to isolate different generations of zircon. In addition, the zircon analyzed may be discordant and thus yield ambiguous results. Many complex dating problems require the analysis of much smaller amounts of zircon than is practical and cost-effective with ID-TIMS. Age determinations by the SHRIMP answer the need for controlled (i.e. in situ) analysis of the smallest possible amounts of material. As will be discussed in Part II, there are other benefits to in situ spot age determinations, but there are some drawbacks too, in particular the poorer analytical precision. It is the opinion of the author that the SHRIMP and ID-TIMS are complementary methods and that it is important for the geochronologist to choose the method that best suits the particular problem, and sometimes both will be required.

The most important application of the SHRIMP at the GSC will be the determination of U-Pb ages of zircons. In 'Part I' of this report, the methods of determining U-Pb ages of zircons are described, including sample preparation, mass spectrometry, data acquisition, age calculations, and error estimation. Also reported are the characteristics of the essential element of this new analytical program, a new in-house zircon standard. In 'Part II', the accuracy and precision of the GSC SHRIMP data are compared to well-determined

ID-TIMS ages for seven different samples spanning 2 Ga, and the relative strengths and weakness of the respective methods are discussed.

## PART I: ANALYTICAL METHODS OF U-Pb-Th ANALYSIS

### Nomenclature

Throughout this paper, the following conventions apply. In discussion of isotopic ratios or ion count rates, those with a '+' sign (e.g.  $^{206}\text{Pb}^+ / ^{238}\text{U}^+$ ) indicate measured values at the collector. The use of a '\*' indicates that the Pb isotope has been corrected for common Pb (e.g.  $^{206*}\text{Pb}^+$ ). Where the '+' sign is omitted (e.g.  $^{206}\text{Pb} / ^{238}\text{U}$ ), it is assumed that all corrections have been applied (common Pb, interelement fractionation, etc.).

Statistical examination of data employs the use of  $\chi^2$ , the reduced chi squared value, sometimes referred to as the mean square of weighted deviates (MSWD). The  $\chi^2$  value is used to assess the likelihood that the data fit a particular model (e.g. single population of numbers, or a fit to a linear regression). Tables of  $\chi^2$  distributions like those in Bevington (1969, Table C-4) can be used to assess the probability (P) that a given  $\chi^2$  value may be exceeded, and P values are indicated throughout the text. The higher the value of P, the more confidence one has that the data fit the particular model. Generally, P should exceed 5% to be considered a valid fit. For assessing the fit to a mean,  $\chi^2$  values were determined using n-1 degrees

of freedom; for fits to a straight line, n-2 degrees of freedom were used; 's' refers to standard deviation, 'se' standard error,  $\sigma$  to 68% confidence interval, and  $2\sigma$  to 95% confidence interval, where  $\sigma$  incorporates several factors in addition to counting errors in assessing the confidence interval.

### The SHRIMP II Ion Microprobe

Figure 1 shows a schematic diagram of the GSC SHRIMP II and periferal devices. The SHRIMP is a Nier-Johnson type double-focusing secondary ion mass spectrometer (SIMS) that analyses secondary ions generated at the target mineral by a beam of primary oxygen ions ( $\text{O}_2^+$ ). A double-focusing mass spectrometer simultaneously corrects for both directional and velocity (kinetic energy) inhomogeneities in a source ion beam (e.g. Roboz, 1968). A single magnetic sector mass spectrometer such as the GSC's MAT 261 used in ID-TIMS analysis of zircon is capable of directional refocusing of ions that have a small angular divergence from the heated Re filament, but there is no capability or requirement for velocity refocusing, as the ions have essentially uniform kinetic energies. In SIMS, the ions generated at the target also have a wide angular divergence, but in addition they have widely different kinetic energies, and it is necessary to employ an additional energy focusing device (electrostatic analyzer). The large size of the SHRIMP (3.5 x 6 m) is required for optimal directional refocusing of the ion beam and to minimize aberrations in the electrostatic and magnetic fields, all necessary for maximum beam transmission.

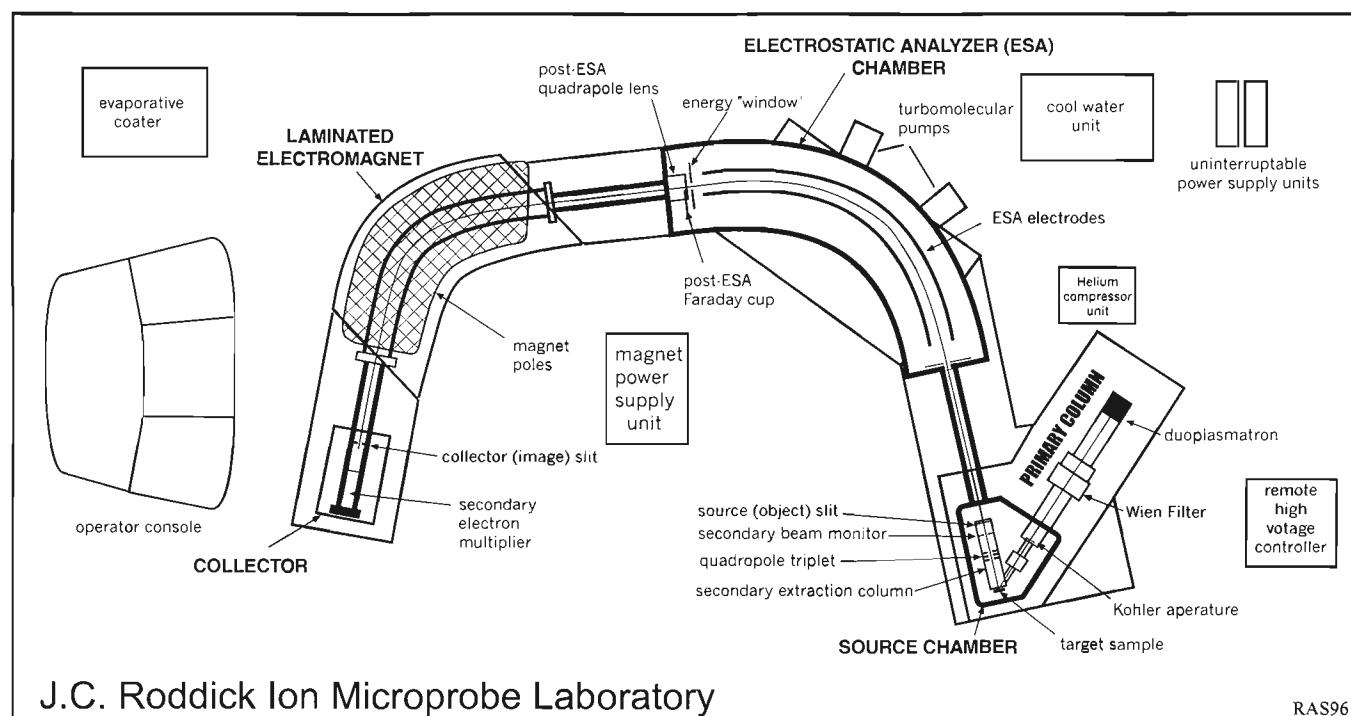


**Figure 1.** Schematic plan view of the J.C. Roddick Ion Microprobe Laboratory, showing the layout of the SHRIMP II and periferal devices.

What follows is a brief description of the main components of the GSC SHRIMP, with emphasis on those factors that have a significant influence on data acquisition.

### Primary column

The purpose of the primary column is to produce a beam of pure  $O_2^+$  ions that can be focused to a spot on the target zircon. The primary oxygen ions are generated in a Kratos Analytical Ltd. duoplasmatron by oxygen gas discharge within a hollow Ni cathode, and are extracted at 10 kV potential. The primary beam is mass filtered by a 'Wien filter' to prevent  $O^-$  or contaminants such as  $NO_2^+$ , or  $OH^+$  from reaching the target. Normal vacuum conditions in the primary column during operation are about  $1.2 \times 10^{-6}$  mbar. The primary column employs Kohler primary ion focusing, which provides radially uniform primary beam density independent of the spot size. The most important practical aspect of Kohler imaging is its influence on the material actually sputtered and analyzed. Perfect Kohler imaging produces flat-bottomed pits, and these are ideal because the material analyzed comes from a uniform depth. Figure 2 shows a profile across a pit in a zircon created with the 200  $\mu m$  Kohler aperture in a typical analysis lasting 18 minutes. Note that the bottom, which is only 0.65  $\mu m$  deep, is flat but it has shallowly sloping edges where the beam was weaker and therefore not in perfect Kohler mode. In practice, perfect Kohler imaging is difficult to achieve and comes at a significant loss in beam transmission. Thus, the sputtered zircon during standard running conditions comes from a dish-shaped depression that is generally only 0.5-1.0  $\mu m$  deep.

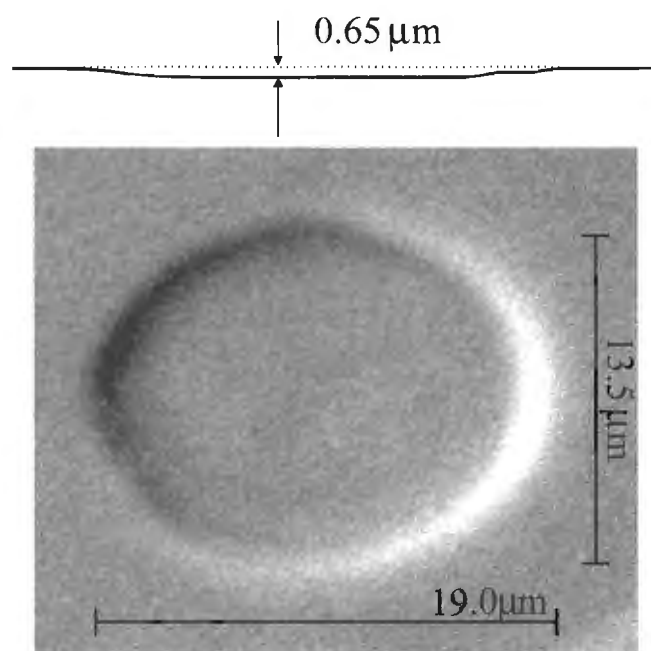


**Figure 2.** Secondary electron image of a pit created with the 100  $\mu m$  Kohler aperture during a routine zircon analysis. At top is a profile of a pit along its long axis, obtained with the use of a Tencor Instruments stylus. Note that the pit is dish-shaped, having flat bottoms and shallow-dipping walls.

**Table 1.** Dimensions of the primary oxygen beam spot.

Kohler aperture diameter ( $\mu m$ )	Spot size, 1 x w ( $\mu m^2$ )	Approx. Spot area ( $\mu m^2$ )	Beam density ( $pA/\mu m^2$ )
200	25 x 33	2592	1.0
100	13.5 x 19	806	1.1
70	8.0 x 12	302	1.4
50	6.0 x 11	207	1.3
30	4 x 6	75	1.0

From the above example, the amount of zircon sputtered for the 200  $\mu m$  aperture is about 8 ng. Using the 100  $\mu m$  aperture, generally preferred in most zircon applications, it is determined that about 2.4 ng of zircon is actually sputtered during the course of a typical analysis (zircon density =  $4.65 \text{ pg}/\mu m^3$ ). Assume, for illustration, that the zircon had 50 ppm of total Pb (highly variable depending on age and U content), then the total amount of Pb sputtered in this case is 0.12 pg, but only 40% of the analysis time is spent analyzing the Pb, so only 0.05 pg of Pb is available for analysis. The very small amount of Pb analyzed is one of major reasons why SHRIMP  $^{207}\text{Pb}/^{206}\text{Pb}$  ages are less precise than those of ID-TIMS. The sputter rates are deliberately low because the objective of the analysis is to analyze as little zircon as possible, within the constraints of the counting statistics of the analyzer system (see 'Error analysis' for further discussion).

The spot size is defined by the particular Kohler aperture inserted into the path of the primary beam. Five different Kohler apertures are available and the resulting spot diameters range from approximately 5 to 30  $\mu m$  (Table 1). The spots are elliptical due to the  $45^\circ$  incidence angle of the cylindrical primary beam with respect to the plane of the target. For the majority of zircon analyses, the 100  $\mu m$  Kohler aperture will be used, producing a spot about  $13.5 \times 19 \mu m$  in dimension. In Kohler mode the sputter rate is dependent only on beam density ('brightness'), not spot size. Primary beam brightness decreases over a period of several days of running as the duoplasmatron becomes clogged with nickel oxides. The beam density for typical run conditions averages about  $1.0 \pm 0.2 \text{ pA}/\mu m^2$ . The rate of penetration of the primary beam into zircon can be reported as depth (nm) per minute per beam density, and for typical conditions is about 42 nm/min/( $pA/\mu m^2$ ).

As an example calculation, suppose a particular zircon was sputtered for 15 minutes using the 200  $\mu m$  Kohler aperture while monitoring a primary current of 3.0 nA. The beam density using the spot areas of Table 1 is  $1.16 \text{ pA}/\mu m^2$ . The depth of penetration would be  $42 \times 15 \times 1.16 = 732 \text{ nm} = 0.73 \mu m$ .

### Source chamber

The source chamber houses part of the primary column, the sample target, and the secondary extraction column. The source chamber is pumped by a 1200 L/s CTI Cryogenics Helium cryopump and is normally at a pressure of  $6 \times 10^{-8}$  mbar. Two samples are permitted within the source chamber, and a further three may be stored in the sample lock above the

source chamber. Positive secondary ions generated during the mechanical sputtering of the mineral (e.g.  $\text{Zr}^+$ ,  $\text{Pb}^+$ ,  $\text{U}^+$ ,  $\text{Th}^+$ ) are extracted at  $90^\circ$  from the surface of the sample by a 750 V potential and accelerated through a total 10 kV potential to Earth ground. Focusing and steering of the secondary ions is accomplished by an array of three quadrupole lenses. A Faraday plate that partially intersects the secondary beam (the 'secondary beam monitor') is used to measure the intensity of the total secondary ion emission from the target. The secondary ions are focused on the back side of the adjustable 'source slit', which is the ion optical object of the analyzer system. For zircon analysis, the source slit is kept at a nominal 100  $\mu\text{m}$  width. The ribbon-shaped beam of secondary ions passing through the source slit is steered by deflecting plates prior to entry into the drift tube to the electrostatic analyzer.

### Electrostatic analyzer

The secondary ions enter the electrostatic analyzer (ESA) chamber, which is a 1272 mm radius,  $90^\circ$  cylindrical electrostatic sector, for filtering and focusing according to the kinetic energy of the ion. The vacuum is held at about  $5 \times 10^{-8}$  mbar by twin Alcatel 450 L/s turbomolecular pumps. The ion beam passes between two cylindrical aluminum plates, 2.5 cm thick and 30 cm high, spaced 6 cm apart, between which a potential of 950 V is placed (positive on the outer radius). Ions of identical energy will be focused at the same point on a plane beyond the electrostatic field. A mechanically-adjustable slit situated on the energy focal plane of the ESA is used to select a particular portion of the energy spectrum to pass through to the mass analyzer, termed the 'energy window'. Presently, this energy window is set at 2.5 mm, equivalent to  $\Delta 20$  eV. A pneumatically-driven Faraday plate immediately beyond the energy window can be inserted in order to measure the intensity of the energy-filtered secondary beam. A quadrupole lens situated at the exit to the ESA chamber permits steering and adjustment of the apparent position of ion optical object of the magnetic sector.

### Magnetic sector

The secondary ions enter a 1000 mm radius,  $72.5^\circ$  magnetic sector at a  $15^\circ$  angle for mass dispersion and refocusing. Ions of identical mass are refocused to the same point on the magnet focal plane beyond the magnet. The GSC SHRIMP uses a prototype laminated electromagnet (Buckley Systems Ltd., New Zealand), designed for improved speed of switching. Control of the magnetic field is through four Hall Effect probes.

### Detector

The mass-dispersed ions pass through the resolving (collector) slit, normally set at a width of 100  $\mu\text{m}$ , located on the focal plane of the magnet. The position of the collector assembly can be rapidly translated along its axis during analysis to optimize focusing of individual isotopes. Ion collection in zircon analysis is accomplished with a single

secondary electron multiplier (ETP model AF150H) into which the isotopes of interest are sequentially stepped. Each arrival of an ion at the first dynode of the electron multiplier generates a pulse of secondary electrons that, if above a selectable threshold value, is converted into one ion 'count' by an Ortec 9302 Discriminator/Preamplifier. The number of counts generated in a specified period is measured by an Ortec 994 Dual Counter/Timer and subsequently used in data processing. The rate of arrival of counts is measured and converted to an analogue signal by the 'ratemeter' for use by the operator in tuning the secondary beam transmission. A typical count rate for  $^{206}\text{Pb}^+$  in zircon would be 500 c/s (counts per second), which represents an ion current of  $8 \times 10^{-17}$  A. Such a signal is orders of magnitude smaller than the typical  $^{206}\text{Pb}^+$  ion beams used in thermal ionization mass spectrometry of zircon, and hence the need to use an electron multiplier under all conditions of zircon analysis. Vacuum for the collector assembly is provided by an Alcatel 450 L/s turbomolecular pump, and is normally about  $7 \times 10^{-9}$  mbar.

### Mass resolution and peak shape

The SHRIMP is designed to operate routinely at high mass resolutions with the flat-topped peaks required for precise isotopic analysis. For U-Pb age determinations of zircon, a mass resolution 'R' of greater than 5000 ( $R = M/\Delta M @ 1\%$  peak height; M is mass in amu) is required to separate the isotopes of interest from interfering isotopes of nominally identical integral mass number. The peak shape has been examined and optimized using Pb-feldspar, and the width of the flat tops is 0.012-0.014 amu at the normal operating resolution of about 5500. See below for further discussion.

### Sensitivity

In order that the widest possible beam of secondary ions extracted from the target can be analyzed, large radius electrostatic ( $r = 1.3$  m) and magnetic ( $r = 1.0$  m) sectors are required (Matsuda, 1974). Compared to other ion microprobes, the SHRIMP is, therefore, highly sensitive to the presence of U and Pb (and other elements) in the mineral sample. An experiment conducted using the zircon SL13 revealed the following percentages of the total secondary ions transmitted to various points in the flight path:

- at target surface: 100%
- to secondary beam monitor (SBM): 37.5%
- through SBM: 37.1%
- through source slit: 37.0%
- through energy window: 5.6% (energy analyzed beam)

Thus, about 63% of the generated secondary ions fail to be transmitted through to the source slit. By the time the energy analyzed beam has passed through the energy window, only 5.6% of the original complement of secondary ions are present. Calculations using estimates of the mass of zircon eroded

show that about 0.3% of the sputtered Pb atoms are actually detected at the collector, a figure that, while low, is similar to TIMS analysis of Pb.

A useful gauge of sensitivity and thus overall performance of the GSC SHRIMP is the count rate of  $^{206}\text{Pb}^+$  at the collector, normalized to the  $^{206}\text{Pb}$  content of the zircon in ppm, normalized to the primary beam intensity (c/s/ppm/nA). Sensitivity for the GSC SHRIMP, assessed with the assumption that the SL13 standard zircon has 19 ppm  $^{206}\text{Pb}$ , normally ranges between 20 and 26 c/s/ppm/nA, a similar range as reported for the ANU SHRIMP II.

## Samples

The SHRIMP is capable of accepting grain mounts, standard polished thin sections, or rock slabs. Grain mounts of zircon are by far the most common method of sample preparation, as literally hundreds of zircons can be mounted on a single epoxy disk. Zircons are picked from the heavy liquid concentrate and divided into magnetic fractions with a Frantz separator. The zircons within each magnetic fraction are further subdivided by morphology and size, identical to the procedure followed for an ID-TIMS analysis. Perhaps differing slightly from the ID-TIMS procedure, however, is that one seeks out the morphologically complex grains, such as those with cores and rims, as these may record the complex history of the rock. Also, depending on the recovery and complexity, grains with a range of magnetic properties are often selected, as there is a desire not to bias the results by selecting only the least magnetic ones. The grains are not abraded, as this action could potentially wipe out age complexities that are sought.

Once selected, the zircons are transferred by pipette or tweezers to the surface of a piece of sticky tape (3M 666) located on the bottom of a custom Teflon mounting assembly. The zircons are packed as closely as possible without touching one another into neat, rectilinear matrices, with individual fractions separated by larger spaces. A few fragments of the

standard zircon are also included on the mount. The zircons are then covered with Struers Epofix epoxy resin and allowed to cure overnight, yielding an epoxy disk 2.5 cm in diameter and 7 mm thick. The mid-points of the zircons are exposed with 9  $\mu\text{m}$ , 6  $\mu\text{m}$ , and finally 1  $\mu\text{m}$  diamond polishing compounds.

Following polishing, the zircons on the mount are photographed in transmitted and reflected light. The mount is then washed with soap by hand, rinsed with deionized water, air blown to remove water droplets, and allowed to dry under a heat lamp. The mount is then coated with 4.0 nm of high purity Au (Aesar 99.9999%) using an Edwards Auto 306 coater. This amount of Au is sufficient for cathodoluminescence (CL) and back-scattered electron (BSE) imaging of the zircons at GSC's electron microbeam facility. Cathodoluminescence and back-scattered electron imaging may reveal internal structures of the zircon not observable with visible light (e.g. Hanchar and Miller, 1993), and these images are used to locate suitable areas for analysis. Subsequently, the mount is repolished lightly with 1  $\mu\text{m}$  diamond paste to remove the Au, cleaned, and recoated with 7.0 nm of Au. Clamped into its stainless steel holder, the resistance across the surface of the sample measured with a multimeter is less than 50  $\Omega/\text{cm}$ .

The sample is then loaded into the sample lock of the SHRIMP and held under high vacuum ( $1 \times 10^{-7}$  mbar) for a minimum of 24 hours prior to transfer into the sample chamber for analysis.

## Mass spectra of zircon

The mass spectrum of zircon generated by the sputtering process is quite complex, as almost any combination of metal ions and oxides may form. The majority of ions are believed to be in the +1 electronic state. Although +2 ions may also be present, none are known to inhabit the part of the spectrum of interest in U-Pb analysis of zircon. An example of a zircon

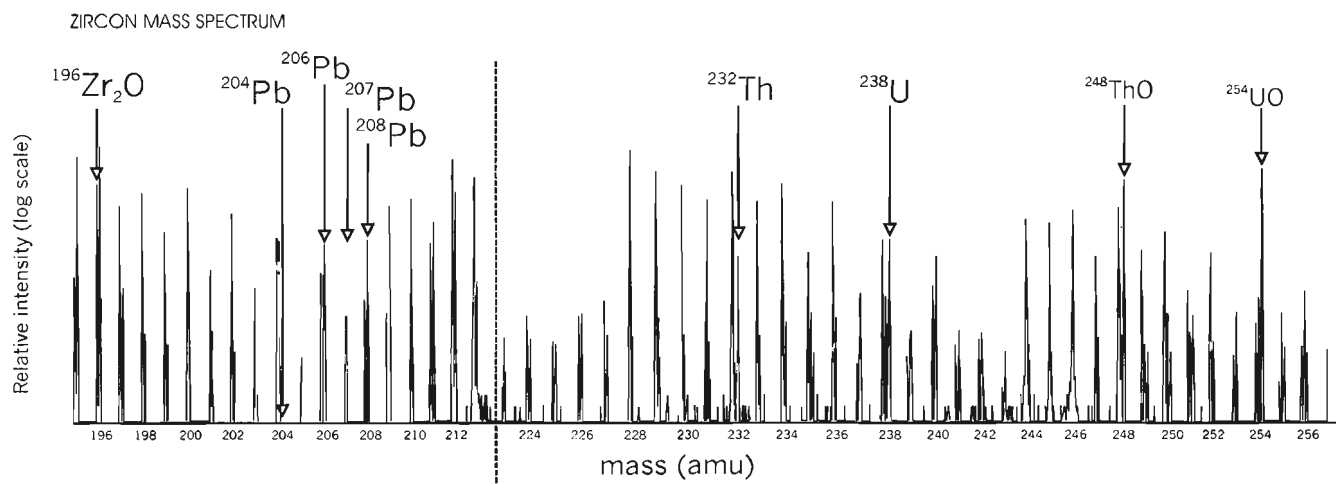


**Figure 3.** Mass spectrum of Kipawa zircon between 194 to 256 amu. Note the complexity of the mass spectrum and the position of the peaks of interest.

mass spectrum (Kipawa zircon) in the mass range of interest (196-254 amu) for zircon analysis is shown in Figure 3. Highlighted are the positions of the nine peaks used in zircon analysis. Figure 4 shows more detailed mass spectra near the peaks of interest. Note that the Pb, U, and Th isotopes are always the peaks of greatest mass in any one region. The most significant nearest neighbours are Hf-Si-Zr-O isobars, all readily separated from the Pb isotopes at a resolution of 5500.

The Pb hydrides  $^{206}\text{Pb}^1\text{H}$  and  $^{207}\text{Pb}^1\text{H}$  are a potential problem in SHRIMP analysis because the masses of the hydrides are almost identical to the metals. The mass of  $^{206}\text{Pb}^1\text{H}$  is 206.9822 amu, which is only 0.0064 amu higher than  $^{207}\text{Pb}$  at 206.9758 amu. A mass resolution of about 32 000 would be required to separate these isobars. Similarly, the mass of  $^{207}\text{Pb}^1\text{H}$  is only 0.0071 amu higher than  $^{208}\text{Pb}$ . The effect of hydrides is to increase the measured  $^{207}\text{Pb}^+ / ^{206}\text{Pb}^+$  value. It is possible to test for the presence of hydrides by comparing the measured  $^{207*}\text{Pb}^+ / ^{206*}\text{Pb}^+$  value

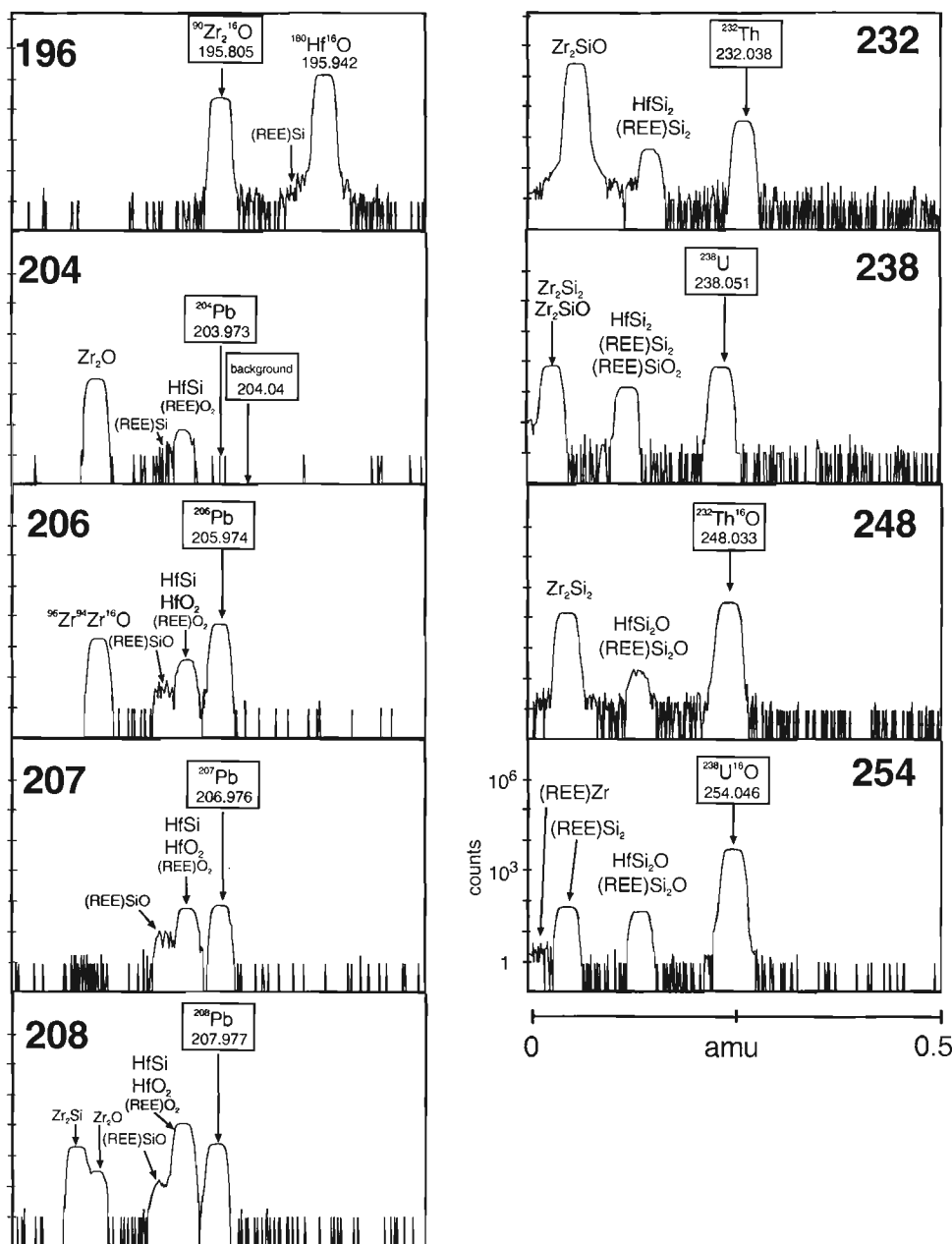


**Figure 4.** More detailed mass spectra (vertical log scale) of Kipawa zircon in ( $\pm 0.25$  amu intervals) centred on the isotopes of interest. Mass resolution is about 5500. Note that the Pb, U, and Th isotopes are always the heaviest within the region of interest.

for a zircon with the accepted value for that zircon. A significantly higher value for  $^{207}\text{Pb}^+/^{206}\text{Pb}^+$  could indicate that hydrides were present during analysis. Previous experience at ANU has shown that hydrides present as contaminants on the sample surface are usually undetectable after the sample mount has been at high vacuum for 24 hours. Accordingly, all zircon mounts remain at high vacuum in the sample lock for a minimum of 24 hours prior to analysis. The primary beam is also mass separated to avoid hydrides in the primary beam (e.g.  $\text{OH}^-$ ) hitting the target. The results of tests on several different zircons with the GSC SHRIMP suggest no statistically significant difference in the  $^{207}\text{Pb}^+/^{206}\text{Pb}^+$  values with the accepted values (see 'Part II'). It is possible that an increase in the  $^{207}\text{Pb}^+/^{206}\text{Pb}^+$  due to hydrides could be counterbalanced by mass fractionation (which would lower the ratios), but at the present time there is no reason to suspect that hydrides are a problem.

**Table 2.** Mass stations ('peaks') visited in a SHRIMP zircon age analysis.

Peak	Actual mass (amu)	typical count time (s) per scan
$^{90}\text{Zr}^{16}\text{O}$	195.805	2
$^{204}\text{Pb}$	203.973	20
background	204.040	20
$^{206}\text{Pb}$	205.974	15
$^{207}\text{Pb}$	206.976	25
$^{208}\text{Pb}$	207.977	15
$^{232}\text{Th}$	232.038	5
$^{238}\text{U}$	238.051	5
$^{232}\text{Th}^{16}\text{O}$	248.033	3
$^{238}\text{U}^{16}\text{O}$	254.046	3

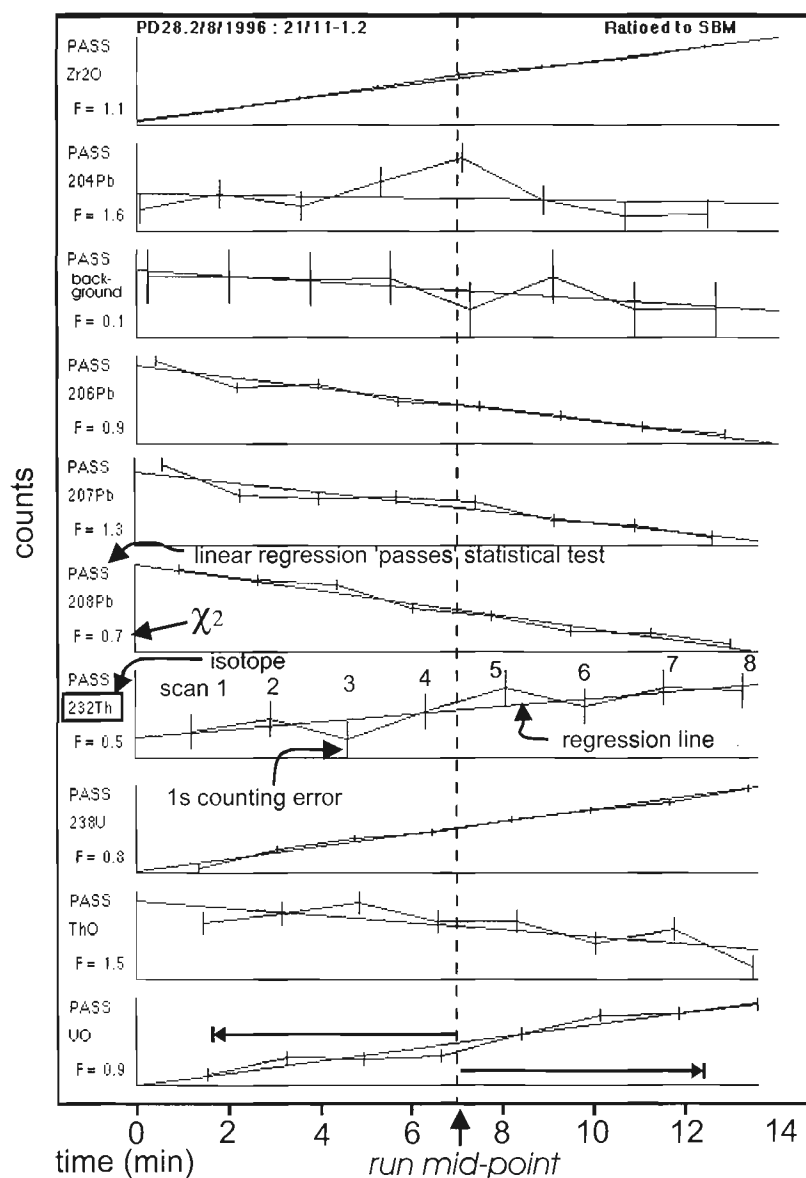


**Figure 5.**

Typical time-series record for each of the 10 mass stations visited during a zircon analysis. Peak intensity either increases, decreases, or remains constant during an analysis. A linear regression is used to calculate the count rate at the mid-point time for each isotope.



## Overview of the zircon analysis

The single most important aspect of the routine analysis of a zircon is the following: the objective of an analysis is to determine the isotopic composition of the zircon at the mid-point of the run. In other words, one is trying to obtain an estimate of the zircon age at a specific depth and time during the analysis. Although it is possible to do depth profiling, where one is specifically interested in the compositional changes of the zircon with depth, the SHRIMP is really not designed for this approach. It is commonly found that the composition of the zircon during the course of the analysis is essentially constant, due to the very small amounts of material analyzed. Sputtering is a very slow and controlled process compared to other *in situ* sampling methods, such as laser ablation, and it is generally not necessary to account for changing target composition. Nevertheless, with some zircons, typically those with fine oscillatory zoning, compositional changes are observed despite the shallow penetration.

A routine run is divided into normally 6 to 8 'scans', each comprising a series of ten mass stations ('peaks') that are sequentially visited for a specified period of time (Table 2). A certain total number of counts will be received at the collector for each peak during the specified time period. As the run proceeds, variations in the secondary ion yields of each isotope will normally occur as a consequence of the deepening of the hole and fluctuations in the intensity of the primary beam. Nevertheless, variations in secondary ion intensity can be corrected for by normalizing the counts on a peak to the total secondary ion beam current as measured at the secondary beam monitor (SBM) within the sample chamber (Fig. 1).

Figure 5 shows an example of an 8 scan, 10 peak zircon analysis, obtained over a 20 minute period. Throughout the run the signal intensity either increases ( $^{196}\text{Zr}_2\text{O}^+$ ,  $^{232}\text{Th}^+$ ,  $^{238}\text{U}^+$ ,  $^{254}\text{UO}^+$ ) or decreases ( $^{206}\text{Pb}^+$ ,  $^{207}\text{Pb}^+$ ,  $^{208}\text{Pb}^+$ ,  $^{248}\text{ThO}^+$ ), generally in a linear fashion. The results for each isotope can be treated as a linear 'time series'. If rastering of the spot prior to analysis was not totally effective,  $^{204}\text{Pb}^+$  may fall off after the first one or two scans. A linear regression is performed on the eight scans for each peak, and the mid-point count rate calculated for each isotope. The isotope ratios are then calculated using the statistically determined mid-point count rates (see 'Error analysis' for further discussion). Changes in either the isotopic composition (i.e. apparent age) or elemental abundances of U or Th of the zircon during the erosion of the pit would result in more complex, nonlinear time series, and a spline fitting procedure is available for such cases.

Initial data processing is done on-line immediately following termination of an analysis using software provided by the manufacturer, and this gives the analyst the first-pass isotope ratios and ages. However, complete processing of the data and final age determinations are done off-line using two custom software applications and various spreadsheet applications. Control of the SHRIMP and offline processing are accomplished with Power Macintosh computers.

## Secondary ion production of $\text{Pb}^+$ , $\text{U}^+$ , and $\text{Th}^+$

In order to determine the  $^{206}\text{Pb}/^{238}\text{U}$ ,  $^{207}\text{Pb}/^{235}\text{U}$ , and  $^{208}\text{Pb}/^{232}\text{Th}$  ages of an unknown spot sample of zircon, both the isotopic composition of Pb and the Pb/U and Pb/Th ratio (weight or atomic) must be determined. While the determination of the Pb isotopic composition is straightforward (see below), the precise determination of the Pb/U and Pb/Th values presents some difficulties. For example, under typical SHRIMP analytical conditions, the measured  $^{206}\text{Pb}^+/\text{U}^+$  in a zircon is normally two to five times the actual  $^{206}\text{Pb}/^{238}\text{U}$  value, varying from spot to spot and from sample mount to sample mount (i.e.  $[^{206}\text{Pb}^+/\text{U}^+]/[^{206}\text{Pb}/^{238}\text{U}] = 2$  to 5). Similarly,  $[^{208}\text{Pb}^+/\text{U}^+]/[^{208}\text{Pb}/^{232}\text{U}] = 3$  to 8. Thus, Pb is enhanced over U and Th as a consequence of the SHRIMP analysis, and it is understanding and controlling this instrumental effect that is discussed next.

## Understanding the relative ionization Yields of Pb, U, and Th

The crucial parameter in any age determination is the secondary ion current of an element or molecular species  $e$  (e.g.  $^{206}\text{Pb}^+$ ,  $^{238}\text{U}^+$ ),  $s_{i_e}$ , measured at the collector while sputtering is occurring, where

$$s_{i_e} = \text{PI}_e Y_e \alpha_e \theta_e \eta_e \quad (1)$$

and  $\text{PI}_e$  is the primary particle flux (ions/second) during measurement of the isotope  $e$ ,  $Y_e$  is the total number of secondary particles of  $e$  removed per primary particle impact or 'sputter yield',  $\alpha_e$  is the ionization probability of  $e$ ,  $\theta_e$  is the fractional concentration of  $e$  in the surface layer, and  $\eta_e$  is the transmission of  $e$  in the analysis system. In order for  $[^{206}\text{Pb}^+/\text{U}^+]/[^{206}\text{Pb}/^{238}\text{U}] = 1$ ,  $s_{i_{206}}/s_{i_{238}}$  must equal  $\theta_{206}/\theta_{238}$ , and for this to occur,  $\text{PI}_{206} = \text{PI}_{238}$ ,  $Y_{206} = Y_{238}$ ,  $\alpha_{206} = \alpha_{238}$ , and  $\eta_{206} = \eta_{238}$ . In other words, if the measured isotopic ratio is to equal the ratio in the sample, the primary particle flux, the sputter yield, the ionization probability, and the transmission of each isotope must be identical at all times. As it has already been stated,  $[^{206}\text{Pb}^+/\text{U}^+]/[^{206}\text{Pb}/^{238}\text{U}]$  is not equal to unity and also varies, and therefore one or more of  $\text{PI}_e$ ,  $Y_e$ ,  $\alpha_e$ , and  $\eta_e$  must be different between isotopes and also variable. Let us now consider each of these factors to determine what may be causing this particular analytical problem.

## Primary particle flux, $\text{PI}_e$

The primary ion current may fluctuate by several per cent over the course of an analysis due to uncontrollable variations in  $\text{O}_2^-$  ion production in the duoplasmatron, but there is no systematic relationship between the intensity of the primary ion beam with the particular isotope being measured. Furthermore, primary beam intensity fluctuations are largely cancelled out by normalizing the collected ion beam to the total secondary ion signal ('secondary ion normalization'), and thus in practice it can be assumed that  $\text{PI}_{206} = \text{PI}_{238}$  and  $\text{PI}_{208} = \text{PI}_{232}$ .

### Sputter yield, $Y_e$

Sputtering is a complex subject in its own right (see, for example, Benninhoven et al., 1987). In brief, an incoming high energy  $O_2^-$  ion is thought to penetrate the surface of the target and loses energy through elastic collisions with the target atoms. The target atoms in turn strike other target atoms, generating a 'collision cascade' of target atoms, causing considerable disruption of the crystal structure. A fraction of the jostled target particles, those having sufficient momentum to overcome the surface binding energy and the correct vector, will be ejected backwards from the surface (i.e. sputtered) about  $10^{-14}$  to  $10^{-12}$  s after primary impact. The sputtered particles include both atomic and molecular species, and are thought to be derived from the upper 1-2 nm of the surface. Sputtering is essentially a surface process (Williams, 1983), whereas lattice damage may extend to 10-25 nm.

The sputter yield  $Y_e$  is governed by a number of factors, including kinetic energy of the primary beam, the primary particle mass and charge, angle of incidence of the primary beam, and the nature of the target. All except the last factor may be considered as constants in the SHRIMP, i.e., the accelerating voltage of the primary beam is kept at 10 kV, the primary beam is mass filtered and consists of only  $O_2^-$  ions, and the angle of incidence is fixed at  $45^\circ$ .

The sputter yields from chemically complex targets are dependent on the binding energy of the element, which in turn is dependent on its mass, charge, crystal structural configuration, and neighbouring elements. In zircon analysis we should not expect that  $Y_{206}$  should be the same as  $Y_{238}$ . However, as explained by Shimizu and Hart (1982), once the crater has been eroded down to the interaction depth of the beam, a steady state will exist whereby the composition of the sputtered particles will be equivalent to that of the undisturbed bulk solid. The analysis of Shimizu and Hart (1982) would suggest steady state is reached after 4 nm depth penetration, which occurs after about 6 seconds of burn time in the case of the SHRIMP. Consequently, differential sputter yields between Pb, U, and Th are not important in explaining differential ion yields of these elements during a typical SHRIMP run lasting several minutes.

### Ionization probability, $\alpha_e$

As it is only charged (positively, in the current SHRIMP configuration) particles that can be electrostatically extracted from the sample, accelerated, and mass analyzed, the formation of secondary ions from the sputtered particles is a crucial, but highly complex and controversial issue. There is no generally accepted model for secondary ion formation, such as whether ion formation occurs within or above the sample surface (e.g. Williams, 1979). Nevertheless, it is this factor that may be largely responsible for the differing secondary ion yields of Pb, U, and Th.

The ionization probability of an element depends upon:

- a. Ionization potential. The first ionization potential of Pb is 7.42 eV whereas that of U is 6.08 eV and Th is 6.95 eV. As Pb has the higher ionization potential, all things being

equal one would expect it to be less easily ionized, opposite to the observed relationship. Clearly, factors other than the ionization potential are at work.

- b. Electronic state of the target. The ionization probabilities of Pb and U are enhanced in the presence of an electronegative element such as oxygen at the sample surface. Oxygen reduces the availability of electrons that could otherwise recombine with the positively charged ions of interest. In SHRIMP, deliberate increases in the partial pressure of oxygen in the sample chamber result in a relative increase in the ionization probability of Pb compared to U. From day to day there are variations in the partial pressure of oxygen in the sample chamber, and there may be local variations in oxygen activity on the sample surface. Thus, the relative yields of  $Pb^+$ ,  $U^+$ , and  $Th^+$  appear to be influenced by variations in oxygen partial pressure.
- c. Primary particle reactivity. Use of  $O_2^-$  as the primary particle provides an electronegative element to the target zone that enhances ionization, but this can be assumed to be relatively constant from sample to sample and spot to spot.
- d. Target composition. The ionization probability of an element is dependent upon the composition and crystal structure of the target, a phenomenon termed the "matrix effect" (Shimizu and Hart, 1982). Highly metamict and annealed zircon, comprising silica and baddeleyite phases, shows enhanced  $Pb^+$  yields compared to nonmetamict zircon (McLaren et al., 1994). It is important that the matrix remain constant from spot to spot, which is usually, but not necessarily, true during an analysis of an unknown zircon.
- e. Energy distributions. It is well known that the relative proportions of secondary ions vary as a function of their kinetic energy. Most of the secondary ions have rather low energies (1-10 eV), but their proportions change as their energy increases. In the GSC SHRIMP, the energy bandpass to the magnet is about 20 eV (-5/+15 eV relative to maximum transmission), which is not as wide as desirable, but required to meet the acceptance of the magnet. In theory it might be possible to select a specific, narrow energy bandpass in which there was no discrimination of the Pb/U and Pb/Th ions. However, the ion intensities would be too low and the instrumental setup would be very sensitive to any changes in the position of the energy spectrum (discussed below).

### Transmission, $\eta_m$

The main function of the Au conducting layer on the sample mount is to maintain a surface of equal potential (about +750 V) with respect to the first extraction electrode. Excess electrons at the sputter site, originating from the primary  $O_2^-$  beam and from positively charged secondary ions, are conducted across the Au-coated sample surface in order to maintain this extraction potential. An accumulation of negative charge at a particular spot on the sample surface would have the effect of lowering the overall extraction potential, and

thus the overall 10 kV accelerating potential of the secondary ions. Lowering the accelerating potential would cause a shift in the position of the energy spectrum at the exit to the ESA chamber, potentially altering the relative intensities of the isotopes transmitted to the magnet through the energy window. Furthermore, the relative extraction efficiencies of  $\text{Pb}^+$ ,  $\text{U}^+$ , and  $\text{Th}^+$  probably vary with the extraction potential.

Although the conditions of secondary energy and mass analysis are constant, it appears that each sample mount is slightly different in the way that charge is dissipated across its surface. The quality of the Au coating, the presence of irregularities on the mount (e.g. scratches, pits, and grain edges), the depth of the pit, and the nature of the electrical contact established between the steel sample holder and the Au-coated surface all appear to have a role. Consequently, sample mounts can be subtly different in the conditions under which secondary ions are extracted from their surfaces. Transmission conditions of Pb, U, and Th cannot be assumed to be constant from sample mount to sample mount. However, studies at the GSC have shown that the transmission conditions over the surface of a single mount can be stabilized, and remain so indefinitely.

### Mitigation of the variable relative elemental yields

The factors causing the ratio  $[\text{}^{206}\text{Pb}^+/\text{}^{238}\text{U}^+]/[\text{}^{206}\text{Pb}/\text{}^{238}\text{U}]$  to be greater than one and variable from mount to mount and spot to spot are the ionization probabilities ( $\alpha_c$ ) and transmission efficiencies ( $\eta_m$ ) of Pb, U, and Th. These difficulties have been largely overcome by the following analytical practices:

1. A standard zircon having a normal zircon crystal structure and well known and constant Pb/U and Pb/Th is included within each sample mount. It is found that the relative yields of  $^{206}\text{Pb}^+/\text{}^{238}\text{U}^+$  and  $^{208}\text{Pb}^+/\text{}^{232}\text{Th}^+$  are systematic with  $\text{UO}^+/\text{U}^+$  and  $\text{ThO}^+/\text{Th}^+$  for any particular mount (see below). These calibration or 'working' curves are established on the standard to correct for the spot-to-spot variations in the relative yields of  $^{206}\text{Pb}^+/\text{}^{238}\text{U}^+$  and  $^{208}\text{Pb}^+/\text{}^{232}\text{Th}^+$  on the mount. The relative ion yields determined for the standard at the  $\text{UO}^+/\text{U}^+$  and  $\text{ThO}^+/\text{Th}^+$  of the unknown are applied to the unknown spot. These practices ensure that there is no bias of the Pb/U and Pb/Th data due to calibration from a separate mount. The calibration curves established differ slightly between mounts, but do not for change with time. Consequently, once the calibration curves have been established they remain valid as long as the mount is not removed from its steel holder.
2. To minimize variation in depth penetration and resultant changes in secondary ion extraction efficiencies, the burn time and primary beam currents are kept as similar as possible between all spots.

### Kipawa standard zircon

The requirements of a suitable ion microprobe zircon standard are stringent. The zircon must be homogeneous in Pb/U and Pb/Th ratios to within 1% at the scale of tens of micrometres across and a few micrometres deep, requiring the zircon to have undergone virtually no lead loss since crystallization. The  $^{206}\text{Pb}/\text{}^{238}\text{U}$ ,  $^{207}\text{Pb}/\text{}^{235}\text{U}$ , and  $^{208}\text{Pb}/\text{}^{232}\text{Th}$  ratios must also have been determined by an independent method, normally isotope dilution thermal ionization mass spectrometry. Abundance levels of radiogenic Pb should be 20 ppm or greater to ensure good counting statistics. The zircon crystal structure should be matched with the unknowns; if nonmetamict zircons will be analyzed then the standard should be nonmetamict. The zircon should be plentiful, free of inclusions, and occur in pieces at least 50  $\mu\text{m}$  in dimension, suitable for mounting with unknowns having a range of thicknesses. Ideally, the zircon should be homogeneous in abundance levels of Pb, U, and Th in order that it can be used to calibrate their abundance levels in the unknowns, although this is not required to determine accurate ages.

A number of candidate zircons from among the GSC's collection were considered over several months before adopting material from the Kipawa Syenite Complex (Currie and van Breemen, 1996). The zircon occurs at a rare mineral site in a skarn-like unit at the margins of the syenite body. The reader is referred to Currie and van Breemen (1996) for a description of the geology and occurrence of rare minerals at this site. Zircon crystals reach several centimetres in diameter in pegmatitic patches within amphibolite, and such material was collected and analyzed by Currie and van Breemen (1996) for age dating purposes.

The original zircon material (Z2430) was further investigated in this study in order to determine its utility as a SHRIMP standard. Fragments of the least-magnetic, optically clear zircon from sample Z2430 were mounted in epoxy, polished, and C-coated in order to perform cathodoluminescence imaging. The purpose of the cathodoluminescence imaging was to determine the degree of heterogeneity in U contents in the fragments. It is been found that bright cathodoluminescence zones correlate with zircon of low U content and vice versa. About 30–40% of the zircon fragments are unzoned, and these are preferred targets for SHRIMP analyses. The abundance levels of U and Th in the grains that have a uniform cathodoluminescence are, however, not sufficiently uniform to be suitable as an abundance standard. Both U and Th average about 250 ppm, with ranges of about  $\pm 25\%$  and  $\pm 50\%$ , respectively. In a later section it is demonstrated that the Kipawa zircon is suitably homogeneous in Pb/U and Pb/Th ratios.

### Isotope dilution analysis

Results of six isotope dilution analysis of six clear, colourless fragments of the Kipawa zircon sample Z2430 are summarized in Table 3 and plotted in Figure 6. Fractions A, B, and C are from Currie and van Breemen (1996) and were air abraded prior to analysis, whereas D, E, and F were unabraded for this work. The fragments weighed from 22 µg to 74 µg each. The results show that the bulk fragments are slightly discordant, from 0.1 to 0.3% relative to the origin. The weighted mean ratios and 95% confidence limits are as follows:  $^{207}\text{Pb}/^{206}\text{Pb} = 0.072265 \pm 0.000041$  or  $993.4 \pm 0.7$  Ma,  $^{206}\text{Pb}/^{238}\text{Pb} = 0.16632 \pm 0.00015$  or  $991.4 \pm 1.1$  Ma. The fact that the grains show some discordance, albeit small, suggests that some Pb loss may be observed in the SHRIMP analyses, and indeed, this is the case; a small fraction of SHRIMP spots of the Kipawa zircon can be recognized as having anomalously low Pb/U and Pb/Th and are omitted from the calibration. For the purpose of calibrating the  $^{206}\text{Pb}/^{238}\text{Pb}$  and  $^{208}\text{Pb}/^{232}\text{Th}$  results, Kipawa zircon Z2430 is assumed to have an age of 993 Ma.

### Pb/U and Pb/Th calibration using the Kipawa standard zircon

We have seen above that the raw  $^{206}\text{Pb}+^{238}\text{U}+$  and  $^{208}\text{Pb}+^{232}\text{Th}+$  values of unknowns by themselves would be of little use, as for any one spot we have no independent way of determining the elemental discrimination conditions that existed during the analysis. The concurrent measurement of a standard zircon, however, provides a solution to this problem. Extensive analysis of the Kipawa zircon standard was carried out for two main reasons: firstly, to examine the reliability of the zircon (i.e., the extent to which random samples of this zircon are concordant from spot to spot and grain to grain) and secondly, to establish the characteristics of the Pb/U and Pb/Th calibration lines for the GSC SHRIMP.

Hinthorne et al. (1979) were the first to use  $\text{UO}^+/\text{U}^+$  to correct for the changing relative yields of  $^{206}\text{Pb}^+$  and  $^{238}\text{U}^+$ . Based on the sputtering model of Anderson and Hinthorne (1973), which related the ion yields to temperature, electron density, and composition of a plasma, Hinthorne et al. (1979) established an exponential relationship between  $^{206}\text{Pb}+^{238}\text{U}+$  and  $\text{UO}^+/\text{U}^+$ . Compston et al. (1984) initially used a linear relationship for the ANU SHRIMP I, and later a quadratic function was adopted (Williams and Claesson, 1987). Recently, Claoue-Long et al. (1995) have recommended the use at ANU of a power law relationship for  $\text{UO}^+/\text{U}^+ - \text{Pb}/\text{U}$  (i.e.  $^{206}\text{Pb}+^{238}\text{U}+=0.005(\text{UO}^+/\text{U}^+)^2$ ). The results to date from the GSC SHRIMP using Kipawa zircon, however, indicate that a simple linear relationship is all that is required at the present time, i.e.:

$$^{206}\text{Pb}+^{238}\text{U}^+ = m(\text{UO}^+/\text{U}^+) + b \quad (2)$$

$$^{208}\text{Pb}+^{232}\text{Th}^+ = m(\text{ThO}^+/\text{Th}^+) + b \quad (3)$$

where m is the slope and b is the y-intercept.

Table 3. ID-TIMS data for Kipawa zircon (Z2430).

Fraction size	Wt. 10 <sup>-6</sup> g	U ppm <sup>a</sup>	Th/U <sup>b</sup>	Pb* ppm <sup>a</sup>	$^{206}\text{Pb}/^{238}\text{Pb}$	Pb pg <sup>c</sup>	$^{208}\text{Pb}/^{232}\text{Th}$	$^{206}\text{Pb}/^{238}\text{Pb}$	$^{208}\text{Pb}/^{232}\text{Th}$	Corr. Coeff.	$^{207}\text{Pb}/^{235}\text{U}$	$^{207}\text{Pb}/^{206}\text{Pb}$	Age (Ma) $^{207}\text{Pb}/^{235}\text{U}$	Age (Ma) $^{206}\text{Pb}/^{238}\text{Pb}$	% Disc <sup>d</sup>	U blank pg	Pb blank pg
A	74	405	0.946	79	23549	13	0.2881	0.1664±.09%	1.657±.10%	0.9419	1.657±.10%	0.07225±.03%	992.2	993.0±1.4	0.09	3	10
B	69	481	1.15	98	24447	14	0.3511	0.1666±.10%	1.661±.11%	0.9683	1.661±.11%	0.07231±.03%	993.5	994.6±1.2	0.12	3	10
C	75	412	1.06	82	10775	29	0.3241	0.1665±.09%	1.660±.10%	0.9524	1.660±.10%	0.07229±.03%	992.7	994.2±1.3	0.16	3	10
D	66	281	0.954	55	11927	16	0.2907	0.1662±.08%	1.656±.10%	0.9522	1.656±.10%	0.07224±.03%	991.4	992.7±1.2	0.14	1	3
E	22	305	0.914	59	9067	8	0.2783	0.1661±.08%	1.655±.10%	0.936	1.655±.10%	0.07227±.03%	990.5	993.5±1.4	0.33	1	3
F	60	144	0.524	25	13068	7	0.1596	0.1663±.09%	1.656±.10%	0.9399	1.656±.10%	0.07223±.03%	991.4	992.4±1.4	0.1	1	3
WT. MEAN 95% CL								0.16632 ± 0.00015				0.072265 ± 0.000041	993.4 ± 0.7	991.4 ± 1.1			

Fractions A, B, C from O. van Breemen (pers. comm., 1996); D, E, F this study  
 Errors are 1 standard error of the mean in % except  $^{207}\text{Pb}/^{235}\text{U}$  age error which are 2 se in Ma; \* = radiogenic Pb  
 a=include sample weight error of ±0.001 mg in concentration uncertainty  
 b=from  $^{206}\text{Pb}/^{238}\text{Pb}$  ratio and calculated at  $^{207}\text{Pb}/^{206}\text{Pb}$  age  
 c=total common Pb in analysis  
 d=discordance relative to chord through origin

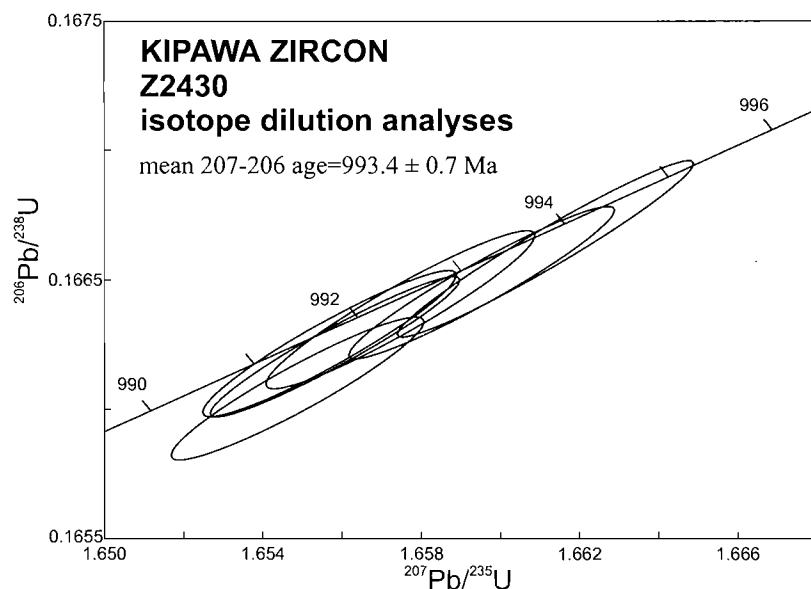


**Figure 6.**

Concordia plot showing ID-TIMS data on six fragments of Kipawa zircon. Data from O. van Breemen (pers. comm., 1996) and this study. Error ellipses are at 95% confidence level.

Figure 7 shows an example of  $^{238}\text{U}^{16}\text{O}^+ / ^{238}\text{U}^+$  versus  $^{206}\text{Pb}^+ / ^{238}\text{U}^+$  and  $^{232}\text{Th}^{16}\text{O}^+ / ^{232}\text{Th}^+$  versus  $^{208}\text{Pb}^+ / ^{232}\text{Th}^+$  (abbreviated as 'UO/U-Pb/U' and 'ThO/Th-Pb/Th' in the following discussion) and 1 se error bars for the Kipawa zircon. The data were obtained by analyzing 25 separate spots on a single zircon fragment over a two day period, and the Pb isotopes have been corrected for common Pb. In the UO/U-Pb/U plot (Fig. 7a), the  $\text{UO}^+/\text{U}^+$  values range from 7 to 8, and corresponding  $^{206}\text{Pb}^+ / ^{238}\text{U}^+$  values from 0.46 to 0.58. A least-squares linear regression, in which  $^{206}\text{Pb}^+ / ^{238}\text{U}^+$  is the dependent variable, yields a correlation coefficient (R) of 0.984, slope (m) of  $0.126 \pm 0.005$  (1 se), and intercept (b) of -0.43. The 1 s of  $^{206}\text{Pb}^+ / ^{238}\text{U}^+$  about the line is 1.4%. Similarly for the ThO/Th-Pb/Th plot (Fig. 7b),  $R=0.967$ ,  $m=0.0466 \pm 0.0026$ ,  $b=-0.277$ , and 1 s for  $^{208}\text{Pb}^+ / ^{232}\text{Th}^+=2.1\%$ .

Similar experiments as this one were carried out periodically over several months on different Kipawa zircon fragments on different sample mounts, and the results are summarized in Table 4. The first observation is that the degree of scatter about a best-fit straight line differs between experiments. For example, the 1s of  $^{206}\text{Pb}^+ / ^{238}\text{U}^+$  relative to the predicted value at the measured  $\text{UO}^+/\text{U}^+$  ranges from 0.9% to 2.9%, and for  $^{208}\text{Pb}^+ / ^{232}\text{Th}^+$  it is 1.5% to 3.6%. When enough data are available for any particular experiment it is sometimes apparent that certain spots fall below the main trend. Low  $^{206}\text{Pb}^+ / ^{238}\text{U}^+$  is usually correlated with low  $^{208}\text{Pb}^+ / ^{232}\text{Th}^+$ , and appear to be spots in which Pb loss has occurred. Such obvious outliers have been excluded from the results in Table 4. Nevertheless, the fact that the degree of fit varies depending on the grains analyzed suggests that the effects of Pb loss cannot always be avoided. Variations in the quality of the zircon grains rather than instrumental effects appear to govern the degree of coherence in the Kipawa zircon to a best fit straight line.

The slope of the calibration line versus mean  $\text{UO}^+/\text{U}^+$  and  $\text{ThO}^+/\text{Th}^+$  values for each analytical session indicated in Table 4 are plotted in Figure 8. For both isotopic systems

there is no apparent correlation of slope with  $\text{UO}^+/\text{U}^+$  or  $\text{ThO}^+/\text{Th}^+$ , indicating that higher order functions are not required within the range of  $\text{UO}^+/\text{U}^+$  and  $\text{ThO}^+/\text{Th}^+$  considered. For UO/U-Pb/U (Fig. 8a), the weighted mean slope is  $0.125 \pm 0.005$  (2 se) and  $\chi^2 = 1.04$  ( $P=40\%$ ). The slopes for ThO/Th-Pb/Th show more scatter (Fig. 8b), but still may be considered a single population with a weighted mean slope of  $0.0438 \pm 0.0022$  and  $\chi^2 = 1.73$  ( $P=10\%$ ). The y-intercepts range from -0.35 to -0.54 for UO/U-Pb/U and -0.16 to -0.44 for ThO/Th-Pb/Th. The correlation lines shift slightly up or down with each sample mount, causing the y-intercepts to differ. It is possible that a power law relationship would better describe the relationship over more extensive ranges in  $\text{UO}^+/\text{U}^+$  and  $\text{ThO}^+/\text{Th}^+$ . As the vast majority of analyses of unknown zircons will be within the range of mean  $\text{UO}^+/\text{U}^+$  and  $\text{ThO}^+/\text{Th}^+$  values shown, a linear fit has been adopted for the time being.

The mean slopes determined for the Pb/U and Pb/Th calibration lines are not fundamental properties of SIMS analysis of zircon, but instead depend, in part, on the particular instrumental setup of the GSC SHRIMP. Changes in the slope can be affected by adjusting the width of the ESA energy window, or by using a different type of sample holder. For example, analyses of Kipawa zircon mounted on a thin section gave  $\text{UO}^+/\text{U}^+$  values between 4 and 5, and a calibration line with a slope of about 0.09 in one analytical session.

The observed positive correlations between  $^{238}\text{U}^{16}\text{O}^+$  and  $^{206}\text{Pb}^+$ , and  $^{232}\text{Th}^{16}\text{O}^+$  and  $^{208}\text{Pb}^+$  may result from their similar ionization probabilities and similar energy distributions. A high  $\text{UO}^+/\text{U}^+$  or  $\text{ThO}^+/\text{Th}^+$  at a particular spot indicates that, for whatever reason,  $\text{UO}^+$  and  $\text{ThO}^+$  are being ionized and/or transmitted relatively more efficiently. One can think of  $\text{UO}^+/\text{U}^+$  and  $\text{ThO}^+/\text{Th}^+$  as the monitors of the 'run conditions' for any particular spot, with the relative yields of  $^{206}\text{Pb}^+ / ^{238}\text{U}^+$  and  $^{208}\text{Pb}^+ / ^{232}\text{Th}^+$ , respectively, being (linearly) dependent on spot run conditions.

The scatter of data about the Pb/U and Pb/Th calibration lines for the Kipawa zircon is the main source of propagated error in determining the  $^{206}\text{Pb}/^{238}\text{U}$  and  $^{208}\text{Pb}/^{232}\text{Th}$  ages for the unknowns (see below). Consequently, a great deal of attention has been paid in this report to understanding and mitigating the factors that could produce scatter in these curves. The Kipawa zircon, while not a perfect solution, appears to be sufficiently reliable in terms of the concordancy of random spots. It is recommended that at least ten analyses be obtained for each sample mount to obtain the best control on the Pb/U and Pb/Th ages.

### Calculation of $^{206}\text{Pb}/^{238}\text{U}$ , $^{207}\text{Pb}/^{235}\text{U}$ , and $^{208}\text{Pb}/^{232}\text{Th}$ ratios in the unknowns

Once the UO/U-Pb/U and ThO/Th-Pb/Th calibration lines for the standard have been determined, the  $^{206}\text{Pb}/^{238}\text{U}$  and  $^{208}\text{Pb}/^{232}\text{Th}$  values of the unknowns can be calculated from the  $^{206}\text{Pb}^+ / ^{238}\text{U}^+$  and  $^{208}\text{Pb}^+ / ^{232}\text{Th}^+$  values by applying the following simple ratio relationship:

$$\frac{(^{206}\text{Pb}^+ / ^{238}\text{U}^+)_{\text{unk}}}{(^{206}\text{Pb} / ^{238}\text{U})_{\text{unk}}} = \frac{(^{206}\text{Pb}^+ / ^{238}\text{U}^+)_{\text{std}}}{(^{206}\text{Pb} / ^{238}\text{U})_{\text{std}}} \quad (4)$$

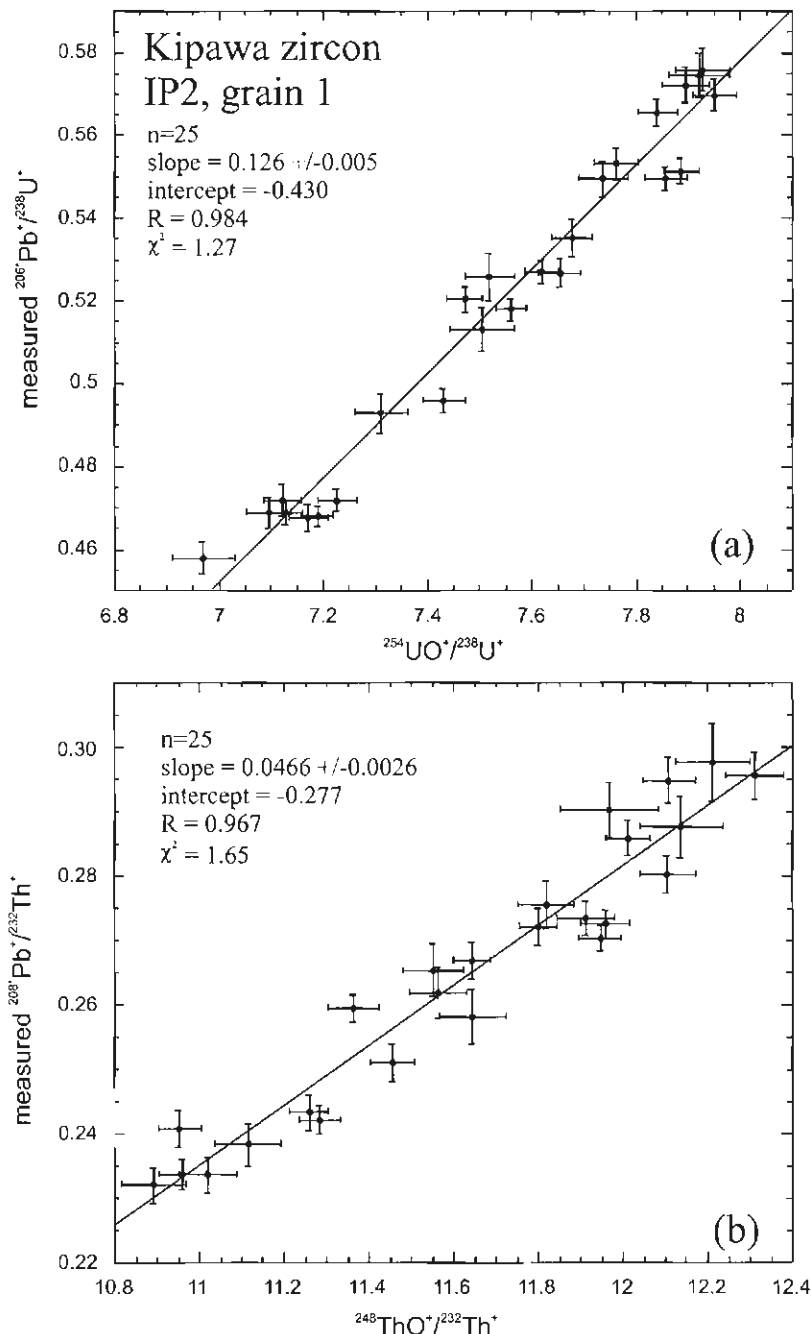


**Figure 7.**

- a) Measured  $^{254}\text{UO}^+ / ^{238}\text{U}^+$  versus  $^{206}\text{Pb}^+ / ^{238}\text{U}^+$  for Kipawa zircon during a good analytical session. Each datum (with 1 se errors) represents a single spot determination. The excellent linear correlation of the data indicates stable analytical conditions and a high degree of internal concordancy for the zircon.
- b) Measured  $^{248}\text{ThO}^+ / ^{232}\text{Th}^+$  versus  $^{208}\text{Pb}^+ / ^{232}\text{Th}^+$  for the Kipawa zircon.

Table 4. Summary of Pb/U and Pb/Th slope calibrations for nine different mounts in which Kipawa zircon was analyzed.

	# grains analyzed	CALIBRATION OF Pb/U RATIO						CALIBRATION OF Pb/Th RATIO						<sup>207</sup> Pb/ <sup>206</sup> Pb DATA				U AND Th CONTENTS			
		# spots	slope on UO/U vs. Pb/U	1 se slope	y-intercept	R	%1 s <sup>206</sup> Pb/ <sup>238</sup> U about line	wt. mean UO/U	# spots	slope on ThO/Th vs. Pb/Th	1 se slope	y-intercept	R	%1 s <sup>206</sup> Pb/ <sup>232</sup> Th about line	%1 s <sup>206</sup> Pb/ <sup>232</sup> Th age about line	wt. mean <sup>207</sup> Pb/ <sup>206</sup> Pb age (Ma)	2 se error (Ma)	1 s U (ppm) average	Th (ppm) average	1 s Th (ppm)	
26/06/96	6	21	0.140	0.009	-0.543	0.968	1.4	7.925	20	0.0464	0.007	-0.282	0.909	3.5	3.6	12.448	994.6	19			
06/02/96	5	16	0.123	0.010	-0.420	0.962	1.6	7.842	16	0.0592	0.008	-0.441	0.891	2.5	2.6	12.246	1003.0	21	206	36	201
06/04/96	1	7	0.119	0.009	-0.385	0.989	1.3	7.507	7	0.0362	0.003	-0.161	0.979	1.8	1.8	11.597	995.6	33	261	22	342
06/05/96	3	17	0.133	0.008	-0.489	0.980	0.9	7.658	17	0.0493	0.006	-0.312	0.895	1.8	1.8	11.793	995.2	17	237	51	238
06/10/96	3	17	0.132	0.010	-0.463	0.960	2.9	7.243	17	0.0470	0.005	-0.275	0.930	3.6	3.7	11.103	999.8	21	211	36	163
19/07/96	1	25	0.126	0.005	-0.430	0.984	1.4	7.519	25	0.0466	0.003	-0.277	0.967	2.1	2.2	11.602	997.1	13	318	59	343
08/09/96	3	34	0.119	0.004	-0.347	0.988	1.6	6.618	25	0.0430	0.001	-0.232	0.991	1.5	1.5	10.853	996.6	10	232	70	224
28/09/96	2	22	0.129	0.007	-0.428	0.976	1.8	7.925	25	0.0458	0.003	-0.274	0.968	2.7	2.8	11.581	999.5	17	206	27	154
18/09/96	1	14	0.127	0.005	-0.438	0.985	1.6	7.271	14	0.0458	0.003	-0.274	0.968	2.7	2.8	11.581	1010.0	22	285	21	371

Therefore,

$$\frac{(^{206}\text{Pb}/^{238}\text{U})_{\text{unk}}}{(^{206}\text{Pb}/^{238}\text{U})_{\text{std}}} = \frac{(^{206}\text{Pb}/^{238}\text{U})_{\text{unk}}}{(^{206}\text{Pb}/^{238}\text{U})_{\text{std}}} \times \quad (5)$$

where,

$(^{206}\text{Pb}/^{238}\text{U})_{\text{unk}}$  is measured ratio in the unknown, corrected for common Pb,

$(^{206}\text{Pb}/^{238}\text{U})_{\text{std}}$  is the standard value, calculated from the UO/U-Pb/U calibration line of the standard at the UO<sup>+</sup>/U<sup>+</sup> of the unknown,

$(^{206}\text{Pb}/^{238}\text{U})_{\text{unk}}$  is the value of interest,

and  $(^{206}\text{Pb}/^{238}\text{U})_{\text{std}}$  equals 0.1666 for Kipawa zircon.

And similarly,

$$\frac{(^{208}\text{Pb}/^{232}\text{Th})_{\text{unk}}}{(^{208}\text{Pb}/^{232}\text{Th})_{\text{std}}} = \frac{(^{208}\text{Pb}/^{232}\text{Th})_{\text{unk}}}{(^{208}\text{Pb}/^{232}\text{Th})_{\text{std}}} \times \quad (6)$$

Therefore,

$$\frac{(^{208}\text{Pb}/^{232}\text{Th})_{\text{unk}}}{(^{208}\text{Pb}/^{232}\text{Th})_{\text{std}}} = \frac{(^{208}\text{Pb}/^{232}\text{Th})_{\text{unk}}}{(^{208}\text{Pb}/^{232}\text{Th})_{\text{std}}} \times \quad (7)$$

where  $(^{208}\text{Pb}/^{232}\text{Th})_{\text{std}}$  is assumed to be 0.05038 for Kipawa zircon.

These simple relationships assume that the Pb<sup>+</sup>/U<sup>+</sup> and Pb<sup>+</sup>/Th<sup>+</sup> elemental discrimination of the unknown is the same as that of the standard under the same analytical conditions. The 'same analytical conditions' means that the unknown and standard are compared at the same UO<sup>+</sup>/U<sup>+</sup> and ThO<sup>+</sup>/Th<sup>+</sup> values, which are those of the unknown. The  $(^{206}\text{Pb}/^{238}\text{U})_{\text{std}}$  and  $(^{208}\text{Pb}/^{232}\text{Th})_{\text{std}}$  values have to be calculated from the linear approximations, as it would be fortuitous if a standard had actually been analyzed at exactly the same UO<sup>+</sup>/U<sup>+</sup> or ThO<sup>+</sup>/Th<sup>+</sup> value as the unknown.

The  $(^{207}\text{Pb}/^{235}\text{U})_{\text{unk}}$  follows from the  $(^{206}\text{Pb}/^{238}\text{U})_{\text{unk}}$ , i.e.,

$$\frac{(^{207}\text{Pb}/^{235}\text{U})_{\text{unk}}}{^{207}\text{Pb}/^{206}\text{Pb}} = \frac{(^{206}\text{Pb}/^{238}\text{U})_{\text{unk}}}{^{238}\text{U}/^{235}\text{U}} \times \quad (8)$$

where  $^{238}\text{U}/^{235}\text{U}=137.88$  and the Pb isotopes have been corrected for common Pb.

### Common Pb corrections

The potential sources of common Pb in a SHRIMP analysis of zircon include the Au coating and the initial Pb in the zircon itself. In an isotope dilution analysis of Pb, the isotopic composition of the common Pb in any total Pb analysis must be inferred, usually chosen as a blend of the laboratory 'blank' and an estimate of the intrinsic common Pb in the zircon. The situation in a SHRIMP analysis is not that different, except that the counting statistics on <sup>204</sup>Pb are much less favourable. Not only are smaller amounts of zircon analyzed, but also the probe spot can be placed deliberately in optically clean areas of the zircon, away from cracks or inclusions, where the amount of intrinsic common Pb is usually very small. Common Pb corrections tend to be most

important for Neoproterozoic to Phanerozoic zircons and those of any age with low U contents, i.e. where the quantities of radiogenic Pb are low.

Table 5 reports measurements of the Pb isotopic composition of the surface blank for the sample mounts and the pure Au used in the evaporative coating procedure (data from B. Davis, pers. comm., 1996). To obtain the measurement of the surface blank, a 15 mL Savillex beaker was washed in soap, rinsed in deionized water, dried under a heat lamp, and then the inside was evaporatively coated with Au, a

procedure identical to the treatment of the sample mounts. The beaker and its contents were then dissolved in 3 N HNO<sub>3</sub> and spiked with <sup>205</sup>Pb prior to Pb column chemistry. The pure Au sample was cleaned in acetone and H<sub>2</sub>O, dissolved in 3 N HNO<sub>3</sub>, and prepared unspiked. The total Pb determined from the analysis of the surface blank was 180 pg. A replicate analysis yielded a similar result. The isotopic composition of the pure Au is identical to the composition of the surface blank, indicating that the common Pb on the sample surface is accountable entirely by the Au coating.

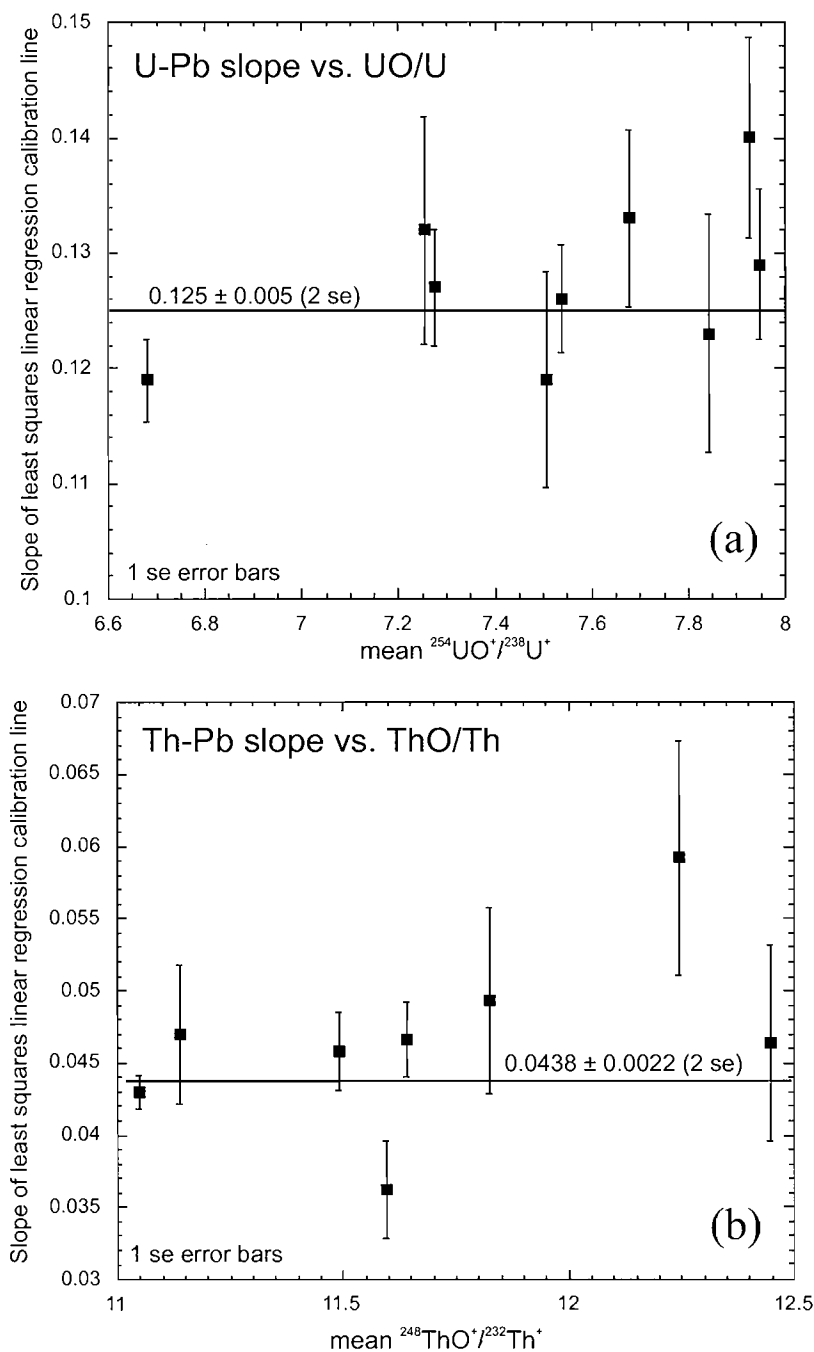


**Figure 8.**

Summary of **a)** UO/U-Pb/U and **b)** ThO/Th-Pb/Th calibration line slopes versus mean UO/U and ThO/Th, respectively, for Kipawa zircon from several different mounts.



**Table 5.** TIMS Pb isotopic analysis of surface blank and pure Au (B. Davis, pers. comm., 1996).

	$^{206}\text{Pb}/^{204}\text{Pb}$	$^{204}\text{Pb}/^{206}\text{Pb}$	$^{207}\text{Pb}/^{204}\text{Pb}$	$^{208}\text{Pb}/^{204}\text{Pb}$	$^{207}\text{Pb}/^{206}\text{Pb}$	$^{208}\text{Pb}/^{206}\text{Pb}$	Total Pb (pg)*
pure Au	17.335	0.05769	15.516	37.077	0.895	2.138	
surface blank	17.476	0.05722	15.503	36.981	0.887	2.116	180

2 se external precision in ratios is estimated at <0.5%  
 \* total Pb deposited on the surface of the sample

In most unknowns the levels of common Pb are either undetectable or at a consistently low level from sample to sample, and it is inferred that the common Pb composition of these samples is that of the Au coating. Such reasoning is similar to that commonly followed in isotope dilution analysis where there is an assumption about the expected levels of blank in each unknown analysis. This assumption is validated here by the observation that the common Pb content decreases with rastering time of the area around the spot prior to an analysis. Common Pb is undetectable or very nearly so after complete removal of the Au. It is not always time efficient, however, to raster for the amount of time needed to eliminate the surface blank, and hence the need to make a correction. Keeping the Au coating to the absolute minimum is very important in this regard.

Most zircon analyses yield a count rate for  $^{204}\text{Pb}$  (background corrected) of 0.1–0.3 c/s. For the unknowns, a  $^{204}\text{Pb}$  count rate of 1 c/s has been selected as the cutoff value, below which the surface blank composition is used, and above which the isotopic composition of the common Pb follows the model of Cumming and Richards (1975).

Two separate ways to determine the quantity of common Pb (here used to mean total nonradiogenic Pb) in an analysis are discussed next. In both of these calculations, three factors  $f_{206}$ ,  $f_{207}$ , and  $f_{208}$  can be derived, where:

$f_{206}$  = fractional amount of total  $^{206}\text{Pb}$  which is common Pb

$$\begin{aligned} &= ^{206}\text{Pb from common Pb} / ^{206}\text{Pb total} \\ &= ^{206}\text{Pb}_c / ^{206}\text{Pb}_t \end{aligned} \quad (9)$$

$$\begin{aligned} f_{207} &= ^{207}\text{Pb}_c / ^{207}\text{Pb}_t \\ &= f_{206} \times (^{207}\text{Pb}/^{206}\text{Pb})_c / (^{207}\text{Pb}/^{206}\text{Pb})_t \end{aligned} \quad (10)$$

$$\begin{aligned} f_{208} &= ^{208}\text{Pb}_c / ^{208}\text{Pb}_t \\ &= f_{206} \times (^{208}\text{Pb}/^{206}\text{Pb})_c / (^{208}\text{Pb}/^{206}\text{Pb})_t \end{aligned} \quad (11)$$

where 't' is the measured (total) Pb, and 'c' is the common Pb.

These factors are used to correct the measured isotopic ratios for the presence of the common Pb, e.g.:

$$^{206}\text{Pb}^+ / ^{238}\text{U}^+ = (1 - f_{206}) \times (^{206}\text{Pb}^+ / ^{238}\text{U}^+) \quad (12)$$

$$\begin{aligned} ^{207}\text{Pb}^+ / ^{206}\text{Pb}^+ &= (^{207}\text{Pb}^+ / ^{206}\text{Pb}^+) \\ &\times (1 - f_{207}) / (1 - f_{206}) \end{aligned} \quad (13)$$

$$^{208}\text{Pb}^+ / ^{232}\text{Th}^+ = (1 - f_{208}) \times (^{208}\text{Pb}^+ / ^{232}\text{Th}^+) \quad (14)$$

### $^{204}\text{Pb}$ method of common Pb correction

This method uses the measured  $^{204}\text{Pb}$  isotope to determine the proportion of common Pb, similar to the methodology employed in an isotope dilution analysis. The  $^{204}\text{Pb}$  count rate is calculated as the  $^{204}\text{Pb}$  total count rate minus the 'background' count rate measured at a nominal mass of 204.04 amu where there are no known isotopes present. The background count rate is normally one-quarter to one-half of the total  $^{204}\text{Pb}$  count rate. The difficulty with this method is the large error in the correction that results from the few counts of  $^{204}\text{Pb}$  in most zircons (see further discussion in 'Error analysis'). The calculation of  $^{204}f_{206}$ , the fraction of  $^{206}\text{Pb}$  that is common Pb determined by the '204 method', is as follows:

$$^{204}f_{206} = (^{204}\text{Pb}/^{206}\text{Pb})_t / (^{204}\text{Pb}/^{206}\text{Pb})_c = \quad (15)$$

The advantage of this method is that only  $(^{204}\text{Pb}/^{206}\text{Pb})_c$  has to be assumed (i.e. the isotopic composition of the common Pb). The '204 method' is used in cases where one wants to make no assumptions about the Pb/U, Pb/Th, and  $^{207}\text{Pb}/^{206}\text{Pb}$  ages of the analyzed zircon. The 204 method is always the one used for studies of zircons older than about 1.5 Ga and in any study in which assessment of concordancy is an issue.

### $^{207}\text{Pb}$ method of common Pb correction

The 207 correction for common Pb compares the measured  $^{207}\text{Pb}^+ / ^{206}\text{Pb}^+$  value with the expected radiogenic  $^{207}\text{Pb}^+ / ^{206}\text{Pb}^+$  value for the zircon, i.e.,

$$^{207}f_{206} = [(^{207}\text{Pb}^+ / ^{206}\text{Pb}^+) - (^{207}\text{Pb}^+ / ^{206}\text{Pb}^+)] / [(^{207}\text{Pb}^+ / ^{206}\text{Pb}^+)_c - (^{207}\text{Pb}^+ / ^{206}\text{Pb}^+)_c] \quad (16)$$

In addition to the common Pb composition, this method also requires the  $^{207}\text{Pb}^+ / ^{206}\text{Pb}^+$  to be specified. This method is generally used only for certain Phanerozoic zircons that are thought to be near concordant based initially on the 204 correction. The idea here is that the difference in  $^{207}\text{Pb}^+ / ^{206}\text{Pb}^+$  in zircons up to about 500 Ma is relatively small, and therefore it is possible to estimate the  $^{207}\text{Pb}^+ / ^{206}\text{Pb}^+$  value in such a zircon with sufficient accuracy. Young zircons have low  $^{207}\text{Pb}^+$ , which results in large propagated errors in the  $^{207}\text{Pb}^+ / ^{206}\text{Pb}^+$  ratio using the 204 method. Although discussed here as an option, in general this method is not favoured at the GSC due to a desire to utilize the  $^{207}\text{Pb}/^{206}\text{Pb}$  ratio despite its relatively high uncertainty. Analyses of young zircons, for which the common Pb contribution is significant and variable, can be assessed using a Terra-Wasserburg diagram, in which the uncorrected

$^{207}\text{Pb}/^{206}\text{Pb}$  values are plotted against the uncorrected  $^{238}\text{U}/^{206}\text{Pb}$  values and a regression line fitted through the data.

### $^{232}\text{Th}/^{238}\text{U}$ Ratios and Th abundances

Although it contains no age information, the  $^{232}\text{Th}/^{238}\text{U}$  value is useful in petrogenetic interpretations of zircon and is also used to calculate the elemental abundance of thorium. For a zircon that has remained a closed system since crystallization,

$$^{208}\text{Pb}^*/^{206}\text{Pb}^* = \left[ \frac{^{232}\text{Th}/^{238}\text{U}}{(e^{\lambda_{238}t} - 1)} \right] \quad (17)$$

For the 993 Ma Kipawa zircon the second term is a constant:

$$^{208}\text{Pb}^*/^{206}\text{Pb}^* = [^{232}\text{Th}/^{238}\text{U}]0.30236 \quad (18)$$

Consequently, if there are variations in the Th/U ratio in the Kipawa zircon, and the secondary ion yields of  $^{232}\text{Th}^+$  and  $^{238}\text{U}^+$  (or  $^{248}\text{ThO}^+$  and  $^{254}\text{UO}^+$ ) are identical (i.e. no instrumental fractionation), a plot of  $^{232}\text{Th}^+/^{238}\text{U}^+$  (or  $^{248}\text{ThO}^+/^{254}\text{UO}^+$ ) versus  $^{208}\text{Pb}^*/^{206}\text{Pb}^*$  will yield a straight line through the origin of slope=0.30236. The species  $^{248}\text{ThO}^+$  and  $^{254}\text{UO}^+$  are normally used because the ion intensities are considerably greater than for  $^{232}\text{Th}^+$  and  $^{238}\text{U}^+$ . Figure 9 is such a plot for 179 spots from several different grains of Kipawa zircon. The mean slope of a line forced through the origin is  $0.33108 \pm 0.000471$  (1 se), which is significantly greater than 0.30236. Thus, at a given  $^{208}\text{Pb}^*/^{206}\text{Pb}^*$  the measured  $^{248}\text{ThO}^+/^{254}\text{UO}^+$  is too low, with  $^{254}\text{UO}^+$  ionized in preference to  $^{248}\text{ThO}^+$ . Thus,

$$^{208}\text{Pb}^*/^{206}\text{Pb}^* = f_{\text{ThO-UO}} \times 0.30236 \times \left( \frac{^{248}\text{ThO}^+}{^{254}\text{UO}^+} \right) \quad (19)$$

where  $f_{\text{ThO-UO}} = 0.33108/0.30236 = 1.095 \pm 0.0209$  (1 se)

Therefore,

$$\begin{aligned} ^{232}\text{Th}/^{238}\text{U} &= f_{\text{ThO-UO}} \times (^{248}\text{ThO}^+/^{254}\text{UO}^+) \\ &= 1.095 (^{248}\text{ThO}^+/^{254}\text{UO}^+) \quad (20) \end{aligned}$$

This analysis uses the variable  $^{208}\text{Pb}^*/^{206}\text{Pb}^*$  to independently assess the  $\text{ThO}^+/\text{UO}^+$  discrimination factor ( $f_{\text{ThO-UO}}$ ), and it assumes that fractionation of the Pb isotopes (i.e.,  $^{208}\text{Pb}^*/^{206}\text{Pb}^*$ ) is insignificant (see justification below). The factor  $f_{\text{ThO-UO}}$  is only weakly dependent on  $\text{UO}^+/\text{U}^+$  values for a particular sample mount. An average of several mounts is as follows:

$$f_{\text{ThO-UO}} = 0.0318[\text{UO}^+/\text{U}^+] + 0.859 \quad (21)$$

Generally, data for any one mount show considerable scatter about such a line, indicating that  $\text{UO}^+/\text{U}^+$  is not the best monitor of the relative ionization yields of  $\text{ThO}^+$  and  $\text{UO}^+$ . As the  $^{232}\text{Th}/^{238}\text{U}$  ratio is not used for any age calculations, a better predictive model for  $f_{\text{ThO-UO}}$  is really not required. Consequently, the measured  $^{248}\text{ThO}^+/^{254}\text{UO}^+$  values in unknowns are multiplied by the constant  $1.095 \pm 0.0209$  (1 se) to obtain the true  $^{232}\text{Th}/^{238}\text{U}$  values. Higher precision in the  $^{232}\text{Th}/^{238}\text{U}$  is not required, as this ratio is not used to calculate  $^{208}\text{Pb}/^{232}\text{Th}$  ages at the GSC laboratory, as can be done. From  $^{232}\text{Th}/^{238}\text{U}$  it is straightforward to convert this atomic ratio to a weight ratio, i.e.,  $\text{Th}/\text{U}$  (wt.) =  $^{232}\text{Th}/^{238}\text{U} \times 0.968$ , and hence the Th concentration from the U abundance (see below).

A fixed  $\pm 2\%$  (1 se) uncertainty in  $f_{\text{ThO-UO}}$  is added in quadrature with the counting statistical error on  $^{248}\text{ThO}^+/^{254}\text{UO}^+$  (typically 0.5%) to derive the errors in the  $^{232}\text{Th}/^{238}\text{U}$  and  $\text{Th}/\text{U}$  weight ratios. The Th abundance is assigned a blanket 1 SD error of  $\pm 10\%$  due to the error in the U concentration of the SL13 zircon standard (see below).

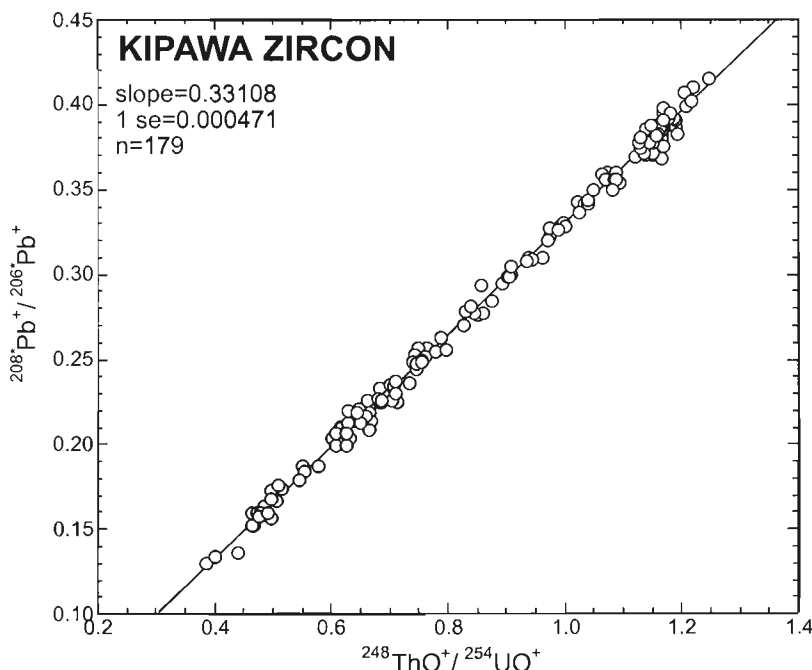


**Figure 9.**

$^{248}\text{ThO}^+/^{254}\text{UO}^+$  versus  $^{208}\text{Pb}^*/^{206}\text{Pb}^*$  for Kipawa zircon. This correlation allows the relative instrumental fractionation of  $^{248}\text{ThO}^+$  from  $^{254}\text{UO}^+$  to be calculated (see text for details), used in determining the Th abundances.

### U and Pb abundances

Although the main aim of SHRIMP zircon analysis is the determination of isotopic ratios of Pb, U, and Th, the abundances of these elements in the zircons can also be determined. Only the interelement isotopic ratios are necessary for an age calculation, and in a SHRIMP analysis the interelement isotopic ratios of Pb, U, and Th are directly *measured*. By contrast, in isotope dilution U-Pb and Th-Pb analyses, the interelement ratios are *calculated* from precise measurements of the abundances of each of Pb, U, and Th and the isotopic composition of Pb in the sample. The comparatively imprecise SHRIMP method of determining U and Pb abundances is described next (see above for Th).

To determine the U abundance in an unknown, a standard with known U content must be present on the sample mount. The standard is analyzed as usual and its  $^{196}\text{Zr}_2\text{O}^+ / ^{238}\text{U}^+$  and  $\text{UO}^+ / \text{U}^+$  values are determined. The  $^{238}\text{U}^+$  is ratioed with  $^{196}\text{Zr}_2\text{O}^+$  under the assumption that the Zr abundance is equal in all zircons and that the collected  $^{196}\text{Zr}_2\text{O}^+$  signals of standard and unknown will be of equal intensity when measured under exactly the same analytical conditions, i.e.:

$$\begin{aligned} & (^{196}\text{Zr}_2\text{O}^+ / ^{238}\text{U}^+)_{\text{unk}} / (^{196}\text{Zr}_2\text{O}^+ / ^{238}\text{U}^+)_{\text{std}} = \text{U}_{\text{std}} / \text{U}_{\text{unk}} \\ & \text{U}_{\text{unk}} (\text{ppm}) = \text{U}_{\text{std}} (\text{ppm}) / \\ & [ (^{196}\text{Zr}_2\text{O}^+ / ^{238}\text{U}^+)_{\text{unk}} / (^{196}\text{Zr}_2\text{O}^+ / ^{238}\text{U}^+)_{\text{std}} ] \end{aligned} \quad (22)$$

As previously explained,  $\text{UO}^+ / \text{U}^+$  is a monitor of the analytical conditions, and it is important to compare standard and unknown at the same  $\text{UO}^+ / \text{U}^+$  value. Consequently, as we have seen for Pb/U, the  $(^{196}\text{Zr}_2\text{O}^+ / ^{238}\text{U}^+)_{\text{std}}$  has to be calculated at the  $\text{UO}^+ / \text{U}^+$  of the unknown. Claoue-Long et al. (1995) reported a power law relationship between  $^{196}\text{Zr}_2\text{O}^+ / ^{238}\text{U}^+$  and  $\text{UO}^+ / \text{U}^+$  (i.e.  $^{196}\text{Zr}_2\text{O}^+ / ^{238}\text{U}^+ = a(\text{UO}^+ / \text{U}^+)^{0.66}$ ). Attempts were made with the GSC SHRIMP to independently determine the form of the  $(^{196}\text{Zr}_2\text{O}^+ / ^{238}\text{U}^+)$

versus  $\text{UO}^+ / \text{U}^+$  working curve using SL13 zircon, but it was found that the relationship was poorly defined owing to the known  $>\pm 10\%$  variation in U content of that zircon. Nevertheless, during analysis of a particular grain of Kipawa zircon the relationship shown in Figure 10 was observed. Only seven spots were visited, but they lie along a least squares straight line ( $\chi^2=0.53$ ,  $P=75\%$ ) with  $m=0.496 \pm 0.026$  (1 se),  $b=0.755$  and  $R=0.993$ . Analysis of other parts of this grain during subsequent sessions worsened the excellent correlation observed. Although the linear correlation has not been duplicated in other grains since, it appears that the seven analyses of that particular day by chance hit a part of the grain having identical U contents. Such a correlation line will be difficult to confirm, as few zircons are sufficiently homogeneous in U content to conduct such an experiment. There is a  $\pm 6\%$  difference in the discrimination factor between  $^{196}\text{Zr}_2\text{O}^+$  and  $^{238}\text{U}^+$  over the range of  $\text{UO}^+ / \text{U}^+$  values shown in Figure 10, so that the variations in zircon U abundance for such a study would need to be  $<<\pm 6\%$ . Despite the fortuitous results of Figure 10, Kipawa zircon is otherwise too heterogeneous in U content (e.g. Table 3) to be used in determining the  $\text{UO}^+ / \text{U}^+$ -Zr/U calibration line for a particular mount.

Instead, the  $\text{UO}^+ / \text{U}^+$ -Zr/U calibration line is established by analyzing SL13 zircon on a second 'standard' mount ( $\text{U} = 238 \pm 23$  ppm (1 se); I. Williams, pers. comm., 1996). This is not an ideal situation, as it is likely that each mount has a unique  $\text{UO}^+ / \text{U}^+$ -Zr/U calibration line (i.e. the y-intercepts vary), and compounding the problem is the fact that SL13 zircon has only moderately uniform U contents. Thus, the form of the  $\text{UO}^+ / \text{U}^+$ -Zr/U calibration line determined above is of little value at the present time, being overwhelmed by the required use of SL13 on a separate mount. The external reproducibility of U contents is estimated to be  $\sim \pm 10\%$  (1 se) with this method.

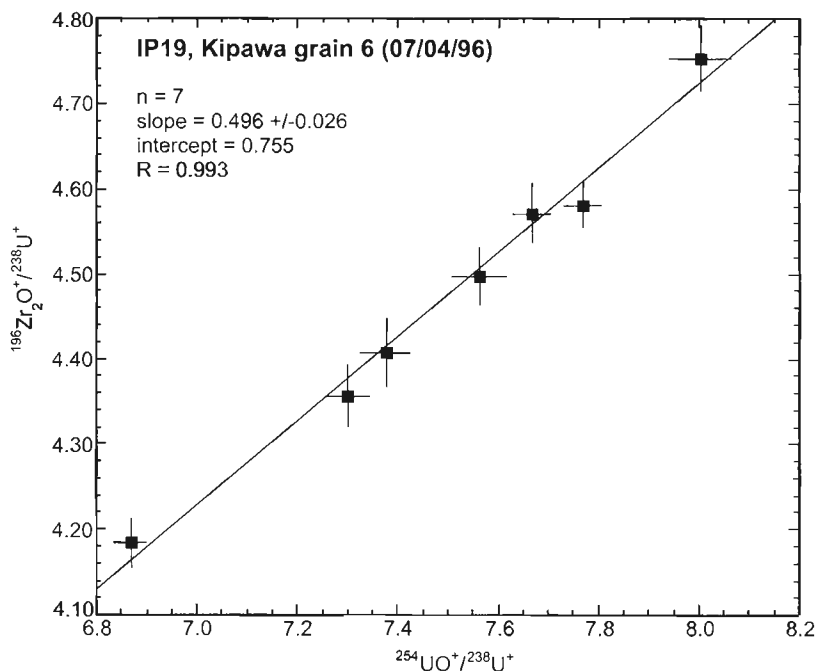


**Figure 10.**

$^{254}\text{UO}^+ / ^{238}\text{U}^+$  versus  $^{196}\text{Zr}_2\text{O}^+ / ^{238}\text{U}^+$  for a single fragment of Kipawa zircon. This correlation shows that the relative instrumental fractionation of  $^{196}\text{Zr}_2\text{O}^+$  from  $^{238}\text{U}^+$  varies systematically with  $^{254}\text{UO}^+ / ^{238}\text{U}^+$ . The  $^{196}\text{Zr}_2\text{O}^+ / ^{238}\text{U}^+$  parameter is used to determine the U abundance in an unknown.

Total Pb contents follow from the  $^{206}\text{Pb}/^{238}\text{U}$  and U abundance (in  $\mu\text{g}/\text{g}^{-1}$ ) i.e.,

$$\begin{aligned}^{206}\text{Pb } \mu\text{mol}/\text{g}^{-1} &= ^{238}\text{U } \mu\text{mol}/\text{g}^{-1} \times ^{206}\text{Pb}^*/^{238}\text{U} \\ &= (\text{U } \mu\text{g}/\text{g}^{-1}/238.0289 \text{ g/mol}^{-1}) \times \\ &\quad 0.992743 \times ^{206}\text{Pb}^*/^{238}\text{U} \quad (23)\end{aligned}$$

$$^{207}\text{Pb } \mu\text{mol}/\text{g}^{-1} = ^{207}\text{Pb}/^{206}\text{Pb} \times ^{206}\text{Pb } \mu\text{mol}/\text{g}^{-1} \quad (24)$$

$$^{208}\text{Pb } \mu\text{mol}/\text{g}^{-1} = ^{208}\text{Pb}/^{206}\text{Pb} \times ^{206}\text{Pb } \mu\text{mol}/\text{g}^{-1} \quad (25)$$

Totalling and converting to weights:

$$\begin{aligned}\text{Total radiogenic Pb } (\mu\text{g}/\text{g}) &= (205.974 \text{ g/mole}^{-1} \times \\ &\quad ^{206}\text{Pb } \mu\text{mol}/\text{g}^{-1}) + (206.976 \text{ g/mol}^{-1} \times ^{207}\text{Pb } \mu\text{mol}/\text{g}^{-1}) + \\ &\quad (207.977 \text{ g/mol}^{-1} \times ^{208}\text{Pb } \mu\text{mol}/\text{g}^{-1}) \quad (26)\end{aligned}$$

### Error analysis

In estimating the total uncertainty of  $(^{206}\text{Pb}/^{238}\text{U})_{\text{unk}}$ ,  $(^{207}\text{Pb}/^{235}\text{U})_{\text{unk}}$ ,  $(^{208}\text{Pb}/^{232}\text{Th})_{\text{unk}}$ , and  $(^{207}\text{Pb}/^{206}\text{Pb})_{\text{unk}}$  on a single spot, the following separate errors need to be incorporated:

- error due to the standard calibration;
- counting errors,
- common and background Pb corrections,
- composition of the common Pb,
- mass fractionation of Pb isotopes, and
- isobaric interferences (hydrides).

Note that for ease of calculation all errors on ratios, ages, and elemental abundances for single spots are quoted as  $\pm 1\sigma$  (68% confidence interval). Only summary age calculations are quoted at the 95% confidence interval ( $2\sigma$ ).

#### a. standard calibration

Here we are concerned with the fit of the  $\text{UO}/\text{U}-\text{Pb}/\text{U}$  and  $\text{ThO}/\text{Th}-\text{Pb}/\text{Th}$  calibration lines and determining the error in the calculated  $(^{206}\text{Pb}/^{238}\text{U})_{\text{std}}$  and  $(^{208}\text{Pb}/^{232}\text{Th})_{\text{std}}$  at the  $\text{UO}^+/\text{U}^+$  and  $\text{ThO}^+/\text{Th}^+$  of the unknown (used in equations 5 and 7). The error is essentially the standard deviation of the measured  $^{206}\text{Pb}^+/\text{U}^+$  and  $^{208}\text{Pb}^+/\text{Th}^+$  of the standard about the linear regression line, augmented by factors that depend on the number of points in the regression (e.g. Mendenhall and Sincich, 1995). Note that a simple, unweighted least squares linear regression is used, that is, with minimization of  $(^{206}\text{Pb}^+/\text{U}^+)_{\text{std}}$  or  $(^{208}\text{Pb}^+/\text{Th}^+)_{\text{std}}$  as the dependent variable. More sophisticated regressions that involve weighting, two-variable linear regression, and error correlations have been compared with the simple linear regression and not found to be sufficiently beneficial to offset the inconvenience associated with carrying out such a regression with the current setup for data reduction. From a simple linear regression it is straight forward (see Mendenhall and Sincich, 1995) to calculate the 68% confidence interval of an individual value of  $y$  (i.e.  $^{206}\text{Pb}^+/\text{U}^+$ ) at a specified value of  $x$  (i.e.  $\text{UO}^+/\text{U}^+$ ):

$$1\sigma_{\text{std}} = \pm t_{0.16} \times s \times [1 + 1/n + (x_p - x_m)^2/SS_{xx}]^{1/2} \quad (27)$$

where  $t_{0.16}$  is the  $t$  multiplier for  $n-2$  degrees of freedom (from statistical tables),  $n$  is the number of data points (e.g. spots on the standard),  $s = [\sum_{i=1}^n (y_m - y_p)^2 / (n-1)]^{1/2}$  is the standard deviation of measured values ( $y_m$ ) relative to predicted values ( $y_p$ ),  $x_p$  is the  $x$  value of the calculation,  $x_m$  is the mean  $x$  value, and  $SS_{xx} = \sum_{i=1}^n (x_i - x_m)^2$ . The third term in the square brackets is generally of secondary importance and has been ignored because the  $\text{UO}^+/\text{U}^+$  or  $\text{ThO}^+/\text{Th}^+$  of the unknown is never very far from the mean of the standard calibration line. Thus, the above equation can be simplified as,

$$1\sigma_{\text{std}} = \pm t_{0.16} \times s \times (1 + 1/n)^{1/2} \quad (28)$$

Average  $1\sigma_{\text{std}}$  for  $(^{206}\text{Pb}^+/\text{U}^+)_{\text{std}}$  and  $(^{208}\text{Pb}^+/\text{Th}^+)_{\text{std}}$  are 1.6% (range 0.9 to 2.9%) and  $\pm 2.5\%$  (range 1.5-3.7%), respectively. The  $1\sigma_{\text{std}}$  determined for a particular sample mount is applied as a blanket error to the unknowns and is usually the major source of error in the final  $(^{206}\text{Pb}/^{238}\text{U})_{\text{unk}}$  values. Note that no reference calibration is necessary for the Pb isotopes, and they are not detectably fractionated from each other (see below).

#### b. counting errors

'Counting errors' refers to the uncertainties that result from instrumental effects during the run. In understanding how counting errors are calculated, it is important to recall that normally the objective of an analysis is to determine the isotopic composition of the zircon at the mid-point of the run. During each visit to a peak, a certain total number of counts will be received at the collector. The uncertainty associated with each visit to a mass station ( $i$ ) is modelled by Poisson distribution as  $1s = (n_i)^{1/2}$ , where  $n$  is the number of counts received in the count period.

It is obvious, but needs to be emphasized, that no two visits to a mass station occur at exactly the same time period. Consequently, the ratios of the isotopes have to be calculated at the same arbitrary time, chosen as the mid-point of the run. The mid-point time occurs at the half way point between the last mass station of the first scan and the first mass station of the last scan. The error in calculating from a linear regression the total number of counts at the mid-point of the time series is as follows. An unweighted least-squares linear regression is calculated for each time series analysis of an isotope. Outliers may be recognized and omitted. A  $\chi^2$  value is determined for the fitted line. The mid-point count value for the isotope is calculated,  $n_{\text{mid}}$ . The total counting error associated with the time series of a particular isotope is  $(n_{\text{tot}})^{1/2}$ , where  $n_{\text{tot}}$  is the total number of counts in the time series ( $\sum n_i$ ). Therefore, the fractional counting error associated with any one mass station is:

$$(n_{\text{tot}})^{1/2}/n_{\text{tot}} = 1/(n_{\text{tot}})^{1/2} \quad (29)$$

Therefore, for  $n_{\text{mid}}$  the  $1s$  uncertainty is:

$$n_{\text{mid}} \times 1/(n_{\text{tot}})^{1/2} \quad (30)$$

The 1 s error is augmented by the degree of fit of the line, i.e.,

$$\pm 1 s = (\chi^2)^{1/2} \times n_{\text{mid}} \times 1/(n_{\text{tot}})^{1/2} \quad (31)$$

To obtain a 1 s error in the midpoint count rate,  $n_{\text{mid}}$  is divided by the count period to obtain  $(c/s)_{\text{mid}}$ , which has a counting error of:

$$\pm 1 s = (\chi^2)^{1/2} \times (c/s)_{\text{mid}} \times 1/(n_{\text{tot}})^{1/2} \quad (32)$$

Once the errors for each of the mid-point count rates have been calculated, any additional errors, including the errors associated with the common Pb and background correction (see below), are added quadratically. Then the ratios of the isotopes are calculated and the %1 s count rate errors are summed. For example, for the  $^{206}\text{Pb}/^{238}\text{U}$  ratio the total counting error in per cent is  $[(\pm 1 s_{206\text{Pb}}\%)^2 + (\pm 1 s_{238\text{U}}\%)^2]^{1/2}$ .

### c. common Pb and background corrections

The common Pb and background corrections introduce additional errors in the count rates for  $^{206}\text{Pb}$ ,  $^{207}\text{Pb}$ , and  $^{208}\text{Pb}$ . Take for example an analysis with a total count rate for  $^{204}\text{Pb}$  of 0.14 c/s. If  $^{204}\text{Pb}$  is monitored for about 100 s then the 1 s counting error is about  $0.14 \times 1/(14)^{1/2} = \pm 0.037$  c/s. Assuming, in this example, a background of 0.047 c/s collected over the same period, then the 1 s counting error for background would be about  $\pm 0.022$  c/s. Thus, the error in the background corrected  $^{204}\text{Pb}$  count rate (0.093 c/s) for this spot is  $[(0.037)^2 + (0.022)^2]^{1/2} = \pm 0.043$  c/s ( $\pm 46\%$ ). Assuming that the common Pb has the composition of the Au, the count rates and errors for  $^{206}\text{Pb}$ ,  $^{207}\text{Pb}$ , and  $^{208}\text{Pb}$  due to the common Pb would be  $1.61 \pm 0.74$  c/s,  $1.44 \pm 0.66$  c/s, and  $3.44 \pm 1.58$  c/s, respectively, with errors calculated at  $\pm 46\%$  as determined above in this example.

The factors  $f_{206}$ ,  $f_{207}$ , and  $f_{208}$  and their total uncertainties, taking into account the errors associated with the common Pb and background correction, would normally be calculated next from the required isotopic ratios and counting errors (e.g. see equations 9, 10, 11, 15). Typical raw (uncorrected)  $^{206}\text{Pb}$ ,  $^{207}\text{Pb}$ , and  $^{208}\text{Pb}$  count rates and counting uncertainties for Kipawa zircon are  $500 \pm 2.5$  c/s,  $36 \pm 0.4$  c/s, and  $180 \pm 1.1$  c/s, respectively. Gathering the appropriate count rates, we obtain  $^{204}\text{c}f_{206} = ^{206}\text{Pb}/^{206}\text{Pb}_t = 1.61/500 = 0.0032$ , which has a fractional uncertainty of  $[(0.74/1.61)^2 + (2.5/500)^2]^{1/2} = 0.46$ . Following identical measures for the other isotopes, we obtain:

$$^{204}\text{c}f_{206} = 0.0032 \pm 0.0015$$

$$^{204}\text{c}f_{207} = 0.040 \pm 0.018$$

$$^{204}\text{c}f_{208} = 0.019 \pm 0.009$$

As an example of how  $^{204}\text{c}f_{206}$  is used, consider that in this example the measured  $^{206}\text{Pb}^+/^{238}\text{U}^+$  value is  $0.500 \pm 0.004$ , and we wish to convert this to the radiogenic ratio with errors. The conversion to a radiogenic  $^{206}\text{Pb}^+/^{238}\text{U}^+$  is  $(1 - ^{204}\text{c}f_{206}) \times ^{206}\text{Pb}^+/^{238}\text{U}^+$ . The uncertainty in the radiogenic  $^{206}\text{Pb}^+/^{238}\text{U}^+$  can be shown to be equal to  $[(1 - ^{204}\text{c}f_{206})(\pm 1 s_{6/38})]^2 + ((^{206}\text{Pb}^+/^{238}\text{U}^+)(\pm 1 s_{f_{206}}))^2]^{1/2} = [(1 -$

$0.0032)(0.004))^2 + ((0.500)(0.0015))^2]^{1/2} = \pm 0.00406$ . In this case it can be seen that the common Pb correction does not significantly increase the uncertainty in the  $^{206}\text{Pb}^+/^{238}\text{U}^+$  value, and this is true for most zircons.

Now consider the calculation of the uncertainty in the radiogenic  $^{207}\text{Pb}^+/^{206}\text{Pb}^+$  ratio from a measured value of  $^{207}\text{Pb}^+/^{206}\text{Pb}^+ = 0.07200 \pm 0.00087$ , with error based on counting statistics. The radiogenic  $^{207}\text{Pb}^+/^{206}\text{Pb}^+ = ^{207}\text{Pb}^+/^{206}\text{Pb}^+ \times (1 - f_{207})/(1 - f_{206}) = 0.06934$  and the quadratic summation of the errors (not shown) yields  $\pm 0.00155$ . The error in the  $^{207}\text{Pb}^+/^{206}\text{Pb}^+$  went from  $\pm 1.2\%$  to  $\pm 2.2\%$  after common Pb correction, which is a significant increase. The common Pb correction will noticeably increase the error in the  $^{207}\text{Pb}^+/^{206}\text{Pb}^+$  value for most zircons less than 1.5 Ga, but generally has only a minor influence on Archean zircons. The  $^{208}\text{Pb}$  isotope ratios are usually affected to a moderate extent, but usually less than  $^{207}\text{Pb}$ .

### d. common Pb composition

At this point in the analytical program no errors have been assigned to the isotopic composition of the common Pb. The errors associated with this factor are much less than the errors that are typically associated with estimating the common Pb ratios based on measurement of  $^{204}\text{Pb}$ . For instance, in the previous example, the uncertainties due to counting statistics alone on the  $^{206}\text{Pb}/^{204}\text{Pb}$ ,  $^{207}\text{Pb}/^{204}\text{Pb}$ , and  $^{208}\text{Pb}/^{204}\text{Pb}$  values of the common Pb are  $\pm 65\%$ , much greater than the uncertainty in the common Pb composition.

### e. mass fractionation of the Pb isotopes

The issue of mass fractionation of the Pb isotopes in SHRIMP has been addressed by several workers (Compston et al., 1984; Williams and Claesson, 1987; Wiedenbeck and Watkins, 1993; Roddick and van Breemen, 1994), and to date there has been no convincing case made for significant mass fractionation. The results from tests comparing isotope dilution and GSC SHRIMP  $^{207}\text{Pb}/^{206}\text{Pb}$  ages of several different ages suggest no detectable mass discrimination (see 'Part II', this report). Consequently, no additional uncertainty due to mass fractionation is applied to the data.

### Summary

The following is a summary of the factors considered in the calculation of uncertainties in the important isotopic ratios and elemental abundances, arranged in decreasing importance:

- $(^{206}\text{Pb}/^{238}\text{U})_{\text{unk}}$ : uncertainty in the standard calibration (UO/U-Pb/U regression), counting statistics, common Pb and background corrections
- $(^{207}\text{Pb}/^{235}\text{U})_{\text{unk}}$ : uncertainty in  $(^{206}\text{Pb}/^{238}\text{U})_{\text{unk}}$  and  $(^{207}\text{Pb}/^{206}\text{Pb})_{\text{unk}}$
- $(^{207}\text{Pb}/^{206}\text{Pb})_{\text{unk}}$ : uncertainty due to counting statistics, common Pb and background corrections

**Table 6.** Summary of age results for test samples using SHRIMP and ID-TIMS. Errors are at the 95% confidence level.

Sample #	ID-TIMS: best concordant age estimate (Ma)	SHRIMP: best concordant age estimate (Ma)	ID-TIMS data source
Z3940	476 ± 2	481 ± 8	V. McNicoll (pers. comm., 1996)
Z2170 (SL13)	572.1 ± 0.2 (206-238) 576.2 ± 0.7 (207-206)	578 ± 6	Roddick and van Breemen (1994)
Z3053	1161 ± 2	1164 ± 17	O. van Breemen (pers. comm., 1996)
Z3134	1856 ± 2	1857 ± 11	Stern and Lucas (1994)
Z3371	2589 ± 1	2587 ± 6	M. Villeneuve (pers. comm., 1996)
Z3935	2667 ± 1	2660 ± 11	O. van Breemen (pers. comm., 1996)
Z1242	2681 ± 1.9/-1.4	2680 ± 6	Mortensen and Card (1993)

- ( $^{208}\text{Pb}/^{232}\text{Th}$ )<sub>unk</sub>: uncertainty due to standard calibration (ThO/Th-Pb/Th regression), counting statistics, common Pb correction, and background correction
- U, Pb, and Th abundances: blanket error of ±10%.
- Th/U ratio: ±2% uncertainty in the ThO-UO fractionation factor, counting statistics.

## PART II: PERFORMANCE EVALUATION

In 'Part I' of this report, the methods of determining U-Pb-Th ages and errors using the GSC SHRIMP were presented. In order to validate the analytical methodologies employed and to examine the precision and accuracy of the isotopic ages under routine analytical conditions, a series of tests were performed upon seven different zircon samples over a period of three months. Published and unpublished isotope dilution data derived from the GSC laboratory exist for each of the test samples and, for most, the isotope dilution ages are very precise and unambiguous.

### Test samples and analytical method

Table 6 summarizes the rock types, isotope dilution ages, and data sources for each of the test samples. The sample numbers and Pb/U ages are as follows: Z3940 (476 Ma), Z2170 (572 Ma), Z3053 (1161 Ma), Z3134 (1856 Ma), Z3371 (2589 Ma), Z3935 (2667 Ma), Z1242 (2681 Ma). Concordia plots of each are shown in Figure 11. With the exception of sample Z2170 (SL13), which is metamorphic in origin, all the zircon ages represent crystallization events.

Zircons selected from the same mineral fractions used to obtain the ID-TIMS ages were mounted (5-30 grains) along with several Kipawa zircon fragments on three separate epoxy disks (IP2, IP19, IP25). Routine mounting, imaging, and coating protocols were followed for each. The samples were then analyzed using the SHRIMP, and at least six spot analyses were obtained per sample. The number of scans ranged from six to eight, and peak collection times varied slightly between samples, but was similar to that shown in Table 2. The calibration line for Kipawa zircon on each

mount was established with ten or more analyses from one or more fragments. The data were reduced as described in 'Part I', with the  $^{204}\text{Pb}$  method used for common Pb correction. No special treatments were employed in the analyses of the test zircons, as the objective was to investigate the performance under routine conditions.

### Test results

Table 7 summarizes the 204-corrected isotopic data for the test samples. Figure 11 shows Wetherill concordia plots of the SHRIMP data plotted alongside the ID-TIMS data at the same scale. Note that the SHRIMP data for individual spots are plotted as 68% confidence level error polygons, whereas the ID-TIMS data for the zircon fractions are shown as 95% confidence level ellipses or crosses for clarity. It is immediately obvious that a SHRIMP datum (a spot) is significantly less precise than an ID-TIMS datum (a fraction). The reasons for this difference have been eluded to in 'Part I'. Firstly, the count rates for the abundant Pb or U isotopes at the collector in an ID-TIMS analysis are usually on the order of  $10^6$  c/s, whereas in a SHRIMP analysis the count rates are typically  $10^2$  to  $10^3$  c/s, i.e. the ion signals in a SHRIMP analysis are at least 1000 times weaker. This difference reflects the approximately  $10^3$  smaller mass of zircon analyzed in a SHRIMP analysis. As the uncertainty in the intensity of an ion beam is inversely proportional to the square root of the total number of arrivals (see 'Part I'), it is an unavoidable fact of Poisson counting statistics that SHRIMP data will be less precise over approximately the same counting period.

Secondly, the method of determining the Pb/U ratios in a SHRIMP analysis, that is, by reference to standard, is fundamentally less precise than an isotope dilution determination (further discussion below). The standard zircon is not perfectly concordant everywhere, and the method of correction for changing interelement fractionation from spot to spot is only an approximation. The uncertainty in the Pb/U ratio of the unknown can be no better than the Pb/U ratio determined for the standard, which is usually ~1.5% ( $1\sigma$ ) per spot. The interelement ratios in an ID-TIMS analysis are referenced back to precisely calibrated reference solutions and the uncertainties in the interelement ratios are almost entirely due to (favourable) counting statistics.

Because the uncertainty in the SHRIMP Pb/U ratio has a lower limit, but the Pb-isotope ratios do not (being determined principally by the Pb-isotope counting statistics and the common Pb correction), the dimensions of the error polygons on a conventional concordia plot will vary depending on the concentrations of radiogenic Pb in the zircon. Long, skinny error polygons result from analyzing zircons with lots of radiogenic Pb (e.g. >1.5 Ga magmatic zircons), whereas equant or flattened ones result from zircons with smaller amounts of radiogenic Pb (e.g. <1.5 Ga zircons).

### *SHRIMP single and grouped ages*

The approaches used to derive final ages from SHRIMP data vary depending on the age of the sample and the nature of the data. As in ID-TIMS work, there is a desire to rely as much as possible on concordant data. In the case of SHRIMP, however, a single concordant spot determination may or may not be sufficiently precise for certain applications. As a general rule, for zircons <1.5 Ga the age on an individual spot cannot be determined to better than about  $\pm 4\%$  ( $2\sigma$ ), the error on the most precisely determined ratio ( $^{206}\text{Pb}/^{238}\text{U}$ ) in younger zircons. For zircons >1.5 Ga, where the  $^{207}\text{Pb}/^{206}\text{Pb}$  age is more precisely determined, the  $2\sigma$  age error in a single spot will typically be about  $\pm 2\%$  to  $\pm 0.5\%$ , depending on age and Pb content. The age errors are discussed in more detail below.

When higher precision on a SHRIMP age is required a number of SHRIMP concordant analyses can be statistically pooled together or discordant analyses may be linearly regressed in the conventional way. Some analysts new to SHRIMP may feel uncomfortable with statistical pooling, but in fact the methods are fundamentally no different than existing approaches used in ID-TIMS. In both analytical methods there is commonly an attempt to improve the final age estimate by multiple analysis of the sample. There are actually very few zircon samples in which a geological age determination could be made on the basis of a single ID-TIMS analysis, whether concordant or not, and there are few analysts who would be satisfied with just one data point no matter how precise. Attempts to replicate a concordant or near-concordant analysis is always preferred, as the analyst gains a better understanding about possible internal geological age variations in the sample that may affect the final age and uncertainty estimate. For example, an old core may not have been detected in the first, single, near-concordant ID-TIMS analysis, and only revealed through multiple analyses.

As it is relatively easy and fast (~20 min) to collect a SHRIMP analysis, an attempt is normally made to analyze the zircon of interest in various places or on several grains. The analyst attempts to collect a sample of the population, as large as practicable in the given time, perhaps 10-20 spots if a high-precision age is required. This is not only good analytical practice, but it is also useful because the number of data points is sufficiently large that statistical processing is meaningful. Attempts at collecting such a large number of analyses on a single age population in ID-TIMS would be infrequent and costly. The larger sample size in a SHRIMP data set has certain analytical advantages, in that it usually inspires more confidence in assessing whether one or more age populations

exist, as long as the ages are sufficiently different. However, the greater sample size comes at a price, as each datum is less precise. Nevertheless, if the sample yields statistical evidence of being a single population of ages, a final result can be calculated that, while never reaching the precision of a good ID-TIMS analysis, can be within a factor of five or so.

The statistical methods of analyzing SHRIMP data are a subject for future application papers. For the test samples older than 1.5 Ga, final weighted mean ages and 95% confidence errors were calculated by pooling the  $^{207}\text{Pb}/^{206}\text{Pb}$  data for all spots <3% discordant (Table 7). For zircons <1.5 Ga, where shallow discordance is difficult to assess with SHRIMP data, final ages rely upon accumulating and analyzing a sufficient number of data points such that the concordant  $^{206}\text{Pb}/^{238}\text{U}$  age can be statistically distinguished. Such an analysis is assisted by the use of logarithmic probability plots of the  $^{206}\text{Pb}/^{238}\text{U}$  ages, where a grouping of concordant spots will form a 'plateau' of ages, through which a line can be drawn of constant slope. Probability plots are included as insets in Figure 11, and the one for Z3940 illustrates well the concordant age plateau and the trailing off to low  $^{206}\text{Pb}/^{238}\text{U}$  ages of spots that have suffered Pb loss. Such points have been omitted from the final age calculation.

### *SHRIMP versus ID-TIMS ages*

How well do the SHRIMP compare, assuming that the 'true' ages are represented by the ID-TIMS data? Plotted in Figure 12 are the ratios of the SHRIMP isotopic age to the ID-TIMS age, for each isotopic system. Errors are shown at the 95% confidence level and incorporate the errors in both the SHRIMP and ID-TIMS ages. A line is drawn across the diagrams at a value of 1.0, indicating perfect agreement of the SHRIMP and ID-TIMS results. A value greater than 1 indicates the fractional amount that the SHRIMP age is older than the ID-TIMS age, etc. The final SHRIMP ages have been corrected for common Pb by the  $^{204}\text{Pb}$  method, and for reference a small dash indicates the data prior to correction.

The  $^{207}\text{Pb}/^{206}\text{Pb}$  age data (Fig. 12a) all lie within the 95% confidence limits of 1.0, indicating that, within the precision of the analyses the  $^{207}\text{Pb}/^{206}\text{Pb}$  ages are in perfect agreement with the accepted ages. For the young zircons, the  $^{207}\text{Pb}/^{206}\text{Pb}$  ages are not particularly useful owing to the paucity of  $^{207}\text{Pb}$  and the large correction for common Pb, but for the Archean samples the data are more useful as there is practically no effect due to common Pb. Also plotted are data for approximately 100 analyses of the Kipawa standard accumulated over several months. On the basis of these data it is concluded that fractionation of the Pb isotopes is not significant. Furthermore, the results indicate that the 204 method of common Pb correction is a suitable method of estimating the common Pb, and that there are no significant isobaric interferences on the Pb isotopes.

Plotted at the same scale in Figure 12b are the  $^{206}\text{Pb}/^{238}\text{U}$  data. Once again, all analyses fall about a value of 1.0 within error. Note that the correction for common Pb is insignificant for most test samples, and that the errors are similar

regardless of age. On the basis of this diagram, it is concluded that the calibration of the Pb/U ratio is valid using the Kipawa zircon standard as a reference.

Looking more closely at the data, there is an apparent negative trend to the data, with young samples showing  $^{206}\text{Pb}/^{238}\text{U}$  ages about 1% higher than the accepted values and one old sample giving a  $^{206}\text{Pb}/^{238}\text{U}$  age about 1% lower. It is not certain from the limited number of samples whether this effect is due to some unknown analytical problem

associated with Pb/U calibration or a real geological effect. For example, for the Archean zircons, it is quite reasonable to suppose that the pooled  $^{206}\text{Pb}/^{238}\text{U}$  ages include spots that have suffered a small amount of Pb loss, too small to be recognized and omitted for the pooled final ages, but skewing the data to slightly younger ages. The ID-TIMS analyses, for that matter, do show varying degrees of Pb loss. For the younger SL13, it has been shown by Roddick and van Breemen (1994) that the ID-TIMS data are, in fact, slightly discordant.

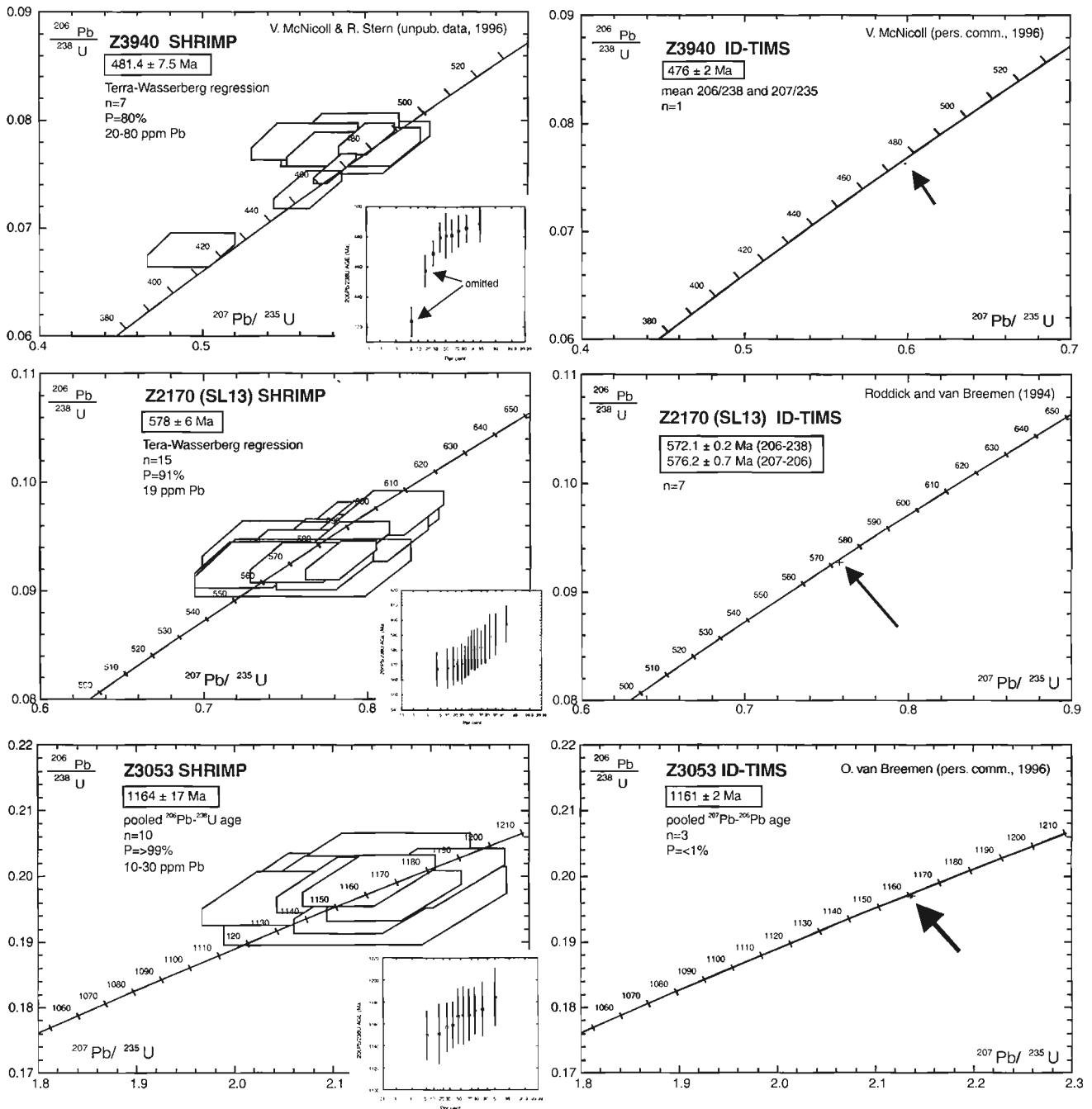


**Figure 11.** Concordia plots showing paired SHRIMP and ID-TIMS results at the same scale for seven test zircon samples of differing age. SHRIMP data are shown with  $1\sigma$  error polygons, whereas ID-TIMS data are at  $2\sigma$ .



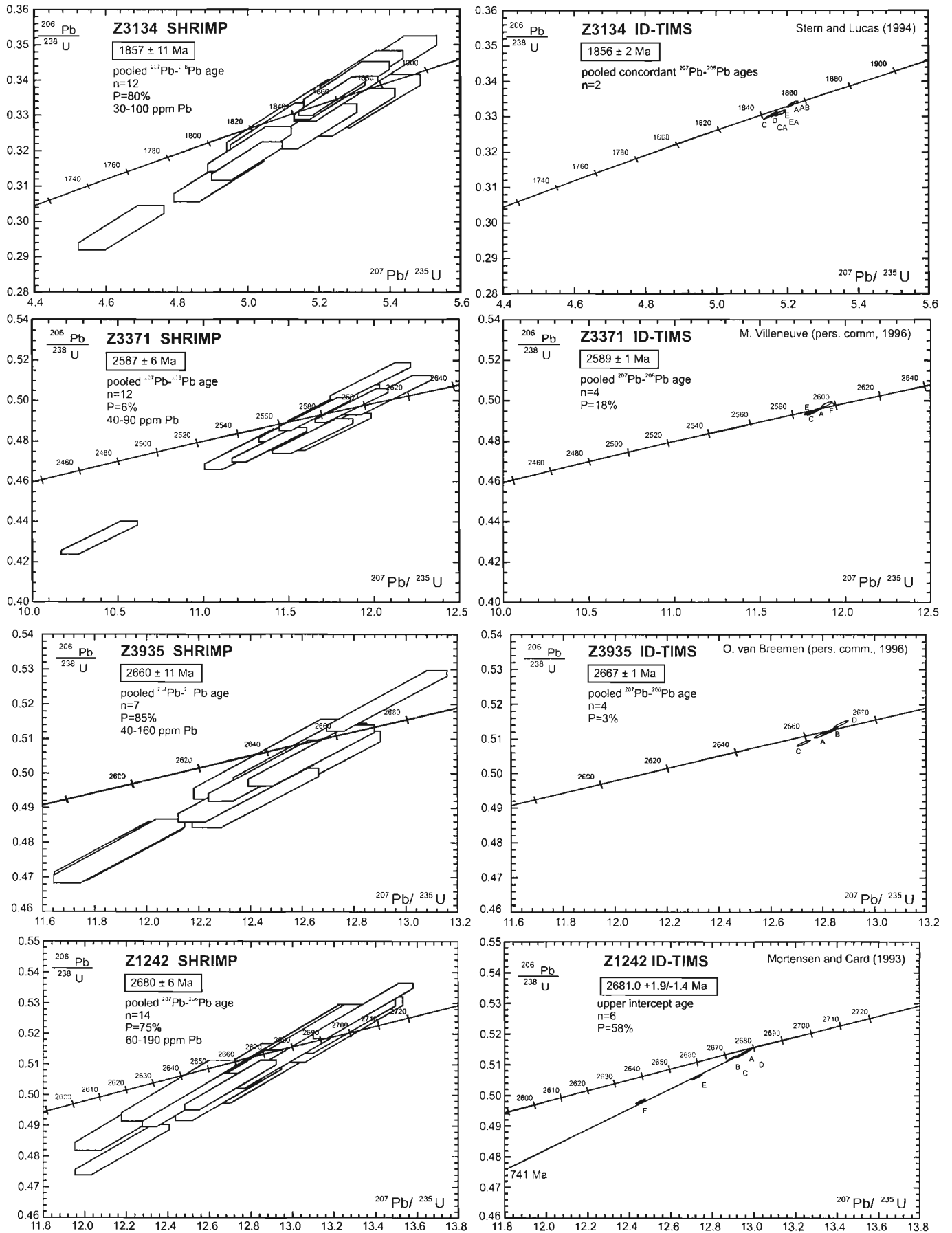
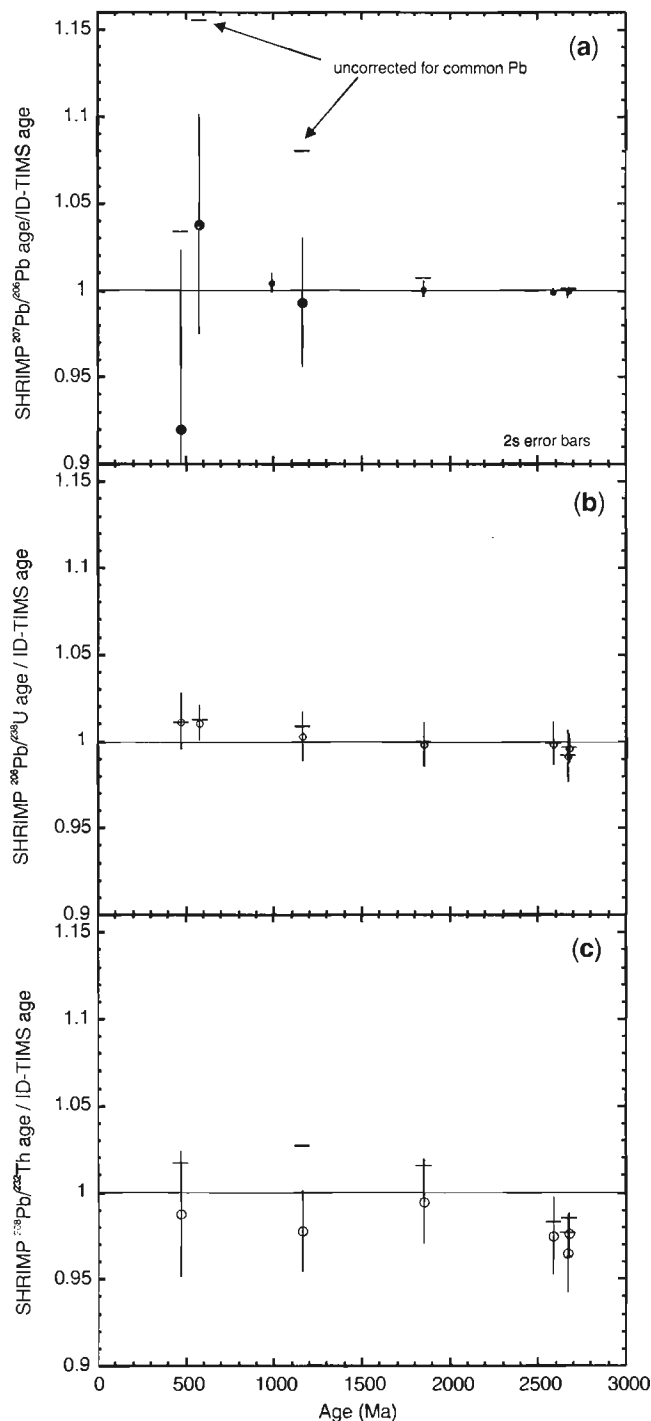


Figure 11. (cont.)

**Table 7. SHRIMP analytical data (corrected for common Pb using 204 method) for test samples.**  
All errors are 1 $\sigma$ .

SPOTS	U ppm	Th ppm	Th/U	Pb* ppm	<sup>204</sup> Pb/ <sup>206</sup> Pb	$\pm^{204}\text{Pb}/^{206}\text{Pb}$	<sup>206</sup> Pb/ <sup>204</sup> Pb	f206	$\pm$ f206	f207	f208	<sup>208</sup> Pb/ <sup>206</sup> Pb	$\pm^{208}\text{Pb}/^{206}\text{Pb}$	<sup>206</sup> Pb/ <sup>232</sup> Th	$\pm^{206}\text{Pb}/^{232}\text{Th}$
3940/10-3.2	322	152	0.47	26	3.21e-04	8.11e-05	3118	0.00556	0.00141	0.0849	0.0783	0.1407	0.0035	0.0227	0.0009
3940/10-13.1	253	176	0.70	22	2.84e-05	1.17e-04	35224	0.00049	0.00202	0.0077	0.0047	0.2223	0.0050	0.0239	0.0009
3940/10-16.1	799	573	0.72	69	2.52e-05	4.08e-05	39620	0.00044	0.00071	0.0070	0.0043	0.2191	0.0023	0.0245	0.0008
3940/10-13.2	197	112	0.57	16	3.03e-04	2.15e-04	3301	0.00525	0.00372	0.0786	0.0634	0.1668	0.0085	0.0224	0.0014
3940/10-16.2	985	763	0.77	83	1.00e-05	1.00e-05	100000	0.00017	0.00017	0.0028	0.0016	0.2389	0.0015	0.0236	0.0007
3940/10-4.1	161	71	0.44	13	3.38e-04	1.56e-04	2954	0.00587	0.00271	0.0915	0.0915	0.1252	0.0062	0.0224	0.0014
3940/10-1.1	226	131	0.58	19	1.78e-04	1.39e-04	5607	0.00309	0.00241	0.0487	0.0365	0.1749	0.0060	0.0238	0.0012
2170-2.3	213	19	0.09	18	4.70e-04	1.17e-04	2130	0.00814	0.00202	0.1096	0.3789	0.0288	0.0046	0.0300	0.0033
2170-2.4	217	20	0.09	19	2.24e-04	2.40e-04	4474	0.00387	0.00416	0.0549	0.2235	0.0289	0.0093	0.0296	0.0075
2170-2.5	203	19	0.09	19	7.63e-05	8.85e-05	13101	0.00132	0.00153	0.0191	0.0738	0.0355	0.0037	0.0287	0.0349
2170-2.6	216	20	0.09	19	2.56e-04	1.28e-04	3902	0.00444	0.00222	0.0651	0.2617	0.0269	0.0050	0.0278	0.0041
2170-2.7	219	19	0.09	19	1.75e-04	1.40e-04	5716	0.00303	0.00243	0.0427	0.2007	0.0259	0.0054	0.0287	0.0050
2170-2.8	210	19	0.09	19	1.33e-04	1.49e-04	7511	0.00231	0.00259	0.0330	0.1268	0.0341	0.0060	0.0187	0.0081
2170-2.9	218	20	0.09	19	2.00e-04	1.24e-04	5013	0.00346	0.00214	0.0492	0.2054	0.0287	0.0050	0.0204	0.1166
2170-1.1	215	20	0.09	19	9.88e-05	1.19e-04	10122	0.00171	0.00206	0.0252	0.1197	0.0270	0.0046	0.0288	0.0048
2170-1.2	217	20	0.09	19	1.00e-05	1.00e-05	100000	0.00017	0.00017	0.0026	0.0122	0.0301	0.0015	0.0261	0.0609
2170-1.3	212	19	0.09	19	1.00e-05	1.00e-05	100000	0.00017	0.00017	0.0026	0.0119	0.0307	0.0018	0.0334	0.0020
2170-1.4	207	18	0.09	18	6.61e-06	6.60e-05	151286	0.00011	0.00114	0.0017	0.0078	0.0311	0.0027	0.0174	0.0082
2170-1.5	200	18	0.09	17	2.03e-04	8.57e-05	4934	0.00351	0.00149	0.0515	0.2364	0.0243	0.0034	0.0218	0.0492
2170-1.6	231	21	0.09	20	2.14e-04	9.13e-05	4672	0.00371	0.00158	0.0559	0.2630	0.0223	0.0036	0.0224	0.0030
2170-1.7	243	21	0.09	21	1.00e-05	8.00e-05	100000	0.00017	0.00139	0.0025	0.0124	0.0296	0.0032	0.0317	0.0039
2170-1.8	225	20	0.09	20	1.00e-05	1.00e-05	100000	0.00017	0.00017	0.0025	0.0123	0.0297	0.0012	0.0309	0.0021
3053-4.1	86	71	0.82	19	3.38e-04	1.67e-04	2958	0.00586	0.00289	0.0647	0.0515	0.2320	0.0077	0.0566	0.0023
3053-4.2	54	32	0.60	11	8.51e-04	2.07e-04	1175	0.01474	0.00358	0.1447	0.1550	0.1745	0.0088	0.0573	0.0032
3053-4.4	117	100	0.85	27	3.71e-04	9.88e-05	2693	0.00644	0.00171	0.0694	0.0540	0.2427	0.0046	0.0567	0.0016
3053-4.5	107	85	0.79	23	3.86e-04	1.46e-04	2593	0.00668	0.00253	0.0736	0.0625	0.2157	0.0062	0.0549	0.0021
3053-4.6	95	76	0.79	21	6.20e-04	1.50e-04	1613	0.01075	0.00259	0.1123	0.0910	0.2320	0.0064	0.0590	0.0021
3053-4.7	105	81	0.78	23	1.46e-04	1.04e-04	6863	0.00253	0.00181	0.0276	0.0233	0.2265	0.0049	0.0590	0.0018
3053-4.8	88	70	0.79	20	2.44e-04	1.60e-04	4103	0.00422	0.00277	0.0470	0.0368	0.2373	0.0066	0.0611	0.0022
3053-4.9	97	76	0.78	22	2.96e-04	1.35e-04	3384	0.00512	0.00234	0.0561	0.0459	0.2287	0.0059	0.0585	0.0021
3053-4.10	120	103	0.86	27	2.39e-04	1.12e-04	4192	0.00413	0.00193	0.0447	0.0350	0.2451	0.0053	0.0552	0.0017
3053-4.11	94	76	0.81	21	2.82e-05	9.61e-05	35524	0.00049	0.00167	0.0055	0.0043	0.2406	0.0045	0.0586	0.0018
3134-8.2	86	27	0.31	29	1.00e-05	1.00e-05	100000	0.00017	0.00017	0.0014	0.0042	0.0889	0.0016	0.0969	0.0041
3134-8.4	115	33	0.28	38	1.33e-05	5.37e-05	75472	0.00023	0.00093	0.0018	0.0061	0.0797	0.0022	0.0914	0.0038
3134-7.1	93	28	0.31	32	8.19e-05	6.74e-05	12210	0.00142	0.00117	0.0111	0.0348	0.0844	0.0028	0.0938	0.0044
3134-7.2	96	29	0.30	33	1.81e-06	6.52e-05	552486	0.00003	0.00113	0.0002	0.0008	0.0838	0.0027	0.0943	0.0042
3134-7.3	87	23	0.27	30	1.20e-04	6.50e-05	8324	0.00208	0.00113	0.0159	0.0554	0.0761	0.0027	0.0973	0.0055
3134-3.2	200	80	0.40	72	7.59e-05	3.65e-05	13184	0.00131	0.00063	0.0103	0.0248	0.1109	0.0016	0.0969	0.0024
3134-3.3	122	38	0.31	39	1.56e-05	5.40e-05	64103	0.00027	0.00094	0.0021	0.0065	0.0883	0.0022	0.0908	0.0034
3134-13.1	137	47	0.34	47	1.98e-05	4.98e-05	50403	0.00034	0.00086	0.0027	0.0074	0.0990	0.0020	0.0947	0.0029
3134-14.1	162	70	0.43	58	5.27e-05	4.91e-05	18990	0.00091	0.00085	0.0072	0.0157	0.1223	0.0020	0.0962	0.0027
3134-14.2	88	27	0.30	30	1.80e-04	9.87e-05	5555	0.00312	0.00171	0.0241	0.0775	0.0797	0.0038	0.0898	0.0047
3134-8.5	146	50	0.34	45	6.75e-05	6.46e-05	14819	0.00117	0.00112	0.0092	0.0269	0.0908	0.0025	0.0814	0.0031
3134-11.1	175	70	0.40	60	2.07e-04	5.59e-05	4836	0.00358	0.00097	0.0278	0.0618	0.1168	0.0030	0.0938	0.0035
3134-8.1	134	58	0.44	48	3.12e-05	2.54e-05	32031	0.00054	0.00044	0.0042	0.0092	0.1250	0.0018	0.0949	0.0033
3134-13.1	155	61	0.39	52	8.60e-05	3.42e-05	11629	0.00149	0.00059	0.0116	0.0271	0.1145	0.0021	0.0921	0.0030
3134-19.1	271	128	0.47	98	1.72e-05	1.39e-05	58005	0.00030	0.00024	0.0024	0.0046	0.1385	0.0013	0.0979	0.0021
3134-19.2	287	137	0.48	103	6.07e-05	2.69e-05	16464	0.00105	0.00047	0.0083	0.0164	0.1349	0.0017	0.0945	0.0028
3134-19.3	100	27	0.27	35	7.26e-05	5.41e-05	13770	0.00126	0.00094	0.0099	0.0344	0.0756	0.0025	0.0954	0.0045
3371-A9.1	183	37	0.20	93	1.00e-05	1.00e-05	100000	0.00017	0.00017	0.0009	0.0066	0.0557	0.0008	0.1287	0.0041
3371-A9.2	164	32	0.20	86	1.37e-05	1.24e-05	72993	0.00024	0.00022	0.0012	0.0092	0.0545	0.0007	0.1351	0.0037
3371-A2.1	59	19	0.32	31	3.99e-05	2.46e-05	25038	0.00089	0.00043	0.0035	0.0162	0.0901	0.0016	0.1307	0.0047
3371-A4.1	164	90	0.55	92	1.43e-05	1.70e-05	69881	0.00025	0.00029	0.0013	0.0035	0.1519	0.0017	0.1318	0.0029
3371-B1.1	101	37	0.37	56	2.38e-05	3.43e-05	41946	0.00041	0.00059	0.0021	0.0087	0.1013	0.0017	0.1338	0.0038
3371-B7.1	89	35	0.39	49	2.47e-05	2.29e-05	40453	0.00043	0.00040	0.0022	0.0084	0.1080	0.0015	0.1339	0.0051
3371-B5.1	78	29	0.37	41	1.00e-05	1.00e-05	100000	0.00017	0.00017	0.0009	0.0036	0.1024	0.0012	0.1285	0.0042
3371-B10.1	83	35	0.42	47	4.46e-05	2.92e-05	22422	0.00077	0.00051	0.0040	0.0142	0.1147	0.0018	0.1361	0.0049
3371-B15.2	88	35	0.40	46	3.55e-05	2.74e-05	28145	0.00062	0.00048	0.0032	0.0118	0.1102	0.0024	0.1282	0.0045
3371-B9.1	113	40	0.35	61	1.00e-05	1.00e-05	100000	0.00017	0.00017	0.0009	0.0038	0.0974	0.0011	0.1323	0.0033
3371-B6.1	99	34	0.34	47	3.62e-05	3.64e-05	27609	0.00063	0.00063	0.0032	0.0141	0.0936	0.0020	0.1152	0.0042
3371-B14.1	94	33	0.35	50	1.93e-05	2.20e-05	51733	0.00034	0.00038	0.0017	0.0073	0.0975	0.0015	0.1322	0.0040
3371-B10.2	88	36	0.41	48	6.57e-05	2.68e-05	15232	0.00114	0.00046	0.0059	0.0211	0.1132	0.0016	0.1347	0.0046
3371-B8.1	81	39	0.48	44	5.21e-05	3.16e-05	19205	0.00090	0.00055	0.0046	0.0147	0.1299	0.0028	0.1315	0.0047
3935-3.2	141	157	1.11	89	1.10e-05	3.16e-05	90580	0.00019	0.00055	0.0009	0.0014	0.3013	0.0028	0.1331	0.0073
3935-2.2	241	263	1.09	155	2.90e-05	2.13e-05	34471	0.00050	0.00037	0.0025	0.0036	0.2972	0.0023	0.1374	0.0026
3935-2.3	195	155	0.79	118	1.46e-04	3.22e-05	6846	0.00253	0.00056	0.0124	0.0245	0.2158	0.0021	0.1372	0.0031
3935-3.3	223	179	0.80	132	8.46e-05	3.46e-05	11822	0.00147	0.00060	0.0071	0.0143	0.2163	0.0028	0.1323	0.0033
3935-17.1	78	50	0.64	46	6.78e-05	5.65e-05	14751	0.00117	0.00098	0.0057	0.0144	0.1717	0.0033	0.1324	0.0044
3935-6.1	64	47	0.74												

$^{206}\text{Pb}/^{238}\text{U}$	$\pm^{206}\text{Pb}/^{238}\text{U}$	$^{207}\text{Pb}/^{235}\text{U}$	$\pm^{207}\text{Pb}/^{235}\text{U}$	$^{207}\text{Pb}/^{206}\text{Pb}$	$\pm^{207}\text{Pb}/^{206}\text{Pb}$	AGE (Ma)	$\pm$ age (Ma)	AGE (Ma)	$\pm$ age (Ma)	AGE (Ma)	$\pm$ age (Ma)	AGE (Ma)	$\pm$ age (Ma)	AGE (Ma)	$\pm$ age (Ma)	%
$^{206}\text{Pb}/^{238}\text{U}$	$\pm^{206}\text{Pb}/^{238}\text{U}$	$^{207}\text{Pb}/^{235}\text{U}$	$\pm^{207}\text{Pb}/^{235}\text{U}$	$^{207}\text{Pb}/^{206}\text{Pb}$	$\pm^{207}\text{Pb}/^{206}\text{Pb}$	$^{206}\text{Pb}/^{232}\text{Th}$	$^{206}\text{Pb}/^{232}\text{Th}$	$^{206}\text{Pb}/^{238}\text{U}$	$^{206}\text{Pb}/^{238}\text{U}$	$^{207}\text{Pb}/^{235}\text{U}$	$^{207}\text{Pb}/^{235}\text{U}$	$^{207}\text{Pb}/^{235}\text{U}$	$^{207}\text{Pb}/^{235}\text{U}$	$^{207}\text{Pb}/^{235}\text{U}$	$^{207}\text{Pb}/^{235}\text{U}$	CONC
0.0772	0.0016	0.5739	0.0213	0.0539	0.0015	453.0	18.4	479.6	9.5	460.6	13.9	366.7	65.4	130.8		
0.0774	0.0024	0.6096	0.0307	0.0571	0.0020	476.7	18.5	480.6	14.6	483.3	19.6	496.0	80.3	96.9		
0.0782	0.0015	0.6011	0.0172	0.0557	0.0011	490.1	15.4	485.5	8.9	477.9	11.0	441.6	43.4	109.9		
0.0774	0.0018	0.5916	0.0428	0.0554	0.0036	447.4	27.9	480.8	10.7	471.9	27.7	428.8	153.7	112.1		
0.0755	0.0014	0.5818	0.0128	0.0559	0.0006	471.3	14.2	469.1	8.2	465.6	8.2	448.8	23.5	104.5		
0.0779	0.0017	0.5633	0.0326	0.0524	0.0027	447.7	27.0	483.7	10.3	453.7	21.4	304.2	120.2	159.0		
0.0787	0.0019	0.5883	0.0327	0.0542	0.0025	474.4	23.3	488.3	11.5	469.8	21.1	380.0	109.1	128.5		
0.0926	0.0019	0.7617	0.0329	0.0597	0.0021	597.7	64.1	570.7	10.9	575.0	19.2	591.8	79.8	96.4		
0.0921	0.0022	0.7608	0.0580	0.0599	0.0042	588.9	147.9	567.8	13.0	574.5	34.0	600.8	158.1	94.5		
0.0971	0.0020	0.8138	0.0333	0.0608	0.0020	572.7	674.5	597.5	12.0	604.6	18.8	631.4	71.9	94.6		
0.0923	0.0021	0.7300	0.0360	0.0573	0.0023	553.6	80.0	569.4	12.6	556.6	21.3	504.5	92.2	112.9		
0.0948	0.0022	0.7983	0.0396	0.0611	0.0025	571.5	98.8	584.0	12.7	595.9	22.6	641.1	91.6	91.1		
0.0957	0.0025	0.7994	0.0450	0.0606	0.0028	375.2	161.0	588.9	14.8	596.5	25.7	625.5	103.8	94.2		
0.0926	0.0022	0.7666	0.0398	0.0601	0.0026	409.1	2186.8	570.9	13.2	577.8	23.2	605.2	96.1	94.3		
0.0944	0.0022	0.7740	0.0355	0.0595	0.0022	573.0	95.2	581.3	13.0	582.0	20.5	584.9	81.4	99.4		
0.0942	0.0022	0.7597	0.0252	0.0585	0.0012	521.6	1166.1	580.1	13.0	573.8	14.7	549.0	46.2	105.7		
0.0959	0.0023	0.7997	0.0344	0.0605	0.0020	664.4	39.3	590.5	13.6	596.7	19.6	620.1	72.3	95.2		
0.0945	0.0019	0.7876	0.0264	0.0605	0.0015	349.1	163.5	581.8	11.1	589.8	15.1	620.7	53.9	93.7		
0.0935	0.0021	0.7481	0.0319	0.0581	0.0019	436.0	950.4	576.0	12.6	567.1	18.7	531.7	74.5	108.3		
0.0942	0.0023	0.7313	0.0316	0.0563	0.0019	447.4	58.4	580.3	13.3	557.3	18.7	464.5	75.1	124.9		
0.0920	0.0019	0.7744	0.0295	0.0611	0.0018	630.4	76.1	567.3	11.1	582.3	17.0	641.2	65.3	88.5		
0.0928	0.0018	0.7841	0.0218	0.0613	0.0011	615.1	41.1	572.2	10.5	587.8	12.5	648.8	38.5	88.2		
0.1986	0.0048	2.0900	0.1018	0.0763	0.0030	1113.4	44.5	1168.0	25.9	1145.5	34.0	1103.2	80.8	105.9		
0.1955	0.0050	2.1334	0.1255	0.0792	0.0040	1126.7	60.3	1151.0	26.8	1159.7	41.5	1175.9	102.2	97.9		
0.1994	0.0039	2.1369	0.0677	0.0777	0.0018	1115.2	30.5	1171.8	21.1	1160.8	22.2	1140.3	45.5	102.8		
0.1966	0.0041	2.0539	0.0872	0.0758	0.0026	1080.8	40.3	1157.0	21.9	1133.6	29.4	1089.1	71.0	106.2		
0.1985	0.0045	2.1022	0.0943	0.0768	0.0028	1157.6	39.2	1167.1	24.4	1149.5	31.4	1116.6	73.3	104.5		
0.1996	0.0045	2.1962	0.0797	0.0798	0.0021	1158.4	33.5	1173.3	24.2	1179.8	25.7	1191.7	51.9	98.5		
0.2017	0.0049	2.1401	0.1005	0.0770	0.0029	1198.3	42.8	1184.3	26.1	1161.9	33.0	1120.2	76.5	105.7		
0.1987	0.0042	2.1261	0.0829	0.0776	0.0023	1149.3	40.3	1168.3	22.8	1157.3	27.3	1136.9	61.0	102.8		
0.1953	0.0041	2.1383	0.0778	0.0794	0.0022	1086.7	33.2	1149.8	21.9	1161.3	25.5	1182.7	55.2	97.2		
0.1970	0.0038	2.1632	0.0686	0.0796	0.0018	1169.2	33.5	1159.1	20.6	1169.3	22.3	1188.1	45.7	97.6		
0.3263	0.0071	5.0826	0.1335	0.1130	0.0014	1870.0	76.4	1820.2	34.5	1833.2	22.5	1848.0	22.5	98.5		
0.3204	0.0063	5.0026	0.1171	0.1133	0.0012	1768.6	70.5	1791.5	30.7	1819.7	20.0	1852.2	19.3	96.7		
0.3327	0.0068	5.2245	0.1466	0.1139	0.0019	1813.0	81.1	1851.3	33.0	1856.6	24.2	1862.6	30.7	99.4		
0.3309	0.0068	5.2770	0.1324	0.1157	0.0014	1822.1	77.6	1842.6	32.8	1865.2	21.6	1890.4	22.2	97.5		
0.3339	0.0075	5.3308	0.1500	0.1158	0.0017	1875.9	101.2	1857.4	36.5	1873.8	24.3	1892.0	25.9	98.2		
0.3421	0.0061	5.3170	0.1157	0.1127	0.0012	1869.8	43.8	1896.8	29.6	1871.6	18.8	1843.8	18.7	102.9		
0.3124	0.0068	4.9164	0.1251	0.1141	0.0012	1756.8	62.2	1752.5	33.4	1805.1	21.7	1866.3	19.7	93.9		
0.3268	0.0064	5.1780	0.1241	0.1149	0.0014	1827.8	53.9	1822.9	31.0	1849.0	20.6	1878.5	21.4	97.0		
0.3388	0.0064	5.2737	0.1195	0.1129	0.0012	1856.9	49.1	1880.8	31.0	1864.6	19.5	1846.6	18.7	101.9		
0.3331	0.0070	5.2053	0.1507	0.1134	0.0020	1737.3	86.8	1853.2	33.7	1853.5	25.0	1853.8	32.2	100.0		
0.2981	0.0064	4.6427	0.1191	0.1130	0.0013	1582.1	57.3	1681.7	31.8	1757.0	21.7	1847.7	21.3	91.0		
0.3262	0.0063	5.0613	0.1224	0.1125	0.0014	1812.5	64.7	1820.0	30.6	1829.7	20.7	1840.6	22.7	98.9		
0.3347	0.0065	5.2448	0.1172	0.1137	0.0010	1832.1	61.8	1861.0	31.7	1859.9	19.2	1858.7	15.7	100.1		
0.3170	0.0054	4.9944	0.1000	0.1143	0.0010	1780.8	55.3	1774.9	26.6	1818.4	17.1	1868.5	15.4	95.0		
0.3353	0.0055	5.2330	0.0948	0.1132	0.0007	1887.1	39.3	1864.2	26.8	1858.0	15.6	1851.0	10.4	100.7		
0.3343	0.0058	5.2262	0.0999	0.1134	0.0007	1824.7	51.8	1859.3	27.9	1856.9	16.4	1854.2	11.7	100.3		
0.3457	0.0068	5.3962	0.1303	0.1132	0.0014	1842.3	83.3	1913.8	32.5	1884.3	20.9	1851.8	21.7	103.3		
0.4775	0.0085	11.3920	0.2184	0.1730	0.0009	2446.6	73.5	2516.3	37.2	2555.8	18.1	2587.2	8.8	97.3		
0.4965	0.0096	11.7440	0.2472	0.1715	0.0011	2560.6	66.5	2598.9	41.6	2584.2	19.9	2572.7	10.4	101.0		
0.4838	0.0092	11.7380	0.2475	0.1760	0.0013	2483.6	84.2	2543.7	39.9	2583.8	19.9	2615.4	12.0	97.3		
0.4927	0.0082	11.6550	0.2080	0.1716	0.0008	2502.4	52.4	2582.2	35.4	2577.1	16.8	2573.0	8.1	100.4		
0.5020	0.0097	12.0800	0.2573	0.1745	0.0012	2538.5	68.3	2622.3	41.9	2610.7	20.2	2601.7	11.3	100.8		
0.4984	0.0086	11.8090	0.2230	0.1719	0.0010	2540.2	90.9	2606.9	37.1	2589.4	17.8	2575.7	9.8	101.2		
0.4817	0.0087	11.6420	0.2338	0.1753	0.0012	2443.1	75.0	2534.7	37.8	2576.1	19.0	2608.8	11.7	97.2		
0.5086	0.0092	11.9810	0.2362	0.1709	0.0010	2578.3	87.0	2650.7	39.5	2602.9	18.6	2566.0	9.8	103.3		
0.4752	0.0096	11.2690	0.2576	0.1720	0.0013	2438.1	80.0	2506.4	42.9	2545.6	21.6	2577.1	12.9	97.3		
0.4965	0.0083	11.8690	0.2127	0.1734	0.0008	2511.3	59.4	2598.8	36.0	2594.1	16.9	2590.4	7.6	100.3		
0.4316	0.0083	10.3960	0.2228	0.1747	0.0013	2203.6	76.9	2312.7	37.5	2470.7	20.1	2603.4	12.3	88.8		
0.4834	0.0086	11.5460	0.2220	0.1732	0.0010	2509.0	71.7	2542.0	37.3	2568.3	18.1	2589.2	9.5	98.2		
0.4884	0.0095	11.5720	0.2424	0.1719	0.0010	2553.4	82.5	2563.7	41.1	2570.4	19.8	2575.7	10.0	99.5		
0.4873	0.0110	11.6890	0.2986	0.1740	0.0017	2497.5	83.3	2559.2	47.8	2579.8	24.2	2596.0	16.0	98.6		
0.4953	0.0095	12.3830	0.2600	0.1813	0.0012	2525.5	129.7	2593.5	40.9	2633.9	19.9	2665.0	11.1	97.3		
0.5051	0.0089	12.6380	0.2432	0.1815	0.0011	2601.9	46.6	2635.6	38.3	2653.1	18.3	2666.4	9.7	98.8		
0.5008	0.0089	12.4830	0.2424	0.1808	0.0011	2597.8	54.3	2617.1	38.2	2641.4	18.4	2660.1	10.0	98.4		
0.4928	0.0086	12.4210	0.2437	0.1828	0.0013	2511.2	58.6	2582.7	37.2	2636.8	18.6	2678.5	11.9	96.4		
0.5009	0.0113	12.5860	0.3180	0.1822	0.0016	2513.4	78.2	2617.6	48.7	2649.2	24.1	2673.4	14.9	97.9		
0.5040	0.0116	12.5080	0.3242	0.1800	0.0017	2495.4	95.3	2630.9	50.0	2643.3	24.7	2652.8	15.5	99.2		
0.4775	0.0086															



**Figure 12.** SHRIMP ages for test samples normalized to the ID-TIMS age versus age. Error bars are 95% confidence level. Small ticks above the datum indicate no correction for common Pb. **a)**  $^{207}\text{Pb}/^{206}\text{Pb}$  ages, **b)**  $^{206}\text{Pb}/^{238}\text{U}$  ages, **c)**  $^{208}\text{Pb}/^{232}\text{Th}$  ages.

Although beyond the scope of this report to discuss the complexity and controversy over the age of SL13, it is interesting to note that the SHRIMP mean  $^{206}\text{Pb}/^{238}\text{U}$  age of 578 Ma is more consistent with the ID-TIMS  $^{207}\text{Pb}/^{206}\text{Pb}$  age of 576 Ma rather than the  $^{206}\text{Pb}/^{238}\text{U}$  age of 572 Ma.

In Figure 12c, it can be seen that the SHRIMP mean  $^{208}\text{Pb}/^{232}\text{Th}$  ages range from 0.5-3.0% younger than the accepted ages. Although none of the test samples has been analyzed for  $^{208}\text{Pb}/^{232}\text{Th}$  isotopes, it is inconceivable that all the test samples would have preferentially lost  $^{208}\text{Pb}$  or gained  $^{232}\text{Th}$  to similar extents. Presently, the age discrepancy is interpreted to be due to an unknown analytical bias. Preliminary analyses of the  $^{208}\text{Pb}/^{232}\text{Th}$  ratios in the Kipawa standard by ID-TIMS (B. Davis, pers. comm., 1996) indicate an age similar to the concordant Pb/U age, and therefore, the problem may not be the Kipawa zircon. More work is needed to verify the ID-TIMS data and to investigate possible systematic errors in the data reduction procedure.

### Comparison of SHRIMP and ID-TIMS age errors

The 95% confidence intervals for the SHRIMP ages for the zircon test samples are compared with the ID-TIMS errors for the same samples in Figures 13 and 14. The absolute values of the 95% confidence errors in Ma are shown in Figure 13 for each of the  $^{207}\text{Pb}/^{206}\text{Pb}$ ,  $^{206}\text{Pb}/^{238}\text{U}$ , and  $^{208}\text{Pb}/^{232}\text{Th}$  SHRIMP ages. The ID-TIMS data have  $2\sigma$  errors of 1-2 Ma regardless of age and are consistently better than the SHRIMP data, for reasons explained previously. For the SHRIMP data, the absolute error depends on the age of the sample and the isotopic system being considered. For zircons <1.5 Ga the  $^{206}\text{Pb}/^{238}\text{U}$  data provide the most precise ages, with  $2\sigma$  errors of 5-8 Ma at 500 Ma, whereas, for zircons >1.5 Ga similar absolute errors are instead derived from the  $^{207}\text{Pb}/^{206}\text{Pb}$  data.

The same data for the test samples are plotted in Figure 14 as the  $2\sigma$  error in the age as a percentage of the absolute age. For the ID-TIMS data, the  $2\sigma$  errors in age drop from roughly 0.2% at 500 Ma to about 0.05% at 2700 Ma. The errors in the SHRIMP  $^{206}\text{Pb}/^{238}\text{U}$  ages for zircons <1.5 Ga are 1-1.5% and are the best that can be achieved for zircons of this age. For zircons >1.5 Ga, a final age can be determined to a  $2\sigma$  precision of 1.0% to 0.2%, decreasing with increasing age. The interesting feature of Figure 14 is that, regardless of the absolute age, it is generally possible to derive a SHRIMP age that has an error about a factor of five times-greater than the ID-TIMS error. Thus, if  $\sigma$  errors of 1-2 Ma were obtained in an ID-TIMS analysis, then errors of 5-10 Ma can be expected from SHRIMP.

## CONCLUSIONS

Since the delivery of the SHRIMP in November, 1995, the principal objective of the first year has been to establish zircon geochronology as a routine analytical method. Despite numerous technical difficulties encountered during the first six months, including an exhaustive search for potential zircon standard materials, the results in this report demonstrate that the zircon geochronology program is now in place. An

attempt has been made here to bring together the basic concepts, approaches, and analytical methods presently employed in determining U-Pb-Th isotopic ages in zircon. There is no doubt that the analytical methods will be refined and improved with time, and consequently this report should not be taken as the last word on subject. For example, while the Kipawa zircon is a suitable zircon standard, the search continues for even better material that may someday take its place.

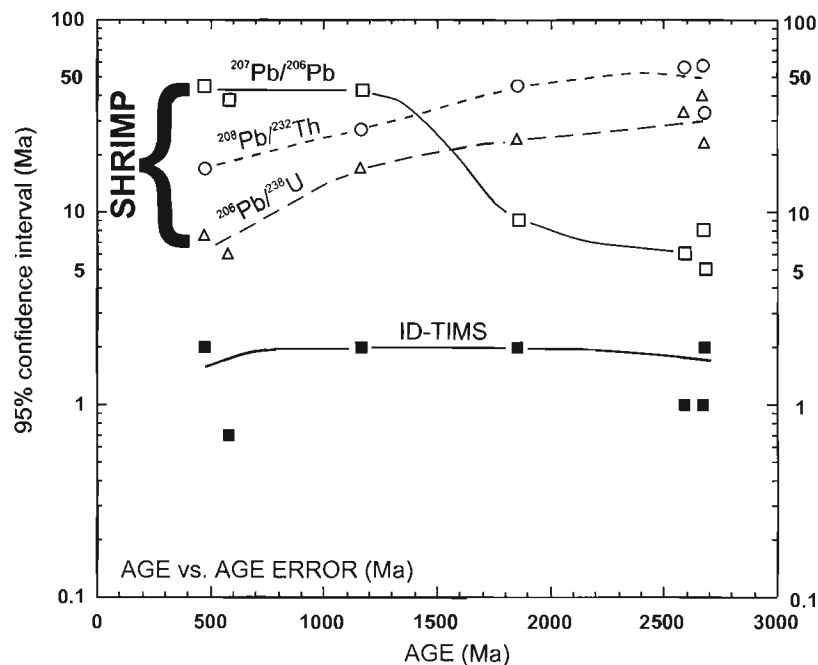
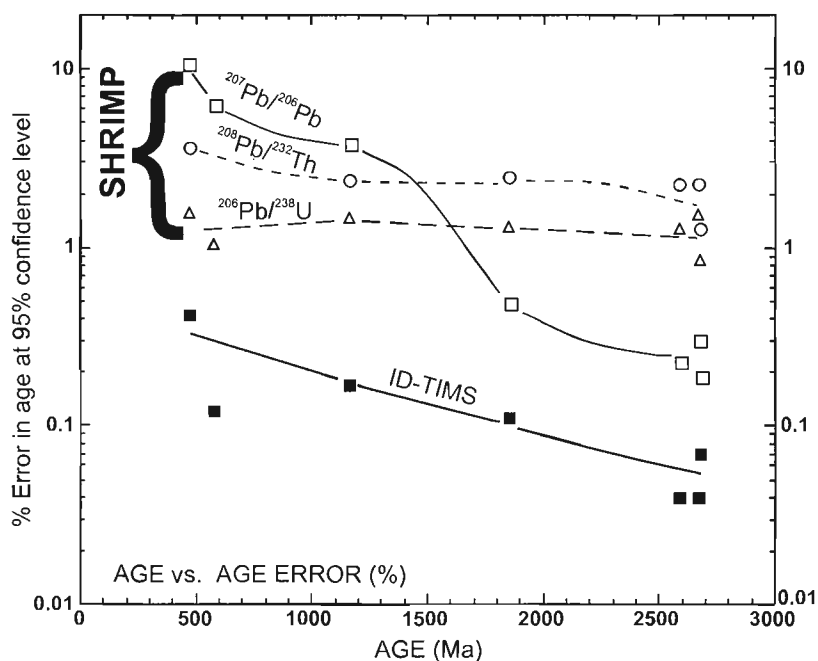


**Figure 13.**

Age versus 95% confidence level errors (Ma) of SHRIMP and ID-TIMS ages for test samples.

**Figure 14.**

Age versus percentage  $2\sigma$  age error of SHRIMP and ID-TIMS.



Throughout this report it has been necessary and useful to compare and contrast the data obtained by SHRIMP with isotope dilution thermal ionization mass spectrometry (ID-TIMS). Table 8, after Stern (1996), presents a summary of the relative strengths and weaknesses of these two methods. It is apparent that in many ways the techniques are complementary. SHRIMP excels at geochronology in complex zircon targets, such as those with complex inheritance or Pb loss, or in cases where zircon must be analyzed in situ. SHRIMP is also the technique of choice for rapid surveys of large zircon populations, such as in the study of provenance characteristics of detrital zircon suites. Isotope dilution still remains the method of choice for obtaining the highest precision analysis of homogeneous, near concordant zircons. It is unlikely that any technology now or in the future will be able to match the precision of a good ID-TIMS analysis. What the SHRIMP brings to the GSC laboratory is a rapid method of obtaining age information with unprecedented horizontal and vertical (depth) spatial resolution. The SHRIMP is an interactive geochronological tool that allows the geochronologist to respond in real time to the age data being generated. Hypotheses can be tested, modified, rejected, or confirmed over the space of a few hours. In the author's view, it is this element of interactivity that clearly distinguishes the SHRIMP analysis from an ID-TIMS analysis.

## ACKNOWLEDGMENTS

A great many people were involved in acquiring the SHRIMP, but it was principally the vision of the late J.C. Roddick. I wish to thank R. Parrish and Otto van Breemen for their encouragement and support following Chris' death in February, 1995. M. Gerasimoff provided crucial logistical and technical assistance in establishing the laboratory infrastructure and in testing and installing the instrument; its enhanced performance and many of the customized features of the GSC SHRIMP are, in part, due to his efforts. B. Davis is thanked for analyzing the Pb isotopes in gold, and for his unpublished Th-Pb data on the Kipawa zircon. M. Villeneuve, V. McNicoll, R. Theriault, and P. Hunt all provided help and advice at various stages. Student S. Wilkinson contributed to the documentation of the Kipawa zircon. The staff of Australian Scientific Instruments and the Research School of Earth Sciences provided all manner of advice, data, and logistical support in transferring the SHRIMP technology to Canada. I would especially like to thank W. Compston, I. Williams, A. Rastawicki, H. Persing, T. Ireland, S. Clement, and A. Nutman for spending so much of their time with me in Australia and Ottawa to ensure the success of this endeavor.

**Table 8.** Comparison of relative performance of GSC SHRIMP II and ID-TIMS in U-Pb zircon dating (after Stern, 1996).

	SHRIMP	ID-TIMS*
Mass of zircon analyzed	1-10 ng per spot	>1000 ng per fraction
typical mass of Pb analyzed	~0.1 pg per spot	>100 pg per fraction
Reproducibility (1 $\sigma$ ) of $^{206}\text{Pb}/^{238}\text{U}$ age	~1.5% per spot	0.2% per fraction
Reproducibility (1 $\sigma$ ) of $^{207}\text{Pb}/^{206}\text{Pb}$ age	0.5-10.0% per spot (depends on age)	0.05-0.08% per fraction
Overall instrumental Pb sensitivity (collected Pb/total Pb)	0.3%	0.6%
# data points in one year (GSC potential)	4000 (20 spots/day * 200 days)	1200
Ability to determine precise (<0.1% 2 se) ages of geological events	possible in some cases, but resource intensive	routine in many cases, but difficult if zircon is complex
Ability to tackle complex dating problems (inheritance, Pb-loss, overgrowths, etc.)	very strong, if sufficient age contrasts exist	possible in some cases; resource intensive; may be uncertainties in age interpretation
ability to tackle detrital studies	excellent for rapid surveys of protolith ages; weaker at precise determination of youngest zircon	highly resource intensive; excellent for precise determination of youngest zircon
ability to carry out in situ (contextual) studies	excellent: thin sections and rock slabs	not possible
fate of analyzed material	essentially nondestructive	sample destroyed
*isotope dilution statistics from B. Davis and M. Villeneuve (pers. comm., 1996)		

## REFERENCES

- Andersen, C.A. and Hinthorne, J.R.**  
1973: Thermodynamic approach to the quantitative interpretation of sputtered ion in mass spectra; *Analytical Chemistry*, v. 45, p. 1421-1438.
- Benninghoven, A., Rudenauer, F.G., and Werner, H.W.**  
1987: Secondary ion mass spectrometry: basic concepts, instrumental aspects, applications and trends; *Chemical Analysis*, v. 86, Wiley, 1227 p.
- Bevington, P.R.**  
1969: *Data Reduction and Error Analysis for the Physical Sciences*; McGraw-Hill, New York, 336 p.
- Bowring, S.A., Williams, I.S., and Compston, W.**  
1989: 3.96 Ga gneisses from the Slave province, Northwest Territories, Canada; *Geology*, v. 17, p. 971-975.
- Claoue-Long, J.C., Compston, W., Roberts, J., and Fanning, C.M.**  
1995: Two Carboniferous ages: a comparison of SHRIMP zircon dating with conventional zircon ages and  $^{40}\text{Ar}/^{39}\text{Ar}$  analysis; in *Geochronology, time scales and global stratigraphic correlation*, (ed.) W.A. Berggren, D.V. Kent, M-P. Aubry, and J. Hardenbol; Society for Sedimentary Geology, Special Publication, v. 54, p. 3-21.
- Clement, S.W.J. and Compston, W.**  
1989: SIMS at high sensitivity and high mass resolution; in *Proceedings of the Seventh International Conference on Secondary Ion Mass Spectrometry Conference*, (ed.) A. Benninghoven, C.A. Evans, K.D. McKeegan, H.A. Störms, and H.W. Werner; Wiley, New York, p. 815-819.
- Clement, S.W.J., Compston, W., and Newstead, G.**  
1977: Design of a large, high resolution ion microprobe; in *Proceedings of the International Secondary Ion Mass Spectrometry Conference*, (ed.) A. Benninghoven; Springer-Verlag, 12 p.
- Compston, W., Williams, I.S., and Clement, S.W.J.**  
1982: U-Pb ages within single zircons using a sensitive high mass-resolution ion microprobe; 30th Annual Conference of the American Society of Mass Spectrometry, p. 593-595.
- Compston, W., Williams, I.S., and Meyer, C.**  
1984: U-Pb geochronology of zircons from lunar breccia 73217 using a sensitive high mass-resolution ion microprobe; *Journal of Geophysical Research*, v. 89, p. B525-B534.
- Cumming, G.L. and Richards, J.R.**  
1975: Ore lead ratios in a continuously changing Earth; *Earth and Planetary Science Letters*, v. 28, p. 155-171.
- Currie, K.L. and van Breemen, O.**  
1996: The origin of rare minerals in the Kipawa Syenite Complex, western Quebec; *Canadian Mineralogist*, v. 34, p. 435-451.
- Froude, D.O., Ireland, T.R., Kinney, P.D., Williams, I.S., Compston, W., Williams, A.R., and Myers, J.S.**  
1983: Ion microprobe identification of 4,100-4,200 Myr-old detrital zircons; *Nature*, v. 304, p. 616-618.
- Hanchar, J.M. and Miller, C.F.**  
1993: Zircon zonation patterns as revealed by cathodoluminescence and backscattered electron images: implications for interpretation of complex crustal histories; *Chemical Geology*, v. 110, p. 1-13.
- Hinthorne, J.R., Andersen, C.A., Conrad, R.L., and Lovering, J.F.**  
1979: Single-grain  $^{207}\text{Pb}/^{206}\text{Pb}$  and U/Pb age determinations with a 10- $\mu\text{m}$  spatial resolution using the ion microprobe mass analyzer; *Chemical Geology*, v. 25, p. 271-303.
- Matsuda, H.**  
1974: Double focussing mass spectrometers of second order; *International Journal of Mass Spectrometry and Ion Processes*, v. 14, p. 219-233.
- McLaren, A.C., Fitzgerald, J.D., and Williams, I.S.**  
1994: The microstructure of zircon and its influence on the age determination from Pb/U isotopic ratios measured by ion microprobe; *Geochimica et Cosmochimica Acta*, v. 58, p. 993-1005.
- Mendenhall, W. and Sincich, T.**  
1995: *Statistics for Engineering and the Sciences*; Prentice-Hall, New Jersey, U.S.A., 1182 p.
- Mortensen, J.K. and Card, K.D.**  
1993: U-Pb age constraints for the magmatic and tectonic evolution of the Pontiac Subprovince, Quebec; *Canadian Journal of Earth Sciences*, v. 30, p. 1970-1980.
- Roboz, J.**  
1968: *Introduction to Mass Spectrometry Instrumentation and Techniques*; John Wiley and Sons, New York, 539 p.
- Roddick, J.C. and van Breemen, O.**  
1994: U-Pb zircon dating: a comparison of ion microprobe and single grain conventional analyses; in *Radiogenic Age and Isotopic Studies: Report 8; Geological Survey of Canada, Current Research 1994-F*, p. 1-9.
- Shimizu, N. and Hart, S.R.**  
1982: Applications of the ion microprobe to geochemistry and cosmochemistry; *Annual Reviews of Earth and Planetary Sciences*, v. 10, p. 483-526.
- Stern, R.A.**  
1996: A SHRIMP II ion microprobe at the Geological Survey of Canada; *Geoscience Canada*, v. 23, p. 73-76.
- Stern, R.A. and Lucas, S.B.**  
1994: U-Pb zircon age constraints on the early tectonic history of the Flin Flon accretionary collage, Saskatchewan; in *Radiogenic Age and isotopic Studies: Report 8; Geological Survey of Canada, Current Research 1994-F*, p. 75-86.
- Wiedenbeck, M. and Watkins, K.P.**  
1993: A time scale for granitoid emplacement in the Archean Murchison Province, Western Australia, by single zircon geochronology; *Precambrian Research*, v. 61, p. 1-26.
- Williams, I.S. and Claesson, S.**  
1987: Isotopic evidence for the provenance and Caledonian Metamorphism of high grade paragneisses from the Seve Nappes, Scandinavian Caledonides: ion microprobe zircon U-Th-Pb; *Contributions to Mineralogy and Petrology*, v. 97, p. 205-217.
- Williams, P.**  
1979: The sputtering process and sputtered ion emission; *Surface Science*, v. 90, p. 588-643.
- 1983: Secondary ion mass spectrometry; *Applied Atomic Collision Physics*, v. 4, p. 327-377.





# Modified chemical procedures for the extraction and purification of uranium from titanite, allanite, and rutile in the Geochronology Laboratory, Geological Survey of Canada

W.J. Davis<sup>1</sup>, V.J. McNicoll<sup>1</sup>, D.R. Bellerive<sup>1</sup>, K. Santowski<sup>1</sup>, and D.J. Scott<sup>1</sup>

*Davis, W.J., McNicoll, V.J., Bellerive, D.R., Santowski, K., and Scott, D.J., 1997: Modified chemical procedures for the extraction and purification of uranium from titanite, allanite, and rutile in the Geochronology Laboratory, Geological Survey of Canada; in Radiogenic Age and Isotopic Studies: Report 10; Geological Survey of Canada, Current Research 1997-F, p. 33-35.*

---

**Abstract:** A procedure for the extraction and purification of U from Fe-, Ca-, and Ti-bearing minerals using U/TEVA•SPECT<sup>TM</sup> extraction chromatographic material is described. The procedure has several advantages over previous techniques: it requires less time, uses much smaller quantities of high-purity acids, and yields improved U analysis by thermal ionization mass spectrometry.

**Résumé :** Le présent rapport consiste en une description d'une méthode d'extraction et de purification de U contenu dans des minéraux à Fe, à Ca et à Ti qui utilise le matériau chromatographique d'extraction U/TEVA•SPECT<sup>TM</sup>. Cette méthode offre plusieurs avantages par rapport aux techniques précédemment utilisées : elle requiert moins de temps, utilise de plus petites quantités d'acides de haute pureté et produit de meilleurs résultats quant aux analyses de U par spectrométrie de masse à thermoionisation.

---

<sup>1</sup> Geological Survey of Canada, 601 Booth Street, Ottawa, Ontario K1A 0E8

## INTRODUCTION

This paper describes a new procedure adopted for the routine extraction and purification of uranium (U) from minerals that contain important quantities of iron (Fe), such as titanite, rutile, allanite, and perovskite. The method uses U/TEVA•SPEC<sup>TM</sup> extraction chromatographic material (Eichrom Industries, Inc., Darien, Illinois), a substance specifically designed for the selective sorption of U and tetravalent actinides from acidic nitrate media (Horwitz et al., 1992). The principal difficulty in U-Pb analyses of Fe-bearing minerals is that inefficient chemical separation of U from other cations, in particular Fe, results in poor ionization and measurement of U by thermal ionization mass spectrometry (Parrish et al., 1992). Previous procedures to separate U from Fe at the GSC laboratory involved time consuming column chemistry using anion exchange resins in 8 N HNO<sub>3</sub> (Parrish et al., 1992). The method used large quantities of ultra-pure 8 N HNO<sub>3</sub> and did not consistently result in satisfactory mass spectrometric analysis. The method described here uses much smaller quantities of HNO<sub>3</sub>, requires a single column procedure for U purification, provides low U blanks, and routinely yields good quality U signals during thermal ionization mass spectrometry.

## CHEMICAL PROCEDURES

Mineral selection, weighing, spiking, and dissolution follow procedures outlined in Parrish et al. (1987, 1992). Following dissolution in HF-HNO<sub>3</sub>, the sample is taken up in 6.2 N HCl, evaporated to dryness and dissolved in 0.20 mL 3.1 N HCl. This solution is added to Teflon<sup>TM</sup> columns containing 0.25 mL of 200-400 mesh BioRad Laboratories<sup>TM</sup> AG1X8 anion exchange resin (bed length = 1.5-2.0 cm). Cleaning of the resin follows methods described by Parrish et al. (1992).

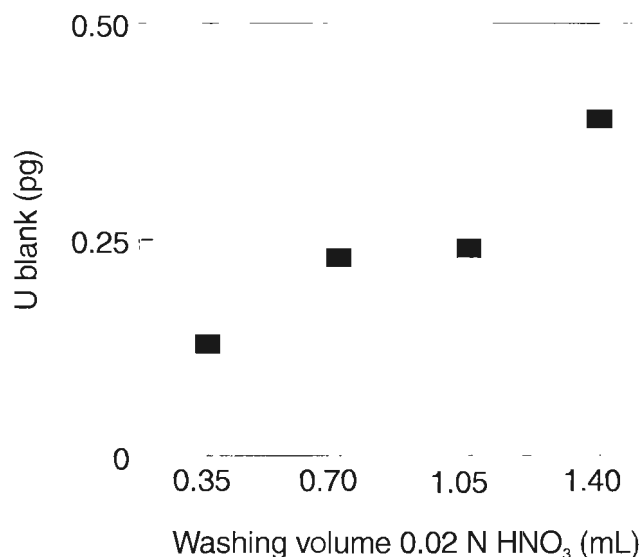


**Figure 1.** Total U blank versus washing volume of 0.02 N HNO<sub>3</sub>.

**Table 1.** Procedure for the extraction of U using U/TEVA•SPEC<sup>TM</sup> material.

<b>Column washing</b>
Wash columns (stored in HCl) with HNO <sub>3</sub> and H <sub>2</sub> O
Add 50 µL of U/TEVA•SPEC <sup>TM</sup> resin
Wash with 0.35 mL of 0.02N HNO <sub>3</sub>
Add 0.15 mL 2N HNO <sub>3</sub> to condition
<b>Add sample and collect U</b>
Add sample to column
Add: 0.02 mL 2N HNO <sub>3</sub>
0.02 mL 2N HNO <sub>3</sub>
0.02 mL 2N HNO <sub>3</sub>
0.40 mL 2N HNO <sub>3</sub>
Replace with U collection beakers
Add: 0.02 mL 0.02N HNO <sub>3</sub>
0.02 mL 0.02N HNO <sub>3</sub>
0.02 mL 0.02N HNO <sub>3</sub>
0.35 mL 0.02N HNO <sub>3</sub>
0.01 mL H <sub>3</sub> PO <sub>4</sub>
Evaporate to dryness

After initial elution in 3.1 N HCl, which removes Ti and Ca but retains U, Fe, and Pb, U is separated from Pb and collected along with Fe in 1 N HBr. Lead is further purified in HBr and collected in 6.2 N HCl as described by Parrish et al. (1992). The HBr solution containing Fe and U is evaporated on a hot plate and the precipitate dissolved in 0.15 mL 2 N HNO<sub>3</sub>.

### Uranium extraction

The U purification procedure uses U/TEVA•SPEC<sup>TM</sup>, an extraction chromatographic resin made up of diamyl amylphosphonate sorbed on a polymeric substrate of Amberlite XAD-7. A full description of the material and its properties is given by Horwitz et al. (1992). The Teflon<sup>TM</sup> columns have a reservoir volume of 50-55 µL and a resin bed length of 12 mm. The recommended loading capacity for 50 µL of U/TEVA•SPEC<sup>TM</sup> chromatographic material is 0.2 to 0.4 mg of U, several orders of magnitude greater than U contents of the sample material. There is no jeopardy of overloading the columns, even with large U-rich samples.

U/TEVA•SPEC<sup>TM</sup> chromatographic material (100-200 µm) is washed in 15 mL Savillex<sup>TM</sup> capsules by repeated rinsing and decanting with 2 N HNO<sub>3</sub> and 0.02 N HNO<sub>3</sub> (4 or 5 cycles). The material undergoes hydrolysis if stored for long periods in H<sub>2</sub>O which can inhibit stripping of U from the material (Eichrom Industries, pers. comm., 1996). For this reason, the material is stored dry and small batches of material are cleaned and prepared prior to use.

The chemical procedure is detailed in Table 1. The Teflon<sup>TM</sup> columns are cleaned in 6 N HCl, and rinsed with HNO<sub>3</sub> and H<sub>2</sub>O prior to addition of the U/TEVA•SPEC<sup>TM</sup> material. The precleaned resin is added to the column and 0.35 mL of 0.02N HNO<sub>3</sub> is passed through the column to further clean it. The effectiveness of this cleaning procedure has been

evaluated in an experiment in which four columns were washed with variable amounts of 0.02 N HNO<sub>3</sub>, ranging from 0.35 mL to 1.4 mL. The U content of each of the four washes was measured by isotope dilution (Fig. 1). All of the blank determinations were less than 1 pg and the blank did not decrease with larger washing volumes. Four separate sample batches have been processed between May and September 1996 using this cleaning procedure; 13 of 15 blank determination are less than 1 pg, and all are less than 4 pg.

Prior to adding the sample the resin is equilibrated with 0.15 mL of 2 N HNO<sub>3</sub>. Iron and other cations are eluted in 0.46 mL of 2 N HNO<sub>3</sub>, whereas U is strongly retained on the U/TEVA•SPEC<sup>TM</sup> material. Uranium is then stripped and collected in a total of 0.41 mL of 0.02 N HNO<sub>3</sub>. One drop of phosphoric acid is added to the solution prior to evaporation. The sample is then ready for analysis by thermal ionization mass spectrometry.

---

## SUMMARY

The procedure using U/TEVA•SPEC<sup>TM</sup> extraction chromatographic material results in precise and stable uranium analyses on the mass spectrometer. A total of 102 titanite, 20 rutile and 2 allanite fractions have been processed using this technique with consistently good results and total procedural blanks. The main advantages of the technique are the very efficient separation of uranium from other cations, in particular Fe, the significantly reduced quantities of ultra-pure nitric acid required by the procedure, and improved quality of U signal measured on the mass spectrometer.

---

## REFERENCES

- Horwitz, E.P., Dietz, M., Chiarizia, R., Diamond, H., Essling, A.M., and Graczyk, D.**  
 1992: Separation and preconcentration of uranium from acidic media by extraction chromatography; *Analytica Chimica Acta*, v. 266, p. 25-37.
- Parrish, R.R., Bellerive, D., and Sullivan, R.W.**  
 1992: U-Pb chemical procedures for titanite and allanite in the Geochronology Laboratory, Geological Survey of Canada; in *Radiogenic Age and Isotopic Studies: Report 5*; Geological Survey of Canada, Paper 91-2, p. 187-190.
- Parrish, R.R., Roddick, J.C., Loveridge, W.D., and Sullivan, R.W.**  
 1987: Uranium-lead analytical techniques at the geochronology laboratory, Geological Survey of Canada; in *Radiogenic Age and Isotopic Studies: Report 1*; Geological Survey of Canada, Paper 88-2, p. 3-7.



## 2.70-2.58 Ga plutonism and volcanism in the Slave Province, District of Mackenzie, Northwest Territories<sup>1</sup>

M.E. Villeneuve<sup>2</sup>, J.R. Henderson<sup>2</sup>, R.B. Hrabi<sup>3</sup>, V.A. Jackson<sup>4</sup>,  
and C. Relf<sup>5</sup>

*Villeneuve, M.E., Henderson, J.R., Hrabi, R.B., Jackson, V.A., and Relf, C., 1997: 2.70-2.58 Ga plutonism and volcanism in the Slave Province, District of Mackenzie, Northwest Territories; in Radiogenic Age and Isotopic Studies: Report 10; Geological Survey of Canada, Current Research 1997-F, p. 37-60.*

---

**Abstract:** New U-Pb zircon age dates are reported from eleven plutonic and seven volcanic rocks sampled in five greenstone belts in the Slave Province. Three of these belts are in the northwestern Slave Province (High Lake greenstone belt, Anialik River volcanic belt, and Napaktulik Lake volcanic belt) and the other two are located in the central Slave Province (Winter Lake supracrustal belt, Courageous Lake volcanic belt). Locally, the volcanic and plutonic rocks help constrain structural and depositional history within a belt, define the age of metallogenesis and allow for inter-belt correlation of units. Regionally, the age data support previous data sets, with the ages of volcanic rocks from greenstone belts falling between 2705 Ma and 2671 Ma. Plutonic rocks are in accord with general evolution from predeformational 2.70-2.64 Ga tonalites and diorites to 2.62-2.59 Ga K-feldspar megacrystic granites and finally to postdeformational 2.60-2.58 Ga two-mica granites. A distinct break in magmatic activity between 2.640 and 2.625 Ga remains evident in the data set for the plutons. The data also highlight inconsistencies in the time of formation of deformational fabrics recorded by plutonic rocks, suggesting that local strain regimes play a major role in fabric development, even within a single belt.

**Résumé :** Dans la Province des Esclaves, onze roches plutoniques et sept roches volcaniques provenant de cinq ceintures de roches vertes échantillonnées ont été datées selon la méthode U-Pb sur zircon. Trois des ceintures de roches vertes s'étendent dans le nord-ouest de la Province des Esclaves (ceinture de roches vertes de High Lake, ceinture de roches volcaniques d'Anialik River et ceinture de roches volcaniques de Napaktulik Lake) et les deux autres sont situées dans le centre de celle-ci (ceinture de roches supracrustales de Winter Lake, ceinture de roches volcaniques de Courageous Lake). À l'échelle locale, les roches volcaniques et plutoniques nous fournissent des renseignements qui nous aident à reconstituer l'évolution structurale et sédimentaire de la ceinture dans laquelle elles se trouvent, à dater l'époque de la métallogenèse et à corrélérer des unités d'une ceinture à l'autre. À l'échelle régionale, les datations s'intègrent bien aux ensembles de données radiométriques antérieurs et permettent de situer entre 2 705 et 2 671 Ma l'âge des roches

---

<sup>1</sup> Contribution to Canada-Northwest Territories Mineral Initiatives (1991-1996), an initiative under the Canada-Northwest Territories Economic Development Cooperation Agreement/Contribution to Slave NATMAP Project

<sup>2</sup> Geological Survey of Canada, 601 Booth Street, Ottawa, Ontario K1A 0E8

<sup>3</sup> Department of Geological Sciences, Queen's University, Kingston, Ontario K7L 3N6

<sup>4</sup> NWT Geology Division, Department of Indian Affairs and Northern Development, Box 1500, Yellowknife, NWT, X1A 2R3

<sup>5</sup> Canada-NWT Mineral Initiatives Office

volcaniques à l'intérieur des ceintures de roches vertes. Les roches plutoniques s'insèrent dans un schéma général d'évolution, qui débute par des tonalites et de diorites antérieures à la déformation datées de l'intervalle 2,70-2,64 Ga, se poursuit par des granites à gros phénocristaux de feldspath potassique d'un âge de 2,62-2,59 Ga et se termine par des granites à deux micas postérieurs à la déformation remontant à 2,60-2,58 Ga. Un arrêt bien net de l'activité magmatique entre 2,640 et 2,625 Ga demeure évident dans les ensembles de données tirées des plutons. Les données mettent également en lumière des incohérences dans la chronologie de l'apparition des fabriques de déformation qui touchent les roches plutoniques, ce qui laisse supposer que les régimes de déformation locaux ont joué un rôle important dans la formation des fabriques, même au sein d'une seule ceinture.

## INTRODUCTION

The Slave Province, an Archean granite-greenstone-turbidite terrane located in the northwestern Canadian Shield has been the focus of a number of geoscientific studies operating under the umbrella of the Slave NATMAP project. Most of

the mapping was centred along a north-south corridor that roughly approximates the extension of an isotopic boundary defined by Nd (Davis and Hegner, 1992) and Pb (Thorpe et al., 1992) isotopic compositions, separating values exhibiting components of old crust in the west from more juvenile signatures in the east (Fig. 1).

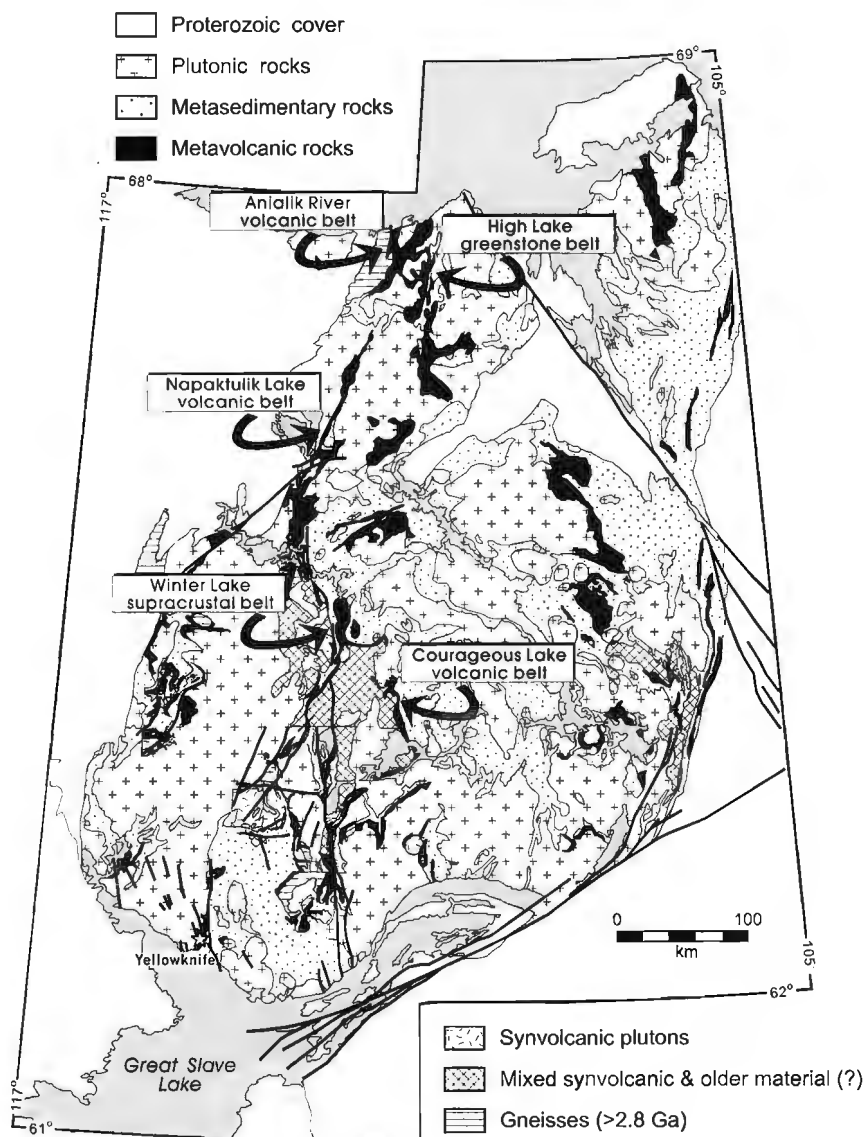


**Figure 1.**

*Regional map of the Slave Province with location of mapping projects.*

The geology of the Slave Province can be roughly subdivided into four main categories. Gneisses, volcanic rocks, and tonalites older than ca. 2.8 Ga form basement inliers throughout the western Slave Province. Included in these are the ca. 3.96 Ga Acasta gneisses (Bowring et al., 1989a, b) of the west-central Slave Province, the 3.15 Ga Augustus granite at Point Lake (Henderson et al., 1982), the ca. 2.9 Ga Sleepy Dragon Complex (Henderson et al., 1987) northeast of Yellowknife, as well as 3.3–3.1 Ga rhyolites in the Winter Lake belt and Napaktulik Lake volcanic belt (Villeneuve et al., 1993; Villeneuve and van Breemen, 1994). Other scattered occurrences of rocks older than 2.8 Ga are present throughout the western Slave Province, but, as of yet, none have been found in the east, providing a general geological basis for the east-west dichotomy of isotopic compositions.

Unconformably and structurally overlying the basement rocks are 2.71–2.66 Ga greenstone volcanic-turbidite belts that form the Yellowknife Supergroup (Henderson, 1970). This association was first described from stratigraphic studies in the Yellowknife area, but the similarity of the associations within many of the greenstone volcanic-turbidite belts has led to its application on a province-wide basis. In general, age dating has borne out the temporal similarities inferred from the lithological associations (Mortensen et al., 1988; van Breemen et al., 1992). The volcanic and associated synvolcanic intrusions consist of a bimodal suite of tholeiitic basalts and andesites, and a calc-alkaline suite of intermediate to felsic volcanic and volcanoclastic rocks. The first suite has been termed the Yellowknife type (Padgham, 1992), after its type locality, and the latter the Hackett River type (Padgham, 1992) after the prototypal succession in the central and eastern Slave Province. On the surface, ages of dated volcanic rocks from any given belt do not display a noticeable bias towards a unique age range (van Breemen et al., 1992). Such statements, however, must be tempered by the relatively small data set of ages (<40 U-Pb ages on felsic volcanics) and regional scale of mapping that is the norm for many of the greenstone belts.

Associated with, and forming the dominant part of, the supracrustal successions in the Slave Province are large accumulations of turbidite deposits principally derived from volcanic and plutonic sources. Dating of interlayered felsic volcanic units (Henderson et al., 1987; Mortensen et al., 1988; van Breemen et al., 1992; Bleeker and Villeneuve, 1995) indicates that many of the turbidite sequences are coeval with volcanism younger than 2.70 Ga. Detrital zircon geochronology on some of these packages highlight sources from within the volcanic and synvolcanic plutons of the Yellowknife Supergroup as well as detritus sourced in the prevolcanic basement units (Villeneuve et al., 1994; Villeneuve and van Breemen, 1994).

Recent mapping in the Slave Province, coupled with new U-Pb geochronology has defined a period of volcanism and sediment deposition around 2.62–2.60 Ga that postdates the volcano-turbidite successions that are typical of the Yellowknife Supergroup. Primarily recognized in the field by units of polymictic boulder conglomerate that unconformably overlie volcanic and turbidite sequences, detrital dating of these rocks indicate an age younger than 2.6 Ga

(Isachsen and Bowring, 1994; Villeneuve et al., 1994; van Breemen et al., 1994). Of special note, the central portion of the High Lake volcanic belt contains a sequence of felsic to intermediate volcanic rocks associated with chemically deposited sedimentary rocks, black slates, poorly bedded volcanic- and shale-clast conglomerates, and psammitic greywackes (Henderson et al., 1995). Ongoing dating within this part of the belt shows that this supracrustal package was deposited between 2.62 and 2.61 Ga (Henderson et al., 1995; M. Villeneuve, unpub. data, 1996).

Lastly, plutonic activity was prevalent from 2.72 to 2.58 Ga, although there appears to be evidence for a hiatus in plutonic activity between 2640 and 2625 Ma (van Breemen et al., 1992). Age dates of plutons suggests that the bulk of activity took place after 2625 Ma (van Breemen et al., 1992 and references therein), with these plutons forming the seas of granite between greenstone turbidite belts. The composition of the postvolcanic plutonic rocks progressed from metaluminous hornblende±biotite diorite and tonalite at 2.63 Ga through to K-feldspar megacrystic biotite granites at ca. 2.61 Ga through to smaller plutons of peraluminous two mica megacrystic granites at 2.59 Ga until cessation of magmatism at 2.58 Ga (Davis et al., 1994).

Some of the results of an age dating program carried out as part of the Slave NATMAP program are described below. For the most part, these samples build on the original regional data set and groundbreaking work of Mortensen et al. (1988), Isachsen et al. (1991), and van Breemen et al. (1992). The results herein represent some of the first age dates produced from the various map areas in the Slave Province and, as such, were chosen primarily to address questions of local significance such as age of deposition or constraining the timing of deformation. The significance of each age within the context of local geology is given after each sample and the contributions to the broader regional problems are dealt with in a brief discussion at the end.

## ANALYTICAL METHODS

Following the separation of heavy minerals using heavy liquids, samples were passed through a Frantz LB-1 magnetic separator to purify zircon and titanite. Zircon crystals were selected for analysis based on criteria that optimized for their clarity, lack of cloudiness and colour, and lack of fractures. All zircons were abraded prior to analysis to increase concordance by removing the outer portions of the grains where much of the Pb-loss and alteration take place (Krogh, 1982).

Following abrasion, photography, and final mineral selection, mineral fractions were analyzed according to methods summarized in Parrish et al. (1987). Data have been reduced and errors have been propagated using software written by J. C. Roddick; error propagation was done by numerical methods (Roddick, 1987; Parrish et al., 1987). Error ellipses on concordia diagrams are shown at the  $2\sigma$  (95% confidence) level of uncertainty. Final errors are indicated on Table 1. Linear regressions on discordant arrays of data use a modified York (1969) method that takes into account the

Table 1. U-Pb data.

Fraction <sup>a</sup>	Wt. <sup>b</sup> μg	U ppm	Pb <sup>c</sup> ppm	<sup>206</sup> Pb/ <sup>204</sup> Pb <sup>d</sup>	Pb <sup>e</sup> pg	<sup>208</sup> Pb/ <sup>206</sup> Pb <sup>f</sup>	Radiogenic ratios (±1 σ, %) <sup>f</sup>			<sup>207</sup> Pb/ <sup>206</sup> Pb Age (Ma) <sup>g</sup>	Discord. <sup>h</sup> %
							<sup>207</sup> Pb/ <sup>235</sup> U	<sup>206</sup> Pb/ <sup>238</sup> U	<sup>207</sup> Pb/ <sup>206</sup> Pb		
Anialik river volcanic belt											
CR-99-0558 Anialik tonalite (Z2788; 67.7954°N 110.8660°E)											
A (Z)	5	60	33	351	26	0.23	10.645±0.39	0.4556±0.34	0.16945±0.18	2552±6	6.2
I (Z)	16	60	34	1604	14	0.22	11.105±0.15	0.4681±0.14	0.17207±0.05	2578±2	4.8
J(Z)	8	42	25	1220	9	0.25	11.805±0.15	0.4901±0.15	0.17469±0.06	2603±2	1.49
R-36-91 Northern rhyolite (Z2348; 67.7616°N 110.9455°E)											
A (Z)	46	38	23	1952	29	0.19	13.139±0.20	0.5177±0.21	0.18406±0.10	2690±3	0.01
B (Z)	24	26	16	1232	4	0.16	13.069±0.15	0.5161±0.15	0.18367±0.09	2686±3	0.17
C (Z)	20	32	19	1125	3	0.16	13.120±0.17	0.5180±0.17	0.18369±0.08	2686±3	-0.2
E (Z)	10	46	27	816	17	0.16	13.132±0.18	0.5179±0.18	0.18392±0.10	2689±3	-0.07
High Lake volcanic belt											
R-30-91 High Lake granite (Z2415; 67.3884°N 110.8532°E)											
A (Z)	5	141	86	1208	20	0.24	12.140±0.19	0.5007±0.18	0.17584±0.07	2614±2	-0.013
B (Z)	16	78	46	3460	7	0.2	11.907±0.13	0.4934±0.12	0.17503±0.03	2606±1	0.98
C(Z)	6	106	60	1286	16	0.17	11.830±0.19	0.4894±0.18	0.17533±0.06	2609±2	1.92
94-HSAJ-244 High Lake rhyolite (Z3889; 67.3566°N 110.8039°E)											
A (Z)	7	41	25	657	15	0.16	13.429±0.33	0.5247±0.30	0.18562±0.10	2704±3	-0.7
B (Z)	5	63	37	1871	2	0.15	13.215±0.14	0.5155±0.14	0.18593±0.06	2707±2	1.2
D (Z)	5	116	69	2571	8	0.16	13.222±0.11	0.5165±0.10	0.18567±0.04	2704±1	0.9
E (Z)	6	62	38	1150	12	0.16	13.320±0.16	0.5205±0.14	0.18559±0.07	2704±2	0.1
93-HSA-J389 Rush rhyolite (Z3275; 67.3947°N 110.9650°E)											
A(Z)	7	53	31	2852	4	0.14	13.309±0.11	0.5195±0.10	0.18579±0.05	2705±2	0.37
C (Z)	6	59	36	2814	4	0.17	13.401±0.12	0.5232±0.11	0.18577±0.04	2705 ±1	-0.34
D (Z)	4	59	35	943	9	0.15	13.284±0.18	0.5184±0.18	0.18585±0.09	2706 ±3	0.61
R-40-91 James River rhyolite (Z2414; 67.1714°N 110.9654°E)											
A (Z)	10	138	83	2308	2	0.15	13.234±0.11	0.5196±0.10	0.18471±0.04	2696±1	-0.09
B (Z)	13	71	42	2080	14	0.15	13.097±0.15	0.5143±0.14	0.18471±0.04	2696±1	0.94
C (Z)	11	84	49	2429	12	0.17	12.309±0.14	0.4944±0.13	0.18056±0.04	2658±1	3.12
D (Z)	9	238	145	1863	36	0.18	13.165±0.31	0.5177±0.30	0.18444±0.04	2693±1	0.18
Canoe Lake rhyolite (Z1183; 67.1425°N 111.6000°E)											
3a (Z)	24	121	71	4557	21	0.15	13.114±0.10	0.5154±0.09	0.18454±0.03	2694±1	0.66
3b (Z)	20	155	92	5507	18	0.17	12.889±0.10	0.5084±0.09	0.18385±0.03	2688±1	1.72
3c (Z)	27	157	90	4315	31	0.17	12.445±0.10	0.4891±0.09	0.18455±0.03	2694±1	5.73
A (Z)	5	98	59	1144	13	0.16	13.127±0.21	0.5154±0.21	0.18473±0.08	2696±3	0.74
B (Z)	5	145	87	3339	0	0.16	13.175±0.11	0.5179±0.10	0.18451±0.04	2694±1	0.17
92-HSA-727 Hood River rhyolite (Z2765; 66.8868°N 110.2843°E)											
A (Z)	32	17	10	1616	1	0.08	12.740±0.13	0.5100±0.13	0.18119±0.05	2664±2	0.34
B (Z)	13	30	17	1485	6	0.11	12.809±0.16	0.5110±0.15	0.18181±0.06	2669±2	0.39
D (Z)	6	99	56	3249	6	0.09	12.854±0.12	0.5124±0.10	0.18194±0.04	2671±1	0.17
E (Z)	11	61	35	1427	15	0.1	12.870±0.12	0.5135±0.11	0.18179±0.05	2669±2	-0.1
92-HSA-728 Ulu granite (Z3060; 66.8956°N 110.9124°E)											
C (Z)	2	116	65	451	13	0.19	11.315±0.38	0.4741±0.36	0.17310±0.14	2588±5	4.02
E (Z)	2	125	61	739	3	0.15	10.278±0.24	0.4300±0.23	0.17333±0.12	2590±4	13.04
F (Z)	2	105	60	357	14	0.19	11.693±0.35	0.4894±0.35	0.17328±0.17	2590±6	1.01
R-33-91 Foliated quartz diorite (Z2635; 67.6270°N 110.8376°E)											
A (Z)	11	154	92	4488	7	0.25	11.689±0.12	0.4865±0.11	0.17427±0.03	2599±1	2.03
B (Z)	5	142	84	2799	7	0.25	11.646±0.18	0.4823±0.17	0.17511±0.04	2607±1	3.23
C (Z)	11	138	81	3154	15	0.24	11.523±0.13	0.4796±0.13	0.17425±0.04	2599±1	3.41
E (Z)	6	114	70	796	27	0.25	11.980±0.17	0.4968±0.14	0.17488±0.08	2605±3	0.23
D (Z)	5	289	179	2694	16	0.31	11.677±0.11	0.4853±0.10	0.17449±0.04	2601±1	2.36
R-32-91 Two mica granite (Z2634; 67.6279°N 110.8305°E)											
A (Z)	4	152	79	1283	12	0.22	10.302±0.22	0.4363±0.21	0.17128±0.07	2570±2	10.95
F (Z)	1	321	149	551	15	0.17	9.570±0.36	0.4023±0.36	0.17255±0.15	2583±5	18.36
C-tip (Z)	6	199	56	2266	9	0.07	4.574±0.13	0.2739±0.12	0.12113±0.06	1973±2	23.5
D (Z)	1	124	55	285	6	0.16	9.058±0.93	0.3897±0.85	0.16857±0.41	2544±14	19.44
E (Z)	1	654	254	717	26	0.15	7.984±0.22	0.3432±0.19	0.16875±0.11	2545±4	29.12



Table 1 (cont.)

Fraction <sup>a</sup>	Wt. <sup>b</sup> μg	U ppm	Pb <sup>c</sup> ppm	<sup>206</sup> Pb/ <sup>204</sup> Pb <sup>d</sup>	Pb <sup>e</sup> pg	<sup>208</sup> Pb/ <sup>206</sup> Pb <sup>f</sup>	Radiogenic ratios (±1 σ, %) <sup>f</sup>			<sup>207</sup> Pb/ <sup>206</sup> Pb Age (Ma) <sup>g</sup>	Discord. <sup>h</sup> %
							<sup>207</sup> Pb/ <sup>235</sup> U	<sup>206</sup> Pb/ <sup>238</sup> U	<sup>207</sup> Pb/ <sup>206</sup> Pb		
Napaktulik Lake volcanic belt											
91-VJ-4400 Mirror Lake granite (Z2486; 66.5851°N 112.3598°E)											
A (Z)	1	1678	771	1686	25	0.140	9.540±0.13	0.4066±0.11	0.17016±0.05	2559±2	16.57
B (Z)	4	1321	645	204	792	0.190	9.402±0.51	0.4181±0.15	0.16308±0.43	2488±14	11.22
C (Z)	7	1191	432	2557	65	0.070	7.246±0.11	0.3442±0.10	0.15268±0.05	2376±2	22.77
E (Z)	5	652	276	564	156	0.100	8.676±0.22	0.3923±0.10	0.16038±0.17	2460±6	15.55
D (Z)	3	1311	632	1104	100	0.090	10.411±0.20	0.4459±0.18	0.16936±0.07	2551±2	8.17
F (Z)	3	3278	1487	408	671	0.060	9.425±0.26	0.4339±0.11	0.15754±0.21	2430±7	5.20
H (Z)	1	1311	522	840	39	0.110	8.074±0.15	0.3641±0.11	0.16081±0.08	2464±3	21.79
J (Z)	3	2893	1376	661	334	0.080	10.111±0.19	0.4460±0.12	0.16441±0.12	2502±4	5.92
K (Z)	2	569	260	162	211	0.220	8.747±0.67	0.3831±0.17	0.16558±0.56	2514±19	19.65
91-VJ-4401 Hood River granite (Z2487; 66.6095°N 112.2912°E)											
A (Z)	5	273	175	804	57	0.310	12.343±0.15	0.5000±0.11	0.17905±0.08	2644±3	1.40
B (Z)	1	242	166	524	10	0.480	11.468±0.29	0.4840±0.26	0.17186±0.17	2576±6	1.47
C (Z)	1	215	138	719	4	0.380	11.442±0.22	0.4812±0.20	0.17247±0.13	2582±4	2.32
D (Z)	4	129	85	957	12	0.400	11.508±0.16	0.4841±0.15	0.17240±0.07	2581±2	1.68
E (Z)	5	51	36	180	47	0.500	11.747±0.50	0.4936±0.43	0.17263±0.33	2583±11	-0.13
F (Z)	4	58	37	266	26	0.460	10.821±0.41	0.4562±0.28	0.17203±0.30	2578±10	7.20
91-VJ-4403 Eastern granite (Z2488; 66.6834°N 112.0584°E)											
A (Z)	6	117	59	1260	16	0.110	10.932±0.14	0.4593±0.13	0.17262±0.06	2583±2	6.82
C (Z)	2	135	51	591	12	0.080	7.734±0.22	0.3537±0.20	0.15857±0.15	2441±5	23.14
E (Z)	3	92	51	413	24	0.160	11.696±0.44	0.4880±0.38	0.17384±0.26	2595±9	1.54
F-FRAG (Z)	62	63	36	12502	10	0.180	11.786±0.10	0.4915±0.09	0.17390±0.04	2596±1	0.85
G-FRAG (Z)	47	60	35	6151	11	0.180	11.875±0.10	0.4947±0.09	0.17409±0.03	2597±1	0.29
TBM-122 Football granite (Z3059; 66.6587°N 112.2553°E)											
A (Z)	9	187	105	5581	9	0.150	12.001±0.12	0.4949±0.11	0.17587±0.03	2614±1	1.03
B (Z)	2	117	71	539	12	0.260	11.942±0.54	0.4933±0.52	0.17560±0.21	2612±7	1.26
E (Z)	5	90	35	484	20	0.220	7.554±0.22	0.3291±0.18	0.16646±0.13	2522±5	31.28
F (Z)	6	141	54	1187	14	0.250	7.013±0.14	0.3133±0.13	0.16233±0.07	2480±2	33.23
TITAN-X(T)	101	232	145	2279	316	0.300	11.963±0.13	0.4942±0.12	0.17556±0.04	2611±1	1.04
TITAN-Y (T)	104	258	170	3952	212	0.360	12.109±0.10	0.4993±0.09	0.17591±0.03	2615±1	0.19
Winter Lake volcanic belt											
HLB-92-B0021A Eastern gneiss leucosome (Z3415; 64.2539°N 112.6404°E)											
A (Z)	2	445	215	792	40	0.060	11.341±0.17	0.4513±0.11	0.18226±0.12	2674±4	12.19
B (Z)	2	751	402	1473	28	0.050	12.700±0.13	0.5042±0.12	0.18270±0.07	2678±2	2.08
C (Z)	1	186	104	1819	4	0.120	12.463±0.13	0.4982±0.13	0.18144±0.05	2666±2	2.73
D (Z)	1	223	114	407	17	0.070	11.803±0.27	0.4748±0.26	0.18031±0.14	2656±5	6.87
E (Z)	1	146	83	633	10	0.110	12.850±0.28	0.5145±0.14	0.18114±0.20	2663±7	-0.57
F (Z)	2	132	70	1899	3	0.120	11.874±0.13	0.4754±0.13	0.18117±0.05	2664±2	7.09
VN-93-03 Providence granite (Z3375; 64.7667°N 112.2333°E)											
B (Z)	2	104	63	1477	5	0.220	12.529±0.16	0.5071±0.14	0.17921±0.09	2646±3	0.07
D (Z)	5	91	56	1258	6	0.210	12.746±0.16	0.5100±0.16	0.18127±0.07	2665±2	0.37
C (Z)	4	93	58	2390	1	0.240	12.508±0.13	0.5061±0.13	0.17925±0.06	2646±2	0.27
Courageous Lake volcanic belt											
Deb rhyolite (Z3416; 64.0011°N 111.2317°E)											
A (Z)	1	212	123	844	2	0.130	13.151±0.23	0.5158±0.22	0.18492±0.14	2698±4	0.73
C (Z)	2	217	127	968	14	0.130	13.243±0.15	0.5190±0.15	0.18504±0.08	2699±3	0.16
E (Z)	4	157	92	5767	4	0.130	13.251±0.11	0.5186±0.10	0.18533±0.03	2701±1	0.37
F (Z)	2	99	57	1798	1	0.110	13.235±0.13	0.5176±0.13	0.18544±0.07	2702±2	0.59

<sup>a</sup>All zircon fractions are abraded; (Z)=Zircon, (T)=Titanite<sup>b</sup>Error on weight = ±0.001 mg<sup>c</sup>Radiogenic Pb<sup>d</sup>Measured ratio corrected for spike and Pb fractionation of 0.09±0.03‰AMU<sup>e</sup>Total common Pb on analysis corrected for fractionation and spike, of blank model Pb composition<sup>f</sup>Corrected for blank and spike Pb and U and common Pb (Stacey-Kramers model Pb composition equivalent to the <sup>207</sup>Pb/<sup>206</sup>Pb age)<sup>g</sup>Age error is ±2 se in Ma<sup>h</sup>Discordance along a discordia to origin.

scatter of the points about the line (see a discussion in Parrish et al., 1987). Fraction letters shown on concordia diagrams are keyed to the fraction letters in Table 1.

## ANIALIK RIVER VOLCANIC BELT

The Anialik River volcanic belt, together with the adjacent Kangguyak gneiss belt (McEachern, 1993) represents the northernmost project in the western Slave Province (Fig. 1). The doubly-plunging antiformal structure in the northern part of the belt is cored by the synvolcanic Anialik River igneous complex (Fig. 2), a composite pluton of tonalite-trondjemite-granodiorite suite rocks, with phases dated at  $2703 \pm 1$  Ma,  $2693 \pm 2$  Ma and  $2683 \pm 3$  Ma (Abraham et al., 1994). This complex has an intrusive contact with the volcanic belt at its southern end and is in tectonic contact on its eastern and western margins (Relf, 1995). Part of the western contact is cut by the  $2602 \pm 2$  Ma (Abrahams et al., 1994) Chin Lake stock, an undeformed, leucocratic, two-mica quartz monzonite.

The volcanic rocks enveloping the Anialik River volcanic belt have been subdivided into three general units by Relf (1995) that comprise: 1) massive and pillowed basaltic to andesitic flows, breccias, and minor volcanoclastic sediments forming a mafic unit; 2) dacites, rhyodacites, and fragmental volcanic rocks forming an intermediate to felsic unit; and 3) rhyolite flows and tuffs forming a felsic unit. Apart from the sample of dacite reported herein, two other felsic volcanic rocks from the felsic unit on the west side of the belt were dated by Abraham et al. (1994). An age of  $2677 \pm 3$  Ma was obtained on a felsic tuff and a similar age of  $2678 \pm 2$  Ma was obtained on a quartz-feldspar porphyry, displaying a temporal correlation with other volcanic rocks of the Yellowknife Supergroup.

Sedimentary rocks make up only a minor component of the belt. Synvolcanic sedimentation takes the form of thin slaty lenses and brown-weathering carbonates interbedded with intermediate to felsic volcanic rocks (Relf, 1995) and discontinuous silicate, oxide, and carbonate facies iron-formation. The most distinctive unit in the Anialik River volcanic belt consists of lenses of clast-supported granite and volcanic boulder conglomerate, with rounded boulders embedded in a fine grained, chloritic matrix displaying a pronounced throughgoing foliation. Tirrul and Bell (1980) proposed that the unit rests unconformably on the underlying volcanic rocks. A syenite boulder from the conglomerate yielded a poorly defined age of  $2590 \pm 10$  Ma (Villeneuve and van Breemen, 1994), corroborating this interpretation. Further mapping in the belt yielded several other lens-shaped examples of clast-rich polymictic orthoconglomerate, generally occurring adjacent to faults. The youngest detrital zircon grain analyzed in a subsequent sample, has a concordant age of  $2600 \pm 3$  Ma (Villeneuve and van Breemen, 1994), suggesting that these conglomerates were deposited late in the tectonic history of the Slave Province.

In fault contact along the western side of the Anialik River volcanic belt are the amphibolite-facies ortho- and paragneisses of the Kangguyak gneiss belt (McEachern, 1993; Relf, 1995).

Tonalite gneiss and granitic gneiss make up the bulk of the exposure within the belt and have produced ages ranging from 3.3 Ga to 2.95 Ga (Isachsen and Bowring, 1994; M. Villeneuve, unpub. data, 1995), suggesting that the gneisses form part of a basement complex in the northwestern Slave Province. Isolated occurrences of paragneiss consists of migmatitic biotite schist, quartzite, and metamorphosed conglomerate containing cobbles of granite, quartzite, and amphibolite in a multiply deformed coarse hornblende-rich matrix (Relf, 1995). Detrital zircon geochronology indicates a maximum depositional age of  $2880 \pm 2$  Ma for the conglomerate (Villeneuve and van Breemen, 1994) and a poorly defined maximum age (due to discordance of analyses) of 3.15 Ga for the quartzite (Relf et al., 1994a). There is an abundance of 3.3-3.1 Ga zircons in both units (Villeneuve and van Breemen, 1994). Although contact relationships were not observed between the paragneisses and orthogneisses, the presence of detrital zircons with ages correlative to the orthogneiss units suggests that the orthogneisses are basement to the paragneisses.

The Kangguyak gneisses are separated from the Anialik River volcanic belt by the Tohokatak fault (Relf et al., 1994a). Early fault movement, interpreted to be Archean (Relf et al., 1994a; Relf, 1995), consists of complex, ductile dip-slip and strike-slip motion, possibly consisting of multiple episodes of movement between 2.64 Ga and 2.60 Ga (Relf, 1995). Overprinting brittle-ductile greenschist grade fault fabrics suggests later reactivation of the fault during the Proterozoic, coincident with orogeny in nearby Wopmay Orogen.

The Kangguyak gneiss belt and Anialik River volcanic belt appear to have separate structural histories until ca. 2.64 Ga (Relf et al., 1994a; Relf, 1995) whereupon the main cleavage forming event in the Anialik River volcanic belt ( $D_2$  in Anialik River volcanic belt,  $D_3$  in Kangguyak gneiss belt) can be correlated with movement along the Tohokatak fault (Relf, 1995). The overall geometry of the Anialik River volcanic belt is controlled by the development of north-northeast-trending, upright folds that form  $D_3$  in the volcanic belt. Timing of the  $D_3$  deformation is constrained by intrusion and subsequent deformation of a carbonatite intrusion complex (Relf et al., 1994b; Relf, 1995), emplaced around 2600 Ma. Timing of peak metamorphic conditions in the Kangguyak gneiss belt and western Anialik River volcanic belt is determined from titanite geochronology on igneous plutons (Abraham et al., 1994; Villeneuve and van Breemen, 1994; Relf et al., 1994a) that give ages around 2.65-2.64 Ga, in agreement with a hornblende  $^{40}\text{Ar}/^{39}\text{Ar}$  age of 2.64 Ga from the Kangguyak gneiss belt (H. Sandeman, unpub. data in Relf, 1995). Peak metamorphic conditions in the eastern Anialik River volcanic belt are synchronous with intrusion of ca. 2.61 Ga granites (Relf, 1995), suggesting a diachronous event across the belt.

For this study, two samples have been dated from the Anialik River volcanic belt that augment the previous geochronological work of Abraham et al. (1994) and help constrain timing of volcanism and deformation.

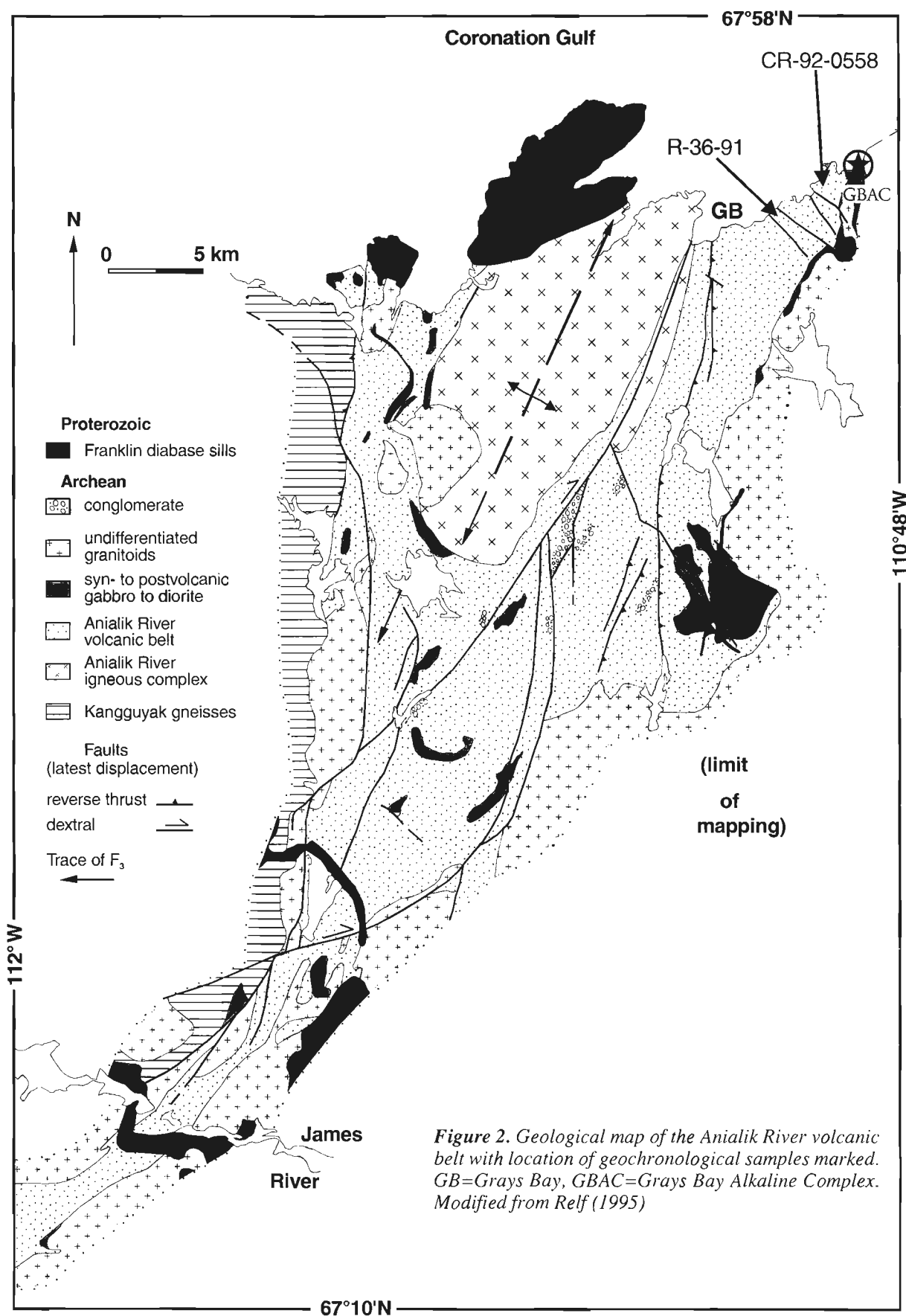


*Figure 2. Geological map of the Anialik River volcanic belt with location of geochronological samples marked. GB=Grays Bay, GBAC=Grays Bay Alkaline Complex. Modified from Relf (1995)*

### Anialik tonalite

A sample of equigranular, medium grained biotite tonalite (CR-92-0558) was collected from a dyke located about 500 m west of Grays Bay (Fig. 2). The dyke, one of a series that are up to 30 cm wide, both cuts the foliation in the surrounding mafic volcanic rocks and is folded about it (Relf, 1995) in isoclinal folds with north-northeast fold axes, suggesting that it was intruded post- $S_2$  ( $D_2$ ) and deformed by the north-northeast-trending, fold-forming event ( $D_3$  of Relf, 1995).

Zircons from the sample are subequant, multifaceted, euhedral clear crystals with relatively low U content. Although of good optical quality, analysis of one to three grain fractions indicates that Pb loss plays a role in the U-Pb systematics of the zircons, with results being 2-11% discordant (Fig. 3a). Fractions A through H have larger than normal error ellipses due to the low U content coupled with elevated lab blank levels (up to 30 pg) during the period of the analyses. Additional analysis of two other multigrain fractions (I, J), gave results that are both lower in error and more concordant. Regression of all six analyses yield an upper intercept age of  $2613 \pm 6$  Ma (MSWD=2, lower intercept= $1041 \pm 90$  Ma). The age of the Anialik tonalite is interpreted as the time of intrusion, and represents the minimum age for the  $D_2$  cleavage forming event.

Because the tonalite dyke emplacement is interpreted to be syn- $D_3$  and a nearby 2600 Ma carbonatite intrusion (Grays Bay Alkaline Complex, Fig. 2) is interpreted as deformed by  $D_3$  (Relf, 1995) it suggests that the formation of the open folds that define the overall shape of the belt may have occurred, either sporadically or continually, over a 10 Ma period. This 2600 Ma age is slightly at odds with the  $2602 \pm 2$  Ma age of the Chin Lake stock, interpreted to be a post-tectonic pluton (Abraham et al., 1994). The fact that the post-2600 Ma String Lake conglomerate carries a strong foliation in the matrix, suggests that  $D_3$  deformation continued after emplacement of the Chin Lake stock. The combination of ages suggests that  $D_3$  may also represent strain partitioning on a belt-wide scale, such that the last deformational fabrics were not recorded during emplacement of the Chin Lake stock.

### Northern rhyolite

A foliated biotite dacite porphyry was collected from the northeast side of the Anialik River volcanic belt, just inshore from Grays Bay. This sample is a plagioclase-quartz eye porphyry located in the centre of a complex of rhyolite to dacite dykes marked by self-intrusion and a carbonate-matrix rhyolite breccia around the margins, suggesting that the sample is part of a high level intrusion within a rhyolite dome complex. Biotite (5%), euhedral plagioclase phenocrysts (10%), and quartz eyes (10%) are distributed within a fine grained matrix displaying minor carbonate alteration.

Zircons from the sample are clear, euhedral, low-U prisms, with a typical magmatic morphology. Uranium content is around 25-40 ppm, with all fractions giving concordant, reproducible results (Fig. 3b). The weighted average of the  $^{207}\text{Pb}/^{206}\text{Pb}$  ages is  $2687 \pm 2$  Ma.

The  $2687 \pm 2$  Ma age on the northern rhyolite from the east side is 10 Ma older than the  $2678 \pm 2$  Ma and  $2677 \pm 3$  Ma determined from felsic volcanic rocks on the west side of the belt (Abraham et al., 1994). Although the small number of dated volcanics in the belt prevents working out detailed stratigraphy, it is clear that volcanism spanned at least 10 Ma and correlates with the age of other Yellowknife Supergroup volcanic rocks throughout the Slave Province.

### HIGH LAKE GREENSTONE BELT

The High Lake greenstone belt abuts the eastern side of the Anialik River volcanic belt at Grays Bay (Fig. 4) and then diverges from the Anialik River volcanic belt by taking a southerly trend as opposed to the southwesterly trend of the Anialik River volcanic belt. Separating the two belts is a composite pluton that contains sporadic, small remnants of greenstone belts (Jackson, 1989). The High Lake greenstone belt continues southward, is transected by the James River, and terminates south of the Hood River.

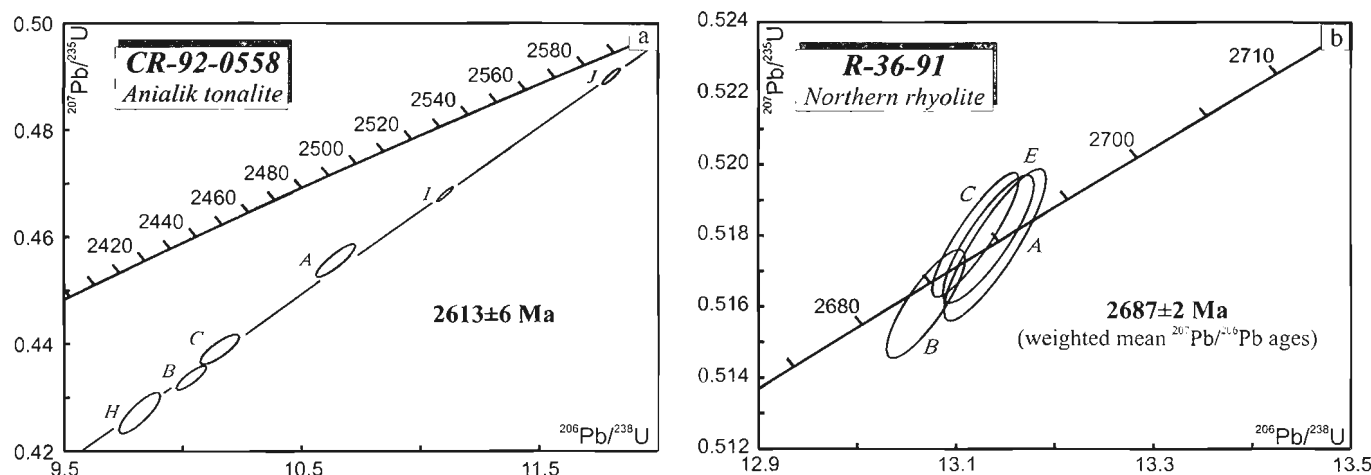


**Figure 3.** Concordia plots for samples from the Anialik River volcanic belt (ARVB). Error ellipses are at the  $2\sigma$  level of uncertainty.

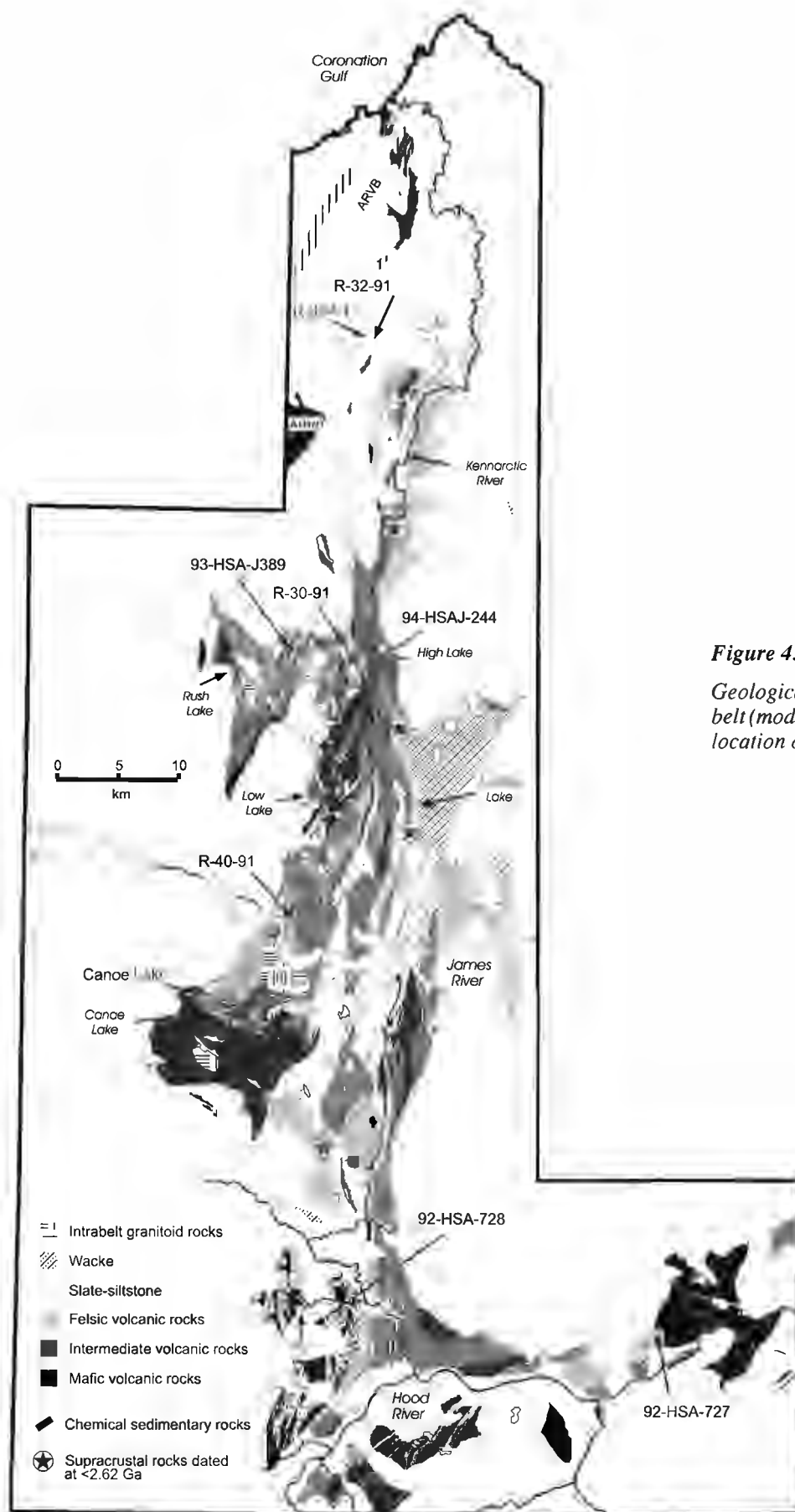


**Figure 4.**

*Geological sketch map of High Lake greenstone belt (modified from Henderson et al., 1994) with location of geochronological samples marked.*

The High Lake greenstone belt has been divided into three broad north-trending parts by Henderson et al. (1995). The western volcanic domain forms the western margin of the belt from Canoe Lake northwards (Fig. 4). It comprises intermediate to felsic volcanic rocks and nonbedded volcanoclastic rocks, as well as subordinate occurrences of mafic volcanic rocks in the area between Rush Lake and High Lake (Henderson et al., 1993b, 1995).

The eastern boundary of the western volcanic domain coincides with the Kennarctic River. East of the boundary, the central mixed domain is a band of mixed banded iron-formation and marbles that can be traced from Canoe Lake to High Lake (Henderson et al., 1995). The central mixed domain is several kilometres wide north of High Lake, pinches to a few hundred metres width at High Lake, and gradually widens to around 10 km south of the James River (Henderson et al., 1995). Mafic, intermediate and felsic volcanics are capped by chemical sedimentary rocks (marbles, including stromatolite-bearing carbonates (Henderson, 1975), chert iron-formation), that are, in turn, overlain by graphitic shales (Henderson et al., 1993a, 1995). Black slate-grey siltstone turbidite couplets and poorly-bedded conglomerate containing volcanic and shale clasts are interbedded with and overlie felsic volcanic and volcanoclastic rocks (Henderson et al., 1993a, 1995).

Uranium-lead zircon dating of three felsic volcanic rocks and detrital zircon dating of a grey siltstone clearly show that the central mixed domain is much younger than other volcanic belts dated in the Slave Province. Three felsic volcanic rocks, collected from widely spaced localities, give overlapping ages of  $2616 \pm 3$  Ma (Henderson et al., 1995) and  $2616 \pm 1$  Ma and  $2612 \pm 3$  Ma (M. Villeneuve, unpub. data, 1996). Detrital zircons from a grey siltstone layer collected from within the domain contains five concordant zircon analyses with ages of 2618 to 2608 Ma and two concordant analyses at 2667 and 2658 Ma (Villeneuve, unpub. data, 1996), suggesting that some parts of the central mixed domain are younger than 2608 Ma.

Although other occurrences of young supracrustal rocks have been previously noted in the Slave Province, (Isachsen and Bowring, 1994; Villeneuve et al., 1994; Villeneuve and van Breemen, 1994), these have generally been restricted to cobble and boulder conglomerates of limited extent, unconformably overlying 2.71–2.67 Ga Yellowknife Supergroup rocks. The uniqueness of the central mixed domain lies in the presence of a supracrustal package containing extrusive rocks interbedded with distinct sedimentary facies, coupled with the broad areal extent of the domain. Further geochronological work is underway in an attempt to distinguish the tectonic and depositional environments represented by this domain.

The third domain, the eastern volcanic domain (Henderson et al., 1995) is defined by a package of mafic and intermediate volcanic rocks similar to the western volcanic domain (Henderson et al., 1995). It starts as a narrow 2 km wide zone at the James River and stretches to the Hood River where it forms most of the width of the High Lake greenstone belt (Henderson et al., 1995), with a western boundary consisting of a high-strain zone (Fig. 4). In addition, a package of turbiditic sediments east of Snofield Lake, which is

lithologically similar to other Yellowknife Supergroup assemblages, may also be part of this domain, as it contains detrital zircons with ages from ca. 2.73 Ga to 2.67 Ga. These ages are indicative of, but not exclusive to, a correlation with turbidite packages common throughout the Slave Province.

Dates presented here focus on the western and eastern volcanic domains and associated plutons. Data for the central domain will be presented elsewhere, pending the outcome of ongoing studies focused in that area.

### *High Lake diorite and rhyolite*

Along the western shore of High Lake (Fig. 4) a synvolcanic, massive sulphide Cu-Zn-Pb±Au±Ag deposit is located within highly gossanized and sheared intermediate to felsic volcanic rocks (Jackson, 1989; Henderson et al., 1994). Intruding the mineralized volcanic rocks is a small pluton of weakly foliated hornblende-biotite diorite (R-30-91), interpreted to be an apophysis of a larger diorite pluton (Henderson et al., 1993a) that intruded the greenstone belt to the west. Zircons are sharply terminated, multifaceted and clear with little to no internal growth zoning. One concordant single grain fraction (A) and two discordant two-grain fractions (B and C) result in a discordia (Fig. 5a) with an extremely poor fit (MSWD=19), possibly due to minor inheritance in fraction C. Regressing using a Davis (1982) technique that places greater emphasis on the concordant analysis, results in the interpreted crystallization age of  $2613 \pm 5$  Ma (lower intercept =  $796 \pm 1250$  Ma, probability of fit = 41%).

A sample of hydrothermally altered rhyolite (94-HSAJ-244) was collected from the north end of High Lake. Although the sampled unit is unmineralized, it is correlated with the mineralized, sheared, and hydrothermally altered volcanic and volcanoclastic rocks that host the massive sulphide deposit. Zircons from this unit are  $<100 \mu\text{m}$ , clear, colourless, prismatic, subhedral to euhedral grains, often with ragged edges. Uranium content is low and analysis of four multigrain fractions resulted in three analyses less than 1% discordant (Fig. 5b) and one reversely discordant fraction (A, -0.7% discordant). Although the outer surface of the zircons is roughened by the intense alteration of the rhyolite by postdepositional fluids, the U-Pb systematics results in a crystallization age of  $2705 \pm 1$  Ma (lower intercept =  $-420 \pm 800$  Ma, MSWD=1.8).

The age of the two units indicates that the diorite body intruding into the package of felsic volcanics hosting the High Lake deposit is not synvolcanic in age. It has been suggested that the mineralization at High Lake is related to synvolcanic, mainly hydrothermally-driven processes (Henderson et al., 1995), marked by the occurrence of "dalmatianite". A review of "dalmatianite" occurrences, as mapped by Henderson et al. (1993a) shows that this alteration texture occurs in intermediate volcanic rocks spatially related to diorite plutons (e.g. eastern margin of Rush Lake sequence, High Lake, and west of the High Lake diorite) and therefore likely represents a contact metamorphic effect in hydrothermally altered intermediate volcanic rocks. As such,  $2613 \pm 5$  Ma represents the minimum age for the alteration that gave rise to the massive sulphide mineralization at High Lake.

### ***Rush rhyolite***

The Rush Lake sequence is a sequence of intermediate to felsic volcanic rocks that have a general northwest strike and form a distinct angular discordance with the northerly striking main part of the western volcanic domain (e.g. the area west of High Lake). The Rush Lake volcanic units are then cut by northerly striking, deformed mafic dykes interpreted as possible feeders to the unconformably overlying pillowed volcanics (Henderson et al., 1994).

The Rush rhyolite (93-HSAJ-389) is a quartz-phyric felsic volcanic rock, with large quartz eyes and lath-shaped plagioclase phenocrysts up to 4 mm long, a classic example of Slave Province felsic volcanic rocks. Embayed quartz phenocrysts are generally monocrystalline and feldspars are fresh. Clots of fine grained, altered biotite are scattered throughout. The groundmass consists of very fine grained, evenly distributed biotite, feldspar, and quartz, with a foliation defined by alignment of the fine biotite flakes. Zircons range from elongate ( $l:w > 4:1$ ) to stubby ( $l:w = 1:1$ ), prismatic, clear crystals with sharp terminations. Minor fluid inclusions can be seen in some crystals. Three multigrain fractions are all between 0.6% and -0.3% discordant, resulting in a well constrained age of  $2705 \pm 1$  Ma (Fig. 5c) for the unit.

This age is identical to the age of the rhyolite at High Lake. Because the unconformably overlying mafic pillowed volcanics are intruded by the  $2613 \pm 5$  Ma High Lake diorite, they are constrained to between 2705 Ma and 2613 Ma. Two possible scenarios present themselves to explain the angular unconformity between the older felsic volcanic rocks and the overlying mafic volcanic rocks and their intrusive equivalents: 1) the Rush Lake sequence may have been formed elsewhere and amalgamated to the main part of the western volcanic domain to be intruded and overlain by the mafic rocks or 2) it may have formed as the basal part of the main western volcanic domain sequence and rotated (deformed?) relative to the rest of the domain, prior to extrusion of the mafic volcanic rocks.

### ***James River rhyolite and Canoe Lake rhyolite***

The James River rhyolite and Canoe Lake rhyolite are located in the western volcanic domain (Henderson et al., 1995), almost due south of High Lake. The James River rhyolite (R-40-91), collected from a crystal-rich portion of a red-weathering, massive quartz-feldspar porphyritic rhyodacite, immediately north of the James River, yielded a small number of clear, stubby, euhedral zircons with sharp terminations and edges. Four fractions of three to four crystals each (A, B, D, F) were analyzed, with fraction A giving a concordant analysis at  $2696 \pm 3$  Ma (Fig. 5d) and the other fractions forming a discordia with an upper intercept age of  $2695 \pm 2$  Ma (MSWD=4, lower intercept= $-11 \pm 200$  Ma). Fraction C, consisting of a single large, dark brown, subhedral equant crystal is morphologically anomalous when compared to the remainder of the zircon population. Analysis of this crystal resulted in a 3% discordant fraction that plots to the left of the discordia line formed by the other fractions. The most likely scenario, due to the clearly distinct morphology, would

suggest that this crystal was a xenocryst with a different Pb-loss trajectory than the other crystals, resulting in an apparent younger  $^{207}\text{Pb}/^{206}\text{Pb}$  age. Alternatively, it is possible that fractions B, D, and F contain inherited components and that the "true" discordia runs through fractions C and A. In either case, fraction A provides a general pinning of the age to ca. 2695 Ma.

Preliminary data for the Canoe Lake rhyolite was reported in Mortensen et al. (1988). Three analyzed fractions were not collinear (3a, 3b, 3c), but suggested an age of between 2.70 and 2.69 Ga. Zircon separates from the original sample were used to form two additional fractions (A and B), both of which proved to be less than 1% discordant (Fig. 5e). Ignoring the most discordant fraction (3c), a regression results in a crystallization age of  $2696 \pm 4/-3$  Ma (MSWD=6, lower intercept= $771 \pm 355$  Ma). The Canoe Lake rhyolite, as described by Mortensen et al. (1988) is a massive, unfoliated, quartz-feldspar porphyry, with partially recrystallized quartz phenocrysts.

Both these samples represent rhyolites from the southern portion of the western volcanic domain (Henderson et al., 1995). Although slightly younger than rhyolites in the southern portions of the western volcanic domain, these data are still consistent with age correlations with the Yellowknife Supergroup. The ca. 10 Ma difference in ages between the more northern and southern parts of the domain may point towards formation in separate magmatic centres or differing stratigraphic exposures.

### ***Hood River rhyolite***

The Hood River rhyolite (92-HSA-727) represents the only sample collected from the eastern volcanic domain. The sample is a biotite-quartz-feldspar porphyry crowded with altered biotite phenocrysts, sericitized plagioclase phenocrysts, and recrystallized quartz-eyes in a fine grained matrix of quartz and feldspar. Zircons from the sample are clear, crack-free, colourless euhedral crystals with slightly resorbed edges and terminations. Fluid inclusions near the surface of the grains are common, but are rare in the interior. Although most crystals are less than 150  $\mu\text{m}$  in length, one extremely large (ca. 600  $\mu\text{m}$  diameter), broken crystal was included in the zircons chosen for air abrasion and analysis. During abrasion this crystal fragment broke into two parts, of which fraction A ultimately was analyzed. The three other fractions all have, within error, the same  $^{207}\text{Pb}/^{206}\text{Pb}$  age of 2670 Ma and are all less than 0.4% discordant (Fig. 5f). Fraction A is 0.3% discordant but has a slightly younger  $^{207}\text{Pb}/^{206}\text{Pb}$  age of 2664 Ma. This discrepancy is interpreted to be the result of insufficient removal of zircon material along the zone of weakness where the large crystal broke apart, resulting in parts of the crystal that experienced minor Pb loss being retained in the analysis, possibly coupled with insufficient abrasion due to the large size of the crystal. As such, the crystallization age is interpreted to be represented by the weighted average of the  $^{207}\text{Pb}/^{206}\text{Pb}$  ages of the other fractions and equal to  $2670 \pm 1$  Ma.

This age is the youngest of the five volcanic rocks analyzed in the study area. As such, it may represent a young part of western volcanic domain's homoclinal sequence or it could represent a tectonically separate package of volcanic rocks in the eastern volcanic domain that bears no genetic relation to those in the western volcanic domain.

### Ulu granite

The Ulu gold property of BHP Minerals consists of gold-bearing dilatant zones within massive basalt in the western volcanic domain. Henderson et al. (1995) suggested that gold deposition was synchronous with the development of the northeast-striking,  $S_3$  cleavage in the country rocks. This

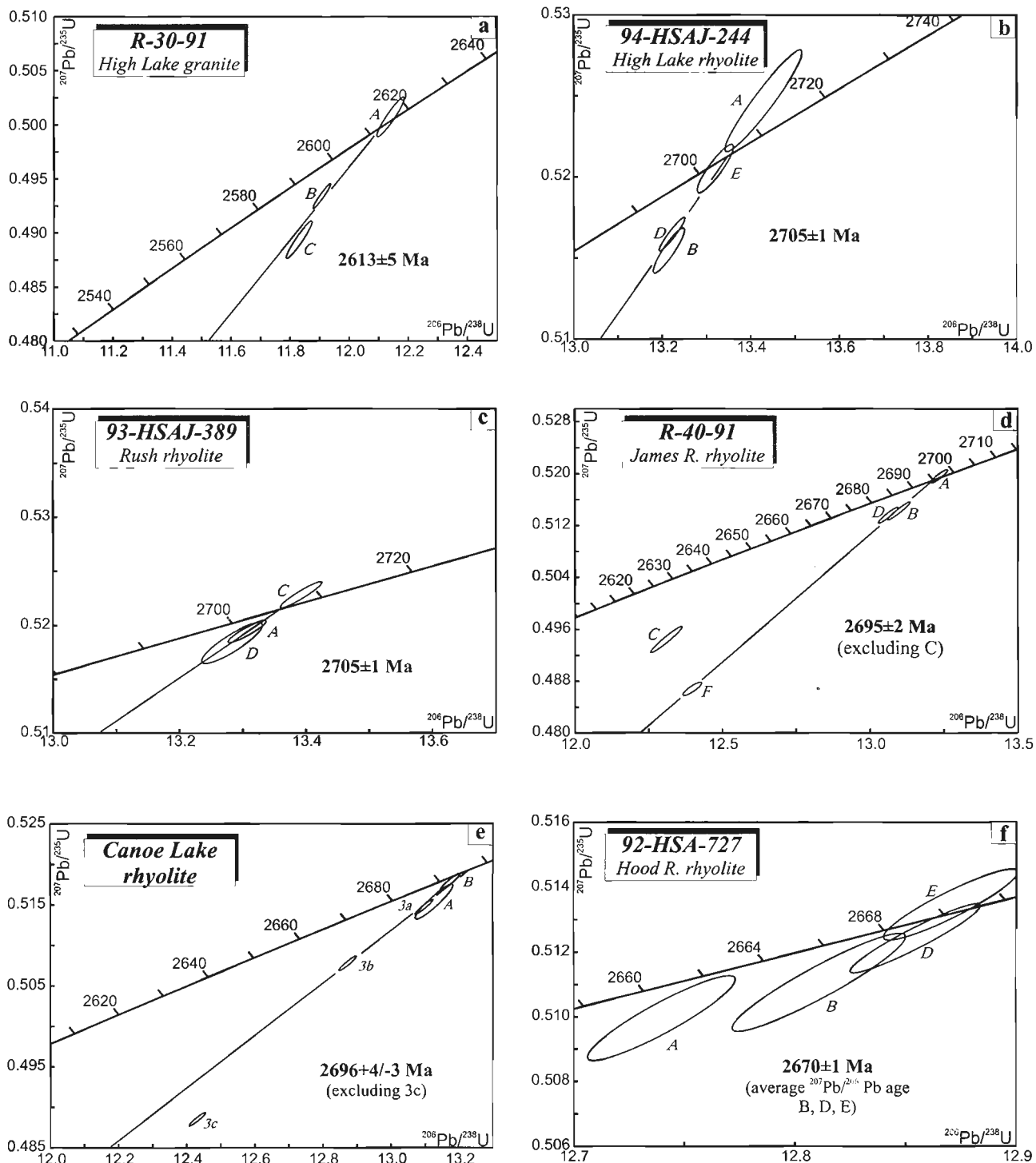


Figure 5. Concordia plots for samples from the High Lake greenstone belt. Error ellipses are at the  $2\sigma$  level of uncertainty; qtz = quartz.



cleavage is truncated by an intrusive contact with the Ulu granite (93-HSA-728), a two-mica granodiorite with recrystallized megacrysts of K-feldspar as well as coarse grained quartz and plagioclase. Biotite forms the bulk of the mica in the rock. Three fractions of clear, euhedral zircons resulted in analyses that are 1 to 3% discordant, but collinear (Fig. 5g). Regression of all three points results in an age of crystallization of  $2588 \pm 4$  Ma (MSWD=0.4, lower intercept =  $-27 \pm 112$  Ma). As such, the gold mineralization and  $S_3$  cleavage development are interpreted to be older than 2588 Ma.

### *Two-mica granite and foliated quartz diorite*

These two granites were collected within 1 km of each other, from the granitic terrane north of the High Lake greenstone belt and east of the northwestern side of the Anialik River volcanic belt. The foliated quartz diorite (R-33-91) is a coarse grained, hornblende-biotite quartz diorite that contains a moderate to strong north to north-northeast-striking, steeply dipping mineral foliation, principally defined by alignment of biotite. Recrystallized, coarse-grained hornblende forms 15% of the rock and biotite approximately 5%, with large, partially to wholly sericitized plagioclase and minor quartz forming the remainder. A small, elongate two-mica granite body (R-32-91) intrudes into the main body of the foliated quartz diorite to the west. The straight, sharply defined

contact between the two is exposed along the base of a hill, with little evidence for chill margin in the foliated quartz diorite or intermixing of the two intrusive bodies. The sharp truncation of foliation by the two-mica granite constrains the timing of deformation. The two-mica granite is similar in lithology to the  $2602 \pm 2$  Ma Chin Lake stock (Abraham et al., 1994) that intrudes the western margin of the 2705-2683 Ma Anialik River igneous complex (Abraham et al., 1994). It is a coarse grained, muscovite-rich (ca. 15-20%) quartz monzonite displaying recrystallized quartz and variably altered K-feldspar.

The foliated quartz diorite contained slightly pink, clear, euhedral prismatic zircons with sharp edges and terminations. Analysis of five one (A, B) to three grain (E) fractions resulted in linear array of four analyses (Fig. 5h), with fraction E being concordant. Fraction B, was a darker grain whose data falls to the right of the discordia line defined by the other fractions, suggesting that it may be xenocrystic. Regression of the other four fractions gives an upper intercept age of  $2603 \pm 6/-4$  Ma (MSWD=6.0, lower intercept =  $315 \pm 396$  Ma), interpreted to be the age of crystallization.

The two-mica granite gave a very low yield of pink to red, subhedral, moderate to poor quality zircons with a heterogeneous morphology ranging from subrounded to elongate prismatic. Even after heavy abrasion, all the zircon fractions yielded discordant results, with four of the fractions arranged

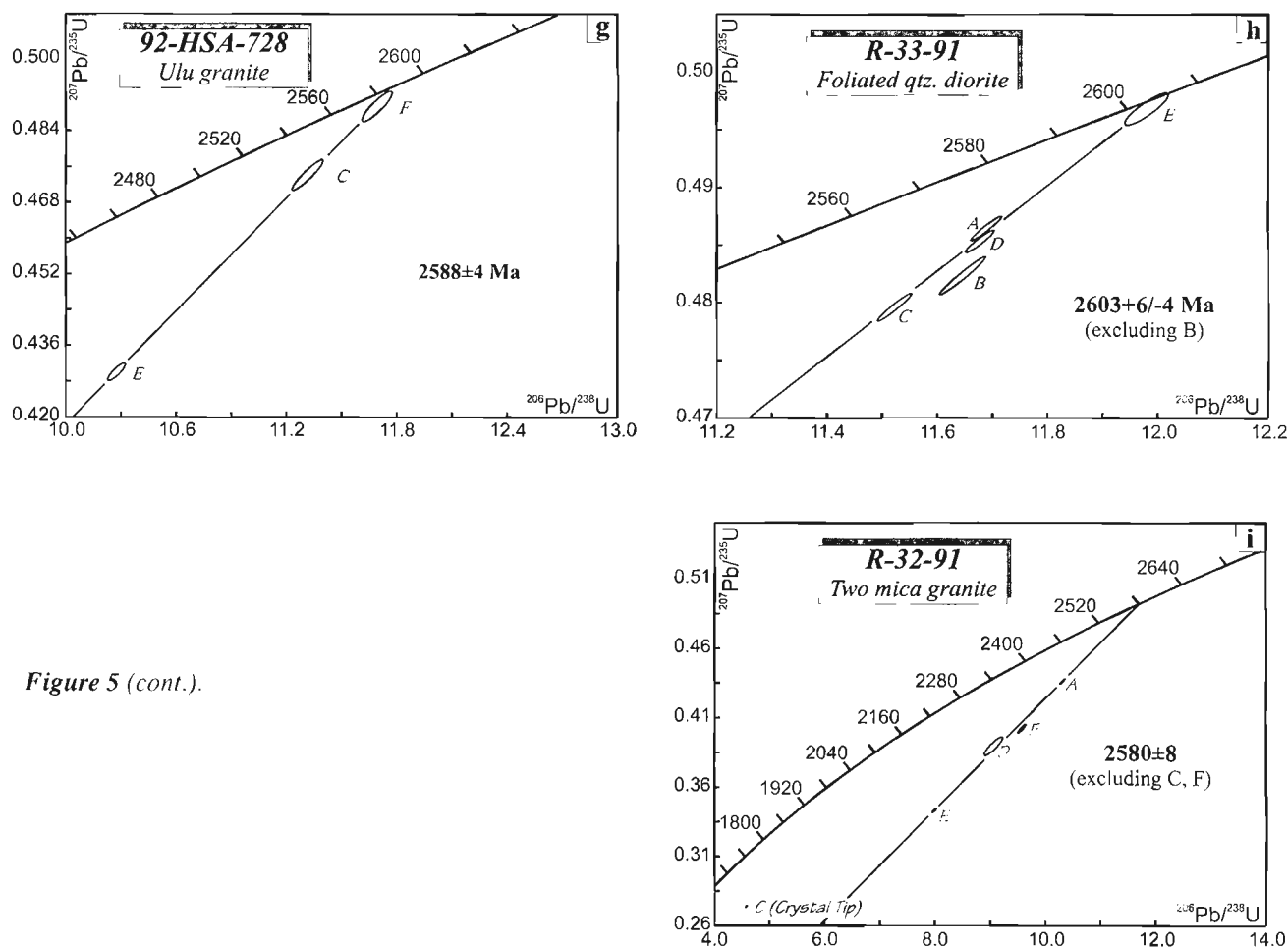
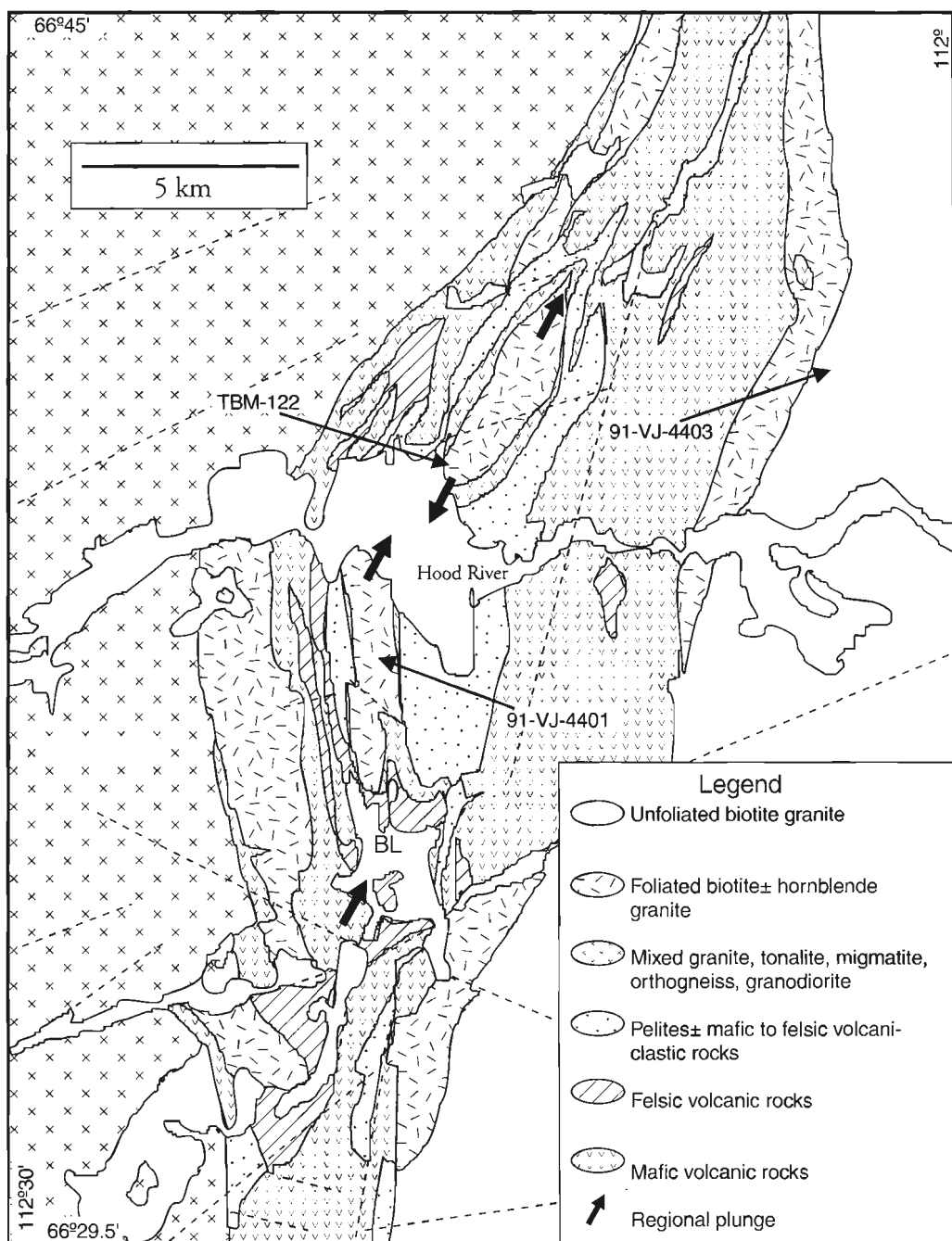


Figure 5 (cont.).

in a poorly defined linear pattern (Fig. 5i). Fraction C, a broken tip of a larger zircon appears to have been affected by a secondary Pb-loss event that has moved it off the Pb-loss trajectory displayed by the other crystals. Fraction F, a dark red crystal that stood out from the other fractions of clear, pink crystals, probably contained an inherited core, and was analyzed separately for this reason. Ignoring fraction C and F, linear regression of the other three fractions gives an age of  $2580 \pm 8$  Ma (MSWD=5.0, lower intercept =  $199 \pm 77$  Ma).

The larger than normal error is the result of regression of three discordant fractions coupled with potentially complex Pb-loss histories as evidenced by fraction C.

The age of the foliated quartz diorite is similar to the age range given for the Mistake Lake Suite (Relf, 1995). The age of the two mica granite is in accord with other ages of muscovite-bearing granites throughout the Slave Province, although it is 20 Ma younger than the nearby Chin Lake stock.



**Figure 6.** Geological sketch map for the Napaktulik Lake volcanic belt with location of geochronological samples marked.

The age of the foliated quartz diorite is further evidence of a post-2605 Ma deformational event that can be correlated to D<sub>3</sub> deformation in the Anialik River volcanic belt.

## NAPAKTULIK LAKE VOLCANIC BELT

The Napaktulik Lake volcanic belt is located just east of Napaktulik Lake (formerly Takijuk Lake, Fig. 6). The belt consists of mainly mafic volcanic and turbiditic sedimentary rocks that contain minor intervening felsic volcanic rocks. The belt strikes broadly north-south, varies in width from 1-8 km (Fig. 1) and has undergone metamorphism at medium to low grade (Jackson and Falck, 1991).

The belt is separated from the Tree River volcanic belt to the northeast by less than a kilometre of granitoid rocks. The Tree River volcanic belt is, in turn, continuously exposed until it merges with the southernmost, highly attenuated portion of the Anialik River volcanic belt (Tirrul and Bell, 1980; Relf, 1995). The Anialik River volcanic belt appears to contain far less meta-sedimentary material than either the Tree River volcanic belt or the Napaktulik Lake volcanic belt, and is bounded to the west by a major fault structure, the Tohokatak Fault Zone (Relf et al., 1994a; Relf, 1995). The southern Napaktulik Lake volcanic belt narrows to less than a kilometre in width, but is continuous with the Hanikahamijuk Lake volcanic belt (Gebert, 1994). The Hanikahamijuk Lake volcanic belt differs from the Napaktulik Lake volcanic belt in a number of respects. It contains a much higher proportion of felsic volcanic rocks, less turbiditic sedimentary rocks and it is characterized by a pronounced northeast trend, as opposed to the more northerly trend of the Napaktulik Lake volcanic belt. Detailed correlations between the two belts remain uncertain at this time. Isachsen and Bowring (1994) report a 3.0 Ga age on tonalites and 2.7-2.66 Ga volcanics that contain older inheritance from the southern extension of the Napaktulik Lake volcanic belt.

The belt is bounded to the east by a medium- to coarse-grained biotite K-feldspar megacrystic granite (informally named the eastern granite), that contains a very weak deformational fabric. The west side of the belt consists of mixed lithologies of biotite-hornblende tonalite, granodiorite, and granitic gneiss. High grade supracrustal rocks are also present along the western side of the belt. Hence, the Napaktulik Lake volcanic belt straddles the boundary between a little deformed granitoid terrane to the east and a terrane consisting of highly deformed migmatites and gneisses to the west.

Internally, the belt is intruded by plutons that form elliptical map patterns. These plutons are more highly deformed than their external counterparts to the east and they contain inconsistent mineral lineations, suggesting that their initial map patterns have been modified by later deformation.

The rocks contain a predominant, bedding-parallel fabric, that also contains pre- to syndeformational growth of cordierite and amphibole porphyroblasts. This fabric is deformed about open to tight folds with northwest- or northeast-striking axial surfaces. The plunge of the axes of the northeast folds alternate from north to south, over the distance of a few kilometres. It is possible that some of these fold reversals are

indicative of east-west Proterozoic crossfolding, similar to fold patterns recognized further south along the west margin of the Slave Province (King et al., 1992). Due to the lack of Proterozoic rocks, this deformation can only be restricted to the Late Archean or younger (Jackson and Villeneuve, 1993).

## Hood River granite

This unit (91-VJ-4401) is a biotite granite that weathers to buff. The granite is compositionally homogenous, medium- to coarse-grained, and contains irregular K-feldspar phenocrysts up 1.5 cm long with micropertthitic texture. Plagioclase is sericitized and commonly zoned. Quartz is clear and displays undulose extinction and annealed textures. Traces of anhedral garnets (<1 mm diameter) are present. The rock contains a moderate to strong foliation.

Zircons from this sample are stubby, sharply terminated, and relatively free of inclusions. A few fractures traverse some crystals. Five of six fractions form a collinear array (Fig. 7a), anchored by a concordant analysis (fraction E). The large error on fraction E is due to the high proportion of common Pb in the analysis; exacerbated by low U content and small sample size of the single grain. By regressing all the analyses, apart from fraction A, an age of  $2582 \pm 5/-4$  Ma (MSWD = 1.2, lower intercept =  $128 \pm 401$  Ma) is obtained. Fraction A has a minimum age of 2644 Ma, and is interpreted to contain an inherited component.

The K-feldspar megacrysts, minor garnet, and age of the granite show that this pluton is correlative with the group 3 granites (Davis et al., 1994), representative of the one of the last phases of magmatism in the Slave Province. Although the nature of the pluton is suggestive of the C6b suite (King et al., 1991), the Hood River granite contains a pronounced penetrative foliation, showing that a component of deformation in parts of the Napaktulik Lake volcanic belt is younger than 2582 Ma.

## Eastern granite

This rock (91-VJ-4403) is a medium- to coarse-grained biotite granite, with sparse (5-10%), 1-2 cm long rectangular K-feldspar phenocrysts, set in an equigranular ground mass of K-feldspar, zoned and sericitized plagioclase, and clear quartz. The quartz has undulose extinction, but in general the pluton is isotropic to weakly foliated. The granite is a large body that forms the eastern boundary of the Napaktulik Lake volcanic belt and extends southwards into the adjacent Contwoyto Lake map area and northwards into the Hepburn Island map area.

Zircons are stubby, euhedral crystals, generally devoid of fractures, but containing minor clear inclusions. In addition, a large, clear crystal was broken apart during sample preparation. Two of the largest fragments (F and G), each more than 250  $\mu$ m across, were analyzed separately and were 0.9% and 0.3% discordant with small individual errors (Fig. 7b). An analysis of a 74  $\mu$ m single crystal (fraction E) gave similar results, but with larger error, while a similar single grain analysis (fraction C) was significantly more discordant. A

regression through these four points results in a tight constraint on the age of crystallization of  $2599 \pm 1$  Ma (MSWD = 0.4, lower intercept =  $790 \pm 24$  Ma). Fraction A, not included in the regression, plots to the right of the discordia line and is interpreted to contain a component of slightly older inherited zircon. Alternatively, by regressing the most concordant fractions and assuming that fraction C has large and complex Pb-loss patterns, an age of  $2598 \pm 1$  Ma is calculated, overlapping within error of the other regression. To cover both possibilities, an age of  $2598 \pm 3$  is estimated for the age of the rock.

### Football granite

This unit (TBM-122) is a lozenge-shaped two-phase pluton comprising an older, grey tonalite that is crosscut by deformed granitic and pegmatitic veins. The tonalitic phase, which is dated here, is texturally and compositionally similar to that found in parts of the gneissic terrane along the west side of the Napaktulik Lake volcanic belt.

The composite pluton stretches northwards from a south-pointing apex on the north shore of the Hood River and forms a doubly plunging antiformal structure that plunges shallowly southwest at the southern end. The regional plunge then reverses across the Hood River, such that the Hood River granite displays a northerly plunge. Age dating places a maximum

age of 2.58 Ga on the crossfolding event in the Napaktulik Lake volcanic belt (Jackson and Villeneuve, 1993). However, the plunge reversals define fold hinges with the same orientation and frequency as Early Proterozoic crossfolds noted elsewhere in the Slave Province and the overlying ca. 1.86 Ga Wopmay Orogen (King, 1986). As such, the elliptical shape of this pluton may be partly the result of post-Slave events.

Two populations of zircon are present in the sample. Large, subhedral to anhedral, clear inclusion and crack-free crystals up to 200  $\mu\text{m}$  diameter form the minority population, while the remaining zircons are small (<74  $\mu\text{m}$ ) clear crystals. Dark brown titanite is also present. Analysis of two large crystals (fractions A and B) resulted in near concordant points (Fig. 7c) and analysis of two smaller crystals resulted in extremely discordant results (fractions E and F). The degree of discordance suggests that the smaller crystals may have been more prone to Pb loss than the larger crystals due to their decreased surface:volume ratio. All the points are roughly collinear, and a modified York (1969) regression results in an age of crystallization of  $2617 \pm 8$  Ma (MSWD=42, lower intercept=460 Ma). Because of the high MSWD, a Davis (1982) regression, which gives more weight to near concordant analyses was used for the zircon regression. The resulting age is  $2617 \pm 2$  Ma (probability of fit=2%, lower intercept=460 Ma).

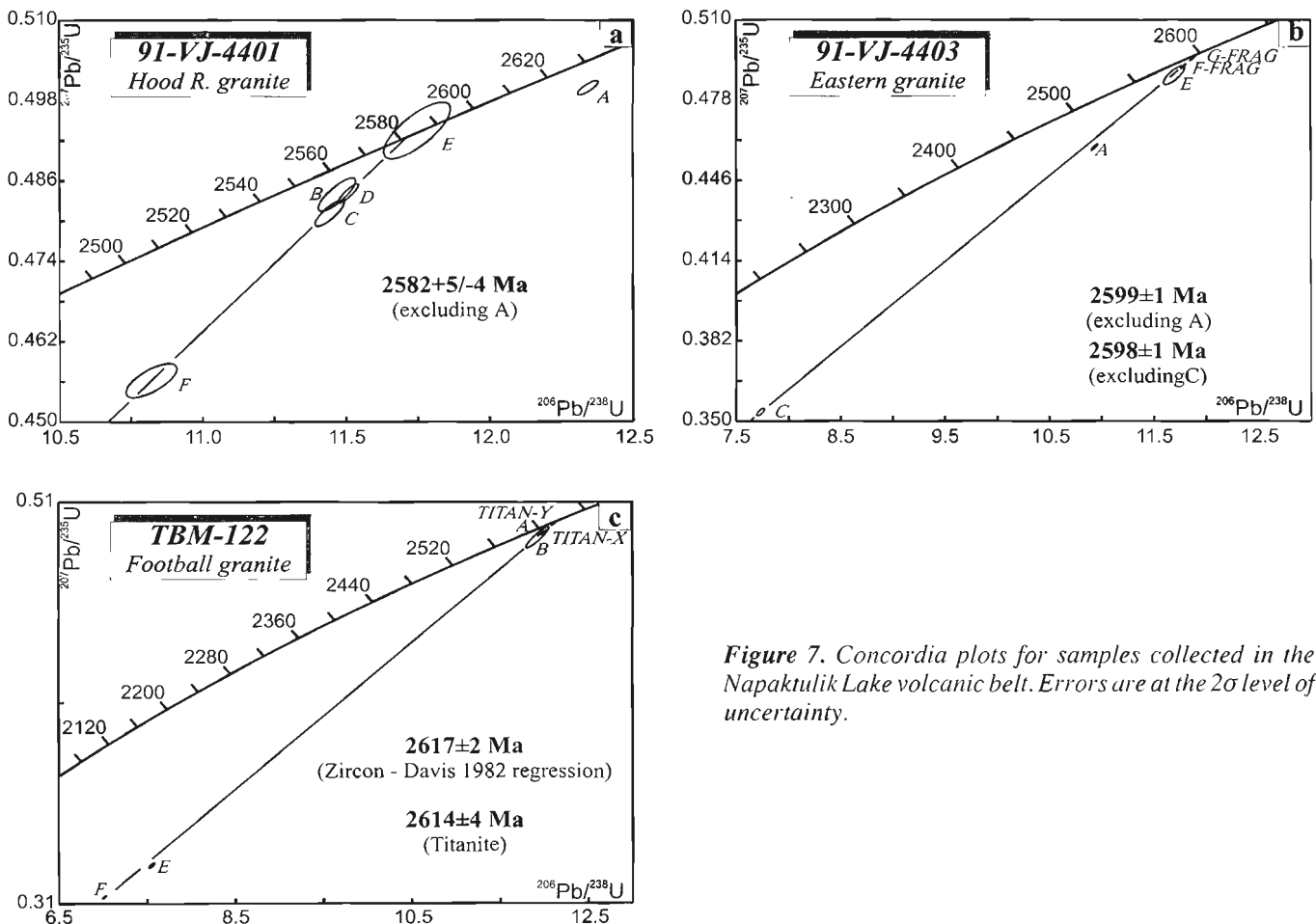


**Figure 7.** Concordia plots for samples collected in the Napaktulik Lake volcanic belt. Errors are at the  $2\sigma$  level of uncertainty.

Analysis of two fractions of titanite yielded one concordant and one near-concordant analysis. A regression through the two titanite analyses results in an age of  $2614 \pm 4$  Ma, indistinguishable from the age given by the zircons. Regression of all the zircon and titanite data gives an age of  $2615 \pm 4$  Ma (MSWD=24, lower intercept= $485 \pm 37$  Ma), which is interpreted to be the crystallization age for the tonalite component of the Football granite.

## WINTER LAKE SUPRACRUSTAL BELT

The Winter Lake supracrustal belt is volcano-sedimentary belt that merges with supracrustal assemblages at Point Lake and continues southward for 100 km (Fig. 8). The 1:250 000 scale mapping of the Winter Lake supracrustal belt by Fraser (1969) and more recently by Thompson (1992) and Thompson et al. (1993, 1994) have placed the belt within a regional depositional and metamorphic framework. In addition, the more recent mapping of Thompson et al. (1993, 1994) has outlined the geology of the granitic-gneiss complex lying east of the Winter Lake supracrustal belt. Concurrent with the more recent work, 1:50 000 mapping in the belt has highlighted not only a broad time-span for the deposition of stratigraphic sequences in the belt, but also the distinctly different character of the eastern and western portions (Fig. 9) of a 5–10 km wide supracrustal belt (Hrabi et al., 1993, 1994, 1995).

The structural base of the eastern side of the Winter Lake supracrustal belt is comprised of variably deformed felsic and mafic volcanic rocks up to 4 km thick (Hrabi et al., 1993, 1994). Well exposed to the south and west of Newbigging Lake, the felsic volcanic rocks are primarily massive, siliceous rhyolites and tuffs and include a fiamme-bearing unit from which an age of  $3118 \pm 11/-8$  Ma was derived (Villeneuve and van Breemen, 1994). Directly above the basal unit, a discontinuous, thin unit of crossbedded orthoquartzite contains discordant zircons with a narrow range of  $^{207}\text{Pb}/^{206}\text{Pb}$  ages between 3.16 and 3.14 Ga, although its contact relationship with the underlying felsic volcanic rocks is unclear because of localized high strain at the contact. The absence of detrital zircons younger than 3.1 Ga implies correlation with the lowermost felsic volcanic (Hrabi et al., 1993, 1994). Also associated with this band of localized high strain and overlying both the orthoquartzite and 3.1 Ga felsic volcanics is pillowed komatiitic basalt (Hrabi et al., 1993, 1994, 1995). This unit, originally grouped with the lowermost structural sequence (Hrabi et al., 1993) was reinterpreted as being in conformable contact with the overlying folded package of massive and pillowed mafic volcanics that dominate the central stratigraphy of the Winter Lake supracrustal belt (Hrabi et al., 1994).

The mafic volcanics within the eastern sequence have a tholeiitic affinity and are correlated with Yellowknife Supergroup strata based upon lithological associations and geochemistry (Hrabi et al., 1993, 1994). A sequence of polymictic conglomerates and associated arkoses rest unconformably on the mafic volcanics and extensive turbidite deposits and are preserved in a steeply-plunging structural basin (Hrabi et al., 1995). This unit was deposited after the  $D_1$  deformation that is evident in the underlying turbidite

section, but is deformed about later upright  $F_2$  folds (Hrabi et al., 1995). Detrital dating has confirmed an age younger than 2670 Ma for this sequence, but the depositional and lithological similarity of the units, coupled with the distinct structural history of the sequence suggests that they are correlative to the ca. 2.6 Ga boulder conglomerates found elsewhere in the Slave Province (Villeneuve et al., 1994; Isachsen and Bowring, 1994; Relf, 1995). Although the maximum depositional age remains unresolved, the sediments are cross-cut by a small, undeformed pegmatitic leucogranite that has produced a monazite U/Pb crystallization age of  $2548 \pm 2$  Ma (Villeneuve, unpub. data, 1995).

The western side of the Winter Lake supracrustal belt resembles the eastern side but differs in some important details. The structural base of both sides of the belt are made up primarily of felsic to intermediate volcanics (Hrabi et al., 1995), but on the western side, the felsic volcanics are  $3305 \pm 2$  Ma (Villeneuve, unpub. data, 1995). Orthoquartzite is joined by iron-formation in a thin unit that separates the old volcanics at the base from a thick homoclinal package of pillowed and massive mafic volcanics (Hrabi et al., 1995). These flows, unlike those on the eastern side, have both tholeiitic and calc-alkaline affinities and display geochemical evidence of crustal contamination (Hrabi et al., 1994; Hrabi et al., 1995). Locally, the top of the mafic volcanic rocks is demarcated by a late fault zone, above which sits a heterogeneous assemblage of mafic and ultramafic volcanic flows, volcanoclastic rocks, and clastic and chemical sedimentary rocks, all intruded by gabbro and peridotite sills (Hrabi et al., 1995). Rapid facies changes are the norm and many of the ultramafic rocks are medium- to coarse-grained tremolite-bearing schists (Hrabi et al., 1995). The top of this section, on the east, is sharply marked by another late fault.

Dating in the Winter Lake supracrustal belt has concentrated on the felsic volcanic rocks at the structural base and the detrital units unconformably overlying the pillowed volcanic rocks of the eastern section. This is primarily due to the paucity of dateable units in the mafic volcanic rocks that make up the central portion of the stratigraphy. Apart from the units detailed below, two other units were dated from just east of the margin of the belt. A strongly foliated biotite monzogranite gave a zircon U/Pb age of  $2720 \pm 8/-7$  Ma and a titanite U/Pb age of  $2659 \pm 5$  Ma (Villeneuve, 1993). An undeformed leucocratic dyke that crosscuts the thin layer of amphibolites wrapping around the margin of monzogranite, gave a monazite U/Pb age of  $2587 \pm 2$  Ma (Villeneuve, 1993).

### *Eastern gneiss leucosome*

This sample (HLB-92-B0021A), collected from the gneiss terrane along the eastern margin of the Winter Lake belt represents the leucocratic portion of a fine grained, banded biotite granitic gneiss. Banding is defined by alignment of biotite and flattening of quartz grains. The sample is part of a larger granite-gneiss complex that is bounded to the west by the Winter Lake supracrustal belt and to the east by the Courageous Lake volcanic belt. Comprising mixed migmatitic gneisses, granitic gneisses, and crosscutting undeformed granites (Thompson et al., 1995), parts of this complex are interpreted

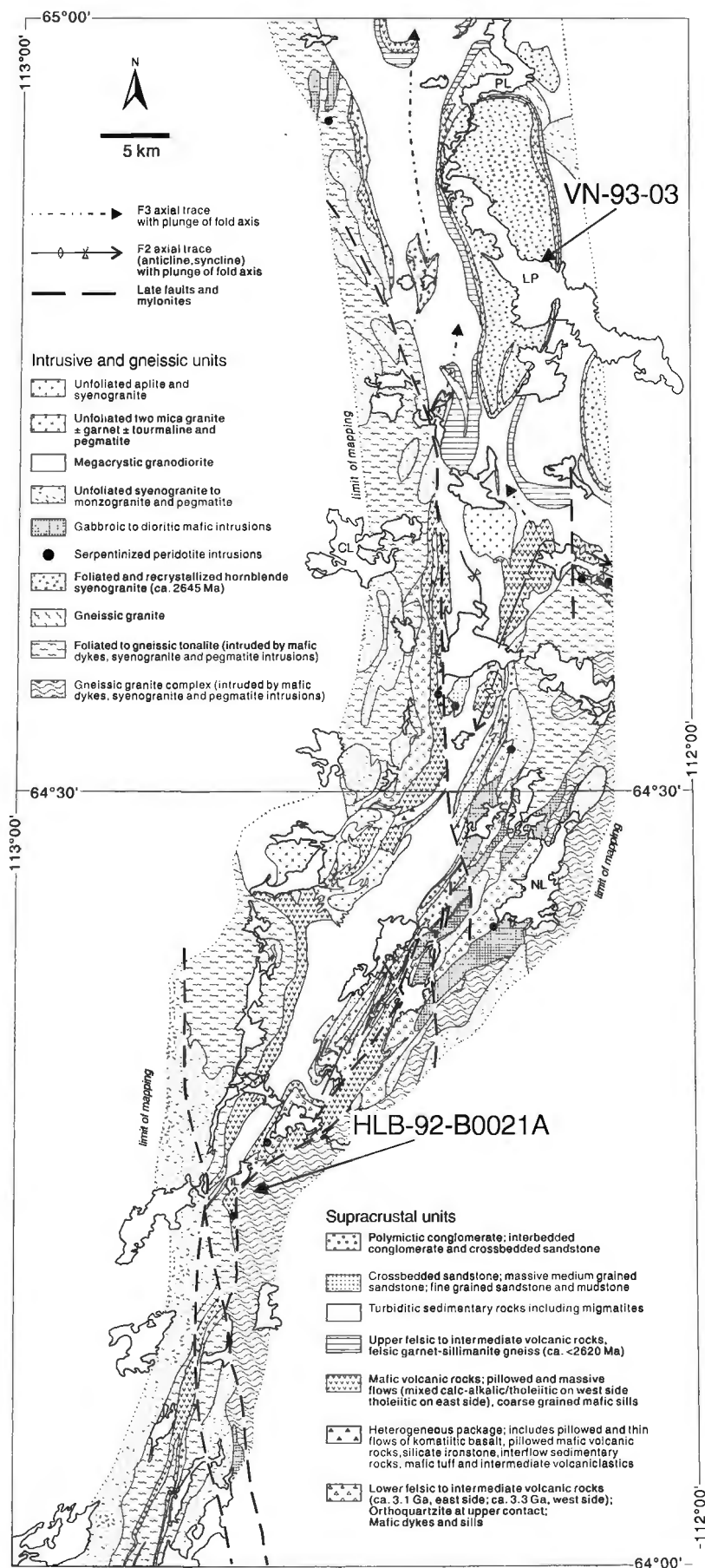


**Figure 8.**

Geological map of the northern and southern halves of the Winter Lake supracrustal belt (modified from Hrabi et al., 1995). Location of geochronological samples are marked.

as basement to the Yellowknife Supergroup strata (Thompson et al., 1995). The sampled granitoid gneiss has an irregular gneissosity that becomes abruptly transposed parallel with the margin of the Winter Lake supracrustal belt near the contact (Hrabi et al., 1993). This culminates in occurrences of mylonite along the boundary, with structural indicators displaying evidence for complex movements along that zone (Hrabi et al., 1993), suggesting that the Winter Lake

supracrustal belt may be (at least in part) allochthonous with respect to the structurally underlying granitic gneisses (Hrabi et al., 1993).

The zircons from the sample are a relatively homogenous population of colourless to very pale pink, euhedral prismatic crystals with L:W of around 2:1. They are clear, have somewhat blunt terminations and edges and contain minor clear inclusions and minor fractures. Six single-grain fractions

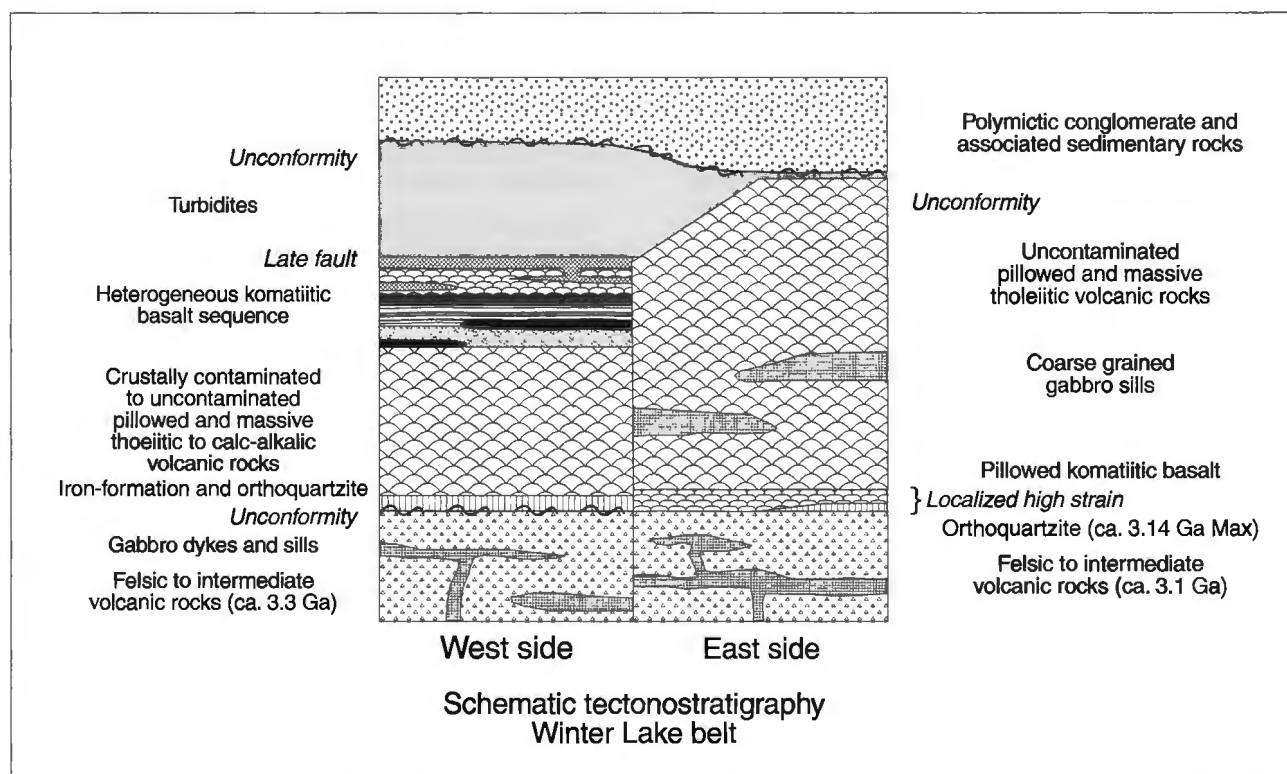


Figure 9. Schematic tectonostratigraphy of the Winter Lake supracrustal belt (modified from Hrabi et al., 1995).

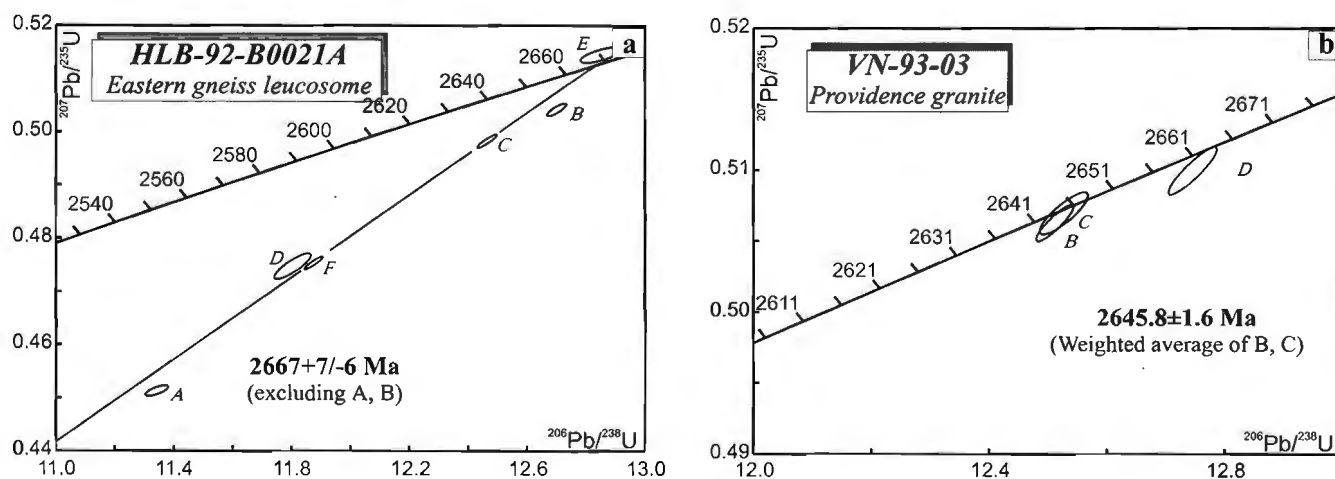


Figure 10. Concordia plots for samples collected from the Winter Lake supracrustal belt. Errors are at the  $2\sigma$  level of uncertainty.

give a poorly defined linear array at varying degrees of discordance (Fig. 10a). Taking the four rightmost fractions, including fraction E that plots slightly above concordia, results in an age of  $2667 \pm 7/-6$  Ma (MSWD=5.7, lower intercept= $144 \pm 248$  Ma). Although it is assumed that fractions A and B contain a cryptic component of inherited Pb, if they are included in the regression, they have very little effect on the interpreted age ( $2670 \pm 12/-9$  Ma, MSWD=29, lower intercept= $149 \pm 375$  Ma).

It is possible that the zircons in the leucosome are metamorphic in origin and that 2667 Ma marks the time of peak metamorphic conditions. However, given the euhedral, homogenous nature of the zircon population and morphology typical of magmatic rocks, it is more likely that this age represents the time of crystallization of the granitic magma. In addition, 2667 Ma is significantly older than ages ascribed to peak metamorphic conditions, such as an age of ca. 2.61 Ga for thermal peak metamorphic conditions in the nearby Contwoyto Lake area (King et al., 1992; Relf, 1992) or 2.65-2.64 Ga in the more distant Aniak River volcanic belt (Relf, 1995). For these reasons,  $2667 \pm 7/-6$  Ma is considered to be the age of granite crystallization.

The age of the large area of granitoid-gneiss complex east of the Winter Lake supracrustal belt and the evidence for the presence of crust significantly older than the Yellowknife Supergroup strata is one of the important unresolved questions in the Slave Province. This age clearly shows that some of this complex is coeval with Yellowknife Supergroup volcanism and highlights the role of late Archean tectonics in emplacing supracrustal belts adjacent to apparent basement complexes.

### Lake Providence pluton

Collected along the shoreline of Lake Providence, this large pluton of variably foliated hornblende syenogranite (VN-93-03) has a thin, conformable veneer of amphibolite-grade

supracrustal rocks around the margins (Thompson et al., 1993; Hrabí et al., 1994). The foliation in the pluton increases in intensity towards the margins and, apart from at the very northern end, is conformable with the foliation in the surrounding metamorphosed supracrustal rocks.

The sample gave a good yield of elongate, very clear, inclusion-free prismatic zircons. Slight irregularities on flat faces coupled with rounding of terminations and edges are evidence of minor, late resorption. Two of three fractions gave reproducible, concordant results (B, C; Fig. 10b) at 2646 Ma and a third three-grain fraction (D) has an error ellipse that grazes concordia at 2664 Ma. It is interpreted that age of the pluton is given by the two younger, most concordant fractions with an weighted average  $^{207}\text{Pb}/^{206}\text{Pb}$  age of  $2645.8 \pm 1.6$  Ma and that the slightly more discordant fraction D contains a component of inherited Pb.

The age of this pluton, coupled with the map pattern suggests that this body represents an intrusion into mafic volcanics of the Yellowknife Supergroup.

## COURAGEOUS LAKE VOLCANIC BELT

The Courageous Lake volcanic belt (Fig. 1) is a typical Slave Province greenstone belt comprising metamorphosed mafic volcanic and volcanoclastic rocks punctured by rhyolite intrusions. Mapped in detail by Dillon-Leitch (1984), the belt was divided into an upper cycle on the eastern side and a lower cycle on the western side of the belt. The lower cycle is partly recognized by the abundance of high level felsic porphyries that form irregular bodies within the mafic succession. Gold mineralization is common within the belt and past-producing mines include the Salmita and Tundra mines on the east shore of Matthews Lake. Previous geochronology in the belt is sparse, but Villeneuve (1993) reported two ages on felsic porphyries from each cycle. One, located on Courageous Lake within the lower cycle, returned an age of  $2729 \pm 8/-7$  Ma and is among the oldest dated Yellowknife Supergroup volcanic

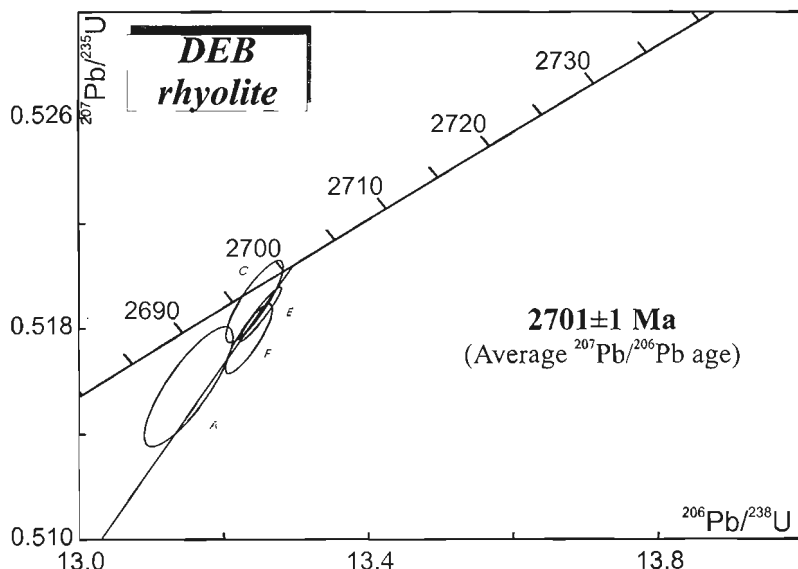


**Figure 11.**

Concordia plot for DEB volcanic sample. Errors are at the  $2\sigma$  level of uncertainty.



rocks. The other sample, from a body midway down the western shore of Matthews Lake gave an age to the upper cycle of  $2671 \pm 5/4$  Ma.

### DEB rhyolite

The DEB massive sulphide (Cu, Zn, Pb, and Ag) deposit is located about 5 km south of the  $2671 \pm 5/4$  Ma rhyolite and 5 km west of the Tundra mine within the lower cycle (Dillon-Leitch, 1984).

A specimen from a large diameter drill core was selected for dating purposes. The sample is a typical quartz-eye rhyolite porphyry that yielded elongate, clear, sharply terminated prismatic crystals and crystal fragments. Pieces of zircon with ends removed due to the presence of transverse fractures are the most common form and all zircons are less than 80  $\mu\text{m}$  long. Heavy air abrasion results in four fractions plotting within 0.7% of concordia (Fig. 11), all with the same  $^{207}\text{Pb}/^{206}\text{Pb}$  ages. By taking a weighted average of the  $^{207}\text{Pb}/^{206}\text{Pb}$  ages, a crystallization age of  $2701 \pm 1$  Ma is inferred.

This age falls between the previously dated rhyolite samples and because of the absence of intrusive or extrusive relationships in the sampled core, indicates that this part of the stratigraphy is older than  $2701 \pm 1$  Ma and is probably correlated with the older, lower succession as suggested by Dillon-Leitch (1984).

## SUMMARY AND CONCLUSIONS

Although geochronological studies carried out in conjunction with the mapping studies described here turned up new and interesting departures from pre-1992 conceptions of Slave Province geology (e.g. ca. 3.1 Ga volcanic rocks, <2.62 Ga supracrustal rocks), much of the data from these areas serves to reinforce and refine the conclusions of earlier workers. Chief among these are the continued evidence for the dominance of the Yellowknife Supergroup (Henderson, 1970) strata within almost every greenstone belt of the Slave Province and that the evolution of the plutonic suites tends to follow the pattern described by Davis et al. (1994). In general, the data presented here agrees with data produced by previous geochronological studies. Mortensen et al. (1988) provided broad regional coverage of many of the volcanic belts, Isachsen et al. (1991) produced a timeframe for deposition of the type section of Yellowknife Supergroup rocks in the Yellowknife basin, and van Breemen et al. (1992) provided the temporal relations between the plutonic suites.

Figure 12a compiles age data for volcanic rocks from throughout the Slave Province, separated into volcanic belts associated with basement inliers >2.8 Ga in age (Western domains) and volcanic belts that do not have evidence for significantly older basement (Eastern domains). This division is also based on the east-west dichotomy in the north-central Slave Province pinpointed by the isotopic work of Davis and Hegener (1992). Data from domains that straddle the boundary between the two types of volcanic belts are separated out. These include ages on volcanic rocks from the Courageous

Lake belt (Villeneuve, 1993), Point Lake belt, Hanikahamijuk Lake belt (Mortensen et al., 1988), and the Anialik River volcanic belt.

Data from the western domains mostly represent ages from a single belt. The Yellowknife greenstone belt serves as a model for the level of geochronology required to pinpoint definitive timeframes and episodes of volcanism. The best evidence for younger and older volcanic rocks comes from near Yellowknife, where there is a clear concentration of age dates, coupled with a one of the longest histories of geological

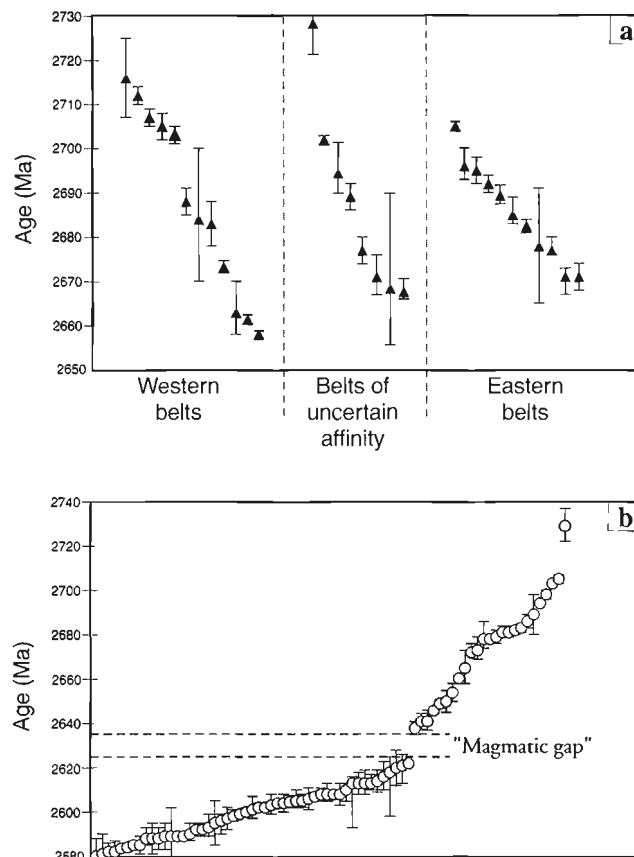


**Figure 12.** *a*) Plot of age of volcanic rocks dated in the Slave Province. Western belts are generally proximal to older (>2.8 Ga) basement, rocks from eastern belts do not have isotopic or age data for proximal older basement. Data from the western domain is dominated by dating in the Yellowknife belt (Isachsen et al., 1991) while data from the eastern domains represent a few ages from a number of widely scattered belts (Villeneuve and van Breemen, 1994 and references therein). The volcanic data forms a smooth continuum of ages between ca. 2.72 Ga and 2.66 Ga and argues against a distinct, Slave Province-wide hiatus in volcanic activity. *b*) Plot of age of plutonism in order of ascending age. This plot is an updated version of one presented by van Breemen et al. (1992) and includes new data presented herein as well as data listed in Villeneuve and van Breemen (1994). The magmatic gap, first noted by van Breemen et al. (1992) continues to be evident in the plutonic age data.

mapping. The approximately ten ages on volcanic rocks from within the Yellowknife belt (Mortensen et al., 1988; Isachsen et al., 1991) clearly point to a hiatus in volcanic activity between 2700 Ma and 2685 Ma.

The data from the eastern domains appears to show a shorter timespan but more continuous activity for volcanism. However, data from the eastern domains generally represents a few analyses from a number of widely scattered belts, with none having the degree of detailed mapping and geochronological control found in the Yellowknife belt. Because the oldest volcanic units at Yellowknife (Kam Group) are dominated by mafic volcanism and required careful mapping to find felsic units suitable for age dating (Isachsen et al., 1991), the lack of older age dates may simply represent a sampling bias within the eastern domains.

The overall data in Figure 12a shows that although an age gap is present at Yellowknife, it is not a pan-Slave phenomenon, since volcanic rocks from the Anialik River volcanic belt, the Back River volcanic belt, Hanikahamijuk Lake volcanic belt (Mortensen et al., 1988) and the High Lake greenstone belt have ages that fall within this timespan. As such, there is a remarkable continuum of ages within the volcanic rocks on a regional basis, although, as evidenced by the Yellowknife belt, a hiatus may be present locally. One final feature of Figure 12a overrides all of the other factors. With less than thirty-five age dates covering >500 km<sup>2</sup> of geology, and with approximately one-third of the ages coming from the Yellowknife belt, the aforementioned points are but sweeping generalizations pending future extension of the current mapping, especially within the eastern Slave Province.

The ages presented for the plutonic rocks closely match the ages predicted by the detailed studies of plutonic suites in the Contwoyto Lake area (King et al., 1991, van Breemen et al., 1992; Davis et al., 1994). In essence, a tripartite breakdown approximating that of Davis et al. (1994) holds, with ca. 2.70 Ga to 2.64 Ga equigranular, foliated hornblende±biotite tonalites, diorites, and trondjemites followed by 2.62 Ga to 2.59 Ga megacrystic biotite granites and finally with 2.60 Ga to 2.58 Ga two-mica, post-tectonic, coarse grained granites.

The addition of eleven new ages on intrusive rocks (out of a total of >80 plutons dated) has not filled the ca. 2640-2625 Ma magmatic gap (Fig. 12b) first noted by van Breemen et al. (1992). This magmatic gap continues to be a Slave Province-wide phenomenon and represents a break between minor plutonism associated with major volcanism and major plutonism associated with minor volcanism (e.g. High Lake).

One of the more interesting phenomena highlighted by the intrusive suite age data revolves around the timing of regional deformation. Taken as a whole, this data shows some striking anomalies, with plutons such as the 2602 Ma Chin Lake stock of the Anialik River volcanic belt being undeformed, yet the nearby <2600 Ma String Lake conglomerate and ca. 2600 Ma Grays Bay alkaline complex (Relf et al., 1994b; Relf, 1995) displaying a strong penetrative foliation that can be correlated on a regional scale. The syn-D<sub>3</sub> age of the 2613 ± 6 Ma Anialik tonalite can be contrasted with the 2600 Ma age of carbonatite intrusion and the 2605±6/-4 Ma

of the foliated quartz diorite, both of which are also deformed about a regional north-northeast-trending axis. In a similar light, the relatively undeformed 2599 Ma eastern granite of the Napaktulik Lake volcanic belt is 15 Ma older than the foliation-bearing Hood River granite. Given the large size of the eastern granite, this may illustrate partitioning of strain around the margins of such large isotropic bodies.

As such, the foliation-forming deformation event recorded in the Hood River granite or the lack of foliation in the Chin Lake stock highlights the importance of localized strain states within the more regional deformation events. Alternatively, these cases may illustrate a strong episodicity to the terminal deformational event in the Slave Province. As is aptly illustrated by rocks in the High Lake greenstone belt and Anialik River volcanic belt, major deformational events (in this case) may occur over a period of several million years, either episodically or continuously. Clearly, care must be taken in comparing degrees of foliation between plutons to ensure similarity in lithology of the plutons and surrounding country rocks, as well as the size and age of the plutons to accurately gauge the presence and timing of a major deformational event.

## ACKNOWLEDGMENTS

Klaus Santowski, Diane Bellerive, and Jack MacRae are thanked for their invaluable assistance in shepherding the samples through the laboratory and producing the excellent analyses. Janet King is thanked for insights and input, as well as her patience and support during the Slave NATMAP Project. Ralph Thorpe is thanked for collecting the DEB rhyolite sample and providing a geological context. Bill Davis freely gave excellent suggestions and insights into the regional significance of much of the Slave geochronology data and is thanked for a thoughtful and constructive review of the manuscript.

## REFERENCES

- Abraham, A.P.G., Davis, D.W., Kamo, S.L., and Spooner, E.T.C.  
1994: Geochronological constraints on late Archean magmatism, deformation and gold-quartz vein mineralisation in the northwestern Anialik River greenstone belt and igneous complex, Slave Province, N.W.T.; Canadian Journal of Earth Sciences, v. 31, p. 1365-1383.
- Bleeker, W. and Villeneuve, M.  
1995: Structural studies along the Slave portion of the SNORCLE transect; in Slave-Northern Cordillera Lithosphere Experiment (SNORCLE), Transect Meeting (April 8-9, 1995), University of Calgary, (comp.) F. Cook and P. Erdmer; Lithoprobe Report Number 44, p. 8-13.
- Bowring, S.A., King, J.E., Housh, T.B., Isachsen, C.E., and Podosek, F.A.  
1989a: Neodymium and lead isotope evidence for enriched early Archean crust in North America; Nature, v. 340, p. 222-225.
- Bowring, S.A., Williams, I.S., and Compston, W.  
1989b: 3.96 Ga gneisses from the Slave Province, N.W.T., Canada; Geology, v. 17, p. 971-975.
- Davis, D.W.  
1982: Optimum linear regression and error estimation applied to U-Pb data; Canadian Journal of Earth Sciences, v. 19, p. 2141-2149.

- Davis, W.J. and Hegner, E.**  
1992: Neodymium isotopic evidence for the tectonic assembly of Late Archean crust in the Slave Province, northwest Canada; *Contributions to Mineralogy and Petrology*, v. 111, p. 493-504.
- Davis, W.J., Fryer, B.J., and King, J.E.**  
1994: Geochemistry and evolution of Late Archean plutonism and its significance to the tectonic development of the Slave craton; *Precambrian Research*, v. 67, p. 207-241.
- Dillon-Leitch, H.C.H.**  
1984: Geology of the Courageous-Mackay Lake Greenstone Belt, NWT, parts of 75M/14, 15: 76D/2, 3, 4, 5; Northwest Territories Geology Division, Department of Indian and Northern Development, EGS 1984-4a, b, c, d, scale 1:24 000.
- Fraser, J.A.**  
1969: Winter Lake, District of Mackenzie; Geological Survey of Canada, Map 1219A, scale 1:253 440.
- Gebert, J.**  
1994: Final summary of mapping in the Hanikahimijak Lake area, a portion of the Point Lake volcanic belt, west-central Slave Province (86I/1, 2; 86H/14, 15); in *Exploration Overview*, Department of Indian Affairs and Northern Development, Northwest Territories Geology Division, Yellowknife, p. 35-36.
- Henderson, J.B.**  
1970: Stratigraphy of the Yellowknife Supergroup, Yellowknife Bay-Prosperous Lake area, District of Mackenzie; Geological Survey of Canada, Paper 70-26, 12 p.  
1975: Archean stromatolites in the northern Slave Province, Northwest Territories; *Canadian Journal of Earth Sciences*, v. 12, p. 1619-1630.
- Henderson, J.R., Henderson, M.N., and Kerswill, J.A.**  
1993a: Preliminary geological map of the north central High Lake Greenstone Belt, N.W.T., NTS 76M/6 East, 76M/7; Geological Survey of Canada, Open File 2782, scale 1:50 000.
- Henderson, J.B., Loveridge, W.D., and Sullivan, R.D.**  
1982: A U-Pb study of zircon from granitic basement beneath the Yellowknife Supergroup, Point Lake, district of Mackenzie; in *Rb-Sr and U-Pb Isotopic Age Studies, Report 5*; in *Current Research, Part C*; Geological Survey of Canada, Paper 82-1C, p. 173-178.
- Henderson, J.B., van Breemen, O., and Loveridge, W.D.**  
1987: Some U-Pb zircon ages from Archean Basement, supracrustal and intrusive rocks, Yellowknife-Hearne Lake area, District of Mackenzie, N.W.T.; in *Radiogenic Age and Isotopic Studies: Report 1*; Geological Survey of Canada, Paper 87-2, p. 111-121.
- Henderson, J.R., Henderson, M.N., Kerswill, J.A., Arias, Z., Lemkow, D., Wright, T.O., and Rice, R.**  
1993b: Geology and mineral occurrences of the southern part of High Lake greenstone belt, Slave Province, Northwest Territories; in *Current Research, Part C*; Geological Survey of Canada, Paper 93-1C, p. 125-136.  
1994: Geology and mineral occurrences of the central part of High Lake greenstone belt, Archean Slave Province, Northwest Territories: a preliminary account of an unconformity between two volcanic sequences; in *Current Research 1994-C*; Geological Survey of Canada, p. 81-90.
- Henderson, J.R., Kerswill, J.A., Henderson, M.N., Villeneuve, M., Petch, C.A., Dehls, J.F., and OKeefe, M.D.**  
1995: Geology, geochronology and metallogeny of the High Lake greenstone belt, Archean Slave Structural Province, Northwest Territories; in *Current Research 1995-C*; Geological Survey of Canada, p. 97-106.
- Hrabi, R.B., Grant, J.W., Berclaz, A., Duquette, D., and Villeneuve, M.E.**  
1994: Geology of the northern half of the Winter Lake supracrustal belt, Slave Province, Northwest Territories; in *Current Research 1994-C*; Geological Survey of Canada, p. 13-22.
- Hrabi, R.B., Grant, J.W., Godin, P.D., Helmstaedt, H., and King, J.E.**  
1993: Geology of the Winter Lake supracrustal belt, central Slave Province, District of Mackenzie, Northwest Territories; in *Current Research, Part C*; Geological Survey of Canada, Paper 93-1C, p. 71-81.
- Hrabi, R.B., Nelson, M.D., and Helmstaedt, H.**  
1995: Diverse metavolcanic sequences and late polymictic conglomerate-associated metasedimentary rocks in the Winter Lake supracrustal belt, Slave Province, Northwest Territories; in *Current Research 1995-E*; Geological Survey of Canada, p. 137-148.
- Isachsen, C.E. and Bowring, S.A.**  
1994: Evolution of the Slave craton; *Geology*, v. 22, p. 917-920.
- Isachsen, C.E., Bowring, S.A., and Padgham, W.A.**  
1991: U-Pb zircon geochronology of the Yellowknife volcanic belt, NWT, Canada: new constraints on the timing and duration of greenstone belt magmatism; *Journal of Geology*, v. 99, p. 55-67.
- Jackson, V.A.**  
1989: Preliminary geological compilation of the Hepburn Island map area (76M); Indian and Northern Affairs Canada, Geology Division, Yellowknife, EGS 1989-11, map with marginal text and figures, scale 1:125 000.
- Jackson, V.A. and Falck, H.**  
1991: Geology of part of the Napaktulik Lake area (86I), Slave Structural Province: preliminary investigation. in *Exploration Overview*, Department of Indian Affairs and Northern Development, Northwest Territories Geology Division, Yellowknife, p. 26-28.
- Jackson, V.A. and Villeneuve, M.E.**  
1993: Late Archean to Proterozoic deformation of granite in the Napaktulik Lake area, northwestern Slave Structural Province (SSP); Geological Association of Canada, Program with Abstracts, v. 18, p. A-48.
- King, J.E.**  
1986: The metamorphic internal zone of Wopmay Orogen (Early Proterozoic), Canada: 30 km of structural relief in a composite section based on plunge projections; *Tectonics*, v. 5, p. 973-994.
- King, J.E., Davis, W.J., and Relf, C.**  
1992: Late Archean tectonomagmatic evolution of the central Slave Province, northwest Territories; *Canadian Journal of Earth Sciences*, v. 29, p. 2156-2170.
- King, J.E., van Nostrand, T., Bethune, K.M., Wingate, M.J., and Relf, C.**  
1991: Final field report on the Contwoyto-Nose Lakes map area, central Slave Province, District of Mackenzie; in *Current Research, Part C*; Geological Survey of Canada, Paper 91-1C, p. 99-108.
- Krogh, T.E.**  
1982: Improved accuracy of U-Pb zircon ages by the creation of more concordant systems using an air abrasion technique; *Geochimica et Cosmochimica Acta*, v. 46, p. 637-649.
- McEachern, S.J.**  
1993: Structural reconnaissance of gneissic tectonites in the western Hepburn Island map sheet, northernmost Slave Province, Northwest Territories; in *Current Research, Part C*; Geological Survey of Canada, Paper 93-1C, p. 103-113.
- Mortensen, J.K., Thorpe, R.I., Padgham, W.A., King, J.E., and Davis, W.J.**  
1988: U-Pb zircon ages for felsic volcanism in the Slave Province, N.W.T.; in *Radiogenic Age and Isotope Studies: Report 2*; Geological Survey of Canada, Paper 88-2, p. 85-95.
- Padgham, W.A.**  
1992: Mineral deposits in the Archean Slave Structural Province; lithological and tectonic setting; in *Precambrian Metallogeny related to Plate Tectonics*, (ed.) G. Gaál and K. Schultz; *Precambrian Research*, v. 58, p. 1-24.
- Parrish, R.R., Roddick, J.C., Loveridge, W.D., and Sullivan, R.W.**  
1987: Uranium-lead analytical techniques at the geochronology laboratory, Geological Survey of Canada; in *Radiogenic Age and Isotope Studies: Report 1*; Geological Survey of Canada, Paper 87-2, p. 3-7.
- Relf, C.**  
1992: Two distinct shortening events during the late Archean orogeny in the west-central Slave Province, Northwest Territories, Canada; *Canadian Journal of Earth Sciences*, v. 29, p. 2104-2117.  
1995: Geology, mineral potential and tectonic setting of the Anialik River volcanic belt and the Kanguyyak gneiss belt, northwestern Slave Province, N.W.T.; Canada-NWT Mineral Initiatives Office, Report EGS 1995-7, Yellowknife, N.W.T., 113 p.
- Relf, C., Chouinard, A., Sandeman, H., and Villeneuve, M.E.**  
1994a: Contact relationships between the Anialik River volcanic belt and the Kanguyyak gneiss belt, northwestern Slave Province, Northwest Territories; in *Current Research 1994-C*; Geological Survey of Canada, p. 49-59.
- Relf, C., Villeneuve, M.E., and Helmstaedt, H.**  
1994b: Discovery of an Archean carbonatite-bearing alkaline complex in the northern Slave Province: tectonic and economic implications; in *Exploration Overview*, Geoscience Forum Abstracts, Northwest Territories Geology Division, Department of Indian Affairs and Northern Development, Yellowknife, p. 53-54.

**Roddick, J.C.**

- 1987: Generalized numerical error analysis with applications to geochronology and thermodynamics; *Geochimica and Cosmochimica Acta*, v. 51, p. 2129-2135.

**Thompson, P.E.**

- 1992: The Winter Lake-Lac de Gras regional mapping project, central Slave Province, District of Mackenzie, Northwest Territories; in *Current Research, Part C*; Geological Survey of Canada, Paper 92-1C, p. 41-46.

**Thompson, P.E., Ross, D., and Davidson, A.**

- 1994: Regional geology of the Winter Lake-Lac de Gras area, central Slave Province, District of Mackenzie, Northwest Territories; in *Current Research 1994-C*; Geological Survey of Canada, p. 1-12.

**Thompson, P.E., Ross, D., Froese, E., Kerswill, J.A., and Peshko, M.**

- 1993: Regional geology in the Winter Lake-Lac de Gras area, central slave Province, District of Mackenzie, Northwest Territories; in *Current Research, Part C*; Geological Survey of Canada, Paper 93-1C, p. 61-70.

**Thompson, P.E., Russell, I., Paul, D., Kerswill, J.A., and Froese, E.**

- 1995: Regional geology and mineral potential of the Winter Lake-Lac de Gras area, central Slave Province, Northwest Territories; in *Current Research 1995-C*; Geological Survey of Canada, p. 107-119.

**Thorpe, R., Cummings, G.L., and Mortensen, J.K.**

- 1992: A significant Pb isotopic boundary in the Slave Province and its probable relationship to ancient basement in the western Slave Province; in *Project Summaries, Canada-Northwest Territories Mineral Development Agreement 1987-91*, Geological Survey of Canada, Open File 2484, p. 179-184.

**Tirrul, R. and Bell, I.**

- 1980: Geology of the Anialik River greenstone belt, Hepburn Island map area, District of Mackenzie; in *Current Research, Part A*; Geological Survey of Canada, Paper 80-1A, p. 157-164.

**van Breemen, O., Davis, W.J., and King, J.E.**

- 1992: Temporal distribution of granitoid plutonic rocks in the Archean Slave Province, northwest Canadian Shield; *Canadian Journal of Earth Sciences*, v. 29, p. 2186-2199.

**van Breemen, O., Henderson, J.R., Jefferson, C.W., Johnstone, R.M., and Stern, R.A.**

- 1994: U-Pb age and Sm-Nd isotopic studies in Archean Hood River and Torp Lake supracrustal belts, northern Slave Province, Northwest Territories; in *Radiogenic Age and Isotope Studies: Report 8*; Geological Survey of Canada, Current Research 1994-F, p. 1-16.

**Villeneuve, M.E.**

- 1993: Preliminary geochronological results from the Winter Lake-Lac de Gras Slave Province NATMAP project, N.W.T.; in *Radiogenic Age and Isotopic Studies: Report 7*; Geological Survey of Canada, Paper 93-2, p. 29-38.

**Villeneuve, M.E. and van Breemen, O.**

- 1994: A compilation of U-Pb age data from the Slave Province; Geological Survey of Canada, Open File 2972, 53 p.

**Villeneuve, M.E., Hrabi, R.B., and Jackson, V.A.**

- 1994: Ages of detrital zircons from supra crustal sequences in the Slave Province, NWT, Canada: implications for age of basement; *Geological Society of America, Annual Meeting, Program with Abstracts*, v. 26, p. A232.

**Villeneuve, M.E., Jackson, V.A., and Thompson, P.H.**

- 1993: Geochronological evidence for the existence of pre-Yellowknife Supergroup supracrustal sequences in the Slave Province; *Geological Association of Canada, Program with Abstracts*, v. 18, p. A107.

**York, D.**

- 1969: Least squares fitting of a straight line with correlated errors; *Earth and Planetary Science Letters*, v. 5, p. 320-324.

# Sm-Nd isotopic study on mafic volcanic rocks from the Rankin Inlet and Tavani regions, District of Keewatin, Northwest Territories<sup>1</sup>

R.J. Thériault<sup>2</sup> and S. Tella<sup>2</sup>

*Thériault, R.J. and Tella, S., 1997: Sm-Nd isotopic studies on mafic volcanic rocks from the Rankin Inlet and Tavani regions, District of Keewatin, Northwest Territories; in Radiogenic and Isotopic Studies: Report 10; Geological Survey of Canada, Current Research 1997-F, p. 61-66.*

---

**Abstract:** Sm-Nd isotopic compositions are presented on eleven Late Archean mafic volcanic whole rock samples of the Rankin Inlet and Tavani areas of the eastern Rankin-Ennadai greenstone belt. Three samples from the lower volcanic cycle of the Rankin Inlet Group yielded  $\epsilon_{\text{Nd}(2.66 \text{ Ga})}$  values of -1.1 to +1.6, and  $^{147}\text{Sm}/^{144}\text{Nd}$  ratios from 0.1289 to 0.1410, suggesting interaction of the mafic magmas with an older LREE-enriched crustal contaminant. Rocks of the upper volcanic cycle yielded  $\epsilon_{\text{Nd}(2.66 \text{ Ga})}$  values of +1.8 to +4.5 and  $^{147}\text{Sm}/^{144}\text{Nd}$  ratios of 0.1374 to 0.1999, and are relatively uncontaminated compared to the lower volcanic cycle. The presence of crustally contaminated volcanic rocks in the lower volcanic cycle indicates that it may have been underlain by older continental-type basement rocks, or that its mantle source was contaminated with crustally-derived fluids or sediments. Four samples from the Tavani area have  $\epsilon_{\text{Nd}(2.68 \text{ Ga})}$  values of +2.1 to +3.4, indicating derivation from depleted mantle sources, with no obvious interaction with older LREE-enriched crust. One of the five samples from the Tavani area yielded a  $\epsilon_{\text{Nd}(2.68 \text{ Ga})}$  value of +0.6, raising the possibility of minor contamination from an older crustal component.

**Résumé :** Dans le présent rapport, sont fournies les compositions isotopiques du couple Sm-Nd tirées de l'analyse sur roche totale de onze échantillons de roches volcaniques mafiques de l'Archéen tardif provenant des régions de Rankin Inlet et de Tavani, dans la partie est de la ceinture de roches vertes de Rankin-Ennadai. Trois échantillons provenant du cycle volcanique inférieur du Groupe de Rankin Inlet ont donné des valeurs  $\epsilon_{\text{Nd}(2.66 \text{ Ga})}$  de -1,1 à +1,6 et des rapports  $^{147}\text{Sm}/^{144}\text{Nd}$  de 0,1289 à 0,1410, ce qui indique une interaction des magmas mafiques avec un contaminant crustal plus ancien, enrichi en terres rares légères. Les roches du cycle volcanique supérieur ont produit des valeurs  $\epsilon_{\text{Nd}(2.66 \text{ Ga})}$  de +1,8 à +4,5 et des rapports  $^{147}\text{Sm}/^{144}\text{Nd}$  de 0,1374 à 0,1999, et elles sont relativement peu contaminées par rapport à celles du cycle volcanique inférieur. La présence de roches volcaniques contaminées par des matériaux crustaux dans le cycle volcanique inférieur portent à croire que les roches de ce cycle se sont déposées peut-être sur des roches de socle de type continental plus anciennes ou que la source du magma dans le manteau a été contaminée par des fluides provenant de la croûte ou des sédiments. Quatre échantillons provenant de la région de Tavani affichent des valeurs  $\epsilon_{\text{Nd}(2.68 \text{ Ga})}$  de +2,1 à +3,4, ce qui indique qu'ils sont issus de sources mantelliques appauvries et qu'aucune interaction évidente ne s'est produite avec une croûte plus ancienne qui aurait été enrichie en terres rares légères. L'un des cinq échantillons de la région de Tavani a produit une valeur  $\epsilon_{\text{Nd}(2.68 \text{ Ga})}$  de +0,6, ce qui soulève la possibilité d'une faible contamination par une composante crustale plus ancienne.

---

<sup>1</sup> Contribution to Canada-Northwest Territories Mineral Initiatives (1991-1996), an initiative under the Canada-Northwest Territories Economic Development Cooperation Agreement.

<sup>2</sup> Geological Survey of Canada, 601 Booth Street, Ottawa, Ontario K1A 0E8

## INTRODUCTION

Because the Sm-Nd isotopic system remains undisturbed throughout most crustal processes, it is a powerful tool for identifying source regions of volcanic rocks, and for understanding the nature of the crust at the time of volcanism. The Rankin-Ennadai belt is an Archean greenstone-granite-gneiss terrane in the Hearne Province of the Churchill Structural Province (Fig. 1). Due to largely reconnaissance level studies, paleogeographic reconstructions of the Rankin-Ennadai belt have been imprecise. Before detailed reconstructions can be established, and before viable comparisons can be made with other Archean cratons, a more sophisticated geological, geochronological, and isotopic data set is required. The goals of this paper are to report the results of an Sm-Nd study of volcanic rocks from the northeast segment of the Rankin-Ennadai belt, in the Rankin Inlet and Tavani regions (Fig. 1), and to consider the magmatic sources and possible contaminants from which these volcanic rocks evolved.

## GEOLOGICAL SETTING

The Rankin-Ennadai greenstone-granite-gneiss belt extends approximately 700 km, from Rankin Inlet on Hudson Bay to northeastern Saskatchewan (Fig. 1). Supracrustal sequences include mafic to felsic volcanic rocks, turbiditic sandstones and mudstones, iron-formation, and local conglomerate, carbonate, and mature siliciclastic rocks. For much of its extent, rocks of the Rankin-Ennadai belt are unconformably overlain by Paleoproterozoic sedimentary rocks of the Hurwitz Group. Reconnaissance geological investigations were carried out by several workers (e.g. Wright, 1967 and references therein). The results of most recent regional bedrock mapping have been reported by Tella et al. (1986, 1992), Tella (1994), and Asper and Chiaranzelli (1996a).

### Rankin Inlet

Different stratigraphic names have been applied to different geographic regions of the Rankin-Ennadai belt. In the Rankin Inlet area, the Rankin Inlet Group is a polydeformed

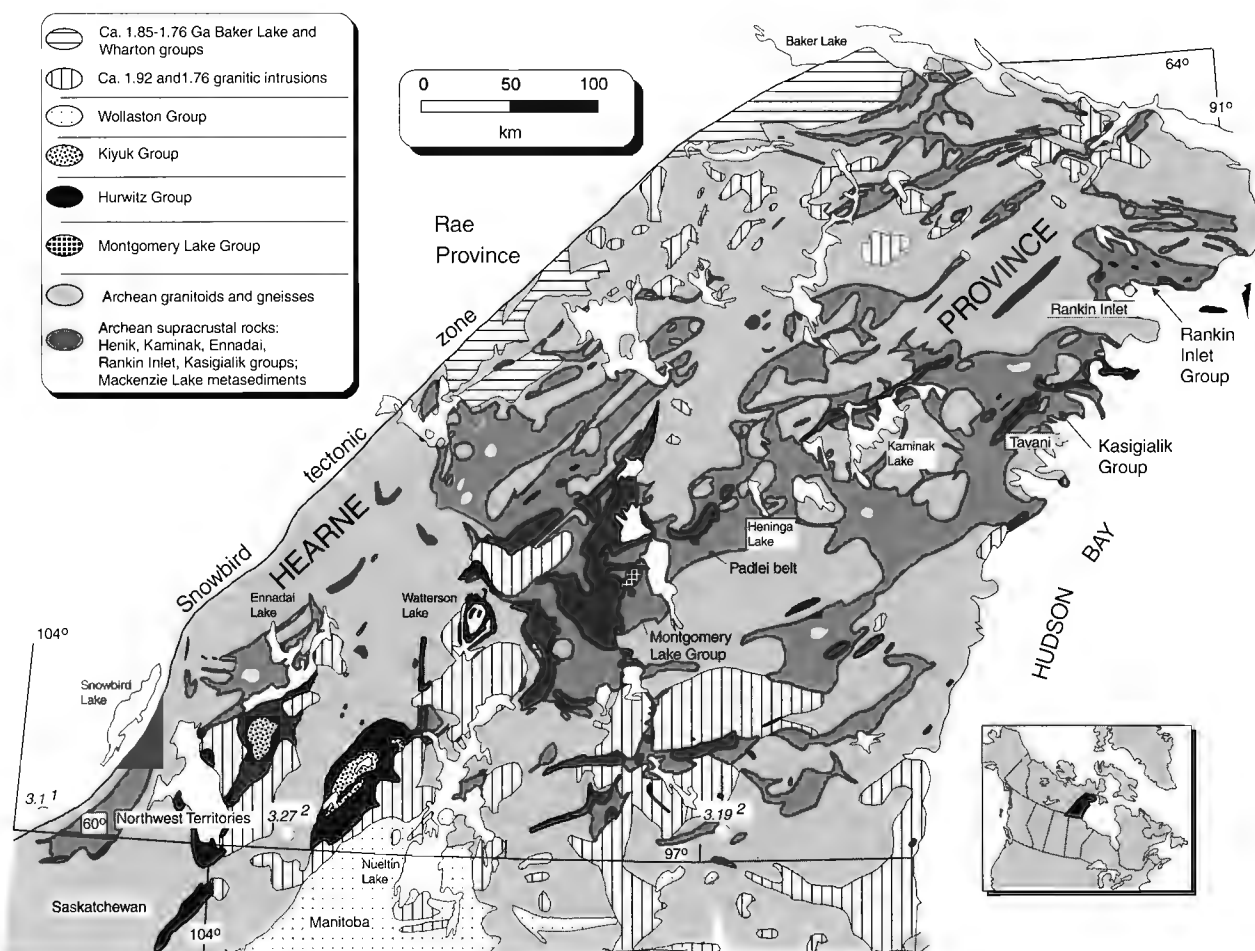


**Figure 1.** Sketch map showing lithostratigraphy of the Hearne Province. Locations of pre-3 Ga rocks are shown, after Asper and Chiaranzelli, 1996b. (<sup>1</sup>Hammer et al., 1995; 3.1-3.3 Ga granulites, <sup>2</sup>Loveridge et al., 1988; 3190 (?) Ma granulite orthogneiss, 3274 ± 18 Ma Kasba granodiorite gneiss).

metavolcanic-metasedimentary supracrustal sequence that consists of massive and pillowed mafic volcanic flows, felsic volcanic rocks, interflow sediments, quartz-magnetite iron-formation, and minor mafic and felsic tuffs, pyroclastics, volcanic breccia, and gabbro sills (Tella et al., 1986). The main rock types are sheared and carbonatized mafic metavolcanic rocks (chlorite schist, amphibolite), minor intercalated mafic and felsic tuffs, and greywacke. The metamorphic grade of the Rankin Inlet Group is greenschist facies, and both deformation and metamorphism are considered to be Archean because structurally overlying Proterozoic rocks were unaffected by penetrative deformation and metamorphism. The volcanic rocks and associated gabbroic bodies are tholeiitic, and display compositional features of MORB, (mid ocean ridge basalt) OIB, (ocean island basalt) and continental basalts (S. Tella, unpub. data, 1989).

Two major cycles of volcanism are recognized within the mafic volcanic sequence. The contact between the lower and upper volcanic cycles is, for the most part, conformable. However, sheared contacts between the sequences have also been observed at several localities, thus their present structural position may not reflect their stratigraphic order. Intercalations of felsic volcanic rocks are only in the lower volcanic cycle and represent less than ten per cent of the sequence.

U-Pb isotopic studies on zircon fractions from a felsic volcanic band within the Rankin Inlet Group yielded an upper concordia intercept age of  $2663 \pm 3$  Ma (Tella et al., 1996). Komatiitic sills, in part containing Cu-Ni mineralization, in the upper volcanic cycle have been dated at  $2748 \pm 92$  Ma and  $2776 \pm 88$  Ma, using the Re-Os method on Ni-Cu-PGE ores (Hulbert and Gregoire, 1993).

Two sets of samples, representative of the lower and upper volcanic cycles, were selected for Sm-Nd isotopic analysis. Sampling locations and brief lithological descriptions are given in Table 1.

### Tavani

In the Tavani region, 70 km southwest of Rankin Inlet (Fig. 1), Archean supracrustal rocks are divided into two volcanic and sedimentary sequences, the Kasigialik Group and the Tagiulik Formation (Park and Ralser, 1992). The former is further subdivided into the Atungag, Akliqnaqtuk, and Evi-taruktuk formations which consist of variable proportions of mafic to felsic volcanic rocks and intercalated sedimentary rocks. Archean metamorphic grade varies from subgreenschist to upper amphibolite facies around granitoid complexes. Paleoproterozoic subgreenschist facies and deformational processes affected the Hurwitz Group cover rocks (Park and Ralser, 1992). The mafic volcanic rocks of

**Table 1.** Description, location and Sm-Nd isotopic data of samples from the Rankin Inlet and Tavani areas.  $\epsilon_{\text{Nd}}$  for Rankin Inlet samples calculated at 2.66 Ga, and  $\epsilon_{\text{Nd}}$  for Tavani area calculated at 2.68 Ga.

Sample	Description	Latitude	Longitude	Sm (ppm)	Nd (ppm)	$^{147}\text{Sm}/^{144}\text{Nd}$	$^{143}\text{Nd}/^{144}\text{Nd}$ (2 $\sigma$ )	$\epsilon_{\text{Nd}}$
<b>Rankin Inlet area</b>								
<b>Upper volcanic cycle</b>								
85TX-014	fine grain massive basalt	62°51'51"	92°12'17"	2.97	10.32	0.1742	0.512473(9)	+4.5
85TX-177-1	fine grain pillowed metabasalt	62°40'29"	92°00'43"	1.87	5.65	0.1999	0.512787(11)	+1.8
85TXA-429A	fine grain massive basalt	62°48'26"	92°18'26"	2.62	11.37	0.1394	0.511779(12)	+3.0
<b>Lower volcanic cycle</b>								
85TXA-160	v. fine grain, metabasalt with disseminated sulphide	62°52'51"	92°14'43"	4.08	18.42	0.1339	0.511575(5)	+0.9
85TXA-177	fine- to med.-grain amphibolitic metavolcanic	62°52'59"	91°36'9"	7.64	35.82	0.1289	0.511527(7)	+1.7
85TXA-399A	v. fine grain, fractured metabasalt crosscut by quartz veins	62°47'51"	92°25'5"	4.87	20.89	0.1410	0.511602(5)	-1.1
<b>Tavani area</b>								
89TX-021	fine grain, epidotized pillow basalt	62°09'50"	93°28'1"	2.25	6.74	0.2019	0.512858(9)	+2.5
89TX-050	fine grain, massive basalt flow with minor quartz veining	62°08'45"	93°54'45"	8.75	39.81	0.1329	0.511686(9)	+3.4
89TX-055	fine- to med.-grain andesitic basalt	62°09'30"	93°55'20"	5.26	24.84	0.1279	0.511533(10)	+2.1
89TX-072	med. grain chloritized massive basalt flow	62°07'30"	93°59'0"	5.66	25.12	0.1361	0.511599(10)	+0.6
89TX-081	fine grain, sheared pillow basalt	62°07'50"	93°55'20"	2.96	9.65	0.1857	0.512585(9)	+2.8

the Tavani area resemble those of the Rankin Inlet area geochemically, and correspond to MORB, OIB, and intra-plate type basalts (Park and Ralser, 1992).

Based on U-Pb geochronology and structural studies, volcanism, plutonism, and deformation occurred within a period of 25 Ma, with 2.68 Ga felsic and mafic volcanism, 2.67–2.66 Ga syntectonic granite plutonism and 2.66–2.65 Ga post-tectonic granite plutonism (Tella et al., 1990; Park and Ralser, 1992). The ca. 2.63 Ga age obtained from the felsic volcanic rocks of the Rankin Inlet Group (Tella et al., 1996) suggests that the volcanism and deformation of the Rankin Inlet Group postdates that of the Tavani area by 15–20 Ma.

## ANALYTICAL PROCEDURES

The analytical methods employed are a variant of those described by Richard et al. (1976). Whole rock powders were spiked with a mixed  $^{148}\text{Nd}$ – $^{149}\text{Sm}$  solution and dissolved in an HF–HNO<sub>3</sub> mixture. Separation of bulk rare-earth elements was done by cation exchange chromatography on TruSpec™ resin calibrated for optimal recovery of LREE. Purification of Sm and Nd was done by HDEHP–teflon powder chromatography. Total procedure blanks were approximately 100 pg for Nd and less than 40 pg for Sm. Isotopic compositions were measured on a MAT-261 solid source mass spectrometer in static mode. Neodymium isotopic compositions were normalized to  $^{146}\text{Nd}/^{144}\text{Nd} = 0.7219$  and corrected to LaJolla  $^{143}\text{Nd}/^{144}\text{Nd} = 0.511860$ . Repeated analysis of an Ames Nd metal solution yielded  $^{143}\text{Nd}/^{144}\text{Nd} = 0.512165 \pm 20$  (external  $2\sigma$  error) (equivalent to LaJolla  $^{143}\text{Nd}/^{144}\text{Nd} = 0.511875$ ). The external reproducibility of individual  $\epsilon_{\text{Nd}}$  values is within 0.5  $\epsilon_{\text{Nd}}$  unit. On the basis of replicate analyses,  $^{147}\text{Sm}/^{144}\text{Nd}$  ratios are generally reproducible to 0.3%. The  $\epsilon_{\text{Nd}}$  values were calculated assuming present-day CHUR (Chondritic uniform reservoir)  $^{143}\text{Nd}/^{144}\text{Nd} = 0.512638$  and  $^{147}\text{Sm}/^{144}\text{Nd} = 0.1967$ . Given the  $2663 \pm 3$  Ma age of the felsic volcanic band in the Rankin Inlet Group (Tella et al., 1996),  $\epsilon_{\text{Nd}}$  values for the Rankin Inlet Group were calculated at 2.66 Ga. The  $\epsilon_{\text{Nd}}$  values for the Tavani area were calculated at 2.68 Ga.

## RESULTS

### Rankin Inlet

Six samples of mafic volcanic rocks from the Rankin Inlet Group were analyzed. Three of the six samples were from the lower volcanic cycle, and the remaining three samples were from the upper volcanic cycle. The lower volcanic cycle rocks yielded  $\epsilon_{\text{Nd}}$  values of –1.1, +0.8, and +1.6 (Fig. 2, Table 1), and suggest variable contamination from older crust. The  $^{147}\text{Sm}/^{144}\text{Nd}$  ratios for the lower volcanic cycle range from 0.1289 to 0.1410, indicative of LREE enrichment. The upper volcanic cycle  $\epsilon_{\text{Nd}}$  values range from +1.8 to +4.5, similar to values estimated for Late Archean depleted mantle (e.g. Abitibi belt of the Superior Province, Machado et al., 1986; eastern Slave Province, Davis and Hegner, 1992). The

$^{147}\text{Sm}/^{144}\text{Nd}$  ratios vary from 0.1394 to 0.1999, and given the elevated  $\epsilon_{\text{Nd}}$  values, suggest minor LREE-enrichment upon, or shortly before final eruption.

### Tavani

Four of the five basaltic samples from the Tavani area yielded  $\epsilon_{\text{Nd}}$  values of +2.1 to +3.4, similar to the upper volcanic cycle of the Rankin Inlet area. One sample (89TX-081) has a  $\epsilon_{\text{Nd}}$  value of +0.6, which may indicate a minor, yet undetermined amount of crustal contamination. The  $^{147}\text{Sm}/^{144}\text{Nd}$  ratios of 0.1279 to 0.2019 show that the Tavani samples are variably LREE-enriched to depleted. The Sm–Nd isotopic compositions of the Tavani samples are apparently not associated with structural or stratigraphic position.

## DISCUSSION AND INTERPRETATION

The data from the Rankin Inlet area indicate noticeable differences between the Sm–Nd isotopic compositions of the lower and upper volcanic cycles. The lower volcanic cycle yields  $\epsilon_{\text{Nd}}$  values ranging from –1.1 to +1.6. These values require the involvement of an older LREE-enriched component in the petrogenesis of these mafic rocks. The Nd isotopic compositions of the lower volcanic cycle may indicate that an older basement underlies the Rankin Inlet Group, and that lavas of the lower volcanic cycle were contaminated by older crustal

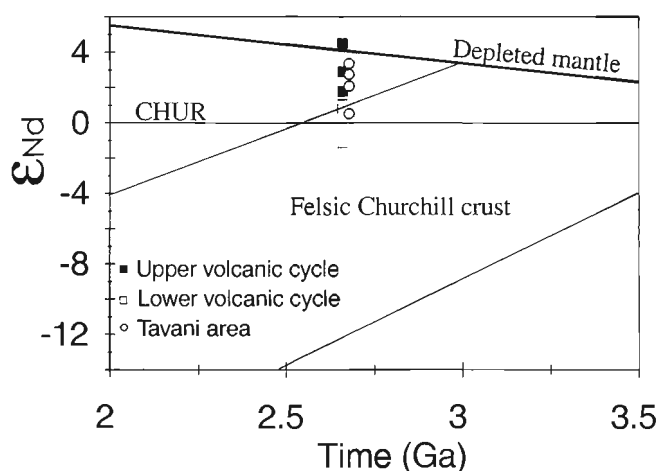


**Figure 2.**  $\epsilon_{\text{Nd}}$  versus Time plot for whole rock samples of the Rankin Inlet and Tavani areas. The  $\epsilon_{\text{Nd}}$  for Rankin Inlet samples calculated at 2.66 Ga, and  $\epsilon_{\text{Nd}}$  for Tavani area calculated at 2.68 Ga. Parameters for  $\epsilon_{\text{Nd}}$  calculations are:  $^{143}\text{Nd}/^{144}\text{Nd}_0(\text{CHUR}) = 0.512638$ ,  $^{147}\text{Sm}/^{144}\text{Nd} = 0.1967$  (Jacobsen and Wasserburg, 1980). Depleted mantle curve depicted according to parameters of Goldstein et al. (1984), where the mantle has evolved linearly since 4.5 Ga to  $\epsilon_{\text{Nd}0} = +10$ . Field for Churchill Province (Rae and Hearne provinces) felsic crust after Crocker et al., 1993; Dudás et al., 1991; Patchett and Arndt, 1986; Stevenson et al., 1989; Thériault, 1992; Thériault et al., 1994. CHUR = chondritic uniform reservoir.



rocks. Alternatively, the more evolved  $\epsilon_{\text{Nd}}$  values of the lower volcanic cycle may reflect contamination of the mantle source by subduction of terrigenous sediments. The  $^{147}\text{Sm}/^{144}\text{Nd}$  ratios, ranging from 0.1289 to 0.1410, indicate that the lower volcanic cycle rocks are enriched in LREE, consistent with the assimilation of a chemically differentiated contaminant. The degree of contamination remains uncertain, and an accurate evaluation of the contribution from an older crustal contaminant requires precise knowledge of the concentration and isotopic composition of the Nd provided by the uncontaminated source and the contaminant. In spite of these limitations, one can speculate on the nature of a potential crustal contaminant to the Rankin Inlet Group. Considering that the  $\epsilon_{\text{Nd}}$  value of -1.1 of sample 85TXA-399A represents an upper limit on the  $\epsilon_{\text{Nd}(2.66\text{ Ga})}$  value of the crustal contaminant, it is possible to estimate a  $T_{\text{DM}}$  model age for this crustal component. Assuming that the crustal component had a typical crust-like  $^{147}\text{Sm}/^{144}\text{Nd}$  ratio of 0.1 and an  $\epsilon_{\text{Nd}(2.66\text{ Ga})}$  value of -1.1, the corresponding  $T_{\text{DM}}$  is 3.01 Ga (using the parameters of Goldstein et al., 1984). It is important to note that the calculated  $T_{\text{DM}}$  age of 3.01 Ga is strictly a lower limit on the  $T_{\text{DM}}$  model age for a potential crustal contaminant, and that its true  $T_{\text{DM}}$  age is likely significantly older, given the fact that sample 85TXA-399A is a contaminated basalt and not the contaminant itself.

Although only three samples from the upper volcanic cycle have been analyzed, the  $\epsilon_{\text{Nd}}$  values of +1.8 to +4.5 indicate derivation from juvenile sources. The absence of obvious crustal contamination in the Nd isotopic compositions of the upper volcanic cycle suggests that the upper and lower volcanic cycles had different petrogenetic histories, and that perhaps they were emplaced in different tectonic settings. The lower volcanic cycle may have been emplaced in or near older continental crust whereas the upper volcanic cycle was emplaced in an environment devoid of older crust. The  $\epsilon_{\text{Nd}}$  values from the Tavani area (+0.6 to +3.4) suggest derivation mostly from juvenile source. One sample with an  $\epsilon_{\text{Nd}}$  value of +0.6 (sample 89TX-081) may indicate minor influence of an older component.

Older continental basement rocks have not been found in the Rankin Inlet and Tavani areas. Furthermore, Aspler and Chiarenzelli (1996b) propose that the Rankin-Ennadai belt was deposited in an oceanic setting which contained only minor fragments of pre-existing continental crust. This proposal is consistent with the Nd isotopic data for the Tavani area and the upper volcanic cycle, but fails to explain the Nd isotopic compositions of the lower volcanic cycle. The existence of Mid- to Early Archean age crystalline rocks in the Rankin-Ennadai belt has only been documented in the southwestern part of the belt, and include 3.3-3.1 Ga mafic granulites in the Athabasca lozenges in the southwestern part of the Snowbird tectonic zone of northern Saskatchewan (Hanmer et al., 1995) and granitic gneisses as old as  $3274 \pm 18$  Ma near Kasba Lake east of the Athabasca lozenges (Loveridge et al., 1988) (cf. Fig. 1). Thus, the nature of a crustal component in the Rankin Inlet Group and Tavani mafic volcanic rocks remains uncertain, and awaits further U-Pb geochronological, geochemical, and isotopic investigations of intercalated felsic volcanic and sedimentary rocks.

## CONCLUSIONS

Mafic volcanic rocks from the lower volcanic cycle of the Rankin Inlet Group yield  $\epsilon_{\text{Nd}}$  values suggesting variable contamination from an older crustal component. This may signify the presence of older basement to the Rankin Inlet Group, or mantle sources which were variably contaminated with continental materials. The  $T_{\text{DM}}$  age of the crustal contaminant is likely older than 3.01 Ga. Upper volcanic cycle rocks do not show compelling evidence of crustal contamination in their Nd isotopic compositions, which are similar to Late Archean depleted mantle signatures documented elsewhere in the Canadian Shield (Davis and Hegner, 1992; Machado et al., 1986; Vervoort et al., 1994). Tavani area mafic volcanic rocks generally give  $\epsilon_{\text{Nd}}$  values similar to those of the upper volcanic cycle of the Rankin Inlet Group, and may have formed remote from older crustal rocks.

## ACKNOWLEDGMENTS

Larry Aspler and Bill Davis are thanked for their constructive and insightful reviews.

## REFERENCES

- Aspler, L.B. and Chiarenzelli, Jeffery R.  
1996a: Geological compilation of the Hearne Province, south-central District of Keewatin, part of NTS areas 55 D-F, K-O. 65 A-D, F-J, P; EGS 1996-02. NWT Geology Division, Department of Indian Affairs and Northern Development, 1 map, scale 1:2 500 000.  
1996b: Stratigraphy, sedimentology and physical volcanology of the Henik Group, central Ennadai-Rankin greenstone belt, Northwest Territories, Canada: late Archean paleogeography of the Hearne Province and tectonic implications; *Precambrian Research*, v. 77, p. 59-89.
- Crocker, C.H., Collerson, K.D., Lewry, J.F., and Bickford, M.E.  
1993: Sm-Nd, U-Pb, and Rb-Sr geochronology and lithostructural relationships in the southwestern Rae province: constraints on crustal assembly in the western Canadian shield; *Precambrian Research*, v. 61, p. 27-50.
- Davis, W.J. and Hegner, E.  
1992: Neodymium isotopic evidence for the tectonic assembly of Late Archean crust in the Slave Province, northwest Canada; *Contributions to Mineralogy and Petrology*, v. 111, p. 493-504.
- Dudás, F.Ö., LeCheminant, A.N., and Sullivan R.W.  
1991: Reconnaissance Nd isotopic study of granitoid rocks from the Baker Lake region, District of Keewatin, N.W.T., and observations on analytical procedures; in *Radiogenic Age and Isotopic Studies: Report 4*; Geological Survey of Canada, Paper 90-2, p. 101-112.
- Goldstein, S.L., O'Nions, R.K., and Hamilton, P.J.  
1984: Sm-Nd isotopic study of atmospheric dusts and particulates from major river systems; *Earth and Planetary Science Letters*, v. 70, p. 221-236.
- Hanmer, S., Williams, M., and Kopf, C.  
1995: Striding--Athabasca mylonite zone: implications for the Archean and Early Proterozoic tectonics of the western Canadian Shield; *Canadian Journal of Earth Sciences*, v. 32, p. 178-196.
- Hulbert, L.J. and Gregoire, D.C.  
1993: Re-Os isotope systematics of the Rankin Inlet Ni ores: an example of the application of ICP-MS to investigate Ni-Cu-PGE mineralization and the potential use of Os isotopes in mineral exploration; *The Canadian Mineralogist, Journal of the Mineralogical Association of Canada*, v. 31, pt. 4, p. 861-876.
- Jacobsen, S.B. and Wasserburg, G.J.  
1980: Sm-Nd isotopic evolution of chondrites; *Earth and Planetary Science Letters*, v. 50, p. 139-155.

**Loveridge, W.D., Eade, K.E., and Sullivan, R.W.**

1988: Geochronological studies of Precambrian rocks from the southern District of Keewatin. Geological Survey of Canada, Paper 88-18, 36 p.

**Machado, N., Brooks, C. and Hart, S.R.**

1986: Determination of initial  $^{87}\text{Sr}/^{86}\text{Sr}$  and  $^{143}\text{Nd}/^{144}\text{Nd}$  in primary minerals from mafic and ultramafic rocks: experimental procedure and implications for the isotopic characteristics of the Archean mantle under the Abitibi greenstone belt, Canada, *Geochimica et Cosmochimica Acta*, v. 50, p. 2335-2348.

**Park, A.F. and Ralser, S.**

1992: Precambrian geology of the southwestern part of the Tavani map area, District of Keewatin, Northwest Territories; Geological Survey of Canada, Bulletin 416, 81 p.

**Patchett, P.J. and Arndt, N.T.**

1986: Nd isotopes and tectonics of 1.9-1.7 Ga crustal genesis; *Earth and Planetary Science Letters*, v. 78, p. 329-338.

**Richard, P., Shimizu, N., and Allègre, C.J.**

1976:  $^{143}\text{Nd}/^{146}\text{Nd}$ , a natural tracer: an application to oceanic basalts; *Earth and Planetary Science Letters*, v. 31, p. 269-278.

**Stevenson, R.K., Patchett, P.J., and Martin, R.F.**

1989: Sm-Nd isochron from a granodiorite-granite complex in the Portman Lake region, Northwest Territories; *Canadian Journal of Earth Sciences*, v. 26, p. 2724-2729.

**Tella, S.**

1994: Geology, Rankin Inlet (55K/16), Falstaff Island (55J/13), and Marble Island (55J/11), District of Keewatin, Northwest Territories; Geological Survey of Canada, Open File 2968, scale 1:50 000.

**Tella, S., Annesley, I.R., Borradile, G.J., and Henderson, J.R.**

1986: Precambrian geology of parts of Tavani, Marble Island and Chesterfield Inlet map areas, District of Keewatin, N.W.T.; Geological Survey of Canada, Paper 86-13, 20 p.

**Tella, S., Roddick, J.C., Park, A.F., and Ralser, S.**

1990: Geochronological constraints on the evolution of the Archean and Early Proterozoic terrane in the Tavani-Rankin Inlet region, District of Keewatin, N.W.T.; Geological Society of America, Abstracts with Programs, v. 22, no. 7, p. A174.

**Tella, S., Roddick, J.C., and van Breemen, O.**

1996: U-Pb zircon age for a volcanic suite in the Rankin Inlet Group, Rankin Inlet map area, District of Keewatin, Northwest Territories; in *Radiogenic Age and Isotopic Studies: Report 9*; Geological Survey of Canada, Current Research 1995-F, p. 11-15.

**Tella, S., Schau, M., Armitage, A.E., Seemayer, B.E., and Lemkow, D.**

1992: Precambrian geology and economic potential of the Meliadine Lake-Barbour Bay region, District of Keewatin, Northwest Territories; in *Current Research, Part C*; Geological Survey of Canada, Paper 92-1C, p. 1-11.

**Thériault, R.J.**

1992: Nd isotopic evolution of the Taltson Magmatic Zone, Northwest Territories, Canada: insights into Early Proterozoic accretion along the western margin of the Churchill Province; *Journal of Geology*, v. 100, p. 465-475.

**Thériault, R.J., Henderson, J.B., and Roscoe, S.M.**

1994: Nd isotopic evidence for early to mid-Archean crust from high grade gneisses in the Queen Maud Block and South of the McDonald Fault, western Churchill province, Northwest Territories; in *Radiogenic Age and Isotopic Studies: Report 8*; Geological Survey of Canada, Current Research 1994-F, p. 37-42.

**Vervoort, J.D., White, W.M., and Thorpe, R.I.**

1994: Nd and Pb isotope ratios of the Abitibi greenstone belt: new evidence for very early differentiation of the Earth; *Earth and Planetary Science Letters*, v. 128, p. 215-229.

**Wright, G.M.**

1967: Geology of the southeastern barren grounds, parts of the District of Mackenzie and Keewatin; Geological Survey of Canada, Memoir 350, 91 p.

# Preliminary U-Pb geochronology of the Hall Peninsula east of Iqaluit, southern Baffin Island

David J. Scott<sup>1</sup>

Continental Geoscience Division

*Scott, D.J., 1997: Preliminary U-Pb geochronology of the Hall Peninsula east of Iqaluit, southern Baffin Island; in Radiogenic Age and Isotopic Studies: Report 10; Geological Survey of Canada, Current Research, 1997-F, p. 67-78.*

---

**Abstract:** A corridor east of Iqaluit has been mapped and sampled for U-Pb geochronology; the initial U-Pb isotopic results of this study are presented here. At the western end of the corridor, an orthopyroxene monzogranite of the Cumberland batholith was emplaced at  $1857 \pm 5/-3$  Ma, and a younger garnetiferous phase at  $1850 \pm 3/-2$  Ma. These rocks intrude the central metasedimentary gneisses that were metamorphosed at ca. 1869 Ma; the metasedimentary rocks are interpreted as the northern continuation of the Tasiuyak gneiss of the Torngat Orogen. The eastern metatonic rocks are Archean, with emplacement ages of ca. 2921 Ma,  $2849 \pm 10/-7$  Ma,  $2844 \pm 6/-5$  Ma, and  $2797 \pm 27/-15$  Ma, and record variable tectonothermal overprints between 1844 and 1736 Ma. Possible correlatives of these rocks in West Greenland and northern Labrador are discussed.

**Résumé:** Un corridor à l'est d'Iqaluit a été cartographié et échantillonné aux fins d'études géochronologiques U-Pb; les résultats des analyses isotopiques par la méthode U-Pb sont livrés dans le présent rapport. À l'extrémité occidentale du corridor, un monzogranite à orthopyroxène du batholite de Cumberland a donné un âge de  $1857 \pm 5/-3$  Ma et une phase à grenat plus récente a été datée à  $1850 \pm 3/-2$  Ma. Ces intrusions recoupent les gneiss métasédimentaires de la partie centrale du corridor, lesquels ont été métamorphisés à environ 1869 Ma et qui constitueraient, selon les interprétations, le prolongement septentrional du gneiss de Tasiuyak de l'orogène de Torngat. Les roches métamorphiques de caractère tonalitique de la partie est sont archéennes, ayant livré des âges de mise en place d'environ 2921 Ma,  $2849 \pm 10/-7$  Ma,  $2844 \pm 6/-5$  Ma et  $2797 \pm 27/-15$  Ma. Ces roches ont conservé également la trace de divers événements tectonothermiques qui se sont déroulés entre 1844 et 1736 Ma. L'auteur discute de corrélations possibles de ces roches avec d'autres du Groenland occidental et du Labrador septentrional.

---

<sup>1</sup> GEOTOP, Université du Québec à Montréal, C.P. 8888, succursale centre-ville, Montréal (Québec) H3C 3P8

## INTRODUCTION

The Precambrian geology of southern Baffin Island comprises Archean metaplutonic rocks as well as Paleoproterozoic metaplutonic and metasedimentary rocks. The bedrock geology of the area was mapped at reconnaissance scale in 1965 (Blackadar, 1967). This investigation clearly outlined the major lithological packages present on the Hall Peninsula (Fig. 1), a poorly known region that links the Ungava and South Baffin orogens with the Torngat and Nagssugtoqidian orogens of northern Labrador and West Greenland. A more detailed examination of the geology of the Hall Peninsula was undertaken along an east-west corridor (Scott, 1996a), in order to evaluate the hypothesis that these rocks represent in part the along-strike continuation of the Torngat Orogen, and to determine the relationship of these rocks to the southeastern margin of the Cumberland batholith.

This work contributes to the Geological Survey of Canada's NE Laurentia program (St-Onge et al., 1996a,b; Hammer et al., 1996a,b; Scott et al., 1996) and the LITHOPROBE Eastern Canadian Shield Onshore-Offshore Transect (ECSOOT), and facilitates a more detailed comparison of geological events in southern Baffin Island with those in northernmost Labrador and northern Quebec.

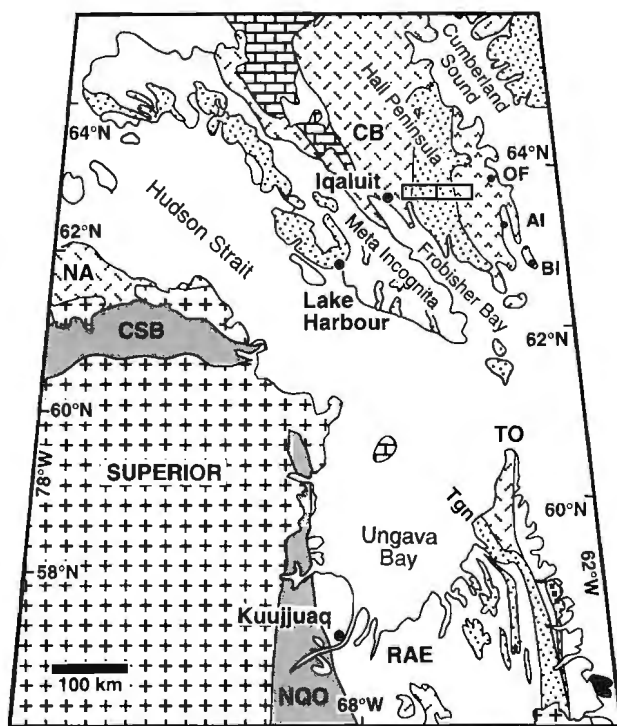


**Figure 1.** Location of study area on Hall Peninsula; rectangle east of Iqaluit outlines area shown in Figure 2. AI = Allen Island; BI = Brevoort Island; CB = Cumberland batholith; CSB = Cape Smith Belt; NA = Narsajuaq Arc; NQO = New Québec Orogen; OF = Okalik Fiord; Tgn = Tasiuyak gneiss; TO = Torngat Orogen. Modified from Hoffman (1989).

## GEOCHRONOLOGY OF THE HALL PENINSULA

The geology of the Hall Peninsula corridor is divisible into three principal lithological domains (Blackadar, 1967; Scott, 1996a, b): a western domain is dominated by orthopyroxene- and garnet-bearing monzogranites of the Cumberland batholith, a central domain comprises siliciclastic metasedimentary rocks (Tasiuyak gneiss) and subordinate metaplutonic rocks, and an eastern domain consists of tonalitic gneisses, monzogranite, and minor metasedimentary rocks (Fig. 2). Detailed descriptions of the rocks in each domain have recently been presented (Scott, 1996b). Initial U-Pb geochronological results are outlined, from west to east, in the following sections. Whereas U-Pb isotopic analysis of some samples is complete, results from other samples are preliminary. Where pending analyses are indicated, the reader is advised that revisions to the stated ages and consequent interpretations are to be expected.

### Analytical methods

Heavy minerals were separated from representative samples by standard crushing, grinding, hydrodynamic, and heavy liquid techniques. Sorting of the heavy mineral concentrates was performed using a Frantz isodynamic separator; highest-quality titanite and monazite were recovered at 0.5-0.75A (10° side slope) and zircon at -0.5 - -1° side slope (1.8A). Unless otherwise stated, only fracture- and inclusion-free crystals were selected for analysis (Table 1). Extraction of Pb and U from zircon and monazite followed the procedure outlined by Parrish et al. (1987); for titanite, a revised purification technique using UTEVA resin was used to purify U (Davis et al., 1997). Most of the zircon analyses are of single crystals or crystal fragments; multi-grain analyses are of restricted populations ( $n < 5$ ). Analytical data were reduced using algorithms developed by Roddick (1987).

### Western plutonic domain

The metaplutonic rocks of this domain have been interpreted as the southernmost exposures of the ca. 1.86 Ga Cumberland batholith (Jackson and Taylor, 1972; Jackson et al., 1990), and are the eastward continuation of the rocks examined by St-Onge et al. (1996a, b) and Scott et al. (1996), interpreted as part of a Paleoproterozoic magmatic arc (e.g. Hoffman, 1990). Whereas the petrogenesis of these rocks, which form one of the most extensive plutonic belts in the northeastern Canadian Shield, is not well known, they intrude the metasedimentary rocks of the central domain (Scott, 1996a). The southwest margin of the batholith (Fig. 1) is in tectonized intrusive contact with rocks of the Meta Incognita Peninsula (St-Onge et al., 1996a).

### Orthopyroxene-biotite monzogranite, Anna Maria Port (D351)

Medium- to coarse-grained orthopyroxene-biotite monzogranite is the dominant rock type in the western plutonic domain (Fig. 2), and indeed is typical of much of the southern exposure of the Cumberland batholith (Scott et al., 1996).

Zircon separated from this sample consists of colourless, short prismatic crystals. Whereas most of the diamagnetic grains are of high quality, some are altered and cracked. Five highly abraded crystals were analyzed individually (Fig. 3a); the five analyses regress to yield an upper intercept of  $1857 \pm 5/-3$  Ma and a lower intercept of 227 Ma. The upper intercept age is interpreted as the time of emplacement of the monzogranite at this location.

### Garnet-biotite monzogranite (D107)

Monzogranite characterized by the presence of biotite and deep-red garnet is a subordinate phase of the Cumberland batholith. Red-garnet monzogranite is commonly associated with variably digested rafts of semipelitic metasedimentary material, suggesting that much of the aluminum required to form garnet is derived from the metasedimentary inclusions (Scott, 1996b; Scott et al., 1996).

A wide variety of rounded zircon grains is present in this sample; due to the association with variably digested metasedimentary material, such grains are suspected to be xenocrysts and hence were not analyzed. Discrete, euhedral zircon overgrowths on some of the rounded crystals are the only euhedral zircon in the sample. Four such overgrowths, removed from their cores and heavily abraded, were analyzed individually. The four analyses are slightly to moderately discordant, and regress to yield an upper intercept of

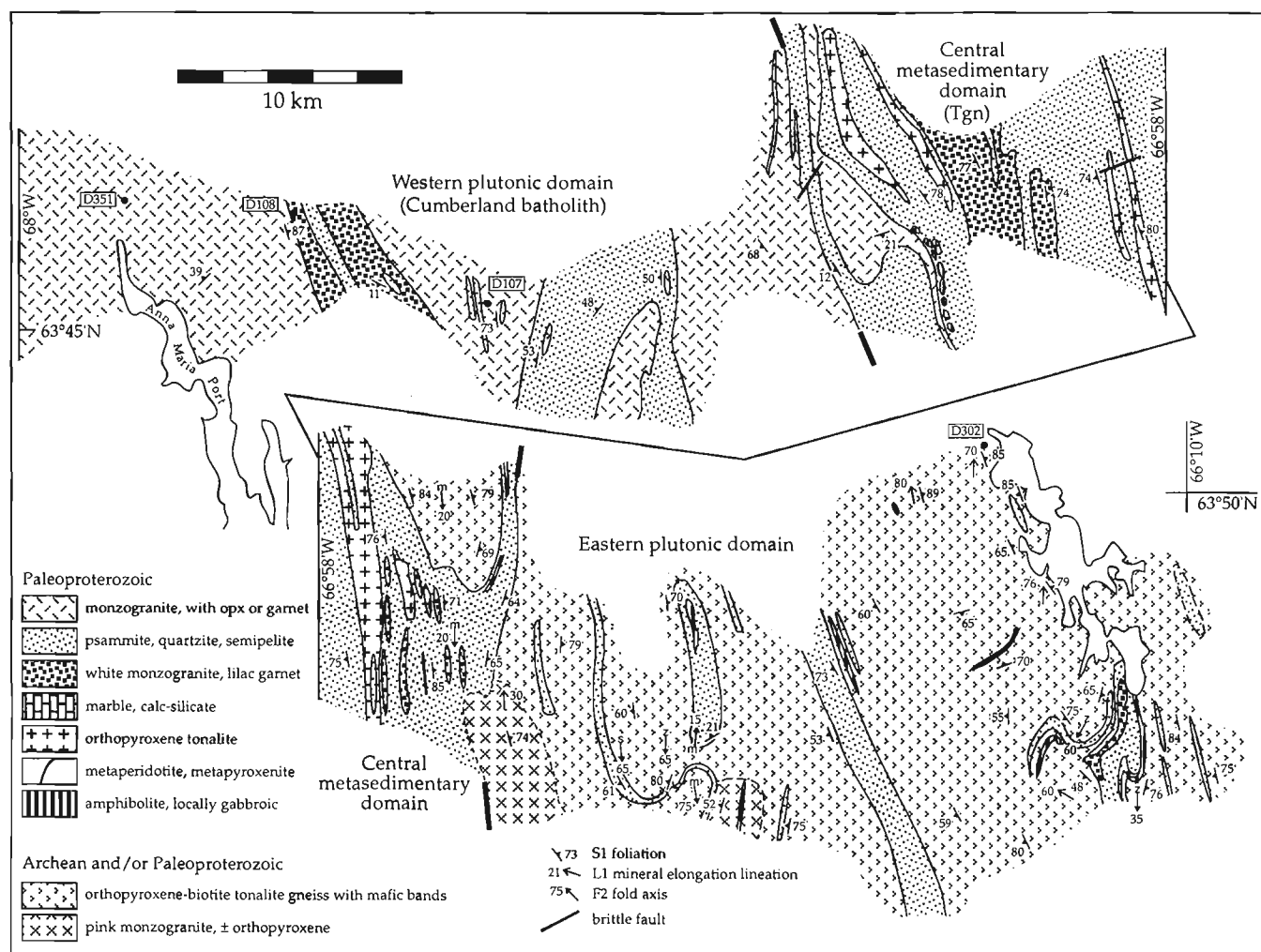


**Figure 2.** Geological map of the corridor examined east of Iqaluit on the Hall Peninsula. Locations of samples D351, D108, D107, and D302 are shown.

Table 1. U-Pb isotopic data.

Fraction			Concentrations			Atomic ratios					Age
Description [1]	# of grains	Weight ( $\mu$ g)	U (ppm) [2]	Pb (rad) (ppm) [2]	Pb (com) (pg) [3]	206 Pb / 204 Pb [4]	208 Pb / 206 Pb [5]	206 Pb / 238U [5] ( $\pm 1\sigma$ , %)	207 Pb / 235U [5] ( $\pm 1\sigma$ , %)	207 Pb / 206Pb [5] ( $\pm 1\sigma$ , %)	207 Pb / 206 Pb (Ma)
<b>Orthopyroxene-biotite monzogranite, Anna Maria Port (D351) 1857 <math>\pm</math> 5/-3 Ma</b>											
1 z, cl, eu, sp, dia	1	9	43	15	3	3401	0.079	0.3334 $\pm$ .10	5.224 $\pm$ .12	0.11364 $\pm$ .06	1858.5
2 z, cl, eu, sp, dia	1	4	47	16	3	1563	0.062	0.3304 $\pm$ .16	5.176 $\pm$ .21	0.11361 $\pm$ .15	1858.0
3 z, cl, eu, sp, dia	1	8	80	7	4	3116	0.094	0.3274 $\pm$ .15	5.125 $\pm$ .17	0.11354 $\pm$ .06	1856.8
4 z, cl, eu, sp, dia	1	7	39	13	2	2566	0.061	0.3312 $\pm$ .11	5.179 $\pm$ .12	0.11341 $\pm$ .06	1854.7
5 z, cl, eu, sp, dia	1	10	47	16	8	1495	0.091	0.3310 $\pm$ .11	5.174 $\pm$ .13	0.11339 $\pm$ .07	1854.5
<b>Garnet-biotite monzogranite (D107) 1850 <math>\pm</math> 3/-2 Ma; mz: ca. 1856 Ma</b>											
1 mz, p gr, eu, fr, IF	1	10	5827	11720	17	73090	5.864	0.3328 $\pm$ .09	5.208 $\pm$ .10	0.11351 $\pm$ .03	1856.3
2 mz, p gr, eu, fr, IF	1	5	6631	12680	6	121300	5.527	0.3325 $\pm$ .09	5.200 $\pm$ .10	0.11343 $\pm$ .03	1855.0
3 z, m br, eu, og, dia	1	6	896	291	5	23300	0.029	0.3306 $\pm$ .09	5.151 $\pm$ .10	0.11300 $\pm$ .03	1848.2
4 z, m br, eu, og, dia	1	4	620	201	5	13770	0.026	0.3292 $\pm$ .09	5.124 $\pm$ .11	0.11288 $\pm$ .03	1846.3
5 z, m br, eu, og, dia	1	6	1003	328	6	16940	0.036	0.3304 $\pm$ .09	5.141 $\pm$ .10	0.11287 $\pm$ .03	1846.1
6 z, m br, eu, og, dia	1	6	1044	331	6	15200	0.026	0.3236 $\pm$ .09	5.011 $\pm$ .10	0.11229 $\pm$ .03	1836.8
<b>White monzogranite (D108) 1869 <math>\pm</math> 9/-3 Ma; mz: 1862 <math>\pm</math> 3 Ma</b>											
1 z, m br, eu, og, dia	1	6	1782	579	4	47800	0.012	0.3352 $\pm$ .09	5.279 $\pm$ .10	0.11421 $\pm$ .03	1867.4
2 z, m br, eu, og, dia	1	5	3691	1186	6	65720	0.008	0.3332 $\pm$ .09	5.242 $\pm$ .10	0.11412 $\pm$ .03	1866.0
3 z, m br, eu, og, dia	1	5	1126	370	3	49630	0.023	0.3327 $\pm$ .08	5.229 $\pm$ .10	0.11398 $\pm$ .03	1863.7
4 mz, p yl, eu, IF	1	9	4334	6305	14	62390	3.913	0.3343 $\pm$ .09	5.250 $\pm$ .10	0.11391 $\pm$ .03	1862.6
5 mz, p yl, eu, IF	1	11	2519	7064	10	59070	8.561	0.3345 $\pm$ .08	5.247 $\pm$ .10	0.11379 $\pm$ .03	1860.8
<b>Orthopyroxene-biotite tonalite (D302) 2797 <math>\pm</math> 27/-15 Ma</b>											
1 z, cl, eu, sp, dia	3	8	302	189	4	22630	0.178	0.5306 $\pm$ .08	14.100 $\pm$ .09	0.19274 $\pm$ .03	2765.7
2 z, cl, eu, sp, dia	1	6	284	182	6	9565	0.215	0.5280 $\pm$ .09	13.963 $\pm$ .10	0.19178 $\pm$ .03	2757.5
3 z, cl, eu, sp, dia	3	12	298	188	9	1216	0.156	0.5250 $\pm$ .08	13.806 $\pm$ .12	0.19072 $\pm$ .06	2748.4
4 z, cl, eu, sp, dia	3	13	153	94	13	5143	0.163	0.5246 $\pm$ .09	13.784 $\pm$ .10	0.19057 $\pm$ .03	2747.1
5 z, cl, eu, sp, dia	4	6	227	139	7	6412	0.171	0.5204 $\pm$ .10	13.612 $\pm$ .11	0.18970 $\pm$ .03	2739.6
<b>Foliated tonalite, Brevoort Island (D352A) 2844 <math>\pm</math> 6/-5 Ma</b>											
1 z, cl, eu, sp, dia	1	3	115	71	2	5361	0.106	0.5447 $\pm$ .11	15.011 $\pm$ .11	0.19988 $\pm$ .04	2825.2
2 z, cl, eu, sp, dia	1	4	45	27	4	1620	0.088	0.5368 $\pm$ .13	14.649 $\pm$ .13	0.19793 $\pm$ .06	2809.2
3 z, cl, eu, sp, dia	3	6	77	51	36	382	0.096	0.5355 $\pm$ .14	14.505 $\pm$ .24	0.19645 $\pm$ .17	2796.9
4 z, cl, eu, sp, dia	1	3	88	51	4	2007	0.075	0.5314 $\pm$ .14	14.367 $\pm$ .14	0.19610 $\pm$ .07	2794.0
5 z, cl, eu, sp, dia	3	6	118	65	6	3406	0.080	0.5024 $\pm$ .10	13.064 $\pm$ .11	0.18860 $\pm$ .04	2730.0
<b>Granitic vein in tonalite, Brevoort Island (D352B) (2820 <math>\pm</math> 5 Ma) og: 1842 <math>\pm</math> 4/-2 Ma</b>											
1 z, cl, eu, sp, dia	3	7	102	62	10	2238	0.097	0.5362 $\pm$ .10	14.632 $\pm$ .11	0.19792 $\pm$ .04	2809.1
2 z, cl, eu, sp, dia	1	4	146	83	4	5264	0.064	0.5280 $\pm$ .09	14.147 $\pm$ .10	0.19433 $\pm$ .03	2779.1
3 z, cl, eu, sp, dia	4	4	218	129	8	3233	0.097	0.5286 $\pm$ .09	14.144 $\pm$ .10	0.19405 $\pm$ .03	2776.8
4 z, cl, eu, sp, dia	4	4	258	154	11	3543	0.136	0.5182 $\pm$ .09	13.803 $\pm$ .10	0.19317 $\pm$ .03	2769.4
5 z, p br, eu, og, dia	1	5	1131	357	4	31150	0.001	0.3297 $\pm$ .08	5.116 $\pm$ .10	0.11257 $\pm$ .03	1841.3
6 z, p br, eu, og, dia	1	6	3086	975	8	47470	0.003	0.3293 $\pm$ .10	5.107 $\pm$ .10	0.11247 $\pm$ .03	1839.6
7 z, p br, eu, og, dia	1	8	1749	549	11	31030	0.002	0.3271 $\pm$ .09	5.069 $\pm$ .10	0.11239 $\pm$ .03	1838.4
<b>Foliated tonalite, Allen Island (D353A) (ca. 2921 Ma) og: ca. 1844 Ma</b>											
1 z, cl, eu, eq, dia	1	10	96	62	6	9557	0.116	0.5650 $\pm$ .09	16.363 $\pm$ .10	0.21005 $\pm$ .03	2905.9
2 z, cl, eu, eq, dia	1	9	89	58	7	3987	0.134	0.5586 $\pm$ .09	16.067 $\pm$ .11	0.20860 $\pm$ .03	2894.7
3 z, p br, eu, og, dia	1	3	734	231	12	3331	0.002	0.3257 $\pm$ .09	5.062 $\pm$ .10	0.11273 $\pm$ .04	1843.9
<b>Granitic vein in tonalite, Allen Island (D353B) 2835 <math>\pm</math> 11 Ma; og: ca. 1760 Ma; t: 1736 <math>\pm</math> 2 Ma</b>											
1 z, cl, eu, sp, dia	1	15	79	48	5	9034	0.091	0.5471 $\pm$ .10	15.101 $\pm$ .11	0.20019 $\pm$ .04	2827.8
2 z, p br, eu, sp, dia	1	8	131	77	5	6624	0.092	0.5281 $\pm$ .11	14.239 $\pm$ .12	0.19555 $\pm$ .03	2789.4
3 z, p br, eu, sp, dia	1	7	100	59	6	4080	0.089	0.5286 $\pm$ .11	14.236 $\pm$ .12	0.19532 $\pm$ .03	2787.5
4 z, m br, eu, og, dia	1	3	1202	387	3	2327	0.062	0.3129 $\pm$ .08	4.644 $\pm$ .11	0.10763 $\pm$ .05	1759.6
5 t, m br, eu, fr, IF	4	32	205	66	43	2976	0.095	0.3100 $\pm$ .17	4.543 $\pm$ .19	0.10630 $\pm$ .04	1736.8
6 t, m br, eu, fr, IF	4	30	203	65	45	3066	0.084	0.3075 $\pm$ .10	4.504 $\pm$ .11	0.10624 $\pm$ .05	1735.9
<b>Foliated tonalite, Okalik Fiord (D354A) 2849 <math>\pm</math> 10/-7 Ma</b>											
1 z, p br, eu, lp-ac, dia	4	5	269	156	6	8990	0.034	0.5473 $\pm$ .09	15.152 $\pm$ .10	0.20079 $\pm$ .03	2832.6
2 z, cl, eu, lp-ac, dia	3	4	325	190	5	9268	0.041	0.5459 $\pm$ .09	15.113 $\pm$ .10	0.20078 $\pm$ .03	2832.5
3 z, p br, eu, lp-ac, dia	1	6	99	57	5	4000	0.027	0.5433 $\pm$ .12	14.945 $\pm$ .12	0.19952 $\pm$ .04	2822.3
4 z, p br, eu, lp-ac, dia	1	6	86	48	5	3395	0.036	0.5270 $\pm$ .10	14.244 $\pm$ .11	0.19601 $\pm$ .04	2793.3

Table 1. (cont.)

Fraction			Concentrations			Atomic ratios					Age
Description	# of grains	Weight (μg)	U (ppm)	Pb (rad) (ppm)	Pb (com) (pg)	206 Pb/ 208 Pb/ 204 Pb	206 Pb/ 238U [5]	207 Pb/ 235U [5]	207 Pb/ 206Pb [5]	207 Pb/ 206 Pb	
[1]			[2]	[2]	[3]	[4]	[5]	(± 1σ, %)	(± 1σ, %)	(± 1σ, %)	(Ma)
Granitic vein in tonalite, Okalik Fiord (D354B) (2768 ± 13 Ma); og: ca. 1829 Ma											
1 z, p br, eu, lp-ac, dia	1	4	975	496	11	10210	0.016	0.4937±.08	12.384±.10	0.18192±.03	2670.5
2 z, p br, eu, lp-ac, dia	1	4	1584	818	11	17120	0.017	0.4876±.08	12.110±.11	0.18014±.05	2654.2
3 z, p br, eu, lp-ac, dia	2	9	1815	856	29	15850	0.024	0.4574±.09	10.848±.10	0.17200±.03	2577.2
4 z, p br, eu, lp-ac, dia	2	7	2428	1114	17	26350	0.021	0.4397±.09	10.251±.11	0.16908±.04	2548.5
5 z, m br, eu, og, dia	1	4	878	275	5	15650	0.004	0.3259±.10	5.010±.11	0.11149±.03	1823.9
6 z, m br, eu, og, dia	1	6	534	160	11	5462	0.008	0.3114±.09	4.659±.10	0.10853±.04	1774.9
[1] Mineral: z = zircon; mz = monazite; t = titanite. Colour: cl = colourless; pk = pink; br = brown; yl = yellow; gr = green; p = pale; m = medium Form: eq = equant; sp = short prism; lp = long prism; ac = acicular; eu = euhedral; og = overgrowth; fr = fragment. Magnetic properties: dia = diamagnetic at -0.5° tilt of Frantz magnetic separator; IF = non-magnetic between 0.5 and 1.0A at 10° side slope.											
[2] Concentrations are known to <10% for sample weights above 20 μg, 10-20% for weights below 20 μg.											
[3] Total common Pb present in analysis corrected for Pb in spike and fractionation.											
[4] Measured ratio, corrected for fractionation and spike.											
[5] Ratios corrected for spike, fractionation, blank, and initial common Pb. Errors quoted are at the 1-sigma confidence level.											

1850±3/-2 Ma (Fig. 3b). Two euhedral fragments of pale greenish-yellow monazite have been analyzed; both are slightly discordant, with analytically indistinguishable  $^{207}\text{Pb}/^{206}\text{Pb}$  ages of 1856.3 and 1855.0 Ma, respectively (Fig. 3b). A possible interpretation of these data is that the age of the zircon overgrowths (1850±3/-2 Ma) represents the crystallization of the monzogranite, and that the two slightly older monazite fragments are xenocrysts inherited from the associated metasedimentary rocks.

### White monzogranite (D108)

Distinctive, white-weathering monzogranite, characterized by the presence of abundant lilac garnets, is intimately associated with the metasedimentary rocks of the western domain (Scott, 1996b). It occurs as diffuse, irregular seams or pods generally parallel to compositional layering and foliation in the clastic rocks, and as discrete, tabular bodies locally discordant to layering. The intimate spatial relationship with the metasedimentary rocks suggests that the monzogranite may be derived locally by anatexis of the host metasedimentary rocks (Scott, 1996b).

The wide variety of rounded zircon crystals present in this sample and the inferred origin by partial melting of metasedimentary material suggests that much of the zircon may be xenocrystic. Euhedral, medium-brown overgrowths are present on many of the rounded zircon crystals, and are essentially the only euhedral zircon in the sample. Three such overgrowths, removed from their cores and heavily abraded, have been analyzed individually. All of the analyses are ~0.2 to 0.8% discordant, with  $^{207}\text{Pb}/^{206}\text{Pb}$  ages between 1867 and 1864 Ma (Fig. 3c). The analyses regress to yield an upper intercept of 1869±9/-3 Ma. Euhedral monazite is present in this sample; two crystals, analyzed individually, have  $^{207}\text{Pb}/^{206}\text{Pb}$  ages of 1862.6 and 1860.8 Ma (Fig 3c). The age of the zircon overgrowths, and probable time of crystallization of the white monzogranite, is interpreted as 1869±9/-3 Ma. The average age of the monazite, 1862 ± 3 Ma, is interpreted

as the time at which the present monzogranite sample cooled through the blocking temperature of monazite (ca. 725°C, Parrish, 1990).

### Central metasedimentary domain

The dominant rock type in the central domain (Fig. 2) is rusty-weathering biotite psammite with ubiquitous lilac garnet, identical to that found as enclaves in the western plutonic domain (Scott, 1996). These rocks physically resemble and are along strike from the ca. 1.93 Ga Tasiuyak paragneiss of the Torngat Orogen (Fig. 1) (Scott and Gauthier, 1996). It has been suggested that the present unit and the Tasiuyak paragneiss are lateral equivalents (Hoffman, 1989; Scott and Gauthier, 1996). Sheets of fine- to medium-grained orthopyroxene-biotite tonalite up to one kilometre thick and several kilometres long (Fig. 2) intrude the metasedimentary rocks of the central domain. An intrusive age of 1890 ± 2 Ma has been determined for one of these bodies (Scott, 1996b), providing a younger bracket on the timing of sedimentation.

Pb-isotopic compositions of detrital zircons extracted from a representative sample of psammite have been analyzed using the Laser Ablation Microprobe ICP-MS technique (Scott and Gauthier, 1996). The  $^{207}\text{Pb}/^{206}\text{Pb}$  ages of fifty-three individual grains were determined; ~60% are younger than ca. 2.0 Ga, and none are older than 2.4 Ga. These data indicate a depositional age younger than 2.0 Ga, and suggest that extensive Archean material was not available in the source region during sedimentation. Zircon overgrowths, removed from rounded detrital grains and analyzed individually using the conventional isotope dilution thermal ionization technique (U-Pb) are 1852 ± 2 Ma (Scott and Gauthier, 1996), interpreted as the age of the thermal peak of metamorphism at this location and possibly coincident with the generation of the white, garnetiferous monzogranites. Monazite recovered from two representative psammite samples will be analyzed in an attempt to quantify the timing of the high-grade metamorphism recorded by these rocks.

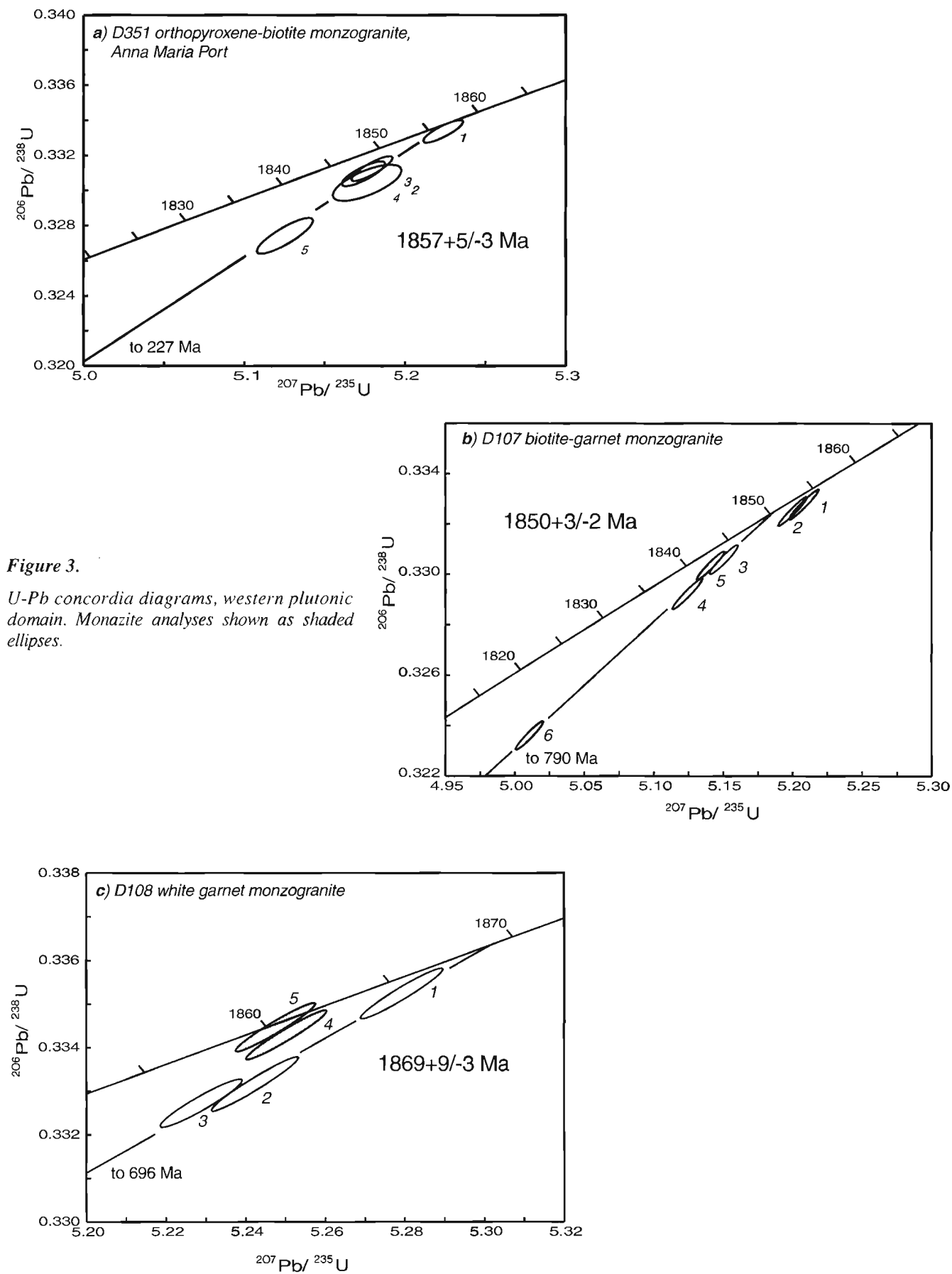


**Figure 3.**

*U-Pb concordia diagrams, western plutonic domain. Monazite analyses shown as shaded ellipses.*



### Eastern plutonic domain

The boundary between the metasedimentary rocks of the central domain and the metaplutonic rocks of the eastern domain is drawn at the easternmost occurrence of continuous panels of metasedimentary rocks (Fig. 2). Similar metasedimentary rocks also occur within the eastern domain. Fine- to medium-grained orthopyroxene-biotite tonalite is the dominant rock type in the eastern plutonic domain. It is commonly finely layered, weakly to moderately foliated, and characterized by the presence of disrupted mafic layers or xenoliths (Scott, 1996a). Pegmatitic granitic veining, predominantly parallel to layering but locally discordant, contributes to the overall streaky, gneissic appearance of these rocks.

### Orthopyroxene-biotite tonalite (D302)

A representative sample of medium-grained, orthopyroxene-biotite tonalite was collected near the eastern edge of the transect area (Fig. 2). Orthopyroxene is extensively retrogressed to hornblende. The diamagnetic fraction of the heavy minerals comprises almost exclusively colourless, short, prismatic zircon crystals, although many are extensively cracked and fragmented, and contain colourless, needle-shaped (fluid?) inclusions.

Four multigrain fractions and one single grain were analyzed. The five analyses regress to yield an upper intercept of  $2797 \pm 27/-15$  Ma and a lower intercept of 2093 Ma (Fig. 4). The upper intercept is interpreted as the age of emplacement of the tonalite; the lower intercept suggests that this sample experienced a Paleoproterozoic tectonothermal event.

### Reconnaissance samples, east coast

Coastal exposures of the eastern tonalitic gneisses were examined at three localities (Fig. 1); logistical considerations precluded geological mapping in these areas, so the following samples were collected for "reconnaissance" age determinations.

At each location, samples of the dominant rock type (foliated to gneissic tonalite) and subordinate granitic veining were collected.

### Foliated tonalite with granitic veins, Brevoort Island (D352)

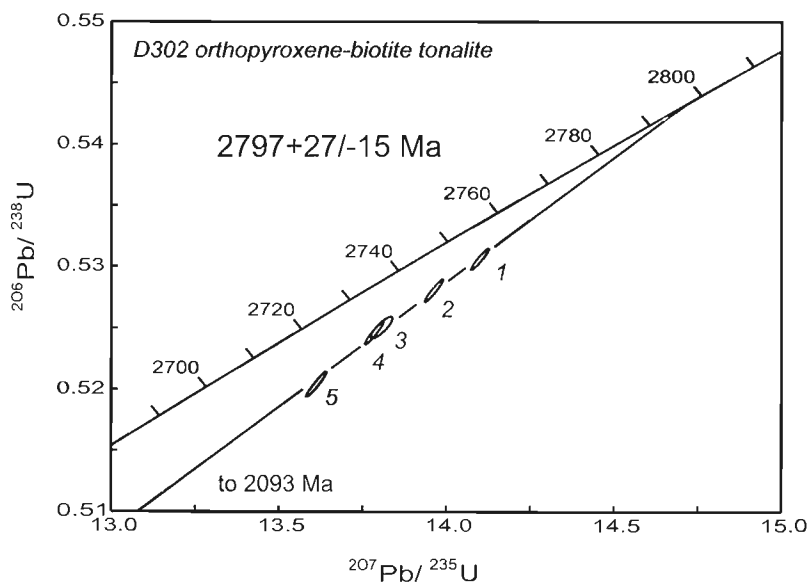
Samples of weakly foliated hornblende-biotite tonalite (D352A) cut by narrow, discrete pink granitic veins (D352B) were collected near the shed adjacent to the airstrip on Brevoort Island (Fig. 1). The host tonalite is slightly more biotite-rich adjacent to the veins, suggesting the veins may have been generated by in situ partial melting of the host tonalite.

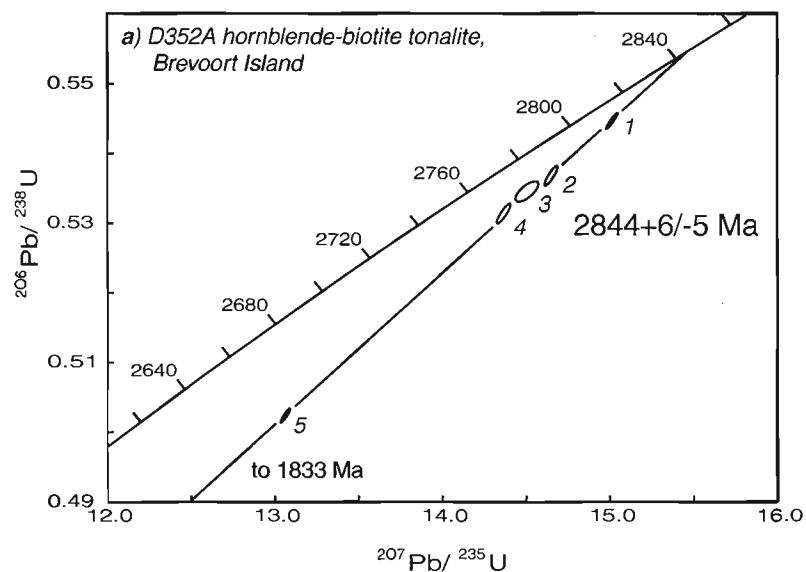
Zircon separated from the foliated tonalite is dominantly colourless and of relatively high quality; short, prismatic crystals are by far the most common morphology. Concentric (growth?) zoning was observed in transmitted light (petrographic microscope, condenser in) in many of the crystals. Three single grain and two multigrain fractions were analyzed (Fig. 5a); they regress to yield an upper intercept of  $2844 \pm 6/-5$  Ma and a lower intercept of 1833 Ma. The upper intercept is interpreted as the emplacement age of the tonalite, while the lower intercept is suggestive of a younger tectonothermal event.

Short prismatic crystals are the dominant zircon morphology recovered from the pink granitic vein sampled (D352B), although many of these grains are overgrown by medium-brown zircon. Three multi-grain and one single grain fractions of colourless prisms were analyzed; all are discordant (1.8–3.4%), with  $^{207}\text{Pb}/^{206}\text{Pb}$  ages between 2809 and 2769 Ma (Fig. 5b). Three fragments of brown overgrowths, physically separated from their respective cores, were extensively abraded and analysed individually. The three analyses regress to yield an upper intercept of  $1842 \pm 4/-2$  Ma, interpreted as the time of formation of the overgrowths. A reference line from the age of the brown overgrowths, 1842 Ma, through the analyses of two of the youngest colourless prisms

**Figure 4.**

*U-Pb concordia diagram, eastern tonalitic gneiss.*



**Figure 5.**

*U-Pb concordia diagrams, east coast reconnaissance samples. Titanite analyses shown as shaded ellipses.*

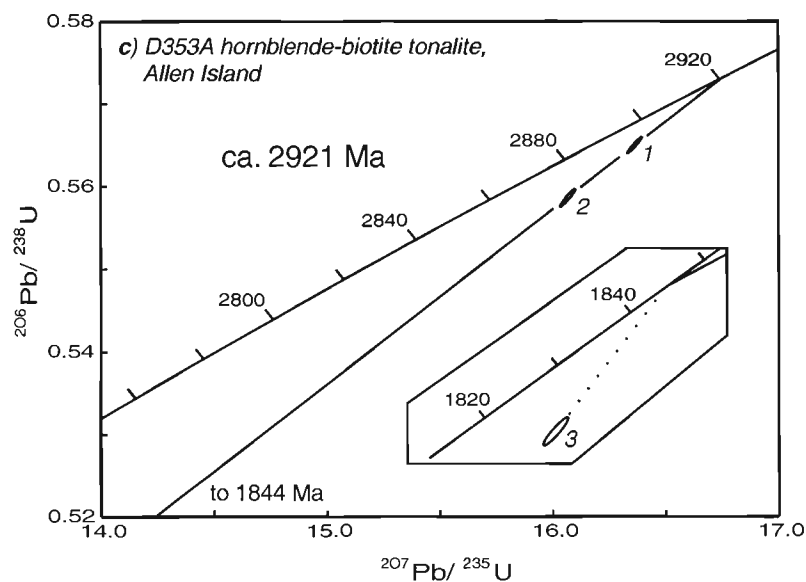
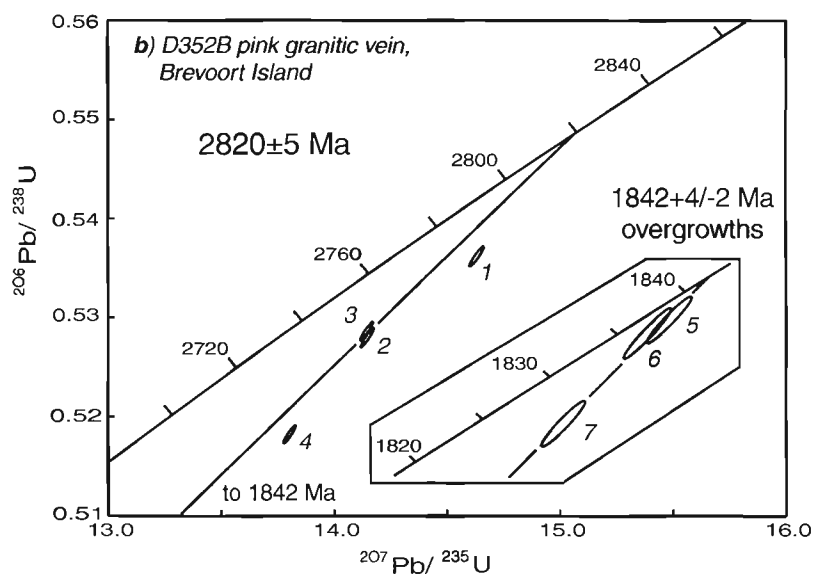
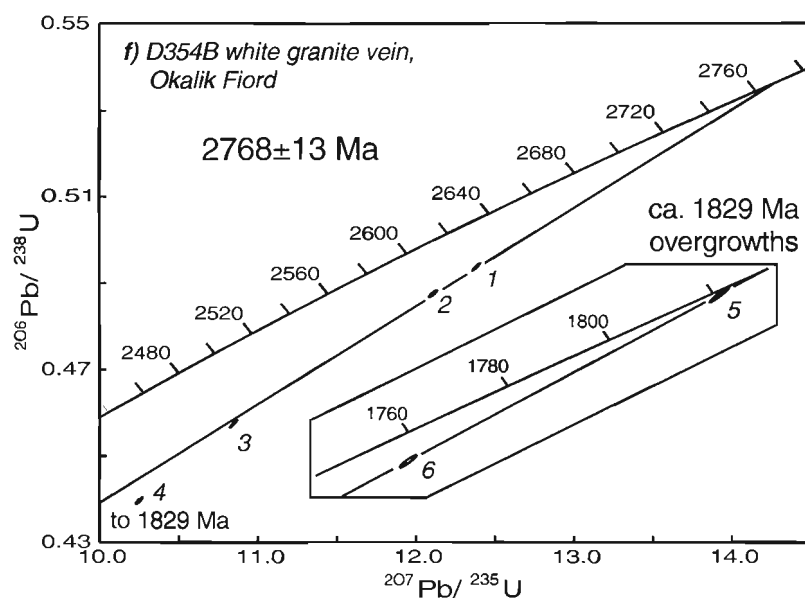
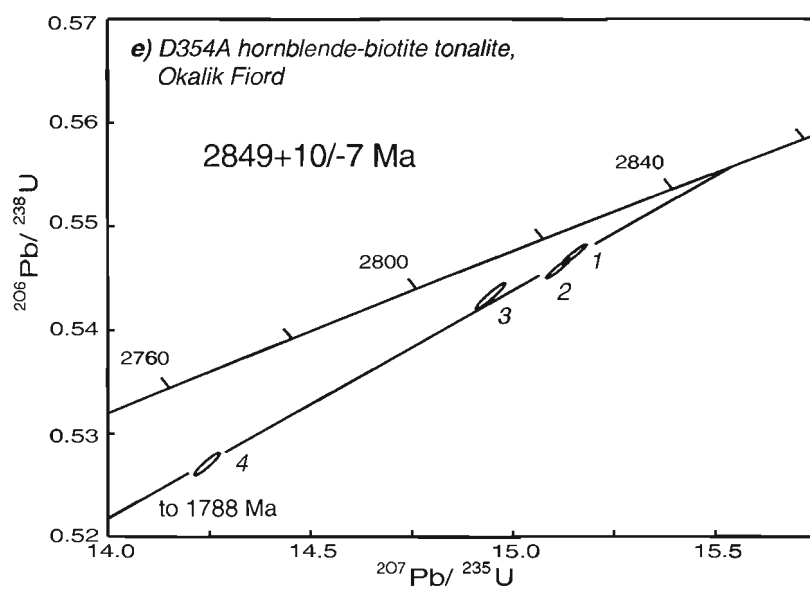
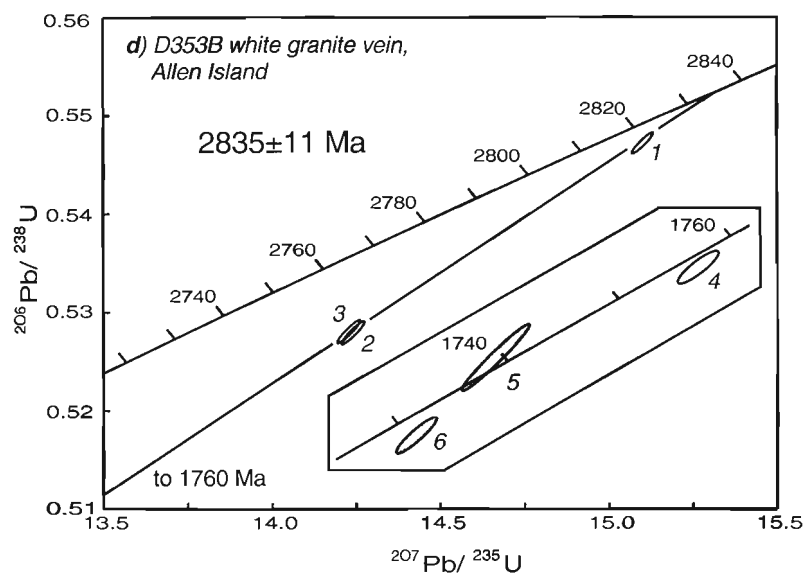


Figure 5. (cont.)



yields an upper intercept with concordia of  $2820 \pm 5$  Ma; this is interpreted as the minimum age of the colourless crystals. It seems reasonable to suggest that  $1842 \pm 4/-2$  Ma represents the age of formation of the granitic veins, possibly by partial melting of the tonalitic host rock, and that the colourless prisms ( $>2820$  Ma) are xenocrysts from the host (2844 Ma) tonalite.

#### **Foliated tonalite with granitic veins, Allen Island (D353)**

Representative samples of foliated hornblende-biotite tonalite (D353A) with narrow, discrete white granitic veins (D353B) were collected from a cliff face on the west side of Allen Island (Fig. 1).

Zircon and titanite were recovered from the foliated tonalite; most of the zircon in the diamagnetic population consists of colourless, euhedral prisms, but medium-brown overgrowths are present on a small proportion of the crystals. Two colourless prisms have been analyzed individually; both are discordant, with  $^{207}\text{Pb}/^{206}\text{Pb}$  ages of 2906 and 2895 Ma (Fig. 5c). A single pale-brown overgrowth is discordant, with a  $^{207}\text{Pb}/^{206}\text{Pb}$  age of 1844 Ma. A reference line from 1844 Ma through the analyses of the two prisms has an upper intercept age of 2921 Ma, interpreted as the minimum age of the colourless zircons. Additional analyses of colourless prisms and overgrowths will refine the above interpretation; analyses of titanite are pending.

Colourless to pale-brown euhedral zircon prisms, some with medium-brown overgrowths, and titanite were recovered from the sampled white granitic vein (D353B). Three colourless prisms, analyzed individually, are variably discordant with  $^{207}\text{Pb}/^{206}\text{Pb}$  ages between 2829 and 2788 Ma (Fig. 5d). An analysis of a single medium-brown overgrowth, removed from its core and heavily abraded, is 0.3% discordant with a  $^{207}\text{Pb}/^{206}\text{Pb}$  age of 1760 Ma. Two multigrain analyses of titanite are identical in age at  $1736 \pm 2$  Ma. A regression of the three colourless prism analyses, forced through 1760 Ma, yields a discordia with an upper intercept of  $2835 \pm 11$  Ma, interpreted as the minimum crystallization age of the colourless zircon. The 1760 Ma age of the overgrowth is tentatively interpreted as the age of a significant tectonothermal event. The titanite age may represent final cooling through ca. 700°C (Scott and St-Onge, 1995) following this event. One possible explanation of these data is that the veins were formed at  $2835 \pm 11$  Ma, and strongly metamorphosed at ca. 1760–1736 Ma; alternatively, the colourless zircons may be xenocrysts in a vein formed at ca. 1760 Ma, subsequently metamorphosed at  $1736 \pm 2$  Ma. Additional analyses of both types of zircon are pending.

#### **Foliated tonalite with granitic veins, Okalik Fiord (D354)**

Samples of foliated hornblende-biotite tonalite (D354A) with discrete white granitic veins (D354B) parallel to the foliation were collected at the head of Okalik Fiord (Fig. 1).

Zircon recovered from the foliated tonalite consists dominantly of short, prismatic to acicular crystals that range from colourless to pale brown. Two multigrain fractions and two single crystals analyzed individually regress to yield a discordia with an upper intercept of  $2849 \pm 10/-7$  Ma and a lower intercept of 1788 Ma (Fig. 5e). The upper intercept is interpreted as the emplacement age of the tonalite, whereas the lower intercept strongly suggests the effects of a significant Paleoproterozoic tectonothermal event are recorded. Titanite recovered from this sample has yet to be analyzed.

Much of the zircon separated from the white granitic vein (D354B) is physically similar to that in the host tonalite, principally pale-brown, short, prismatic to needle-like crystals. Medium-brown overgrowths are present on many of the short, prismatic grains. Two single crystals and two two-grain fractions have been analyzed; all are significantly discordant (3.8–9.3%), with  $^{207}\text{Pb}/^{206}\text{Pb}$  ages between 2671 and 2549 Ma (Fig. 5f). Two medium-brown overgrowths, removed from their cores, strongly abraded and analyzed individually, have  $^{207}\text{Pb}/^{206}\text{Pb}$  ages of 1823.9 Ma (0.3% discordant) and 1774.9 Ma (1.8% discordant), respectively. A reference line through the two analyzed overgrowths has an upper intercept of 1829 Ma, interpreted as an estimate of the crystallization age of the zircon overgrowths. A reference line from 1829 Ma through the analyses of the two most concordant short prismatic crystals has an upper intercept of  $2768 \pm 13$  Ma, interpreted as an estimate of the minimum age of the pale-brown prisms. One explanation of these data is that the white granitic veins formed at  $2768 \pm 13$  Ma, and were metamorphosed at ca. 1829 Ma; alternatively, the pale-brown prisms may be xenocrysts in a vein formed at ca. 1829 Ma. Titanite recovered from this sample has yet to be analyzed.

## **DISCUSSION**

The metaplutonic rocks of the western domain represent the southern continuation of the ca. 1.86 Ga Cumberland batholith (Jackson and Taylor, 1972; Jackson et al., 1990). The eastern limit of the batholith is an intrusive contact with the metasedimentary rocks of the central domain; the southwest margin is a tectonized intrusive contact with gneisses of the Meta Incognita Peninsula (St-Onge et al., 1996a; Scott et al., 1996). The present results suggest that the main orthopyroxene-biotite phase of the monzogranite (D351) was emplaced at  $1857 \pm 5/-3$  Ma, whereas the subordinate red-garnet phase (D107) was emplaced at  $1850 \pm 3/-2$  Ma. Generation of the lilac-garnet white monzogranite (D108) in the host metasedimentary rocks may have occurred ca. 1869 Ma, suggesting that these rocks were metamorphosed prior to emplacement of the Cumberland batholith.

The Archean rocks of the eastern domain, and the those sampled along the coast, collectively document a protracted history of late Archean tonalitic magmatism, from possibly as old as ca. 2.92 Ga (D353A), to 2.80 Ga (D302). The two intermediate-aged samples are identical within error at 2.85 Ga (D352A and D354A). The U-Pb systematics of all of these samples show evidence of substantial disruption in the

Paleoproterozoic. Formation of subordinate granitic veins at 1.84-1.83 Ga (D352B, D354B) and ca. 1.76 Ga (D353B) documents a period of penetrative and widespread metamorphism during this period. Titanite at 1.74 Ga (D353B) may bracket the waning stages of this event. The possible significance of these observations is discussed below.

## REGIONAL CORRELATIONS

Based on similarities in lithological assemblage, metamorphic grade, along-strike continuity of aeromagnetic anomaly patterns (Hoffman, 1989), and detrital zircon ages (Scott and Gauthier, 1996), it seems reasonable to concur with Hoffman's (1989) suggestion that the rocks of the central domain may represent the northern continuation of the Tasiuyak gneiss complex of the Torngat Orogen (northern Labrador). The 1.89 Ga orthopyroxene-biotite tonalite sheets in the central metasedimentary rocks are identical in age to similar rocks that intrude the Tasiuyak gneiss in northern Labrador (Scott and Machado, 1995; Scott, 1995a). Metamorphism of the metasedimentary rocks occurred between ca. 1869 Ma (D108) and 1850 Ma (Scott and Gauthier, 1996), corresponding to the end of extensive felsic plutonism in the Torngat Orogen. The 1.84-1.76 Ga thermal event documented in the eastern Archean rocks is synchronous with movement within the Abloviak and Komaktorvik shear zones in northern Labrador (Bertrand et al., 1993; Scott and Machado, 1995).

Whereas the Paleoproterozoic tectonic link between northern Labrador and southern Baffin appears reasonable, the tectonic significance and cratonic affinity of the Archean metaplutonic rocks of the eastern domain and coastal region are not clear. Several possibilities have been suggested. These rocks may represent: 1) a distinct Archean microcontinent (Burwell craton, Hoffman, 1989); 2) reworked Archean gneisses of the Nagsugtoquidian Orogen of West Greenland (Jackson et al., 1990); or 3) the northern continuation of the Archean Nain craton (Scott and Campbell, 1993). The metasedimentary rocks within the eastern domain, although physically similar to the Paleoproterozoic units of the central domain, are of unknown age and affinity.

The southern continuation of Hoffman's (1989) Burwell craton has been shown to comprise rocks of the Nain craton and 1.91-1.87 Ga intrusions (Scott, 1995a, b), thus the existence of a discrete Burwell craton is considered doubtful. Scott and Campbell (1993) have suggested that the Archean Nain craton may in part continue northward onto the Hall Peninsula, based in large part on the northward continuity of Paleoproterozoic units. Although synchronous tonalitic magmatism has been documented in northern Labrador (Scott, 1995b), discordant mafic dykes, which are characteristic of the Nain craton in Labrador and correlative southern parts of the North Atlantic craton in West Greenland, have not been observed during reconnaissance of the eastern coastal area.

Jackson et al. (1990) have correlated the rocks of the eastern domain with reworked Archean gneisses of the Nagsugtoquidian Orogen in West Greenland. Recent reconnaissance SHRIMP

U-Pb analyses in West Greenland by Kalsbeek and Nutman (1995) has begun to document the limited extent of ca. 1.9 Ga metaplutonic rocks in ca. 2.9-2.6 Ga essentially dyke-free tonalitic gneisses. Detailed conventional U-Pb dating by Connelly and Mengel (1996) documents an Archean magmatic evolution (2.88-2.84 Ga) strongly overprinted by Paleoproterozoic tectonothermal activity (1.85-1.83 Ga); the timing of these magmatic and thermal events strongly resemble that of the eastern gneisses, and supports a correlation across Davis Strait.

The timing of amalgamation of potentially distinct Archean blocks in West Greenland is the subject of current debate (e.g. Connelly and Mengel, 1996). The apparent northward continuity of Paleoproterozoic features onto Baffin Island suggests that the Archean rocks of the Hall Peninsula and those of northern Labrador were part of the same "craton" prior to Torngatian orogenesis (1.91 Ga). If the proposed Hall-Nagsugtoquidian and Nain-North Atlantic craton correlations are correct, much of the Archean material in this region must have been assembled prior to 1.91 Ga.

## ACKNOWLEDGMENTS

Logistical support for fieldwork provided by the Polar Continental Shelf Project (Contribution number 00497), the Science Institute of the Northwest Territories, and the GSC is gratefully acknowledged. Jack MacRae, Diane Bellerive, and Klaus Santowski are warmly thanked for the excellence of their technical support. Reviews of this manuscript by M. St-Onge, R. Thériault, and N. Wodicka have improved the clarity of the ideas presented.

## REFERENCES

- Bertrand, J.-M., Roddick, J.C., Van Kranendonk, M.J., and Ermanovics, I.  
1993: U-Pb geochronology of deformation and metamorphism across a central transect of the Early Proterozoic Torngat Orogen, North River map area, Labrador; *Canadian Journal of Earth Sciences*, v. 30, p. 1470-1489.
- Blackadar, R.G.  
1967: Geological reconnaissance, southern Baffin Island, District of Franklin; Geological Survey of Canada, Paper 66-47, 32 p.
- Connelly, J. and Mengel, F.C.  
1996: U-Pb ages of Archean rocks from the northwestern part of the Nagsugtoquidian Orogen, West Greenland; in *Proceedings, 2nd DLC Workshop on Nagsugtoquidian geology*, (ed.) F.C. Mengel: Report of 1996 Workshop on the Nagsugtoquidian Orogen, Danish Lithosphere Centre Report, p. 71-73.
- Davis, W.J., McNicoll, V.J., Bellerive, D.R., Santowski, K., and Scott, D.J.  
1997: Modified chemical procedures for the extraction and purification of U from titanite, allanite, and rutile in the Geochronology Laboratory, Geological Survey of Canada; in *Radiogenic Age and Isotopic Studies: Report 10*; Geological Survey of Canada, Current Research 1997-F.
- Hammer, S., St-Onge, M.R., and Scott, D.J.  
1996a: Geology, White Strait, District of Franklin, Northwest Territories; Geological Survey of Canada, Open File 3192, scale 1:100 000.  
1996b: Structural geology of the Meta Incognita thrust belt, south Baffin Island, Northwest Territories; in *Current Research 1996-C*; Geological Survey of Canada, p. 73-81.

**Hoffman, P.F.**

- 1989: Precambrian geology and tectonic history of North America; in *The Geology of North America -- An Overview*, (ed.) A.W. Bally and A.R. Palmer; Geological Society of America; *The Geology of North America*, v. A, p. 447-512.
- 1990: Dynamics of the tectonic assembly of northeast Laurentia in geon 18 (1.9-1.8 Ga); *Geoscience Canada*, v. 17, p. 222-226.

**Jackson, G.D. and Taylor, F.C.**

- 1972: Correlation of major Archean rock units in the northeastern Canadian Shield; *Canadian Journal of Earth Sciences*, v. 9, p. 1650-1669.

**Jackson, G.D., Hunt, P.A., Loveridge, W.D., and Parrish, R.R.**

- 1990: Reconnaissance geochronology of Baffin Island, N.W.T.; in *Radiogenic Age and Isotopic Studies: Report 3*; Geological Survey of Canada, Paper 89-2, p. 123-148.

**Kalsbeek, F. and Nutman, A.**

- 1995: Reconnaissance SHRIMP U-Pb dating: assistance for lithological mapping and understanding the tectonothermal evolution of the Nagssugtoqidian orogen; in *Proceedings of the DLC Workshop "Nagssugtoqidian Geology 1995"*, (ed.) F.C. Mongel, M. Marker, and J. van Gool; Danish Lithosphere Centre, p. 29-33.

**Parrish, R.R.**

- 1990: U-Pb dating of monazite and its application to geological problems; *Canadian Journal of Earth Sciences*, v. 27, p. 1431-1450.

**Parrish, R.R., Roddick, J.C., Loveridge, W.D., and Sullivan, R.W.**

- 1987: Uranium-lead analytical techniques at the geochronology laboratory, Geological Survey of Canada; in *Radiogenic Age and Isotopic Studies: Report 1*; Geological Survey of Canada, Paper 87-2, p. 3-7.

**Roddick, J.C.**

- 1987: Generalized numerical error analysis with application to geochronology and thermodynamics; *Geochimica et Cosmochimica Acta*, v. 51, p. 359-362.

**Scott, D.J.**

- 1995a: U-Pb geochronology of a Paleoproterozoic continental magmatic arc on the western margin of the Archean Nain craton, northern Labrador, Canada; *Canadian Journal of Earth Sciences*, v. 32, p. 1870-1882.
- 1995b: U-Pb geochronology of the Nain craton on the eastern margin of the northern Torngat Orogen, Labrador; *Canadian Journal of Earth Sciences*, v. 32, p. 1859-1869.

**Scott, D.J. (cont.)**

- 1996a: Geology of the Hall Peninsula east of Iqaluit, southern Baffin Island Northwest Territories; in *Current Research 1996-C*; Geological Survey of Canada, p. 83-91.

- 1996b: Geology of the Hall Peninsula and preliminary U-Pb results: implications for correlations with Labrador and West Greenland; in *Report of 1996 ECSOOT Transect Meeting*, (ed.) R.J. Wardle and J. Hall; Lithoprobe Report No. 57, p. 192-203.

**Scott, D.J. and Campbell, L.M.**

- 1993: Evolution of the Paleoproterozoic Torngat orogen, Labrador Canada: recent advances using U-Pb geochronology and Nd isotopic systematics; *Geological Society of America, Abstracts with Program*, v. 25, p. A-237.

**Scott, D.J. and Gauthier, G.**

- 1996: Comparison of TIMS (U-Pb) and Laser Ablation Microprobe ICP-MS (Pb) techniques for age determination of detrital zircons from Paleoproterozoic metasedimentary rocks from northeastern Laurentia, Canada, with tectonic implications; *Chemical Geology*, v. 131, p. 127-142.

**Scott, D.J. and Machado, N.**

- 1995: U-Pb geochronology of the northern Torngat Orogen, Labrador Canada: a record of Paleoproterozoic magmatism and deformation; *Precambrian Research*, v. 70, p. 169-190.

**Scott, D.J. and St-Onge, M.R.**

- 1995: Constraints on Pb closure temperature in titanite based on rocks from the Ungava Orogen, Canada: implications for U-Pb geochronology and P-T-t path determinations; *Geology*, v. 23, p. 1123-1126.

**Scott, D.J., St-Onge, M.R., and Hanmer, S.**

- 1996: Geology, Frobisher Bay, District of Franklin, Northwest Territories; Geological Survey of Canada, Open File 3193, scale 1:100 000.

**St-Onge, M.R., Hanmer, S., and Scott, D.J.**

- 1996a: Geology of the Meta Incognita Peninsula, south Baffin Island, Northwest Territories: tectonostratigraphic units and regional correlations; in *Current Research 1996-C*; Geological Survey of Canada, p. 63-72.
- 1996b: Geology, Soper River, District of Franklin, Northwest Territories; Geological Survey of Canada, Open File 3191, scale 1:100 000.

# Timing of early deformation within the long-lived Elbow Lake Shear Zone, Trans-Hudson Orogen, Manitoba<sup>1,2,3</sup>

Kevin M. Ansdell<sup>4</sup> and James J. Ryan<sup>5</sup>

*Ansdell, K.M. and Ryan, J.J., 1997: Timing of early deformation within the long-lived Elbow Lake Shear Zone, Trans-Hudson Orogen, Manitoba; in Radiogenic Age and Isotopic Studies: Report 10; Geological Survey of Canada, Current Research 1997-F, p. 79-88.*

---

**Abstract:** The Elbow Lake Shear Zone forms a strand within a high strain corridor in the central Flin Flon belt that records an episodic deformational history in excess of 100 Ma. Three new U-Pb zircon ages are presented to bracket the timing of the earliest deformation within this zone, and their significance is interpreted in terms of the development of the Amisk collage. The earliest recognized fabrics ( $S_1$ ) are mylonites within gabbro-diabase-basalt assemblages which are crosscut at right angles by a suite of pink tonalite dykes. Zircons from one of these dykes yielded discordant ages, which suggest that the dyke could be as old as  $1870 \pm 2$  Ma. In the same region, a pair of grey tonalite dykes both yielded high precision ages of about 1866 Ma, but they have different amounts of strain. The earlier dyke was intensely sheared, then intruded by the weakly foliated dyke. Both dykes then formed boudins at a scale of tens of metres during subsequent shear episodes. The variable states of strain in dykes of the same age is good evidence for synkinematic ( $D_2$ ) dyke emplacement at 1866 Ma, during initial shortening of the successor arc built upon the Amisk collage.

**Résumé :** La zone de cisaillement d'Elbow Lake, qui forme un cordon au sein d'un corridor d'intense déformation dans le centre de la ceinture de Flin Flon, témoigne de déformations épisodiques qui se sont déroulées sur une période de plus de 100 millions d'années. La présent rapport fournit les résultats de trois nouvelles datations U-Pb sur zircon qui permettent d'encadrer l'époque de la déformation initiale à l'intérieur de cette zone et contient une interprétation de ces résultats qui s'insère dans le contexte de l'évolution du collage d'Amisk. La fabrique la plus ancienne observée ( $S_1$ ) est fournie par des mylonites formées au sein d'assemblages de gabbro-diabase-basalte qui sont recoupés à angle droit par une suite de dykes de tonalite rose. Des zircons extraits de l'un de ces dykes ont livré des âges discordants, qui nous permettent de supposer que l'âge de ce dyke remonterait aussi loin qu'à  $1870 \pm 2$  Ma. Dans la même région, une paire de dykes de tonalite grise ont livré des âges très précis d'environ 1866 Ma, mais leur état de déformation diffère. Le dyke le plus ancien a été intensément cisailé et a été recoupé par le dyke à faible foliation. Les deux dykes ont ensuite été segmentés en boudins d'une dizaine de mètres au cours d'épisodes de cisaillement subséquents. Les états de déformation variables de ces dykes d'âge semblable sont des indices probants d'une mise en place syncinématique ( $D_2$ ) à 1866 Ma, durant l'épisode de raccourcissement initial de l'arc qui s'est édifié sur le collage d'Amisk.

---

<sup>1</sup> Contribution to the Shield Margin NATMAP Project

<sup>2</sup> Contribution to Canada-Manitoba Partnership Agreement on Mineral Development (1990-1995), a subsidiary agreement under the Canada-Manitoba Economic and Regional Development Agreement.

<sup>3</sup> Contribution to Canada-Saskatchewan Partnership Agreement on Mineral Development (1990-1995), a subsidiary agreement under the Canada-Saskatchewan Economic and Regional Development Agreement.

<sup>4</sup> Department of Geological Sciences, University of Saskatchewan, 114 Science Place, Saskatoon, Saskatchewan S7N 5E2

<sup>5</sup> Centre for Deformation Studies in the Earth Sciences, Department of Geology, University of New Brunswick, P.O. Box 4400, Fredericton, New Brunswick E3B 5A3

## INTRODUCTION

The Flin Flon belt (Fig. 1) in the Paleoproterozoic Trans-Hudson Orogen comprises a variety of volcanic-dominated tectonostratigraphic assemblages (1.92 to 1.88 Ga) that are unconformably overlain by fluvial sedimentary rocks (ca. 1.85 to 1.83 Ga) and intruded by felsic to ultramafic intrusive rocks (ca. 1.89 to 1.83 Ga) (e.g. Stern et al., 1993, 1995a, b; Ansdell, 1993; Whalen and Stern, 1996; David et al., in press). The belt is segmented into distinct blocks by a system of shear zones (e.g. Bailes and Syme, 1989; Ryan and Williams, 1994; Fedorowich et al., 1995). Detailed structural analysis of some of these shear zones indicate that they have had complex and protracted histories (e.g. Ryan and Williams, 1996a; Lucas et al., 1996). The early stages of deformation in these shear zones are difficult to identify and notoriously difficult to date. The study of Lucas et al. (1996)

identified an 1866 Ma pluton that crosscuts a fabric in the Meridian-West Arm shear zone and represents the only other study to address the timing of early fabric development in the Flin Flon belt. They suggest that this shear zone is one of a number that were active at that time, and which juxtaposed disparate tectonostratigraphic assemblages to form the Amisk collage (Fig. 1).

The Elbow Lake Shear Zone is a major structure that dissects the central part of the Flin Flon belt, and extends from Athapapuskow Lake to the southern flank of the Kiseynew Belt (Fig. 1) where it appears to root in amphibolite grade high strain zones (Ryan and Williams, 1995b). The complex deformational history of the Elbow Lake Shear Zone has been unravelled in the Elbow Lake area (Fig. 2), where six distinct ductile fabrics have been characterized (Ryan and Williams, 1996a). The relationship between the various deformation fabrics, peak metamorphism, and granitoid plutons in the

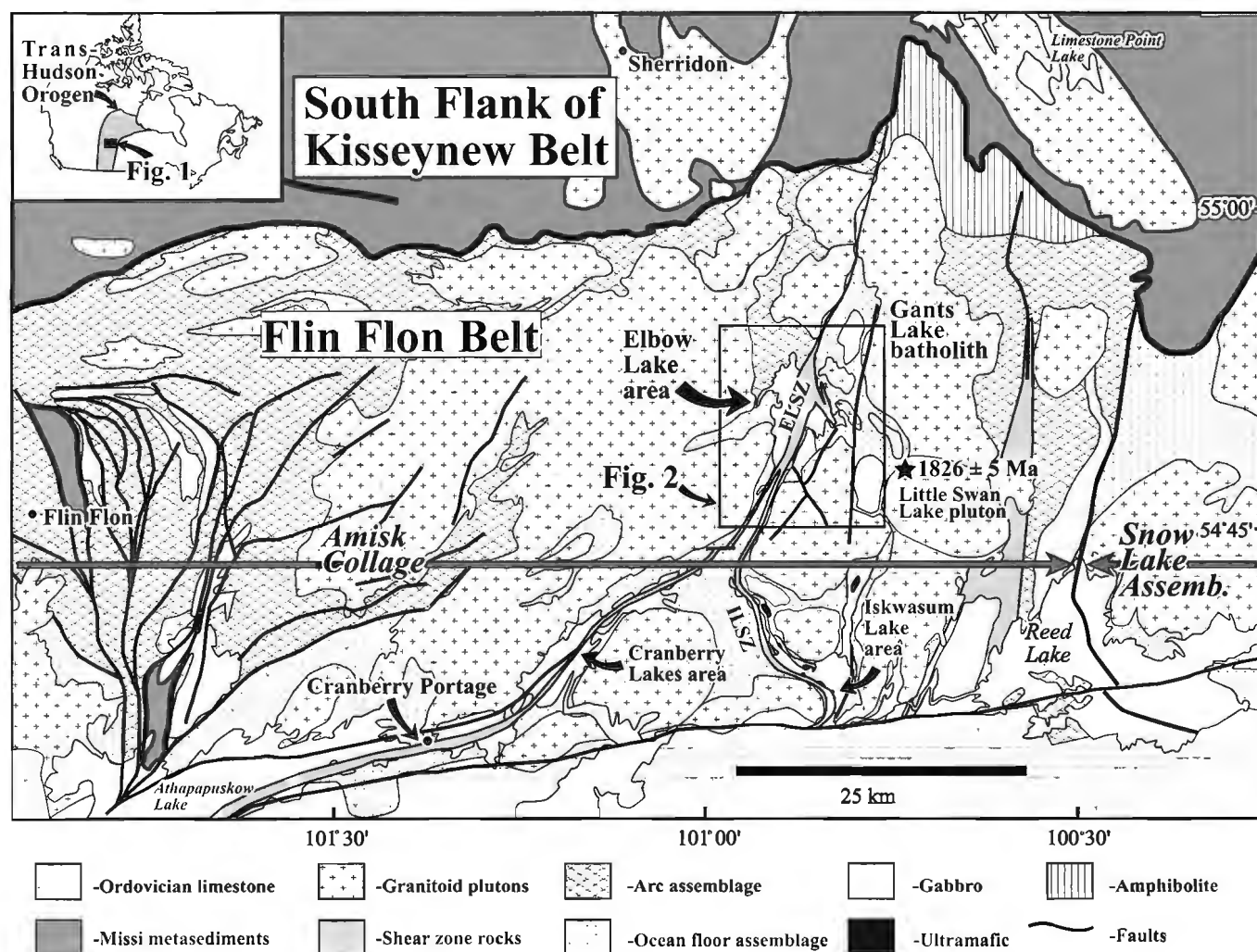


**Figure 1.** Location map of the central Flin Flon belt, between the Kiseynew Belt to the north and Paleozoic cover to the south. The boundary between the Amisk collage and the Snow Lake Assemblage is the Morton Lake fault zone, taken from Syme et al. (1995). The Elbow Lake area is highlighted and is shown in detail in Figure 2. The main Elbow Lake Shear Zone trends southwest and continues through Cranberry Portage. The strand that bends to the southeast is the Iskwasum Lake shear zone (ILSZ).



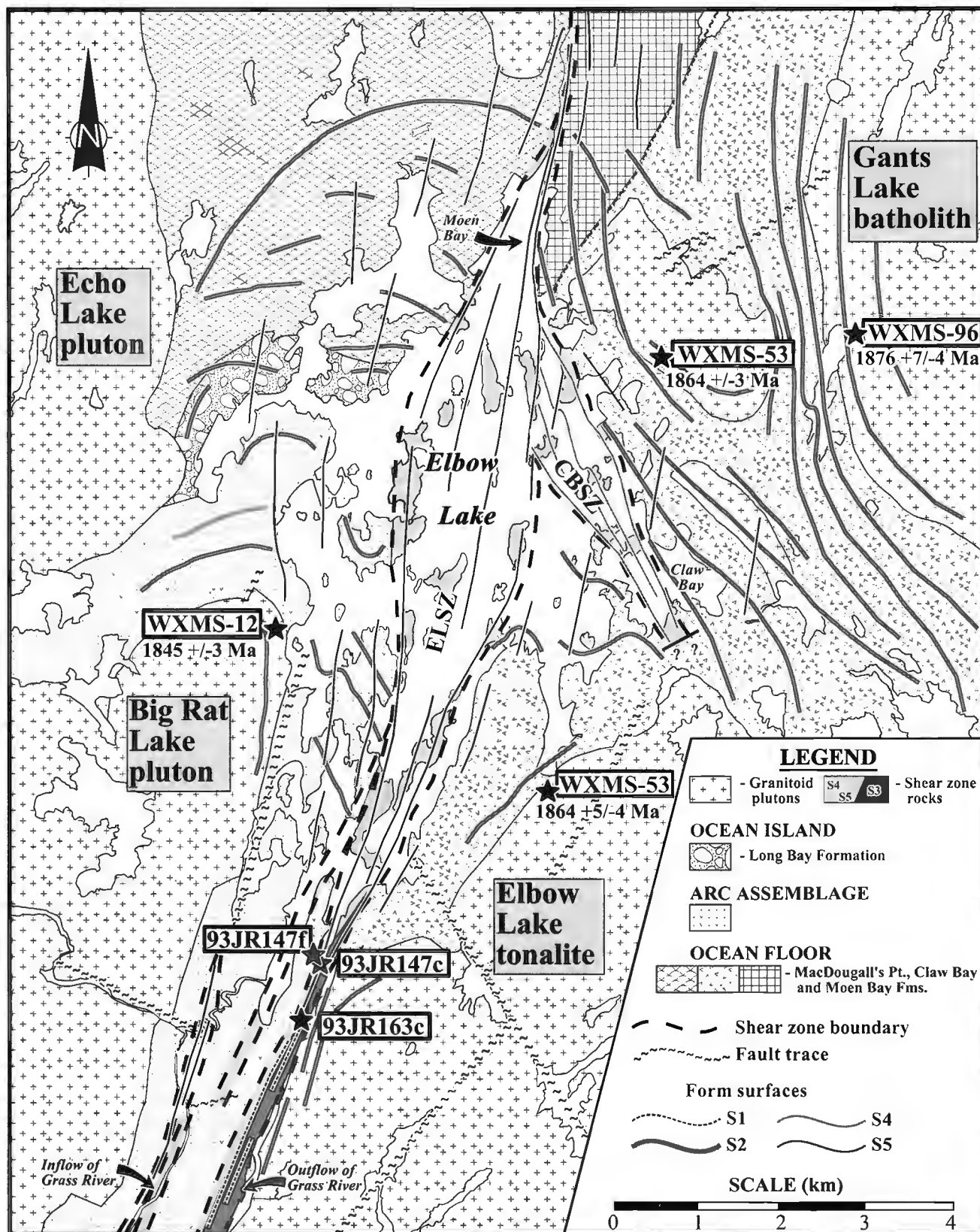


**Figure 2.** Simplified geology map of Elbow Lake illustrating the main rock types and simplified form surface traces. Sample locations for U/Pb geochronology are marked with a star. Samples for the present study have the prefix 93JR-, whereas samples of Whalen and Hunt (1994) are denoted by WXMS. CBSZ = Claw Bay Shear Zone, ELSZ = Elbow Lake Shear Zone.

area indicates that parts of the shear zone had been active at intervals over a period of at least 100 Ma (Ryan and Williams, 1995a). Detailed structural mapping within the shear zone has identified an intimate relationship between early deformation and dyke emplacement. The objective of this paper is to provide geochronological data on the age of deformed dykes, which aid in bracketing the timing of the earliest deformation within the Elbow Lake Shear Zone. The data indicates that a significant early deformation history can be recognized in the Amisk collage, in spite of masking by later deformational fabrics.

## GEOLOGICAL AND STRUCTURAL SETTING OF THE ELBOW LAKE AREA

The Elbow Lake area (Fig. 2) hosts 1.90 Ga juvenile arc, ocean floor, and ocean island tectonostratigraphic assemblages (Syme, 1992; Stern et al., 1995a, b) intruded by voluminous tonalitic to granodioritic intrusions ranging in age from 1876 to 1845 Ma (Whalen, 1992; Whalen and Hunt, 1994). The structural history of the Elbow Lake area is briefly reviewed here to provide background for the discussion of the geochronological data. A more complete account of the structural features in the central Flin Flon belt can be found in Ryan and Williams (1996a). Detailed structural mapping at Elbow Lake has identified six ductile and one brittle-ductile to brittle generations of structures by relating fabrics to metamorphic minerals and dated intrusive rocks (Ryan and Williams 1996a, and references therein).

With rare exceptions, all fold axes, lineations, and foliation elements in the Elbow Lake area are vertical. Simplified form surfaces traces for  $S_1$ ,  $S_2$ ,  $S_4$ , and  $S_5$  are shown in Figure 2. The earliest fabric ( $S_1$ ) occurs as mylonites in gabbro, diabase, and basalt, and as a rare bedding parallel fabric within interflow sedimentary units in the volcanic rocks. The  $S_1$  can be convincingly identified only in areas which are cut by a suite of pink tonalite dykes (Fig. 3a, b). The second generation of fabrics ( $S_2$ ) developed during a progressive east-west shortening episode that produced a north-south structural grain and regional foliation across the central Flin Flon belt (Ryan and Williams, 1996b). The  $D_2$  deformation episode appears to have been prolonged, and accompanied the 1.87 to 1.84 Ga plutonism across the area. The  $S_2$  fabrics are more intensely developed in the 1864 Ma plutons than the 1845 Ma plutons, suggesting that the bulk of the strain developed early in  $D_2$ . The youngest timing of  $S_2$  is pinned by the Little Swan Lake pluton (Fig. 1) which crosscuts  $S_2$  structures and yielded a U/Pb titanite age of  $1826 \pm 5$  Ma (Whalen and Hunt, 1994). Locally preserved, shallow  $F_2$  folds indicate that  $D_2$  was the deformation episode responsible for the steepening of strata and  $S_1$  fabrics (Ryan and Williams, 1996a, b). The  $S_2$  varies in character from a flattening fabric, to a differentiated crenulation cleavage where it overprints  $S_1$  or bedding at a high angle.

The third generation of structures ( $S_3$ ) is a regional mylonite zone (Iskwasum Lake shear zone) best exposed in the Iskwasum Lake area (Fig. 1). At Elbow Lake,  $S_3$  shreds the suite of pink tonalites, and has a unique relationship to

regional metamorphism (Ryan and Williams, 1996a). Unlike  $S_1$  and  $S_2$  mylonites,  $S_3$  mylonites are still relatively fine grained but annealed, indicating that they developed coincident with regional metamorphism.

The remaining structural features postdate peak regional metamorphism. Fourth generation structures include the north-northwest-trending Claw Bay shear zone on the eastern side of Elbow Lake (Fig. 2) and an early manifestation of the east-trending Berry Creek Shear Zone which transects the southern extremity of the exposed Flin Flon belt (Fig. 1). Fifth generation structures ( $S_5$ ) are pervasive across the map area (Fig. 2), comprising the dominant fabric in the Elbow Lake Shear Zone, and they developed during retrograde metamorphic conditions. Throughout most of the Elbow Lake Shear Zone, earlier fabrics have been obliterated by  $S_5$ , and a pervasive  $S_5$  crenulation cleavage developed in the wall rocks. The  $S_6$  structures are restricted to the southern extremity of the exposed Flin Flon belt, and are associated with reactivation of the Berry Creek Shear Zone. Brittle-ductile and brittle structures are broadly grouped in a seventh generation, and vary from north-northeast- to north-northwest-trending with insignificant offset. The brittle-ductile structures may have developed at about 1760 Ma, which is the K-Ar and Ar-Ar age obtained from a number of biotite and hornblende samples in the Elbow Lake area (Whalen and Hunt, 1994). These ages represent cooling ages and are interpreted to coincide with the transition to brittle-ductile deformation in the crust during exhumation of the Flin Flon belt (Ryan and Williams, 1995a).

## ANALYTICAL TECHNIQUES

The samples, which are described in detail below and located on Figure 2, were collected from sites where the structural relationships were well constrained and would thus solve specific problems. The samples were jaw-crushed and swing-milled, and zircons separated using conventional Wilfley Table, heavy liquid, and magnetic separation techniques. Selected zircons were abraded, spiked with a mixed  $^{205}\text{Pb}$ - $^{233}\text{U}$ - $^{235}\text{U}$ , and dissolved in Teflon microcapsules. The complete U-Pb analytical methods, including column chemistry, mass spectrometry, and data reduction procedures, used at the Geological Survey of Canada are described in Parrish et al. (1987) and Roddick et al. (1987). Lead procedural blanks associated with these samples were generally less than 15 pg. The U and Pb concentrations and U-Pb isotopic data for zircon fractions are presented in Table 1. The error ellipses on the concordia diagrams are at the  $2\sigma$  level.

## SAMPLE DESCRIPTIONS AND RESULTS

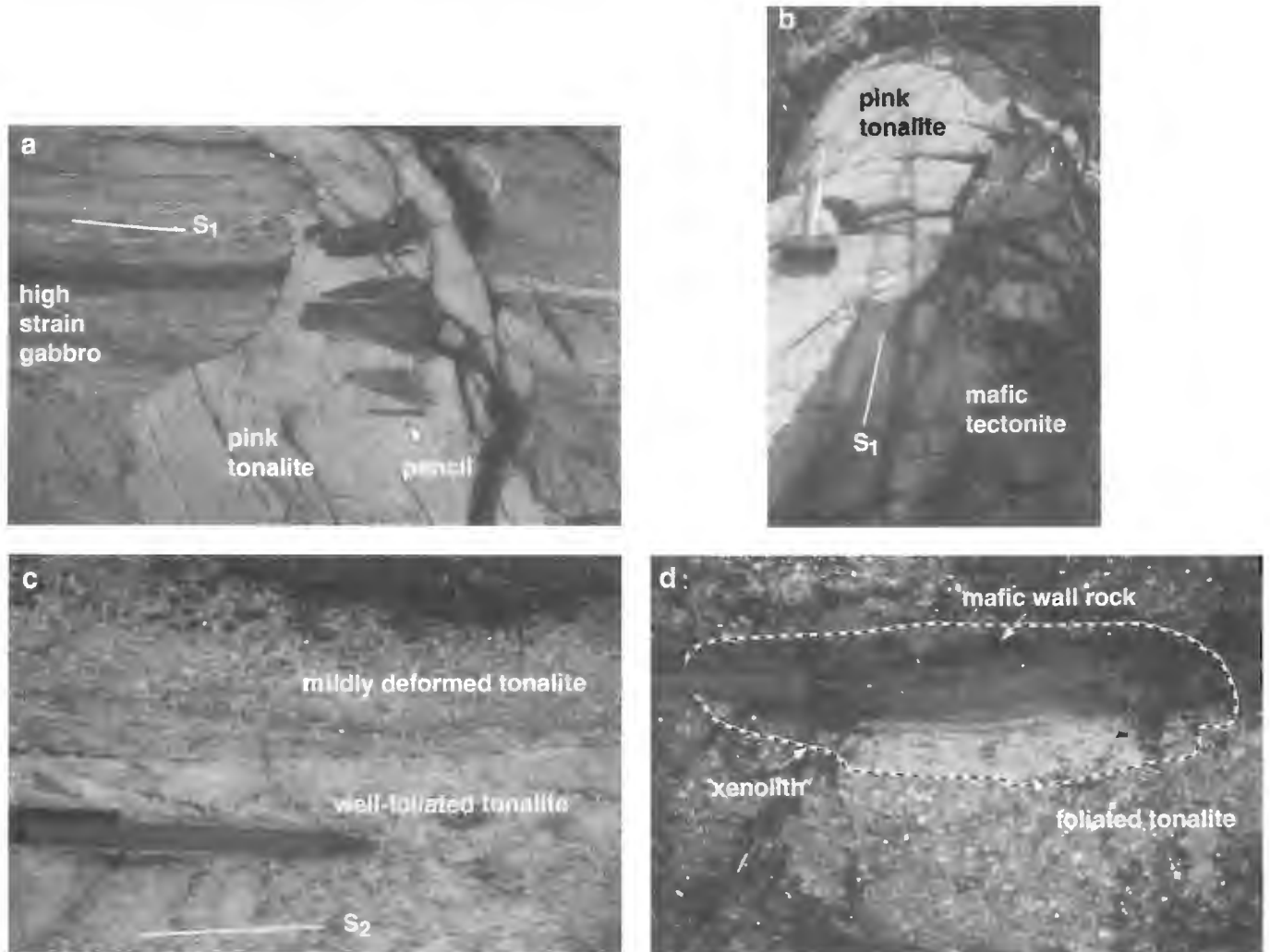
### *Pink tonalite (93JR163c)*

A pink weathering, equigranular quartz-plagioclase tonalite dyke was collected from a suite of dykes in the southern Elbow Lake area that crosscut the  $S_1$  mylonite foliation in gabbro, diabase, and basalt at a high angle (Fig. 3a, 3b). The dykes vary in width from 20 cm to 1 m, and have fairly irregular margins. These high angle dykes are weakly folded

by  $F_2$  folds, developing a weak  $S_2$  flattening of quartz. The dykes are locally intensely deformed by post- $S_2$  deformation. They thus provide an excellent constraint on the minimum age of  $S_1$  development. Ryan and Williams (1996a) suggest that the textural and compositional characteristics of this suite are similar to the larger Elbow Lake tonalite, which has been dated at  $1864 \pm 5/-4$  Ma (Whalen and Hunt, 1994).

Zircons are euhedral prismatic, exhibit magmatic zoning, have abundant fractures and inclusions, and poor clarity (Fig. 4a). They were subdivided into two groups based on magnetic characteristics, and abraded separately. Fractions A to C are less magnetic than fractions D and E. Fractions D and

E are more discordant (5.4 to 6.6% discordant) than the less magnetic fractions (1.6 to 3.6% discordant), although there is no relationship between uranium concentrations, which range from 183 to 629 ppm, and  $^{207}\text{Pb}/^{206}\text{Pb}$  age. A regression line constructed through all five fractions yields an upper intercept age of  $1868 \pm 21/-12$  Ma (Fig. 5), although they are not collinear as indicated by an MSWD of 62.6. Fraction A consists of a single zircon grain and yields the oldest  $^{207}\text{Pb}/^{206}\text{Pb}$  age of  $1870 \pm 2$  Ma. However, this analysis is discordant and so the  $^{207}\text{Pb}/^{206}\text{Pb}$  age represents a minimum crystallization age. The poor quality of the zircons suggests



- a)  $S_1$  mylonite in gabbro and diabase which is crosscut at  $90^\circ$  by a pink tonalite dyke. The mafic xenoliths in the dykes also have a mylonitic fabric. The dyke is weakly  $F_2$  folded and has a weak  $S_2$  fabric. Note mechanical pencil for scale.
- b) The sample collection site for 93JR163c. Note the  $F_2$  folds in the thin wisps of dyke material which cut across the mafic tectonite. The sledge hammer is about 40 cm long.

- c) The well-foliated grey tonalite is intruded by the more mildly deformed quartz phryic grey tonalite. Both dykes yielded almost exact ages.
- d) Xenolith of the well-foliated tonalite and its contact with the mafic wall rocks, within the later, less deformed quartz phryic grey tonalite.

**Figure 3.** Photographs from sample collection sites.

that they may have been susceptible to variable lead loss during the prolonged deformation, metamorphic, and fluid history of the Elbow Lake Shear Zone. Note that any partial resetting likely occurred within 100 Ma after dyke intrusion, since there is no geological, structural, or isotopic evidence for later resetting events. The most conservative estimate for the age of the tonalite is about 1868 Ma. However, there is no morphological or compositional evidence to suggest that the grain analyzed in fraction A was inherited, and so we suggest that the dyke is likely older than 1870 Ma.

### Grey/beige porphyritic tonalite (93JR147c)

This sample is a beige-weathering plagioclase-hornblende-blue quartz eye porphyritic tonalite dyke. The dyke is about 1 m wide and is best exposed within a low-strain lozenge in the Elbow Lake Shear Zone. The core of the dyke is essentially unfoliated, but grades very rapidly into mylonite at its margins indicating significant postemplacement ductile deformation. Isolated porphyroclasts of plagioclase and blue quartz scattered throughout the mylonite indicate that much of the mylonite may be derived from this unit.

The zircons consist of generally colourless, prismatic grains with indistinct growth zonations (Fig. 4b). They are commonly cracked, contain mineral inclusions, and are relatively magnetic. Zircons were separated into two large fractions, and abraded separately. Fractions A and B came from

one large fraction which had length/width ratios of about 4:1, whereas fractions C to E were from the other fraction which consisted of stubbier grains. However, the distinction between the fractions is not obvious, and thus are considered to have formed part of the same morphological group, although the more elongate zircons had lower U contents (32–72 ppm) than the more stubby grains (148–180 ppm). Nevertheless, all fractions are less than 1% discordant, and yield identical  $^{207}\text{Pb}/^{206}\text{Pb}$  ages suggesting that they grew at the same time. The analysis of fraction B is imprecise and is not plotted on Figure 6. A discordia line through these points yields an age of  $1866\pm 2/-1$  Ma, which is interpreted as the crystallization age of the tonalite.

### Foliated beige tonalite (93JR147f)

A sample of a lighter coloured, plagioclase-hornblende porphyritic tonalite was collected 10 m west of 93JR147c. This tonalite is a little finer grained, lacks the abundant blue quartz eyes and has a more intense foliation. This sample, 93JR147f, is in intrusive contact with a tonalite which is similar in appearance to 93JR147c (Fig. 3c) and which contains xenoliths of the intensely foliated 93JR147f material. One xenolith of the intensely foliated dyke preserves the intrusive contact between 93JR147f and the mafic wall rocks (Fig. 3d). These relationships indicate that 93JR147f is older than 93JR147c, and more deformed.

**Table 1.** U-Pb zircon analytical data.

Zircon fraction <sup>a</sup>	Wt <sup>b</sup> ( $\mu\text{g}$ )	U (ppm)	Pb <sup>c</sup> (ppm)	$^{206}\text{Pb}/^{204}\text{Pb}$ <sup>d</sup>	Pb <sup>e</sup> (pg)	$^{208}\text{Pb}$ (%)	$^{206}\text{Pb}/^{238}\text{U}$ <sup>f</sup>	$^{207}\text{Pb}/^{235}\text{U}$ <sup>f</sup>	$^{207}\text{Pb}/^{206}\text{Pb}$ <sup>f</sup>	$^{207}\text{Pb}/^{206}\text{Pb}$ <sup>g</sup> age (Ma)
<b>93JR147C Porphyritic tonalite</b>										
A	10	72	25	1679	3	6.7	$0.3353\pm 0.11\%$	$5.274\pm 0.13\%$	$0.11407\pm 0.07\%$	$1865\pm 3$
B	8	32	11	216	19	6.5	$0.3355\pm 0.26\%$	$5.226\pm 0.60\%$	$0.11297\pm 0.49\%$	$1848\pm 18$
C	8	164	56	4867	1	5.5	$0.3354\pm 0.10\%$	$5.276\pm 0.11\%$	$0.11410\pm 0.04\%$	$1866\pm 2$
D	20	180	61	9332	2	6.3	$0.3335\pm 0.10\%$	$5.245\pm 0.11\%$	$0.11406\pm 0.03\%$	$1865\pm 1$
E	13	148	51	6165	1	6.8	$0.3332\pm 0.09\%$	$5.240\pm 0.10\%$	$0.11406\pm 0.03\%$	$1865\pm 1$
<b>93JR147F Foliated tonalite</b>										
A	4	70	25	1058	2	9.4	$0.3352\pm 0.19\%$	$5.276\pm 0.21\%$	$0.11417\pm 0.09\%$	$1867\pm 3$
B	5	118	42	950	10	8.0	$0.3374\pm 0.12\%$	$5.307\pm 0.17\%$	$0.11405\pm 0.10\%$	$1865\pm 4$
C	7	166	56	2784	4	8.2	$0.3243\pm 0.09\%$	$5.093\pm 0.11\%$	$0.11388\pm 0.05\%$	$1862\pm 2$
D	5	78	30	79	111	12.3	$0.3510\pm 0.45\%$	$5.518\pm 1.80\%$	$0.11402\pm 1.53\%$	$1865\pm 55$
E	7	127	45	3518	1	9.0	$0.3355\pm 0.09\%$	$5.276\pm 0.11\%$	$0.11406\pm 0.04\%$	$1865\pm 2$
F	8	37	13	346	11	10.2	$0.3355\pm 0.18\%$	$5.274\pm 0.33\%$	$0.11402\pm 0.25\%$	$1864\pm 9$
<b>93JR163C Pink tonalite</b>										
A	6	183	62	3218	1	7.2	$0.3259\pm 0.11\%$	$5.139\pm 0.12\%$	$0.11438\pm 0.06\%$	$1870\pm 2$
B	5	311	103	6370	0.1	4.9	$0.3288\pm 0.09\%$	$5.150\pm 0.11\%$	$0.11359\pm 0.03\%$	$1858\pm 1$
C	3	193	63	1006	3	5.6	$0.3213\pm 0.12\%$	$5.026\pm 0.17\%$	$0.11344\pm 0.12\%$	$1855\pm 4$
D	5	192	60	3998	1	5.1	$0.3084\pm 0.11\%$	$4.779\pm 0.12\%$	$0.11240\pm 0.05\%$	$1839\pm 2$
E	6	629	204	983	70	6.5	$0.3171\pm 0.10\%$	$4.985\pm 0.16\%$	$0.11401\pm 0.11\%$	$1864\pm 4$
<sup>a</sup> All fractions air abraded <sup>b</sup> Weighing uncertainty - 1 $\mu\text{g}$ <sup>c</sup> Radiogenic Pb <sup>d</sup> Measured ratio corrected for fractionation and spike <sup>e</sup> Total common Pb in analysis corrected for fractionation and spike <sup>f</sup> Corrected for blank Pb and U, and common Pb (Stacey-Kramers model Pb composition at the interpreted age of the zircons); errors are 1 standard error of the mean in percent <sup>g</sup> Corrected for blank and common Pb; errors are 2 standard errors of the mean in Ma										

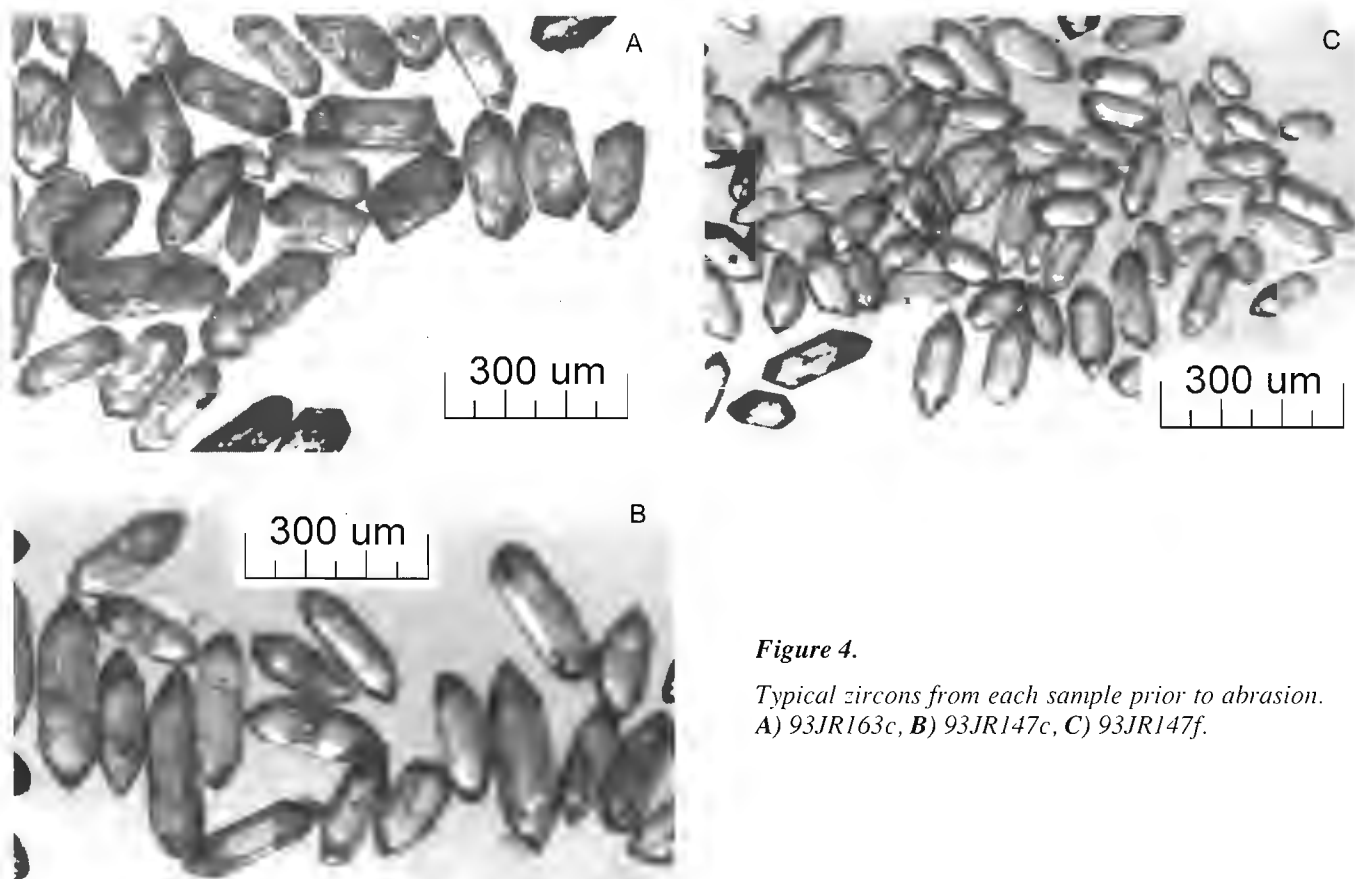
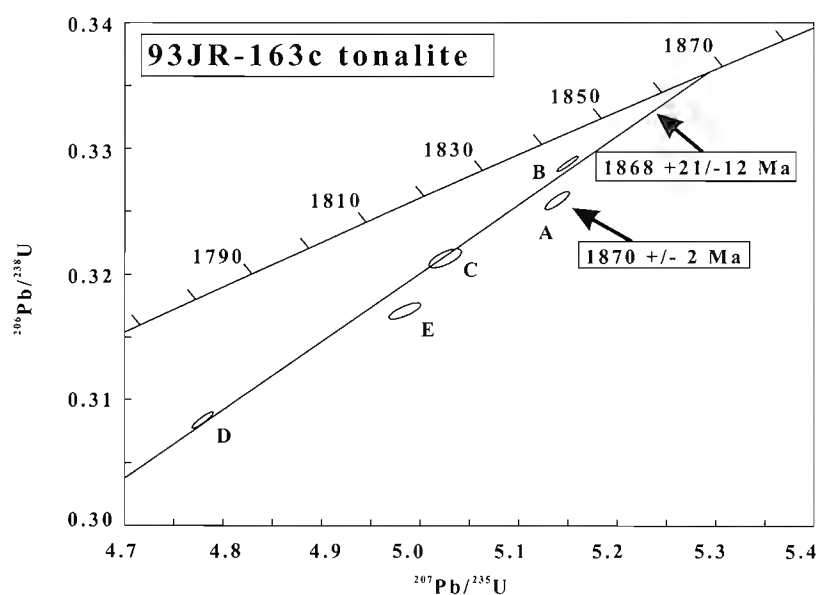


**Figure 4.**

Typical zircons from each sample prior to abrasion.  
A) 93JR163c, B) 93JR147c, C) 93JR147f.

**Figure 5.**

Concordia diagram showing U-Pb data for the pink tonalite dyke 93JR163c.



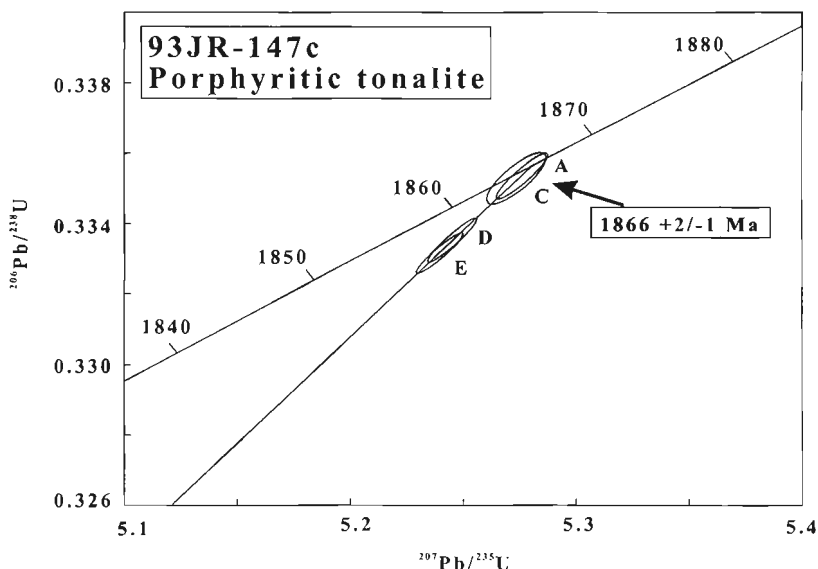
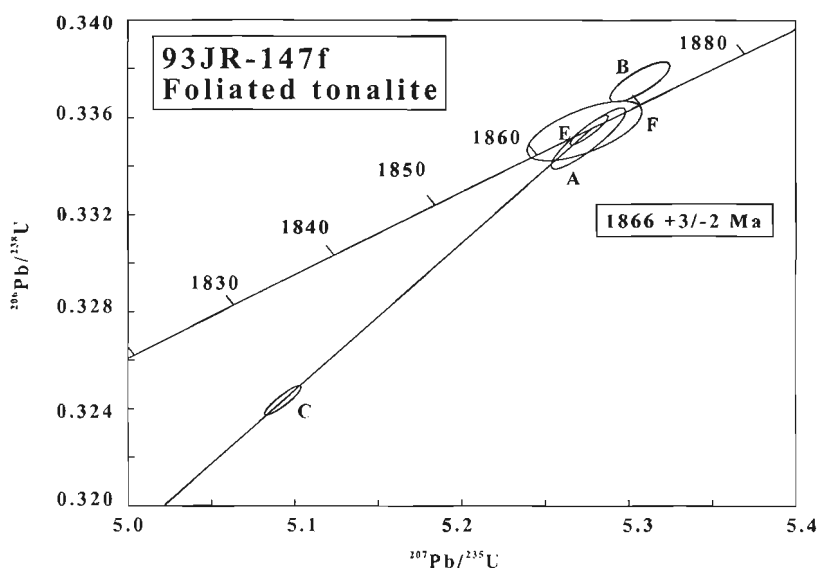


**Figure 6.**

Concordia diagram showing U-Pb data for the porphyritic tonalite dyke 93JR147c.

**Figure 7.**

Concordia diagram showing U-Pb data for the foliated tonalite dyke 93JR147f.



The zircons are clear, prismatic, well-faceted, and speckled with inclusions (Fig. 4c). Prior to abrasion the zircons were separated into stubby grains with a length/width ratio of about 3:1, and more elongate euhedral grains. After abrasion, three fractions (A to C) were picked from the former group, and three from the latter (D to F). There is no distinct difference in the U concentrations between the two groups. Fractions E and F are concordant, and have  $^{207}\text{Pb}/^{206}\text{Pb}$  ages of  $1865 \pm 2$  and  $1864 \pm 9$  Ma, respectively. Fraction C yielded the most discordant analysis (3.2% discordant), and a  $^{207}\text{Pb}/^{206}\text{Pb}$  age of  $1862 \pm 2$  Ma. Fraction D was excluded from the regression calculations, and is not plotted on Figure 7, because the analysis was extremely imprecise. The other fractions are collinear and yield an upper intercept age of  $1866 \pm 3/-2$  Ma, which is interpreted as the age of crystallization of the tonalite.

## DISCUSSION AND CONCLUSIONS

Field and petrographic relationships in the Elbow Lake area have identified several generations of structural fabrics. The relative timing of these fabrics has been constrained using crosscutting relationships between fabrics and plutons, and their relation with metamorphic mineral growth. Together these observations suggest that the Elbow Lake Shear Zone was active for more than 100 million years (Ryan and Williams, 1996a). During detailed structural mapping, tonalitic dykes were identified within the Elbow Lake Shear Zone that crosscut early fabrics but are themselves deformed, making them useful for constraining the early history of the shear zone.

The first generation of structures ( $S_1$ ) consist of mylonites which developed in gabbro, diabase, and basalt, and which are crosscut at a high angle by the tonalite sample 93JR163c. The age of the Elbow-Athapapuskow ocean floor assemblage

is fairly well constrained to ca. 1.90 Ga by a synvolcanic diabase sill and a gabbro pegmatite (Stern et al., 1995b). Zircons from the pink tonalite dyke, which contains an  $S_2$  fabric, yielded discordant ages with an imprecise upper intercept of 1868 Ma. A fraction consisting of a single grain yielded an age of  $1870 \pm 2$  Ma, and this is interpreted as the most likely minimum age of the tonalitic dyke. The scatter about the regression line is likely due to redistribution and partial loss of Pb during later regional metamorphism or fluid movement during deformation. This effect has also been observed in the Cleunio Lake area in the southern flank of the Kiseeynew Domain, and attributed to the same process (Ansdell and Norman, 1995). The poor quality zircons in the tonalite dyke were probably particularly susceptible to Pb loss during metamorphism. The tonalite dyke is considered to be an offshoot of the Elbow Lake tonalite, which yielded similar poor quality zircons and an upper intercept age of  $1864 \pm 5/-4$  Ma (Whalen and Hunt, 1994).

The  $S_1$  mylonites thus developed after 1.90 Ga, the age of the ocean floor assemblage, but prior to 1.87 Ga, the age of the crosscutting pink tonalite dykes. These mylonites juxtapose ocean floor assemblages of differing affinities, but lie within a high-strain corridor which was reactivated at several intervals throughout a complex deformation history. Lucas et al. (1996) showed that the early fabrics associated with some structures in the Flin Flon area developed at about 1.88 to 1.87 Ga, and proposed that distinct volcanic assemblages were juxtaposed at this time during the development of the Amisk collage accretionary complex. The similarity in timing between the structures in the Flin Flon area and the  $S_1$  mylonites in the Elbow Lake Shear Zone suggests that they may represent part of a suite of structures that were active during the construction, or accretion of the Amisk collage. Although the 1870 Ma tonalite dyke is the only dated intrusion that stitches early structures in the central Flin Flon belt, the timing of accretion in this area may also be constrained by the Gants Lake batholith, one of the largest plutons in the Flin Flon belt (Fig. 1). The oldest phase of this composite body is  $1876 \pm 7/-4$  Ma (Whalen and Hunt, 1994), only slightly younger than synvolcanic intrusions dated at 1880 Ma in the Snow Lake arc and the 1885 Ma shoshonites near Flin Flon. Although there is no direct evidence that the collage was accreted prior to 1876 Ma, the Gants Lake batholith is similar to other medium-potassium, calc-alkaline arc-type plutons in the belt, suggesting that it too intruded an already thickened, and thus accreted, volcanic pile. Therefore, a possibility is that the  $S_1$  shear zones predate 1876 Ma, with the likely scenario that arc volcanism and accretion were coeval during the development of the accretionary complex.

The similar age of 1866 Ma for the north-trending dykes, which record different amounts of ductile strain, is strong evidence for synkinematic ( $D_2$ ) dyke emplacement at that time. The ca. 1870 Ma tonalite dyke was intruded at a high angle to the  $S_1$  mylonitic fabric, whereas the ca. 1866 Ma dykes were intruded subparallel to  $S_2$ . These observations suggest that there was a distinct, albeit short, period of tectonic quiescence between  $D_1$  and  $D_2$ . The 1866 Ma date probably marks the initiation of  $D_2$  deformation, although this deformation phase is protracted since  $S_2$  fabrics are also observed in 1845 Ma

plutons in the Elbow Lake area. The fact that there is a concentration of dykes in shear zones that predate regional metamorphism is strong testament that  $S_2$  shear zones preferentially channelled magma.

These new ages constrain the timing of a significant early fabric in the Elbow Lake area which was probably related to accretion of distinct volcanic assemblages, and indicate that the bulk of the north-south structural grain in the central Flin Flon belt developed early in the tectonic history through a combination of accretion ( $D_1$ ) and east-west shortening ( $D_2$ ) of the postaccretion successor arc built upon the collage. Since  $S_2$  is more intensely developed in the 1.87-1.86 Ga plutons than the 1.845 Ga plutons,  $D_2$  is interpreted to have been in its waning stages by 1845 Ma. The combination of voluminous plutonism and  $D_2$  deformation between 1.87-1.84 Ma probably contributed significantly to crustal thickening, uplift, and erosion at that time, with the resulting detritus collecting in fluvial basins on the emergent accretionary complex (Lucas et al., 1996; Ryan and Williams, 1996b).

## ACKNOWLEDGMENTS

The samples were collected with the assistance of Sandra MacDougall. Melodi Kujawa and Melissa Kujawa assisted with crushing, milling, and zircon separation. Jack Macrae, Diane Bellerive, Klaus Santowski, and Richard Stern are thanked for their expertise in chemistry, mass spectrometry, and data reduction. This study is a contribution to the Geological Survey of Canada NATMAP Shield Margin Project under the Canada-Manitoba and Canada-Saskatchewan Partnership agreements on Mineral Development (1990-1995), and to the LITHOPROBE Trans-Hudson Orogen Transect. This study was partially funded by a LITHOPROBE grant to Ansdell, while Ryan acknowledges support from a LITHOPROBE grant to Paul Williams. Constructive comments on the manuscript were made by R. Stern and S. Lucas. LITHOPROBE Publication Number 794.

## REFERENCES

- Ansdell, K.M.  
1993: U-Pb constraints on the timing and provenance of fluvial sedimentary rocks in the Flin Flon and Athapapuskow basins, Flin Flon domain, Trans-Hudson Orogen, Manitoba and Saskatchewan; in *Radiogenic Age and Isotopic Studies: Report 7; Geological Survey of Canada, Paper 93-2*, p. 49-57.
- Ansdell, K.M. and Norman, A.R.  
1995: U-Pb geochronology and tectonic development of the southern flank of the Kiseeynew Domain, Trans-Hudson Orogen, Canada; *Precambrian Research*, v. 72, p. 147-167.
- Bailes, A.H. and Syme, E.C.  
1989: Geology of the Flin Flon-White Lake area; Manitoba Energy and Mines, Geological Report GR87-1, 313 p.
- David, J., Bailes, A.H., and Machado, N.  
in press: Evolution of the Snow Lake portion of the Paleoproterozoic Flin Flon and Kiseeynew belts, Trans-Hudson Orogen, Manitoba, Canada; *Precambrian Research*.
- Fedorowich, J.S., Kerrich, R., and Stauffer, M.R.  
1995: Geodynamic evolution and thermal history of the central Flin Flon domain, Trans-Hudson Orogen: constraints from structural development,  $^{40}\text{Ar}/^{39}\text{Ar}$ , and stable isotope geothermometry; *Tectonics*, v. 14, p. 472-503.

- Lucas, S.B., Stern, R.A., Syme, E.C., Reilly, B.A., and Thomas, D.J.**  
1996: Intraoceanic tectonics and the development of continental crust: 1.92-1.84 Ga evolution of the Flin Flon Belt, Canada; *Geological Society of America, Bulletin*, v. 108, no. 5, p. 602-629.
- Parrish, R.R., Roddick, J.C., Loveridge, W.D., and Sullivan, R.W.**  
1987: Uranium-lead analytical techniques at the geochronology laboratory, Geological Survey of Canada; in *Radiogenic Age and Isotope Studies: Report 1*; Geological Survey of Canada, Paper 87-2, p. 3-7.
- Roddick, J.C., Loveridge, W.D., and Parrish, R.R.**  
1987: Precise U-Pb dating of zircon at the sub-nanogram Pb level; *Chemical Geology (Isotope Geoscience Section)*, v. 66, p. 111-121.
- Ryan, J.J. and Williams, P.F.**  
1994: Tectonometamorphic history of the Elbow Lake Shear Zone, Flin Flon-Snow Lake greenstone belt, Manitoba; in *Proceedings, Lithoprobe, Trans-Hudson Orogen Transect, Saskatoon, Report No. 38*, p. 221-229.
- 1995a: The Elbow Lake area: a long-lived deformation corridor; in *Proceedings, Lithoprobe, Trans-Hudson Orogen Transect, Regina, Report No. 48*, p. 156-161.
- 1995b: Structural mapping in the Elbow-Cranberry-Iskwasum lakes area, Flin Flon Belt, Manitoba (parts of NTS 63K/10, 11, and 15); in *Manitoba Energy and Mines, Minerals Division, Report of Activities*, p. 71-73.
- 1996a: The structural anatomy of the central Flin Flon Belt, northern Manitoba; in *Current Research 1996-C*, Geological Survey of Canada, p. 105-116.
- 1996b: Pre-Missi deformation in the central Flin Flon Belt: the steepening of strata and crustal thickening, in *Proceedings, Lithoprobe, Trans-Hudson Orogen Transect, Saskatoon Report No. 55*, p. 50-59.
- Stern, R.A., Lucas, S.B., Syme, E.C., Bailes, A.H., Thomas, D.J., Leclair, A.D., and Hulbert, L.**  
1993: Geochronological studies in the Flin Flon Domain, Manitoba-Saskatchewan, NATMAP Shield Margin Project area: Results for 1992-1993; in *Radiogenic Age and Isotopic Studies: Report 7*; Geological Survey of Canada, Paper 93-2, p. 59-70.
- Stern, R.A., Syme, E.C., Bailes, A.H., and Lucas, S.B.**  
1995a: Paleoproterozoic (1.90-1.86 Ga) arc volcanism in the Flin Flon Belt, Trans-Hudson Orogen, Canada; *Contributions to Mineralogy and Petrology*, v. 119, p. 117-141.
- Stern, R.A., Syme, E.C., and Lucas, S.B.**  
1995b: Geochemistry of 1.9 Ga MORB- and OIB-like basalts from the Amisk collage, Flin Flon Belt, Canada: evidence for intra-oceanic origin; *Geochimica et Cosmochimica Acta*, v. 59, p. 3131-3154.
- Syme, E.C.**  
1992: Elbow Lake project - Part A: supracrustal rocks and their structural setting; in *Manitoba Energy and Mines, Minerals Division, Report of Activities*, p. 32-46.
- Syme, E.C., Bailes, A.H., and Lucas, S.B.**  
1995: Geology of the Reed Lake area (parts of 63K/9 and 63K/10); in *Manitoba Energy and Mines, Minerals Division, Report of Activities*, p. 42-60.
- Whalen, J.B.**  
1992: Elbow Lake project - Part B: Granitoid rocks; in *Manitoba Energy and Mines, Minerals Division, Report of Activities*, p. 47-51.
- Whalen, J.B. and Hunt, P.A.**  
1994: Geochronological study of granitoid rocks in the Elbow Lake map area, Manitoba: a portion of the Flin Flon Domain of the Trans-Hudson Orogen; in *Radiogenic Age and Isotopic Studies: Report 8*; Geological Survey of Canada, *Current Research 1994-F*, p. 87-96.
- Whalen, J.B. and Stern, R.A.**  
1996: Geochemical and Nd isotopic features of granitoid magmatism within the Flin Flon Belt of the Trans-Hudson Orogen; *Geological Association of Canada-Mineralogical Association of Canada, Program with Abstracts*, v. 21, p. A101.



# Thermochronology of hornblende and biotite from the Wekusko Lake area, Flin Flon Domain, Trans-Hudson Orogen, Manitoba<sup>1</sup>

D. Marshall<sup>2</sup>, K. Connors<sup>3</sup>, and K. Ansdell<sup>4</sup>

*Marshall, D., Connors, K., and Ansdell, K., 1997: Thermochronology of hornblende and biotite from the Wekusko Lake area, Flin Flon Domain, Trans-Hudson Orogen, Manitoba; in Radiogenic Age and Isotopic Studies: Report 10; Geological Survey of Canada, Current Research 1997-F, p. 89-100.*

---

**Abstract:** Geothermobarometry results from the central region of the Wekusko Lake area of the eastern Trans-Hudson Orogen yield temperatures ranging from 575 to 625°C and estimated pressures of 1 to 3.8 kbar. These conditions were reached at ca. 1820-1805 Ma. However, cooling below the Ar closure temperatures for hornblende (i.e. ~500°C) and biotite (~350°C) did not occur until ca. 1755 Ma (range 1764 to 1747 Ma). The six samples analyzed in this study show evidence of hydrothermal degassing and, therefore, must be considered as minimum ages. However, these results from Wekusko Lake are consistent with Ar-Ar ages for hornblende and biotite throughout the eastern Trans-Hudson Orogen suggesting, therefore that post-peak metamorphic exhumation was delayed over a significant area or Ar diffusion was relatively homogeneous throughout the eastern Trans-Hudson Orogen. If this delay is attributed to collision with the Superior craton during or soon after peak metamorphism, then overthrusting of the eastern Trans-Hudson orogen by the Superior craton prevented the typical exhumation cycle which should follow thrust stacking and regional, burial metamorphism.

**Résumé :** La présente étude fournit de nouveaux résultats de géothermobarométrie relatifs à la partie centrale de la région du lac Wekusko, dans l'est de l'orogène trans-hudsonien. Les températures obtenues sont comprises entre 575 et 625 °C et les pressions estimées, entre 1 et 3,8 kbar. Ces conditions ont été atteintes à environ 1 820-1 805 Ma. Cependant, le refroidissement subséquent au-dessous des températures de fermeture de la hornblende (~500 °C) et de la biotite (~350 °C) à l'égard de l'argon n'a eu lieu que vers 1 755 Ma (1 764 à 1 747 Ma). Les six échantillons analysés dans le cadre de la présente étude révèlent des signes de dégazage hydrothermal et, par conséquent, les âges obtenus doivent être considérés comme minimaux. Cependant, les résultats obtenus dans la région du lac Wekusko sont en bon accord avec les données Ar-Ar existantes pour les hornblendes et biotites de l'ensemble de la partie est de l'orogène trans-hudsonien, ce qui suggère que l'exhumation ultérieure au pic thermique du métamorphisme a été retardée dans un vaste secteur, ou que la diffusion de Ar a été relativement homogène dans toute la partie est de l'orogène trans-hudsonien. Si ce retard est attribué à une collision avec le craton de la Province du lac Supérieur pendant, ou peu après, le pic du métamorphisme, alors le chevauchement de la partie est de l'orogène trans-hudsonien par le craton de la Province du lac Supérieur aura empêché le déroulement normal du cycle d'exhumation consécutif à l'empilement des nappes et au métamorphisme régional d'enfouissement associé.

---

<sup>1</sup> Contribution to the Shield Margin NATMAP Project

<sup>2</sup> Department of Earth Sciences, Carleton University, Ottawa, Ontario K1S 5B6

<sup>3</sup> Etheridge Henley Williams, Suite 34A, Walters Drive, Herdsman Business Park, Osborne Park, Western Australia, 6017 Australia

<sup>4</sup> Department of Geological Sciences, University of Saskatchewan, 114 Science Place, Saskatoon, Saskatchewan S7N 0W0

## INTRODUCTION

The Wekusko Lake study area occurs along the faulted boundary between the Flin Flon and Kisseynew belts in the eastern part of the Paleoproterozoic Trans-Hudson Orogen in central Canada. This orogen represents the broad collision zone between the Archean Superior and Rae-Hearne provinces (Hoffman 1989; Fig. 1a). The juvenile rocks of the Trans-Hudson Orogen are dominated by three principal tectonostratigraphic packages: i) volcano-plutonic rocks of the Amisk collage (Flin Flon belt); ii) File Lake Formation turbidites of the Kisseynew belt; and iii) alluvial-fluvial sandstones of the Missi suite (Stauffer, 1990) which occur in both belts.

The arc and ocean floor volcanic rocks of the Amisk collage (Fig. 1) were amalgamated and were subsequently intruded by numerous 1.87-1.84 Ga plutons (Lucas et al., 1996). The extensive turbidite basin of the Kisseynew belt developed partly within the Amisk collage. The 1.86-1.84 Ga turbidites (David et al., in press) are overlain by sandstones of the 1.85-1.83 Ga (Ansdell and Connors, 1994; Ansdell and Norman, 1995) Missi suite and may be laterally equivalent to coarse grained facies of the Kisseynew suite. Prior to 1832 Ma, D<sub>2</sub> compressional deformation resulted in basin inversion and southwest-directed thrusting of the Kisseynew turbidites over the older rocks of the Amisk collage (Connors, 1996). This stage of fold and thrust belt development continued until peak metamorphism (ca. 1820-1805 Ma). Although peak metamorphic conditions are considered to result, at least partly, from crustal thickening during D<sub>2</sub> thrust stacking (e.g. Ansdell et al., 1995), the high temperature, low to medium pressure conditions require additional heat input (Gordon et al., 1990).

The northwest-southeast D<sub>3</sub> shortening started at approximately 1800 Ma and resulted in at least two phases of upright folds that overprint the D<sub>2</sub> thrust stack. Microstructures indicate that conditions remained within the sillimanite stability field during the first stage of D<sub>3</sub> folding and at least within the biotite stability field (or higher) during the second stage of upright folding (Connors, 1996). Interpretation of geochronological and structural data from the Thompson Nickel belt to the east suggests that D<sub>3</sub> northwest-southeast shortening and associated transpressional deformation were active at 1780-1770 Ma and may have continued until ca. 1700 Ma (W. Bleeker, unpub. data, 1990). The D<sub>3</sub> deformation is considered to be the result of collision between the juvenile rocks of the Trans-Hudson Orogen and the Archean Superior craton, whereas the earlier D<sub>2</sub> fold-thrust belt development is attributed to collision with the buried Archean Saskatchewan craton (Ansdell et al., 1995; Lewry et al., 1996).

Uranium-lead zircon ages, interpreted as metamorphic, range from 1810-1803 Ma (Hunt and Zwanig, 1993; David et al., in press) whereas zircon ages from plutons interpreted as anatectic, and therefore synchronous with peak metamorphism, range from 1818-1814 Ma (Gordon et al., 1990; Ansdell and Norman, 1995). Interpreted U-Pb cooling ages from titanites range from 1810-1790 Ma, and Ar-Ar and K-Ar cooling ages cluster around 1850-1750 Ma for hornblende and 1830-1740 Ma for biotite near the Flin Flon-Kisseynew boundary and within the central Kisseynew belt (Fedorowich et al., 1995). Gordon (1989) proposed slow cooling for the high grade rocks of the Kisseynew belt, from 750°C and 550 MPa at approximately 1815 Ma to 280°C at ca. 1705 Ma, and calculated an uplift rate of 60-110 mm/Ma (about 4°C/Ma; Fedorowich et al., 1995). Fedorowich et al. (1995) interpreted an Ar-Ar hornblende age of ca. 1815 Ma as the

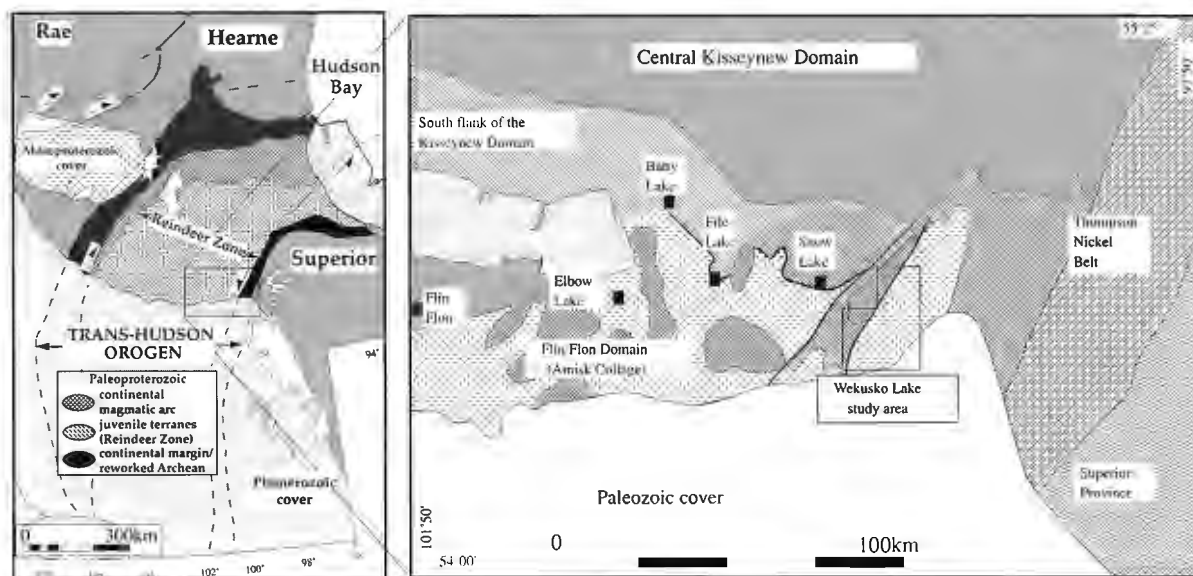


**Figure 1.** Geological map showing the location of the study area relative to the major litho-tectonic features in the Trans-Hudson Orogen.

age of peak metamorphism in the Flin Flon area, and calculated cooling rates which varied from 5 to 2.5°C/Ma from peak metamorphism to ca. 1690 Ma.

The main aim of this study has been to collect more data in an effort to better constrain the age and conditions of peak metamorphism and the cooling history of the eastern

Trans-Hudson Orogen. This work has included metamorphic petrology, calculation of thermobarometric conditions, and Ar-Ar studies in the Wekusko Lake area (Fig. 2) where a 3-5 km oblique section of crust is exposed. Recent structural analyses of the File Lake area and adjacent

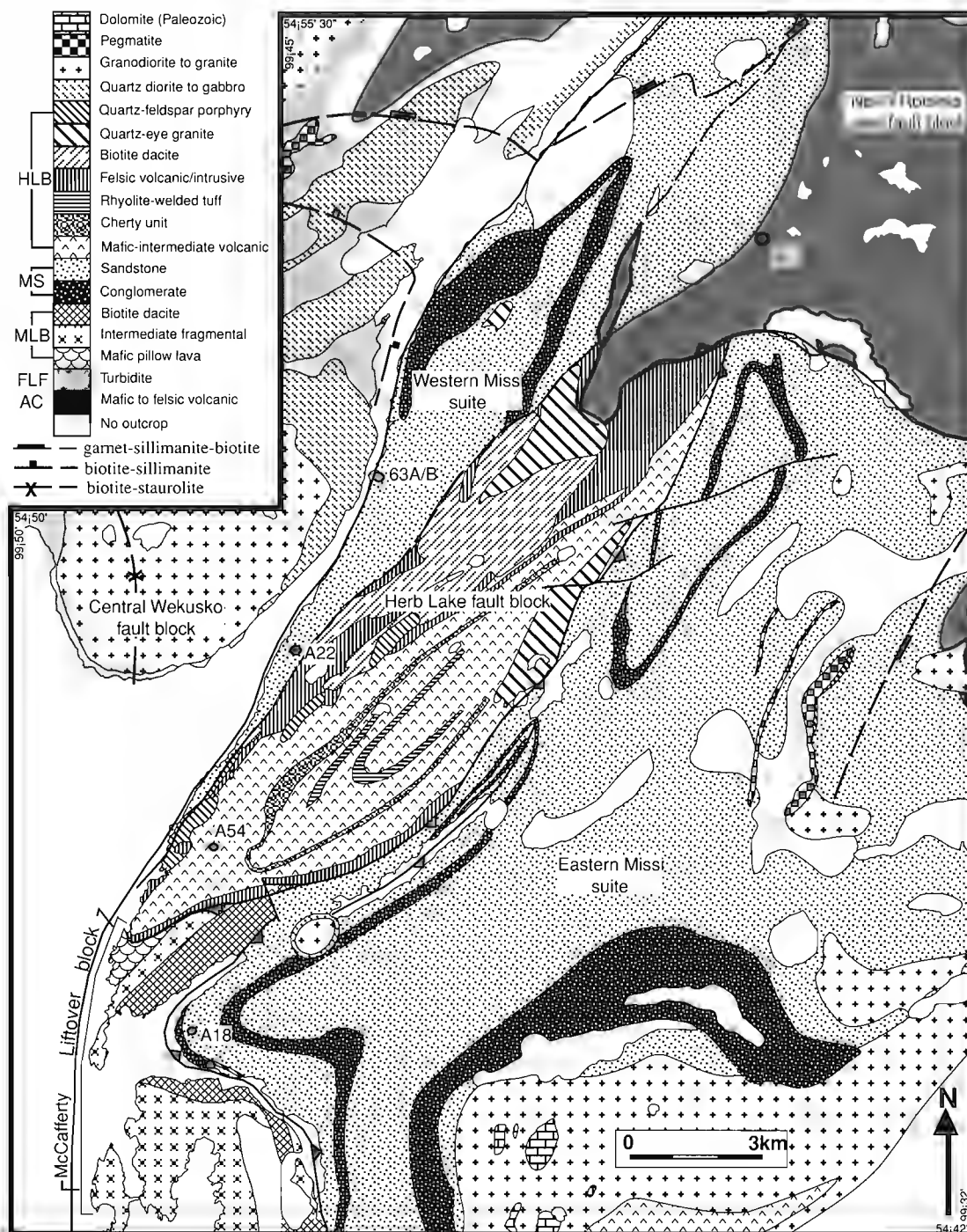


**Figure 2.** Simplified geological map of the east Wekusko Lake area (based on Armstrong, 1941; Frarey, 1950; Gordon and Gall, 1982; Connors, 1996). Argon sample locations are shown as dots (sample numbers abbreviated: A22=AY-93-22, 381= CRA-93-381 etc.). HLB=Herb Lake Block, MS=Missi Suite, MLB=McCafferty Liftover Block, FLF=File Lake Formation, AC=Amisk collage.

region provide the necessary background information for relating the thermal history to the deformation history (e.g. Ansdell and Connors, 1994).

## GEOOTHERMOMETRY

All samples chosen for geochronology and/or geothermometry were composed of fresh minerals in textural equilibrium and exhibited no obvious signs of alteration. Sample locations and rock types are listed in Table 1. Of the six samples chosen for Ar studies only two samples (CRA-93-63A and B) contained divariant mineral assemblages suitable for geothermobarometry.

Sample CRA-93-63A is from the Missi suite sandstone near the Crowduck Bay Fault and contains coexisting garnet, biotite, quartz, and plagioclase (Fig. 3). The almandine garnet porphyroblasts ranging in size up to 5 mm and the biotite porphyroblasts of similar size appear to be in textural equilibrium. The biotite defines the main fabric, generally deformed around the garnets, with the occasional biotite porphyroblast

cutting the main fabric. The matrix of the metamorphic minerals is quartzofeldspathic. Quartz constitutes approximately 50% of the rock. The plagioclase feldspar is partially sericitized and makes up approximately 30% of the rock. The garnet and biotite exist in equal proportions each comprising 10% of the sample.

Sample CRA-93-63B is from the same outcrop, but from within a more mafic compositional band centimetres from sample CRA-93-63A. It contains fresh hornblende porphyroblasts (Fig. 4). Some of the hornblende porphyroblasts define a weak fabric in the rock, while others grow at random orientations across the fabric. Hornblende comprises 40% of the sample, with 35% quartz, 23% mildly sericitized plagioclase feldspar, and 2% iron-titanium oxides.

Electron microprobe investigations of the biotite, garnet, and hornblende within the two samples used for geothermobarometry from the Wekusko Lake study area yielded no evidence of compositional zoning, due to multistage mineral growth or subsequent alteration. The averages of the individual porphyroblasts are shown in Table 2.

**Table 1.** Sample locations and rock types.

Sample #	Location	NTS Map	UTM-N	UTM-E	Rock type	Formation
CRA-93-63A	Crowduck Bay, Wekusko Lake	63J/13	6077200	453650	Metasandstone	Western Missi Suite
CRA-93-63B	Crowduck Bay, Wekusko Lake	63J/13	6077200	453650	Metasandstone	Western Missi Suite
CRA-93-381	Roberts Lake	63J/13	6081050	461580	Conglomerate	Robert Lake block
AY-93-18	Puella Bay, Wekusko Lake	63J/12	6065950	450250	Metasandstone	Eastern Missi Suite
AY-93-22	Crowduck Bay, Wekusko Lake	63J/13	6073850	452050	Metasandstone	Western Missi Suite
AY-93-54	West shore, Wekusko Lake	63J/13	6069900	450200	Mafic-intermediate Volcanic rock	Herb Lake block

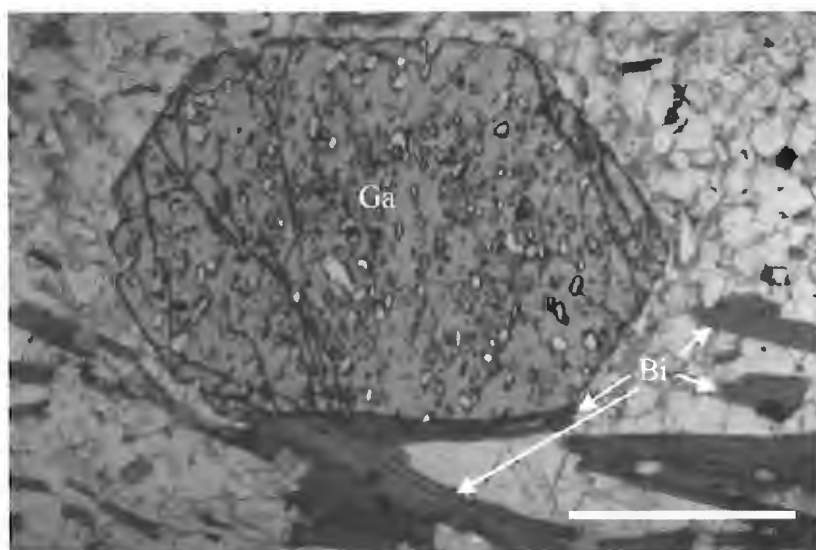


**Figure 3.**

Coexisting garnet (Ga) and biotite (Bi) in a matrix of Missi metasandstone (sample CRA-93-63A). Photo taken in plane polarized light. Scale bar is 0.1 mm.

**Figure 4.**

*Fresh hornblende (Hb) porphyroblasts in Missy metasandstone matrix (sample CRA-93-63B). Photo taken in plane polarized light. Scale bar is 0.1 mm.*

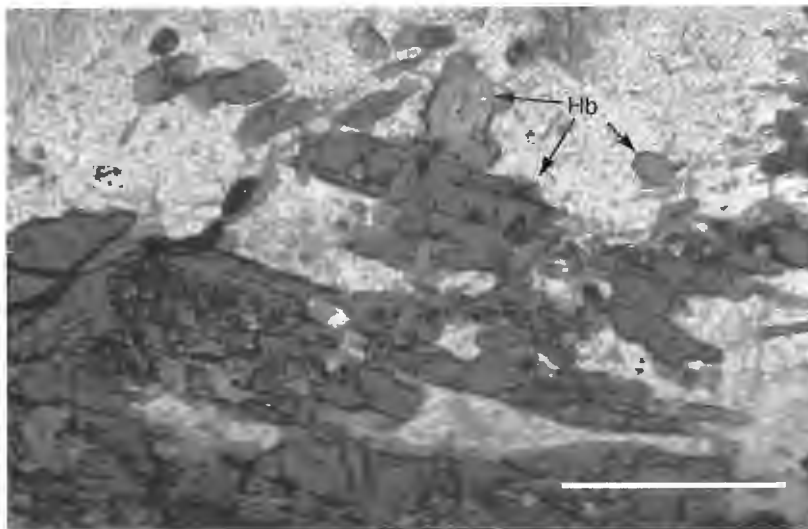


**Table 2.** Electron microprobe analyses: averages from six garnet-biotite pairs and amphibole samples from the same outcrop.

Garnet (CRA 93-63A)						
SiO <sub>2</sub>	37.38	37.14	37.22	36.63	37.49	37.56
Al <sub>2</sub> O <sub>3</sub>	21.04	20.97	20.88	20.64	21.06	21.06
TiO <sub>2</sub>	0.02	0.05	0.05	0.05	0.02	0.04
Cr <sub>2</sub> O <sub>3</sub>	0.04	0.05	0.07	0.03	0.03	0.03
FeO	34.58	34.41	33.69	34.30	35.00	34.94
MnO	1.91	2.25	2.65	2.16	1.88	2.00
MgO	2.74	2.66	2.56	2.56	2.80	2.58
CaO	2.74	2.59	2.95	2.58	2.54	2.50
Total	100.45	100.12	100.07	98.95	100.82	100.71
Biotite (CRA 93-63A)						
SiO <sub>2</sub>	35.65	35.53	35.71	35.63	35.56	35.84
Al <sub>2</sub> O <sub>3</sub>	18.21	18.07	18.17	18.08	18.32	18.37
TiO <sub>2</sub>	1.77	1.72	1.64	1.69	1.57	1.76
Cr <sub>2</sub> O <sub>3</sub>	0.08	0.07	0.09	0.14	0.06	0.12
FeO	20.89	21.46	21.51	20.64	21.28	21.10
MnO	0.06	0.04	0.05	0.04	0.06	0.07
MgO	9.33	9.23	9.35	9.40	9.15	8.78
CaO	0.02	0.04	0.02	0.04	0.02	0.04
K <sub>2</sub> O	9.31	9.23	9.21	9.07	9.32	9.32
Na <sub>2</sub> O	0.01	0.02	0.02	0.00	0.00	0.00
Cl	0.00	0.00	0.00	0.00	0.00	0.00
Total	95.33	95.42	95.77	94.73	95.34	95.40
Amphibole (CRA 93-63B)						
SiO <sub>2</sub>	44.32	42.75	42.94	44.23	44.70	
Al <sub>2</sub> O <sub>3</sub>	14.82	16.17	15.98	14.73	14.10	
TiO <sub>2</sub>	0.27	0.35	0.33	0.24	0.21	
Cr <sub>2</sub> O <sub>3</sub>	0.01	0.01	0.00	0.02	0.00	
FeO	15.00	15.34	15.08	14.82	14.74	
MnO	0.30	0.30	0.25	0.28	0.29	
MgO	10.72	9.95	10.03	10.93	11.02	
K <sub>2</sub> O	0.11	0.12	0.08	0.13	0.11	
CaO	11.68	11.39	11.59	11.54	11.69	
Na <sub>2</sub> O	1.27	1.41	1.33	1.23	1.04	
Cl	0.02	0.01	0.00	0.02	0.00	
Total	98.52	97.79	97.60	98.17	97.90	
Each of the averages above represents the average of 6 analyses from a single porphyroblast for garnet and biotite, and the average of 5 analyses for amphibole						

Gordon and Gall (1982) and Briggs and Foster (1992) were able to map the garnet-sillimanite-biotite, biotite-sillimanite, and biotite-staurolite isograds in the Crowduck Bay area of Wekusko Lake. There is a general trend of increasing metamorphic grade towards the north. The strike of the isograds is approximately east-west in the northern region of the study area, but the isograds show some deflection to the south near the Crowduck Bay Fault. Due to the lack of suitable metamorphic minerals Gordon and Gall (1982) were unable to extend the isograds to the east of the Crowduck Bay Fault into the Missi Sandstone. In an effort to improve our understanding of the metamorphic conditions east of the Crowduck Bay Fault, six coexisting garnet-biotite pairs from sample CRA-93-63A and adjacent amphiboles from sample CRA-93-63B were analyzed (Table 2). The compositions of the coexisting garnet-biotite pairs and adjacent amphiboles were input into a software package (Berman, 1991), using the thermodynamic data of Berman (1988, 1990).

The garnet-biotite pairs define a 575-640°C temperature range (Fig. 5), while the garnet-amphibole-quartz-plagioclase geobarometers of Mader and Berman (1992) yielded pressures in the 1 to 3.8 kbar range (Fig. 5). These

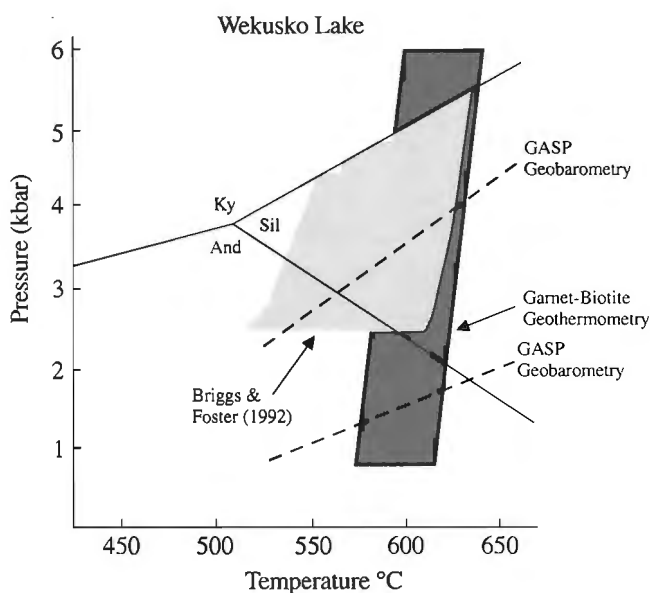


**Figure 5.** Pressure-temperature diagram for the Wekusko Lake area, Trans-Hudson Orogen (samples CRA-93-63A and B). The pressure and temperature constraints are based on garnet-biotite thermometry and garnet-amphibole-quartz-plagioclase (GASP) geothermobarometry. Thermodynamic data are from Berman (1991) with mineral activity models from Berman (1990) and McMullin et al. (1991) for garnet and biotite respectively. Data from Briggs and Foster (1992) are derived from garnet-aluminosilicate-quartz-plagioclase equilibria and coexisting garnet and biotite in the Niblock Lake area. The GASP geobarometric data was calculated using the activity and end-member reactions in Mader and Berman (1992) and thermodynamic data of Berman (1991). Ky=kyanite, Sil=sillimanite, And=andalusite.

data are consistent with the pressures and temperatures of sillimanite stability field as reported by Gordon and Gall (1982) directly to the north. The lack of a stable aluminosilicate phase may result from changes in the local bulk rock composition. However, the pressure and temperatures are consistent with the P-T stability field of sillimanite, thus extending the sillimanite-biotite isograd into the Missi suite conglomerates and sandstones on the southeastern shore of Crowduck Bay, with a deflection along the Crowduck Bay Fault consistent with the deflection of the other isograds.

## <sup>40</sup>Ar/<sup>39</sup>Ar TECHNIQUE AND RESULTS

Six samples containing hornblende and biotite were selected for <sup>40</sup>Ar/<sup>39</sup>Ar analysis. These samples are from throughout the study area and show no obvious signs of alteration. Sample treatment as in Roddick (1988) with an irradiation period of 3.1487 days. Data reduction is as outlined in Roddick (1990).

The resulting step heating data are reported in Table 3 and the incremental release spectra are shown in Figure 6. With the exception of the hornblende sample CRA93-63B (plateau age 1757 ± 11 Ma, 55% of the radiogenic Ar) all the spectra exhibit mid-spectral dips and bumps that are consistent with hydrothermally degassed argon release spectra (Hess et al., 1987) or analyses by some older mass spectrometers. These five spectra do not form consistent plateaus comprised of greater than 55% of total radiogenic argon and no correlation was observed between the argon release spectra and the presence of other elements such as K, Ca, and Cl. This is consistent with the mineral separates being pure. However, Hess et al. (1987) showed that chlorite layers in biotite at the sub-micrometre scale are sufficient to produce Ar-release spectra similar to those from the study area. Such small amounts of alteration are not visible at the magnifications attainable with scanning electron or petrographic microscopes.

The spectra are not consistent with the normal saddle shaped spectra derived from excess Ar. The data do not define consistent isochrons on a <sup>40</sup>Ar/<sup>36</sup>Ar versus <sup>39</sup>Ar/<sup>36</sup>Ar plot nor display linear patterns on <sup>36</sup>Ar/<sup>40</sup>Ar versus <sup>39</sup>Ar/<sup>40</sup>Ar correlation plots and cannot be interpreted as having inherited argon. Both the biotite and hornblende spectra yield similar total gas ages within experimental error, but fail to produce classic plateau ages. These relatively consistent ca. 1760 Ma (Ar ages) have been reported across the Trans-Hudson Orogen from hornblende and biotite for peak metamorphic conditions (M3) in the western Flin Flon area (Fedorowich et al., 1995). These spectra can be interpreted as consistent with rapid uplift rates, submicrometre mineral alteration products (Hess et al., 1987), or some type of irregular degassing behavior under vacuum conditions (Hess et al., 1987; Lee, 1992). Based on these observations, the spectra obtained in this study are difficult to interpret. However, the ages obtained may be used to define minimum ages, assuming that no excess argon has been incorporated into the minerals subsequent to the time the minerals cooled below their respective closure temperatures. Supporting evidence for the validity of this assumption is the lack of "saddle shaped" spectra commonly associated with excess argon.

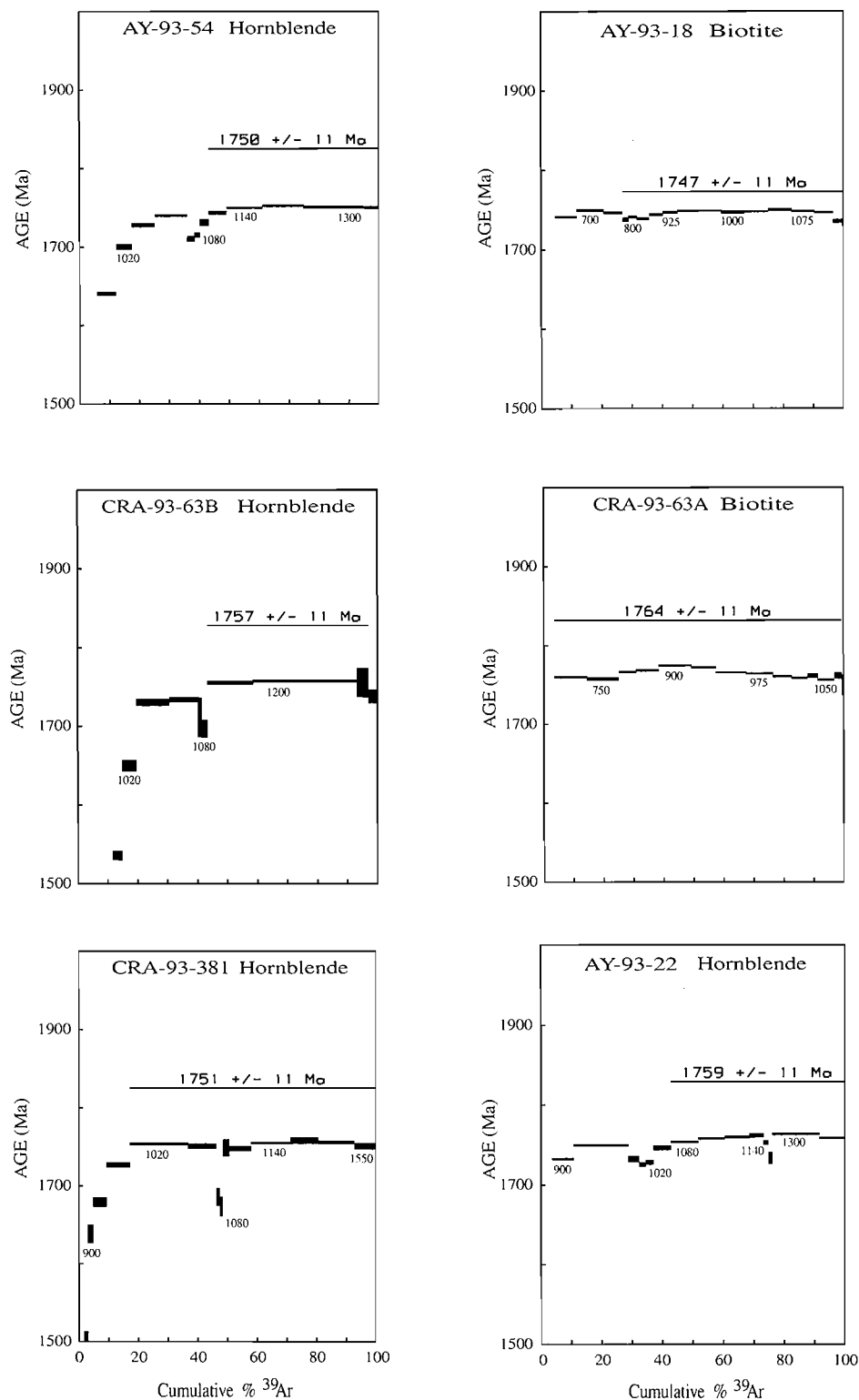


**Figure 6.** Argon release spectra for the biotite and hornblende samples of the Wekusko Lake area. All of the spectra except CRA93-63B are “bumpy” spectra characteristic of hydrothermal alteration (Hess et al., 1987). Sample CRA93-63B yields a plateau consisting of 55% of the radiogenic Ar released. The step temperatures are shown in degrees Celsius below some of the individual steps.

**Table 3.** Wekusko Lake biotite and hornblende argon step heating data.

Temp C	$^{36}\text{Ar}_{\text{tr}}$	$^{37}\text{Ar}_{\text{Ca}}$	$^{38}\text{Ar}_{\text{Cl}}$	$^{39}\text{Ar}_{\text{K}}$	$^{40}\text{Ar}^*/^{39}\text{Ar}$	%Atmos $^{40}\text{Ar}$	Apparent Age Ma $\pm 2$	$^{39}\text{Ar}$ (%)
<b>CRA-93-63B Hornblende J=0.018275 <math>\pm</math> 0.5 % (1 se) 61.58 mg</b>								
700	0.203	2.673	0.362	0.301	30.339	86.78	795.8 $\pm$ 57.9	4.53
800	0.014	1.505	0.027	0.089	64.508	42.75	1405.1 $\pm$ 52.2	1.34
900	0.010	4.374	0.018	0.176	57.267	23.41	1292.0 $\pm$ 19.8	2.65
975	0.006	6.236	0.022	0.206	64.463	11.72	1404.4 $\pm$ 13.4	3.10
1000	0.003	7.392	0.025	0.211	73.484	6.06	1536.0 $\pm$ 6.1	3.18
1020	0.003	11.104	0.034	0.315	81.842	3.75	1650.0 $\pm$ 7.1	4.74
1040	0.003	25.796	0.050	0.732	88.050	1.42	1730.2 $\pm$ 4.4	11.04
1060	0.003	21.536	0.037	0.636	88.323	1.58	1733.6 $\pm$ 3.3	9.59
1080	0.001	2.674	0.011	0.075	86.542	5.06	1711.0 $\pm$ 25.3	1.13
1100	0.004	4.822	0.017	0.133	85.411	8.71	1696.5 $\pm$ 11.3	2.00
1140	0.009	37.442	0.122	1.012	90.061	2.69	1755.4 $\pm$ 2.3	15.26
1200	0.011	79.907	0.333	2.298	90.217	1.60	1757.3 $\pm$ 1.6	34.64
1300	0.005	8.721	0.051	0.250	90.046	6.29	1755.2 $\pm$ 18.6	3.76
1550	0.017	7.053	0.062	0.200	88.633	21.72	1737.5 $\pm$ 8.4	3.02
Total:	0.292	221.23	1.170	6.630				100.00
<b>AY-93-22 Hornblende J=0.018375 <math>\pm</math> 0.5 % (1 se) 60.17 mg</b>								
700	0.038	3.676	0.334	0.613	38.792	31.96	970.9 $\pm$ 7.7	2.58
800	0.008	2.435	0.096	0.27	56.648	12.84	1287.0 $\pm$ 6.0	1.13
900	0.007	18.084	0.054	1.663	87.742	1.49	1732.3 $\pm$ 1.4	6.99
975	0.004	47.790	0.065	4.284	89.093	0.28	1749.4 $\pm$ 1.3	18.02
1000	0.004	10.278	0.013	0.845	87.737	1.56	1732.2 $\pm$ 3.6	3.55
1020	0.001	6.165	0.008	0.518	87.210	0.78	1725.6 $\pm$ 2.7	2.18
1040	0.001	6.499	0.009	0.605	87.410	0.77	1728.1 $\pm$ 2.8	2.54
1060	0.002	14.368	0.017	1.359	88.865	0.39	1746.5 $\pm$ 3.0	5.71
1080	0.001	23.759	0.028	2.158	89.450	0.20	1753.9 $\pm$ 1.3	9.08
1100	0.001	24.030	0.033	2.077	89.764	0.16	1757.8 $\pm$ 1.4	8.73
1120	0.001	23.355	0.040	1.925	89.923	0.25	1759.8 $\pm$ 1.4	8.1
1140	0.002	13.522	0.022	1.088	90.085	0.72	1761.8 $\pm$ 2.6	4.58
1180	0.003	5.037	0.008	0.407	89.354	2.09	1752.7 $\pm$ 2.8	1.71
1220	0.006	3.564	0.007	0.292	87.859	6.65	1733.8 $\pm$ 7.4	1.23
1300	0.006	46.610	0.054	3.675	90.218	0.53	1763.5 $\pm$ 1.4	15.45
1551	0.020	24.495	0.029	2.000	89.807	3.17	1758.4 $\pm$ 1.3	8.41
Total:	0.085	273.670	0.820	23.78				100.00
<b>CRA-93-381 Hornblende J = 0.0184 <math>\pm</math> 0.5 % (1 se) 64.50 mg</b>								
700	0.034	1.045	0.126	0.264	37.605	50.57	948.7 $\pm$ 12.4	2.05
800	0.005	0.619	0.010	0.109	69.853	15.83	1491.1 $\pm$ 21.3	0.85
900	0.004	3.129	0.007	0.244	80.404	6.13	1638.2 $\pm$ 11.8	1.89
975	0.005	15.798	0.012	0.581	83.509	3.15	1679.3 $\pm$ 6.0	4.52
1000	0.004	30.511	0.020	1.015	87.186	1.17	1726.8 $\pm$ 3.0	7.89
1020	0.004	66.900	0.044	2.520	89.305	0.47	1753.6 $\pm$ 1.7	19.60
1040	0.001	26.815	0.021	1.220	89.076	0.37	1750.7 $\pm$ 3.2	9.48
1060	0.001	3.423	0.003	0.149	84.004	1.50	1685.7 $\pm$ 11.1	1.16
1080	0.001	3.188	0.004	0.128	83.052	2.56	1673.3 $\pm$ 12.6	1.00
1100	0.001	6.941	0.007	0.281	88.894	1.40	1748.4 $\pm$ 10.7	2.19
1120	0.003	23.645	0.018	0.945	88.822	1.10	1747.5 $\pm$ 3.0	7.35
1140	0.009	43.521	0.033	1.714	89.370	1.76	1754.4 $\pm$ 1.3	13.33
1180	0.002	30.823	0.021	1.196	89.647	0.62	1757.9 $\pm$ 3.8	9.30
1300	0.009	38.087	0.028	1.560	89.428	1.82	1755.1 $\pm$ 2.0	12.13
1550	0.025	22.010	0.019	0.933	89.039	8.30	1750.2 $\pm$ 3.9	7.26
Total:	0.108	316.450	0.370	12.860				100.00



Table 3. (cont.)

Temp C	<sup>36</sup> Ar <sub>tr</sub>	<sup>37</sup> Ar <sub>Ca</sub>	<sup>38</sup> Ar <sub>Cl</sub>	<sup>39</sup> Ar <sub>K</sub>	<sup>40</sup> Ar*/ <sup>39</sup> Ar	%Atmos <sup>40</sup> Ar	Apparent Age Ma±2	<sup>39</sup> Ar (%)
<b>AY-93-18 Biotite J= 0.0183 ± 0.5 % (1 se) 5.93 mg</b>								
600	0.011	0.047	0.091	2.131	69.181	2.20	1475.8 ± 1.7	4.54
650	0.003	0.010	0.025	3.417	88.838	0.33	1741.6 ± 1.3	7.28
700	0.013	0.012	0.026	4.151	89.485	1.06	1749.7 ± 1.4	8.84
725	0.001	0.018	0.016	2.94	89.237	0.16	1746.6 ± 1.5	6.26
750	0.002	0.016	0.005	0.927	88.559	0.54	1738.1 ± 2.5	1.97
800	0.002	0.026	0.008	1.299	88.843	0.46	1741.7 ± 1.7	2.77
850	0.003	0.053	0.011	1.935	88.665	0.46	1739.4 ± 1.7	4.12
900	0.001	0.066	0.012	2.104	89.061	0.18	1744.4 ± 1.5	4.48
925	0.001	0.055	0.013	2.286	89.279	0.10	1747.1 ± 1.5	4.87
950	0.002	0.068	0.020	3.207	89.421	0.20	1748.9 ± 1.3	6.83
975	0.001	0.045	0.019	3.579	89.464	0.04	1749.5 ± 1.4	7.62
1000	0.002	0.035	0.020	3.593	89.275	0.17	1747.1 ± 1.8	7.65
1025	0.001	0.031	0.019	3.667	89.371	0.04	1748.3 ± 1.3	7.81
1050	0.000	0.031	0.019	3.67	89.540	0.00	1750.4 ± 1.5	7.81
1075	0.001	0.047	0.017	3.492	89.371	0.05	1748.3 ± 1.4	7.44
1100	0.001	0.065	0.016	2.914	89.264	0.17	1747.0 ± 1.3	6.21
1200	0.003	0.366	0.008	1.393	88.384	0.79	1735.9 ± 2.3	2.97
1550	0.015	0.081	0.003	0.254	88.471	16.25	1737.0 ± 7.2	0.54
Total:	0.053	1.070	0.350	46.96				100.00
<b>CRA-93-63A Biotite J = 0.0182 ± 0.5 % (1 se) 5.10 mg</b>								
600	0.011	0.011	0.050	1.488	63.942	3.37	1392.5 ± 1.3	3.50
700	0.018	0.000	0.020	4.663	90.784	1.21	1759.7 ± 1.3	10.98
750	0.003	0.000	0.012	4.483	90.612	0.22	1757.6 ± 2.1	10.56
800	0.000	0.001	0.007	2.428	91.302	0.02	1766.1 ± 1.4	5.72
850	0.003	0.000	0.008	3.203	91.484	0.28	1768.4 ± 1.5	7.54
900	0.000	0.000	0.011	4.654	91.997	0.02	1774.7 ± 1.3	10.96
925	0.000	0.006	0.007	3.443	91.775	0.01	1772.0 ± 1.3	8.11
950	0.001	0.017	0.010	4.285	91.28	0.08	1765.9 ± 1.2	10.09
975	0.000	0.000	0.008	3.816	91.147	0.00	1764.2 ± 1.1	8.99
1000	0.001	0.012	0.005	2.654	90.854	0.09	1760.6 ± 1.5	6.25
1025	0.002	0.004	0.004	2.217	90.701	0.33	1758.7 ± 1.3	5.22
1050	0.000	0.006	0.004	1.474	90.922	0.09	1761.5 ± 2.7	3.47
1100	0.001	0.035	0.005	2.329	90.499	0.19	1756.2 ± 1.4	5.49
1200	0.000	0.011	0.003	1.06	90.913	0.04	1761.3 ± 3.8	2.50
1550	0.006	0.094	0.002	0.266	89.921	6.46	1749.0 ± 13.0	0.63
Total:	0.046	0.200	0.160	42.46				100.00
<b>AY-93-54 Hornblende J = 0.0184 ± 0.5 % (1 se) 52.33 mg</b>								
700	0.030	1.963	0.177	0.399	29.070	43.41	773.0 ± 6.4	2.31
800	0.007	1.595	0.058	0.243	52.426	14.42	1218.3 ± 5.2	1.41
900	0.007	4.302	0.053	0.368	66.555	7.31	1442.5 ± 5.2	2.13
975	0.004	17.434	0.204	1.115	80.578	1.44	1640.5 ± 2.5	6.44
1000	0.001	14.794	0.193	0.892	85.134	0.55	1700.4 ± 3.6	5.16
1020	0.004	20.167	0.385	1.338	87.285	0.94	1728.0 ± 2.5	7.74
1040	0.003	27.306	0.435	1.868	88.244	0.47	1740.2 ± 1.5	10.80
1060	0.002	6.323	0.089	0.424	85.920	1.42	1710.6 ± 3.4	2.45
1080	0.001	4.798	0.069	0.314	86.290	1.20	1715.3 ± 3.2	1.82
1100	0.002	7.812	0.113	0.509	87.558	1.01	1731.5 ± 4.4	2.95
1120	0.002	15.718	0.235	1.027	88.536	0.79	1743.9 ± 2.4	5.94
1140	0.005	31.678	0.481	2.075	89.022	0.80	1750.0 ± 1.2	12.00
1180	0.004	36.518	0.561	2.387	89.211	0.48	1752.4 ± 1.4	13.80
1220	0.003	27.956	0.47	1.868	89.094	0.54	1750.9 ± 1.8	10.80
1300	0.002	22.405	0.365	1.503	89.060	0.53	1750.5 ± 1.6	8.69
1550	0.022	14.292	0.238	0.964	89.005	6.92	1749.8 ± 1.5	5.57
Total:	0.081	255.06	4.13	17.29				100.00
all gas quantities are given in units of 10 <sup>-9</sup> cm <sup>3</sup> at standard temperature and pressure, and have been corrected for decay, isotopes derived from minor interfering neutron reactions, and blanks. <sup>36</sup> Ar <sub>tr</sub> denotes trapped Ar, Ca, Cl, and K denote Ar derived from these elements. <sup>40</sup> Ar* denotes radiogenic argon corrected for atmospheric argon. Errors on the individual heating steps do not include the error in the irradiation parameter J.								

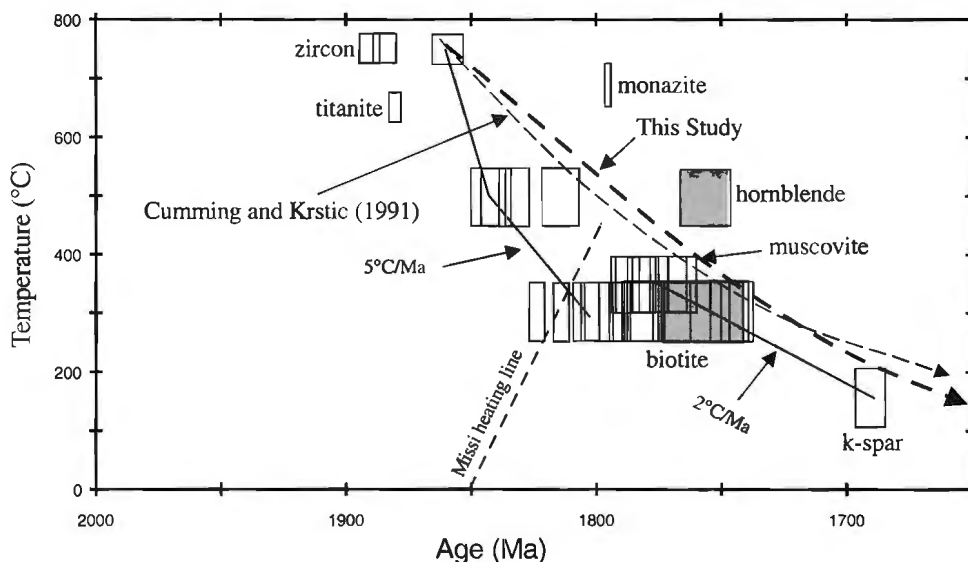


**Figure 7.** Temperature versus time plot for the Flin Flon Domain (after Fedorowich et al., 1995). Data are from Fedorowich et al. (1995), U-Pb monazite (Hunt and Zwanig, 1993) and others (see text). T-t paths shown as a solid line are from Fedorowich et al. (1995). The large-dash T-t path is from Cumming and Krstic (1991). The heavy-signature small-dash T-t path best fits the data from this study and thermochronological data obtained from the eastern Flin Flon Domain. Closure temperature for Ar in K-feldspar (k-spar) from Fedorowich et al. (1995), for Ar in hornblende from Hunziker et al. (1992), for Ar in muscovite from Purdy and Jager (1976), for Ar in biotite from Armstrong et al. (1966) for U-Pb in titanite from Metzger et al. (1992), for U-Pb in monazite from Parrish (1990). The curve from this study is anchored on the previous previously published T-t endpoints of Cumming and Krstic (1991) and Fedorowich et al. (1995). The ranges of data obtained from the four hornblende and two biotite samples in this study are shown in grey.

## DISCUSSION AND CONCLUSIONS

There are two interesting observations arising from the Ar-Ar results for the eastern Trans-Hudson Orogen. The Ar-Ar ages for the hornblende samples are approximately 60 Ma younger than the interpreted age of peak metamorphism. Secondly, the Ar-Ar ages for hornblende samples are similar to those for the biotite. However, before considering the implications of these results we need to examine possible problems with these data.

As discussed above, the samples show evidence of hydrothermal degassing, possibly due to very fine scale degassing. This therefore implies that these results must be considered as minimum ages. However, the ca. 1755 Ma ages obtained in this study are very similar to Ar-Ar and K-Ar data for hornblende and biotite from surrounding areas. It is possible that all of these data sets are reasonably accurate despite some degree of resetting.

It is very difficult to envisage hornblende and biotite samples over such a wide area (Fig. 2) all being subject to an episode of hydrothermal degassing which results in such consistent resetting of the Ar-Ar isotopic systems. It seems unlikely that an alteration event would be that widespread and

that consistent in its effects. It seems more plausible that a regional event such as uplift and cooling could result in widespread ages that are so consistent.

Another problem is similar biotite and hornblende ages in the eastern Trans-Hudson Orogen. Commonly accepted values for closure temperature for Ar in hornblende and biotite are 500°C and 300°C respectively (Hunziker et al., 1992). Therefore, there should be an obvious difference in the Ar-Ar ages for these two minerals for slow to moderate cooling rates. The similarity in the ages for hornblende and biotite may suggest that there was a very rapid period of uplift at ca. 1755 Ma that resulted in rapid cooling through 500°C to below 300°C.

If there was indeed a rapid period of uplift at ca. 1755 Ma, as evidenced by the four hornblende and two biotite samples from this study, then this implies a markedly different temperature-time (T-t) path than that proposed by Fedorowich et al. (1995) for the Flin Flon region approximately 100 km to the west (Fig. 1). There does not appear to be a correlation between Ar-Ar age and metamorphic grade or grain size across the Trans-Hudson Orogen. Of course the paths of argon diffusion (Lee, 1995) are unidentified and it is conceivable that different types of argon diffusion paths are present within the Trans-Hudson Orogen, and this could result in variable Ar closure temperatures across the orogen.

If the Tt path shown in Figure 7 is valid for the eastern Trans-Hudson Orogen then one of the main issues is the slow cooling rate (0602°C/Ma) from the time of peak metamorphism, i.e. ca. 1820–1805 Ma based on present data, to cooling through both hornblende and biotite closure temperatures at ca. 1755 Ma. In most areas, peak temperatures (500–650°C) were not far above hornblende closure temperatures (500°C) and appear to have remained above this temperature until ca. 1760 Ma, when cooling through hornblende and biotite closure temperatures occurred at approximately the same time.

It is possible that the slow cooling rates may be related to the complex collisional history of the Trans-Hudson Orogen. Peak metamorphism is attributed, in part, to thermal re-equilibration after southwest-directed D<sub>2</sub> thrust stacking. This thrust event is interpreted to result from the collision between the Trans-Hudson Orogen and the buried Saskatchewan craton. However, the late cooling ages suggest that the area remained at depth and was not uplifted after peak metamorphism as is typical after thrust stacking. This phenomenon can be explained by the D<sub>3</sub> collision which resulted in the Superior craton to the east overthrusting the Trans-Hudson Orogen. This second overthrusting event of relatively cooler thrust sheets would initially deflect the isotherms downwards, accounting for the relatively flat temperature-time path shown for the eastern Trans-Hudson Orogen. This later collision between the orogen and another Archean craton could have prevented the exhumation of the eastern Trans-Hudson Orogen after the initial D<sub>2</sub> thrust stacking. In contrast, the Flin Flon area, which is farther from the influence of the Superior collision, may have been exhumed as expected after D<sub>2</sub> thrusting.

## ACKNOWLEDGMENTS

Chris Roddick is thanked initiating this project. We gratefully acknowledge the NATMAP Shield Margin Project for funding which covered all aspects of the fieldwork and analyses. K. Connors and K. Ansdell were recipients of National Science and Engineering Research Council Post-doctoral fellowships at Canadian Government Laboratories and D. Marshall was a recipient of National Science and Engineering Research Council Post-doctoral fellowship award 188980. We would like to thank S. Lucas for valuable input throughout our work on the Trans-Hudson Orogen, F. Quigg for performing the analyses, P. Hunt for assistance throughout this project, J.A.R. Stirling and G. Pringle for guiding D. Marshall through the rigors of automated probe analyses, and S. Schaan and I. Russell for assistance during the fieldwork and sampling. Edgar Froese, Mike Villeneuve, and Reg Thériault are thanked for critical reviews of an earlier version of this manuscript.

## REFERENCES

- Ansdell, K.M. and Connors, K.A.  
1994: Lithological and structural relationships in Paleoproterozoic rocks in the east Wekusko Lake area, Trans-Hudson Orogen, Manitoba; in *Current Research 1994-C*; Geological Survey of Canada, p. 193–203.
- Ansdell, K.M. and Norman, A.R.  
1995: U-Pb geochronology and tectonic development of the southern flank of the Kisseynew domain; Trans-Hudson Orogen, Canada; *Precambrian Research*, v. 72, p. 147–67.
- Ansdell, K.M., Lucas, S.B., Connors, K., and Stern, R.A.  
1995: Kisseynew Metasedimentary Gneiss Belt, Trans-Hudson Orogen (Canada)-back-arc origin and collisional inversion; *Geology*, v. 23, no. 11, p. 1039–1043.
- Armstrong, J.E.  
1941: Wekusko, Manitoba; Geological Survey of Canada, Map 665A.
- Armstrong, R.L., Jager, E., and Eberhardt, P.  
1966: A comparison of K-Ar and Rb-Sr ages on Alpine biotites; *Earth and Planetary Science Letters*, v. 1, p. 13–19.
- Berman, R.G.  
1988: Internally-consistent thermodynamic data for stoichiometric minerals in the system Na<sub>2</sub>O-K<sub>2</sub>O-CaO-MgO-FeO-Fe<sub>2</sub>O<sub>3</sub>-Al<sub>2</sub>O<sub>3</sub>-SiO<sub>2</sub>-TiO<sub>2</sub>-H<sub>2</sub>O-CO<sub>2</sub>; *Journal of Petrology*, v. 29, p. 445–522.
- 1990: Mixing properties of Ca-Mg-Fe-Mn garnets; *The American Mineralogist*, v. 75, p. 328–344.
- 1991: Thermobarometry using multiequilibrium calculations: a new technique with petrologic applications; *Canadian Mineralogist*, v. 29, p. 833–855.
- Briggs, W. and Foster, C.T.  
1992: Pressure-temperature conditions of Early Proterozoic metamorphism during the Trans-Hudson Orogen as determined from rocks straddling the Flin-Flin Kisseynew boundary at Niblock and File lakes, Manitoba; *Canadian Journal of Earth Sciences*, v. 29, p. 2497–2507.
- Connors, K.A.  
1996: Unraveling the boundary between turbidites of the Kisseynew domain and the volcano-plutonic rocks of the Flin Flon domain in the eastern Trans-Hudson Orogen, Canada; *Canadian Journal of Earth Sciences*, v. 33, p. 811–829.
- Cumming, G.L. and Krstic, D.  
1991: Geochronology at the Namew Lake Ni-Cu orebody, Flin Flon area, Manitoba, Canada: thermal history of a metamorphic terrane; *Canadian Journal of Earth Sciences*, v. 28, p. 309–325.
- David, J., Bailes, A.H., and Machado, N.  
in press: Evolution of the Snow Lake portion of the Paleoproterozoic Flin Flon and Kisseynew belts, Trans-Hudson Orogen, Manitoba, Canada; *Precambrian Research*.
- Fedorowich, J.S., Kerrich, R., and Stauffer, M.R.  
1995: Geodynamic evolution and thermal history of the central Flin Flon Domain, Trans-Hudson Orogen: constraints from structural development, <sup>40</sup>Ar/<sup>39</sup>Ar, and stable isotope geothermometry; *Tectonics*, v. 14, p. 472–503.
- Frarey, M.J.  
1950: Crowduck Bay, Manitoba. Geological Survey of Canada, Map 987A.
- Gordon, T.M.  
1989: Thermal evolution of the Kisseynew sedimentary gneiss belt, Manitoba: metamorphism at an early Proterozoic accretionary margin; in *Evolution of Metamorphic Belts*, (ed.) J.S. Daly, R.A. Cliff, and B.W.D. Yardley; Geological Society, Special Publication 43, p. 233–243.
- Gordon, T.M. and Gall, Q.  
1982: Metamorphism in the Crowduck Bay area, Manitoba; in *Current Research, Part A*; Geological Survey of Canada, Paper 82-1A, p. 197–201.
- Gordon, T.M., Hunt, P.A., Bailes, A.H., and Syme, E.C.  
1990: U-Pb ages from the Flin Flon and Kisseynew Belts, Manitoba: chronology of crust formation at an Early Proterozoic accretionary margin; *Geological Association of Canada, Special Paper 37*, p. 177–199.
- Hess, J.C., Lippolt, H.J., and Wirth, R.  
1987: Interpretation of <sup>40</sup>Ar/<sup>39</sup>Ar spectra of biotites: evidence from hydrothermal degassing experiments and TEM studies; *Chemical Geology*, v. 66, p. 137–149.
- Hoffman, P.F.  
1989: Precambrian geology and tectonic history of North America; in *The geology of North America: an Overview*, (ed.) A.W. Bailey and A.R. Palmer; Geological Society of America, *The Geology of North America*, v. A, p. 447–512.

**Hunt, P.A. and Zwanzig, H.V.**

1993: U-Pb ages of intrusion, metamorphism and deformation in the Batty Lake area, Keesynew gneiss belt, Manitoba; in *Manitoba Energy and Mines, Minerals Division, Report of Activities, 1993*, p. 34-37.

**Hunziker, J.C., Desmons, J., and Hurford, A.J.**

1992: Thirty-two years of geochronological work in the Central and Western Alps: a review on seven maps; *Memoires de Geologie (Lausanne)*, no. 13, 59 p.

**Lee, J.K.W.**

1992: The argon release mechanisms of hornblende in vacuo; *Chemical Geology*, v. 106, p. 133-170.

1995: Multipath diffusion in geochronology; *Contributions to Mineralogy and Petrology*, v. 120, p. 60-82.

**Lewry, J., Lucas, S., Stern, R., Ansdell, K., and Ashton, K.**

1996: Tectonic assembly and orogenic closure in the Trans-Hudson Orogen; Geological Association of Canada-Mineralogical Association of Canada joint annual meeting, Program with Abstracts, v. 21, p. A56.

**Lucas, S.B., Stern, R.A., Thomas, D.J., Reilly, B.A., Syme, E.C., and Bales, A.H.**

1996: Intraoceanic tectonics and the development of continental-crust, 1.92-1.84 Ga evolution of the Flin Flon belt, Canada; *Geological Society of America, Bulletin*, May, v. 108, no. 5, p. 602-629.

**Mader, U. and Berman, R.**

1992: Amphibole thermobarometry: a thermodynamic approach; in *Current Research, Part E*; Geological Survey of Canada, Paper 92-1E, p. 393-400.

**McMullin D., Berman R.G., and Greenwood H.J.**

1991: Calibration of the SGAM thermobarometer for pelitic rocks using data from phase equilibrium experiments and natural assemblages; *Canadian Mineralogist*, v. 29, p. 889-908.

**Metzger K., Essene E., and Halliday, A.N.**

1992: Closure temperatures for the Sm-Nd system in metamorphic garnets; *Earth and Planetary Science Letters*, v. 113, p. 397-410.

**Parrish, R.R.**

1990: U-Pb dating of monazite and its application to geological problems; *Canadian Journal of Earth Sciences*, v. 27, p. 1431-1450.

**Purdy, J.W. and Jager, E.**

1976: K-Ar ages of fissure minerals from the Swiss Alps; *Schweizerische Mineralogische und Petrographische Mitteilungen*, v. 53, p. 79-98.

**Roddick, J.C.**

1988: The assessment of errors in  $^{40}\text{Ar}/^{39}\text{Ar}$  dating; in *Radiogenic Age and Isotopic Studies: Report 2*; Geological Survey of Canada, Paper 88-2, p. 7-16.

1990:  $^{40}\text{Ar}/^{39}\text{Ar}$  evidence of the age of the New Quebec Crater, northern Quebec; in *Radiogenic Age and Isotopic Studies: Report 3*; Geological Survey of Canada, Paper 89-2, p. 7-16.

**Stauffer, M.R.**

1990: The Missi Formation; Geological Association of Canada, Special Paper 37, p. 121-142.

# U-Pb age constraints on the timing of deposition of the Waugh Lake and Burntwood (Athabasca) groups, southern Taltson magmatic zone, northeastern Alberta<sup>1</sup>

M.R. McDonough<sup>2</sup> and V.J. McNicoll<sup>3</sup>

*McDonough, M.R. and McNicoll, V.J., 1997: U-Pb age constraints on the timing of deposition of the Waugh Lake and Burntwood (Athabasca) groups, southern Taltson magmatic zone, northeastern Alberta; in Radiogenic Age and Isotopic Studies: Report 10; Geological Survey of Canada, Current Research 1997-F, p. 101-111.*

---

**Abstract:** The Waugh Lake and Burntwood groups are dominantly metasedimentary sequences that outcrop in the southern Taltson magmatic zone in northeastern Alberta. The Waugh Lake Group, which forms a small outlier of lower greenschist grade sandstones, pelites, and volcanics exposed in the footwall of the Andrew Lake shear zone, was intruded by 1.97-1.96 Ga plutonic rocks of the Colin Lake and Andrew Lake suites. Detrital zircon ages from a sample of Waugh Lake Group conglomerate and the ages of intrusions constrain the timing of deposition of the lower part of the Waugh Lake Group to be between 2.02 and 1.97 Ga, which is older than previously inferred. Based on isotopic, geochemical, and stratigraphic considerations, the Waugh Lake basin is interpreted as a small intra-arc basin related to the Taltson arc.

The Burntwood group is a section of lower greenschist grade sandstones and pelites exposed in a small outlier on the northwest shore of Lake Athabasca. Detrital zircons from a sample of arkosic hematitic pebbly sandstone indicate that the Burntwood group is younger than ca. 1.92 Ga and therefore not correlative with the Waugh Lake Group. On the basis of U-Pb data, locality, and lithological similarities, we propose reassignment of the Burntwood group to the Athabasca Group.

**Résumé :** Les groupes de Waugh Lake et de Burntwood se composent principalement de séquences métasédimentaires qui affleurent dans la partie sud de la zone magmatique de Taltson, dans le nord-est de l'Alberta. Le Groupe de Waugh Lake, qui forme un petit lambeau de grès, de pélites et de roches volcaniques métamorphisés au faciès des schistes verts inférieur que l'on peut observer dans le mur de la zone de cisaillement d'Andrew Lake, a été recoupé par les roches plutoniques des suites de Colin Lake et d'Andrew Lake à 1,97-1,96 Ga. Les datations effectuées sur des zircons détritiques extraits d'un échantillon de conglomérat du Groupe de Waugh Lake, de même que les âges des intrusions situent la période où a eu lieu le dépôt de la partie inférieure du Groupe de Waugh Lake entre 2,02 et 1,97 Ga, ce qui est plus tôt qu'on ne l'avait d'abord estimé. D'après l'interprétation des données isotopiques, géochimiques et stratigraphiques, le bassin dans lequel a eu lieu le dépôt du Groupe de Waugh Lake serait un petit bassin intra-arc associé à l'arc de Taltson.

---

<sup>1</sup> Contribution to Canada-Alberta Agreement on Mineral Development (1992-1995), a subsidiary agreement under the Canada-Alberta Economic and Regional Development Agreement

<sup>2</sup> SERNAGEOMIN, La Paz 406, Puerto Varas, Chile (Internet: sernageo@reuna.cl)

<sup>3</sup> Geological Survey of Canada, 601 Booth Street, Ottawa, Ontario, K1A 0E8

Le groupe de Burntwood est une succession de grès et de pélites du faciès des schistes verts inférieur qui affleure dans un petit lambeau sur la rive nord-ouest du lac Athabasca. Les zircons détritiques contenus dans un échantillon de grès arkosique à cailloux hématitiques indiquent que le groupe de Burntwood est plus récent que 1,92 Ga environ et qu'il n'est pas, par conséquent, une unité corrélatrice du Groupe de Waugh Lake. En nous basant sur les données U-Pb, le lieu et les similarités lithologiques, nous proposons de réattribuer le groupe de Burntwood au Groupe d'Athabasca.

## INTRODUCTION

The Waugh Lake and Burntwood groups are siliciclastic sequences exposed as outliers in northeastern Alberta within the Taltson magmatic zone (Fig. 1). To date, the age, correlation, and tectonostratigraphic significance of these units has been uncertain. In this paper we present new U-Pb geochronological evidence from detrital and magmatic zircons which brackets deposition of the Waugh Lake Group to the interval between 2.02 and 1.97 Ga and suggest that it formed in an intra-arc setting related to the Taltson arc. We also show that the Burntwood group was deposited after ca. 1.92 Ga, precluding correlation to the Waugh Lake Group (cf. Godfrey, 1980), and propose that it represents the northwest remnant of Athabasca basin, as suggested by Fahrig (1961).

## GEOLOGICAL SETTING

The exposed part of the Taltson magmatic zone is a 300 km long, northerly trending belt of granitic basement gneisses, amphibolite, supracrustal gneisses, and voluminous Paleoproterozoic magmatic rocks underlying northeastern Alberta and the District of Mackenzie. It is bounded to the north by the Great Slave Lake shear zone and to the south, in the subsurface, by the Snowbird tectonic zone (Fig. 1). The Taltson magmatic zone is interpreted as an Andean-type continental magmatic arc and collisional orogen between the subsurface Paleoproterozoic Buffalo Head terrane on the west, and the Archean Churchill Province to the east (Fig. 1, 2; Hoffman, 1989; Ross et al., 1991; Thériault, 1992; Plint and McDonough, 1995). The Taltson magmatic zone forms the southern continuation of the Thelon tectonic zone, a collisional orogen between the Archean Slave and Churchill provinces north of Great Slave Lake (e.g., Hoffman, 1988; Tirrul and Grotzinger, 1990; Henderson and van Breemen, 1991; Hanmer et al., 1992; Fig. 1). Paleoproterozoic magmatic rocks, ranging in age from 1.99–1.92 Ga (Bostock et al., 1987, 1991; Ross et al., 1991; Villeneuve et al., 1993; McNicoll et al., 1994), intrude Archean to earliest Paleoproterozoic gneisses of the Taltson basement complex (McDonough et al., 1995a; V.J. McNicoll and M.R. McDonough, unpub. data, 1996). Enclaves of high-grade pelitic to quartzose gneisses assigned to the 2.13 to 2.08 Ga Rutledge basin (Bostock and van Breemen, 1994) are widespread within plutonic and basement gneisses of the Taltson magmatic zone (Fig. 1). Gneisses and plutonic rocks of the Taltson magmatic zone are deformed by ca. 1930–1935 Ma upper amphibolite to granulite grade shear zones (McDonough et al., 1995b), which are variably overprinted by greenschist grade deformation between 1900 and 1800 Ma (Plint and McDonough, 1995).

## Waugh Lake Group

The Waugh Lake Group forms a small outlier of lower greenschist grade sandstones, pelites, and volcanics in southern Taltson magmatic zone. It is exposed in the footwall of the Andrew Lake shear zone (Fig. 2), a ductile thrust fault that was active at about 1932 Ma, and records oblique, top-to-the-northeast displacement (M.R. McDonough and V.J. McNicoll, unpub. data, 1996). The Andrew Lake shear zone carried Taltson basement complex gneisses in its hanging wall eastward over Andrew Lake granodiorite, rocks of the Colin Lake and Wylie Lake plutonic suites, and the Waugh Lake Group. Hanging wall gneisses are at upper amphibolite to granulite facies, while footwall rocks range from amphibolite facies at the thrust, to lower greenschist facies in the Waugh Lake Group 2 km to the east (McDonough et al., 1995b; Fig. 2). As a result of its low metamorphic grade and its proximity to high grade gneisses of the Andrew Lake thrust sheet, the Waugh Lake Group was previously considered to be the youngest unit of the Taltson magmatic zone (Godfrey, 1986; McDonough et al., 1993). The low metamorphic grade of the rocks of the Waugh Lake Group led Baadsgaard and Godfrey (1972) to interpret a 1780 Ma K-Ar biotite date from a volcanic unit to approximate the age of the basin.

North of the west arm of Waugh Lake, the Waugh Lake Group outlines a broadly synformal feature with a northeast-southwest axis. Formation names have been formally proposed by Iannelli et al. (1995, Fig. 3). The Martyn Lake Formation comprises thin and rhythmically bedded  $T_{bc}$  and  $T_{cd}$  Bouma sequences with abundant way-up criteria. The dominant lithology is dark grey chlorite-bearing slate, which is pelitic in character and indicative of the low grade of metamorphism of the Waugh Lake Group. The argillites have important arsenopyrite occurrences in distinctive bedding-parallel tourmaline veins that contain quartz tension gashes perpendicular to bedding. These veins predate all folding and possibly are diagenetic in character. A second set of arsenopyrite-bearing quartz+tourmaline veins cuts bedding and early veins.

At Doze Lake, the lower conglomerate unit has minor volcanic breccia at its base (Fig. 3), overlain by pebble to boulder conglomerate (debris flow?) with clasts up to cobble size of white quartzite, feldspathic grit, and chlorite schist, all within a matrix of well foliated silty chloritic phyllite interpreted to be pyroclastic by Iannelli et al. (1995). The quartzite and grit cobbles contain rounded millimetre-scale quartz and/or feldspar grains, and therefore are recycled clastics. Coarse pebble to cobble conglomerates from both lower and upper conglomerate units generally contain clasts of white quartzite and granitoid, and intrabasinal clasts from the underlying rhythmite. Rare clasts of tourmaline with quartz tension veins

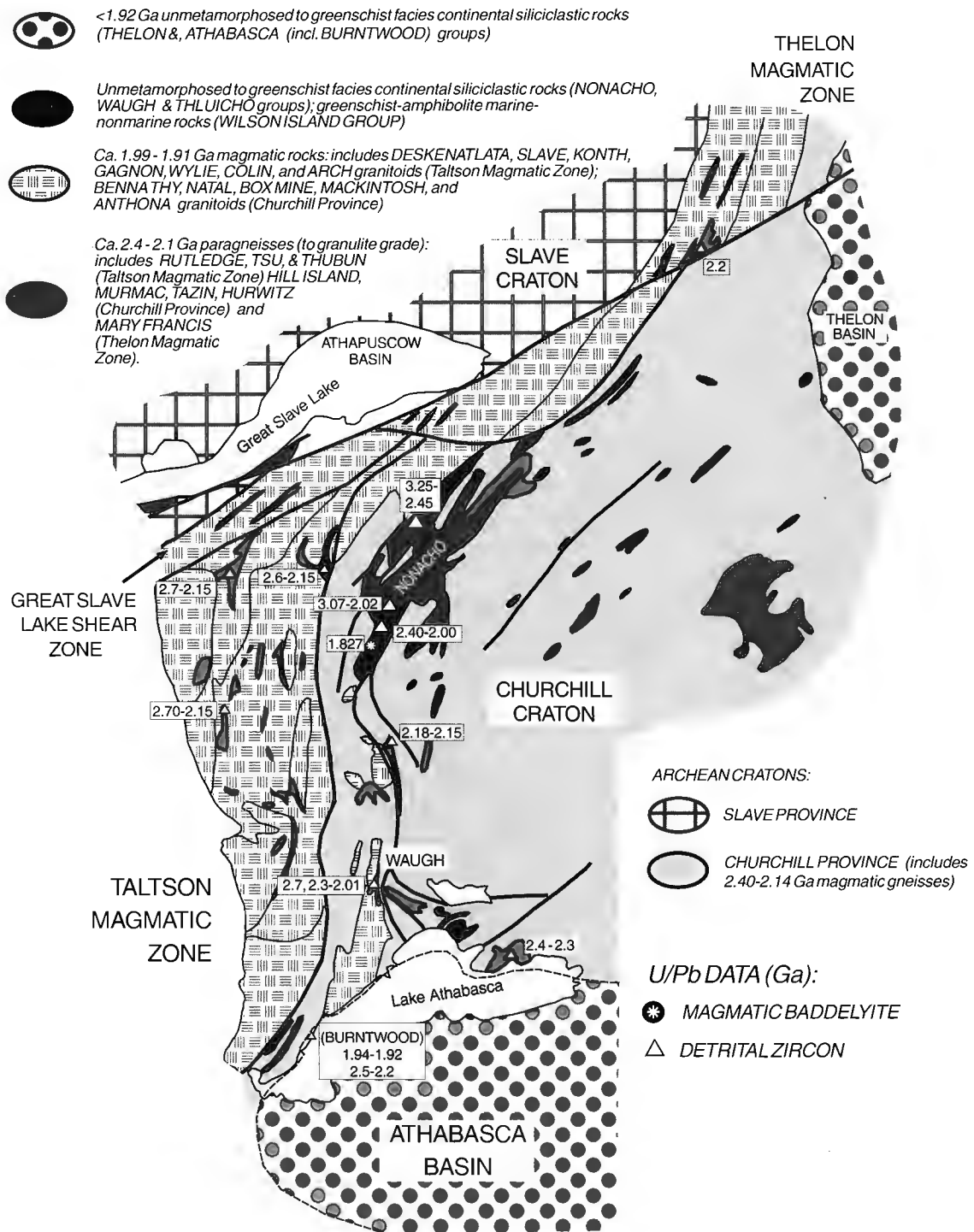


**Figure 1.** Generalized regional geological map of the western Canadian Shield (modified from van Breemen and Aspler, 1994) showing the distribution of supracrustal rocks relative to magmatic and cratonic gneisses. Detrital zircon data are from this study, Bostock and van Breemen (1994), and van Breemen and Aspler (1994). Baddeleyite data are for the Sparrow dykes, which cut the Nonacho Group (Bostock and van Breemen, 1992).

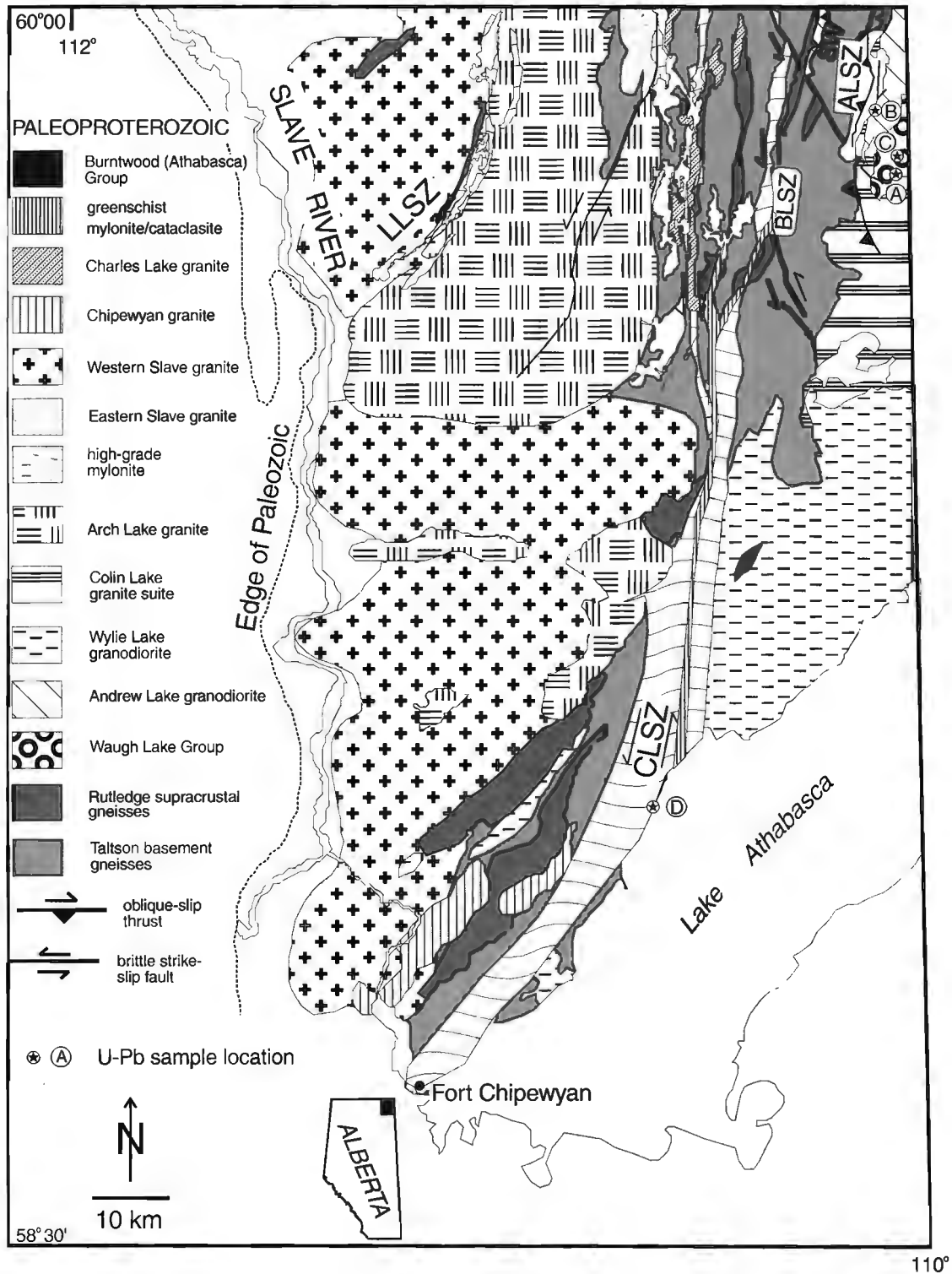


**Figure 2.** Generalized geological map of the southern Taltson magmatic zone modified from Godfrey (1986) and McDonough et al. (1993, 1994) showing locations of U-Pb samples; ALSZ, Andrew Lake shear zone; BLSZ, Bayonet Lake shear zone; CLSZ, Charles Lake shear zone; LLSZ, Leland Lakes shear zone; SW, Swinnerton window.



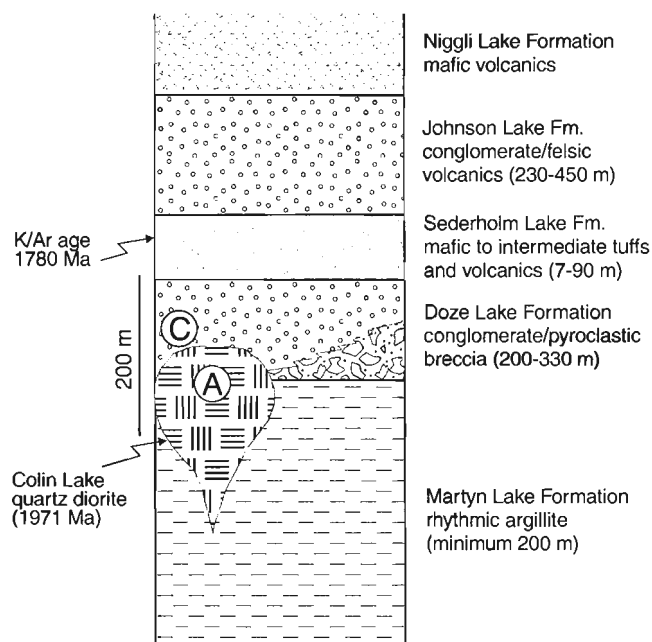


**Figure 3.** Generalized stratigraphic column for the Waugh Lake Group (C.W. Langenberg, pers. comm., 1994; modified from Iannelli et al., 1995). Labels give the approximate stratigraphic position of the Colin Lake quartz diorite (A) and Doze Lake conglomerate (C) U-Pb geochronology samples.

are most probably derived from the distinctive veins in the underlying argillite. The Doze Lake conglomerate has thin-bedded parallel and crossbedded sandstones that grade up into pebbly feldspathic wacke. Sandstones have thin interlayers of fine grained tuffaceous material. Mafic to intermediate flows and pyroclastic breccia interfinger with basal Doze Lake conglomerates.

### Burntwood group

The Burntwood group (informally proposed by Godfrey, 1980, 1986) is an approximately 200 m thick (minimum) section of lower greenschist grade sandstones and pelites exposed in a 100 m wide outlier on the northwest shore of Lake Athabasca (McDonough et al., 1996). The Burntwood group consists of mauve to pink, hematite-cemented, coarse-grained, thick-bedded, locally arkosic, quartz pebble sandstones and quartz sandstones. Sandstones are generally massive, but locally display parallel and trough crossbedding. Minor interbeds of grey-green argillite are within the sandstone. Thicker units of dark green, thinly laminated silty argillite with slaty cleavage and distinctive quartz-hematite veins separate sandstone units. A maximum of 200 m of Burntwood group strata are exposed.

Strata of the Burntwood group were previously included within the Athabasca Group by Fahrig (1961), but were subsequently informally defined and correlated with the Waugh Lake Group by Godfrey (1980) on the basis of depositional features, low metamorphic grade, a lack of hematitic regolith at the basement contact, and resemblance of green pelites to the turbidites of the Martyn Lake Formation.

The Burntwood sliver is bounded to the west by high-grade gneisses of the Taltson basement complex and the ca. 1925 Ma Chipewyan granite (V.J. McNicoll and M.R. McDonough, unpub. data, 1996). A less than 50 m wide brittle postdepositional fault zone separates the Burntwood rocks from the basement (McDonough et al., 1996); bedding in the Burntwood strata dips about 50–70°W toward the fault. Cataclasites consist of Taltson basement complex gneisses and Chipewyan granite on the west, and Burntwood group sandstone with quartz stockwork on the east. The fault is the southern extension of the main brittle fault that forms a central topographic trough along the length of the Charles Lake shear zone (Fig. 2).

## U-Pb GEOCHRONOLOGY

### Analytical methods

The U-Pb analytical methods used in this study are those outlined in Parrish et al., (1987). Treatment of analytical errors follows Roddick (1987), with regression analysis modified after York (1969). Analytical results are presented in Table 1, where errors on the ages are reported at the 2s level, and displayed in the concordia plots (see Fig. 4–7, below). Zircon fractions analyzed are all comprised of single grains that were very strongly air abraded following the method of Krogh (1982). The U-Pb sample locations are displayed in Figure 2 and sample site co-ordinates are provided in Table 1.

The U-Pb isotopic analyses of detrital zircons are reported from samples of conglomeratic sandstone from the Waugh Lake Group and the Burntwood (Athabasca) group. Nine or ten single grains of representative morphology were selected for analysis from each of the two samples; Table 1 includes a description of each zircon grain analyzed. The detrital grains were picked for analysis on the basis of optical clarity and lack of cracks, inclusions, or apparent cores, while at the same time, attempting to ensure that the range of morphological types in each sample was represented. Most of the detrital zircons yielded analyses with low degrees of discordance. The  $^{207}\text{Pb}/^{206}\text{Pb}$  ages of grains that are less than 2.5% discordant are considered to be close to the primary crystallization ages of the source rocks from which they were derived. More discordant analyses are interpreted to represent minimum crystallization ages.

### Waugh Lake Group

A sample of moderately foliated muscovite-bearing feldspathic wacke with centimetre-scale clasts was collected from the Doze Lake Formation of the Waugh Lake Group (sample MRB-MAN-14; location C in Fig. 2, 3). The rock contained colourless to light brown, subrounded to rounded zircon grains and colourless to light brown, equant to prismatic well faceted crystals. The concordant to slightly discordant single grain analyses have  $^{207}\text{Pb}/^{206}\text{Pb}$  ages that are dominantly in the 2.3–2.0 Ga age range, with one grain of ca. 2.7 Ga (Fig. 4). The youngest detrital zircon analyzed is  $2006 \pm 15$  Ma (fraction D); the age of the rock is therefore constrained to be younger than 2.02 Ga.

The Martyn Lake argillite and the Doze Lake conglomerate unit of the Waugh Lake Group are intruded by biotite quartz diorite of the Colin Lake suite on the southern part of the basin, and by the biotite-hornblende Andrew Lake granodiorite on the northern side of the basin (Fig. 2), thereby obliterating potential stratigraphic and/or syndeositional faulting relationships on the margins of the basin. A sample of well foliated biotite-rich Colin Lake quartz diorite gneiss was collected on the north shore of the west arm of Waugh Lake (sample MSB-93-148; location A in Fig. 2, 3). The sample contains well faceted, clear, colourless zircons ranging in shape from equant to prismatic and containing minor inclusions. Five single grains (labelled A-F on Fig. 5) were

analyzed from this rock. A linear regression (MSWD=3.43) through all five analyses has an upper intercept of  $1971 \pm 4$  Ma and is interpreted to be the age of intrusion. The  $^{207}\text{Pb}/^{206}\text{Pb}$  ages of the two most concordant analyses (A, B) are  $1970 \pm 6$  Ma and  $1971 \pm 2$  Ma, which are in agreement with the interpreted age of the rock.

A sample of foliated biotite-hornblende Andrew Lake granodiorite was collected from the east shore of Andrew Lake (sample MRB-MAN-27; location B in Fig. 2). The rock contains equant to prismatic, well faceted zircons with minor inclusions. Zircon fractions C, D, E, and F, which have fairly high U contents (Table 1), are 3-4% discordant. A linear regression through these four single grain analyses has an

**Table 1.** U-Pb analytical data.

Fraction <sup>a</sup>	wt. <sup>b</sup> ug	U ppm	Pb <sup>c</sup> ppm	206Pb <sup>d</sup>	Pb <sup>e</sup> pg	208Pb <sup>f</sup>	Radiogenic ratios ( ± 1σ, %) <sup>g</sup>			Ages (Ma, ± 2σ) <sup>h</sup>			% <sup>i</sup> disc
				204Pb		%	206Pb	207Pb	207Pb	206Pb	207Pb	207Pb	
							238U	235U	206Pb	238U	235U	206Pb	
MRB-MAN-14, Waugh Lake Group conglomerate (UTM 12, 554502E-6630797N; NTS 74M/16)													
A, b,r	1	215.8	133.5	115	86	12.42	0.5290 ± 0.64	13.822 ± 1.60	0.1895 ± 1.28	2737 ± 29	2738 ± 30	2738 ± 41	0
B, b,r	2	133.0	53.10	489	16	5.92	0.3862 ± 0.13	6.985 ± 0.24	0.1312 ± 0.18	2105 ± 5	2110 ± 4	2114 ± 6	0.5
C, c,r	3	169.7	72.06	798	17	10.32	0.3900 ± 0.12	7.248 ± 0.20	0.1348 ± 0.15	2123 ± 4	2142 ± 4	2161 ± 5	2.1
D, c,r	2	132.5	51.57	236	28	11.14	0.3579 ± 0.17	6.088 ± 0.52	0.1234 ± 0.43	1972 ± 6	1989 ± 9	2006 ± 15	1.9
E, c,p,f	1	303.8	126.7	513	17	9.24	0.3855 ± 0.11	7.528 ± 0.22	0.1416 ± 0.17	2102 ± 4	2176 ± 4	2247 ± 6	7.6
F, c,e,f	2	487.2	228.3	208	122	9.31	0.4303 ± 0.16	8.770 ± 0.51	0.1478 ± 0.42	2307 ± 6	2314 ± 9	2321 ± 15	0.7
G, c,p,f	1	209.2	92.33	692	11	11.74	0.3964 ± 0.15	7.759 ± 0.21	0.1420 ± 0.16	2153 ± 5	2204 ± 4	2251 ± 5	5.2
H, c,p,f	2	456.4	177.8	1596	10	5.92	0.3773 ± 0.10	6.753 ± 0.12	0.1298 ± 0.06	2063 ± 3	2080 ± 2	2096 ± 2	1.8
J, c,r	1	296.9	146.4	657	13	13.35	0.4326 ± 0.18	8.802 ± 0.19	0.1476 ± 0.12	2317 ± 7	2318 ± 4	2318 ± 4	0
K, b,e,f	6	370.6	175.7	708	82	11.40	0.4255 ± 0.10	8.642 ± 0.17	0.1473 ± 0.12	2286 ± 4	2301 ± 3	2315 ± 4	1.5
MSB-93-148, Colin Lake quartz diorite, Waugh Lake (UTM 12, 554461E-6629170N; NTS 74M/16)													
A, c,e,f	3	287.6	111.0	602	29	11.10	0.3558 ± 0.12	5.934 ± 0.24	0.1209 ± 0.18	1962 ± 4	1966 ± 4	1970 ± 6	0.5
B, c,e,f	3	132.3	52.68	1303	8	13.78	0.3559 ± 0.10	5.937 ± 0.13	0.1210 ± 0.06	1963 ± 4	1967 ± 2	1971 ± 2	0.5
C, c,p,f	2	241.1	87.78	1819	6	12.54	0.3305 ± 0.11	5.452 ± 0.12	0.1196 ± 0.06	1841 ± 3	1893 ± 2	1951 ± 2	6.5
D, c,p,f	3	264.2	96.37	1325	13	11.56	0.3347 ± 0.12	5.550 ± 0.14	0.1203 ± 0.08	1861 ± 4	1908 ± 2	1960 ± 3	5.8
E, c,e,f	4	183.2	69.93	1827	9	10.60	0.3539 ± 0.12	5.890 ± 0.13	0.1207 ± 0.07	1953 ± 4	1960 ± 2	1967 ± 3	0.8
MRB-MAN-27, Andrew Lake granodiorite, Andrew Lake (UTM 12, 550268E-6635205N; NTS 74M/16)													
A, c,p,f	2	335.6	153.5	1305	9	16.07	0.3900 ± 0.20	7.707 ± 0.22	0.1433 ± 0.11	2123 ± 7	2197 ± 4	2268 ± 4	7.3
C, c,p,f	5	628.5	230.6	7873	9	11.30	0.3382 ± 0.09	5.526 ± 0.10	0.1185 ± 0.03	1878 ± 3	1905 ± 2	1934 ± 1	3.3
D, c,p,f	3	668.8	250.5	2065	19	12.64	0.3340 ± 0.11	5.559 ± 0.13	0.1186 ± 0.05	1887 ± 4	1910 ± 2	1935 ± 2	2.9
E, c,p,f	3	499.4	181.0	3123	10	11.86	0.3322 ± 0.12	5.389 ± 0.13	0.1176 ± 0.05	1849 ± 4	1883 ± 2	1921 ± 2	4.3
F, c,el,f	2	747.7	267.6	2273	17	8.31	0.3410 ± 0.09	5.578 ± 0.11	0.1186 ± 0.05	1891 ± 3	1913 ± 2	1936 ± 2	2.6
MSB-95-45, Athabasca Group conglomeratic sandstone (UTM 12, 520003E-6542999N; NTS 74M/2)													
A, c,r	7	201.5	86.03	2477	12	22.29	0.3442 ± 0.09	5.648 ± 0.11	0.1190 ± 0.05	1907 ± 3	1923 ± 2	1941 ± 2	2.0
B, b,r	6	155.2	70.69	3338	7	12.38	0.4056 ± 0.09	8.025 ± 0.10	0.1435 ± 0.04	2195 ± 3	2234 ± 2	2270 ± 2	3.9
C, b,r	4	462.9	227.9	7883	7	5.98	0.4621 ± 0.09	10.491 ± 0.10	0.1647 ± 0.03	2449 ± 4	2479 ± 2	2504 ± 1	2.5
D, b,r	3	700.3	259.5	3239	13	10.05	0.3466 ± 0.10	5.616 ± 0.11	0.1175 ± 0.05	1919 ± 3	1919 ± 2	1919 ± 2	0
E, c,f	3	65.31	33.87	246	22	17.99	0.4307 ± 0.20	8.721 ± 0.38	0.1469 ± 0.30	2309 ± 8	2309 ± 7	2310 ± 10	0
F, c,f	3	194.9	88.73	2157	6	10.80	0.4132 ± 0.11	8.110 ± 0.12	0.1423 ± 0.06	2230 ± 4	2243 ± 2	2256 ± 2	1.4
G, c,f	2	227.2	110.2	1446	7	12.87	0.4283 ± 0.11	8.644 ± 0.13	0.1464 ± 0.07	2298 ± 4	2301 ± 3	2304 ± 2	0.3
H, c,e,f	1	360.3	160.6	1674	5	12.32	0.3989 ± 0.11	7.597 ± 0.12	0.1381 ± 0.06	2164 ± 4	2184 ± 2	2204 ± 2	2.2
I, b,e,sl	1	368.2	125.8	655	12	5.80	0.3307 ± 0.12	6.011 ± 0.18	0.1318 ± 0.13	1842 ± 4	1977 ± 3	2123 ± 51	15.2

<sup>a</sup> Zircon fractions are all strongly air abraded; c=colourless; b=light brown; e=equant; p=prismatic (length to width ratio of about 2:1); el=elongate; f=well faceted; sf=subfaceted; r=rounded to subrounded

<sup>b</sup> Error on weight = ± 1 μg

<sup>c</sup> Radiogenic Pb

<sup>d</sup> Measured ratio corrected for spike and Pb fractionation of 0.09 ± 0.03%/AMU

<sup>e</sup> Total common Pb on analysis corrected for fractionation and spike

<sup>f</sup> Radiogenic Pb

<sup>g</sup> Corrected for blank Pb and U and common Pb (Stacey-Kramers model Pb composition equivalent to the <sup>207</sup>Pb/<sup>206</sup>Pb age)

<sup>h</sup> Corrected for blank and common Pb

<sup>i</sup> % discordance (to origin)

upper intercept of  $1962 \pm 16/-10$  Ma (MSWD=2.5), which is interpreted to represent the age of crystallization of the rock (Fig. 6). A strongly discordant zircon grain analyzed from this rock (fraction A, not shown; Table 1) is ca. 2.3 Ga in age, and is interpreted to be inherited.

### Burntwood group

A sample of coarse grained, trough crossbedded hematite-cemented quartz pebble sandstone was collected from the northwest shore of Lake Athabasca (Burntwood group of Godfrey, 1980; sample MSB-94-45; location D in Fig. 2) for

detrital zircon geochronology to test possible correlation with the Waugh Lake Group (Godfrey, 1980). The sample contains fairly poor quality zircons; many contain fractures and numerous inclusions. The zircon population is comprised of colourless to light brown, rounded grains and well faceted to subfaceted crystals. Most of the analyses range from concordant to moderately discordant and fall in two  $^{207}\text{Pb}/^{206}\text{Pb}$  age ranges: 2.5–2.2 Ga and 1.94–1.92 Ga (Fig. 7). The younger age range indicates that the Burntwood group is younger than 1.92 Ga and probably received detritus from the emergent plutons of the Taltson magmatic zone.

### MRB-MAN-14, Waugh Lake Group conglomerate

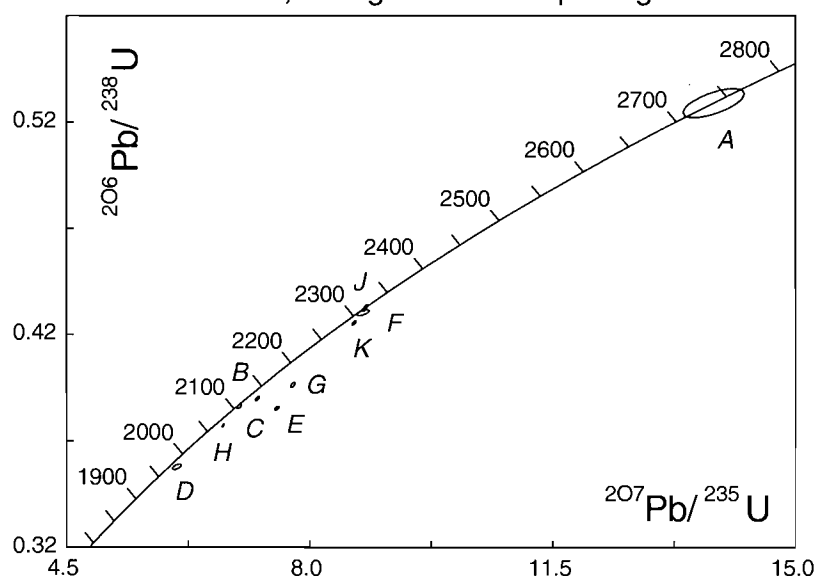
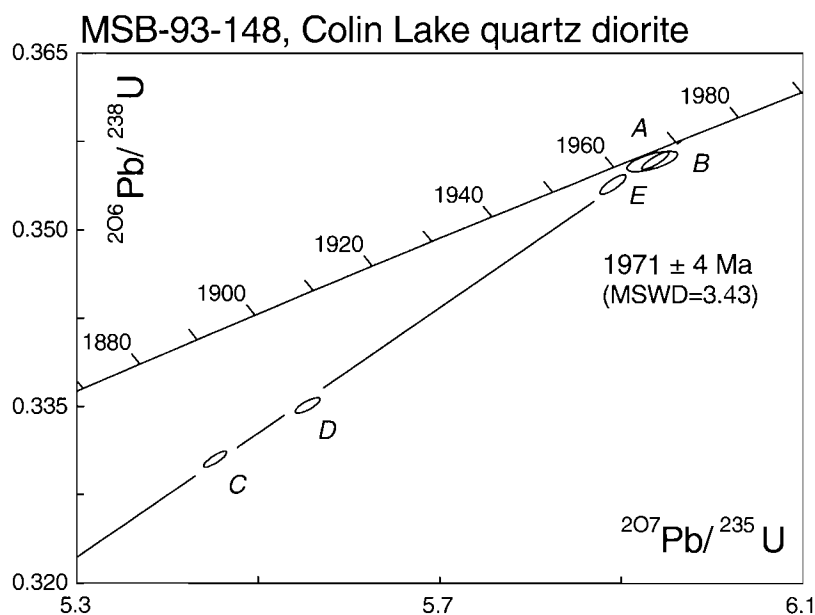


**Figure 4.**

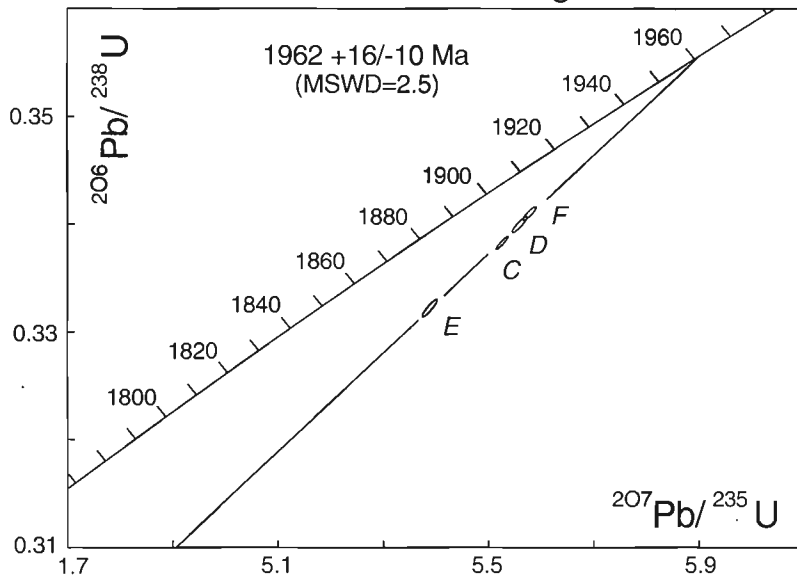
*U-Pb concordia diagram of detrital zircons from the lower conglomerate unit of the Waugh Lake Group (location C in Fig. 2). Single grain analyses have  $^{207}\text{Pb}/^{206}\text{Pb}$  ages that fall mostly in the 2.3 to 2.01 Ga range, with one grain of ca. 2.7 Ga.*

**Figure 5.**

*U-Pb concordia diagram of zircons from the Colin Lake quartz diorite at Waugh Lake (location A in Fig. 2), which intrudes metasediments of the Waugh Lake Group.*



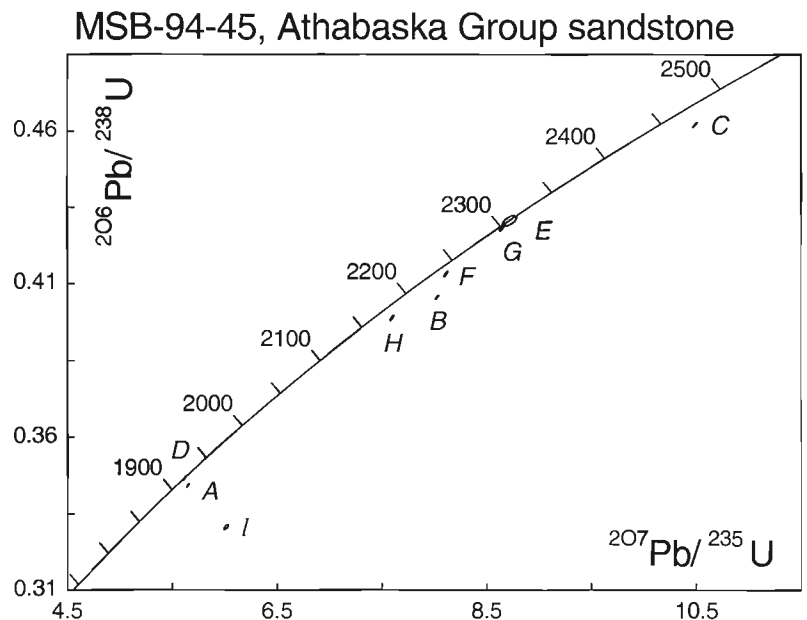
## MRB-MAN-27, Andrew Lake granodiorite

**Figure 6.**

*U-Pb concordia diagram of zircons from the Andrew Lake granodiorite at Andrew Lake (location B in Fig. 2), which intrudes metasediments of the Waugh Lake Group on the north side of the basin.*

**Figure 7.**

*U-Pb concordia diagram of detrital zircons from an arkosic sandstone of the Athabasca Group (Burntwood group; location D in Fig. 2). Single grain analyses have  $^{207}\text{Pb}/^{206}\text{Pb}$  ages that fall in two age ranges: 2.5–2.2 Ga and 1.94–1.92 Ga.*



## DISCUSSION AND CONCLUSIONS

Detrital zircon ages and the ages of intrusions constrain the timing of deposition of the lower part of the Waugh Lake basin to within a 50 Ma period between 2.02 and 1.97 Ga. This age bracket overlaps 1.986 Ga I-type subduction-related magmatism (Deskenatlata gneiss) in the northern Taltson magmatic zone (Bostock et al., 1991; Thériault, 1992). The basement of the Taltson magmatic zone is comprised of 2.44–2.14 Ga magmatic gneisses that intrude Archean gneisses (Bostock et al., 1991; van Breemen et al., 1992; V.J. McNicoll and M.R. McDonough, unpub. data, 1996). Most of the detrital zircons analyzed from the Waugh Lake conglomerate are in the 2.3–2.1 Ga range and were probably derived from the underlying basement. We suggest that development of the basin was the

result of local rifting above a possibly easterly-dipping subduction zone between the Churchill and Buffalo Head cratons (Hoffman, 1989; Fig. 8). The Waugh Lake basin includes bimodal volcanics, intrabasinal conglomerates, thin tuffaceous layers within the conglomerates and is synchronous in timing with I-type magmatism in the Taltson arc. The Waugh Lake basin may represent a small intra-arc basin similar to younger analogues in Taiwan and Japan described by Huang et al. (1995) and Nakayama (1996), respectively. These are small, isolated, siliciclastic and volcanic filled basins formed by a number of extension-generating processes related to arc evolution.

High-grade enclaves of pelitic to quartzose supracrustal gneisses are widespread within plutonic and basement gneisses of the Taltson magmatic zone (Fig. 1, 2). They have detrital zircon  $^{207}\text{Pb}/^{206}\text{Pb}$  ages ranging from Archean to

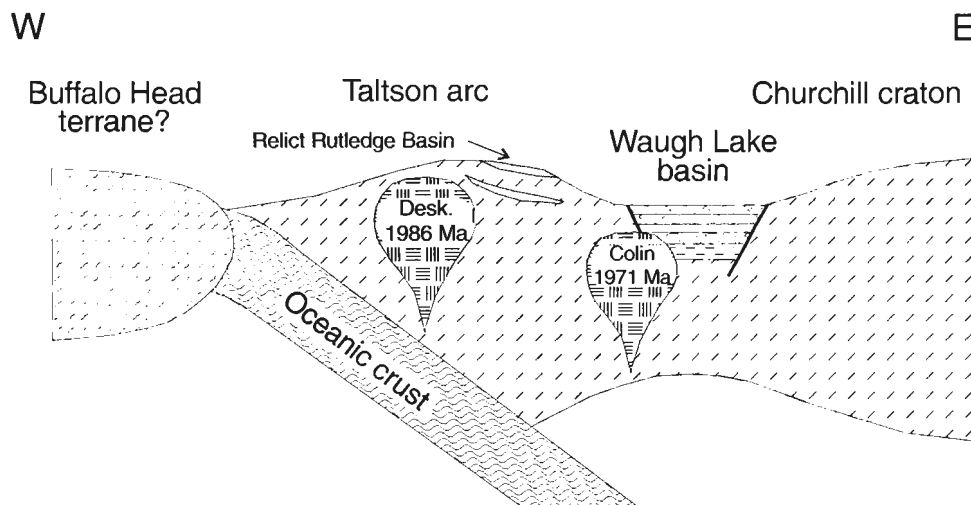


**Figure 8.** Schematic crustal section at about 1970 Ma showing east-dipping subduction beneath the Churchill craton, generation of the Taltson arc, and the subsequent deposition of the Waugh Lake Group in a back arc basin.

2.13 Ga, and were metamorphosed at 2.08–2.05 Ga, and again at 1.93–1.92 Ga (Bostock and van Breemen, 1994). Bostock and van Breemen (1994) interpreted these supracrustal gneisses to have been part of a regionally extensive precollisional basin deposited on the basement between 2.13 and 2.08 Ga, the Rutledge basin. The geochronological data presented here clearly indicate that the Waugh Lake Group is younger than the Rutledge paragneisses (Fig. 1, 8). The recycled quartzite and quartzofeldspathic clasts in conglomerates of the Waugh Lake basin may have been derived from unmetamorphosed equivalents of the Rutledge supracrustal gneisses.

The Nonacho Group consists of a sequence of conglomerate, arkose, and pelite deposited in sinistral strike-slip pull-apart basins in the western Churchill Province (Fig. 1; Aspler and Donaldson, 1985). Detrital zircons from the Nonacho Group have  $^{207}\text{Pb}/^{206}\text{Pb}$  ages ranging from 2.48 to 2.31 Ga and from 2.13 to 2.06 Ga (van Breemen and Aspler, 1994; Fig. 1). The best constraints on the depositional age of the Nonacho Group come from the youngest detritus of 2.06 Ga (van Breemen and Aspler, 1994), and the crosscutting  $1827 \pm 4$  Ma Sparrow diabase dykes (Bostock and van Breemen, 1992; Fig. 1). Bostock and van Breemen (1994) and van Breemen and Aspler (1994) have suggested the age of the Nonacho Group may be synchronous with ca. 1935 to 1906 Ma sinistral faulting in the northern Taltson magmatic zone. However, the isotopic age constraints on the timing of deposition permit correlation of the Waugh Lake and Nonacho groups in a general tectonostratigraphic way. Lithologically the two are by no means a perfect match: the Waugh Lake Group lacks clean heavy mineral-rich beach sands, and the Nonacho Group is virtually devoid of volcanics; however, they both contain a highly variable conglomeratic facies typical of wrench pull-apart basins in arc terranes.

The Burntwood group was informally defined and correlated with the Waugh Lake Group by Godfrey (1980); however, our detrital zircon studies of the Burntwood group indicate that it is younger than 1.92 Ga, and therefore younger than the Waugh Lake Group. The Burntwood group detrital zircons range in age from 2.5–2.2 Ga and from 1.94–1.92 Ga. The older detrital zircons were probably derived from basement rocks of the Taltson magmatic zone that include 2.44–2.14 Ga magmatic gneisses intruding Archean gneisses. Detrital zircon ages in the 1.94–1.92 Ga range indicate sediment provenance from plutons of the emergent Taltson orogen. In addition to the differing age constraints on the timing of deposition for the Waugh and Burntwood groups, lithological differences also exist. Green pelites of the Burntwood group are similar to the Martyn Lake Formation; however, the Burntwood pelites are not rhythmically bedded turbidites, and their quartz-hematite vein mineralogy is completely different than the veins in the Waugh Lake Group. Pebbles in Burntwood sandstone are quartz and minor feldspar; white quartzite, granitoid, and tourmaline-quartz clasts typical of the Doze Lake and Johnson Lake conglomerates are lacking.

The Burntwood group was previously mapped as part of the Athabasca Formation by Fahrig (1961). As shown on Figure 1, the Burntwood group locality is very close to the depositional edge of the Fair Point Formation of the basal Athabasca Group described by Ramaekers (1979) and Wilson (1985). The Burntwood pebbly sandstones bear striking resemblance to the basal Fair Point Formation. Two key lithological characteristics of Godfrey's (1980) Burntwood group are identical to parts of the Fair Point Formation (Fahrig, 1961; Ramaekers, 1979; Wilson, 1985; Langford, 1986): 1) coarse grained, hematite-cemented conglomeratic sandstones with trough crossbedding; and 2) intervening dark green (reduced?) pelite units with quartz-hematite veining. We therefore propose inclusion of the coarse grained hematite

cemented pebbly sandstones in the Fair Point Formation (Fig. 1), and recommend discarding use of the Burntwood group at this locality.

The best age constraints on deposition in the Athabasca basin are from fluorapatite cements in Fair Point and Wolverine formation sandstones that have been U-Pb dated at ca. 1700-1650 Ma (Cumming et al., 1987; Cumming and Krstic, 1992). These early diagenetic cements probably formed shortly after deposition (Cumming et al., 1987), and combined with the new detrital zircon U-Pb data, give limits of ca. 1919 and 1700 Ma for initiation of deposition in the Athabasca basin. Phosphatic cement in the Thelon Formation of the Thelon Basin, which was correlated with the Athabasca basin, was dated at  $1720 \pm 6$  Ma (U-Pb), providing a minimum estimate for Thelon sedimentation (Miller et al., 1989).

Godfrey's (1980) Burntwood locality is on the margins of the Athabasca basin, and directly along strike with the main brittle fault of the Charles Lake shear zone (Fig. 2). The brittle fault may have controlled local deposition of the Burntwood strata, funnelling detritus from the surrounding Taltson magmatic zone into the brittle trough in the centre of the Charles Lake shear zone. Brittle deformation on the shear zone is estimated to have occurred after the rocks of the Taltson magmatic zone cooled below 300°C at 1800 Ma, the age of regional muscovite and biotite cooling ages (Plint and McDonough, 1995). Thus, we suggest that the onset of brittle deformation in the Taltson orogen and local deposition in the Athabasca basin could have been synchronous. If this is the case, time limits for the initiation of deposition in the Athabasca basin could be bracketed between 1800-1700 Ma.

## ACKNOWLEDGMENTS

Discussions with Gerry Ross, Larry Aspler, Reg Thériault, and Willem Langenberg significantly aided completion of this paper. We thank P.G. Guerstein and J.A. van Ham for fieldwork and other assistance. Staff of the Geochronology Lab (in particular Klaus Santowski, Jack MacRae, and Diane Bellerive) are thanked for their assistance in generating the U-Pb data. Critical reviews and constructive comments by Larry Aspler, Otto van Breemen, Hewitt Bostock, and Reg Thériault improved the paper.

## REFERENCES

- Aspler, L.B. and Donaldson, J.A.  
1985: The Nonacho basin (Early Proterozoic), northwest Territories, Canada: sedimentation and deformation in a strike-slip setting; in *Strike-Slip Deformation, Basin Formation and Sedimentation*, (ed.) K.T. Biddle and N. Christie-Blick; Society of Economic Paleontologists and Mineralogists, Special Publication No. 37, p. 193-209.
- Baadsgaard, H. and Godfrey, J.D.  
1972: Geochronology of the Canadian Shield in northeastern Alberta I. Andrew Lake area; *Canadian Journal of Earth Sciences*, v. 4, p. 541-563.
- Bostock, H.H. and van Breemen, O.  
1992: The timing of emplacement, and the distribution of the Sparrow diabase dyke swarm, District of Mackenzie, N.W.T.; in *Radiogenic Age and Isotopic Studies: Report 6*; Geological Survey of Canada, Paper 92-2, p. 49-55.
- 1994: Ages of detrital and metamorphic zircons and monazites from a pre-Taltson magmatic zone basin at the western margin of Rae Province; *Canadian Journal of Earth Sciences*, v. 31, p. 1353-1364.
- Bostock, H.H., van Breemen, O., and Loveridge, W.D.  
1987: Proterozoic geochronology in the Taltson magmatic zone, N.W.T.; in *Radiogenic Age and Isotopic Studies: Report 1*; Geological Survey of Canada, Paper 87-2, p. 73-80.
- 1991: Further geochronology of plutonic rocks in northern Taltson magmatic zone, District of Mackenzie, N.W.T.; in *Radiogenic Age and Isotopic Studies: Report 4*; Geological Survey of Canada, Paper 90-2, p. 67-78.
- Cumming, G.L. and Krstic, D.  
1992: The age of unconformity-related uranium mineralization in the Athabasca basin, northern Saskatchewan; *Canadian Journal of Earth Sciences*, v. 29, p. 1623-1639.
- Cumming, G.L., Krstic, D., and Wilson, J.A.  
1987: Age of the Athabasca Group, northern Alberta; *Geological Association of Canada, Program with Abstracts*, v. 12, p. 35.
- Fahrig, W.F.  
1961: The geology of the Athabasca Formation; *Geological Survey of Canada, Bulletin* 68, 41 p.
- Godfrey, J.D.  
1980: Geology of Fort Chipewyan District, Alberta; *Alberta Research Council, Earth Sciences Report* 78-3.
- 1986: Geology of the Precambrian Shield in northeastern Alberta; *Alberta Research Council, Map EM 180*, scale 1:250 000.
- Hanmer, S., Bowring, S., van Breemen, O., and Parrish, R.  
1992: Great Slave Lake shear zone, NW Canada: mylonitic record of Early Proterozoic continental convergence, collision and indentation; *Journal of Structural Geology*, v. 14, p. 757-773.
- Henderson, J.B. and van Breemen, O.  
1991: K-Ar (hornblende data) from the Healey Lake area, District of Mackenzie: a potential time constraint on the intracratonic indentation of the Slave Province into the Thelon Tectonic Zone; in *Radiogenic Age and Isotopic Studies: Report 4*; Geological Survey of Canada, Paper 90-2, p. 61-66.
- Hoffman, P.F.  
1988: United Plates of America: The birth of a craton; *Annual Reviews of Earth and Planetary Sciences*, v. 16, p. 543-603.
- 1989: Precambrian geology and tectonic history of North America; in *The Geology of North America - An overview*, (ed.) A.W. Bally and A.R. Palmer; Geological Society of America, *The Geology of North America*, v. A, p. 447-512.
- Huang, C., Yuan, P.B., Song, S., Lin, C., Wang, C., Chen, M., Shyu, C., and Karp, B.  
1995: Tectonics of short-lived intra-arc basins in the arc-continent collision terrane of the Coastal Range, eastern Taiwan; *Tectonics*, v. 14, p. 19-38.
- Iannelli, T.R., Langenberg, C.W., and Eccles, R.  
1995: Geology of the Aphebian Waugh Lake Group, northeast Alberta; *Geological Association of Canada, Program with Abstracts*, v. 20, p. A48.
- Krogh, T.E.  
1982: Improved accuracy of U-Pb ages by the creation of more concordant systems using an air abrasion technique; *Geochimica et Cosmochimica Acta*, v. 46, p. 637-649.
- Langford, F.F.  
1986: Geology of the Athabasca Basin; in *Uranium deposits of Canada*, (ed.) E.L. Evans, Canadian Institute of Mining and Metallurgy, Special Volume 33, p. 123-133.
- McDonough, M.R., Grover, T.W., McNicoll, V.J., and Lindsay, D.D.  
1993: Preliminary report of the geology of the southern Taltson magmatic zone, northeastern Alberta (74M/14, 74M/15 and 74M/16); in *Current Research, Part C*; Geological Survey of Canada, Paper 93-1C, p. 221-232.
- McDonough, M.R., Grover, T.W., McNicoll, V.J., Lindsay, D.D., Kelly, K.L., and Guerstein, P.G.  
1994: Revised Geology, Andrew Lake, Alberta-Saskatchewan-NWT (NTS 74M/16); Geological Survey of Canada, Open File 2905, scale 1:50 000.

- McDonough, M.R., McNicoll, V.J., and Thériault, R.J.**  
 1995a: Taltson Basement Complex: basement to a Paleoproterozoic continental collisional and magmatic orogen; Geological Association of Canada, Program with Abstracts, v. 20, p. A68.
- McDonough, M.R., McNicoll, V.J., and Schetselaar, E.M.**  
 1995b: Age and kinematics of crustal shortening and escape in a two-sided oblique-slip collisional and magmatic orogen, Paleoproterozoic Taltson magmatic zone, northeastern Alberta; in Report of LITHOPROBE Alberta Basement Transects Workshop, (ed.) G.M. Ross; LITHOPROBE Report #47, p. 264-308.
- McDonough, M.R., van Ham, J., and Bednarski, J.**  
 1996: Geology, Fletcher Lake, Alberta (NTS 74M/2); Geological Survey of Canada, Open File 3256, scale 1:50 000.
- McNicoll, V., McDonough, M.R., and Grover, T.W.**  
 1994: U-Pb geochronological studies in the southern Taltson magmatic zone, northeastern Alberta; in Report of LITHOPROBE Alberta Basement Transects Workshop, (ed.) G.M. Ross; LITHOPROBE Report #37, p. 270-273.
- Miller, A.R., Cumming, G.L., and Krstic, D.**  
 1989: U-Pb, Pb-Pb, and K-Ar isotopic study and petrography of uraniferous phosphate-bearing rocks in the Thelon Formation, Dubawnt Group, Northwest Territories, Canada; Canadian Journal of Earth Sciences, v. 26, p. 867-880.
- Nakayama, K.**  
 1996: Depositional models for fluvial sediments in an intra-arc basin: an example from the Upper Cenozoic Tokai Group in Japan; Sedimentary Geology, v. 101, p. 193-211.
- Parrish, R.R., Roddick, J.C., Loveridge, W.D., and Sullivan, R.W.**  
 1987: Uranium-lead analytical techniques at the geochronology laboratory, Geological Survey of Canada; in Radiogenic Age and Isotopic Studies: Report 1; Geological Survey of Canada, Paper 87-2, p. 3-7.
- Plint, H.E. and McDonough, M.R.**  
 1995:  $^{40}\text{Ar}/^{39}\text{Ar}$  and K-Ar constraints on shear zone evolution, southern Taltson magmatic zone, northeast Alberta; Canadian Journal of Earth Sciences, v. 32, p. 281-291.
- Ramaekers, P.**  
 1979: Stratigraphy of the Athabasca Basin; in Summary of Investigations 1979, Saskatchewan Geological Survey, Miscellaneous Report 79-10, p. 154-160.
- Roddick, J.C.**  
 1987: Generalized numerical error analysis with applications to geochronology and thermodynamics; *Geochimica et Cosmochimica Acta*, v. 51, p. 2129-2135.
- Ross, G.M., Parrish, R.R., Villeneuve, M.E., and Bowring, S.A.**  
 1991: Geophysics and geochronology of the crystalline basement of the Alberta Basin, western Canada; Canadian Journal Earth Sciences, v. 28, p. 512-522.
- Thériault, R.J.**  
 1992: Nd isotopic evolution of the Taltson magmatic zone, Northwest Territories, Canada: insights into Early Proterozoic accretion along the western margin of the Churchill Province; Journal of Geology, v. 100, p. 465-475.
- Tirrul, R. and Grotzinger, J.P.**  
 1990: Early Proterozoic collisional orogeny along the northern Thelon tectonic zone, Northwest Territories, Canada: evidence from the foreland; Tectonics, v. 9, p. 1015-1036.
- van Breemen, O. and Aspler, L.B.**  
 1994: Detrital zircon ages from Nonacho Basin, western Rae Province, Northwest Territories; in Radiogenic Age and Isotopic Studies: Report 8; Geological Survey of Canada, Current Research 1994-F, p. 49-59.
- van Breemen, O., Bostock, H.H., and Loveridge, W.D.**  
 1992: Geochronology of granites along the margin of the northern Taltson magmatic zone and western Rae Province, Northwest Territories; in Radiogenic Age and Isotopic Studies: Report 5; Geological Survey of Canada, Paper 91-2, p. 17-24.
- Villeneuve, M.E., Ross, G.M., Thériault, R.J., Miles, W., Parrish, R.R., and Broome, J.**  
 1993: Tectonic subdivision and U-Pb geochronology of the crystalline basement of the Alberta Basin, western Canada; Geological Survey of Canada, Bulletin 447, 86 p.
- Wilson, J.A.**  
 1985: Geology of the Athabasca Group in Alberta; Alberta Research Council, Bulletin 49, 78 p.
- York, D.**  
 1969: Least squares fitting of a straight line with correlated errors; Earth and Planetary Science Letters, v. 5, p. 320-324.





## U-Pb zircon ages of Tetagouche Group felsic volcanic rocks, northern New Brunswick<sup>1</sup>

N. Rogers<sup>2</sup>, N. Wodicka<sup>2</sup>, V. McNicoll<sup>2</sup>, and C.R. van Staal<sup>2</sup>

*Rogers, N., Wodicka, N., McNicoll, V., and van Staal, C.R., 1997: U-Pb zircon ages of Tetagouche Group felsic volcanic rocks, northern New Brunswick; in Radiogenic Age and Isotopic Studies: Report 10; Geological Survey of Canada, Current Research 1997-F, p. 113-119.*

---

**Abstract:** Three U-Pb zircon ages of Ordovician volcanic rocks from northern New Brunswick are reported and related into a provisional stratigraphy for the internally imbricated and multiply folded Tetagouche Group. The 471 +5/-3 Ma feldspar-phyric dacites of the Spruce Lake Formation mark the base of the Tetagouche Group, deposited in a Japan Sea-type back-arc basin. Elsewhere in the basin deposition commenced with the calc-arenites and shales of the Vallée Lourdes Formation, which are immediately overlain by the ca. 472 Ma quartz-feldspar porphyries of the Nepisiguit Falls Formation. The association of these units to major massive sulphide deposits indicates that the economically significant syngenetic mineralization occurred early in the Tetagouche Group. The cessation of dominantly subalkalic felsic volcanism is marked by the top of the Flat Landing Brook Formation at 466 ± 2 Ma, after which the alkali basalts of the Boucher Brook Formation were formed.

**Résumé :** Le présent rapport rend compte de trois datations U-Pb sur zircon effectuées sur des roches volcaniques de l'Ordovicien du nord du Nouveau-Brunswick. Ces roches sont intégrées dans un cadre stratigraphique provisoire du Groupe de Tetagouche, une unité dont l'organisation interne est caractérisée par l'existence de nombreuses nappes et de plissements multiples. Les dacites à phénocristaux de feldspath de la Formation de Spruce Lake qui ont été datées à 471 +5/-3 Ma marquent la base du Groupe de Tetagouche, dont le dépôt s'est fait dans un bassin d'arrière-arc semblable à l'actuelle mer du Japon. Ailleurs dans le bassin, la succession sédimentaire a débuté par le dépôt des calcarénites et des shales de la Formation de Vallée Lourdes. Ces roches sont surmontées directement par des unités à phénocristaux de quartz et de feldspath de la Formation de Nepisiguit Falls dont l'âge remonte à environ 472 Ma. L'association de ces unités à d'importants gisements de sulfures massifs indique que la minéralisation syngénétique de grand intérêt économique de cette région s'est formée dans les premiers temps du dépôt du Groupe de Tetagouche. La fin du volcanisme felsique de caractère principalement subalcalin peut être rapportée au sommet de la Formation de Flat Landing Brook, qui a été daté à 466 ± 2 Ma, après quoi se sont déposés les basaltes alcalins de la Formation de Boucher Brook.

---

<sup>1</sup> Contribution to the 1994-1999 Bathurst Mining Camp, Canada-New Brunswick Exploration Science and Technology (EXTECH II) Initiative.

<sup>2</sup> Geological Survey of Canada, 601 Booth Street, Ottawa, Ontario K1A 0E8

## INTRODUCTION

The volcanic dominated, Lower to Middle Ordovician Tetagouche Group mainly occurs in the part of the northern Miramichi Highlands generally known as the Bathurst mining camp (Fig. 1). The Tetagouche Group represents the remnants of the passive side of a Japan Sea-type back-arc basin (van Staal et al., 1991); the structurally overlying Fournier Group representing the oceanic and active side of the marginal basin. This basin closed during the Late Ordovician to Late Silurian (van Staal et al., 1990; van Staal, 1994). During closure the Tetagouche Group was internally imbricated and repeatedly folded, creating a complex geometrical distribution of the rock units (van Staal, 1994). Hence, detailed chronostratigraphy throughout the Bathurst mining camp is essential for structural analysis of the region and for determining the internal geometry of the various rock units. Furthermore, chronologically relating the various dissected structural blocks is economically important, as the Tetagouche Group hosts numerous syngenetic massive sulphide deposits which occur at several stratigraphic horizons (van Staal et al., 1992; Rogers, 1994).

This paper is a continuation of U-Pb zircon geochronology of the Tetagouche Group, summarized by Sullivan and van Staal (1996). However, as each of the volcanic formations contains an internal chemical stratigraphy that may be related to multiple volcanic centres active over a significant

time period (Rogers, 1994, 1995), the ages for the various formations presented herein are likely to be refined as more age determinations become available.

## GEOLOGICAL SETTING

The lower part of the Tetagouche Group consists dominantly of felsic and mafic volcanic rocks, interbedded with minor sedimentary rocks (Fig. 2). These largely volcanic rocks disconformably overlie clastic sediments of the Cambrian to Lower Ordovician Miramichi Group (van Staal and Fyffe, 1991; van Staal et al., 1996). The contact between these two groups, where exposed, is marked by the pre-Tetagouche Group Miramichi mélange at the top of the Miramichi Group and by conglomerate and calcareous psammites and pelites of the Vallée Lourdes Formation (Rice and van Staal, 1992) at the bottom of the Tetagouche Group. The Vallée Lourdes Formation has yielded middle Arenig to early Llanvirn conodonts and brachiopods (Nowlan, 1981; Neuman, 1984) and therefore provides important time constraints on the underlying sedimentary Miramichi Group and overlying volcanic rocks of the Tetagouche Group.

The oldest volcanic rocks in the Tetagouche Group are believed to belong to the Spruce Lake Formation (Rogers and van Staal, 1996). These mainly consist of feldspar-phyric, dacitic to rhyolitic, submarine lava flows and cryptodomes, with subordinate felsic pyroclastic rocks. Whole-rock

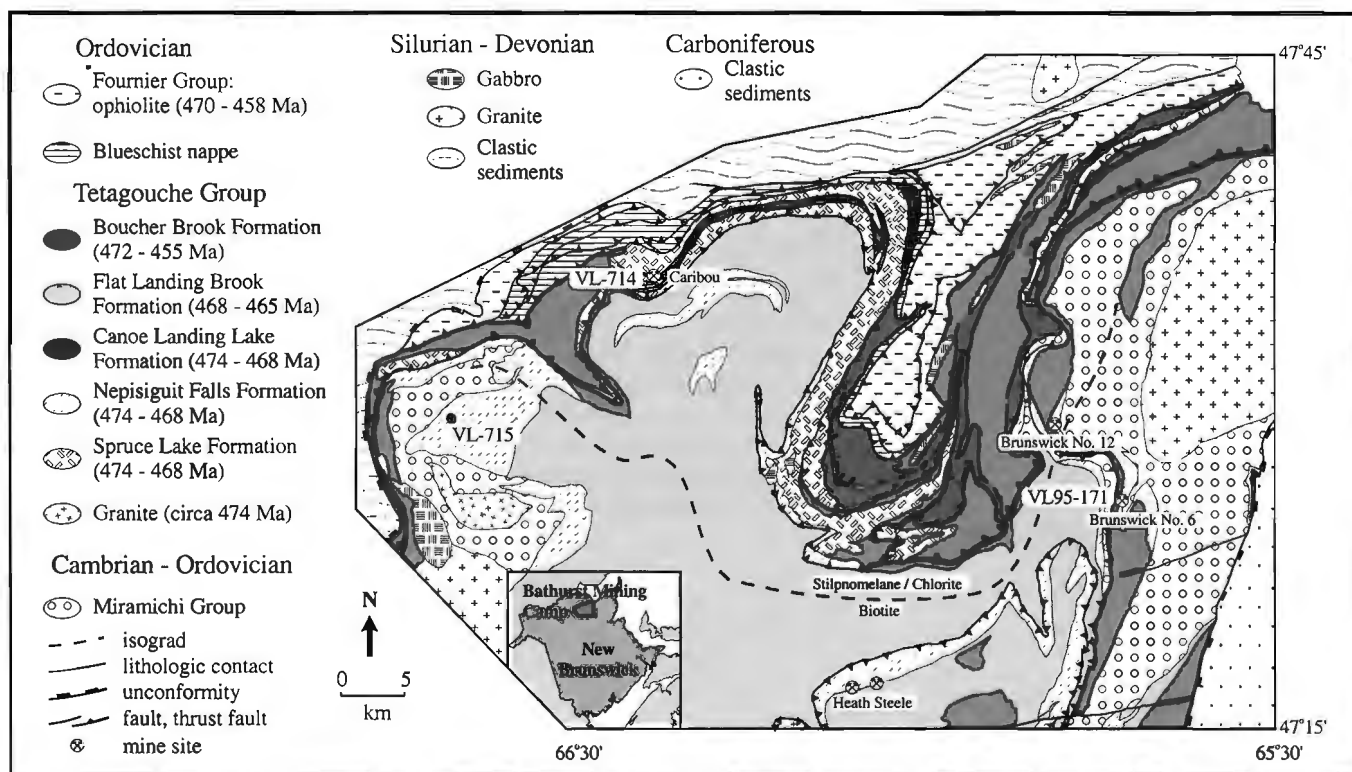


**Figure 1.** Generalized geology of the Bathurst mining camp, northern New Brunswick (modified after Rogers and van Staal, 1996). The age ranges specified represent best estimates based on field relations and all the currently available U-Pb ages (Sullivan and van Staal, 1990; 1993; 1996; this study).

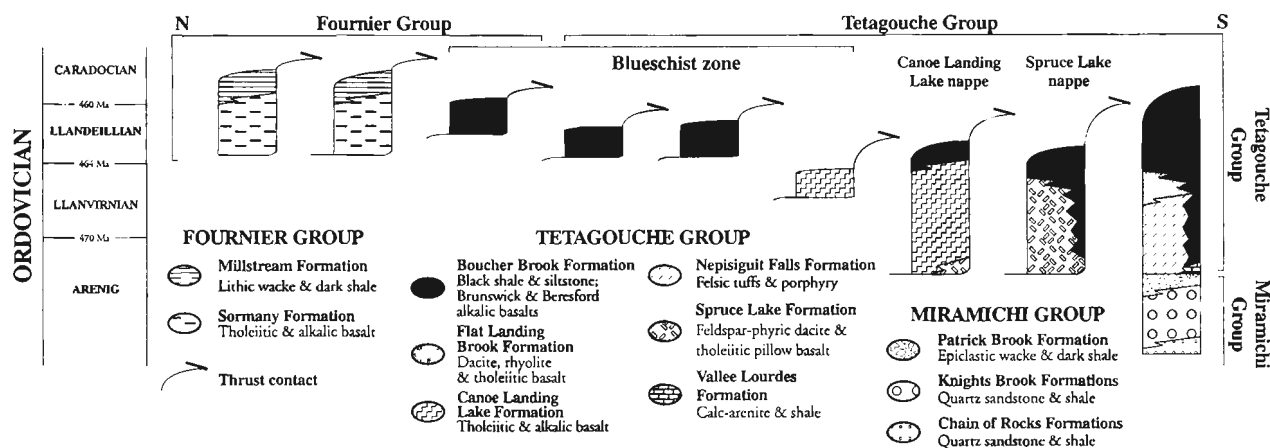


**Figure 2.** Schematic tectonostratigraphy of the Miramichi, Tetagouche, and Fournier groups showing the age relations between the northwardly stacked nappes present in the Bathurst mining camp.

geochemical studies have distinguished several separate suites of felsic volcanic rocks within this formation (Rogers, 1994, 1995). The Orvan Brook suite is of particular interest in that it appears to have a spatial relationship to the Caribou-type massive sulphide deposits that are present within the Spruce Lake Formation (Rogers, 1994, 1995). Sullivan and van Staal (1996) dated an Orvan Brook feldspar porphyry at  $470 \pm 5$  Ma. The felsic volcanic rocks are interlayered with MORB-like tholeiitic pillow basalts of the Forty Mile Brook suite (van Staal et al., 1991). This assemblage is imbricated into several thrust sheets, collectively referred to as the Spruce Lake nappe (C.R. van Staal and N. Rogers, unpublished data, 1996). Contemporary to the Spruce Lake Formation is the structurally overlying Canoe Landing Lake Formation, which consists of chemically distinct alkalic and tholeiitic basalts. The Canoe Landing Lake Formation is similarly internally imbricated and wholly contained within the allochthonous Canoe Landing nappe. In addition to the Canoe Landing Lake Formation this nappe also contains rare dacitic tuffs that are chemically and petrologically identical to the Orvan Brook suite of the Spruce Lake Formation, and yielded a similar age of  $470 \pm 4$ – $2$  Ma (Sullivan and van Staal, 1993). Elsewhere in this nappe a similar situation exists where the Forty Mile Brook tholeiitic pillow lavas of the Spruce Lake Formation are interlayered with the Canoe Landing Lake alkali basalts. Hence, the Spruce Lake and Canoe Landing Lake formations were formed contemporaneously in adjacent parts of the basin. The Spruce Lake and Canoe Landing Lake nappes probably both came from the part of the marginal basin characterized by transitional crust (van Staal et al., 1991).

The pyroclastic dominated felsic volcanic rocks of the Nepisiguit Falls Formation are also at least in part coeval with the Spruce Lake Formation. They have been intruded by Forty Mile Brook tholeiite dykes, and two previously presented U-Pb zircon ages for the Nepisiguit Falls quartz-feldspar porphyries cluster around 470 Ma (Sullivan and van Staal, 1996). The Nepisiguit Falls Formation is also host to a number of major massive sulphide deposits, including the Brunswick-type deposits which occur along the so-called

Brunswick belt (for example, the Brunswick No. 12 and Heath Steele deposits; Fig. 1). The Nepisiguit Falls and Spruce Lake formations are overlain by the regionally extensive rhyolites of the Flat Landing Brook Formation, which are absent in the Spruce Lake and Canoe Landing Lake nappes. These volcanic formations are in turn overlain by the Llandeilo to Caradoc shale and alkali basalt units of the Boucher Brook Formation (van Staal and Fyffe, 1991). The subsequent closure of the Tetagouche basin resulted in a northwardly stacked sequence of internally imbricated nappes, that provide sections through the Tetagouche Group derived from different parts of the basin (Fig. 2).

## ANALYTICAL METHODS

The analytical procedures used in this study for U-Pb isotope dilution analysis are summarized in Parrish et al. (1987). All the zircon fractions were air abraded following the method of Krogh (1982). Treatment of the analytical errors are outlined in Roddick (1987). Procedural blanks for U and Pb ranged from 0 to 1 pg and 3 to 11 pg, respectively. The analytical data are presented in Table 1 and Figures 3 to 5. All of the quoted age uncertainties are at the  $2\sigma$  level.

## SPRUCE LAKE FORMATION: SAMPLE VL-714

Sample VL-714 was collected from the felsic volcanic rocks immediately overlying the ore body in the open pit of the Caribou mine ( $47^{\circ}33'55''$ ,  $66^{\circ}17'54''$ ; Fig. 1). Field relations, petrology, and chemistry all indicate that this sample belongs to the Orvan Brook suite of the Spruce Lake Formation (Rogers, 1994).

The zircon population consists of clear, colourless, euhedral prismatic to acicular crystals with minor inclusions. Six zircon fractions were analyzed, four of which clearly contain a component of inherited Pb (Fig. 3). The other two fractions C and E, which consist of acicular crystals, are probably free

of inheritance. Fraction C has a large error ellipse that overlaps concordia at  $471 \pm 3$  Ma. The nearly concordant fraction E falls within this error ellipse and yields a similar but more precise  $^{206}\text{Pb}/^{238}\text{U}$  age of  $469.0 \pm 0.9$  Ma. It is possible that fraction E lost some Pb and may be indicating an age that is

too young. Thus, an age of  $471 \pm 5/-3$  Ma, based primarily on the  $^{206}\text{Pb}/^{238}\text{U}$  age of concordant fraction C, is estimated for this porphyry. The error assigned takes into account the possibility of Pb loss in these zircons.

**Table 1.** U-Pb zircon analytical data.

							Radiogenic ratios ( $\pm 1\sigma$ , %) <sup>a</sup>			Ages (Ma, $\pm 2\sigma$ ) <sup>h</sup>		
Fraction <sup>f</sup>	Wt. <sup>b</sup> μg	U ppm	Pb <sup>c</sup> ppm	<sup>206</sup> Pb/ <sup>204</sup> Pb <sup>d</sup>	Pb <sup>e</sup> pg	<sup>208</sup> Pb/ %	<sup>206</sup> Pb/ <sup>238</sup> U	<sup>207</sup> Pb/ <sup>235</sup> U	<sup>207</sup> Pb/ <sup>206</sup> Pb	<sup>206</sup> Pb/ <sup>238</sup> U	<sup>207</sup> Pb/ <sup>235</sup> U	<sup>207</sup> Pb/ <sup>206</sup> Pb
Spruce Lake Formation (VL-714)												
A	9	391.0	34.41	517	40	7.45	0.08899±0.23	0.7870±1.0	0.06414±0.94	549.6±2.4	589.5±9.1	746.3±40
B	14	438.3	39.53	4540	8	6.26	0.09244±0.09	0.8107±0.11	0.06360±0.06	570.0±1.0	602.8±1.0	728.4±2.4
C	4	90.5	6.81	139	13	8.48	0.07577±0.35	0.5925±1.0	0.05672±0.88	470.8±3.2	472.5±7.8	480.6±39
D	20	318.8	23.84	4603	7	5.68	0.07760±0.12	0.6124±0.14	0.05724±0.09	481.8±1.1	485.1±1.0	500.7±3.9
E	22	313.3	23.18	5208	6	7.33	0.07547±0.10	0.5890±0.11	0.05661±0.06	469.0±0.9	470.2±0.8	476.2±2.7
F	20	383.8	29.23	3742	10	6.68	0.07817±0.10	0.6171±0.11	0.05725±0.06	485.2±0.9	488.0±0.9	501.2±2.5
Nepisiguit Falls Formation (VL-715)												
A	7	168.9	19.16	1458	6	9.20	0.1117±0.12	1.106±0.17	0.07181±0.13	682.9±1.5	756.4±1.8	980.5±5.2
B	34	177.1	29.67	7221	8	9.65	0.1624±0.08	1.883±0.10	0.08410±0.04	969.9±1.5	1075.0±1.3	1294.9±1.4
C	16	182.0	20.45	848	24	8.13	0.1111±0.11	1.229±0.19	0.08021±0.14	679.4±1.4	813.9±2.1	1202.2±5.3
D	53	198.0	20.04	17780	4	8.56	0.1010±0.08	0.9169±0.10	0.06584±0.03	620.2±1.0	660.7±0.9	801.4±1.3
E	34	120.6	13.73	5959	5	9.38	0.1121±0.10	1.077±0.11	0.06967±0.06	685.1±1.3	742.2±1.1	918.7±2.4
F	20	223.0	16.54	2709	8	6.78	0.07611±0.09	0.5941±0.12	0.05661±0.08	472.8±0.9	473.5±0.9	476.5±3.6
Flat Landing Brook Formation (VL-171)												
A1	20	152.7	12.20	2309	6	14.7	0.07497±0.10	0.5825±0.13	0.05635±0.08	466.0±0.9	466.0±1.0	466.0±3.7
A2	34	151.4	12.08	292	87	14.6	0.07495±0.20	0.5832±0.62	0.05644±0.50	465.9±1.8	466.5±4.6	469.6±22
B	10	129.9	10.51	163	44	15.6	0.07507±0.30	0.5835±1.2	0.05637±1.0	466.6±2.7	466.7±9.0	467.0±47
C	10	175.6	14.08	1807	5	15.2	0.07479±0.10	0.5833±0.22	0.05656±0.18	465.0±0.9	466.5±1.7	474.3±8.1

<sup>a</sup> All zircon fractions were abraded.

<sup>b</sup> Error on weight =  $\pm 1$  μg.

<sup>c</sup> Radiogenic Pb.

<sup>d</sup> Measured ratio corrected for spike and Pb fractionation of  $0.09 \pm 0.03\%$ /AMU.

<sup>e</sup> Total common Pb on analysis corrected for fractionation and spike.

<sup>f</sup> Radiogenic Pb.

<sup>g</sup> Corrected for blank Pb and U and common Pb (Stacey-Kramers model Pb composition equivalent to the <sup>207</sup>Pb/<sup>206</sup>Pb age).

<sup>h</sup> Corrected for blank and common Pb.

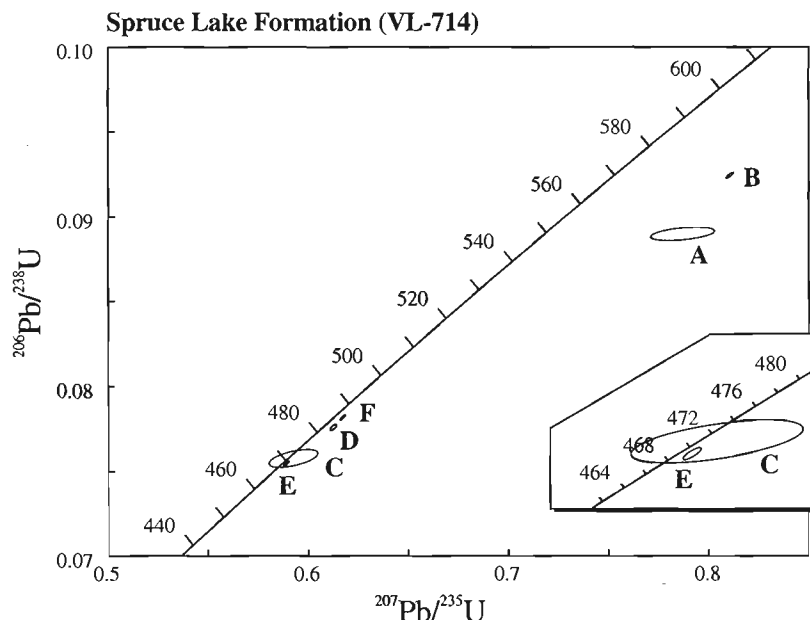


**Figure 3.**

*U-Pb concordia diagram for sample VL-714 from the Spruce Lake Formation.*

## NEPISIGUIT FALLS FORMATION: SAMPLE VL-715

Sample VL-715 is a dacitic quartz-feldspar porphyry identical to the Nepisiguit Falls Formation adjacent to the Heath Steele mine site. Petrographically it consists of black quartz phenocrysts and large, rapidly grown feldspars in a fine grained, recrystallized felsitic, tuffaceous groundmass. Although no massive sulphide deposits are known around the immediate vicinity of this particular sample (47°28'56", 66°28'43"; Fig. 1), chemically similar quartz-feldspar porphyries consistently occur beneath the Brunswick-type massive sulphide showings (Rogers, 1994).

Zircons in this sample are clear, colourless, and range in shape from tablets to prisms and acicular crystals. Five of the six analyzed zircon fractions clearly contain significant inheritance and plot in a scattered array with  $^{207}\text{Pb}/^{206}\text{Pb}$  ages older than ca. 800 Ma (Table 1; Fig. 4). The sixth fraction (F), consisting of acicular crystals, falls just below concordia and yields a  $^{206}\text{Pb}/^{238}\text{U}$  age of  $472.8 \pm 0.9$  Ma. The preferred interpretation for the age of the porphyry is 473 Ma, with an error estimate of  $\pm 3$  Ma assigned to reflect the possibility of Pb loss and inheritance in these zircons.

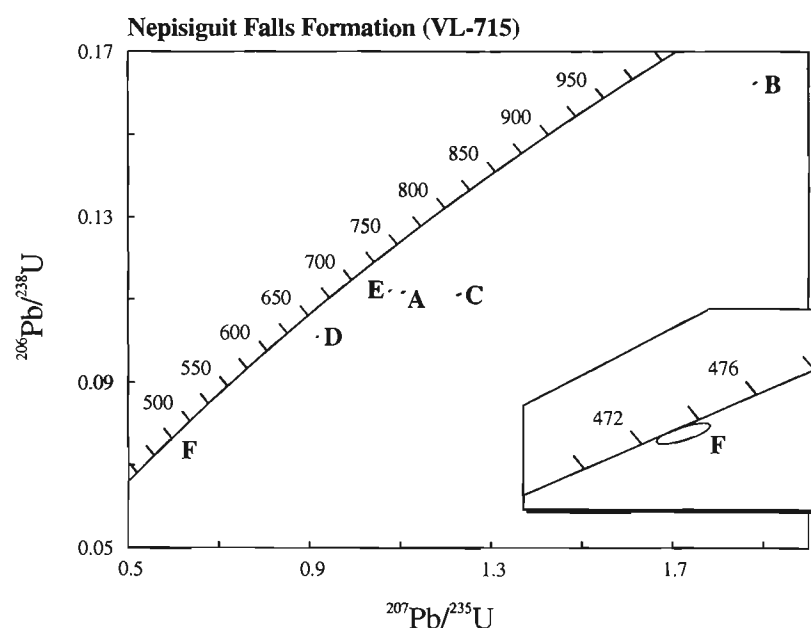
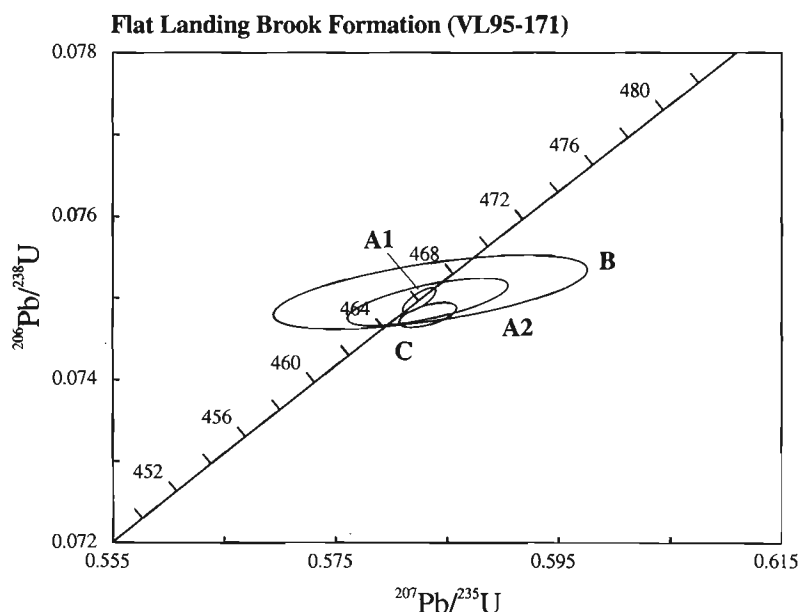


**Figure 4.**

*U-pb concordia diagram for sample VL-715 from the Nepisiguit Falls formation.*

**Figure 5.**

*U-Pb concordia diagram for sample VL95-171 from the Flat Landing Brook Formation.*



## FLAT LANDING BROOK FORMATION: SAMPLE VL95-171

Sample VL95-171 is a fine grained, light grey, aphyric to sparsely feldspar phyric felsic volcanic rock collected from the top of the Flat Landing Brook Formation from a drillhole at the Brunswick No. 6 mine site (47°24'23", 65°49'27", sample from ca. 30 m depth in hole no. 346; Fig. 1). The sample was taken from immediately below a red shale unit that locally marks the base of the Boucher Brook Formation and the transition to regional alkalic volcanism.

The zircon population consists of colourless, well faceted, stubby prisms with minor to abundant bubble and rod-shaped inclusions. Four multigrain fractions were analyzed from this sample; all four of the analyses intersect and overlap each other and concordia (Fig. 5). The best interpretation for the age of the sample is taken to be  $466 \pm 2$  Ma based on the  $^{206}\text{Pb}/^{238}\text{U}$  ages and related uncertainties of concordant zircon fractions A1, A2, and B.

## SUMMARY AND CONCLUSIONS

The three age determinations outlined in this paper provide an improved chronology for the early to middle portion of the Tetagouche Group. During this period numerous volcanic centres were active across a potentially very wide basin that has subsequently been closed with the stacking of several internally imbricated nappes (Fig. 1 and 2). The volcanic stratigraphy can be related, in simple terms, to early Tetagouche Group volcanism being represented by the Canoe Landing Lake, Nepisiguit Falls, and Spruce Lake formations, the middle Tetagouche Group by the Flat Landing Brook Formation, and the upper Tetagouche Group by the Boucher Brook alkali volcanism. However, the overall stratigraphy of the Tetagouche Group is less clearly defined, as sedimentary rocks allocated to the Boucher Brook Formation (van Staal and Fyffe, 1991) are interlayered with the Nepisiguit Falls and Spruce Lake formations (see Fig. 2).

Though somewhat poorly defined, the interpreted U-Pb age of  $471 \pm 5/3$  Ma for sample VL-714 suggests a late Arenig or early Llanvirn age (cf. Tucker et al., 1990) for this Spruce Lake feldspar-phyric porphyry. The age of the porphyry is within the error range of a  $470 \pm 5$  Ma feldspar porphyry, which is also from the Orvan Brook suite (sample VL-644 from Sullivan and van Staal, 1996), and a  $470 \pm 4/2$  Ma porphyritic dacitic tuff from the structurally overlying Canoe Landing Lake Formation (sample VL-7 from Sullivan and van Staal, 1993).

The  $473 \pm 5/3$  Ma age of the Nepisiguit Falls quartz-feldspar porphyry represented by sample VL-715 is similar in age to a  $471 \pm 3$  Ma augen schist also of the Nepisiguit Falls Formation dated by Sullivan and van Staal (1996). However, it is distinctly older than the youngest rock yet dated from this largely volcanic formation, which is a  $469 \pm 2$  Ma quartz- and feldspar-phyric dacite from the Brunswick Belt (sample VL-307 from Sullivan and van Staal, 1996). The apparent disagreement between these two dates for the Nepisiguit Falls Formation may not, however, be as significant as it seems.

These are samples from a dismembered volcanic system, within which it has proved impossible to distinguish distinct eruptive events, let alone each separate pyroclastic unit or lava flow. Such a large volcanic system, as that represented by the felsic volcanic rocks of the Nepisiguit Falls Formation, could easily have produced chemically very similar products for a period of a few million years, potentially at a number of separate centres. Taken together, the U-Pb zircon ages of these felsic volcanic rocks suggest an age of about 472 Ma for the bulk of the Nepisiguit Falls Formation. The chronological overlap between these rocks and those of the Spruce Lake Formation is consistent with the interpretation that these two formations are contemporary (Rogers, 1994).

The age of  $466 \pm 2$  Ma for sample VL95-171 from the top of the Flat Landing Brook Formation is in agreement with a previously determined age of  $466 \pm 5$  Ma for a spherulitic Taylor Brook rhyolite of the Flat Landing Brook Formation (sample VL-74; Sullivan and van Staal, 1990). Although this new age effectively dates the same horizon, the error obtained for sample VL-74 was too great to chronologically distinguish the Flat Landing Brook Formation from the other felsic volcanic formations of the Tetagouche Group. In addition to dating the Flat Landing Brook Formation, this age of  $466 \pm 2$  Ma provides a significant constraint for the base of the overlying Brunswick alkali basalt suite of the Boucher Brook Formation. This is related to the change in source material for the felsic volcanism from dominantly crustal melts to the extreme fractionates represented by the Boucher Brook comendites (Rogers, 1994).

The age relation between the Spruce Lake Formation and the onset of Boucher Brook alkali volcanism (as opposed to Boucher Brook sedimentation) is important as it dictates that a thrust occurs beneath the northward younging Caribou deposit (based on metal zonation in the disseminated massive sulphide). Prior to the recognition of the Spruce Lake Formation, this deposit, which is hosted by thinly bedded siltstone, wacke, and black shale units, was allocated to a portion of the Boucher Brook Formation younger than 465 Ma (van Staal et al., 1992). Despite its large error, sample VL-714 dates the synvolcanic Caribou deposit at ca. 471 Ma, whilst the structurally underlying Boucher Brook alkali basalts exposed to the south of the deposit are believed to be younger than  $466 \pm 2$  Ma (based on relations with the Flat Landing Brook Formation (sample VL95-171) at the Brunswick No. 6 mine). Therefore, the stratigraphy is inverted and hence the need for a thrust between the two formations. This structural relationship is supported by a discrete chemical stratigraphy observed in the associated sediments (Rogers and Brodaric, 1996; Rogers and van Staal, 1996; N. Rogers, unpub. data, 1996), which shows that the Caribou massive sulphide deposit formed very early in the Tetagouche Group. Therefore, it follows that the base of the Spruce Lake Formation, and consequently the Tetagouche Group as a whole, has been identified as  $471 \pm 5/3$  Ma. The top of the Spruce Lake Formation has not yet been dated. However, Spruce Lake feldspar porphyries are cut by, and are therefore younger than, the  $465 \pm 1.5$  Ma Wildcat porphyry (sample VL638 from Sullivan and van Staal, 1996).

With samples VL-714 and VL-715 dating the volcanic rocks associated to the synvolcanic massive sulphide deposits of the Spruce Lake and Nepisiguit Falls formations, respectively, it is noted that all of the economically significant orebodies formed early in the Tetagouche Group, at ca. 473 to 471 Ma. Consequently, even though minor sulphide showings are recognized throughout the Tetagouche Group, it cannot be discounted that the major orebodies (i.e. Brunswick No. 12, Heath Steele, Caribou, etc.) are dissected portions of the same mineralizing event.

## ACKNOWLEDGMENTS

The authors gratefully acknowledge the help of all the staff at the New Brunswick Department of Natural Resources who assisted in the geological investigations. We also thank the staff of the Geochronology Laboratory for their assistance in generating the U-Pb data. The manuscript was critically reviewed by Otto van Breemen and Réginald Thériault.

Neil Rogers is a National Science and Engineering Research Council Visiting Fellow at the Geological Survey of Canada as part of the EXTECH II project.

## REFERENCES

- Krogh, T.E.  
1982: Improved accuracy of U-Pb ages by creation of more concordant systems using an air abrasion technique; *Geochimica et Cosmochimica Acta*, v. 46, p. 637-649.
- Neuman, R.B.  
1984: Geology and palaeobiology of islands in the Ordovician Iapetus Ocean: review and implications; *Geological Society of America, Bulletin* v. 95, p. 1188-1201.
- Nowlan, G. S.  
1981: Some Ordovician conodont faunules from the Miramichi Anticlinorium, New Brunswick; *Geological Survey of Canada, Bulletin* 345, 35 p.
- Parrish, R.R., Roddick, J.C., Loveridge, W.D. and Sullivan, R.W.  
1987: Uranium-lead analytical techniques at the Geochronology Laboratory, Geological Survey of Canada; in *Radiogenic Age and Isotopic Studies: Report 1*; Geological Survey of Canada, Paper 87-2, p. 3-7.
- Rice, R.J. and van Staal, C.R.  
1992: Sedimentological studies in the Ordovician Miramichi, Tetagouche and Fournier groups, Bathurst Camp and Belledune-Elmtree Inlier, northern New Brunswick; in *Current Research, Part D*; Geological Survey of Canada, Paper 92-1D, p. 257-264.
- Roddick, J.C.  
1987: Generalized numerical error analysis with applications to geochronology and thermodynamics; *Geochimica et Cosmochimica Acta*, v. 51, p. 2129-2135.
- Rogers, N.  
1994: The geology and geochemistry of the felsic volcanic rocks of the Acadians Range Complex, Tetagouche Group, New Brunswick; PhD. thesis, Keele University, UK, 420 p.
- Rogers, N. (cont.)  
1995: The petrological variations of the Ordovician felsic volcanic rocks of the Tetagouche Group, New Brunswick; in *Current Research 1995-E*; Geological Survey of Canada, p. 279-286.
- Rogers, N. and Brodaric, B.  
1996: Spatially linked relational database management of petrology and geochemistry using Fieldlog v3.0: a worked example from the Bathurst mining camp, New Brunswick; in *Current Research 1996-E*; Geological Survey of Canada, p. 255-260.
- Rogers, N. and van Staal, C.R.  
1996: The distribution and features of the Spruce Lake Formation, Tetagouche Group, New Brunswick; in *Current Research 1996-D*; Geological Survey of Canada, p. 61-69.
- Sullivan, R.W. and van Staal, C.R.  
1990: Age of a metarhyolite from the Tetagouche Group, Bathurst New Brunswick, from U-Pb isochron analyses of zircons enriched in common Pb; in *Radiogenic Age and Isotopic Studies: Report 3*; Geological Survey of Canada, Paper 89-2, p. 109-117.
- 1993: U-Pb age of the Canoe Landing Lake Formation, Tetagouche Group, New Brunswick; in *Radiogenic Age and Isotopic Studies: Report 7*; Geological Survey of Canada, Paper 93-2, p. 39-43.
- 1996: Preliminary chronostratigraphy of the Tetagouche and Fournier Groups in northern New Brunswick, Canada; in *Radiogenic Age and Isotopic Studies: Report 9*; in Geological Survey of Canada, *Current Research 1995-F*, p. 43-56.
- Tucker, R.D., Krogh, T.E., Ross, R.J., Jr. and Williams, S.H.  
1990: Time-scale calibration by high precision U-Pb zircon dating of interstratified volcanic ashes in the Ordovician and Lower Silurian stratotypes of Britain; *Earth and Planetary Science Letters*, v. 100, p. 51-58.
- van Staal, C.R.  
1994: The Brunswick subduction complex in the Canadian Appalachians: record of the Late Ordovician to Late Silurian collision between Laurentia and the Gander margin of Avalon; *Tectonics*, v. 13, p. 946-962.
- van Staal, C.R. and Fyffe, L.R.  
1991: Dunnage and Gander Zones, New Brunswick; Canadian Appalachian Region; New Brunswick Department of Natural Resources and Energy, Mineral Resources Branch, Geoscience Report 91-2, 39 p.
- van Staal, C.R., Fyffe, L.R., Langton, J.P., and McCutcheon, S.R.  
1992: The Ordovician Tetagouche Group, Bathurst camp, northern New Brunswick, Canada: history, tectonic setting, and distribution of massive sulphide deposits; *Exploration and Mining Geology*, v. 1, p. 93-103.
- van Staal, C.R., Ravenhurst, C.E., Winchester, J.A., Roddick, J.C., and Langton, J.P.  
1990: Evidence for a post-Taconic blueschist suture in northern New Brunswick, Canada; *Canadian Journal of Earth Sciences*, v. 15, p. 207-209.
- van Staal, C.R., Sullivan, R.W., and Whalen, J.B.  
1996: Provenance and tectonic history of the Gander Margin in the Caledonian/Appalachian Orogen: implications for the origin and assembly of Avalonia; in *Avalonian and Related Peri-Gondwanan Terranes of the Circum-North Atlantic*, (ed.) R.D. Nance and M.D. Thompson. Geological Society of America; *Special Paper* 304, p. 347-367.
- van Staal, C.R., Winchester, J.A., and Bédard, J.H.  
1991: Geochemical variations in Middle Ordovician volcanic rocks of the northern Miramichi Highlands and their tectonic significance; *Canadian Journal of Earth Sciences*, v. 28, p. 1031-1049.





# New U-Pb data from the Laberge Group, northwest British Columbia: implications for Stikinian arc evolution and Lower Jurassic time scale calibrations

Gary G. Johannson<sup>1</sup> and Vicki J. McNicoll<sup>2</sup>

*Johannson, G.G. and McNicoll, V.J., 1997: New U-Pb data from the Laberge Group, northwest British Columbia: implications for Stikinian arc evolution and Lower Jurassic time scale calibrations; in Radiogenic Age and Isotopic Studies; Report 10; Geological Survey of Canada, Current Research, 1997-F, p. 121-129.*

---

**Abstract:** New U-Pb data from biostratigraphically well constrained strata of the Laberge Group provide insight into Early Jurassic magmatic and tectonic evolution of the northern Stikinian arc. Ammonite biochronology furnishes sub zonal resolution for coeval strata at two U-Pb geochronology sample sites to the lower part of the early Late Pliensbachian Kunae Zone. A granitic conglomerate clast collected near the Lower-Upper Pliensbachian boundary yielded a crystallization age of  $186.6 \pm 0.5/-1$  Ma and indicates dramatic rates of uplift and pluton exhumation during this time. A rhyodacitic lithic-crystal lapilli tuff yielded an age of  $186 \pm 1$  Ma, indicating eruptive processes were continuing into the early Late Pliensbachian even as comagmatic pluton exhumation was occurring. These data shed light on magmatic and tectonic regimes during the Pliensbachian, indicating a late phase of comagmatic arc building in the northern Stikinian arc followed by rapid tectonically-driven arc dissection. In light of the relative accuracy of these two U-Pb age determinations and their tight biostratigraphic constraints placing them near the Lower-Upper Pliensbachian substage boundary, a reassessment of the current interpolated Pliensbachian-Toarcian boundary of 187 Ma given elsewhere appears necessary.

**Résumé :** De nouvelles datations U-Pb qui ont été menées sur des strates à biostratigraphie bien établie du Groupe de Laberge permettent de jeter un éclairage nouveau sur l'évolution magmatique et tectonique de la partie nord de l'arc stikinien au Jurassique précoce. Une biochronologie des ammonites précise dans des couches contemporaines de celles où deux sites d'échantillonnage ont été datés à l'aide de la méthode U-Pb ont permis de situer ceux-ci à un niveau de précision supérieur à celui de la zone, les plaçant dans la partie inférieure de la Zone à Kunae du début du Pliensbachien tardif. Un claste de conglomérat granitique recueilli près de la limite séparant les parties inférieure et supérieure du Pliensbachien a livré un âge de cristallisation de  $186,6 \pm 0,5/-1$  Ma, ce qui révèle des vitesses spectaculaires de soulèvement et d'exhumation des plutons à cette époque. Un tuf à lapillis à cristaux et à fragments lithiques de composition rhyodacitique a livré un âge de  $186 \pm 1$  Ma, ce qui indique que les processus éruptifs se sont poursuivis au début du Pliensbachien tardif au moment même où le pluton comagmatique était soumis à une exhumation. Ces données ont permis de jeter un regard neuf sur les régimes magmatiques et tectoniques du Pliensbachien, révélant l'existence d'une phase tardive d'édification d'un arc comagmatique dans le nord de l'arc stikinien suivie par la dissection rapide de l'arc par des processus tectoniques. À la lumière de la précision relative de ces deux datations U-Pb et des données biostratigraphiques précises les plaçant près de la limite séparant les sous-étages inférieur et supérieur du Pliensbachien, il semble nécessaire de réévaluer l'âge de la limite Pliensbachien-Toarcien reconnu à l'heure actuelle, que d'autres chercheurs ont situé par interpolation à 187 Ma.

---

<sup>1</sup> 2012 1st St. N.W., Calgary, Alberta T2M 2T4

<sup>2</sup> 601 Booth Street, Ottawa, Ontario K1A 0E8

## INTRODUCTION

The Whitehorse Trough is an arc-marginal marine basin of Mesozoic age that forms a northwest-trending synclinorium, extending approximately 500 km from the south-central Yukon into northern British Columbia within the Intermontane Morphogeological Belt (Fig. 1). The Whitehorse Trough and associated arc, the Late Triassic Stikinian arc (i.e. Stuhini Group in B.C.; Lewes River Group in the Yukon), comprise northern Stikinia. The Whitehorse Trough delimits the eastern extent of Stikinia in the northern Canadian Cordillera, where its strata overlie the major tectonic boundary between the Stikine and Cache Creek terranes. The Lower to Middle Jurassic Laberge Group is widely interpreted to represent an overlap assemblage that was deposited on and links the Stikine and Cache Creek terranes (Wheeler et al., 1988). An understanding of the stratigraphic range and provenance characteristics of this arc-marginal marine sedimentary succession are critical to deciphering Stikine and Cache Creek

terrane interactions. The results presented here form part of a larger regional-scale study into various aspects of Early Jurassic basin evolution of the Whitehorse Trough that include detailed biostratigraphy, provenance characteristics, paleoflow patterns, and clastic diagenesis of the Laberge Group (Johannson, 1994; Johannson et al., in press).

The study area, covering over 500 km<sup>2</sup>, is within the Atlin Lake region of northwestern British Columbia (Fig. 2), mainly within the boundaries of Atlin Lake Wilderness Provincial Park in the southern part of the lake. In the study area the Intermontane Belt is represented by the Stikine terrane which narrows to roughly 35 km in width and the Cache Creek (Atlin) Terrane. In the immediate vicinity of Atlin Lake are four major tectonostratigraphic elements, consisting of the northern Cache Creek terrane to the east, Stikine and Nisling terranes to the west, and the Laberge Group of the Whitehorse Trough (Monger et al., 1991) (Fig. 1 and 2).

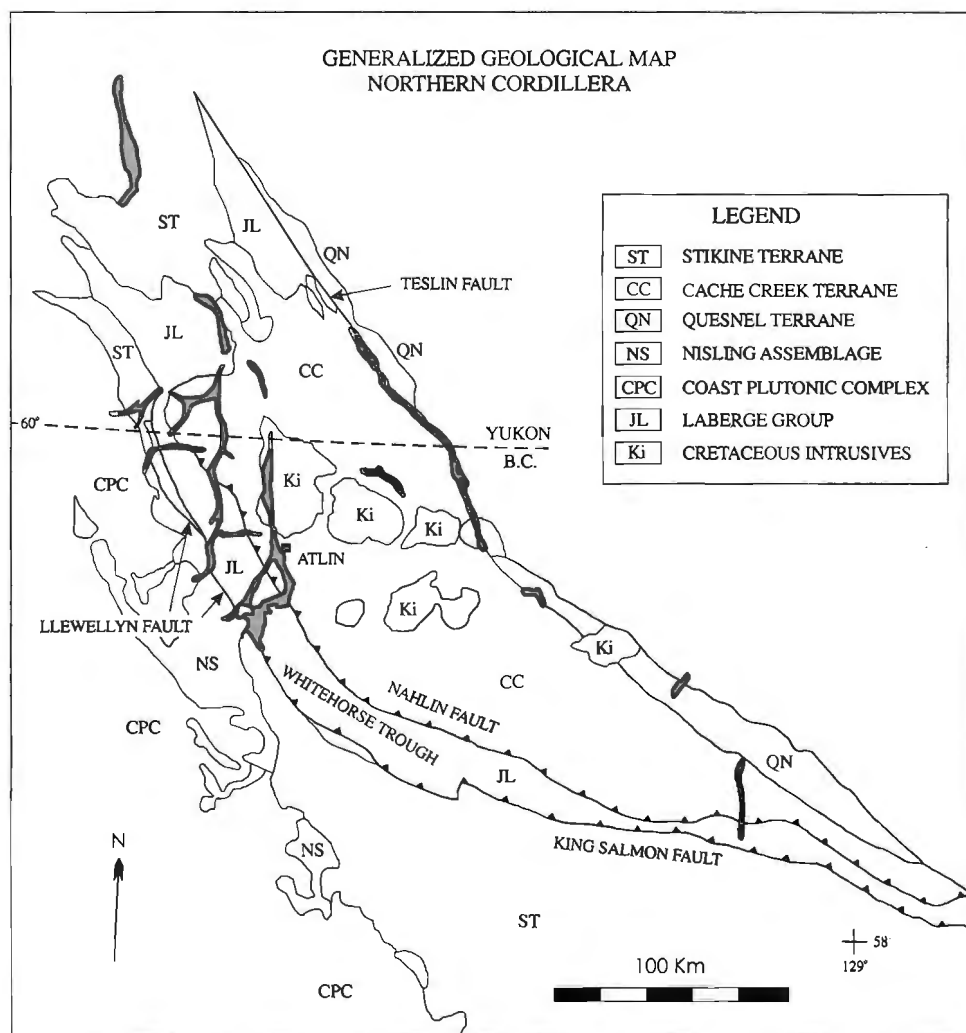


**Figure 1.** Generalized geology of the northern Canadian Cordillera. The Whitehorse Trough (Laberge Group = JL) straddles the British Columbia – Yukon border in the northwest quadrant of the province (modified after Wheeler and McFeely, 1991).

The age of the Laberge Group remains poorly constrained through much of the Whitehorse Trough, hence establishing good biostratigraphic age control was one of the primary aims of the larger regional scale study. Megafauna collected by the senior author include ammonites, nautiloids, belemnoids, bivalves, corals, brachiopods, crinoids, and fish. The ammonites are by far the most numerous and important fossils in the study area and form the basis for biostratigraphic determinations. Well constrained biostratigraphic age determinations have enabled accurate stratigraphic collection of U-Pb samples, that have yielded new data shedding light on the nature and timing of processes governing sedimentation in the Lower Jurassic Whitehorse Trough. In addition, the relatively precise ages of both of the U-Pb samples and their good biostratigraphic constraints allows us to evaluate the age of the upper Pliensbachian stage boundary. It appears that the current interpolated Pliensbachian-Toarcian boundary of 187 Ma given by Harland et al. (1990) needs to be reassessed.

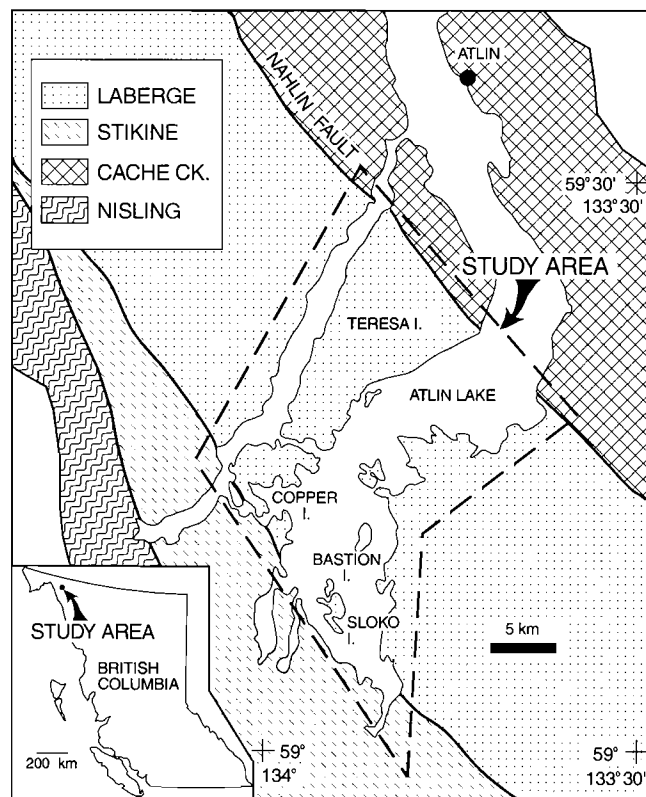


**Figure 2.** Map showing location of study area and regional setting of the Laberge Group in the Atlin Lake area (modified after Wheeler et al., 1991). In the immediate vicinity of Atlin Lake are four major tectonostratigraphic elements, consisting of the northern Cache Creek terrane to the east, Stikine and Nisling terranes to the west, and the Laberge Group of the Whitehorse Trough (Monger et al., 1991). Dashed line marks the boundary of the study area.

## BIOSTRATIGRAPHY AND SEDIMENTOLOGY

The Laberge Group comprises a deep-marine submarine fan succession in the study area. The Laberge Group is composed of the Inklin and Takwahoni formations in B.C. (Souther, 1971); however, the Inklin Formation alone represents the Laberge Group in the immediate region of the study area. Proximal shallow-marine correlatives (i.e. the Takwahoni Formation) are absent. The Inklin Formation in this area is biostratigraphically constrained to an age of Early Sinemurian (Coroniceras Assemblage) to Late Pliensbachian (Kunae Zone) and is interpreted to represent a forearc basin-fill over three kilometres in thickness (Johansson, 1994; Johansson et al., in press). The U-Pb geochronology samples were collected from biostratigraphically well constrained strata of Kunae Zone age and are found within measured sections on Sloko and Copper islands in Atlin Lake (Fig. 1). The stratigraphic level at which the sampled units occur is shown in Figures 3 and 4, respectively.

### Sample GGAJ-92-71

The Sloko Island sample is a monzogranite clast collected from a thick (>12 m) amalgamated Late Pliensbachian conglomerate unit that overlies a fining-upward megasequence of muddy rhythmites (Fig. 3). The composite nature of the unit, its lensoid geometry, closed framework, and mud-poor sandy matrix indicate a mid-fan channel environment with deposition interpreted to result from a series of coarse gravely, high-concentration turbidity currents. Granitic clasts are abundant in this unit, forming almost 70% of the clasts, and display great compositional and textural similarity, suggesting provenance from a single plutonic suite. There is a stratigraphically abrupt and striking change in clast modes in units only slightly older (i.e. late Early Pliensbachian). These units contain predominantly volcanic clasts; plutonic clasts, which are more mafic in composition than the granitic clasts in the Late Pliensbachian conglomerate unit, rarely exceed 10% of the total clasts.

The sampled clast is an orthoclase-megacrystic hornblende-biotite monzogranite, which is a particularly abundant plutonic clast lithology within the Upper Pliensbachian units. The stratigraphic position of the conglomerate unit is about 150 m above a sharply defined Early-Late Pliensbachian boundary marked by the first appearance of ammonites *Fanninoceras* with *Dubariceras freboldi* (Fig. 3). The first appearance of *Fanninoceras* defines the base of the Late Pliensbachian substage while *Dubariceras freboldi* is considered diagnostic of the Freboldi Zone of the late Early Pliensbachian and is rarely found to occur with *Fanninoceras* (Smith et al., 1988). This co-occurrence of ammonites provides a high-resolution marker for the Early-Late Pliensbachian substage boundary.

### Sample GGAJ-92-127

The Copper Island sample is a lithic-crystal lapilli tuff of rhyodacitic composition. It was collected from a thick sequence of predominantly medium to coarse sandstone with

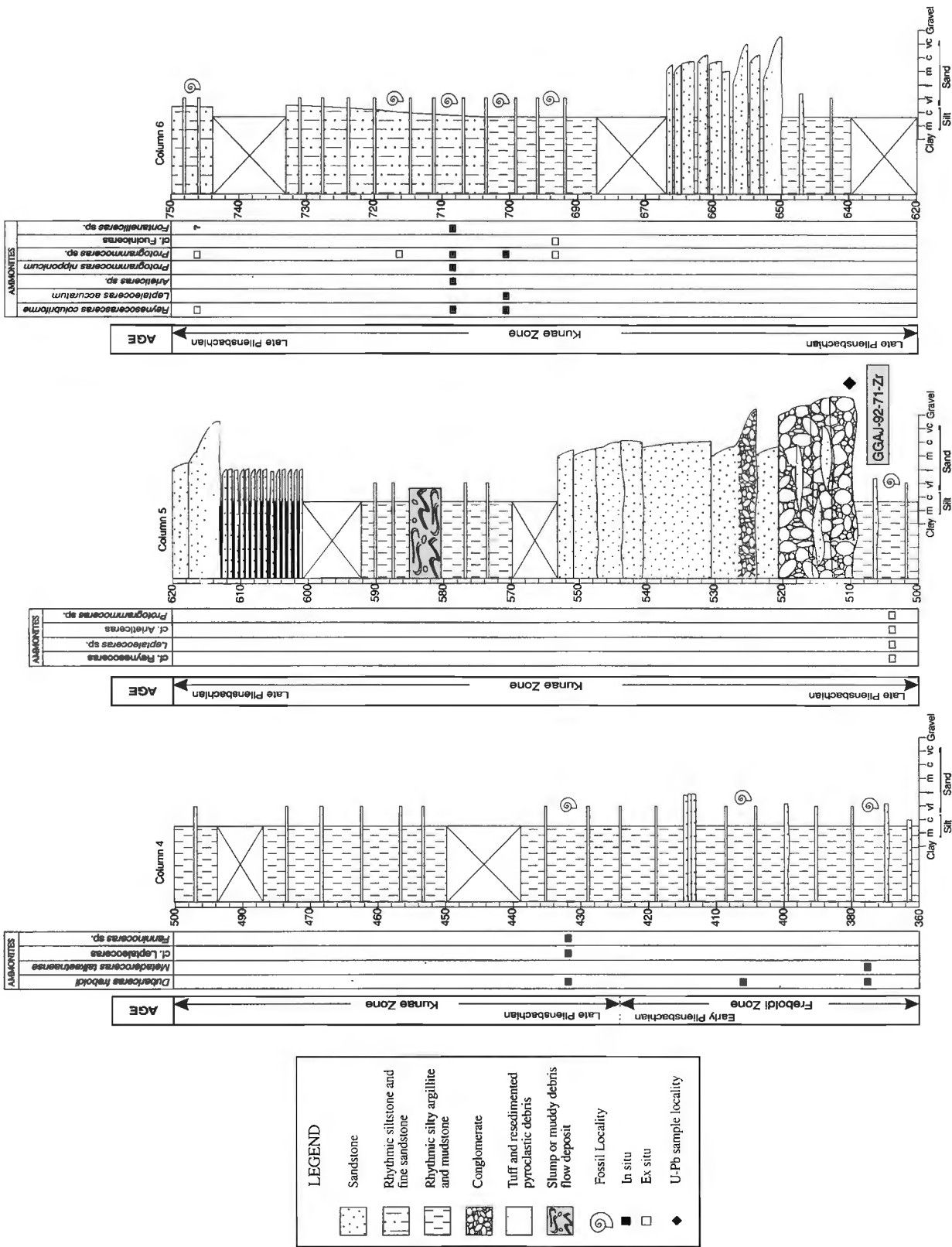


Figure 3. Portion of Sloko Island measured section showing stratigraphic intervals of interest and biostratigraphic constraints. Figure depicts three parts of a column that show the location of the Early-Late Pliensbachian boundary, the U-Pb sample interval (GGAI-92-71-Zr), and the bracketing ammonite collections. Scale is in metres.

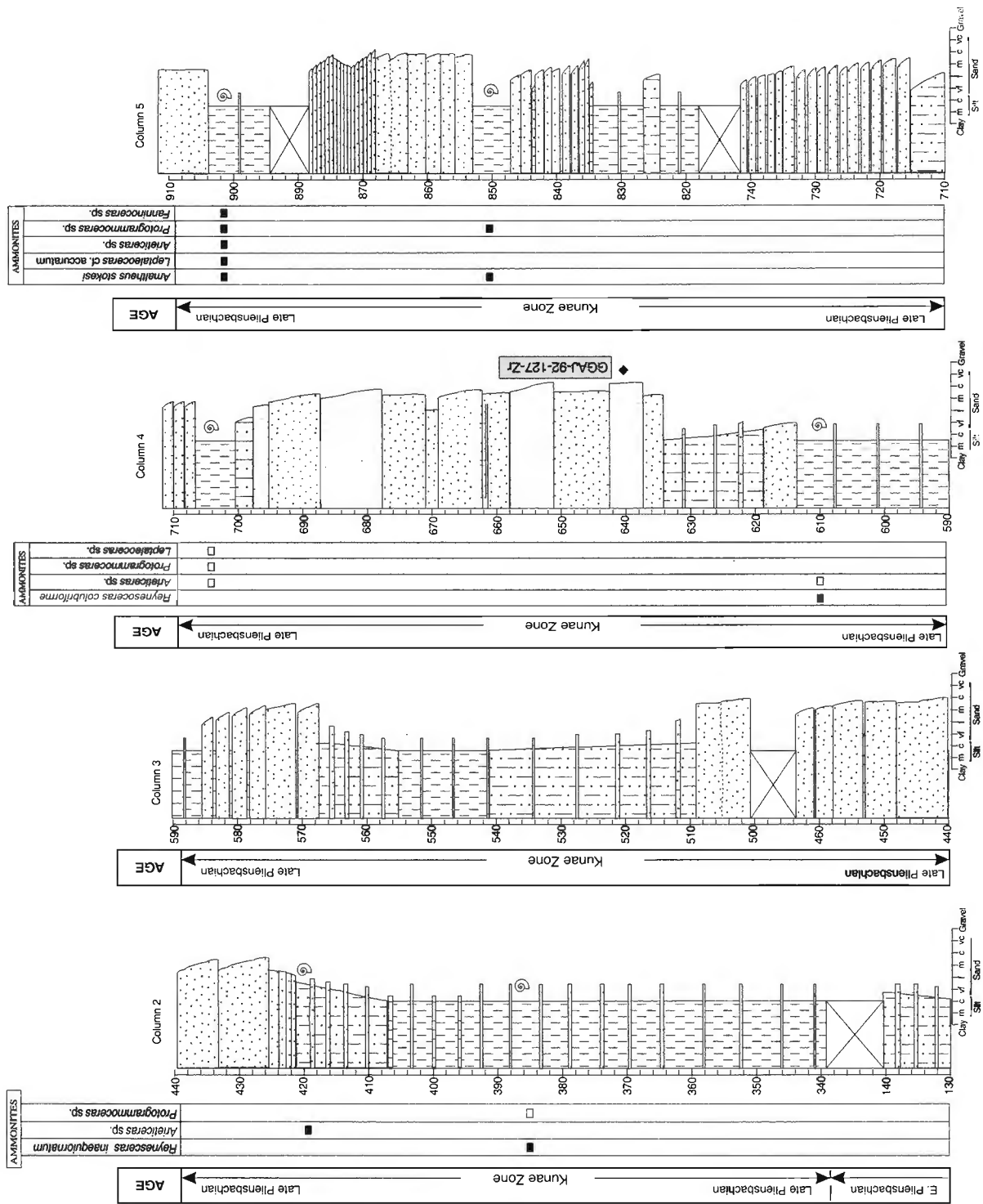


Figure 4. Portion of Copper Island measured section showing stratigraphic intervals of interest and biostratigraphic constraints. Figure depicts four parts of a column that show the location of the interpreted Early-Late Pliensbachian boundary, the U-Pb sample interval (GGAJ-92-127-Zr), and the bracketing ammonite collections. The legend from Figure 3 also applies to this figure. Scale is in metres.

minor interbedded water-lain lapilli tuff and resedimented pyroclastic debris (Fig. 4). The sequence is composed primarily of thick, planar bedded, sheet sands with minor interbedded stacks of thin sand-mud/silt-mud couplets, forming a coarsening-upward megasequence interpreted to represent a prograding mid-fan lobe environment.

The sampled lapilli tuff is crystal-rich and composed predominantly of broken and whole plagioclase euhedra which frequently display normal oscillatory zoning, and minor quartz, hornblende, and accessory biotite. The textural features of the unit are indicative of coeval pyroclastic deposition rather than epiclastic reworking. Modal attributes of the crystal component mimic the composition of the predominantly monolithic volcanic lithic fragments and indicate derivation from the same eruptive event (Smith and Lotosky, 1995). The stratigraphic position of the tuff unit is about 300 m above a well defined Early-Late Pliensbachian boundary and is bracketed by ammonites *Reynesoceras inaequior-natum* 260 m below and *Amaltheus stokesi* at 210 and 260 m above (Fig. 4). Both of these species have very short ranges in the Kunae Zone; *Reynesoceras inaequior-natum* is confined to the base of the Kunae Zone and *Amaltheus stokesi* is confined to the lower third of the zone (Smith et al., 1988).

## U-Pb GEOCHRONOLOGY

The U-Pb analytical methods utilized in this study are those outlined in Parrish et al. (1987). Treatment of analytical errors follows Roddick (1987), with regression analysis modified after York (1969). Analytical results are presented in Table 1, where errors on the ages are reported at the  $2\sigma$

level, and displayed in the concordia plots (Fig. 5 and 6). Zircon fractions analyzed were very strongly air abraded following the method of Krogh (1982). The U-Pb sample locations are displayed in the stratigraphic columns of Figures 3 and 4; sample site co-ordinates are provided in Table 1.

### Sample GGAJ-92-71

The monzogranite clast from the Sloko Island conglomerate (Fig. 3) contains abundant, very high quality zircons. Four multigrain fractions of light brown, sharply faceted, doubly terminated, prismatic crystals were analyzed from the sample. All of the analyses contain a small inherited component. A linear regression including all four analyses has a lower intercept of  $186.6 \pm 0.5/-1$  Ma (MSWD = 0.33) which is interpreted to be the age of the clast (Fig. 5).

### Sample GGAJ-92-127

The lithic-crystal lapilli tuff sampled on Copper Island (Fig. 4) contains abundant colourless to light brown, very sharply faceted, doubly terminated, prismatic zircons. The crystals are very clear and of good quality with some containing minor fluidal inclusions. Four multigrain fractions were analyzed from this sample. All four of the analyses overlap each other and intersect concordia (Fig. 6). Taking into consideration the  $^{206}\text{Pb}/^{238}\text{U}$  ages and the related uncertainties of all four fractions, the age of the rock is interpreted to be  $186 \pm 1$  Ma.

Table 1. U-Pb analytical data.

							Radiogenic ratios ( $\pm 1\sigma$ %) <sup>g</sup>			Ages (Ma, $\pm 2\sigma$ ) <sup>h</sup>		
Fraction <sup>a</sup>	Wt. <sup>b</sup>	U	Pb <sup>c</sup>	<sup>206</sup> Pb <sup>d</sup>	Pb <sup>e</sup>	<sup>208</sup> Pb <sup>f</sup>	<sup>206</sup> Pb	<sup>207</sup> Pb	<sup>207</sup> Pb	<sup>206</sup> Pb	<sup>207</sup> Pb	<sup>207</sup> Pb
	μg	ppm	ppm	<sup>204</sup> Pb	pg	%	<sup>238</sup> U	<sup>235</sup> U	<sup>206</sup> Pb	<sup>238</sup> U	<sup>235</sup> U	<sup>206</sup> Pb
GGAJ-92-71: monzogranite clast <sup>1</sup>												
A, 90	53	495.6	14.85	3605	13	11.26	0.02944 ± 0.09	0.2026 ± 0.13	0.04990 ± 0.07	187.1 ± 0.3	187.3 ± 0.4	190.2 ± 3.5
B, 90	70	403.6	12.11	2096	25	11.30	0.02947 ± 0.09	0.2031 ± 0.13	0.04999 ± 0.08	187.2 ± 0.3	187.7 ± 0.5	194.3 ± 3.8
C, 100	74	493.5	14.81	7729	9	11.01	0.02957 ± 0.09	0.2042 ± 0.11	0.05009 ± 0.05	187.9 ± 0.3	188.7 ± 0.4	199.3 ± 2.1
D, 100	48	424.1	12.74	3836	10	11.21	0.02952 ± 0.11	0.2036 ± 0.13	0.05003 ± 0.09	187.5 ± 0.4	188.2 ± 0.4	196.4 ± 4.1
GGAJ-92-127: lithic-crystal lapilli tuff <sup>2</sup>												
A, 90	74	357.8	10.83	700	74	12.69	0.02927 ± 0.11	0.2016 ± 0.27	0.04995 ± 0.22	186.0 ± 0.4	186.5 ± 0.9	192.4 ± 10
B, 90	64	312.4	9.517	830	47	13.45	0.02919 ± 0.10	0.2010 ± 0.24	0.04995 ± 0.19	185.5 ± 0.4	186.0 ± 0.8	192.5 ± 9.0
C, 100	93	307.2	9.371	555	102	13.34	0.02926 ± 0.13	0.2018 ± 0.31	0.05003 ± 0.25	185.9 ± 0.5	186.7 ± 1.1	196.6 ± 11
D, 90	81	319.4	9.702	9605	5	13.16	0.02920 ± 0.09	0.2013 ± 0.11	0.05000 ± 0.04	185.5 ± 0.3	186.2 ± 0.4	195.2 ± 1.8

<sup>a</sup> All zircon fractions are very strongly abraded; numbers refer to average size of grains in microns

<sup>b</sup> Error on weight =  $\pm 1$  μg

<sup>c</sup> Radiogenic Pb

<sup>d</sup> Measured ratio corrected for spike and Pb fractionation of  $0.09 \pm 0.03\%$ /AMU

<sup>e</sup> Total common Pb on analysis corrected for fractionation and spike

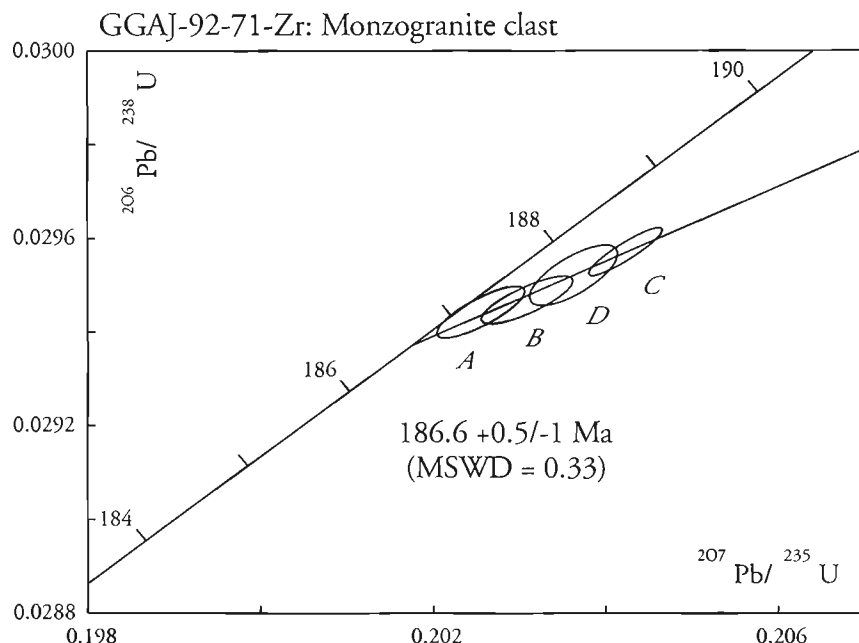
<sup>f</sup> Radiogenic Pb

<sup>g</sup> Corrected for blank Pb and U and common Pb (Stacey-Kramers model Pb composition equivalent to the  $^{207}\text{Pb}/^{206}\text{Pb}$  age)

<sup>h</sup> Corrected for blank and common Pb

<sup>1</sup> Sample locality: Shoreline exposure on Sloko Island, Atlin Lake, northern B.C.; NTS 104N/4; UTM 8, 563600E-6562770N.

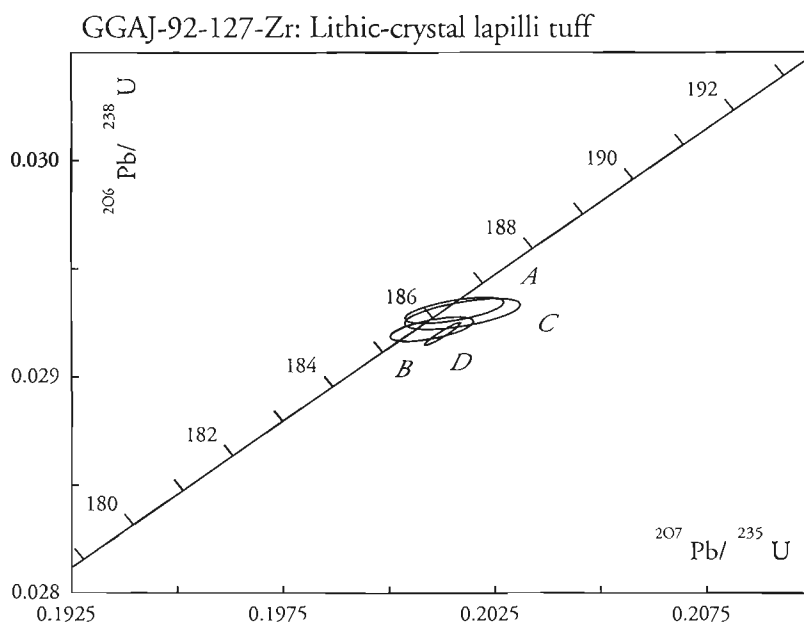
<sup>2</sup> Sample locality: South side of Copper Island, Atlin Lake, northern B.C.; NTS 104N/5; UTM 8, 558400E-6573275N.

**Figure 5.**

*U-Pb concordia diagram of zircon analyses from a monzogranite clast, sample GGAJ-92-71-Zr.*

**Figure 6.**

*U-Pb concordia diagram of zircon analyses from a lithic-crystal lapilli tuff, sample GGAJ-92-127-Zr.*



## DISCUSSION AND CONCLUSIONS

### *Magmatic and tectonic regimes*

These U-Pb data provide important information on active processes within the Stikine arc system during the Pliensbachian. Other macro- and microscopic evidence (Johansson, 1994; Johansson et al., in press) clearly indicate that the bulk of the Lower Pliensbachian sediments are derived from volcanoclastic sources of restricted composition (i.e. dacitic to rhyodacitic) that appear to be broadly coeval with deposition. These pyroclastics are very similar to deposits in the Yukon known as the Nordenskiöld dacite (Cairnes, 1910); however,

their abundance in the Lower Pliensbachian succession at Atlin Lake indicate much more extensive and voluminous eruptions than that recorded by the Nordenskiöld dacite further north. The age of the pyroclastic unit ( $186 \pm 1$  Ma) confirms the interpretation of coeval deposition and further shows that sporadic volcanism continued past the main eruptive episode in the Early Pliensbachian into the early Late Pliensbachian even as comagmatic plutons were being exhumed and eroded.

The age of the granitic clast ( $186.6 \pm 0.5/-1$  Ma) is of particular significance in unraveling tectonic behaviour in the northern Stikine arc. The early Late Pliensbachian marks an abrupt provenance shift in the study area with the influx of

abundant granitic detritus – a source rock conspicuous by its paucity during Early Pliensbachian time. Granitic rocks are primary to prominent secondary detrital modes in Upper Pliensbachian conglomerate and sandstone, and define a distinct petrofacies in the Inklin succession at Atlin Lake. These Pliensbachian granites are likely derived from the Little River batholith in the southern Yukon, northwest of the study area, which is of identical age and composition (Hart, 1994 and references therein). The fact that young Pliensbachian plutons are acting as major clast sources indicates dramatic rates of arc incision and erosion. Since this rapid uplift and erosion is being generated during a regional highstand (Smith and Tipper, 1988) in the northern Canadian Cordillera, it removes eustatic controls as a causative mechanism thereby indicating an accelerated tectonic episode is driving the uplift. There is evidence that indicates that the Little River batholith was offset by strike-slip motion along the Tally-Ho Shear Zone during the Early Jurassic (Hart, 1994). This regional structure is on trend with and interpreted to be an extension of the basin-bounding Llewellyn Fault on southwest Atlin Lake (Hart, 1994). In light of the paleotectonic reconstructions which invoke highly oblique subduction during the Early Jurassic (Engebretson et al., 1985; Umhoefer et al., 1989; Irving and Wynne, 1991) the most plausible mechanism for rapid arc dissection involves intra-arc strike-slip tectonics which commonly generates major uplift along arc segments with restraining bends (Christie-Blick and Biddle, 1985). The Llewellyn Fault was proposed as the intra-arc transform fault along which syndepositional movement occurred (Johannson, 1994; Johannson et al., in press).

### Geochronological-biochronological calibrations

Geochronological-biochronological calibrations embodied in the geological time scale are critical to a host of geological interpretations. This is particularly true of the Jurassic of the Canadian Cordillera which was a period of important regional tectonism. Time scale revisions are a matter of course as new data become available and have led to a number of revised geological time scales in recent decades (e.g. Palmer, 1983; Harland et al., 1990). Geochronological data from this study illustrates the need for revision of the Lower Jurassic segment of the time scale of Harland et al. (1990), currently favored by many Cordilleran workers.

The duration of ammonite biochronozones is variable and nonlinear due to the nonsystematic nature of evolutionary processes such as speciation; however, the duration of Jurassic ammonite zones has been estimated from European ammonite successions using a number of approaches which utilize geochronology and magnetostratigraphy among others (e.g., Hallam et al., 1985). Results have been consistent and indicate individual zone durations range from 1.8 to 0.6 Ma (Kennedy and Cobban, 1976; Westermann, 1984; Hallam et al., 1985). Assuming ammonite biochronozones for North America are of similar duration, it is reasonable to assume that a fraction of Kunae Zone stratigraphic range (i.e.,  $<1/3$ ) represents a time slice in the order of 105 thousand years. As both samples were collected from strata constrained to this lower fraction of the Kunae Zone, they are interpreted to occur in strata temporally close to the Early-Late Pliensbachian boundary. The relatively precise ages of both samples and their good biostratigraphic constraints makes them important for refining the absolute age of the upper Pliensbachian stage boundary. Our findings do not agree with the interpolated Pliensbachian-Toarcian stage boundary of 187.0 Ma given by Harland et al. (1990) and indicate that a younger age for the boundary is required. This discrepancy is noted on Figure 7, a plot of the stratigraphic interval and U-Pb age of the lapilli tuff dated in this study versus the Harland et al. (1990) time scale. In addition the monzogranite clast, which was dated at  $186 \pm 0.5/-1$  Ma, is contained within sediments that should be younger in age than the age of the clast. These observations are reported as preliminary pending the results of an ongoing regional project focused on recalibrating the biochronological and geochronological scales throughout the North American Cordillera (Pálffy et al., 1994; Pálffy, 1995).

### ACKNOWLEDGMENTS

The results presented in this paper form part of the senior author's MSc. thesis. G.G.J. gratefully acknowledges the financial support provided by Natural Sciences and Engineering Research Council (NSERC) grants to P.L. Smith (University of British Columbia) and by GSC Pacific through S.P. Gordey. Staff of the Geochronology Laboratory are thanked for their assistance in generating the U-Pb data. Critical reviews by Mike Villeneuve and Reg Theriault improved the paper.

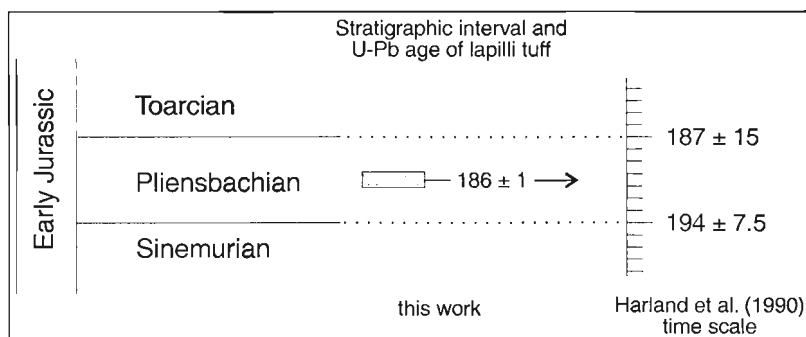


**Figure 7.**

Plot of the stratigraphic interval and U-Pb age of the lapilli tuff determined from this study versus the Harland et al. (1990) time scale. Ages are in Ma.



## REFERENCES

- Cairnes, D.D.**  
1910: Preliminary memoir on the Lewes and Nordenskiöld Rivers coal district; Geological Survey of Canada, Memoir 5, 70 p.
- Christie-Blick, N. and Biddle, K.T.**  
1985: Deformation and basin formation along strike-slip faults; in *Strike-slip Deformation, Basin Formation, and Sedimentation*, (ed.) K.T. Biddle and N. Christie-Blick; Society for Sedimentary Geology, Special Publication 37, p. 1-34.
- Engebretson, D.C., Cox, A., and Gordon, R.G.**  
1985: Relative motions between oceanic and continental plates in the Pacific Basin; Geological Society of America, Special Paper 206, 59 p.
- Hallam, A., Hancock, J.M., La Brecque, J.L., Lawrie, W., and Channell, J.E.T.**  
1985: Jurassic and Cretaceous geochronology and Jurassic to Paleogene magnetostratigraphy; in *The Chronology of the Geological Record*, (ed.) N.J. Snelling; Geological Society of London, Memoir 10, p. 118-140.
- Harland, W.B., Armstrong, R.L., Cox, A.V., Craig, L.E., and Smith, A.G.**  
1990: *A Geologic Timescale 1989*; Cambridge University Press, New York, 280 p.
- Hart, C.J.R.**  
1994: Tectonic and magmatic evolution of the Intermontane Superterrane and Coast Plutonic Complex in southern Yukon Territory; MSc. thesis, University of British Columbia, Vancouver, British Columbia, 198 p.
- Irving, E. and Wynne, P.J.**  
1991: Paleomagnetic evidence for motions of parts of the Canadian Cordillera; *Tectonophysics*, v. 187, p. 259-275.
- Johannson, G.G.**  
1994: Provenance constraints on Early Jurassic evolution of the northern Stikinian arc, Whitehorse Trough, Atlin Lake, northwestern British Columbia; MSc. thesis, University of British Columbia, Vancouver, British Columbia, 299 p.
- Johannson, G.G., Smith, P.L., and Gordey, S.P.**  
in press: Provenance constraints on Early Jurassic evolution of the northern Stikinian arc: evidence from the Laberge Group, Whitehorse Trough, northwestern British Columbia; *Canadian Journal of Earth Sciences*.
- Kennedy, W.J. and Cobban, W.A.**  
1976: Aspects of ammonite biology, biogeography and biostratigraphy; *Special Papers in Palaeontology, Palaeontological Association*, London, v. 17, p. 1-94.
- Krogh, T.E.**  
1982: Improved accuracy of U-Pb ages by the creation of more concordant systems using an air abrasion technique; *Geochimica et Cosmochimica Acta*, v. 46, p. 637-649.
- Monger, J.W.H., Wheeler, J.O., Tipper, H.W., Gabrielse, H., Harms, T., Struik, L.C., Campbell, R.B., Dodds, C.J. Gehrels, G.E., and O'Brien, J.**  
1991: Part B. Cordilleran terranes; in *Upper Devonian to Middle Jurassic assemblages*, Chapter 8 of *Geology of Cordilleran Orogen in Canada*, (ed.) H. Gabrielse and C.J. Yorath; Geological Survey of Canada, *Geology of Canada* no. 4, p. 281-327 also *Geological Society of America, The Geology of North America*, v. G-2).
- Pálffy, J.**  
1995: Development of the Jurassic geochronologic scale; in *GÉCZY Jubilee Volume, Hantkeniana*, v. 1, p. 13-25.
- Pálffy, J., Mortensen, J.K., McNicoll, V.J., Anderson, R.G., Johannson, G.G., and Hart, C.J.R.**  
1994: Towards an improved Jurassic time scale: calibration of ammonite biochronology and U-Pb geochronology in the Canadian Cordillera; Program with Abstracts, 4th International Congress on Jurassic Stratigraphy and Geology, p. 35-36.
- Palmer, A.R.**  
1983: The decade of North American Geology 1983 geologic time scale; *Geology*, v. 11, p. 503-504.
- Parrish, R.R., Roddick, J.C., Loveridge, W.D., and Sullivan, R.W.**  
1987: Uranium-lead analytical techniques at the geochronology laboratory, Geological Survey of Canada; in *Radiogenic Age and Isotopic Studies: Report 1*; Geological Survey of Canada, Paper 87-2, p. 3-7.
- Roddick, J.C.**  
1987: Generalized numerical error analysis with applications to geochronology and thermodynamics; *Geochimica et Cosmochimica Acta*, v. 51, p. 2129-2135.
- Smith, G.A. and Lotosky, J.E.**  
1995: What factors control the composition of andesitic sand? *Journal of Sedimentary Research*, v. A65, p. 91-98.
- Smith, P.L. and Tipper, H.W.**  
1988: Biochronology, stratigraphy and tectonic setting of the Pliensbachian of Canada and the United States; 2nd International Symposium on Jurassic Stratigraphy, p. 119-138.
- Smith, P.L., Tipper, H.W., Taylor, D.G., and Guex, J.**  
1988: An ammonite zonation for the Lower Jurassic of Canada and the United States: the Pliensbachian; *Canadian Journal of Earth Sciences*, v. 25, p. 1503-1523.
- Souther, J.G.**  
1971: Geology and mineral deposits of Tulsequah map-area, British Columbia; Geological Survey of Canada, Memoir 362, 84 p.
- Umhoefer, P.J., Dragovich, J., Carey, J., and Engebretson, D.C.**  
1989: Refinements of the "Baja British Columbia" plate-tectonic model for northward translation along the margin of western North America; in *Deep Structure and Past Kinematics of Accreted Terranes*, (ed.) J.W. Hillhouse; *Geophysical Monograph* 50, International Union of Geodesy and Geophysics, v. 5, p. 101-112.
- Westermann, G.E.G.**  
1984: Gauging the duration of stages: a new approach for the Jurassic; *Episodes*, v. 7, no. 2, p. 26-28.
- Wheeler, J.O. and McFeely, P.**  
1991: Tectonic assemblage map of the Canadian Cordillera; Geological Survey of Canada, Map 1712A, scale 1:2 000 000.
- Wheeler, J.O., Brookfield, A.J., Gabrielse, H., Monger, J.W.H., Tipper, H.W., and Woodsworth, G.J.**  
1988: Terrane map of the Canadian Cordillera; Geological Survey of Canada, Open File 1894.
- York, D.**  
1969: Least squares fitting of a straight line with correlated errors; *Earth and Planetary Science Letters*, v. 5, p. 320-324.



# Laser $^{40}\text{Ar}/^{39}\text{Ar}$ ages of the Babine porphyries and Newman Volcanics, Fulton Lake map area, west-central British Columbia<sup>1</sup>

M.E. Villeneuve<sup>2</sup> and D.G. MacIntyre<sup>3</sup>

*Villeneuve, M.E. and MacIntyre, D.G., 1997: Laser  $^{40}\text{Ar}/^{39}\text{Ar}$  ages of the Babine porphyries and Newman Volcanics, Fulton Lake map area, west-central British Columbia; in Radiogenic Age and Isotopic Studies: Report 10; Geological Survey of Canada, Current Research 1997-F, p. 131-139.*

---

**Abstract:** Laser  $^{40}\text{Ar}/^{39}\text{Ar}$  age dating of the Babine Igneous Suite collected from near central Babine Lake provide control on the age of intrusion of porphyries responsible for Cu ( $\pm$ Au) mineralization. A porphyry sample from north of Saturday Lake gives a hornblende age of  $51.9 \pm 0.7$  Ma and a biotite age of  $51.5 \pm 0.5$  Ma. Two samples of extrusive equivalents from the Newman Peninsula give ages of  $49.9 \pm 0.9$  Ma and  $51.3 \pm 0.6$  Ma, similar to the  $51.2 \pm 0.6$  Ma age of porphyry intrusion at the nearby Granisle past-producing mine. An older age of  $52.6 \pm 0.6$  (hornblende) is derived from a sample collected from Turkey Mountain, suggesting that this sequence represents a volcanic centre separated in time from the units dated on the Newman Peninsula.

The data supports the hypothesis that the Newman Volcanics are extrusive equivalents of the high-level Babine Intrusion porphyries, improves on previously determined K-Ar ages and narrows the age range for intrusion from a potential 10 Ma to less than 3 Ma.

**Résumé :** La datation  $^{40}\text{Ar}/^{39}\text{Ar}$  au laser d'échantillons de la Suite ignée de Babine provenant d'un secteur voisin du centre du lac Babine encadrent l'âge de la mise en place des porphyres responsables de la minéralisation de Cu ( $\pm$ Au) de cette région. Un échantillon de roche porphyrique provenant d'un secteur situé au nord du lac Saturday a livré un âge sur hornblende de  $51,9 \pm 0,7$  Ma, et un âge sur biotite de  $51,5 \pm 0,5$  Ma. Deux échantillons de roches extrusives équivalentes provenant de la péninsule Newman ont livré des âges de  $49,9 \pm 0,9$  Ma et de  $51,0 \pm 0,6$  Ma, ce qui se rapproche de l'âge ( $51,2 \pm 0,6$  Ma) de l'intrusion porphyrique située à proximité dans l'ancienne mine Granisle. Un âge plus ancien de  $52,6 \pm 0,6$  Ma (hornblende) a été établi à partir d'un échantillon prélevé au mont Turkey, ce qui nous laisse supposer que cette séquence représente un centre volcanique séparé dans le temps des unités qui ont été datées dans la péninsule Newman.

Ces données appuient l'hypothèse voulant que les Volcanites de Newman soient des équivalents extrusifs des porphyres de haut niveau de l'Intrusion de Babine, précisent les datations K-Ar effectuées précédemment et réduisent l'intervalle d'âge de mise en place de l'intrusion d'une valeur potentielle de 10 millions d'années à moins de 3 millions d'années.

---

<sup>1</sup> Contribution to the Nechako Plateau NATMAP Project

<sup>2</sup> Continental Geoscience Division, 601 Booth Street, Ottawa, Ontario K1A 0E8

<sup>3</sup> British Columbia Geological Survey Branch, Department of Employment and Investment, Victoria, British Columbia



Oblique plate collision in the Middle Cretaceous resulted in an extensional and transtensional tectonic regime that continued into the latest Eocene. Faults formed during this period provided the conduits for the isolated magmatic centres that define a broad northeast-trending magmatic arc situated between the Bowser basin to the north and Chilcotin extension

complex to the south. Evolution of this magmatic arc began in the Late Cretaceous with emplacement of the Bulkley intrusions (Carter, 1981) and eruption of comagmatic Kasalka Group calc-alkaline volcanic rocks (MacIntyre, 1981). In the Babine Lake area a younger Eocene magmatic event is represented by the small, high

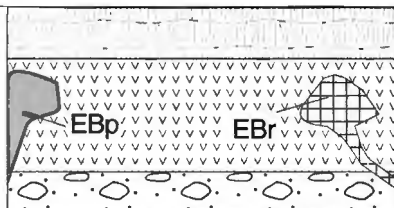
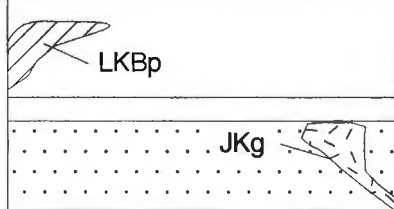
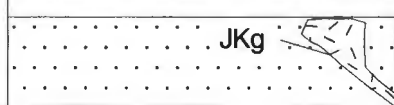
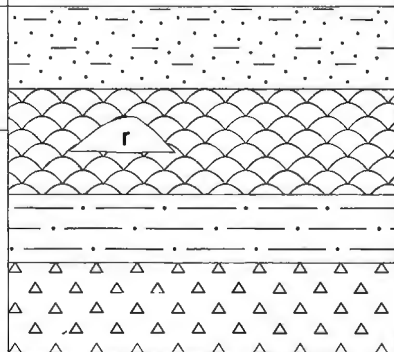
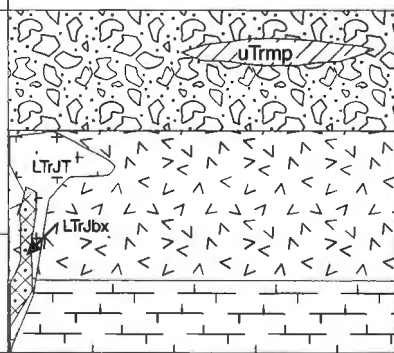
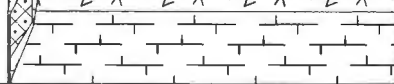
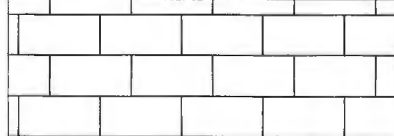
Eocene		Oolite Lk. Gp.	EBc	Endako Gp., Buck Creek Fm. - vesicular basalt
			ENv	Newman Volcanics - lahar, debris flows, volc. breccia, hb-bt-fd porph. flows, sills
			EB	Babine intrusions - bt-fd porph. (EBp), rhyodacite (Ebr), qz-bt-fd porph (EBq)
			PEcg	conglomerate, sandstone
Cretaceous			uKK	Kasalka Gp. - hb-bt-fd porph. flows & breccia
			LKBp	Bulkley intrusions - bt-hb-qz porph. (LKBp)
			IKS	Skeena Gp. - sandstone, shale, siltstone
			JKg	diorite, granodiorite, quartz diorite
M. Jur.		Hazelton Gp.	mJS	Smithers Fm. - fossiliferous feldspathic sandstone, siltstone, conglomerate
			ImJv	basaltic flows and related pyroclastic and volcaniclastic rocks; ash flow tuffs, lapilli tuffs and flow banded rhyolite (r).
L. Jur.			IJN	Nilkitkwa Fm. - siltstone, sandstone, conglomerate, minor limestone
			IJT	Telkwa Fm. - andesitic pyroclastics, andesite, basalt and rhyolite flows, felsic pyroclastics
U. Triassic		M. Triassic	uTrcg	maroon to red conglom. with clasts of megacrystic porphyry, px-fd porph., siltstone megacrystic feldspar porph. flows (uTrmp) banded siltstone, feldspathic sandstone
			LTrJbx	Nose Bay intrusive breccia - breccia with Topley and fd-px porphyry clasts
M. Trias.			LTrJT	Topley intrusions - pink granite, qz. monzonite, monzonite, aplite, rhyolite (EJT)
			uTrp	pyroxene-feldspar porphyry flows, breccia
			mTrs	calcareous siltstone, chert, tuff (M. Triassic radiolarian)
Perm.			Pc	massive, thick-bedded limestone (Middle Penn. Early Permian conodonts)

Figure 1. Legend.

level calc-alkaline plutons of the Babine Igneous Suite and the comagmatic Newman Volcanics (Carter et al., 1995). The youngest units are the Eocene vesicular basalts of the Buck Creek Formation of the Endako Group that form isolated flat sheets resting conformably upon the Newman Volcanics (MacIntyre et al., 1996).

The Eocene Babine Igneous Suite extends from the southern border of the current map area in a northerly swath for approximately 100 km to the northern tip of Babine Lake (Carter, 1981). It is of particular economic interest because there are at least twelve known porphyry Cu ( $\pm$ Au) deposits spatially associated with emplacement of high level porphyry intrusions. The two past-producing mines in the area, Granisle and Bell, occur within and on the north border of the Fulton Lake map sheet respectively (Carter, 1981). Extrusive equivalents of the porphyry intrusions, the Newman Volcanics, occur on the Newman Peninsula near the former mine sites and on the west side of Babine Lake near the town of Granisle (Carter et al., 1995). The volcanics are flat-lying to gently dipping and are contained within a rectilinear, north-trending graben. Lahars and porphyry flows of the Newman Volcanics also underlie Turkey Mountain, which is a broad circular plateau in the northwest corner of the map area that may be the remains of a stratovolcano.

The predominant phase of the Babine intrusions is quartz diorite to granodiorite in composition and typically contains fresh phenocrysts of biotite, hornblende, and feldspar in a quartz-feldspar groundmass. The intrusions associated with the porphyry copper deposits typically have a crowded porphyritic texture with 35 to 40%, 2 to 3 mm phenocrysts of biotite, plagioclase, and occasionally quartz and hornblende in a fine grained groundmass (MacIntyre et al., 1996). These porphyries and related intrusions occur as multiphase intrusive centres comprised of interfingering, pre- and postmineral plugs and dykes (Carter et al., 1995; Dirom et al., 1995) that cut Jurassic to Early Cretaceous volcanic and sedimentary strata (MacIntyre et al., 1995). It is this phase that is interpreted to be the source of copper- and gold-rich magmatic fluids (Dirom et al., 1995; Carter et al., 1995; Ogryzlo et al., 1995), that mixed with circulating meteoric waters to form the copper and gold enriched porphyry copper deposits. Subordinate phases include an apparent older quartz-feldspar $\pm$ biotite porphyry, noted at the Bell mine pit (Dirom et al., 1995), and a transitional rhyodacite intrusive-extrusive complex that outcrops on the Newman Peninsula south of the Bell mine (MacIntyre et al., 1996).

Previously interpreted to be extrusive equivalents of the Babine porphyry intrusions (Carter, 1981; MacIntyre et al., 1996), the calc-alkaline flows, breccias, and lahars of the Newman Volcanics sit discordantly upon Jurassic and Cretaceous volcano-sedimentary rocks (MacIntyre et al., 1996). A general stratigraphy based on sporadic exposures on the Newman Peninsula and at Turkey Mountain suggests the lowermost members of the Newman Volcanics are mainly massive, columnar jointed, flat-lying hornblende $\pm$ biotite $\pm$ feldspar andesite flows and/or sills. One of the best exposures of these rocks occurs along the southwest shore of the Newman Peninsula (Carter, 1981; MacIntyre et al., 1996). Along the eastern side of the Newman Peninsula, the flows grade

upward into a breccia consisting of angular fragments with compositions identical to the underlying flows. The breccia, in turn, becomes interbedded with monolithic lahar and volcanic conglomerate (MacIntyre et al., 1996). The lahar is also well exposed on cliff faces at Turkey Mountain, west of Babine Lake. Here they contain poorly sorted, centimetre- to metre-scale clasts of hornblende-biotite-feldspar porphyry in a poorly consolidated light grey, crystal- and ash-rich matrix (MacIntyre et al., 1996).

### *Previous geochronology*

As part of a larger regional study of porphyry copper deposits in west-central British Columbia in the late 1970s, Carter (1981) obtained and compiled a number of K-Ar ages on the Babine Igneous Suite. Although the ages (all ages revised to conform with decay constant of Steiger and Jager, 1977) range from a low of 45 Ma (Wanless et al., 1974) to a high of 56 Ma (Carter, 1981), most ages tend to be within the 2-3 Ma individual error at around 50 Ma (Wanless et al., 1974; Carter, 1981). Within the Fulton Lake map area, age dating by Wanless et al. (1974) concentrated on exposures north of Saturday Lake and resulted in a hornblende age of  $47 \pm 3$  Ma for hornblende-feldspar porphyry and  $50 \pm 3$  Ma for biotite and hornblende from hornblende-biotite-feldspar porphyry. Dating by Carter (1981) was centred around the Granisle and Bell deposits. At Granisle mine, biotite from four units were dated, giving ages of  $52 \pm 2$  Ma,  $52 \pm 2$  Ma,  $51 \pm 2$  Ma for a series of dykes and veins around the orebody and  $56 \pm 2$  Ma for a Babine biotite-feldspar porphyry from the southwest portion of the orebody (Carter, 1981). Figure 1 shows previously determined K-Ar dates and sample locations for rocks belonging to the Babine Igneous Suite in the map area.

Because of advances in analytical techniques, five samples of the Babine Igneous Suite and Newman Volcanics were collected during the summer of 1995 in an attempt to further constrain the timeframe for magmatism. In particular, it was hoped that a temporal and probable genetic link could be resolved between the extrusive Newman Volcanics and the Babine Porphyry Intrusions at Granisle mine.

Samples were collected from Newman Volcanics on the east and west side of the Newman Peninsula, at Turkey Mountain, and from Babine biotite-feldspar $\pm$ hornblende porphyries at Granisle mine and north of Saturday Lake.

## **METHODOLOGY**

Hand-picked separates of 100-400  $\mu$ m biotite, weighing approximately 0.5 mg and hornblende, weighing 3-6 mg were loaded into aluminum foil packets. These were arranged in an aluminum can 40 mm x 19 mm, along with evenly distributed packets of Fish Canyon Tuff sanidine, ( $28.03 \pm 0.1$  Ma, Renne et al., 1994) as flux monitors. The can was sent to the research reactor at McMaster University for eight hour neutron irradiation in an approximate fast neutron fluence of  $3 \times 10^{16}$  neutrons/cm<sup>2</sup>. This resulted in a calculated J factor

(MacDougall and Harrison, 1988) of 0.00182 to 0.00185, with *J* factor variation along the can interpolated for samples that fell between monitors.

When returned from the reactor, samples were split into three to five aliquots. Each aliquot was placed into separate 1.5 mm diameter x 4 mm deep holes drilled in a Cu planchet. The samples and planchet were then placed under vacuum in a chamber topped with a ZnSe window. This window is transparent to the beam of a Weck CO<sub>2</sub>, 45 W surgical laser. During analysis of the samples, the laser power was stepped in 3–8 increments from 2 W to 45 W power readout, after which the laser beam was attenuated by 20x with an inline optical attenuator. Because power density in the beam forms a broad gaussian distribution, the edges of the beam were clipped by a metal mask to restrict the beam to an approximately 150 µm diameter with roughly constant power distribution at the sample. The beam was manually panned for 1 minute around the hole to provide an even heating of the sample. Crosschecking of gas release spectra on standards step-heated in a temperature calibrated MS-10/double vacuum furnace showed that the increasing CO<sub>2</sub> laser power mimics an increase in furnace temperature. However, quantitative temperature calibration is not possible on the laser system because sample geometry, size, opacity of sample to laser, and other factors shift the heating spectrum to higher or lower absolute temperatures within any given hole. The gas released is cleaned by passive equilibration of the gas with i) a container filled with three SAEST<sup>TM</sup> NP-10 getters of ST707 alloy held at 400°C and ii) a cold getter of SAEST<sup>TM</sup> alloy 201 pellets for 2 to 5 minutes. Total extraction blank is approximately  $2 \times 10^{-12}$  cm<sup>3</sup> STP <sup>40</sup>Ar for all steps.

Mass spectrometry was carried out on a VG3600 mass spectrometer, a magnetic sector mass spectrometer with 60° extended geometry equipped with a faraday collector and electron multiplier. Signal on the latter is measured across a  $1 \times 10^9$  ohm resistor with a resulting gain, relative to faraday, of approximately 50. Sensitivity of the multiplier is gain dependent, but is approximately  $1.900 \times 10^{-9}$  cm<sup>3</sup> STP/V.

Argon peaks are sequentially scanned by computer controlled switching of magnetic field, as monitored by a calibrated Hall probe (see Roddick, 1996 for details). Twelve scans of each mass were measured along with baselines taken 0.4 masses away from <sup>36</sup>Ar peak. Corrections to the measured peak intensities were carried out as described in Roddick (1990).

Initially, each aliquot of a sample is treated as a separate step-heated analysis, with data reduction procedures for each aliquot following Roddick (1988). In most cases, the two aliquots give identical ages (within error) and the data is combined and treated as a single step-heated analysis for data reduction. Further aliquots may be analyzed if more step heating analyses are needed to provide adequate statistical control on the age or if the first two aliquots give different or equivocal ages (perhaps due to impurities in one aliquot by a second mineral phase).

Data interpretation involves utilization of inverse isochron analysis (Roddick et al., 1980, error analysis follows Roddick, 1988) as well as integration of plateau portions of a

gas release spectrum. For reasons outlined in Roddick (1988), error in *J* factor measurement of  $\pm 0.5\%$  is only included in the final age determination.

## AGE DETERMINATIONS

This study represents six age determinations from five samples; analytical results are shown in Table 1 and plotted on Ar step-heating release spectra in Figure 2.

Sample DMA95-106 is a hornblende-biotite-feldspar porphyry collected just north of Saturday Lake. Wanless et al. (1974) reported identical ages of  $50.2 \pm 3$  Ma for biotite and hornblende collected from a small stock of similar lithology in the vicinity. Two aliquots (aliquots B and C) of hornblende from DMA95-106, containing 80% of the total gas, gave total gas ages of 52.3 and 52.1 Ma respectively (Fig. 2a). A third, smaller aliquot (aliquot A) gives a somewhat younger age of 50.3 Ma. Combining gas from all three aliquots results in an age of  $51.9 \pm 0.7$  Ma. All four aliquots of biotite from the same sample yielded virtually identical combined gas ages, with only aliquot C (perhaps due to impurities) not giving a multistep plateau (Fig. 2b). Combining data from aliquots A, B, and D results in an age of  $51.5 \pm 0.5$  Ma, within error of the hornblende age from the same rock. As such, an average age of around  $51.7 \pm 0.6$  Ma is suggested for the unit, an age that is slightly older, but within error of the previous age determinations of Wanless et al. (1974).

Three samples were collected in the vicinity of the Granisle mine. At the mine site, a sample of medium grained hornblende-biotite-feldspar porphyry drill core (DDH-70-11) was taken and biotite was separated for analysis. Combining two aliquots, each with a well defined plateau age, results in an age of  $51.2 \pm 0.6$  Ma (Fig. 2c). This is in agreement with the  $51 \pm 2$  Ma age of Carter (1981) for two samples of biotite-feldspar porphyry with chloritized hornblende collected from the mine. Carter (1981) also collected another sample of biotite-feldspar porphyry in which the biotite is an alteration of primary hornblende. This sample resulted in a substantially older age of  $56 \pm 3$  Ma. Its field relationship to the other samples is uncertain and as such, it cannot be ascertained whether the sample represents an older phase, or if the isotopic systematics have been disturbed. In addition, biotite from a sample of quartz-bornite-chalcopryrite-biotite-apatite vein material gave an age of  $51 \pm 2$  Ma (Carter, 1981), essentially identical to the ages determined for biotite-feldspar porphyries from the mine, suggesting that mineralization occurred concurrently with the main intrusive phase.

In addition to DDH-70-11, two samples of Newman Volcanics were collected from the Newman Peninsula. Sample DMA95-177 is a hornblende-feldspar porphyry that underlies the volcanic breccia member of the well-exposed section along the road on the east side of the peninsula, about 1 km north of the Granisle mine. Combining the multistep plateau portion of three aliquots results in a robust age of  $51.3 \pm 0.6$  Ma (Fig. 2d), making the unit clearly time-correlative to the intrusive porphyry at the mine site.

Table 1.  $^{40}\text{Ar}/^{39}\text{Ar}$  analytical data.

Power <sup>a</sup>	<sup>36</sup> Ar <sub>tr</sub>	<sup>37</sup> Ar <sub>Ca</sub>	<sup>38</sup> Ar <sub>Cl</sub>	<sup>39</sup> Ar <sub>K</sub>	<sup>40</sup> Ar	%Atm.	Apparent Age	<sup>39</sup> Ar
(W)	x10 <sup>-11</sup> cm <sup>3</sup> STP <sup>b</sup>					<sup>40</sup> Ar	Ma±2σ <sup>c</sup>	(%)
DMA-95-106; Z3961; Biotite; J = 0.0018495±0.50% (1 se)								
Aliquot A								
3	0.007	0.006	0.005	0.035	2.39	82.4	39.8 ± 12.9	0.2
5	0.005	0.012	0.066	0.630	11.58	13.2	52.5 ± 1.0	3.2
7	0.004	0.011	0.092	0.952	15.99	6.8	51.5 ± 0.4	4.8
10	0.003	0.022	0.160	1.610	26.06	3.2	51.5 ± 0.8	8.1
12	0.002	0.033	0.073	0.757	12.29	4.0	51.2 ± 0.9	3.8
14	0.001	0.006	0.026	0.291	4.78	5.1	51.2 ± 1.8	1.5
20	0.000	0.003	0.014	0.152	2.54	4.7	52.4 ± 3.3	0.8
30	0.000	0.005	0.009	0.084	1.43	9.0	50.7 ± 2.6	0.4
45	0.000	0.002	0.002	0.025	0.54	3.0	67.6 ± 17.1	0.1
Subtotal <sup>d</sup>	0.022	0.100	0.447	4.536	77.60	8.3	51.6 ± 0.7	22.9
Aliquot B								
3	0.005	0.004	0.005	0.044	2.24	65.7	57.0 ± 16.2	0.2
5	0.006	0.012	0.070	0.718	13.11	13.2	52.2 ± 1.1	3.6
7	0.005	0.012	0.125	1.309	21.93	6.7	51.4 ± 0.7	6.6
10	0.004	0.030	0.155	1.471	24.50	5.0	52.1 ± 0.7	7.4
15	0.002	0.025	0.122	1.200	19.17	2.9	51.0 ± 0.9	6.1
20	0.000	0.013	0.033	0.273	4.30	0.8	51.4 ± 0.7	1.4
45	0.000	0.005	0.012	0.141	2.35	5.2	52.0 ± 2.2	0.7
Subtotal <sup>d</sup>	0.022	0.101	0.522	5.156	87.60	7.5	51.7 ± 0.7	26.0
Aliquot C								
3	0.010	0.009	0.006	0.066	3.56	83.3	29.8±14.1	0.3
5	0.006	0.012	0.077	0.845	15.22	11.2	52.6±0.5	4.3
7	0.002	0.022	0.099	0.962	15.97	4.2	52.3±0.6	4.9
10	0.003	0.027	0.100	0.989	16.50	5.1	52.0±0.6	5.0
15	0.002	0.010	0.145	1.403	22.30	2.2	51.1±0.6	7.1
20	0.000	0.002	0.008	0.081	1.36	8.4	50.8±2.3	0.4
45	0.000	0.002	0.004	0.032	0.52	9.7	48.9±9.9	0.2
Subtotal <sup>d</sup>	0.023	0.084	0.439	4.378	75.43	9.1	51.5±0.6	22.2
Aliquot D								
3	0.004	0.005	0.003	0.016	1.62	74.1	87.8±55.1	0.1
5	0.002	0.010	0.028	0.287	5.27	13.6	52.2±1.7	1.4
7	0.003	0.009	0.086	0.892	14.60	6.0	50.7±0.8	4.5
10	0.006	0.022	0.172	1.771	29.47	5.9	51.5±0.8	8.9
15	0.006	0.030	0.187	1.999	32.88	5.0	51.4±0.6	10.1
20	0.001	0.022	0.054	0.471	7.62	4.2	51.0±0.9	2.4
45	0.001	0.015	0.033	0.290	4.71	5.3	50.7±1.6	1.5
Subtotal <sup>d</sup>	0.023	0.113	0.563	5.726	96.17	7.0	51.4±0.7	28.9
Total <sup>d</sup>	0.09	0.40	1.97	19.79	336.8	7.9	51.5±0.5	100.0
DMA-95-106; Z3961; Hornblende; J = 0.0018424±0.50% (1 se)								
Aliquot A								
3	0.006	0.008	0.004	0.006	2.33	72.2	340.9 ± 174.	0.1
5	0.006	0.186	0.016	0.085	2.94	55.4	50.3 ± 3.4	0.8
10	0.016	3.174	0.214	0.556	13.18	36.6	49.3 ± 1.3	5.1
15	0.005	4.835	0.264	0.733	13.02	12.3	51.1 ± 0.4	6.7
20	0.003	2.349	0.103	0.361	6.31	12.8	50.0 ± 0.9	3.3
30	0.001	1.405	0.069	0.220	3.74	11.8	49.2 ± 1.5	2.0
45	0.000	0.467	0.021	0.068	1.18	12.3	50.2 ± 3.2	0.6
Subtotal <sup>d</sup>	0.037	12.424	0.691	2.029	42.70	26.0	51.0 ± 0.9	18.6
Aliquot B								
5	0.020	0.193	0.015	0.089	7.59	77.7	62.6 ± 19.6	0.8
10	0.037	3.012	0.207	0.525	19.14	56.5	52.0 ± 4.1	4.8
15	0.018	9.158	0.473	1.420	27.68	18.8	51.9 ± 1.0	13.0
20	0.003	4.688	0.215	0.726	12.56	8.0	52.1 ± 1.1	6.7
30	0.003	3.811	0.166	0.570	10.04	9.4	52.3 ± 1.6	5.2
45	0.002	3.135	0.125	0.466	7.86	7.5	51.2 ± 1.5	4.3
Subtotal <sup>d</sup>	0.083	23.997	1.201	3.796	84.87	28.8	52.2 ± 1.0	34.8
Aliquot C								
5	0.028	0.127	0.013	0.096	9.80	84.9	50.3 ± 19.8	0.9
10	0.022	2.806	0.196	0.560	15.36	41.4	52.7 ± 1.8	5.1
15	0.026	9.020	0.532	1.421	30.05	25.1	51.9 ± 1.3	13.0
20	0.007	5.777	0.302	0.881	15.76	12.3	51.5 ± 0.8	8.1
30	0.006	8.329	0.391	1.278	22.14	7.5	52.5 ± 1.8	11.7
45	0.002	5.331	0.262	0.834	14.03	5.1	52.3 ± 1.5	7.7
Subtotal <sup>d</sup>	0.091	31.390	1.696	5.070	107.15	24.8	52.1 ± 0.9	46.5
Total <sup>d</sup>	0.2	67.8	3.6	10.9	234.7	26.5	51.9 ± 0.7	99.9

Power <sup>a</sup>	<sup>36</sup> Ar <sub>tr</sub>	<sup>37</sup> Ar <sub>Ca</sub>	<sup>38</sup> Ar <sub>Cl</sub>	<sup>39</sup> Ar <sub>K</sub>	<sup>40</sup> Ar	%Atm	Apparent Age	<sup>39</sup> Ar
(W)	x10 <sup>-11</sup> cm <sup>3</sup> STP <sup>b</sup>					<sup>40</sup> Ar	Ma±2σ <sup>c</sup>	(%)
DMA-95-200; Z3964; Hornblende; J = 0.0018239±0.50% (1 se)								
Aliquot A								
5	0.166	0.021	0.005	0.005	49.39	99.3	233.3 ± 6183.1	0.0
8	0.033	0.066	0.001	0.010	10.26	95.8	135.2 ± 570.4	0.1
10	0.008	0.044	0.003	0.011	2.74	83.6	135 ± 107.6	0.1
11	0.011	0.060	0.006	0.011	3.52	88.9	116.5 ± 185.5	0.1
12	0.005	0.124	0.016	0.022	1.76	81.9	46.3 ± 32.7	0.2
14	0.009	0.695	0.132	0.124	4.56	58.5	49.4 ± 3.9	1.3
16	0.012	1.970	0.299	0.328	8.63	40.4	50.8 ± 3.3	3.3
18	0.009	2.371	0.341	0.403	8.82	29	50.5 ± 1.0	4.1
20	0.003	1.734	0.244	0.283	5.17	16	49.8 ± 1.3	2.9
25	0.003	2.211	0.304	0.352	6.27	14	49.8 ± 1.5	3.6
30	0.015	3.852	0.710	0.638	14.66	30.6	51.7 ± 2.2	6.4
35	0.001	0.963	0.203	0.132	2.25	10.1	49.8 ± 1.8	1.3
45	0.001	1.657	0.457	0.155	2.68	13.6	48.4 ± 2.0	1.6
Subtotal <sup>d</sup>	0.276	15.768	2.721	2.474	120.71	67.3	51.8 ± 13.0	25.0
Aliquot B								
5	0.110	0.117	0.007	0.023	32.71	99.1	42.8 ± 158.2	0.2
8	0.011	0.215	0.025	0.040	4.01	83.1	54.7 ± 15.6	0.4
10	0.040	1.396	0.212	0.234	15.64	75.9	52.2 ± 4.0	2.4
11	0.023	4.438	0.608	0.733	18.00	38.0	49.4 ± 0.9	7.4
12	0.022	3.420	0.439	0.558	15.05	42.9	49.9 ± 1.8	5.6
14	0.005	1.678	0.218	0.273	5.72	28.1	49 ± 1.7	2.8
16	0.008	2.809	0.367	0.456	9.42	25.7	49.9 ± 1.1	4.6
18	0.002	1.748	0.251	0.275	4.83	13.6	49.4 ± 2.0	2.8
20	0.005	2.130	0.273	0.340	6.56	21.5	49.1 ± 1.4	3.4
25	0.004	1.410	0.258	0.230	4.78	26.8	49.4 ± 1.9	2.3
30	0.001	1.325	0.206	0.194	3.36	11.5	49.7 ± 1.8	2.0
45	0.003	2.101	0.345	0.272	5.03	16.1	50.3 ± 1.0	2.7
Subtotal <sup>d</sup>	0.234	22.787	3.209	3.628	125.11	55.5	49.8 ± 1.3	36.6
Aliquot C								
5	0.127	0.086	0.008	0.016	38.49	97.2	208.2 ± 863	0.2
8	0.042	0.080	0.006	0.015	12.97	94.7	148 ± 426.1	0.1
10	0.016	0.158	0.015	0.028	5.14	91.6	49.3 ± 75.7	0.3
11	0.042	3.652	0.553	0.622	21.88	56.3	49.9 ± 2.3	6.3
12	0.011	2.906	0.405	0.497	10.75	29.2	49.7 ± 1.3	5.0
14	0.004	1.631	0.230	0.272	5.21	21.5	48.7 ± 1.7	2.8
16	0.005	1.808	0.234	0.285	5.66	24.2	48.8 ± 2.2	2.9
18	0.005	1.561	0.181	0.250	5.47	29.6	50.1 ± 1.9	2.5
20	0.010	4.314	0.608	0.720	13.78	20.8	49.2 ± 1.4	7.3
25	0.005	2.252	0.403	0.378	7.37	20.6	50.3 ± 1.5	3.8
30	0.003	1.720	0.279	0.272	5.01	16.3	50 ± 1.3	2.8
35	0.005	1.218	0.185	0.181	4.28	35.3	49.8 ± 3.5	1.8
45	0.002	1.830	0.322	0.260	4.58	13.7	49.3 ± 1.1	2.6
Subtotal <sup>d</sup>	0.277	23.216	3.429	3.796	140.59	57.8	50.7 ± 4.5	38.4
Total <sup>d</sup>	0.8	61.8	9.4	9.9	386.4	60.0	50.6 ± 3.7	100.
DDH-70-11; Z3967; Biotite; J = 0.0018403±0.50% (1 se)								
Aliquot A								
3	0.003	0.003	0.002	0.012	1.14	76.5	75.8 ± 26.1	0.1
5	0.003	0.008	0.025	0.139	3.22	29.5	53.4 ± 4.7	1.3
8	0.004	0.012	0.107	0.606	10.44	10.2	50.6 ± 1.0	5.8
10	0.001	0.007	0.101	0.589	9.66	3.7	51.7 ± 0.8	5.6
12	0.002	0.019	0.308	1.770	28.39	2.2	51.3 ± 0.6	17.0
15	0.001	0.020	0.194	1.083	17.30	1.3	51.6 ± 1.2	10.4
20	0.002	0.037	0.303	1.718	27.07	2.3	50.4 ± 0.4	16.5
30	0.001	0.032	0.180	0.956	15.45	2.1	51.8 ± 0.3	9.2
45	0.001	0.010	0.016	0.086	1.49	10.7	50.8 ± 3.6	0.8
Subtotal <sup>d</sup>	0.018	0.148	1.236	6.959	114.16	4.6	51.3 ± 0.6	66.7
Aliquot B								
3	0.002	0.005	0.003	0.011	0.75	95.9	9.6 ± 56.6	0.1
5	0.005	0.006	0.026	0.136	3.44	44.6	45.8 ± 2.1	1.3
8	0.002	0.007	0.069	0.393	6.75	9.3	51.0 ± 2.4	3.8
10	0.001	0.007	0.074	0.424	6.96	4.7	51.2 ± 1.1	4.1
12	0.002	0.016	0.211	1.190	19.18	2.6	51.4 ± 0.9	11.4
15	0.001	0.016	0.105	0.573	9.23	3.1	51.1 ± 0.9	5.5
20	0.001	0.013	0.115	0.678	10.70	1.8	50.8 ± 1.2	6.5
45	0.000	0.004	0.013	0.067	1.16	12.3	50.0 ± 2.7	0.6
Subtotal <sup>d</sup>	0.014	0.074	0.616	3.472	58.17	7.4	50.8 ± 0.7	33.3
Total <sup>d</sup>	0.03	0.22	1.85	10.43	172.3	5.5	51.1 ± 0.6	100.



Table 1. (cont.)

Power <sup>a</sup>	<sup>36</sup> Ar <sub>tr</sub>	<sup>37</sup> Ar <sub>Ca</sub>	<sup>38</sup> Ar <sub>Cl</sub>	<sup>39</sup> Ar <sub>K</sub>	<sup>40</sup> Ar	%Atm.	Apparent Age	<sup>9</sup> Ar
(W)	x10 <sup>-11</sup> cm <sup>3</sup> STP <sup>b</sup>					<sup>40</sup> Ar	Ma±2σ <sup>c</sup>	(%)
DMA-95-177; Z3963; Hornblende; J = 0.0018331±0.50% (1 se)								
Aliquot A								
5	0.056	0.151	0.008	0.026	16.96	97.9	45.0 ± 221.2	0.2
8	0.007	0.208	0.01	0.027	2.53	86.5	40.9 ± 14.1	0.2
10	0.011	1.426	0.102	0.213	6.35	50.8	48.0 ± 2.4	1.5
11	0.005	4.002	0.209	0.654	11.84	13.5	51.1 ± 2.2	4.7
12	0.001	1.184	0.044	0.201	3.5	8.8	51.8 ± 2.3	1.4
15	0.002	0.917	0.067	0.155	3.06	17.8	52.8 ± 6.0	1.1
25	0.003	2.08	0.136	0.344	6.4	14.6	51.7 ± 2.2	2.5
45	0.002	2.275	0.139	0.37	6.25	9.5	49.9 ± 1.1	2.7
Subtotal <sup>d</sup>	0.087	12.243	0.715	1.990	56.89	45.7	50.6 ± 3.1	14.3
Aliquot B								
5	0.078	0.218	0.013	0.035	24.91	92.2	174.0 ± 123.3	0.3
8	0.009	0.351	0.018	0.044	3.79	69	86.4 ± 24.0	0.3
10	0.012	1.035	0.082	0.165	5.77	63	42.2 ± 3.2	1.2
11	0.016	4.804	0.352	0.723	16.13	29	51.7 ± 1.1	5.2
12	0.009	5.344	0.352	0.85	15.89	16.5	50.9 ± 1.1	6.1
15	0.006	4.612	0.257	0.7	13.03	14.3	52.0 ± 1.2	5.0
25	0.021	12.251	0.696	1.905	36.51	17.2	51.7 ± 0.5	13.7
45	0.022	18.328	0.891	2.865	52.06	12.5	51.8 ± 0.5	20.6
Subtotal <sup>d</sup>	0.173	46.943	2.661	7.287	168.09	30.5	52.3 ± 0.9	52.4
Aliquot C								
5	0.126	0.094	0.012	0.024	37.45	99.2	42.0 ± 211.2	0.2
8	0.045	0.695	0.016	0.089	14.79	88.9	59.9 ± 10.1	0.6
10	0.010	0.937	0.071	0.157	5.69	50.8	58.1 ± 5.3	1.1
11	0.030	5.242	0.367	0.840	21.82	40.3	50.6 ± 1.3	6
12	0.005	2.298	0.133	0.361	6.9	20.3	49.7 ± 1.4	2.6
15	0.006	3.756	0.187	0.623	11.71	15.5	51.8 ± 1.5	4.5
25	0.020	10.128	0.655	1.628	31.57	18.3	51.7 ± 0.6	11.7
45	0.007	5.171	0.300	0.904	15.99	12.6	50.4 ± 0.7	6.5
Subtotal <sup>d</sup>	0.249	28.321	1.741	4.626	145.92	49.9	51.5 ± 1.3	33.2
Total <sup>d</sup>	0.51	87.51	5.12	13.90	370.9	40.5	51.8 ± 0.9	99.9
DMA-95-270 Z3966 Hornblende J = 0.0018465±0.50% (1 se)								
Aliquot A								
5	0.014	0.013	0.001	0.009	4.24	96.0	59.6 ± 174.7	0.1
8	0.001	0.012	0.003	0.015	0.41	39.9	53.1 ± 35.9	0.1
10	0.001	0.022	0.002	0.014	0.34	47.9	41.6 ± 12.4	0.1
11	0.007	0.484	0.064	0.083	3.62	60.5	56.2 ± 9.0	0.6
12	0.002	0.453	0.072	0.075	1.69	35.1	47.9 ± 4.6	0.5
14	0.001	0.723	0.099	0.119	2.05	15.4	47.8 ± 1.8	0.8
16	0.001	0.902	0.093	0.133	2.3	10.8	50.9 ± 2.4	0.9
18	0.000	0.427	0.055	0.062	1.08	11.5	50.8 ± 3.6	0.4
20	0.000	0.314	0.047	0.053	0.86	5.3	50.7 ± 5.5	0.4
25	0.001	0.615	0.086	0.081	1.54	17.1	51.8 ± 4.9	0.6
45	0.004	2.433	0.384	0.397	7.37	17.4	50.4 ± 1.4	2.7
Subtotal <sup>d</sup>	0.032	6.398	0.906	1.041	25.50	37.1	50.6 ± 2.1	7.2
Aliquot B								
5	0.007	0.025	0.002	0.035	2.77	79.9	52.4 ± 24.0	0.2
10	0.002	0.205	0.022	0.093	2.03	31.7	48.9 ± 4.3	0.6
15	0.004	2.193	0.224	0.347	6.65	16.1	52.7 ± 1.4	2.4
20	0.002	1.495	0.138	0.294	4.89	9.7	49.3 ± 1.3	2.0
30	0.002	2.288	0.232	0.36	6.11	8.7	51.0 ± 1.0	2.5
45	0.001	1.386	0.164	0.205	3.44	7.5	51.0 ± 1.7	1.4
Subtotal <sup>d</sup>	0.018	7.592	0.782	1.334	25.89	20.1	50.1 ± 1.1	9.1
Aliquot C								
5	0.015	0.061	0.006	0.030	4.70	91.3	45.3 ± 10.4	0.2
10	0.004	0.618	0.060	0.112	2.85	41.0	49.5 ± 2.3	0.8
15	0.011	3.856	0.401	0.570	12.41	26.7	52.4 ± 0.9	3.9
20	0.001	2.644	0.288	0.393	6.86	6.3	53.6 ± 2.3	2.7
30	0.008	10.971	1.137	1.582	27.98	8.3	53.2 ± 0.9	10.9
45	0.015	20.168	2.230	2.822	49.46	8.7	52.5 ± 0.4	19.5
Subtotal <sup>d</sup>	0.054	38.318	4.122	5.509	104.26	15.2	52.7 ± 0.7	38.0
Aliquot D								
5	0.031	0.063	0.008	0.061	9.88	93.6	34.1 ± 16.0	0.4
15	0.018	6.418	0.754	1.109	23.16	22.7	53.0 ± 0.9	7.7
30	0.014	17.817	2.100	2.755	48.01	8.4	52.4 ± 0.4	19.0
45	0.010	18.536	2.151	2.675	46.00	6.4	52.8 ± 0.7	18.5
Subtotal <sup>d</sup>	0.073	42.834	5.013	6.600	127.05	16.9	52.5 ± 0.6	45.6
Total <sup>d</sup>	0.18	95.14	10.82	14.48	282.7	18.4	52.3 ± 0.6	99.9

<sup>a</sup> Nominal power as measured by beam

<sup>b</sup> Gas quantities corrected for decay, isotopes derived from interfering neutron reactions

<sup>c</sup> Errors are analytical only and do not reflect error in irradiation parameter J

<sup>d</sup> Integrated age, uncertainty includes error in J (0.5% at 1 sigma)

<sup>a</sup>Nominal power as measured by laser, prior to 20x attenuation of beam

<sup>b</sup>Gas quantities corrected for decay, isotopes derived from interfering neutron reactions

<sup>c</sup>Errors are analytical only and do not reflect error in irradiation parameter J

<sup>d</sup>Integrated age, uncertainty includes error in J (0.5% at 1 sigma)

A sample was also collected from the columnar jointed hornblende porphyry flow or sill exposed on the southwest shore of the peninsula (DMA95-200). Carter (1981) collected a sample close to the same outcrop and obtained a K-Ar hornblende age of  $52 \pm 3$  Ma (Carter, 1981). Analysis of three aliquots resulted in three equivalent plateau ages, that when combined give an age of  $49.9 \pm 0.6$  Ma (Fig. 2e), within the larger error of the previously determined K-Ar age.

Sample DMA95-270, a medium- to fine-grained hornblende feldspar porphyry, was collected from near the base of Turkey Mountain. Two small aliquots, representing 17% of the gas, gave poor analytical results. Two larger aliquots each gave a multistep plateau age (Fig. 2f). Combining the plateau fractions of aliquots C and D results in an interpreted age of  $52.6 \pm 0.6$  Ma. This suggests a slightly older age for the Turkey Mountain rocks as opposed to those on the Newman Peninsula and within the Granisle graben. This apparent age difference is consistent with preliminary magnetic studies by Carmel Lowe (pers. comm., 1996) indicating that Turkey Mountain rocks, that have an associated aeromagnetic high, were erupted during a different magnetic cycle than those on the Newman Peninsula which produce a pronounced aeromagnetic low.

## CONCLUSIONS

1. Laser  $^{40}\text{Ar}/^{39}\text{Ar}$  analysis of biotite and hornblende separates from the Babine Igneous Suite has resulted in tighter age control on the duration of magmatism. Previous dating by the K-Ar method had a potential age span of over 15 Ma, but the new data suggests that active magmatism may have been more narrowly focused into a time span of less than 4 Ma. Although further geochronology may reveal units that are younger or older than those analyzed in this study, the samples selected here represent the type examples of the Babine Igneous Suite and should therefore serve as a baseline for analysis of other Babine Igneous Suite rocks located north of the map area.
2. The age similarity between the Newman Volcanics from the east side of the peninsula and the Babine Intrusion at Granisle mine suggest that these represent a subvolcanic intrusion and its extrusive equivalent. The fact that comagmatic volcanics are preserved in such close proximity to their intrusive equivalents suggests the volcano-plutonic centre is exposed at a shallow, subvolcanic level. The absence of Newman Volcanics near other deposits in the district implies that they are eroded to a deeper level and may not have the economic potential of the Bell and Granisle deposits.
3. The columnar jointed porphyry on the southwest side of the Newman Peninsula was originally interpreted as an extrusive body (Carter, 1981; MacIntyre et al., 1996). The younger age of  $49.9 \pm 0.6$  Ma on this unit, relative to the section of Newman Volcanics on the east side of the peninsula, may point towards an intrusive sill-like relationship for this body and possibly marks one of the

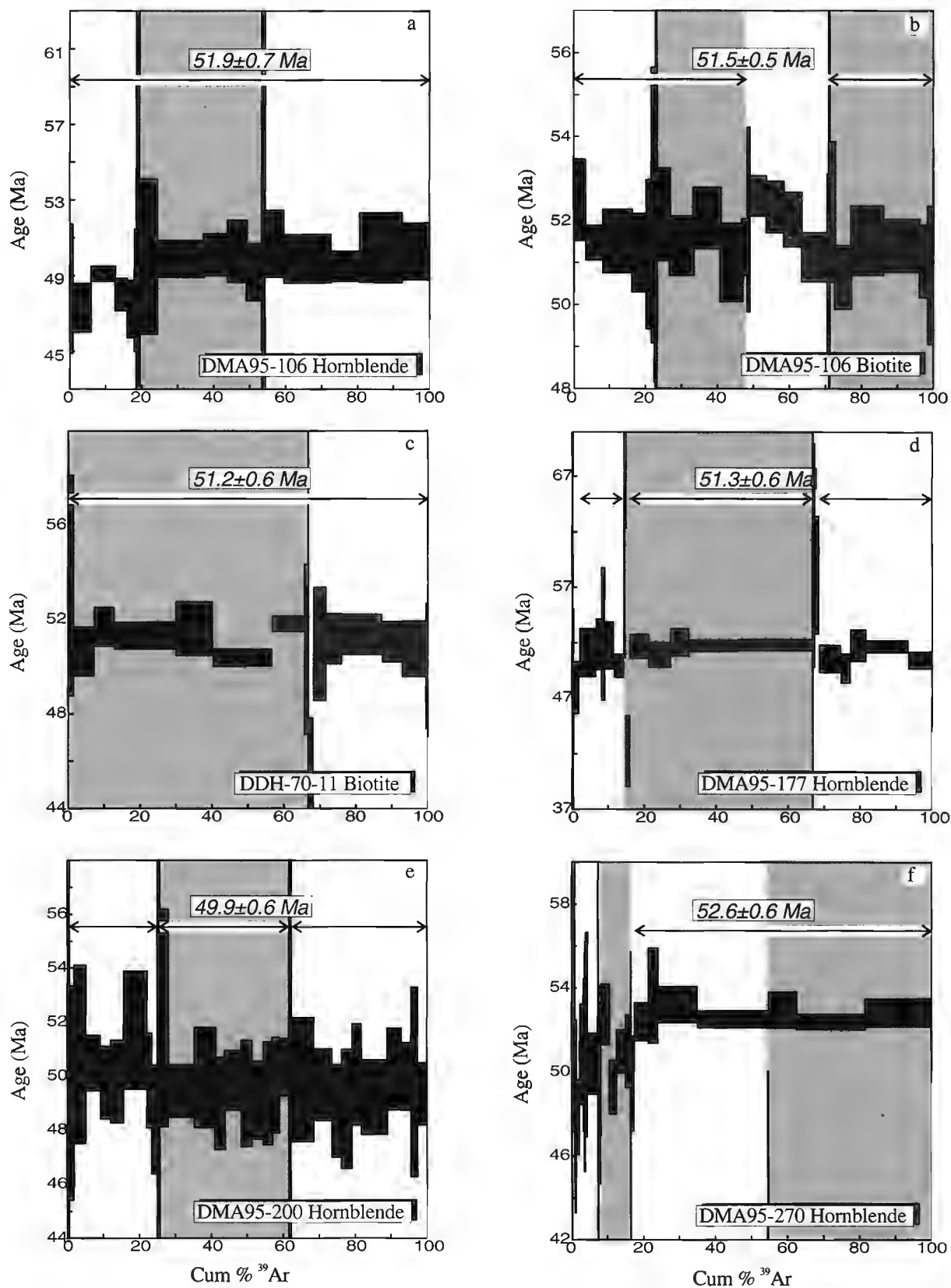


**Figure 2.** Gas release spectra for samples analyzed. Alternating backgrounds indicate different aliquots. Steps used in age calculation are indicated by lines with arrowheads.

last Babine Suite events. Alternatively, the unit may indeed be extrusive and mark either a second volcanic vent or a fault displaced section from stratigraphically on top of the lahar member in the section exposed on the east side of the peninsula.

4. The increased precision in the ages highlights the slightly older age of the suite at Turkey Mountain relative to the ca. 50 Ma events dated on the Newman Peninsula. This suggests derivation from another eruptive center. The Turkey Mountain suite may be the remains of a stratovolcano. This suggests building of stratovolcanoes preceded volcanic collapse, formation of grabens, and development of porphyry copper deposits. Saturday Lake may represent a third centre, but because the age overlaps both Turkey Mountain and Newman Peninsula, it is permissive that the intrusive porphyries may be related to either of these two areas.
5. Redefinition of the age of the hornblende-biotite-feldspar porphyry at Saturday Lake shows that it is correlative with porphyries at Granisle mine.

## ACKNOWLEDGMENTS

Pat Hunt is thanked for her careful sample preparation. Fred Quigg is thanked for his meticulous and comprehensive handling of the analytical aspects of this study. Both have been instrumental in continuing the legacy of Chris Roddick whose vision and massive contributions are not forgotten. Vicki McNicoll and Mike Gerasimoff are thanked for their thoughtful and careful reviews.

## REFERENCES

- Bysouth, G.D. and Wong, G.Y.**  
1995: The Endako molybdenum mine, central British Columbia: an update; in *Porphyry Deposits of the Northwestern Cordillera of North America*, (ed.) T.G. Schroeter, Canadian Institute of Mining, Metallurgy and Petroleum, Special Volume 46, p. 697-703.
- Carter, N.C.**  
1981: Porphyry copper and molybdenum deposits west-central British Columbia; British Columbia Ministry of Energy, Mines and Petroleum Resources, Bulletin 64, 150 p.
- Carter, N.C., Dirom, G.E. and Ogryzlo, P.L.**  
1995: Porphyry copper-gold deposits, Babine region, west-central British Columbia; in *Porphyry Deposits of the Northwestern Cordillera of North America*, (ed.) T.G. Schroeter, Canadian Institute of Mining, Metallurgy and Petroleum, Special Volume 46, p. 247-255.
- Dirom, G.E., Dittrick, M.P., McArthur, D.R., Ogryzlo, P.L., Pardoe, A.J. and Stothart, P.G.**  
1995: Bell and Granisle porphyry copper-gold mines, Babine region, west-central British Columbia; in *Porphyry Deposits of the Northwestern Cordillera of North America*, (ed.) T.G. Schroeter, Canadian Institute of Mining, Metallurgy and Petroleum, Special Volume 46, p. 256-289.
- Gabrielse, H., Monger, J.W.H., Wheeler, J.O., and Yorath, C.J.**  
1991: Part A. Morphogeological belts, tectonic assemblages, and terranes; in Chapter 2 of *Geology of the Cordilleran Orogen in Canada*, (ed.) H. Gabrielse and C.J. Yorath; Geological Survey of Canada, *Geology of Canada*, no. 4, p. 15-28 (also *Geological Society of America, The Geology of North America*, v. G-2).
- MacDougall, I. and Harrison, T.M.**  
1988: *Geochronology and Thermochronology by the  $^{40}\text{Ar}/^{39}\text{Ar}$  Method*; Oxford University Press, New York, 212 p.
- MacIntyre, D.G.**  
1981: Akie River Project (94F); in *Geological Fieldwork 1980*, British Columbia Ministry of Energy, Mines and Petroleum Resources, Paper 1981-1, p. 33-45.
- MacIntyre, D.G., Webster, I.C.L., and Bellefontaine, K.A.**  
1996: Babine porphyry belt project: bedrock geology of the Fulton Lake map area (93L/16), British Columbia; in *Geological Fieldwork 1995*, (ed.) B. Grant and J.M. Newell; British Columbia Ministry of Energy, Mines and Petroleum Resources, Paper 1996-1, p. 1-25.
- Ogryzlo, P.L., Dirom, G.E., and Stothart, P.G.**  
1995: Morrison-Hearne Hill copper-gold deposits, Babine region, west-central British Columbia; in *Porphyry Deposits of the Northwestern Cordillera of North America*, (ed.) T.G. Schroeter, Canadian Institute of Mining, Metallurgy and Petroleum, Special Volume 46, p. 290-303.
- Renne, P.R., Deino, A.L., Walter, R.C., Turrin, B.D., Swisher, C.C., Becker, T.A., Curtis, G.H., Sharp, W.D., and Jaouni, A.-R.**  
1994: Intercalibration of astronomical and radioisotopic time, *Geology*, v. 22, p. 783-786.
- Roddick, J.C.**  
1988: The assessment of errors in  $^{40}\text{Ar}/^{39}\text{Ar}$  dating; in *Radiogenic Age and Isotopic Studies: Report 2*; Geological Survey of Canada, Paper 88-2, p. 7-16.  
1990:  $^{40}\text{Ar}/^{39}\text{Ar}$  evidence for the age of the New Quebec Crater, northern Quebec; in *Radiogenic Age and Isotopic Studies: Report 2*; Geological Survey of Canada, Paper 89-2, p. 7-16.  
1996: Efficient mass calibration of magnetic sector mass spectrometers; in *Radiogenic Age and Isotopic Studies: Report 9*; Geological Survey of Canada, Current Research 1995-F, p. 1-9.
- Roddick, J.C., Cliff, R.A., and Rex, D.C.**  
1980: The evolution of excess argon in alpine biotites — a  $^{40}\text{Ar}/^{39}\text{Ar}$  analysis; *Earth and Planetary Science Letters*, v. 48, p. 185-208.
- Steiger, R.H. and Jäger, E.**  
1977: Subcommittee on geochronology: convention on the use of decay constants in geo and cosmochronology; *Earth and Planetary Science Letters*, v. 36, p. 359-362.
- Wanless, R., Stevens, R.D., LaChance, G.R., and DeLabio, R.N.**  
1974: Age determinations and geological studies, K-Ar isotopic ages, Report 11; Geological Survey of Canada, Paper 73-2, p. 22-23.



## U-Pb geochronology of stranger stones in Neoproterozoic diamictites, Canadian Cordillera: implications for provenance and ages of deposition

Gerald M. Ross<sup>1</sup> and Michael E. Villeneuve<sup>2</sup>

*Ross, G.M. and Villeneuve, M.E., 1997: U-Pb geochronology of stranger stones in Neoproterozoic diamictites, Canadian Cordillera: implications for provenance and ages of deposition; in Radiogenic Age and Isotopic Studies: Report 10; Geological Survey of Canada, Current Research 1997-F, p. 141-155.*

---

**Abstract:** Results of U-Pb zircon dating are presented for crystalline clasts (stranger stones) in diamictites from the Rapitan and Misinchinka groups, which represent two glacial intervals during Neoproterozoic Windermere Supergroup sedimentation in the northern and central Canadian Cordillera. A leucogranite dropstone in the lowermost Sayunei Formation gives an age of  $755 \pm 18$  Ma and provides a maximum depositional age for the Rapitan Group. Gabbro and syenogranite clasts yield nearly concordant ages of  $1857 \pm 3$  Ma and  $1860 \pm 1$  Ma, respectively. The association of ca. 1860 Ma and 755 Ma plutonic rocks suggest an intra-Cordilleran source. Six felsic plutonic and volcanic boulders from the Vreeland Formation (lower Misinchinka Group) yields one discordant age of  $1842 \pm 16/-14$  Ma and the remaining ages in the narrow range of 1865-1862 Ma. The composition and restricted suite of ages for the Vreeland Formation suggest possible derivation from the Fort Simpson High or (less likely) Great Bear Magmatic Zone.

**Résumé :** Le présent rapport fournit les résultats de datations U-Pb sur zircon effectuées sur des clastes de roches cristallines (pierres étrangères) présentes dans les diamictites des groupes de Rapitan et de Misinchinka, qui témoignent de deux intervalles glaciaires survenus au cours du dépôt du Supergroupe de Windermere au Néoprotérozoïque, dans le nord et le centre de la Cordillère canadienne. Un galet de déstage de composition leucogranitique situé dans la partie basale de la Formation de Sayunei a été daté à  $755 \pm 18$  Ma, ce qui établit une limite d'âge maximale à la sédimentation du Groupe de Rapitan. Des clastes de gabbro et de syénogranite ont livré des âges quasi concordants de  $1857 \pm 3$  Ma et de  $1860 \pm 1$  Ma, respectivement. L'association de roches plutoniques ayant livré des âges d'environ 1860 Ma et 755 Ma appuie l'hypothèse d'une source située à l'intérieur de la Cordillère. Six blocs de roches plutoniques et volcaniques de composition felsique présents dans la Formation de Vreeland (partie inférieure du Groupe de Misinchinka) ont été datés. L'un de ceux-ci a donné un âge discordant de  $1842 \pm 16/-14$  Ma alors que les autres âges obtenus s'insèrent dans l'étroit intervalle de 1865-1862 Ma. La composition et l'étendue restreinte des âges des échantillons de la Formation de Vreeland pointent comme source possible la hauteurs de Fort Simpson ou (moins vraisemblablement) la zone magmatique du Grand lac de l'Ours.

---

<sup>1</sup> GSC Calgary, 3303-33rd Street N.W., Calgary, Alberta T2L 2A7

<sup>2</sup> GSC Ottawa, 601 Booth Street, Ottawa, Ontario K1A 0E8

## INTRODUCTION

The Neoproterozoic was an unusual time in Earth history that witnessed the formation of two worldwide, continental ice sheets. The development of these glacial intervals are tied to major tectonic events, such as the break-up of the Neoproterozoic supercontinent Rodinia and the concomitant assembly of Gondwana (e.g. Hoffman, 1991), and major fluctuations in the chemistry of seawater during the appearance and radiation of metazoan life (Knoll and Walter, 1992). In western Canada, each of the two glacial episodes are well-represented within metasedimentary strata of the Windermere Supergroup in the Canadian Cordillera. The Canadian equivalents of the older of the glacial intervals (referred to as "Sturtian" based on occurrences with southern Australia) are the Toby Formation in the southern Cordillera (Aalto, 1971) and the Rapitan Group in the northern Cordillera (Young, 1976). The younger glacial interval (referred to as the "Marinoan" or "Varanger") is represented in the central and northern Cordillera by diamictites within the Vreeland Formation of the Misinchinka Group (McMechan, 1990) and Stelfox Member of the Ice Brook Formation (Aitken, 1991), respectively. The expression of the younger glacial event in the southern Cordillera is limited to a widespread and distinctive condensed interval deposited during the postglacial sea level rise and a less distinctive synglacial lowstand depositional system (Ross and Murphy, 1988; Ross et al., 1995).

Nearly all of the Windermere diamictites characteristically contain clasts composed of sedimentary rocks that are either intrabasinal in origin or derived from older sedimentary rocks that underlie the Windermere; clasts composed of exotic, basement-derived(?) crystalline material are rare. Exceptions include clasts of two mica granite reported from the Toby Formation (basal Windermere Supergroup; Loveridge et al., 1981; Miller, 1994), abundant clasts of coarse granitic material from the Vreeland Formation of the Misinchinka Group (McMechan, 1990) and granitic clasts from glaciogenic strata of the Rapitan Group (Aitken, 1991). Aitken (pers. comm., 1989) has coined the term "stranger stones" to describe these rare crystalline clasts, a term which we adopt as it conveys the unusual and enigmatic nature of the clasts. In this paper we report on the ages of granitic and associated clasts of crystalline rock from the Vreeland Formation and the Rapitan Group. Accurate U-Pb ages of these clasts could provide a fingerprint that would constrain provenance, if the clasts can be linked to known basement provinces, and may provide maximum ages of sedimentation for these poorly constrained, yet critical, sedimentary assemblages.

## GEOLOGICAL SETTING OF THE WINDERMERE SUPERGROUP

The Windermere Supergroup is widespread in the Canadian Cordillera and occurs from southernmost British Columbia north to the Alaska-Yukon border (Fig. 1). It has been interpreted to represent a rift and passive margin succession that formed as a consequence of continental break-up and separation during formation of the proto Pacific Ocean (Stewart, 1972; Ross et al., 1989; Ross, 1991; Gabrielse and

Campbell, 1991). The rift component consists of glaciogenic diamictites, and related sedimentary strata, and local mafic volcanic rocks that accumulated during syndepositional normal faulting. The overlying passive margin sequence is characterized by regionally widespread stratigraphic units that comprise a deep-to-shallow water shoal sequence in the southern Cordillera and a succession of clastic-to-carbonate "Grand Cycles" in the north (Aitken, 1989). Recent overviews and summaries of the Windermere in the northern and southern Canadian Cordillera can be found in papers in the *Geology of North America* series (DNAG) Narbonne and Aitken (1995) and Ross et al. (1995). The Windermere is overlain unconformably by latest Precambrian to Cambrian arkose and quartz arenites that record a younger rift event that led to the Paleozoic passive margin sequence (Devlin and Bond, 1988; Lickorish and Simony, 1995). The stratigraphic intervals investigated in this study consist of diamictites deposited during the older rift event (Rapitan Group and Toby Formation) and younger diamictites deposited during subsequent passive margin sedimentation (Vreeland Formation).

## CRYSTALLINE BASEMENT

Provenance studies of sedimentary strata within the Canadian Cordillera rely on a sound knowledge of the age and distribution of crystalline basement that could have provided sediment. Understanding the structure and tectonic evolution of the sub-Phanerozoic, western Canadian Shield has been the focus of numerous studies over the past years and has laid the framework for provenance studies in the Canadian Cordillera (e.g. Ross and Bowring, 1990; Ross and Parrish, 1991; Gehrels et al., 1995). In particular, recent studies by Ross et al. (1991) and Villeneuve et al. (1993) have delineated Precambrian domains buried beneath Alberta and British Columbia and extrapolated these domains westward beneath the Cordilleran deformation front. Figure 1 shows the present state of knowledge of the age and distribution of autochthonous crystalline basement in western Canada. This compilation is based on studies of the exposed Canadian Shield as well as subsurface studies of the geophysical signature of basement and dating of drill core (Villeneuve et al., 1993).

Exposures of crystalline basement also occur within the Canadian Cordillera but are restricted to structural culminations within the southern Cordillera, in particular Frenchman's Cap-Thor-Odin region of the Monashee Complex (Parkinson, 1991; Armstrong et al., 1991), Malton Complex and associated gneiss bodies (Gold Creek Gneiss, Hugh Allan Gneiss, Blackman Gneiss; McDonough and Parrish, 1991; Murphy et al., 1991), and possible occurrences in the Grand Forks region of southernmost British Columbia (Armstrong et al., 1991) (Fig. 2). In the central Canadian Cordillera, Evenchick et al., (1984) described two occurrences of pre-Windermere crystalline rocks in the Sifton and Deserters Range. There are no known exposures of the crystalline basement that underlie the thick succession of Mesoproterozoic to Neoproterozoic sedimentary strata of the northern Cordillera and it thus remains terra incognita. High quality U-Pb

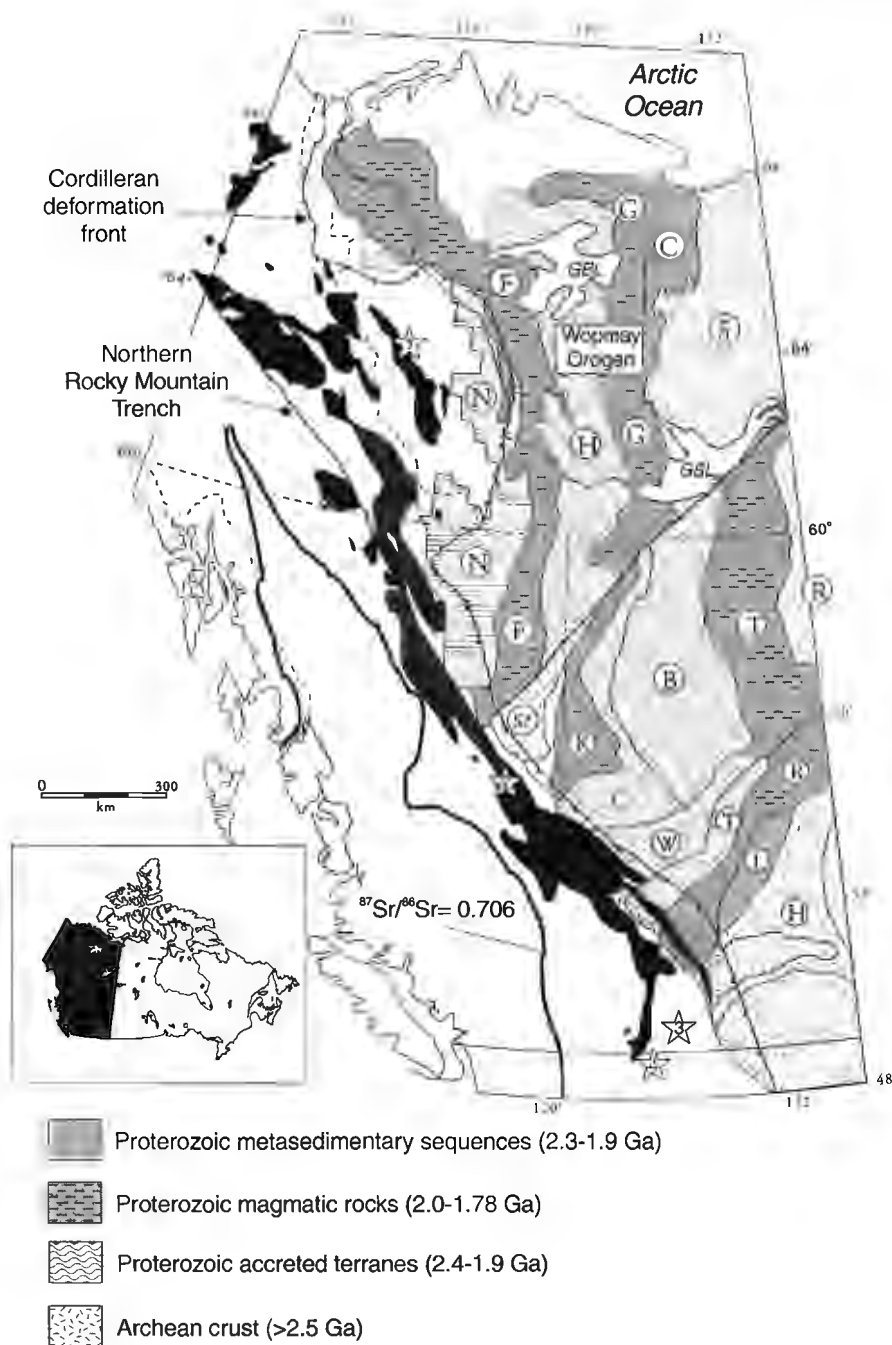


**Figure 1.** Distribution of the Windermere Supergroup (shown in black main figure) in the Canadian Cordillera relative to autochthonous basement domains (modified from Ross, 1991). Numbered stars are localities of diamictites with cobbles of crystalline rock ("stranger stones"): 1: Rapitan Group, Mackenzie Mountains; 2: Vreeland Formation, Misinchinka Range; 3 and 4: Toby Formation, southern British Columbia and northeastern Washington State, U.S.A., respectively. Abbreviations for basement domains: Archean: S-Slave Province; R-Rae Province; H-Hearne Province; Proterozoic accreted terranes: H-Hottah Terrane; C-Chinchaga; B-Buffalo Head; W-Wabamun; T-Thorsby; Proterozoic magmatic terranes: G-Great Bear; F-Fort Simpson; K-Ksituan; T-Taltson; R-Rimbey; Proterozoic metasedimentary terranes: C-Coronation; L-Lacombe. N is the Nahanni domain (Hoffman, 1989), age unknown. GSL-Great Slave Lake; GBL-Great Bear Lake. The strontium "0.706" line is taken from Armstrong (1988) and approximates the western edge of cratonic basement.

geochronology has now been completed on most of these basement rocks and a clear pattern of ages and associations has emerged. Both the Malton and Monashee complexes contain an older mixed paragneiss-orthogneiss assemblage that ranges in age from 2050-1960 Ma that is intruded by ca. 1870-1851 Ma orthogneisses. In the Sifton Range of the central Cordillera, a potassium feldspar augen gneiss gives an upper intercept age of  $1851 \pm 13$  Ma similar to ages obtained from orthogneisses in the southern Cordillera (Evenchick et al., 1984). Nearly all of the Paleoproterozoic basement rocks are associated with younger magmatic rocks that range in age from 740-728 Ma. For example, older gneisses in the Malton Complex are intruded by leucogranite orthogneisses that range from 740-736 Ma and include widespread, weakly foliated sill-like bodies (M.R. McDonough, pers. comm., 1993), suggesting that this igneous event is widespread in the

Malton Complex. In the Deserters Range (central British Columbia; Fig. 2), a mylonitic leucocratic granitic gneiss, dated at  $728 \pm 9/-7$  Ma is nonconformably overlain by Neoproterozoic feldspar-quartz pebble conglomerate and quartzite assigned to the Windermere Supergroup (Evenchick et al., 1984). Similarly, Parrish and Scammell (1988) dated an alkalic gneiss that intrudes core gneisses of Frenchman's Cap at  $740 \pm 36$  Ma. Thus there appears to be evidence for an association of older Proterozoic gneisses (ca. 2.0-1.85 Ga) and younger (ca. 740 Ma) orthogneisses within exposed basement with the Canadian Cordillera. The ages of the younger orthogneisses are similar to ages of magmatic activity believed to be related to Windermere rifting (Fig. 2) suggesting that these younger orthogneisses are part and parcel of that magmatic event.

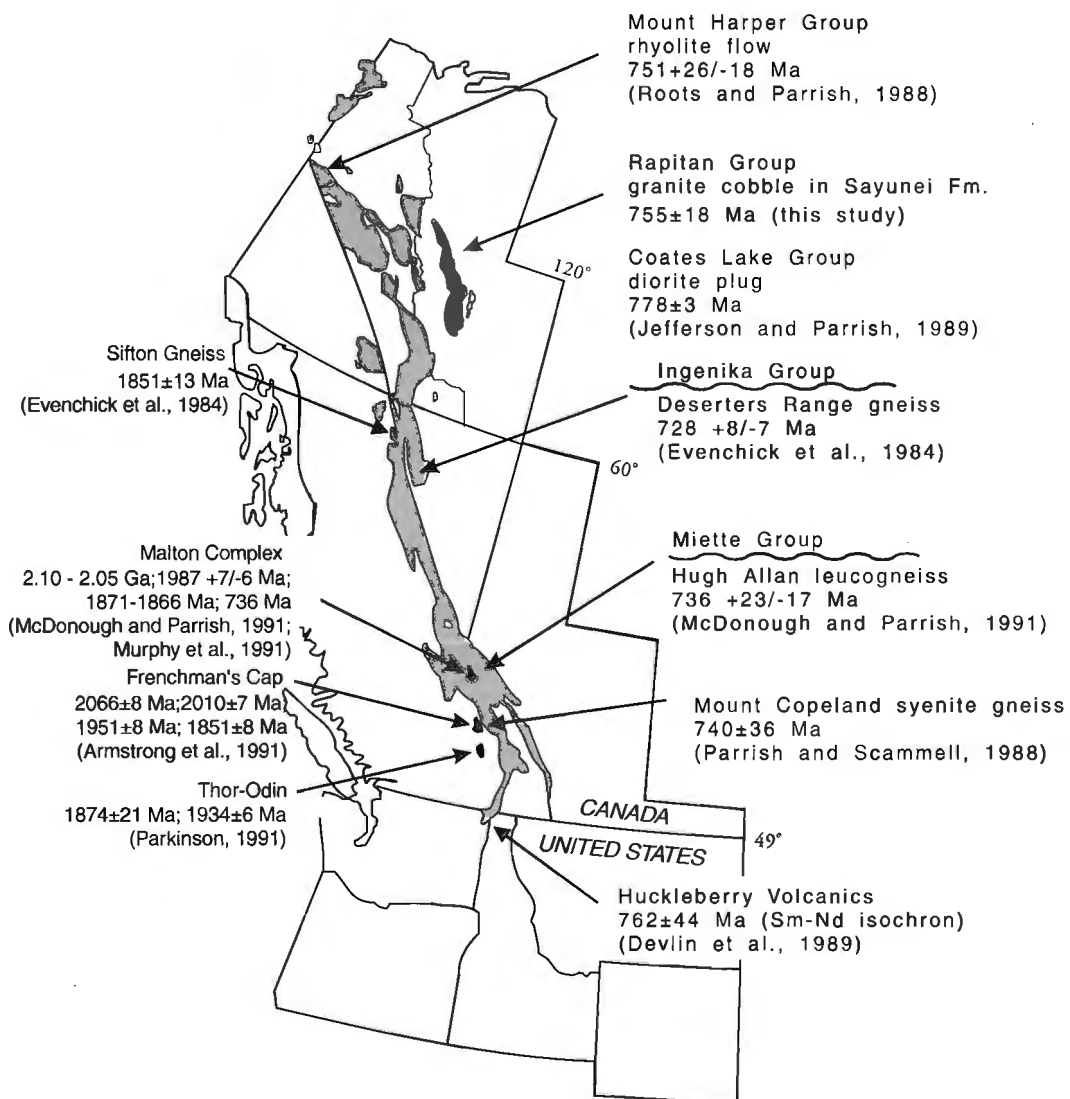


**Figure 2.** Simplified map showing the distribution of crystalline basement within structural culminations within the Canadian Cordillera (black fill) as well as the locations, ages and source of data for magmatic rocks within or immediately underlying the Windermere Supergroup.



## U-Pb METHODOLOGY

Zircons were concentrated from crushed samples using standard techniques of heavy liquid and separation by magnetic susceptibility. Zircon crystals were selected for analysis based on crystal clarity, lack of fractures or inclusions, and colour. All zircons were abraded prior to dissolution in order to remove outer portions of the grains where much of the Pb loss and alteration takes place, and thereby increase concordance (Krogh, 1982). After abrasion, photography, and final mineral selection, individual fractions were analyzed following the methods of Parrish et al. (1987). Data were reduced and errors propagated after the methods of Roddick (1987) and Parrish et al., (1987); analyses plotted as ellipses on concordia diagrams are shown at  $2\sigma$  (95% confidence) level of uncertainty. Final errors are indicated on Table 1. Linear regressions on discordant arrays of data use a method that takes into account the scatter of the points about the line (see discussion in Parrish et al., 1987). Fraction letters shown on concordia plots are keyed to fraction letters in Table 1.

## STRANGER STONES IN THE RAPITAN GROUP

The Rapitan Group is widespread within thrust slices of the Windermere Supergroup in the northern Canadian Cordillera (Fig. 1). The Rapitan Group comprises the local Mount Berg Formation and the widespread Sayunei and Shezal formations which collectively have been interpreted as recording deposition in rift basins (e.g. Eisbacher, 1981; Yeo, 1981). The age of the Rapitan Group is constrained as younger than 778 Ma (Jefferson and Parrish, 1989) (Fig. 3). The Rapitan has long been recognized as having glacially influenced deposition based on the presence of coarse, bouldery diamictites, dropstones, and till pellets (Gabrielse, 1972; Young, 1976; Yeo, 1981; Eisbacher, 1981). The Sayunei Formation, up to 600 m thick, consists of reddish mudstones, interbedded sandstones and conglomerates of deep-water origin. Glacial dropstones are common within the finely bedded facies of the Sayunei Formation. The overlying Shezal Formation, up to 800 m thick, consists of massive to crudely bedded diamictite with subordinate interbeds of sandstone and mudstone (Fig. 4). Studies of paleocurrent indicators suggest variable transport directions but with an overall east-to-west, and local north-to-south transport (Yeo, 1981; Eisbacher, 1981). The Rapitan Group rests unconformably on sedimentary strata of the Mackenzie Mountains Supergroup and in general the clast composition reflects that provenance with an abundance of sedimentary clasts easily correlated with underlying units and local occurrences of clasts of greenstone that can be correlated with the Little Dal Formation basalts and Tsezotene sills. Two exceptions have been noted and these consist of a total of three igneous clasts found within two sections of the Rapitan Group. Two clasts are from the Shezal Formation (88-AC-8-D and AC-540-R) and a single clast occurrence as a dropstone within the turbidites of the Sayunei Formation (88-AC-8-B).

## Sayunei dropstone

Sample 88-AC-8-B is a clast of undeformed leucogranite, about 20 cm in diameter, composed of medium grained, intergrown quartz and alkali feldspar with 5-10% chloritized biotite. The zircons within this sample were not abundant and comprised pale pink, translucent, euhedral, and broken crystals. Single grain fractions A and B each yielded only around 100 pg of radiogenic Pb, resulting in a higher than normal blank Pb/radiogenic Pb ratio and a resulting expansion in analytical uncertainty for each fraction (Table 1; Fig. 5a). Nevertheless, both fractions overlap concordia and taking a weighted average of  $^{207}\text{Pb}/^{206}\text{Pb}$  ages results in an age of  $755 \pm 18$  Ma, which is interpreted as the age of igneous crystallization. A third fraction (Table 1) consisted of two clear, colourless, slightly turbid crystals, distinct from the clear pink grains that make up the majority of the zircon population. This fraction yielded an extremely discordant analysis (58%) with a  $^{207}\text{Pb}/^{206}\text{Pb}$  age of 2.14 Ga, indicating that this fraction contained an inherited older component.

## Shezal Formation

Sample 88-AC-8-D is an approximately 15 cm clast of undeformed biotite gabbro from the upper Shezal Formation, within the same measured stratigraphic section which contained the Sayunei dropstone (Fig. 4; see Fig. 3 in Aitken, 1991 for photograph). The gabbro, which is coarse grained and unfoliated with equant phaneritic texture, produced a good yield of faceted, euhedral, clear to slightly turbid, pale pink zircons. Analysis of six fractions produced five fractions less than 2% discordant and all six fractions fall on a discordia with an upper intercept of  $1860 \pm 1$  Ma (MSWD of 2) which is interpreted as the age of igneous crystallization (Fig. 5b). Zircon with significantly older inheritance or zircons with younger ages are not apparent in any of the analyses.

Sample AC-540-R, also from the Shezal Formation, (located at  $64^{\circ}29'\text{N}$  and  $129^{\circ}17'\text{W}$ ; Aitken et al., 1973) is an approximately 20 cm clast of quartz monzonite composed of zoned grey potassium feldspar crystals, euhedral green plagioclase, anhedral quartz, and intercrystalline greenish mafic minerals (altered biotite) and contained a large number of clear, slightly pink zircons. Four analyses, ranging from 5.7% to 0.3% discordant, scatter about a discordia (MSWD=5.5) with an upper intercept age of  $1857 \pm 3$  (Table 1; Fig. 5c) which is interpreted as the age of crystallization.

## STRANGER STONES IN THE VREELAND FORMATION (MISINCHINKA GROUP)

The Misinchinka Group consists of coarse diamictites, pelites, grits, carbonates, and subordinate amphibolites and is correlative with the Miette Group which is widespread south of  $54^{\circ}\text{N}$  (Evenchick, 1988; McMechan, 1990; Hein and McMechan, 1994) (Fig. 6). In the Deserters Range, the Misinchinka Group unconformably overlies 728 Ma basement (Evenchick et al., 1984) which provides a maximum age constraint. The diamictites are thickest and best exposed in the Ice Mountain-Paksumo Pass area of the Back Ranges of

Table 1. U-Pb data.

Fraction <sup>a</sup>	Wt. <sup>b</sup> μg	U ppm	Pb <sup>c</sup> ppm	<sup>206</sup> Pb/ <sup>204</sup> Pb <sup>d</sup>	Pb <sup>e</sup> pg	<sup>208</sup> Pb/ <sup>206</sup> Pb <sup>f</sup>	Radiogenic ratios (±1σ, %) <sup>g</sup>			<sup>207</sup> Pb/ <sup>206</sup> Pb Age (Ma) <sup>g</sup>	Discord. <sup>h</sup> %
							<sup>207</sup> Pb/ <sup>235</sup> U	<sup>206</sup> Pb/ <sup>238</sup> U	<sup>207</sup> Pb/ <sup>206</sup> Pb		
88-AC-8B Sayunei Formation (Z2652; 64.6839°N 129.8362°E)											
A (Z)	2	337	41	368	12	0.100	1.084 ± 1.74	0.1214 ± 0.45	0.06473 ± 1.59	766 ± 66	3.71
B (Z)	1	663	83	458	14	0.110	1.097 ± 0.51	0.1235 ± 0.18	0.06439 ± 0.44	755 ± 18	0.53
C (Z)	4	496	74	39	709	0.210	1.234 ± 7.81	0.1353 ± 1.81	0.06615 ± 6.68	811 ± 257	-0.90
D (Z)	3	571	104	1147	9	0.160	2.991 ± 0.17	0.1630 ± 0.16	0.13307 ± 0.08	2139 ± 3	58.57
88-AC-8D Sayunei Formation (Z2653; 64.6839°N 129.8362°E)											
A (Z)	29	134	49	6746	12	0.180	5.194 ± 0.10	0.3311 ± 0.09	0.11378 ± 0.03	1861 ± 1	1.04
B (Z)	27	166	61	4128	22	0.180	5.160 ± 0.12	0.3289 ± 0.10	0.11377 ± 0.04	1861 ± 1	1.68
C (Z)	21	146	54	4841	12	0.170	5.234 ± 0.11	0.3339 ± 0.10	0.11370 ± 0.04	1859 ± 2	0.15
D (Z)	21	157	55	2426	26	0.200	4.894 ± 0.14	0.3114 ± 0.13	0.11397 ± 0.05	1864 ± 2	7.10
E (Z)	13	93	36	1082	23	0.220	5.259 ± 0.18	0.3346 ± 0.14	0.11401 ± 0.15	1864 ± 5	0.24
F (Z)	23	143	53	4136	17	0.180	5.224 ± 0.11	0.3327 ± 0.10	0.11388 ± 0.07	1862 ± 3	0.67
AC-540-R Shezal Formation (Z2654; 64°12'N 129°17'E)											
A (Z)	9	90	32	930	17	0.210	4.962 ± 0.21	0.3159 ± 0.18	0.11393 ± 0.11	1863 ± 4	5.72
B (Z)	12	134	48	2735	1	0.140	5.185 ± 0.13	0.3309 ± 0.12	0.11363 ± 0.05	1858 ± 2	0.95
C (Z)	16	190	66	715	87	0.130	5.052 ± 0.17	0.3234 ± 0.11	0.11332 ± 0.11	1853 ± 4	2.92
E (Z)	22	121	45	3169	17	0.200	5.210 ± 0.11	0.3328 ± 0.10	0.11352 ± 0.04	1857 ± 2	0.28
RAR-90-W6 Vreeland Diamictite (Z2417; 54.5900°N 121.5617°E)											
A (Z)	16	150	57	2486	20	0.210	5.223 ± 0.12	0.3327 ± 0.09	0.11387 ± 0.06	1862 ± 2	0.66
B (Z)	15	198	65	3478	2	0.190	4.576 ± 0.11	0.2914 ± 0.10	0.11391 ± 0.05	1863 ± 2	13.02
D (Z)	8	304	82	1253	30	0.170	3.727 ± 0.13	0.2455 ± 0.10	0.11009 ± 0.08	1801 ± 3	23.82
E (Z)	14	278	80	987	66	0.160	4.019 ± 0.15	0.2639 ± 0.10	0.11048 ± 0.10	1807 ± 4	18.46
F (Z)	13	187	61	3807	12	0.170	4.551 ± 0.11	0.2941 ± 0.10	0.11222 ± 0.04	1836 ± 1	10.72
G (Z)	9	305	78	3370	0	0.150	3.560 ± 0.11	0.2372 ± 0.10	0.10886 ± 0.05	1780 ± 2	25.43
RAR-90-W7 Vreeland Diamictite (Z2418; 54.5900°N 121.5617°E)											
B (Z)	5	107	39	1145	10	0.220	4.903 ± 0.23	0.3147 ± 0.21	0.11300 ± 0.11	1848 ± 4	5.22
E (Z)	14	99	35	3836	1	0.200	4.904 ± 0.11	0.3145 ± 0.10	0.11307 ± 0.04	1849 ± 2	5.34
D (Z)	4	131	47	981	11	0.180	5.051 ± 0.19	0.3220 ± 0.18	0.11377 ± 0.14	1861 ± 5	3.76
F (Z)	13	88	34	1799	13	0.250	5.246 ± 0.14	0.3337 ± 0.12	0.11404 ± 0.06	1865 ± 2	0.54
RAR-90-W11 Vreeland Diamictite (Z2419; 54.5900°N 121.5617°E)											
A (Z)	5	326	105	2044	15	0.140	4.654 ± 0.15	0.3000 ± 0.14	0.11253 ± 0.06	1841 ± 2	9.22
B (Z)	6	175	60	1189	17	0.210	4.827 ± 0.20	0.2987 ± 0.18	0.11719 ± 0.08	1914 ± 3	13.58
C (Z)	6	177	53	1312	0	0.180	4.090 ± 0.22	0.2664 ± 0.17	0.11137 ± 0.12	1822 ± 4	18.44
E (Z)	4	302	72	760	22	0.140	3.431 ± 0.32	0.2225 ± 0.25	0.11186 ± 0.20	1830 ± 7	32.23
F (Z)	5	290	84	1782	13	0.220	3.886 ± 0.16	0.2509 ± 0.11	0.11234 ± 0.08	1838 ± 3	23.95
RAR-90-W12 Vreeland Diamictite (Z2420; 54.5900°N 121.5617°E)											
A (Z)	3	120	43	686	11	0.190	5.017 ± 0.19	0.3189 ± 0.14	0.11410 ± 0.12	1866 ± 4	4.98
B (Z)	4	190	72	665	24	0.220	5.215 ± 0.19	0.3314 ± 0.15	0.11414 ± 0.13	1866 ± 5	1.32
C (Z)	4	152	55	1000	2	0.180	5.048 ± 0.19	0.3221 ± 0.15	0.11366 ± 0.12	1859 ± 5	3.62
D (Z)	1	190	77	474	7	0.160	6.885 ± 0.31	0.3627 ± 0.28	0.13769 ± 0.19	2198 ± 7	10.75
F (Z)	4	196	69	1151	14	0.150	5.108 ± 0.14	0.3226 ± 0.11	0.11483 ± 0.09	1877 ± 3	4.56
MBB-88-W12 Vreeland Diamictite (Z1807; 54.5900°N 121.5617°E)											
A	36	194	71	452	334	0.180	5.106 ± 0.20	0.3265 ± 0.15	0.11341 ± 0.10	1855 ± 4	1.60
B	19	131	49	1327	39	0.186	5.259 ± 0.13	0.3347 ± 0.09	0.11397 ± 0.07	1864 ± 3	0.20
C	29	171	60	2150	46	0.184	4.949 ± 0.11	0.3163 ± 0.09	0.11347 ± 0.05	1856 ± 2	5.20
RAR-90-W13 Vreeland Diamictite (Z2421; 54.5900°N 121.5617°E)											
A (Z)	15	173	63	7161	6	0.200	5.069 ± 0.11	0.3238 ± 0.10	0.11355 ± 0.03	1857 ± 1	3.01
B (Z)	20	143	53	8354	6	0.180	5.181 ± 0.10	0.3299 ± 0.09	0.11389 ± 0.03	1863 ± 1	1.51
D (Z)	18	161	59	11978	5	0.180	5.154 ± 0.10	0.3286 ± 0.09	0.11375 ± 0.03	1860 ± 1	1.76
E (Z)	23	170	61	11754	4	0.190	4.995 ± 0.10	0.3199 ± 0.09	0.11327 ± 0.03	1853 ± 1	3.92

<sup>a</sup>All zircon fractions are abraded; (Z) = Zircon<sup>b</sup>Error on weight = ±0.001 mg<sup>c</sup>Radiogenic Pb<sup>d</sup>Measured ratio corrected for spike and Pb fractionation of 0.09 ± 0.03%/AMU<sup>e</sup>Total common Pb on analysis corrected for fractionation and spike, of blank model Pb composition<sup>f</sup>Corrected for blank and spike Pb and U and common Pb (Stacey-Kramers model Pb composition equivalent to the <sup>207</sup>Pb/<sup>206</sup>Pb age)<sup>g</sup>Age error is ±2 se in Ma<sup>h</sup>Discordance along a discordia to origin.

northeast British Columbia where they attain a remarkable thickness (excess of 1 km; Fig. 7A) and coarse clast size (up to 8 m). In contrast to the Rapitan Group, there is little evidence to suggest local fault control of sedimentation within rift basins and additionally, the Vreeland Formation diamictites lie well above the base of the Windermere Supergroup, which led McMechan (1990) to suggest that these diamictites were younger than the Rapitan Group or Toby Formation. McMechan (1990) demonstrated that the Vreeland diamictites pass laterally to the south-southwest into turbiditic grits typical of the McKale Formation of the Miette Group and the Windermere Supergroup of the southern Cordillera in general (e.g. Ross et al., 1989). The Vreeland Formation diamictites thus are interpreted to represent a proximal facies of the Windermere turbidite basin that was deposited along the south flank of the ancestral Peace River Arch, a paleotopographic high that trends at a high angle into the Cordillera.

The Vreeland Formation is up to 1200 m thick and is overlain by argillaceous rocks of the Framstead Formation and carbonates of the Chowika Formation. The Vreeland Formation consists of massive to crudely bedded bouldery diamictite containing unsorted clasts in a cleaved argillaceous matrix (McMechan, 1990; Hein and McMechan, 1994). Local interbeds of laminated siltstone to sandstone are present and contain dropstones of glacial origin (McMechan, 1990). Boulders are up to 8 m across and consist of unfoliated granites and related felsic plutonic rocks, felsic extrusive

rocks, diabase, dolomite, and quartzite of inferred extrabasinal origin as well as abundant intraformational clasts of mudstone and siltstone. The “stranger stones” of crystalline material are most abundant in the upper part of the Vreeland Formation. The igneous rocks comprise two predominant types: massive, unfoliated, phaneritic intrusive rocks that range in composition from tonalite to alkali granite (Fig. 7B, C) and extrusive or hypabyssal rocks that include dacite tuff, flow-banded, spherulitic rhyolite, and felsic porphyry (Fig. 7D, E). This association of rock types is comparable to those expected in the shallow levels of a continental magmatic arc. We collected a total of thirteen different rock types of which six representative samples were chosen for geochronological analysis on the basis of freshness. The diabase clasts were not sampled for this study but range from massive, unfoliated typical dark green diabase to locally pegmatitic texture (Fig. 7B) and should be considered a target for future work.

RAR-90-W6 is a fresh, fine grained, equigranular leucocratic tonalite that yielded a number of stubby, well faceted, high quality, colourless zircons and a few dark brown, clear crystals. Discordance ranges from 0.7% (fraction A, Table 1, Fig. 8a) to 25% (fraction G). Utilizing a Davis (1982) regression technique to take advantage of the near-concordance of fraction A, results in an upper intercept of  $1863 \pm 3$  Ma with a 48% probability of fit. Fraction B is

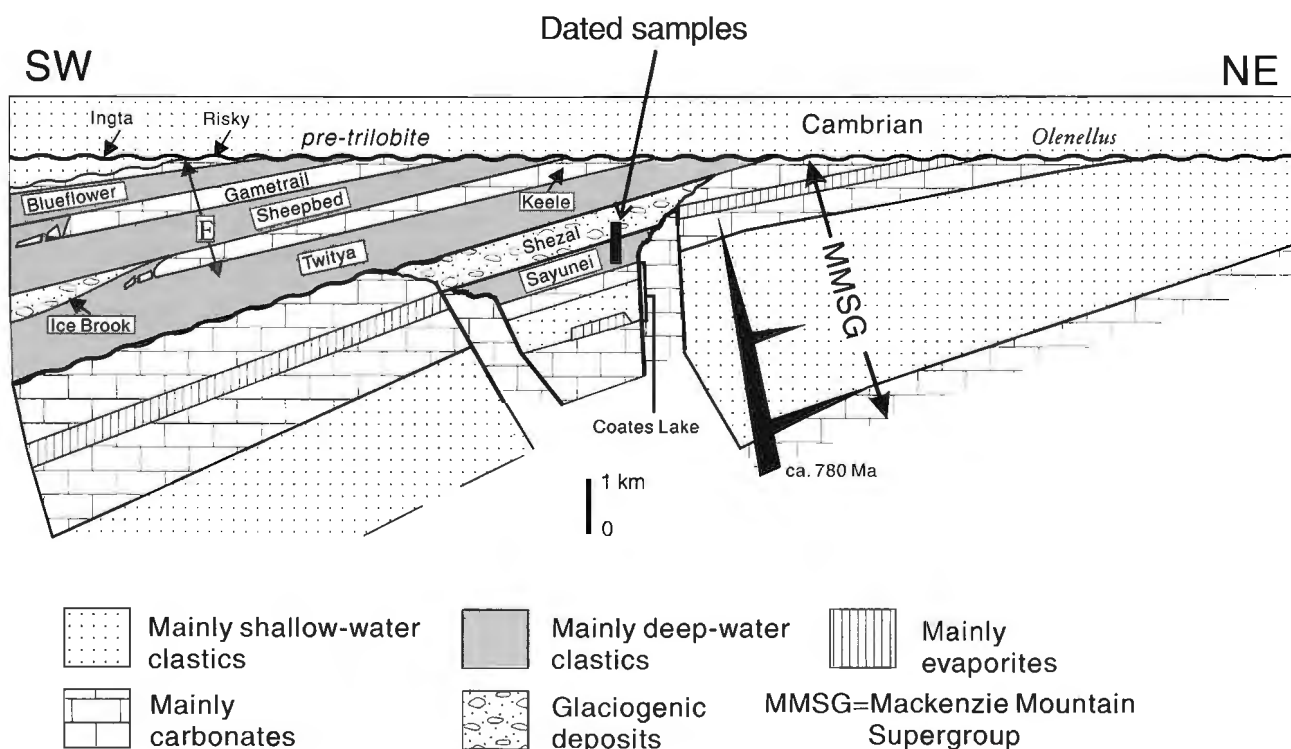


**Figure 3.** Simplified stratigraphic cross-section through the Mackenzie Mountains illustrating the main stratigraphic units, their mutual relationships and the positions of dated samples and magmatic rocks. The two Neoproterozoic glacial intervals are in the Rapitan Group and Ice Brook Formation (from Narbonne and Aitken, 1995).

excluded from the regression as it consists of two dark crystals and clearly plots to right of fraction F, indicative of a xenocrystic-inherited component.

RAR-90-W7 is from a large boulder of equigranular, coarse grained syenogranite that contains magnetite and chloritized mafic phases (Fig. 7C). A small number of stubby, clear, colourless, well faceted crystals were separated from the rock. Four collinear fractions, including fraction F at 0.5% discordance, yielded an upper intercept of  $1867 \pm 3$  Ma, again utilizing a Davis (1982) regression, with a probability of fit of 19% (Table 1; Fig. 8b).

RAR-90-W12 is a leucocratic granite, with potassium feldspar megacrysts up to 3 cm long in a groundmass of medium-grained reddish plagioclase subhedra and quartz (Figure 7D). Six fractions of clear, colourless, euhedral zircon were analyzed, with one fraction (D) displaying

inheritance of a much older component ( $^{207}\text{Pb}/^{206}\text{Pb}$  age of 2198 Ma; Table 1). Three fractions plot near each other at 4-5% discordant and fraction B, which provides the best control on the age, plots at 1% discordance. Fraction F appears to contain a minor inherited Pb component. A discordia through fractions A, B, C, and E results in an upper intercept of  $1867 \pm 13/-9$  Ma ( $\text{LI}=130 \pm 500$  Ma,  $\text{MSWD}=3$ ), interpreted as the age of crystallization (Fig. 8C).

RAR-90-W11 is a fine- to medium-grained, equigranular syenogranite. Zircons from this rock comprised a somewhat heterogeneous population of euhedral to subhedral crystals. The zircons range from dark, clear grains to colourless, rounded and elongate crystals. Most zircons have well defined crystal faces, although some rounding of edges is evident. Two fractions (B and D) display cryptic inheritance and plot to the right of a discordia defined by fractions A, C, E, and F (Fig. 8d). The discordia gives an upper intercept of

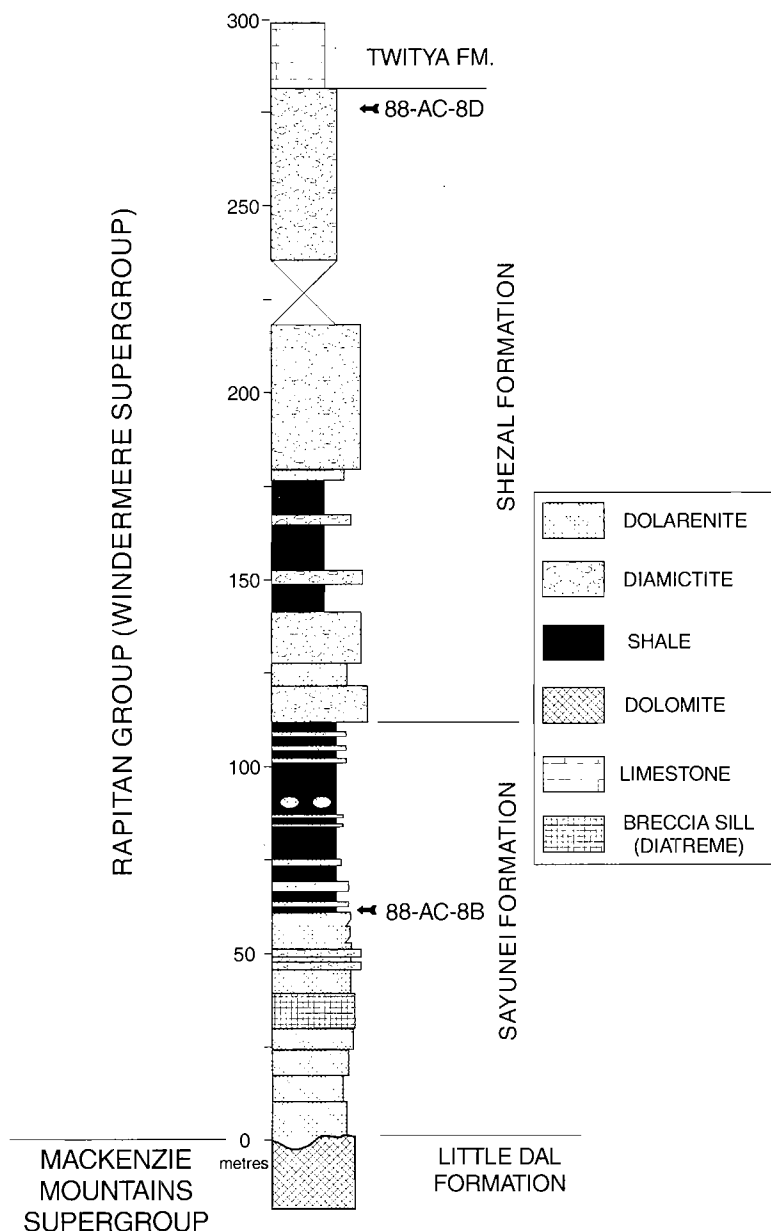


**Figure 4.**

*Measured stratigraphic section through the Rapitan Group with the positions of the dated stanger stones shown. Unpublished section measured by James D. Aitken (location:  $64^{\circ}41'N$ ,  $129^{\circ}49'W$ ).*

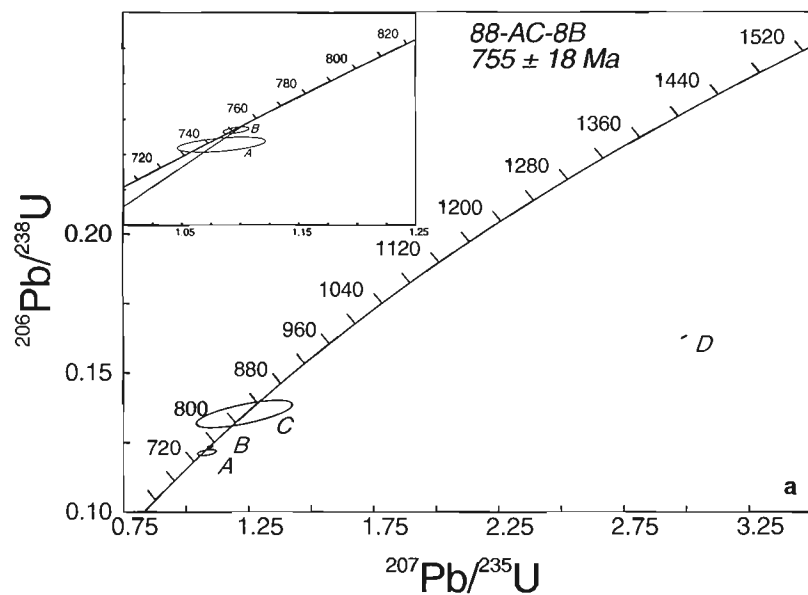
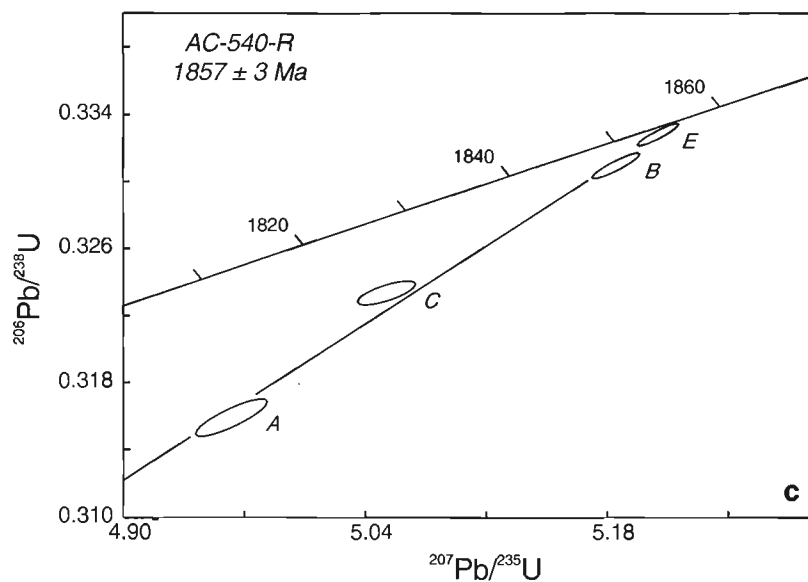
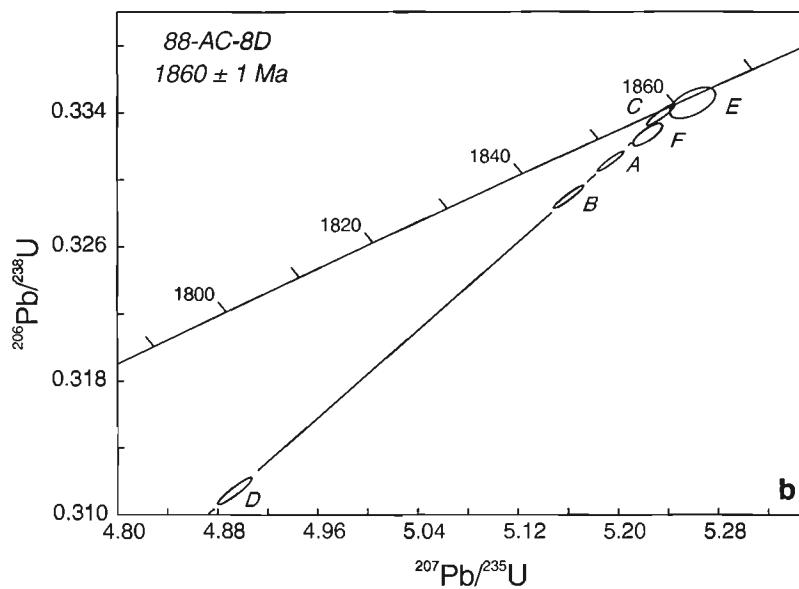


**Figure 5.**

U-Pb concordia plots for samples from the Rapi-tan Group. **a)** is for the Sayunei dropstone (88-AC-8-B) and the inset shows a detail of the two most concordant points. **b)** and **c)** are for stones in the Shezal Formation.



1842±16/-14 Ma (lower intercept =  $53 \pm 125$  Ma, MSWD=25), which is interpreted as an igneous crystallization age.

MBB-88-W12 (collected previously by Margot McMechan from the same locality) is composed of homogeneous unfoliated medium- to fine-grained leucogranite with a massive texture defined by equant subhedral grains of quartz and feldspar and <5% mafic material which has been altered and is now composed of patches of rusty-weathering carbonate. Three single grain fractions of clear, purple zircons resulted in a concordant analysis and two collinear discordant analyses that give  $1864 \pm 4$  Ma (LI=250 ± 130 Ma, MSWD=2.1) as the age of crystallization (Fig. 8e).

RAR-90-W13 represents the only felsic volcanic rock sampled. It is a dacite with subrounded phenocrysts of potassium feldspar in a leucocratic, fine grained greenish matrix (Fig. 7e). Stubby, clear multifaceted zircons proved to have well behaved U/Pb systematics. Four fractions form a collinear array with an upper intercept of  $1867 \pm 2$  Ma (LI=508 ± 68 Ma, MSWD=1.4; Fig. 8f).

## SOURCE AREAS AND PROVENANCE

### Rapitan Group

The ca. 755 Ma granitic cobble within the lower Sayunei Formation provides a maximum age for deposition of the Sayunei Formation and possibly the Rapitan Group in general. Its age is comparable to the ages of magmatism that are

characteristic of the lower Windermere Supergroup throughout western Canada (Fig. 2; see Ross et al., 1995 for a summary) which ranges from ca. 770 Ma to 728 Ma. It is suggested that the cobble that we dated may have been derived from an early rift-related pluton that was unroofed during on-going rifting and deposition of the Rapitan Group. This would suggest a local provenance, in accord with the predominance of clasts derived from immediately subjacent sedimentary strata of the Mackenzie Mountains Supergroup. However, such plutonic rocks have not been observed in the underlying Mackenzie Mountains Supergroup.

The source(s) of the two cobbles in the Shezal Formation with virtually identical ages of 1860 and 1857 Ma is problematic. As noted previously, the Rapitan Group lies unconformably on an older sedimentary succession, the Mackenzie Mountains Supergroup, which in turn lies on the sedimentary strata of the Hornby Bay-Dismal Lakes group succession in the subsurface of the Mackenzie Corridor. Recent subsurface mapping using both drill core and seismic reflection data from petroleum exploration has shown that virtually the entire Mackenzie Valley is underlain by these pre-Windermere sedimentary rocks (Aitken and Pugh, 1984; Cook et al., 1992; Cook and MacLean, 1995). Thus the closest occurrences of known crystalline basement that could have been exposed during Windermere sedimentation would have been the eastern shores of Great Bear Lake, a distance of about 500 km (Fig. 1). There, igneous rocks of the Great Bear Magmatic Zone are exposed as part of an 1865-1840 Ma episutural volcano-plutonic belt along the west part of the ca. 1960-1870 Ma Wopmay Orogen (Hildebrand et al., 1987;

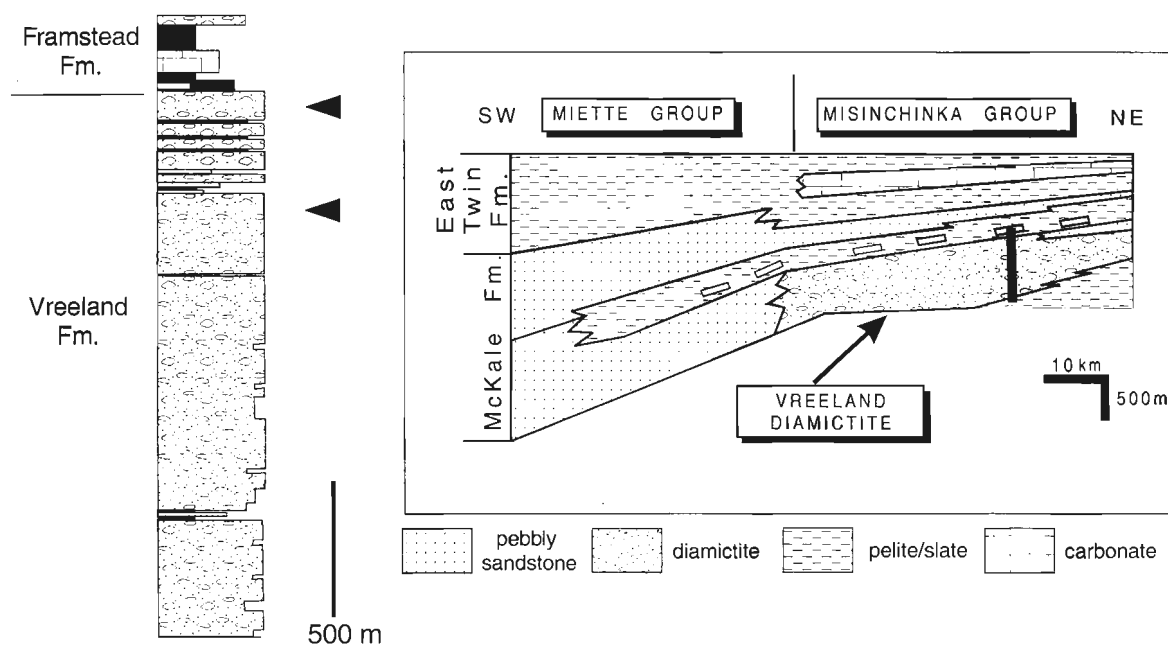


**Figure 6.** Schematic stratigraphic relationships between the Vreeland Formation diamictites and the turbidite facies of the Miette Group. The vertical line shows the approximate position of the measured section illustrated to the left. The stratigraphic section to the left is through the lower Misinchinka Group in the Herrick Creek area and shows the stratigraphic position of dated clasts (from McMechan, 1990 and Hein and McMechan, 1994, respectively).

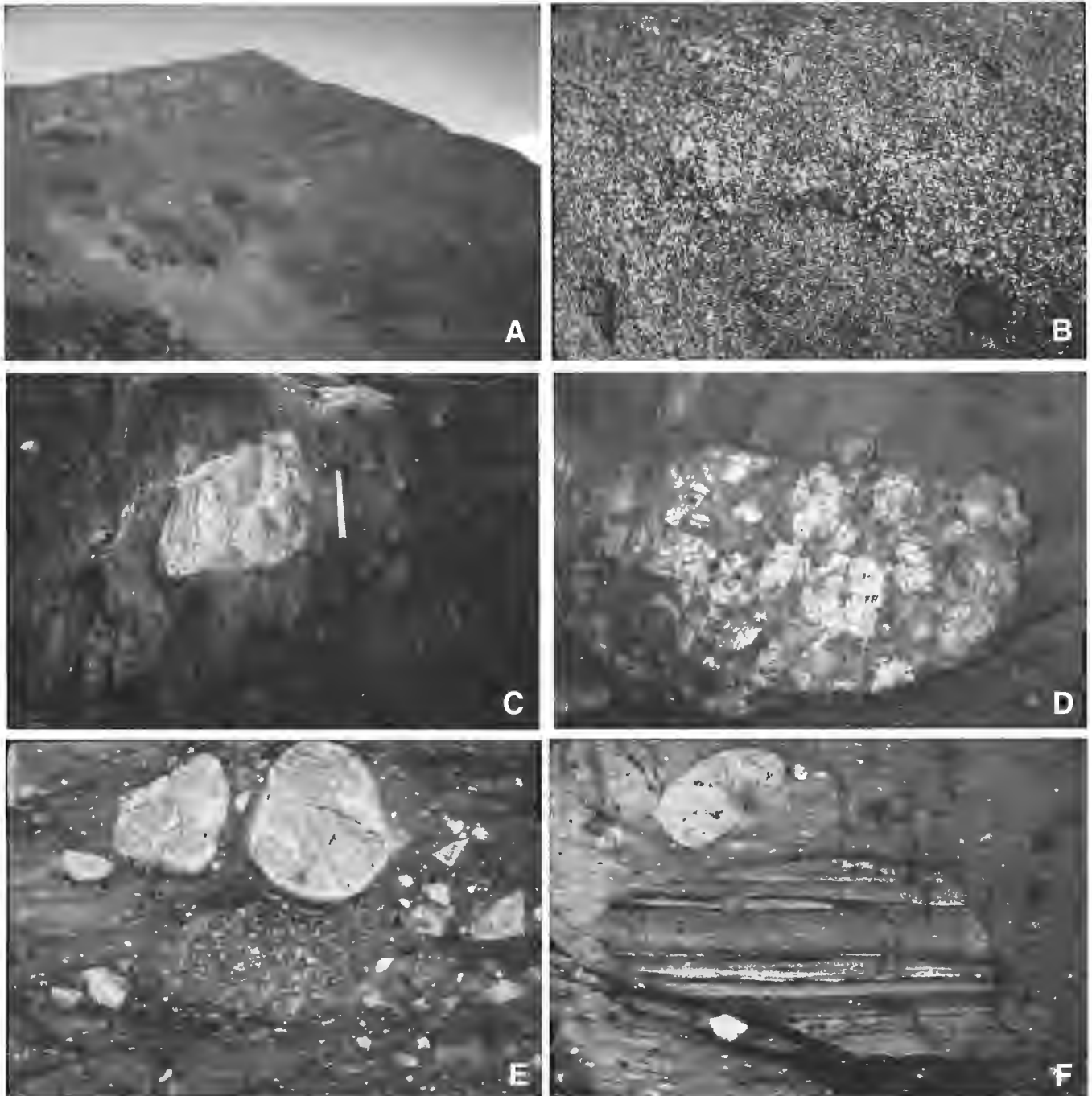


**Figure 7.** Exemplary photos from the Vreeland Formation in the Herrick Creek area (54°35'N; 121°34'W) **A)** Cliffside exposure shallow dipping Vreeland Formation diamictite showing the crude stratification typical of this unit. **B)** Coarse pegmatitic patch within boulder of diabase. **C)** Large stone of equigranular alkali granite in cleaved silty argillaceous matrix (RAR-90-W11). **D)** Stone of potassium feldspar megacrystic granite (RAR-90-W12). **E)** Stones composed of quartzite (light-coloured) and dacite porphyry (RAR-90-W13). Note apparent deformation of dacite stone by compaction and impingement of quartzite boulder. **F)** Undated aphyric rhyolite with flow banding defined by trains of devitrification spherules.

Bowring and Grotzinger, 1992). The ages of plutonic rocks in the Great Bear Magmatic Zone match those in the Shezal Formation and it is conceivable that is the source of the Shezal boulders. It is surprising however, that there are no clasts of volcanic rock, which is abundant in the Great Bear Magmatic Zone, nor are there any clasts of foliated granitoids which are also common in Wopmay Orogen (Hildebrand et al., 1987).

An alternative explanation is that the Rapitan stranger stones were derived from an intra-Cordilleran source. This is supported by two pieces of evidence. First, virtually all of the Rapitan Group clasts are of relatively local derivation and it seems incongruous that only three clasts would have been of long distance transport. Second, the ages of the clasts are nearly identical to the ages of intra-Cordilleran basement

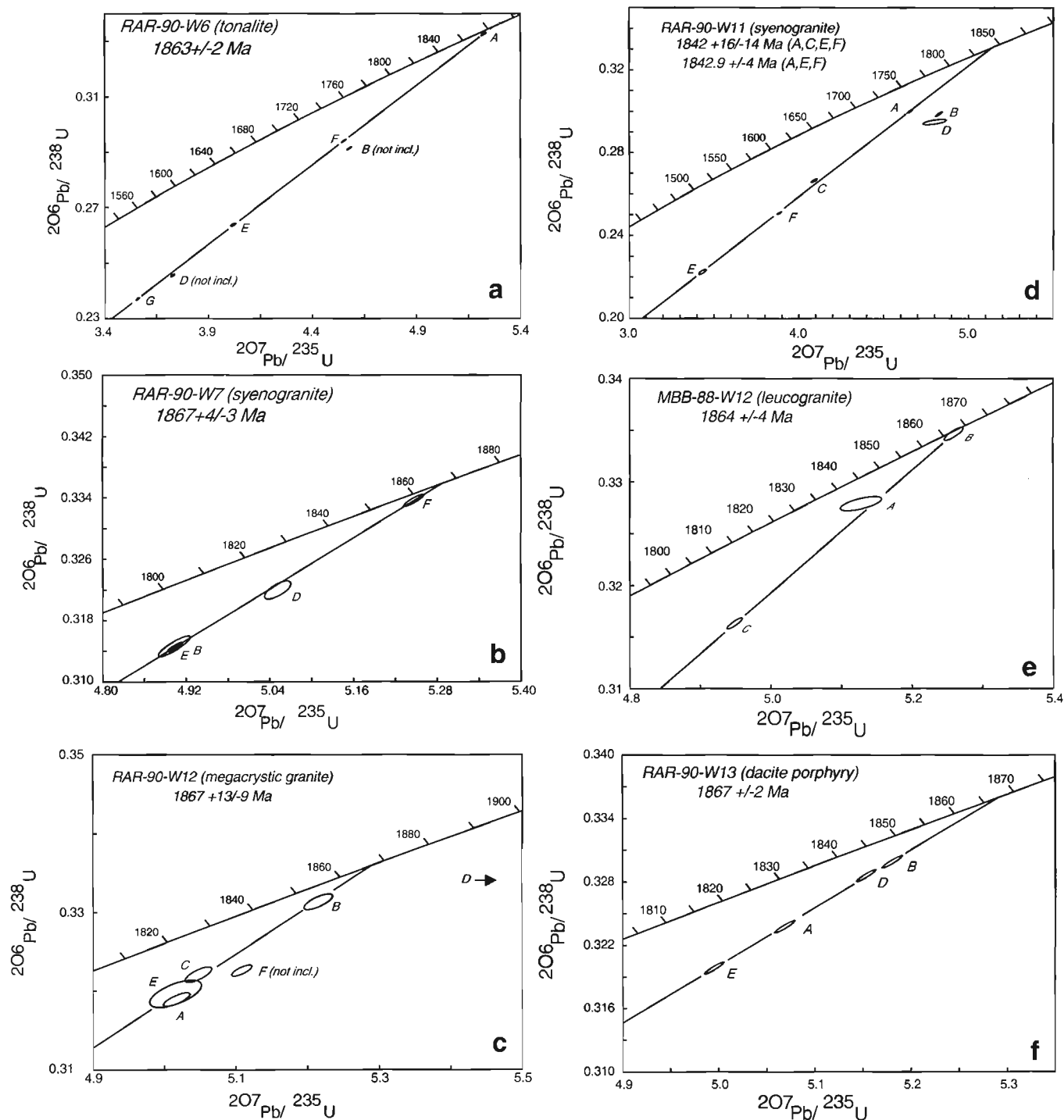


Figure 8. Concordia plots for igneous stones in the Vreeland Formation.



rocks, albeit present much further to the south. Nonetheless we suggest that derivation of the Rapitan stranger stones is more easily explained with an intra-Cordilleran source that may have been exposed locally during rifting

### *Misinchinka Group*

The ages of the igneous rocks dated from the Vreeland Formation diamictites fall into a narrow range of ca. 1867-1863 Ma and one granite dated at 1842 Ma. A number of possible sources of these age rocks are present in the western Canadian Shield. The Great Bear Magmatic Zone is a 100 km wide by 900 km long belt of high level calc-alkaline plutonic and volcanic rocks. It comprises two main magmatic episodes: an 1875-1860 Ma prefolding suite of basalt to rhyolite and biotite-hornblende granite plutons and a syn- to postfolding suite of 1858-1840 Ma biotite syenogranite and subordinate hornblende diorite, quartz diorite, and monzodiorite (Hildebrand et al., 1987). The folding event created macroscopic folds with a gentle northward plunge but little penetrative deformation or metamorphism of rocks of the older plutonic suite, consistent with the lack of deformational fabrics in Vreeland Formation boulders. Another possible source region is a poorly known region of the basement termed the Fort Simpson magnetic high (Hoffman, 1987; Villeneuve et al., 1991) that is about 200 km west of and parallel to the Great Bear Magmatic Zone (Fig. 1). Although buried beneath Phanerozoic sediments, the aeromagnetic signature of this belt is strikingly similar to the calc-alkaline magmatic Great Bear Magmatic Zone suggesting that the Fort Simpson anomaly may be caused by predominantly calc-alkaline plutonic rocks. Little direct information is available from the rocks that comprise the Fort Simpson high as only two hydrocarbon exploration wells drilled to basement. Each recovered undeformed biotite granites from depths of 2.5-3.0 km and although these two samples were separated by 300 km, both gave identical U-Pb ages of 1845 Ma, an age that overlaps with the youngest Great Bear Magmatic Zone plutons and is also present in the Vreeland Formation boulder suite (Villeneuve et al., 1991).

Based solely on the ages and lithologies of dated boulders from the Vreeland Formation, there is little to discriminate between a Great Bear Magmatic Zone source and a Fort Simpson high source. We considered using neodymium (Nd) isotopes signatures of the Vreeland Formation boulders as a test of these contrasting possible source areas but unfortunately the Nd isotopic composition of the Fort Simpson granites is indistinguishable from that of the Great Bear plutonic rocks (Villeneuve et al., 1991). However, as pointed out by McMechan (1990) the Vreeland Formation lies to the southwest of the west flank of the ancestral Peace River Arch which is underlain by the southernmost extent of the Fort Simpson magnetic anomaly (Ross, 1990). Recent seismic reflection data recorded along the western flank of the Fort Simpson High in northeast British Columbia show that

Windermere strata thin and may pinch-out to the northeast, suggesting that the Fort Simpson was exposed during Windermere sedimentation (Cook and Van der Velden, 1993). Thus given the proximity of the Fort Simpson High to the Neoproterozoic margin of western Canada we suggest that it represents the most likely source of the boulders.

## **CONCLUSIONS**

Uranium-lead zircon analysis of stranger stones from glaciogenic strata within the Rapitan Group fall into two ages: ca. 755 Ma and ca. 1860-1857 Ma. The younger date provides a maximum age for deposition of the lower Rapitan Group (Sayunei Formation). In addition the age of 755 Ma is similar to the ages of magmatism that are widespread within or below the lower parts of the Windermere Supergroup in the Canadian Cordillera. We suggest that 755 Ma granite was derived locally from an intra-Cordilleran pluton exposed during rift-related uplift. The two ca. 1860 Ma clasts could have been derived from similar age plutonic rocks of the Great Bear Magmatic Zone, over 500 km to the east in the Canadian Shield. Alternatively, they too may have an intra-Cordilleran source as there appears to be a pattern of ca. 1860 Ma and ca. 740 Ma gneissic rocks within intra-Cordilleran basement in the southern Cordillera. A similar basement association may underlie the northern Cordillera and was exposed during Neoproterozoic rifting.

Stranger stones in the Vreeland Formation diamictites are mostly 1867-1863 Ma with a single clast dated at 1842 Ma. The composition of the clasts is consistent with derivation from shallow level igneous rocks of a continental magmatic arc. In western Canada, two source areas are permissive; the Great Bear Magmatic Zone well to the north (more than 400 km) of the Vreeland Formation or the Fort Simpson high, a buried magmatic arc that is proximal to the Vreeland Formation diamictites. Our preferred explanation is derivation of the Vreeland stranger stones from igneous rocks of the Fort Simpson high which would have been exposed on the western flank of the Peace River Arch during Neoproterozoic sedimentation.

## **ACKNOWLEDGMENTS**

Margot McMechan is thanked for pointing out the occurrence of the granitic boulders in the Vreeland Formation and for providing a stimulating field trip to the remote Herrick Creek area. Jim Aitken provided the samples and context for the stranger stones from the Rapitan Group. The staff at the GSC geochronology lab (Klaus Santkowski and Jack MacRae) are thanked for their help in this project. Jeff Nazarchuk is thanked for sampling of the Vreeland Formation. Rob Rainbird is thanked for his review of this contribution.

## REFERENCES

- Aalto, R.K.**  
1971: Glacial marine sedimentation and stratigraphy of the Toby Conglomerate (Upper Proterozoic), southeastern British Columbia, northwestern Idaho and northeastern Washington; *Canadian Journal of Earth Sciences*, v. 8, p. 753-787.
- Aitken, J.D.**  
1989: Uppermost Proterozoic formations in central Mackenzie Mountains, Geological Survey of Canada, Bulletin 368, 26 p.  
1991: The Ice Brook Formation and post-Rapitan Late Proterozoic glaciation, Mackenzie Mountains, Northwest Territories; Geological Survey of Canada, Bulletin 404, 43 p.
- Aitken, J.D., Macqueen, R.W., and Usher, J.L.**  
1973: Reconnaissance studies of Proterozoic and Cambrian strigraphy, lower Mackenzie River area (Operation Norman), District of Mackenzie; Geological Survey of Canada, Paper 73-9, 178 p.
- Aitken, J.D. and Pugh, D.C.**  
1984: The Fort Norman and Leith Ridge structures: major, buried pre-Cambrian features underlying Franklin Mountains and Great Bear and Mackenzie plains; *Bulletin of Canadian Petroleum Geology*, v. 32, p. 139-146.
- Armstrong, R.L.**  
1988: Mesozoic and early Cenozoic magmatic evolution of the Canadian Cordillera in Processes in continental lithospheric deformation, (ed.) S.P. Clark Jr., B.C. Burchfiel, and J. Suppe; Geological Society of America, Special Publication 218, p. 55-92.
- Armstrong, R.L., Parrish, R.R., van der Heyden, P., Scott, K., Runkle, D., and Brown, R.L.**  
1991: Early Proterozoic basement exposures in the southern Canadian Cordillera: core gneiss of Frenchman Cap, Unit 1 of the Grand Forks Gneiss, and the Vaseaux Formation; *Canadian Journal of Earth Sciences*, v. 28, p. 1169-1201.
- Bowring, S.A. and Grotzinger, J.P.**  
1992: Implications of new chronostratigraphy for the tectonic evolution of Wopmay orogen, northwest Canadian Shield; *American Journal of Science*, v. 292, p. 1-20.
- Cook, D.G. and Maclean, B.C.**  
1995: The intracratonic Paleoproterozoic Forward orogeny, implications for regional correlations, Northwest Territories, Canada; *Canadian Journal of Earth Sciences*, v. 32, p. 1991-2008.
- Cook, F.A. and Van der Velden, A.**  
1993: Proterozoic crustal transition beneath the Western Canada sedimentary basin; *Geology*, v. 21, p. 785-788.
- Cook, F.A., Dredge, M., and Clark, E.A.**  
1992: The Proterozoic Fort Simpson structural trend in northwestern Canada; *Geological Society of America, Bulletin*, v. 104, p. 1121-1137.
- Davis, D.W.**  
1982: Optimum linear regression and error estimation applied to U-Pb data; *Canadian Journal of Earth Sciences*, v. 19, p. 2141-2149.
- Devlin, W.J. and Bond, G.C.**  
1988: The initiation of the early Paleozoic Cordilleran miogeoclinal: evidence from the uppermost Proterozoic-Lower Cambrian Hamill Group of southeastern British Columbia; *Canadian Journal of Earth Sciences*, v. 25, p. 1-19.
- Devlin, W.J., Bruekner, H.K., and Bond, G.C.**  
1989: New isotopic data and a preliminary age for volcanics near the base of the Windermere Supergroup, northeastern Washington, U.S.A.; *Canadian Journal of Earth Sciences*, v. 25, p. 1906-1911.
- Eisbacher, G.E.**  
1981: Sedimentary tectonics and glacial record in the Windermere Supergroup, Mackenzie Mountains, Northwest Territories; Geological Survey of Canada, Paper 80-27, 40 p.
- Evenchick, C.A.**  
1988: Stratigraphy, metamorphism, structure and their tectonic implications in the Sifton and Desererts ranges, Cassiar and northern Rocky Mountains, northern British Columbia; Geological Survey of Canada, Bulletin 376, 90 p.
- Evenchick, C.A., Parrish, R.R., and Gabrielse, H.**  
1984: Precambrian gneiss and late Proterozoic sedimentation in north-central British Columbia; *Geology*, v. 12, p. 233-237.
- Gabrielse, H.**  
1972: Younger Precambrian of the northern Canadian Cordillera. *American Journal of Science*, v. 272, p. 521-536.
- Gabrielse, H. and Campbell, R.B.**  
1991: Upper Proterozoic assemblages, Chapter 6 in *Geology of the Cordilleran Orogen in Canada*, (ed.) H. Gabrielse and C.J. Yorath; Geological Survey of Canada, *Geology of Canada*, no. 4, p. 125-150 (also Geological Society of America, *The Geology of North America*, v. G-2).
- Gehrels, G.E., Dickinson, W.R., Ross, G.M., Stewart, J.H., and Howell, D.H.**  
1995: Detrital zircon reference for Cambrian to Triassic miogeoclinal strata of western North America; *Geology*, v. 23, p. 831-834.
- Hein, F.J. and McMechan, M.E.**  
1994: Proterozoic-Lower Cambrian strata of the Western Canada Sedimentary Basin; in *Geological Atlas of the Western Canada Sedimentary Basin*, (comp.) G.D. Mossop and I. Shetsen; Calgary, Canadian Society of Petroleum Geologists and Alberta Research Council, p. 47-57.
- Hildebrand, R.S., Hoffman, P.F., and Bowring, S.A.**  
1987: Tectono-magmatic evolution of the Great Bear magmatic zone, Wopmay Orogen, northwestern Canada; *Journal of Volcanology and Geothermal Research*, v. 32, p. 99-118.
- Hoffman, P.F.**  
1987: Continental transform tectonics: Great Slave Lake shear zone (ca. 1.9 Ga), northwest Canada; *Geology*, v. 15, p. 785-788.  
1989: Precambrian geology and tectonic history of North America, in *The geology of North America-An overview*, (ed.) A.W. Bally and A.R. Palmer; Boulder, Colorado, Geological Society of America, *Geology of North America*, v. A, p. 447-512.  
1991: Did the breakout of Laurentia turn Gondwanaland inside-out?; *Science*, v. 252, p. 1409-1412.
- Jefferson, C.W. and Parrish, R.R.**  
1989: Late Proterozoic stratigraphy, U-Pb zircon ages and rift tectonics, Mackenzie Mountains, northwestern Canada; *Canadian Journal of Earth Sciences*, v. 26, p. 1784-1801.
- Knoll, A.H. and Walter, M.R.**  
1992: Latest Proterozoic stratigraphy and Earth history; *Nature*, v. 356, p. 673-678.
- Krogh, T.E.**  
1982: Improved accuracy of U-Pb zircon ages by the creation of more concordant systems using an air abrasion technique; *Geochimica et Cosmochimica Acta*, v. 46, p. 637-649.
- Lickorish, W.H. and Simony, P.S.**  
1995: Evidence for late rifting of the Cordilleran margin outlined by stratigraphic division of the Lower Cambrian Gog Group, Rocky Mountain Main Ranges, British Columbia and Alberta; *Canadian Journal of Earth Sciences*, v. 32, p. 860-874.
- Loveridge, W.D., Leech, G.B., Stevens, R.D., and Sullivan, R.W.**  
1981: Zircon and monazite ages of a granitic clast in Toby Conglomerate (Windermere Supergroup), Canal Flats, British Columbia; in *Current Research, Part C*; Geological Survey of Canada, Paper 81-1C, p. 131-134.
- McDonough, M.R. and Parrish, R.R.**  
1991: Proterozoic gneisses of the Malton Complex, near Valemount, British Columbia: U-Pb ages and Nd isotopic signatures; *Canadian Journal of Earth Sciences*, v. 28, p. 1202-1216.
- McMechan, M.E.**  
1990: Upper Proterozoic to Middle Cambrian history of the Peace River Arch: evidence from the Rocky Mountains; *Bulletin of Canadian Petroleum Geology*, v. 38A, p. 36-44.
- Miller, F.K.**  
1994: The Windermere Group and late Proterozoic tectonics in northeastern Washington and northern Idaho; Washington Division of Geology and Earth Resources, Bulletin 80, p. 1-19.
- Murphy, D.C., Walker, R.T., and Parrish, R.R.**  
1991: Gold Creek gneiss, southeastern Cariboo Mountains, British Columbia: age, geological setting, and regional implications; *Canadian Journal of Earth Sciences*, v. 28, p. 1217-1231.
- Narbonne, G.M. and Aitken, J.D.**  
1995: Neoproterozoic of the Mackenzie Mountains, northwestern Canada; *Precambrian Research*, v. 73, p. 101-122.
- Parkinson, D.**  
1991: Age and isotopic character of Early Proterozoic basement gneisses in the southern Monashee Complex, southeastern British Columbia; *Canadian Journal of Earth Sciences*, v. 28, p. 1159-1168.

- Parrish, R.R. and Scammell, R.J.**  
 1988: The age of the Mount Copeland Syenite Gneiss and its metamorphic zircons, Monashee Complex, southeastern British Columbia; in *Radiogenic Age and Isotopic Studies: Report 2*; Geological Survey of Canada, Paper 88-2, p. 21-28.
- Parrish, R.R., Roddick, J.C., Loveridge, W.D., and Sullivan, R.W.**  
 1987: Uranium-lead analytical techniques at the geochronology laboratory, Geological Survey of Canada; in *Radiogenic Age and Isotope Studies: Report 1*; Geological Survey of Canada, Paper 87-2, p. 3-7.
- Roddick, J.C.**  
 1987: Generalized numerical error analysis with applications to geochronology and thermodynamics; *Geochimica et Cosmochimica Acta*, v. 51, p. 2129-2135.
- Roots, C.F. and Parrish, R.R.**  
 1988: Age of the Mount Harper Volcanic Complex, southern Ogilvie Mountains, Yukon; in *Radiogenic Age and Isotopic Studies: Report 2*; Geological Survey of Canada, Paper 88-2, p. 29-35.
- Ross, G.M.**  
 1990: Deep crust and basement structure of the Peace River Arch; *Bulletin of Canadian Petroleum Geology*, v. 38A, p. 25-35.  
 1991: Tectonic setting of the Windermere Supergroup revisited; *Geology*, v. 19, p. 1125-1128.
- Ross, G.M. and Bowring, S.A.**  
 1990: Detrital zircon geochronology of the Windermere Supergroup and the tectonic assembly of the southern Canadian Cordillera; *Journal of Geology*, v. 98, p. 879-893.
- Ross, G.M. and Murphy, D.C.**  
 1988: Transgressive stratigraphy, anoxia and regional correlations in the Late Proterozoic Windermere grit system of the southern Canadian Cordillera; *Geology*, v. 16, p. 139-143.
- Ross, G.M. and Parrish, R.R.**  
 1991: Detrital zircon geochronology of metasedimentary rocks in the southern Omineca Belt, Canadian Cordillera; *Canadian Journal of Earth Science*, v. 28, p. 1254-1270.
- Ross, G.M., Bloch, J.D. and Krouse, H.R.**  
 1995: Neoproterozoic strata of the southern Canadian Cordillera and the evolution of seawater sulfate; *Precambrian Research*, v. 73, p. 71-99.
- Ross, G.M., McMechan, M., and Hein, F.**  
 1989: Proterozoic history: birth of the miogeocline; in *The Western Canada Sedimentary Basin*, (ed.) B.D. Ricketts; Canadian Society of Petroleum Geologists, Calgary, p. 79-104.
- Ross, G.M., Parrish, R.R., Villeneuve, M.E., and Bowring, S.A.**  
 1991: Geophysics and geochronology of the crystalline basement of the Alberta Basin, western Canada; *Canadian Journal of Earth Sciences*, v. 28, p. 512-522.
- Stewart, J.H.**  
 1972: Initial deposits of the Cordilleran geosyncline: evidence of Late Precambrian (<850 m.y.) continental separation; *Geological Society of America, Bulletin*, v. 83, p. 1345-1360.
- Villeneuve, M.E., Theriault, R.J., and Ross, G.M.**  
 1991: U-Pb ages and Sm-Nd signature of two subsurface granites from the Fort Simpson magnetic high, northwest Canada; *Canadian Journal of Earth Sciences*, v. 28, p. 1003-1008.
- Villeneuve, M.E., Ross, G.M., Theriault, R.J., Miles, W., Parrish, R.R., and Broome, J.**  
 1993: Geophysical subdivision, U-Pb geochronology and Sm-Nd isotope geochemistry of the crystalline basement of the western Canada sedimentary basin, Alberta and northeastern British Columbia; *Geological Survey of Canada Bulletin* 447, 86 p.
- Yeo, G.M.**  
 1981: The Late Proterozoic Rapitan glaciation in the northern Cordillera; in *Proterozoic Basins of Canada*, (ed.) F.H.A. Campbell; Geological Survey of Canada, Paper 81-10, p. 25-46.
- Young, G.M.**  
 1976: Iron formation and glaciogenic rocks of the Rapitan Group, Mackenzie Mountains, Yukon and Northwest Territories, Canada; *Precambrian Research*, v. 3, p. 137-158.



## Other publications containing geochronological data generated by the Geochronology Laboratory of the Geological Survey of Canada

**Currie, K.L. and van Breemen, O.**

1996: The origin of rare minerals in the Kipawa syenite complex, western Quebec; *The Canadian Mineralogist*, v. 34, p. 435-451.

**Davis, W.J., Gariépy, C., and van Breemen, O.**

1996: Pb Isotopic composition of late Archean granites and the extent of recycling early Archean crust in the Slave Province, northwest Canada; *Chemical Geology*, v. 130, p. 255-269.

**Henderson, J.R., Kerswill, J.A., Henderson, M.N., Villeneuve, M., Petch, C.A., Dehls, J.F., and O'Keefe, M.D.**

1995: Geology, geochronology and metallogeny of the High Lake greenstone belt, Archean Slave Structural Province, Northwest Territories; in *Current Research 1995-C*, Geological Survey of Canada, p. 97-106.

**Higgins, M.D. and van Breemen, O.**

1996: Three generations of anorthosite-mangerite-charnockite-granite (AMCG) magmatism, contact magmatism and tectonism in the Saguenay-Lac-Saint-Jean region of the Grenville Province, Canada; *Precambrian Research*, v. 79, p. 327-346.

**Lecheminant, A.N., Rainbird, R.H., and Villeneuve, M.E.**

1996: Precambrian geology of northern Wellington Inlier, Victoria Island, Northwest Territories; in *Current Research 1996-C*; Geological Survey of Canada, p. 1-10.

**Pehrsson, S., Hanmer, S., and van Breemen, O.**

1995: U-Pb geochronology of the Raglan gabbro belt, Central Metasedimentary Belt, Ontario: implications for an ensialic marginal basin in the Grenville Orogen; *Canadian Journal of Earth Sciences*, v. 33, p. 691-702.

**Rainbird, R.H., McNicoll, V.J., Thériault, R.J.,**

**Heaman, L.M., Abbott, D.G.F., and Thorkelson, D.J.**

1997: Pan-continental river system draining Grenville Orogen recorded by U-Pb and Sm-Nd geochronology of Neoproterozoic quartzarenites and mudrocks, Northwestern Canada; *Journal of Geology*, v. 105, p. 1-17.

**Rainbird, R.H., Villeneuve, M.E., Cook, D.G., and MacLean, B.C.**

1996: Detrital zircon ages from two wells in the Northwest Territories: implications for the correlation and provenance of Proterozoic subsurface strata; in *Current Research 1996-B*, Geological Survey of Canada, p. 29-38.

**Skulski, T. and Percival, J.A.**

1996: Allochthonous 2.78 Ga oceanic plateau slivers in a 2.72 Ga continental arc sequence: Vizion greenstone belt, northeastern Superior Province, Canada; *Lithos*, v. 37, p. 163-179.

**Thériault, R.J. and Ermanovics, I.**

1997: Sm-Nd isotopic and geochemical characterization of the Paleoproterozoic Torngat orogen, Labrador, Canada; *Precambrian Research*, v. 81, p. 15-37.

**Wodicka, N., Parrish, R.R., and Jamieson, R.A.**

1996: The Parry Sound domain: a far-travelled allochthon? New evidence from U-Pb zircon geochronology; *Canadian Journal of Earth Sciences*, v. 33, p. 1087-1104.

